

**PREDICTION OF SEDIMENTARY ARCHITECTURE AND  
LITHOLOGICAL HETEROGENEITY IN FLUVIAL POINT-BAR  
DEPOSITS**

Catherine Ellen Russell

Submitted in accordance with the requirements for the degree of

Doctor of Philosophy

The University of Leeds

School of Earth and Environment

July 2017





The candidate confirms that the work submitted is her own, except where work which has formed part of jointly-authored publications has been included. The contribution of the candidate and the other authors to this work is explicitly indicated below. The candidate confirms that appropriate credit has been given within the thesis where reference has been made to the work of others.

© 2017 The University of Leeds and Catherine Ellen Russell.

A version of Chapter 2 is under review for the IAS Special Publication 48, and titled “A new universal approach to morphometric analysis of fluvial meander bends”. The authors are as follows (in order): Catherine E. Russell, Nigel P. Mountney, David M. Hodgson, Luca Colombera, and Robert E. Thomas. The candidate set the scientific scope of the work, devised and developed the methodology, collected data from satellite imagery, performed all data analysis, drew all illustrations and graphs, and wrote the text. The co-authors guided the development of the methodology, and provided guidance during the design of the method and feedback on the manuscript.

A version of Chapter 3 is under review for the IAS Special Publication 48, and titled “Prediction of lithological heterogeneity in fluvial point-bar deposits from analysis of meander morphology and scroll-bar pattern”. The authors are as follows (in order): Catherine E. Russell, Nigel P. Mountney, David M. Hodgson, and Luca Colombera. The candidate set the scientific scope of the work, devised and developed the methodology, collected data from satellite imagery and the published literature, performed all data analysis, drew all illustrations and graphs, and wrote the text. The co-authors guided the development of the methodology, and provided guidance during the design of the method and feedback on the manuscript.

## Acknowledgements

First and foremost I would like to acknowledge how grateful I am for the support that I have received from my supervisors Nigel Mountney, David Hodgson, and Luca Colombera. In particular, I would like to thank Nigel for giving me this opportunity, and allowing me the freedom to explore ideas that have been instrumental in shaping this thesis. Also thank you to Robert Thomas for his advice in the development of the Intersection Shape methodology.

I would like to thank my Mum and Dad for their patience because this PhD has been a strain on all of us at times; I would like them to consider it as much their achievement as it is mine. Thank you also to my sister Tish who is always there on the end of the phone and gave me encouragement when I needed it, despite not liking rocks. Thank you to Peter for his patience and believing in me no matter what. I am lucky to have such a big and supportive family, thank you for your unfailing support.

I would like to thank my field assistants Fay McDermott and Matthew Morgan for their support and help in collecting a somewhat tedious dataset, you are patient people. My friends and colleagues (from FRG, Strat, SMRG, TRG, BSG, and the Leeds Quaternary research groups) have helped to make this experience really enjoyable with my personal highlights being the BSRG trip to Barcelona, and the USA road trip of 2015. Particular mentions go to Jen Stuart for helping me kick off the write-up process and her support throughout; Hazel Beaumont for believing in me and sharing an uncommon love for rivers; Lou Proctor for her support and our coffee breaks; and last but by no means least, Maggie whose constant support and friendship has been an integral part of my PhD experience.

This research was funded by the sponsors of the Fluvial & Eolian Research Group: Aker BP, Areva, BHPBilliton, ConocoPhillips, Murphy Oil Corporation, Nexen, Saudi Aramco, Shell, Tullow Oil, Woodside, and YPF.

## Abstract

Point-bar deposits in meandering rivers preserve lithological heterogeneities that influence hydrocarbon production. Here, a series of methodologies are used to determine the lateral extent, accretion history, and internal facies heterogeneity of fluvial point-bar deposits to improve subsurface prediction and reconstructions of exhumed meander belts. A novel quantitative Intersection Shape methodology has been developed to describe the morphology of meandering fluvial reaches using data from 260 active and 10 abandoned meander bends from 13 river reaches in different physiographic environments. The resulting classification scheme describes 25 meander morphologies in 4 parent groups (open asymmetric, angular, bulbous, open symmetric). Results are expressed graphically enabling visual assessment and comparison. The overall scroll-bar pattern type (22 shapes in 8 parent groups) can be divided into growth phases and shapes derived from the Intersection Shape methodology overlain on the scroll-bar pattern to find best-fits and determine a meander-bend accretion history. A map of predicted relative heterogeneity can be constructed that accounts for the bend growth history and downstream fining trends. Abandonment mechanisms that individual meanders undergo (neck cut-off, chute cut-off, neck cut-off on converging limbs) affect the lateral extent of the resultant point-bar deposits. Active point-bar deposits are dominantly equidimensional (1:1) whereas abandoned point-bar deposits exhibit both rounded (1:1) and elongated (1:<1) shapes in near-equal proportion. Focussing on abandoned point-bar deposits in an active reach may lead to underestimation of the lateral dimensions of amalgamated fluvial point-bar deposits. By rigorously describing the shape, dimensions, and relative proportions of point-bar deposits in meandering fluvial systems the methodologies developed here avoid such underestimation and can be applied to: (i) generate testable hypotheses of heterogeneity for modern systems; (ii) develop models of lithological

heterogeneity in ancient systems based on identification of analogous processes between modern and ancient fluvial systems; and (iii) infer the accretion history of exhumed systems.

# Table of Contents

Acknowledgements.....	ii
Abstract .....	iii
1 Introduction .....	1
1.1 Project background and rationale.....	1
1.2 Aims and Objectives .....	20
1.3 Research questions .....	20
1.4 Methods .....	27
1.4.1 Remote sensing.....	27
1.4.2 Outcrop analysis.....	28
1.5 Thesis layout.....	28
2 A new universal approach to morphometric analysis of fluvial meander bends	32
2.1 Chapter Summary .....	32
2.2 Introduction .....	33
2.3 Background.....	36
2.3.1 The description of meander form: Subjective shape classification .....	38
2.3.2 The description of meander form: Simplified sine-generated type curves .....	40
2.3.3 The description of meander form: Radius of Curvature.....	40
2.3.4 The description of meander form: Bend Asymmetry .....	41
2.4 Data and methods.....	42

2.5	Application and results .....	54
2.6	Discussion.....	64
2.7	Conclusions.....	67
3	Prediction of lithological heterogeneity in fluvial point-bar deposits from analysis of meander morphology and scroll-bar pattern .....	70
3.1	Chapter Summary .....	70
3.2	Introduction .....	71
3.3	Background.....	76
3.3.1	Meander shape.....	77
3.3.2	Scroll-bar pattern .....	77
3.3.3	Point-bar heterogeneity.....	79
3.4	Methodology.....	82
3.5	River Selection .....	84
3.5.1	Planform morphometry .....	87
3.5.2	Classification of the surface expression of scroll bar pattern.....	87
3.5.3	Meander-shape classification.....	91
3.5.4	Estimating lithological heterogeneity .....	92
3.6	Results .....	97
3.6.1	Meander shape.....	100
3.6.2	Surface expression of scroll-bar pattern.....	102
3.6.3	Relationships between the data sets.....	104
3.6.4	Observations from planform morphometric constructions .....	105

3.7	Discussion .....	114
3.7.1	Application of heterogeneity prediction to the sub-surface .....	114
3.7.2	Limitations and future development .....	117
3.8	Conclusions .....	118
4	Implications of the variation of mechanisms for fluvial abandonment on the stratigraphic record .....	120
4.1	Chapter Summary .....	120
4.2	Introduction .....	121
4.3	Background.....	126
4.3.1	Causes of meander cut-off .....	126
4.3.2	Channel fill.....	127
4.3.3	Neck cut-off .....	131
4.3.4	Chute cut-off.....	132
4.3.5	Avulsion.....	133
4.3.6	Styles of sandbody stacking .....	137
4.3.7	Lithological heterogeneity of abandoned point-bar deposits .....	137
4.4	Methodology .....	139
4.4.1	Recorded parameters.....	139
4.4.2	Styles of meander abandonment.....	141
4.4.3	Scroll-bar type .....	157
4.5	Results.....	157
4.6	Discussion .....	171

4.6.1	Planform point-bar dimensions .....	171
4.6.2	Controls on cut-off mechanisms.....	172
4.6.3	Preservation potential of point-bar deposits .....	173
4.6.4	Limitations .....	177
4.7	Conclusions.....	177
5	Reconstructing planform point-bar dimensions and palaeo-meander shape from a preserved point-bar deposit in outcrop .....	179
5.1	Chapter Summary .....	179
5.2	Introduction .....	180
5.3	Geological background.....	185
5.4	Methodology.....	194
5.4.1	Lithofacies identification.....	194
5.4.2	Sedimentary graphic logs .....	194
5.4.3	Stratigraphic panels .....	195
5.4.4	Palaeocurrent analysis.....	197
5.5	Data analysis techniques.....	197
5.6	Point-bar reconstruction .....	200
5.7	Results .....	200
5.7.1	Lithofacies .....	200
5.7.2	Facies successions.....	224
5.7.3	FAKTS analysis .....	234
5.7.4	Panels .....	238



5.8	Discussion .....	245
5.8.1	Application of established methodologies .....	245
5.8.2	Application of facies and facies successions .....	251
5.8.3	Application of architectural derivations.....	253
5.8.4	Limitations .....	269
5.9	Conclusions .....	269
6	Discussion .....	271
6.1	Research Question 1 .....	271
	How can meander shapes be geometrically classified, in order to be compared universally, in a repeatable, quantifiable manner?.....	271
6.2	Research Question 2 .....	277
	How does the geometry of a meander and scroll-bar pattern of the point-bar, relate to the heterogeneity of a point-bar deposit? .....	277
6.3	Research Question 3 .....	283
	What is the impact of the timing and mechanism of channel abandonment on geometries of preserved point-bar deposits? .....	283
6.4	Research Question 4 .....	289
	How can planform point-bar dimensions and palaeo meander shape be reconstructed from an exposure of a preserved point-bar deposit. ....	289
6.5	Research Question 5 .....	298
	How can the internal stratigraphic architecture, and geomorphic variability, be predicted from surface morphology, or flattened seismic timeslices? .	298
7	Conclusions and Future Work .....	303

7.1	Conclusions.....	303
7.2	Future Work .....	308
8	List of References .....	312
9	Appendix .....	350

## List of Figures

Figure 1.1 - Fluvial reach morphologies. From Brice 1978, modified by Schumm (1985). .....	2
Figure 1.2 - A graph to show the optimum slope for meandering channels .....	3
Figure 1.3 – Controls on fluvial morphology from Church (2006). .....	4
Figure 1.4 – Meandering fluvial systems on Aeolis Dorsa (153.636°, -6.041°), Mars ....	6
Figure 1.5 - a) A regional scale facies model. From Ghazi and Mountney (2009). .....	8
Figure 1.6 - A consideration of data resolution and coverage for a typical subsurface field (from Howell <i>et al.</i> , 2014). .....	9
Figure 1.7 - A classic cross-section of a point-bar deposit .....	13
Figure 2.1 - A) A demonstration of the variety of meaning for wavelength and amplitude in the literature .....	38
Figure 2.2 - Meander classification schemes modified from A) Ielpi and Ghinassi (2014), B) Bridge (2003), C) Allen (1982), D) Brice (1974).....	39
Figure 2.3 - A step-by-step guide for completion of the Intersection Shape methodology with each of the three outputs highlighted with a red box .....	44
Figure 2.4 – Demonstrations of the definition of a meander .....	45
Figure 2.5 - A) The morphometric parameters measured in each meander for this study; B) the terminology of the “Intersection Shape” methodology.....	47
Figure 2.6 – Implementation of the Intersection Shape methodology.....	50
Figure 2.7 - Four groups of meander and their associated shapes on bivariate plots. .	51
Figure 2.8 - Graphical table of shape properties showing the characteristics by which each type of meander is defined. ....	53
Figure 2.9 - Planform outlines of the three rivers investigated in this paper; the Senegal River, the Irtysh (Ob) River and the Ok Tedi (Fly) River. ....	57

Figure 2.10 - Twenty meanders for three of the meandering reaches plotted onto graphs.....	58
Figure 2.11 - A comparison of meander shapes in their Groups between the Senegal and Irtysh (Ob) rivers. ....	61
Figure 2.12 - A) Three end member models of scroll bar pattern; B) Histograms representing the distribution of upstream and downstream asymmetry / resonance (Upstream limb to Apex - Downstream limb to Apex); C) Histogram representing upstream and downstream migration (Downstream limb to Apex - Downstream limb to MRG) respectively. ....	63
Figure 3.1 - A) Terminology used in the description of fluvial point-bars modified from Chapter 2; B) Inclined Heterolithic Strata (IHS), modified from Thomas <i>et al.</i> , (1987). ....	72
Figure 3.2 - Literature summary of heterogeneity data in point-bars.....	74
Figure 3.3 - A figure to show examples of the literature where meander shape change is depicted; A) Ielpi <i>et al.</i> (2014); B) Hooke (1977); C) Bridge (2003). ....	78
Figure 3.4 - A map of the simplified climate zones modified from (Peel <i>et al.</i> 2007). The rivers selected for this study are plotted. ....	83
Figure 3.5 - A classification of the surface expression of scroll bar pattern. 8 Types have been defined (Table 3.2); 22 sub-types were defined by identifying variations in the overall process described by the Type category.....	89
Figure 3.6 - A demonstration of the construction of a model of heterogeneity from a meander planform image .....	94
Figure 3.7 - A pie chart showing the proportion of each shape in the 260 meander shapes studied.....	101
Figure 3.8 - A pie chart showing the proportion of each scroll bar type in the 260 meander shapes studied.....	103
Figure 3.9 - A graph showing the variety of scroll bar patterns in each meander shape group overall, and for each river studied. ....	104

Figure 3.10 - Pie charts of the proportions of features seen in fluvial meandering systems are shown with planform morphology maps for the Ok Tedi (Fly) River, Papua New Guinea, and the Senegal River, Senegal .....	110
Figure 3.11 – Pie charts of the proportions of features seen in fluvial meandering systems are shown with planform morphology maps for the Murray River, Australia, and the Irtysh (Ob) River Russia.....	112
Figure 3.12 - Interpretations of the heterogeneity types for modern systems .....	113
Figure 3.13 - A comparison of the interpretation of a seismic time slice from the Cretaceous McMurray Formation, Alberta.....	115
Figure 4.1 - A) A figure to demonstrate connectivity of sand-prone sediment in planform and cross-section; B) An isopach map of two scenarios for the spatial distribution of meandering river sandstone bodies (from Donselaar and Overeem 2008).....	122
Figure 4.2 - Prevailing models of cut-off in the literature .....	125
Figure 4.3 - Solid lines are active channel courses, dashed represent abandoned ones. The log represents the vertical accretion which occurs post cut-off.....	128
Figure 4.4 - Schematic representation of the diversion angle ( $\alpha$ ) .....	130
Figure 4.5 - A figure of modern examples of the prevalent mechanisms of cut-off alongside ancient examples of flattened seismic imagery .....	136
Figure 4.6 - A description of the dimensions and ratios used in this study .....	140
Figure 4.7 - Individual cut-off styles .....	144
Figure 4.8 - Group cut-off styles.....	152
Figure 4.9 - A) A graph showing the comparative distributions of point-bar shape dimensions for 216 meander shapes; B) A graph showing a predictive relationship .	158
Figure 4.10 - A) A histogram showing the dimensions of active point-bars .....	159
Figure 4.11 – A graph to show the proportions of abandoned point-bar deposits and the individual cut-off style for each.....	161

Figure 4.12 - A graph to show the individual cut-off style for each abandoned point-bar deposit, and the style of scroll-bar pattern observed for each style. ....	162
Figure 4.13 - A) The proportions of scroll-bar patterns observed for the 110 abandoned point-bar deposits observed; B) Group cut-off styles observed, and the individual cut-off styles observed in each case. ....	165
Figure 4.14 - An assessment of abandoned point-bar deposit dimensions, individual cut-off styles, (with associated scroll-bar patterns), and group cut-off styles, for each of the 11 rivers studied.....	171
Figure 4.15 – Illustration demonstrating the preservational bias of point-bar deposits that are recently abandoned via chute or neck cut-off, as a result of the behaviour of its genetic proto meander. ....	174
Figure 4.16 - A flowchart demonstrating the relationships between the meander shapes described in Chapter 2, and the resulting abandoned point-bar deposit dimensions leading from asymmetric or symmetric cut-off. The code attributed to each meander shape related to those attributed in Figure 2.8. ....	176
Figure 5.1 - A figure to demonstrate the downstream fining of sediment on a meander bend (modified from Fustic et al., 2012). Orange represents mud-prone sediment, whilst yellow represents sand-prone. ....	183
Figure 5.2 - A figure to demonstrate the potential error in interpreting fluvial meander bends in outcrop. ....	184
Figure 5.3 - Location maps and geological setting of Nolton Haven cove.....	186
Figure 5.4 - Stratigraphic column combined from work by Waters et al., (2008), Waters et al., (2009; 2011), Jenkins (1962), Hartley and Warr (1990), with ages derived from Gradstein et al., (2004) .....	188
Figure 5.5 – A) Reconstructed palaeoenvironment of the early and late Westphalian (from Waters et al., 2009); B) A map showing the areas of Wales affected by the Caledonian and Variscan orogenies (from Dunne, 1983) .....	189

Figure 5.6-A planform sketch of the outcrop showing the overall accretion direction.	193
Figure 5.7 - Positions that the sedimentary graphic logs were taken from at Nolton Haven cove. The numbering system shown on the image refers to the logs that were recorded at Nolton Haven cove.....	196
Figure 5.8 - Facies panels describing the facies at the outcrop in detail.....	213
Figure 5.9 - Legends for the following figures. ....	215
Figure 5.10 – Depiction of the probabilities and statistical significance of facies relationships through use of the Walker (1979) methodology.....	228
Figure 5.11 – Figures showing sketch logs, and outcrop examples, of the facies successions identified in this study through use of the Markov chain analyses undertaken.....	231
Figure 5.12 – A bedform phase diagram that relates the mean grainsize to the mean flow velocity. ....	234
Figure 5.13 - A figure to show the average bed thicknesses for a 3 bed thick moving average of each facies.....	235
Figure 5.14 - A) A stacked column to show the probabilities of transition between facies; B) A pie chart describing the probability of each facies transitioning to itself vertically upward. ....	238
Figure 5.15 - A) A field photo of the exposure studied at Nolton Haven; B) a pseudo-3D panel of the detailed facies described in Table 5.1; C) a pseudo-3D panel of the simplified facies according to the FAKTS classification scheme overlain with the erosional surfaces seen, and rose diagrams; D) a pseudo-3D panel of the average lithologic heterogeneity across the point-bar deposit.....	239
Figure 5.16 - A) A field photo of the exposure studied at Nolton Haven; B) a pseudo-3D panel of the relative energy required to deposit each bed; C) a pseudo-3D panel of the interpreted facies successions. ....	239

Figure 5.17 – A visual summary of the numerical deductions that were undertaken using the equations in Table 9 .....	250
Figure 5.18 - A) A panel of the abandoned channel exposure; B) interpretation of the abandoned channel fill exposure.....	256
Figure 5.19 - A figure to show the abandoned channel shape exposed at Nolton Haven cove, compared to data from Smith et al., (2009).....	258
Figure 5.20 - A planform sketch of the outcrop with accretion direction, and flow direction marked on. Outcrop is 123 m long.....	258
Figure 5.21 - An edited version of Figure 4.13A, showing the accretionary styles that exhibit upstream accretion. ....	259
Figure 5.22 - A collation of data relating to each scroll-bar pattern that exhibits upstream accretion. ....	262
Figure 5.23 - A flowchart that shows the possible routes that may be taken to develop scroll-bar pattern 2.3. Routes in colour are the most probable. ....	263
Figure 5.24 - A) the morphology and relative lithologic heterogeneity that would hypothetically be formed if the meander accreted via. Route 1; B) the morphology and relative lithologic heterogeneity that would hypothetically be formed if the meander accreted via. Route 2 .....	264
Figure 5.25 - The reconstructions and predicted facies successions for the two point-bar deposit reconstructions constructed in Figure 5.26. ....	267
Figure 5.26 - A graph of abandoned point-bar deposit dimensions .....	268
Figure 6.1 - A demonstration of the application of the radius-of-curvature methodology for analysis of a variety of meander shapes identified in this study; A) meander shape S1b; B) meander shape S2b; C) meander shape S3f; and D) meander shape S4b (Figure 2.8). ....	272
Figure 6.2 - Pie chart depicting the types of growth observed in 260 active point-bar deposits studied.....	279



Figure 6.3 - A) Pie chart to illustrate the proportions of scroll-bar pattern in abandoned point-bar deposits; B) Pie chart to show the proportions of scroll-bar pattern in active point-bar deposits. ....	285
Figure 6.4 –Pie chart showing proportions of scroll-bar style observed in active bulbous deposits (see also Figure 3.9). Key is the same as in Figure 6.3. n=62.....	285
Figure 6.5 – A) an idealised diagram of a point bar that evolves via expansion and downstream translation resulting in a bulbous shape; B) the sequential development of channel deposits and abandonment; C) the planform interpretation of lateral accretion packages studied between Willow Creek, and Red Deer River, in the Late Cretaceous Bearpaw Formation; D) a model for the channel bend migration of an interpreted point-bar deposit in the Cretaceous Ferron Sandstone Formation, Utah, USA), including its abandonment.....	292
Figure 6.6 – A flowchart of the recommended methodology to assess the range of possible reconstructions of a point-bar deposit. References to “planform” do not imply that the outcrop must be planform, it means that the analysis at that stage of the reconstruction requires a bird’s eye view sketch, or map, or image (e.g. Fig. 5.22)...	295
Figure 6.7 - A flow chart to describe the methodologies for determining the lateral accretion history and heterogeneity for active modern systems, and both accumulated and avulsed seismic reflection imagery.....	301

## List of Tables

Table 1.1 - A table to describe modes of observation of each data set. Green indicates the most likely scenario, whereas red indicates the less likely scenario. ....	16
Table 2.1 - Summary of results depicted as pie-charts in Figure 11 Through comparison of the wide variety of forms in the Senegal and Irtysh (Ob) rivers, similarities and differences are revealed and quantified. ....	59
Table 3.1 - A table to show the rivers selected for this study. ....	86
Table 3.2 - Descriptions of the classifications of scroll-bar styles identified .....	91
Table 3.3 - Meander shape and scroll-bar pattern observed for the 20 meanders studied in each of the 13 meandering reaches studies. A shape reference in brackets indicates that it is an outlier. ....	99
Table 3.4 - A table to demonstrate the markedly different trends seen in Group 3 compared with Groups 1, 2, and 4. ....	105
Table 4.1 - Definitions of individual cut-off types and their geological implications. Also see Figure 4.7. ....	147
Table 4.2 - Definitions of group cut-off types and their geological implications. Also see accompanying Figure 4.8. In Figure 4.8, the scroll-bar and shape variations are selected and used to demonstrate an example, though it is important to note that many shape and scroll-bar styles are possible. ....	156
Table 5.3 – Description of facies characteristics in the deposits of the studied point-bar element at Nolton Haven. ....	224
Table 5.4-Tally matrix for the data considered in this study. ....	224
Table 5.5-A probability matrix for the data considered in this study .....	225
Table 5.6-An independent trials probability matrix. ....	226

Table 5.7 - A difference matrix between the independent trials probability matrix, and the probabilities calculated from the tally matrix. Yellow cells highlight numbers that are statistically significant .....	228
Table 5.8 - A table of the parameters used in the calculations .....	245
Table 5.9 - A table of the parameters and associated equations used in this study...	248



# 1 Introduction

*An overview of the thesis organisation and structure is given in this chapter. The rationale behind the research, the overall aim of the thesis, and the research questions are explained. The structure of this thesis is such that each chapter sequentially builds on the methods and data presented in earlier chapters. Thus, understanding from each prior chapter is used to develop the arguments in each of the subsequent chapters. This structure builds a continuous narrative, so it is suggested that the chapters are not read out of order. In this introductory chapter, each section of the work is outlined to summarise the overall structure of the thematic body of work.*

## 1.1 Project background and rationale

Rivers interact with terrestrial topography both on earth and on other planetary bodies across the solar system (Burr *et al.*, 2009; 2010; 2013; Williams *et al.*, 2013).

Sediment-charged flows in channels may incise (Schumm *et al.*, 1984) or accrete, laterally or vertically (Allen, 1965; Thompson, 1986). The morphology of active fluvial systems is notably varied and complex (Schumm, 1985; Phillips, 2003). Fluvial planform geometry is commonly broadly categorised into braided, and meandering systems; anabranching, anastomosing, and straight rivers also occur but are less common. These classifications may be subdivided to aid description, as described in figure 1.1.

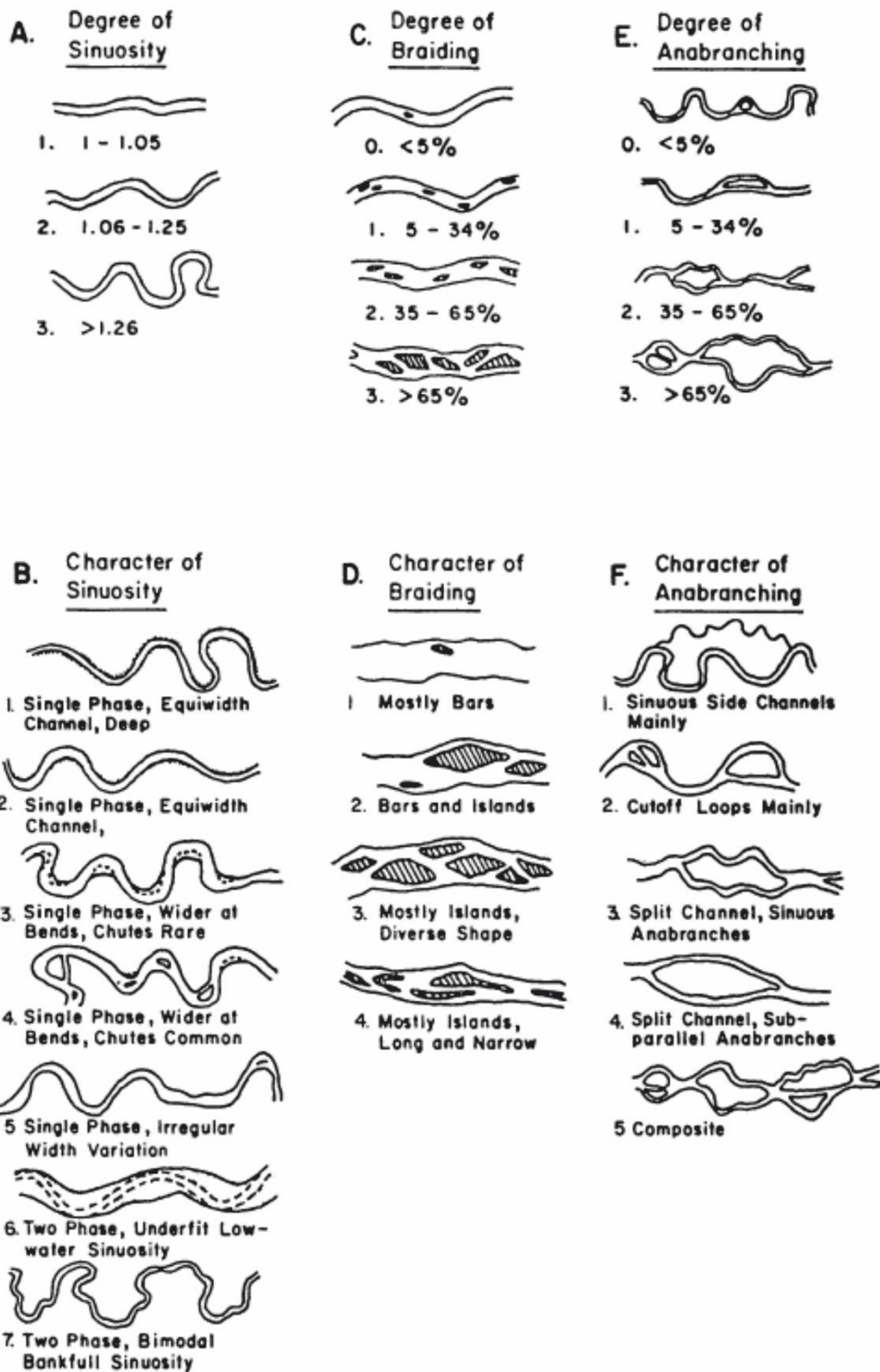
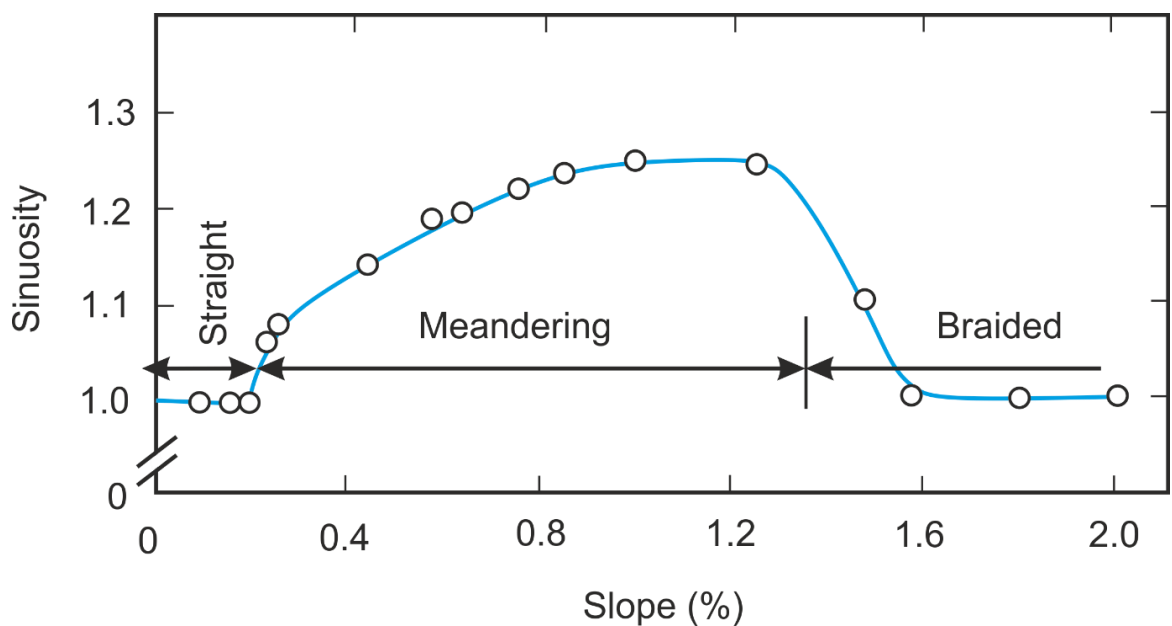


Figure 1.1 - Fluvial reach morphologies. From Brice 1978, modified by Schumm (1985).

Braided fluvial systems are composed of networks of channels that are themselves separated by typically transient islands, known as in-channel bars (Miall, 1977; Bridge, 2003). Meandering fluvial systems are usually composed of a sinuous reach that is a single channel thread. A meandering channel accretes sediment laterally on the inner bank of each meander bend that form point-bar deposits (Allen, 1965), (aside from those that develop as bedrock rivers). The dominant control that dictates whether a fluvial system will develop a meandering or braided plan-form is the ability of the river to approach a quasi-steady equilibrium state whereby it expends the least amount of energy to reach its downstream destination (Church, 2006). In turn, this is controlled by the sediment supply, sediment calibre, transport mechanism of the sediment, as well as stream gradient (Fig. 1.2), (Leopold & Wolman, 1957; Schumm & Khan, 1972; Church, 2006).



**Figure 1.2 - A graph to show the optimum slope for meandering channels. Above a slope of about 1.3%, the river will become braided (modified from Schumm and Khan 1972).**

A fluvial system may transform from braided to meandering, and *vice versa*, along its reach and through time as the dominant controls on the system change (Church, 2006; Hartley *et al.*, 2010; Fig. 1.3).

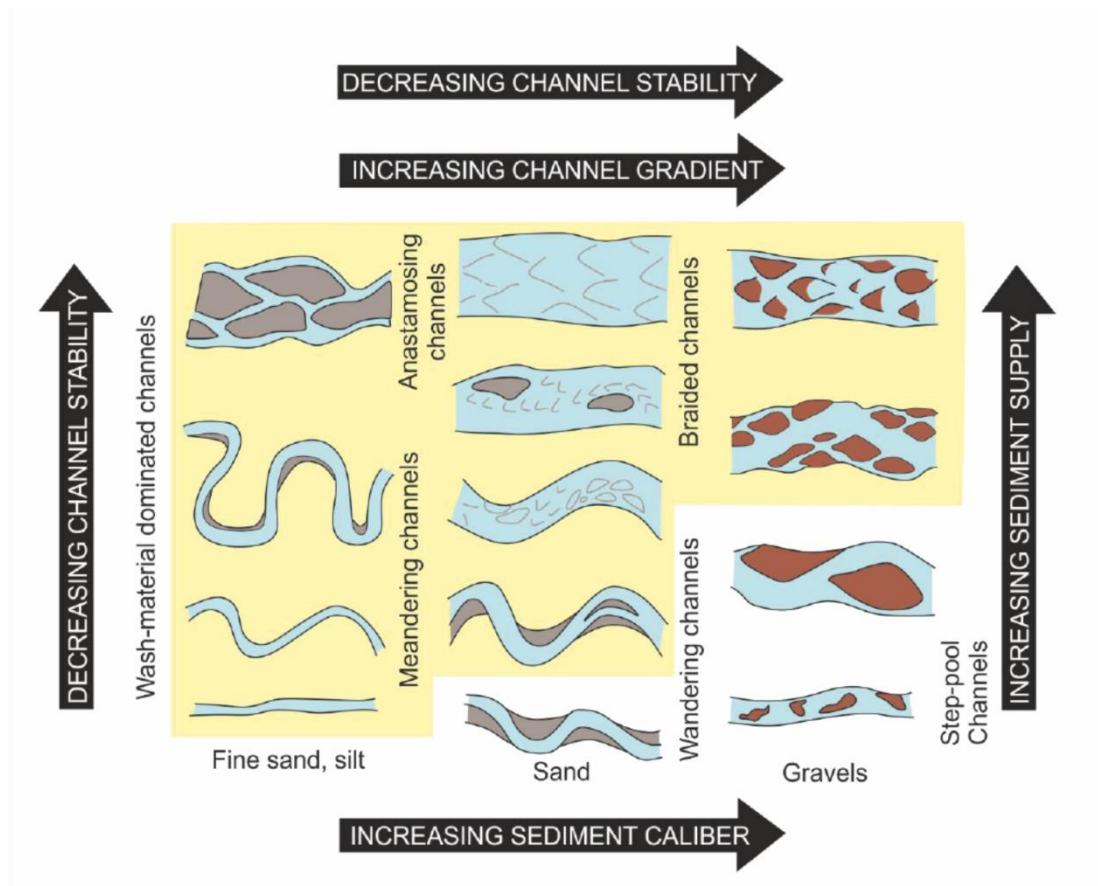
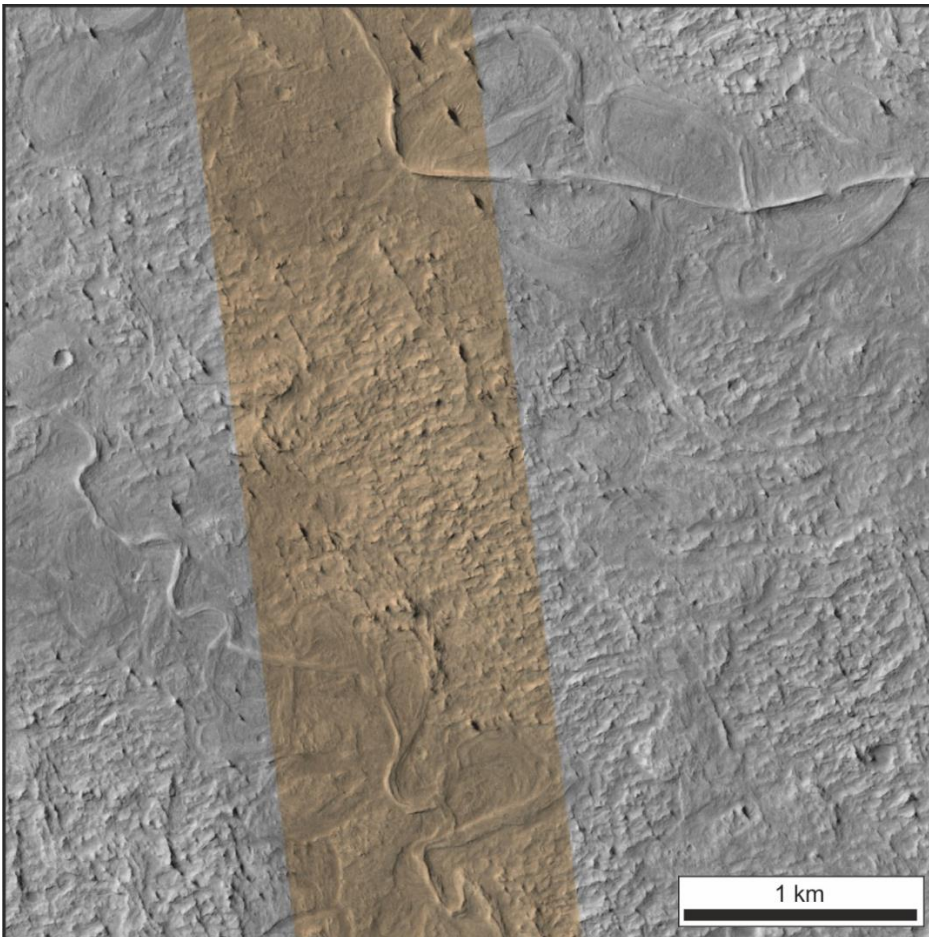


Figure 1.3 – Controls on fluvial morphology from Church (2006).

Typically, meandering systems are viewed as more stable than braided systems although the single thread migrates and laterally accretes sediment. Stability in fluvial systems is encouraged by the inclusion of fine-grained sediment as part of the carried load (Peakall *et al.*, 2007), and by the presence of vegetation that acts to stabilise the substrate on the river banks and floodplain (Perucca *et al.*, 2007; Brooks *et al.*, 2003). A distinct facies shift occurred, i.e. there was a change in the proportions of certain facies types, in the Middle and Late Palaeozoic. This is associated with an increased occurrence of inclined heterolithic strata (IHS; Thomas *et al.*, 1987) in the rock record.



Inclined heterolithic strata is alternating packages of sand-prone and mud-prone material that occurs on inclined surfaces. This facies shift coincides with the terrestrialisation of land plants from the Ordovician to the Devonian (Vecoli *et al.*, 2010; Davies & Gibling 2011; Santos *et al.*, 2017a; 2017b; Davies *et al.*, 2017). The relationship between deep-rooted land plants, and fluvial form is well supported by modern case studies (Abernethy & Rutherford, 1998; Eaton & Giles, 2009; Konsoer *et al.*, 2016). However, early land plants did not have roots that extended to a depth that would have enabled bank stability, and were unlikely to make a sufficiently significant impact in changing fluvial form (Santos *et al.*, 2017a; 2017b). Therefore, another mechanism might potentially be required to induce this stability. Fine-grained sediment is able to influence meandering in a terrestrial fluvial system and its presence alone can result in the generation of IHS (Sweet, 1988; Peakall *et al.*, 2007; Van de Lageweg *et al.*, 2014; Santos *et al.*, 2017a; 2017b). This is supported by the fact that preserved deposits of meandering fluvial systems are evident on Mars (Burr *et al.*, 2013; Fig. 1.4). Comparison of processes between the earth and other planets has been considered problematic due to a lack of ground-truthing, i.e. IHS may not necessarily be present (Davies *et al.*, 2017). Yet the fundamental observation of meandering single-thread channels on Mars, complete with preserved associated point-bar deposits supports the argument that vegetation is not required to stabilise a meandering system (Santos *et al.*, 2017a; 2017b).



**Figure 1.4 – Meandering fluvial systems on Aeolis Dorsa (153.636°, -6.041°), Mars. From NASA/JPL/University of Arizona, (Image Ref: ESP\_034189\_1740\_MRGB)**

River channels are just one of many elements of meandering fluvial systems (Fig. 1.5). An element is a morphological component that is deposited by an environmental condition (i.e. a suite of related processes). Fluvial elements typically give rise to bodies of accumulated strata that themselves possess a distinctive set of lithofacies characteristics (Allen, 1965). Accumulated fluvial elements may be divided into two distinct groups: those that accrete vertically (e.g. levees, crevasse-splays, floodplain deposits), and those that accrete laterally (e.g. point-bars, crevasse splay channels, channel bars) (Leopold & Wolman, 1957, Fenneman, 1906). However, some element types, such as channel fills, may fall into either category (Allen, 1965; Toonen *et al.*, 2012).

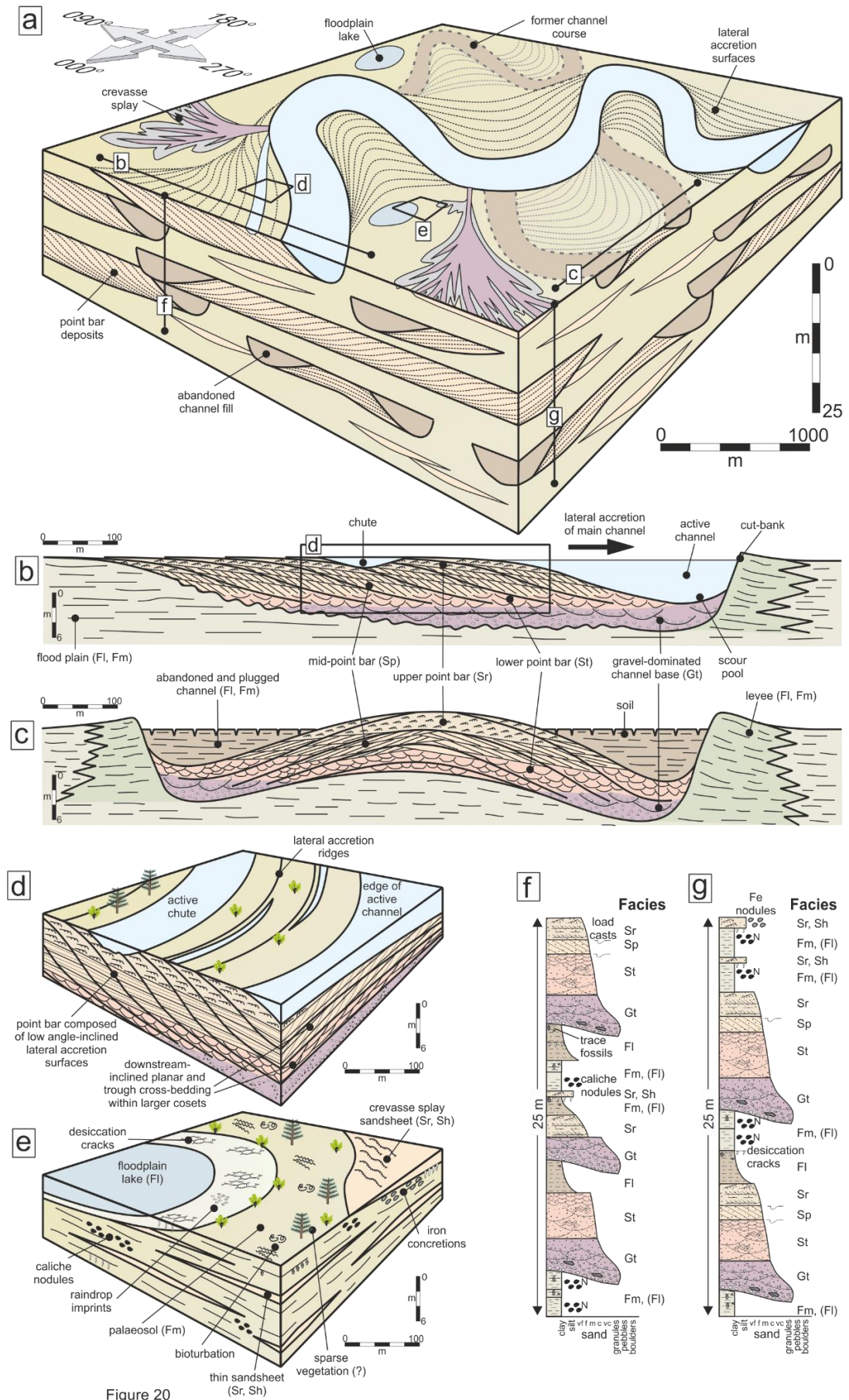


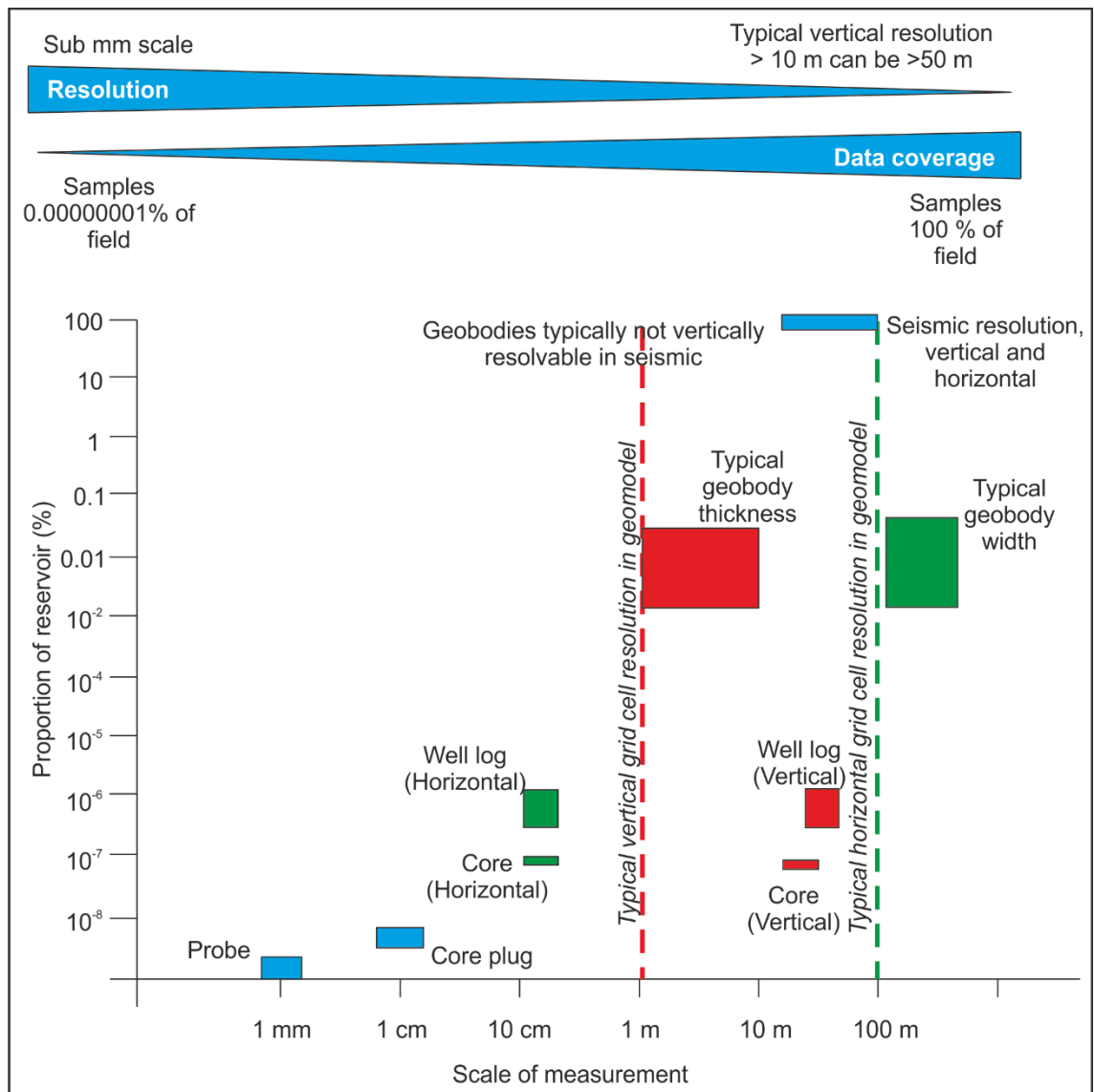
Figure 20

**Figure 1.5 - a) A regional scale facies model. Example from the Permian Warchha Sandstone, Salt Range, Pakistan. From Ghazi and Mountney (2009).**

Fluvial elements develop and accumulate in response to different levels of energy during their formation (Allen, 1965; Miall, 1985). This influences the dominant grain size (Middleton & Southard, 1978). For example, point-bar elements that accumulate in response to deposition of sediment from high-energy flows are commonly sand prone (Allen, 1965; Miall, 1985). This contrasts with sediment that is deposited from low-energy flows, such as floodplain elements, which are commonly characterised by mud-prone deposits.

This study focuses on fluvial meandering river reaches bound by alluvial floodplains (i.e. not bedrock confined systems), and their accumulated deposits preserved in the ancient rock record. Identifying mud- and sand-prone elements in meandering fluvial deposits is of importance to the petroleum industry because sand-prone elements in fluvial successions can form excellent reservoirs (Fielding & Crane, 1987; Tye, 2004). The preserved depositional architecture that forms the record of meandering fluvial systems typically comprises sand-prone elements including channel deposits, point-bar deposits, levee deposits, and crevasse-splay deposits (Allen, 1965). During exploration for new prospects, many data sets are typically collected; these yield information at a range of resolutions and cover different scales. Seismic data encapsulate information about the entire prospect but at a resolution that is usually too low to identify individual element geometries. Core data provide high resolution, but are limited in that the data are effectively only one-dimensional, and therefore provide poor lateral coverage (Howell *et al.*, 2014 – Fig. 1.6).





**Figure 1.6 - A consideration of data resolution and coverage for a typical subsurface field (from Howell *et al.*, 2014).**

As a result, for subsurface fluvial successions, it is difficult to determine the lateral extent, geometry and internal lithofacies distribution of architectural elements, and therefore the gross-scale architecture of the larger fluvial succession of which they form a part (Tye, 2004; Miall, 2006; Hartley *et al.*, 2015). This has a significant impact on our ability to assess and predict the interconnectivity of sand-prone deposits in subsurface successions. For example, large, sand-prone channel-fill deposits that are visible on

seismic datasets may be interconnected via thin crevasse splay deposits (Burns *et al.*, 2017) that themselves remain undetected by seismic surveys.

Factors that control the morphological and architectural variability in freely meandering fluvial systems may be internal or intrinsic to the system (autogenic), or may be external to the system (allogenic) (Rosgen, 1985; Miall, 1988). It can be hard to determine causative processes of observed facies relationships, and some autogenic controls are not entirely independent of allogenic controls. Autogenic processes include: (i) chute cut-off, which splits the flow and therefore erosive power (Camporeale *et al.*, 2005); and (ii) flood repeat frequency (Knighton 1998); (iii) riparian biomass density (Brooks *et al.*, 2003; Perucca *et al.*, 2007; Davies *et al.*, 2017) which, as it increases, reduces the erodability of the bank; and (iv) log jams, which can cause flow-deflection and increase channel complexity (Abbe & Montgomery, 2003), or ice jams (Gay *et al.*, 1998). Allogenic processes include: (i) sediment calibre (Schumm, 1969; 1985); (ii) gradient (Schumm & Khan, 1972); (iii) climate (Alford & Holmes, 1985, Blum & Törnqvist, 2000); (iv) tectonics (Schwab, 1976; Ghinassi *et al.*, 2016); (v) subsidence (Ouchi, 1985); and (vi) sea-level change (Shanley & McCabe, 1994; Tye, 2004).

Identifying the dominant control in a system is challenging (Ethridge & Schumm, 1998) because multiple controls commonly act and interact on a freely meandering fluvial system, and each has a changing degree of influence over time (Alford & Holmes, 1985, Blum & Törnqvist, 2000).

The fundamental controls on the initiation and evolution of meandering fluvial systems are not fully understood. The two main competing theories are Bend Theory (Gorycki, 1973), and Bar Theory (Ikeda, 1981). Bend Theory argues that the development of meanders occurs in response to natural variations in the turbulence of a river flow, as demonstrated by Gorycki (1973). By contrast, Bar Theory argues that inconsistencies in the river bank, or uneven deposition of sediment, are responsible for causing the

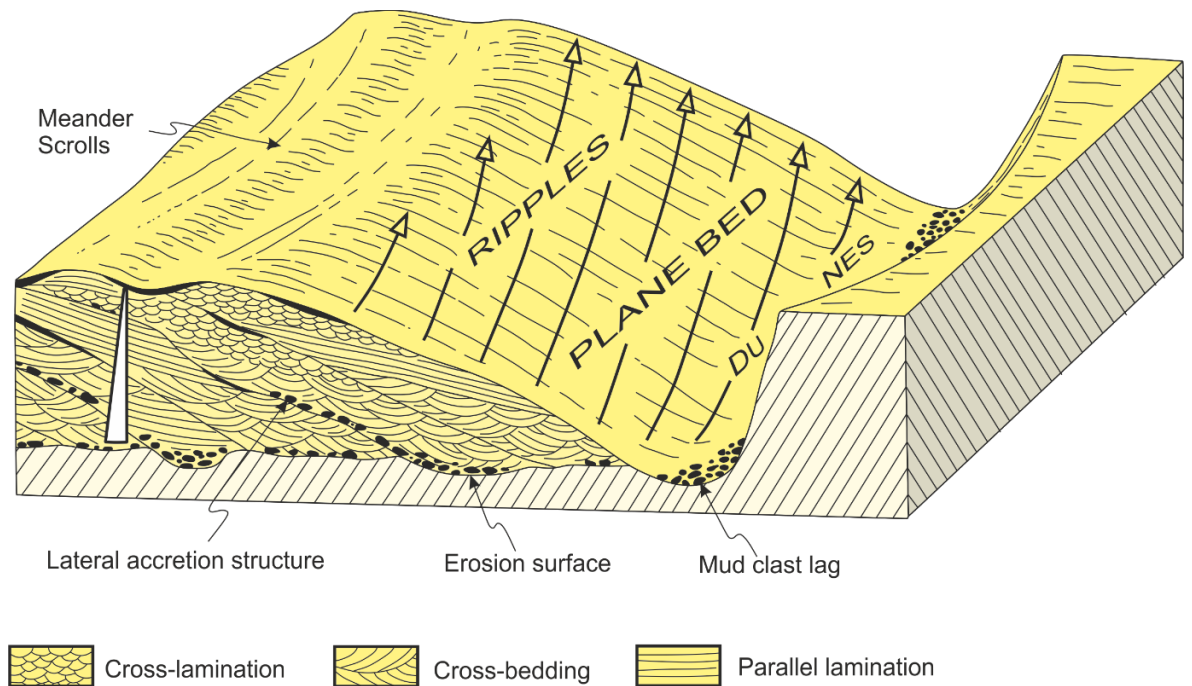
meander to develop by forcing the river to deviate from its preferred course, in turn influencing flow behaviour and thereby permitting formation of incipient point bars (Ikeda, 1981). A major failing of Bar Theory (Ikeda, 1981) is that rivers are able to form meanders where no sediment is present, such as those in glaciers (Leopold & Wolman, 1960), or bedrock. This highlights that, without recourse to external agents, a river can still commence meandering behaviour. However, in the natural world this scenario is rare and sediment, and its calibre, usually plays a major role in influencing the system, whereby flow processes cause sediment to shift position over time on the channel bed, notably during flood events (Hooke, 1977b; Knighton, 1988). In the natural world, both Bend Theory and Bar Theory are likely important drivers for meander generation.

A point-bar is a bank-attached element that undertakes lateral accretion (or related downstream-oriented accretion in some cases), that is deposited in response to the growth of a fluvial meander. The deposits of many fluvial point bars are sand prone (Allen, 1965), and therefore preserved examples of point-bar elements can make good petroleum reservoirs (Jordan & Pryor, 1992). The architectural variability of point bars is extensive, and this variability may be observed in both planform, and in cross-section view. Assessment of the variability of form of point-bars in freely meandering systems is key to predicting the geometry and heterogeneity of such preserved elements in ancient successions (Fielding & Crane 1987; Miall, 1988; Mackey & Bridge, 1995). It is important to gain improved understanding of this variability to better interpret the controls on meandering systems (Bridge, 1993b; Miall, 2006; Engel & Rhoads, 2012; Lotsari *et al.*, 2014). Point-bar deposits accrete on the inside bend of a meander, and down-stream fining of this sediment is commonly observed due to the flow moving at different speeds around the meander bend (Thompson, 1986; Leopold & Wolman, 1960; Thomas *et al.*, 1987; Fustic *et al.*, 2012). This causes lithologic heterogeneity. In this study, heterogeneity refers to spatial variations in porosity and permeability. In

general, sand-prone sediment is typically more porous and permeable than mud-prone sediment (Keogh et al., 2014). Lithological end-members are clean sand (e.g. Donselaar and Overeem, 2008) and mudstone (e.g. Miall, 1978). In a lithologically heterogeneous sediment deposit, mud- and sand-prone sediment may be interbedded on a range of scales, the transition may be gradational with a systematic variation in the mud content, or some combination of the two may occur. Variable flow in a meandering stream also leads to small-scale heterogeneity; mud-prone, and sand-prone beds, or laminations are known as inclined heterolithic strata (IHS) (Thomas *et al.*, 1987). Lithologic heterogeneity refers to the overall heterogeneity based on proportions of mud- and sand-prone sediment in a deposit. Collectively, these heterogeneities significantly impact the preferred flow directions for large-scale hydrocarbon sweeps, so understanding where lithological heterogeneities of different types occur is therefore important. There is potentially a predictable relationship between the presence of IHS, and its distribution in point-bar deposits. Improved understanding of the controls on this distribution would benefit petroleum engineers. Heterogeneity can be observed in sub-surface settings through gamma-ray wireline log interpretation (e.g. Hubbard *et al.*, 2011; Labrecque *et al.*, 2011). Gamma-ray log-response maps are not always available and only provide 1D data. Inclined heterolithic strata is not generally observable at seismic resolution; therefore lithologic heterogeneity, must be predicted by making deductions from available data.

Workers originally sought to develop facies models that described typical facies trends described by associations and successions of genetically related lithofacies (Allen, 1965; 1984; Miall, 1978). One commonly depicted facies succession (from bottom to top), is erosion surface with pebble / mud clast lag, cross-bedding, parallel lamination, and cross-lamination; facies successions are found within lateral accretion structures that are uniformly spaced (Allen, 1984 – Fig. 1.7).





**Figure 1.7 - A classic cross-section of a point-bar deposit. Modified from Allen (1984).**

However, these prevalent and widely applied point-bar models (e.g. Schumm, 1963; Allen, 1964; 1965; 1982; McGowen & Garner, 1970), do not capture the full range of facies variability described from studies of modern systems (Ghinassi *et al.*, 2016, Shiers *et al.*, in review). These facies models depict end-member scenarios that are useful to understand concepts, but are limited in their suitability as tools for application directly to inform geologic models. There is a growing body of work describing the variability of the internal structure of point-bar deposits (e.g., Labrecque *et al.*, 2011; Durkin *et al.*, 2015; Ghinassi *et al.*, 2016; Shiers *et al.*, in review). Indeed, “classic” facies models are not adequate, for the description of the broad range of observed morphologies and architectures given many different facies arrangements can occur depending on the processes that operated over the bar at the time of accretion (Durkin *et al.*, 2015; Ghinassi *et al.*, 2016). It is important to study point-bar deposits in cross-section because they may capture and record information relating to element architecture and internal lithofacies distribution (Miall, 1978; Reijnenstein *et al.*, 2011).

A commonly recognised feature in a cross-section of a point-bar deposit is a scroll bar. A scroll bar is an individual feature on a point bar, adjacent to the direction of past and present meander growth (Sundborg, 1956; Allen, 1965). Scroll-bar deposits record the incremental growth (accretion) of point bars through expansion, translation, rotation, or combinations thereof (Daniel, 1971). This behaviour results in the development of consecutively laterally accreted packages to form scroll bars (Schumm, 1963; Allen, 1965; e.g. Bridge, 2003; Ielpi *et al.*, 2014). Scroll-bar deposits are typically preserved in the geological record as coarsening upwards, metre-scale, inclined beds (Ielpi & Ghinassi, 2014). Classification schemes for planform scroll-bar pattern enable change of form to be recorded via observations of channel migration (Daniel, 1971; Hooke, 1977a; Knighton, 1998; Ielpi *et al.*, 2014). Change of meander form is broadly categorised as expansion, translation, and expansion and rotation (Daniel, 1971). However, many of the methods used in classifications only assess the most recent accretion. Typically, when meander growth processes are modelled, the channel form in plan view begins with a sinusoidal shape (Leopold & Wolman, 1960; Daniel, 1971; Hooke, 1977b; Willis & Tang, 2010), rather than representing growth from a straight reach (Lewin, 1976; Thompson, 1986). It is important to accurately capture variations in meander shape due to its potentially predictable relationship with the distribution of inclined heterolithic strata (IHS). Overarching simplistic descriptions of morphological characteristics are used to distinguish variabilities (Schumm, 1985; Figs 1.5 and 1.6). However, more detail is required to determine the distribution of mud-prone sediment in individual point-bar deposits.

There are three main ways in which the geometry (i.e. size and 3D shape), of accumulated fluvial point-bar successions can be examined: (i) through analysis of active and recently cut-off examples in modern systems; (ii) through the imaging of deposits using reflection seismic data; and (iii) through examination of outcrops that

reveal ancient preserved successions (Table 1.1). In active fluvial successions, point-bar architecture can be assessed and related to measured velocity, discharge and grain-size (Thompson, 1986; Erskine *et al.*, 1992). In planform, remotely sensed imagery can be used to describe size, radius-of-curvature, and planform shape (Sambrook Smith *et al.*, 2016). Underlying recent alluvial architecture can be assessed with approaches that include stratigraphic columns (Erskine *et al.*, 1992; Smith *et al.*, 2009), trench cuts (Moody & Meade, 2014), parametric echo sounding (Sambrook Smith *et al.*, 2016), and GPR (Bridge *et al.*, 1995). In the ancient record, formative processes can only be inferred from preserved deposits. Point-bar deposits may be recognised in the ancient record via their architecture (e.g. Fig. 1.3), and facies distributions (Allen, 1965; Miall, 1978, Ielpi *et al.*, 2014). Observations that may be made in outcrop include palaeoflow indicators, and determination of scroll-bar accretion direction bounded by erosional surfaces (Allen, 1964; Miall, 1985; Durkin *et al.*, 2015; Wu *et al.*, 2015). It is unlikely that both planform and cross-section are available from one site, though exceptions do occur (e.g. Reijenstein *et al.*, 2011; Ielpi *et al.*, 2014; Hartley *et al.*, 2015; Ghinassi *et al.*, 2015; 2016). For a sub-surface deposit, planform shape, core logs, and 3D seismic imagery (e.g. Reijenstein *et al.*, 2011), is typically available.

	<b>Planform</b>	<b>Cross-section</b>
<b>Active modern systems</b>	Global coverage is available at a high resolution.	Only where specific studies are undertaken (e.g. Moody & Meade 2014).
<b>Reflection seismic</b>	Where reflection seismic data is available, it may be flattened to observe a fluvial channel (e.g. Hubbard <i>et al.</i> , 2011).	Available as 1D core. Full cross-sections only observable in exceptional circumstances where a 3D dataset is available (Reijnenstein <i>et al.</i> , 2011).
<b>Outcrop</b>	Only where exceptional outcrop is available (Ielpi <i>et al.</i> , 2014; Ghinassi <i>et al.</i> , 2015; 2016; Wu <i>et al.</i> , 2015)	An outcrop exposure is typically cross-sectional (e.g. Donselaar & Overeem 2008; Durkin <i>et al.</i> , 2015).

**Table 1.1 - A table to describe modes of observation of each data set. Green indicates the most likely scenario, whereas red indicates the less likely scenario.**

Predictions of fluvial architecture and heterogeneity are made through cross-referencing datasets, enabling a greater understanding of the fluvial system. Computer simulations have been developed to better understand the controls on fluvial systems that lead to their development, through this process inevitably simplifies, and eliminates some detailed aspects of primary observation (Camporeale *et al.*, 2005; Colombera *et al.*, 2013; Yan *et al.*, 2017). However, this simplification is necessary so that large data sets can be handled easily (e.g. FAKTS; Colombera *et al.*, 2013).

However, before predictions can be undertaken, accurate, and repeatable, observations must be made in either cross-sectional, or planform exposure. Analysis of meander planform shape is difficult because the natural form of a fluvial meandering reach can be complex and variable (Phillips, 2003; Miall, 2006). Popular existing approaches include shape matching methods (e.g. Brice, 1974; Allen, 1982; Bridge, 2003; Ielpi & Ghinassi, 2014), the radius-of-curvature methodology (Nanson & Hickin 1983), and sinuosity measurements (Hooke, 2004). These methodologies may be used to make observations; however, they are limited in their applicability and in their ability to meaningfully determine and classify meander shapes. There exists a wide range of spatial variability and temporal evolution style for different types of fluvial meander bends (e.g., Miall, 2006; Lotsari *et al.*, 2014). Many studies use sinuosity to study meanders (Howard & Hemberger, 1991; Bledsoe & Watson, 2001; Brooks *et al.*, 2003). Sinuosity alone provides only a limited indication of shape compared to methods based on analysis of radius-of-curvature. Radius-of-curvature is the radius of the circle that best approximates the curve at that point; in this context, it is used to quantify the curve of a meander bend around its apex. The radius-of-curvature methodology is also known to have a relationship with bend migration rate (Hickin & Nanson, 1984). Hooke (2007) used sinuosity and range of sinuosity to quantify fluvial morphologies. However, shape characteristics cannot be captured through this method. Curve fitting, a variation on the radius-of-curvature methodology, was introduced by Brice (1974), though Hooke (1984) states that curve-fitting is difficult and so the methodology has not found common usage. Many of these methodologies are limited in their repeatability as they are based on individual case studies (Andrle, 1994; Chen & Duan, 2004).

Studies carried out on modern systems show that meander forms change over observable time scales (i.e. years to decades), such as the River Dane (Hooke, 2004), Skirden Beck (Thompson, 1986), and the Río Bermejo (Sambrook Smith *et al.*, 2016).

In these examples, change in meander form has been assessed by studying: (i) the formation of pools and riffles (Thompson, 1986); (ii) mechanisms of meander cut-off (Gay *et al.*, 1998), using velocity, discharge, grainsize data (Erskine *et al.*, 1992), and sinuosity (Hooke, 2004); and (iii) use of the radius-of-curvature methodology (Nanson & Hicken, 1983, Hudson & Kesel, 2000, Sambrook Smith *et al.*, 2016). Changes in larger systems may be observed through observation of satellite imagery (e.g. the Ucayali River – Sylvester, 2014).

Lessons learned from observation of modern systems, may aid in the interpretation of the ancient record. However, the methods outlined above remain insufficient to both quantifiably record modern meander morphology and then implement it to aid rock-record interpretation and prediction (Tye, 2004; Miall, 2006). As a result, reconstructions of planform meander forms from geological exposures are limited in their variability (Durkin *et al.*, 2015; Wu *et al.*, 2015). A data set from outcrop is typically limited, and so morphometric extrapolations are commonly undertaken that extend beyond what is directly observed (e.g. Ghinassi *et al.*, 2016). If such limited data were able to generate a full range of variabilities via statistical deductions, then interpretations of the rock record may be better informed (Tye, 2004). From a geological perspective, a predictive model is required to determine the distribution of mud-prone IHS sediment packages. This is important in applied hydrocarbon geology because mudstone and sandstone have contrasting porosity and permeability characteristics, so understanding their relative positions is important for siting production and injection wells (Miall, 1988, Fielding & Crane, 1987; Tye, 2004; 2013), and therefore important for production engineers (Miall, 1988; Pranter *et al.*, 2000; Labrecque *et al.*, 2011).

There is a recognised relationship between position on the meander bend, and the grainsize deposited (Fustic *et al.*, 2012). However, meanders grow in complex ways

and so predicting such trends in meandering fluvial systems is not straightforward. For example, downstream fining around a meander bend has been recognised extensively in the rock record (e.g. Fustic *et al.*, 2012; Durkin *et al.*, 2015; Wu *et al.*, 2015; Ghinassi *et al.*, 2016), including in the sub-surface (Hubbard *et al.*, 2011; Labrecque *et al.*, 2011). Therefore, by harnessing an understanding of processes by which heterogeneity occurs, predictive models to describe the relative distribution of heterogeneity in a freely meandering fluvial system may be developed. This approach is based on the premise that the accretion history ought to be established to predict this heterogeneity. This can be challenging because a floodplain may be reworked over thousands of years, throughout which dominant controls may change significantly and affect the river style and internal character of the resulting ancient deposit (Ethridge & Schumm, 1998; Blum & Törnqvist 2000). This resulting amalgamated complex fluvial deposit may be observed in the ancient record through seismic imagery (e.g. Hubbard *et al.*, 2011); such data are challenging to interpret.

By improving the techniques by which ancient successions are interpreted, the prediction of the lateral extent of a point-bar deposit, its accretion history, its internal facies and bounding surface arrangements, and its related heterogeneity may be interpreted. Effective and detailed observations of the complexity and variety of the morphology of modern meandering fluvial systems should be obtained to gain improved understanding for prediction of accretion histories and heterogeneity (Bridge, 1993a; Miall, 2006; Engel & Rhoads, 2012; Lotsari *et al.*, 2014).

## 1.2 Aims and Objectives

The fundamental aim of this thesis is to devise a series of methodologies that can be used to determine the lateral extent, accretion history, and heterogeneity of point-bar deposits where that information is not otherwise directly available. The purpose of this will be to address issues of prediction of the location of sand-prone areas in point-bar deposits, at a level of detail that has not hitherto been possible. The specific research objectives to be tackled by the subsequent chapters of this thesis are as follows:

- To geometrically classify meander shapes from a range of fluvial environments;
- To consider the relationship between meander shape and scroll-bar pattern, and determine a method by which heterogeneity may be predicted;
- To assess the processes of meander abandonment, and how each may affect the geometries of preserved point-bar deposits
- To apply the understanding gained from answering the previous three objectives to an exposed point-bar deposit in order to more accurately reconstruct the lateral extent and heterogeneity variations of a point-bar deposit, by determining the accretion history.
- To devise a workflow by which the internal stratigraphic architecture, and geomorphic variability, may be predicted from surface morphology, and flattened seismic timeslices.

## 1.3 Research questions

The following research questions have been developed so that the aim and objectives of this research can be met. These questions are explored in the following chapters, and explicitly answered in Chapter 6 (Discussion):



**How can meander shapes be geometrically classified, in order to be compared universally, in a repeatable, quantifiable manner?**

*Rationale:*

Methodologies for meander description that are established in the literature are qualitative, semi-quantitative, or fully quantitative. Qualitative description is based on “shape matching” (Brice, 1974; Allen, 1982; Bridge, 2003; Ielpi & Ghinassi, 2014). This enables some initial observations to be made, but monitoring change is difficult because these parameters are not quantified (Hooke, 1984). Semi-quantitative methods, such as the radius-of-curvature method, measure channel curvature to define a metric that is related to bend migration rate (Nanson & Hickin, 1983). These methodologies describe the curvature, but are unable to provide differentiation between simple and complex shapes. Quantitative methods are limited in that they work most effectively in the reaches for which they were developed and are consequently difficult to apply universally (e.g. Brice 1973; 1974; Gustavson, 1978; Andrieu, 1994; Van De Berg, 1995). Meander shape is commonly associated with a specific form of scroll bars, i.e. a sine-wave-like shape is often related to expansion (Ielpi & Ghinassi, 2014; Frascati & Lanzoni, 2010; Bridge 2003). Scroll bars record evolutionary changes in meander shape, migration direction, bend evolution, and sedimentary architecture (Allen, 1965; Daniel, 1971; Hickin & Nanson, 1975; Bridge, 2003; Miall, 2006; Chen & Duan, 2006). There is a lack of an appropriate tool for quantitative architectural analysis; by developing a quantitative procedure for determining the shape of a meander bend, different shapes may be distinguished. This is of importance for providing clues regarding the interplay of autogenic and allogenic controls (Rosgen, 1994; Miall, 2006; Gutierrez & Abad, 2014). Given the potential applicability of this work to better understanding stratigraphy, the relationship between meander shape and scroll-bar pattern needs to be considered. Aerial imagery can be analysed to determine

a relationship between meander shape and scroll-bar pattern. Quantification of meander shape, via a universal and repeatable method, may provide a means to compare disparate systems, and thereby form the basis for the development of an improved understanding of the controls on the spatio-temporal evolution of meandering reaches in modern systems, and for the establishment of criteria for recognition and interpretation of preserved point-bar deposits in ancient successions.

**How does the geometry of a meander and scroll-bar pattern of the point-bar, relate to the heterogeneity of a point-bar deposit?**

*Rationale:*

Preserved fluvial point-bar deposits are laterally discontinuous (Allen, 1965), and characterised by a complex distribution of lithofacies (e.g. Thomas, 1987; Tye, 2004; Miall, 2006; Durkin *et al.*, 2015). The majority of such bodies are sand-rich architectural elements that contain packages of mud-prone strata (i.e. with clay and/or silt). Such heterolithic packages of strata influence permeability pathways (Fielding & Crane, 1987; Miall, 1988; Tye, 2004), and consequently influence oil and gas production (e.g. Brown & Fisher, 1980; Putnam & Oliver, 1980; Mossop & Flach, 1983; Hubbard *et al.*, 2011). Geological models of fluvial point-bar deposits are routinely used to inform reservoir models. However, many such models simplify or even ignore this lithological heterogeneity variability (Fielding & Crane, 1987; Jordan & Pryor, 1992; Pranter *et al.*, 2009; Hassanpour *et al.*, 2013). Inclined heterolithic strata (IHS; Thomas, 1987) – mud-prone deposits that alternate with sand-prone deposits commonly in a manner that forms couplets – comprise mud components that are laterally and vertically discontinuous (Thomas, 1987; Miall, 1988). Therefore, predicting their distribution is challenging, but ought to be considered. There is a recognised relationship between

the distribution of mud-prone sediment, and the position of deposition on the meander bend (Fustic *et al.*, 2012). The weaker secondary helical flow caused by the change in flow direction from the meander-bend apex to the downstream inflection point, causes the deposition of material on the down-stream limb of the meander bend, which is relatively finer grained than the material deposited elsewhere on the inner bank of the point-bar deposit (Jackson, 1976; Fustic *et al.*, 2012). This leads to the proportion of sand-prone sediment decreasing downstream of the meander apex, whereas mud-prone sediment increases in proportion downstream (Bridge *et al.*, 1995; Fustic *et al.*, 2012). Extensive data have been collected from meandering fluvial reaches that recognise down-stream fining relationships (e.g. Leopold & Wolman, 1960; Jackson, 1975; Thompson, 1876; Bridge & Jarvis, 1982; Thomas *et al.*, 1987; Labrecque *et al.*, 2011; Fustic *et al.*, 2012). Scroll-bars serve to record past positions of evolving meander apices in an accumulated point-bar deposit (Allen, 1965; Ielpi *et al.*, 2014). Therefore, if the scroll-bar geometry can be determined, past mud- and sand-prone zones may be inferred. Development of a methodology to account for the relationship between point-bar morphology and the resultant stratigraphic heterogeneity of modern fluvial meandering reaches, might have significant impact on approaches to petroleum exploration.

### **What is the impact of the timing and mechanism of channel abandonment on geometries of preserved point-bar deposits?**

#### *Rationale:*

Meandering fluvial systems undertake meander loop abandonment (e.g. Fisk, 1947; Allen, 1965; Hooke, 2004; Camporeale, 2005), and this repeated process typically results in an amalgamated and cannibalised partial record of fluvial point-bar deposits

(Fielding & Crane, 1987; Mackey & Bridge, 1995; Miall, 2006). Interpreting these partially preserved deposits is not straightforward (Durkin, 2015). Therefore modern and recent systems, for which bar deposits with distinct and recognisable plan forms that remain exposed at the surface, are observed to better understand the mechanisms involved (Fisk, 1947; Erskine *et al.*, 1992; Gay *et al.*, 1998; Hooke, 2004; 2007). There are three main types of meander abandonment recognised in the literature: (i) neck cut-off, where the inner banks of both the up- and down-stream limbs erode, tighten, and converge (Fisk, 1947; Mosley, 1975; Allen, 1965); (ii) chute cut-off, where a division of the flow from the main channel exploits a depression across the point-bar surface as a cut-through (Fisk, 1947; Kulemina, 1973; Brice, 1977; Lewis & Lewin, 1983; Gagalino & Howard, 1984; Hooke, 1984; Gay *et al.*, 1998); and (iii) avulsion, where an entire meandering reach of several or many meander loops relocates in response to upstream nodal avulsion (Fisk, 1947; Allen, 1965; Erskine *et al.*, 1992). A data set from recently abandoned systems for which preserved meander forms are still evident at the surface should be assessed. Improved understanding of cut-off mechanism and resultant form should be combined with the outcomes of Research Questions 1 and 2 to determine the accretion histories and consequently heterogeneity distribution of abandoned point-bar deposits. By developing an informed technique whereby the style of cut-off may be deduced from limited data, the accretion history may be deduced, and thereby the expected likely heterogeneity distribution of the resultant deposit may be inferred. This is important because the understanding and prediction of the connectivity of the fluvial point-bar deposits is key for reservoir prediction in hydrocarbon exploration (Fielding & Crane, 1987; Gibling, 2006).

**How can planform point-bar dimensions and palaeo meander shape be reconstructed from an exposure of a preserved point-bar deposit?**

*Rationale:*

The thicknesses of ancient preserved point-bar deposits in the subsurface can usually be determined from core or wireline log data. However, such data cannot usually be used to provide direct measurements of lateral extents of such elements; yet, the geometry of these elements is required to inform 3D geological models (Tye, 2004, e.g. Ekeland, 2007). Outcrop data considered analogous to subsurface successions have long been used as proxies to predict likely lateral extent (Tye, 2004; Miall, 2006; Keogh *et al.*, 2014). However, determining the lateral geometry and process of palaeo-accretion of a point-bar element from a two-dimensional cliff exposure is challenging (Geehan & Underwood, 1993, Mjøs *et al.*, 1993; Bridge *et al.*, 2000; Tye, 2004; Miall, 2006; Ekeland, 2007). Accurate interpretation of the history of palaeo-accretion is important and must ideally be undertaken in three dimensions because such reconstructions govern predictions of the distribution of lithological heterogeneities. Ancient preserved point-bar deposits tend to be laterally discontinuous and internally complex (Moody & Mead 2014), making it difficult to determine facies relationships, especially in three dimensions. A point-bar deposit may be studied in detail through assessment of its internal facies types and their distribution in relation to likely formative processes, and also through detailed analysis of palaeocurrent indicators (Miall 1978; 1988; Ekeland, 2007). Palaeohydraulic parameters (mean and maximum bankfull depth, bankfull width, width to depth ratio, sinuosity, mean annual discharge, mean annual flood, channel slope, meander wavelength, and mean flow velocity) may be estimated through the input of measurements made at the outcrop to documented empirical relationships (Hjulström, 1935; Leopold & Wolman, 1960; Schumm, 1960; 1963; 1972; Carlston, 1965; Leeder, 1973; Ethridge & Schumm, 1977; Middleton &

Southard, 1978). However, determining the lateral dimensions of a point-bar deposit remains a challenge so modern analogues are commonly utilised to constrain these dimensions (e.g. Miall & Tyler, 1991; Dalrymple, 2001; Durkin *et al.*, 2015; Colombera *et al.*, 2017). Analogues are commonly selected from active reaches, and based on subjective visual matching between the meander shapes of modern systems and the exposed scroll-bar patterns of ancient preserved successions; such matching is not necessarily undertaken using a statistically robust approach (Tye, 2004). The exposed section of a point-bar deposit that is studied at the outcrop may represent a portion of the point-bar that was (i) deposited exclusively on the downstream limb; (ii) deposited exclusively on the upstream limb; and (iii) deposited on parts of both the up- and downstream limbs. In order for palaeohydraulic parameters to be accurately inferred, the position of the outcrop with respect to its position in the entire preserved point-bar deposit should be determined. The methods and results from preceding chapters will be applied to a point-bar succession studied at outcrop so as to reconstruct its likely lateral original extent, geometry and internal facies distribution in three dimensions.

**How can the internal stratigraphic architecture, and geomorphic variability, be predicted from surface morphology, or flattened seismic timeslices?**

*Rationale:*

Reflection seismic imagery provides a method of planform observation of preserved fluvial successions (e.g. Carter, 2003; Hubbard *et al.*, 2011; Labrecque *et al.*, 2011). The preserved succession may be either an avulsed reach (Carter, 2003; Fachmi & Wood, 2005), or an amalgamated succession (Hubbard *et al.*, 2011). From this imagery, the lateral extent and plan-form geometry of each point-bar deposit may be directly measured, though where cannibalisation has occurred in amalgamated

deposits, these measurements may be underestimated due to the preservation of only partial remnants of the original elements (Bhattacharya *et al.*, 2015). The lateral extent and thickness of these point-bar deposits may be directly integrated into fluvial reservoir models (e.g. Yan *et al.*, 2017). However, determining the accretion history and heterogeneity of the imaged preserved point-bar deposit is more challenging. Predicting these characteristics is important due to the ability of IHS to influence the direction of fluid flow during hydrocarbon sweeps (Fielding & Crane, 1987; Miall, 1988; Tye, 2004). Analogues are found in modern fluvial reaches, and are most commonly used as a means to deduce the missing attributes of a preserved meandering fluvial system (e.g. Posamentier *et al.*, 2004). This direct dependency is of limited accuracy as no two meandering reaches are the same, although modern systems are able to provide proof of concept. By integrating complicated observations of active fluvial systems through the methodologies developed as part of this research study, seismic interpretation may be of benefit for successions that describe either accumulated, or avulsed fluvial systems.

## **1.4 Methods**

The chapters of this thesis are intended to be read as standalone pieces of work that collectively build upon an overarching research theme. Therefore, the methods used in each chapter are specific to that chapter and, as such, are explained therein and are merely introduced and described in brief below. The point-bar analysis undertaken by this study has employed techniques in both remote sensing and outcrop sedimentology and facies analysis.

### *1.4.1 Remote sensing*

Remote sensing techniques were undertaken using Google Earth Pro software (version 7.1.7). The imagery was observed for clarity and then each point-bar to be studied was

marked, and the latitude and longitude recorded (Appendix A and B). The “Path” tool was used to measure distances; nodes were placed, and the distance found by selecting the path in the “Places” list, opening the object menu, selecting line “Properties” and selecting the “Measurements” tab. The “Polygon” tool was used to measure areas; the procedure for placing nodes and recording measurements is identical to using the “Path” tool. The tool for viewing historical imagery was used in order to determine mechanisms for modes of meander abandonment.

#### *1.4.2 Outcrop analysis*

Outcrop analysis was undertaken through: i) lithofacies identification; ii) construction of sedimentary graphic logs; iii) construction of 2D panels, and pseudo-3D panels; and iv) palaeocurrent analysis. Lithofacies were defined by observing and recording the rock properties; grain size, texture, lithology, colour, sedimentary structures and fossil content (Middleton, 1973; 1978; Lindholm, 1987). Sedimentary graphic logs were constructed and record grain size, sedimentary structures, bed thickness, lithology, fossils, and other distinguishable features. Stratigraphic panels were constructed from the base data; such panels enable the lateral and vertical relationships to be established, and individual sedimentary graphic logs to be related to each other. Palaeocurrents were recorded from accretion surfaces, ripple crests, trough axes, channel axes, and cross bedding foresets.

### **1.5 Thesis layout**

Within this thesis, chapter 1 introduces the research and its rationale; furthermore, it outlines the thesis structure. The research questions are addressed in four chapters (2-5); the first three of these chapters (2-4) establish a series of methodologies and a data set that may then be applied. These methodologies aim to integrate data from active and abandoned meandering fluvial channels which are present in both modern



systems and which occur preserved in the ancient record. Chapter 5 is the application of these methodologies and knowledge, to an outcrop exposure (Pennsylvanian, Nolton Haven, Pembrokeshire, Wales, UK). The research questions are then discussed and cross-referenced in the thesis discussion (Chapter 6), and consolidated in the conclusions (Chapter 7).

### ***Chapter 1: Introduction***

Chapter 1 introduces the research rationale and background knowledge for the study. It includes the aim, objectives, research questions, and methodologies.

### ***Chapter 2: A new universal approach to morphometric analysis of fluvial meander bends***

This chapter describes the rationale and specific methodology for the novel Intersection Shape methodology. The procedure is outlined in detail, and is summarised in a flowchart that may be easily implemented; each step of the method is described succinctly. The methodology quantifies fluvial meander shapes and may be used universally. A comparison is included to demonstrate how the methodology is able to highlight morphological differences between two different fluvial reaches.

### ***Chapter 3: Prediction of lithological heterogeneity in fluvial point-bar deposits from analysis of meander morphology and scroll-bar pattern***

This chapter outlines the methodologies that are required to predict the heterogeneity of a fluvial point-bar deposit in an active meander bend. These methods are: i) the observation of overall scroll-bar morphology; ii) the mapping of the positions of relative heterogeneity around a point-bar deposit; iii) the overlaying of these individual maps; and iv) comparison of the attributes of a meandering fluvial system in order to determine the most appropriate analogue(s).

**Chapter 4:** *Implications of the variation of mechanisms for fluvial abandonment on the stratigraphic record*

Chapter 4 highlights the difference in the point-bar dimensions in an active fluvial meandering reach, and an abandoned one. Through assessment of a series of parameters on abandoned meander loops from 11 different river reaches, and by combining the understanding with parameters from active systems measured in Chapters 2 and 3, an improved understanding of amalgamated successions may be gained.

**Chapter 5:** *Reconstructing planform point-bar dimensions and palaeo-meander shape from a preserved point-bar deposit in outcrop*

An exposed point-bar in Nolton Haven, Pembrokeshire, UK – an ancient meandering fluvial succession of Pennsylvanian age – has been studied to determine its three-dimensional accretion history, lithofacies heterogeneity distribution and geometry. This has been achieved through the detailed application of the methods outlined in Chapters 2, 3, and 4.

**Chapter 6:** *Discussion*

This chapter answers the research questions posed in Chapter 1.3 by integrating the information that has been gained through all of the preceding chapters of the thesis. The discussion describes the advances that have been made in this research and critiques the validation of the approaches in terms of methodology and resulting data. The strengths, improvements, and weaknesses are highlighted.

**Chapter 7:** *Conclusions and future work*

This chapter summarises the consolidated understanding drawn from this thesis. Some of the main topics for future work are presented.



## 2 A new universal approach to morphometric analysis of fluvial meander bends

### 2.1 Chapter Summary

River meanders are inherently complex morphological features. Quantifying and classifying the natural variability of meander-bend shape in single river reaches, and across different fluvial systems in a repeatable manner, is challenging. Here, a novel morphometric method, the “Intersection Shape” methodology, has been developed and implemented to quantify and classify the morphology of any meander bend via the relationship between meander shape and scroll-bar pattern. The method uses planform images to identify geometrically-defined points up- and downstream of the point on the inner bank where the most recent scroll bar is widest, between meander-bend inflection points. Channel-perpendicular lines are then constructed from these points into the planform area. A polygon is defined where multiple lines intersect within the confines of the meander body. The ratio of the area of this polygon and the product of its perimeter, is normalised using the average channel width and plotted against the ratio of the length of meander migration trajectory to the meander width. These data are used to quantify the relationship between meander shape and scroll-bar pattern determined by the direction of meander growth. Based on application of this method to 260 active bends from 13 globally-distributed river reaches, meander forms have been classified into four groups representing overall shape: open asymmetric, angular, bulbous, and open symmetric. Within each of these four groups, different meander shapes plot in discrete fields. This provides the basis for a novel quantitative classification scheme representing shape variety across twenty-five subdivisions of the four main groups. Application of the method is demonstrated by classification of twenty active meanders in reaches of each of the Irtysh (Ob) River, Russia, Senegal River,

Senegal, and the Ok Tedi (Fly) River, Papua New Guinea. Quantifiable morphological differences between the meanders of each of these systems are identified. The “Intersection Shape” methodology is generic, repeatable, permits appropriate numerical and graphical comparison, and enables visualisation of different river meander patterns. The resultant bivariate plots can be used to describe and understand how meanders evolve under different sets of controls, and can be applied to investigate geological and stratigraphic problems.

## 2.2 Introduction

Capturing complexity of form in nature is notoriously difficult (Phillips, 2003). The identification and classification of the natural variability of fluvial meander shapes in a meaningful way is no exception (Miall, 2006). The differentiation of meander-bend morphology is significant because the observed wide variety of meander forms are governed by the interplay of many autogenic and allogenic controls (Rosgen, 1994; Miall, 2006, Gutierrez & Abad 2014). Early approaches to the quantification of meander shape were based on physical field measurement (e.g. Towl, 1935; Leighly, 1936; Fisk, 1947), followed in the 1970s and 1980s by the analysis of aerial imagery of limited spatial extent (see Hooke, 1997 for review), and variable quality, resolution and availability (e.g. Nanson and Hickin, 1983). Establishment of links between meander shape and their controls remains an on-going research challenge.

Meander shape is known to be influenced by a number of controls, such as the size and calibre of transported sediment (Allen, 1965), the timing and frequency of meander-loop cut off (Hooke, 2004; Lewis & Lewin, 2009), variations in the erodibility of the floodplain (Hooke, 2004; Gunesalp & Marston, 2012), the ratio of mean annual river discharge to meander wavelength (Carlston, 1965), the abundance and type of riparian vegetation (Millar & Quick, 1993; Rowntree & Dollar, 1999; Perucca *et al.*,

2007; Ielpi *et al.*, 2014), and climate change (Leopold & Wolman, 1957; Alford & Holmes, 1985).

Established methods for meander description can be broadly categorised as qualitative, semi-quantitative, or fully quantitative. Qualitative description is predominantly reliant on "shape matching" (Brice, 1974; Allen, 1982; Bridge, 2003; Ielpi & Ghinassi, 2014). Some parameters describing form are able to be quantified but analysing change is difficult with these existing methods (Hooke, 1984). Semi-quantitative methods, such as the radius-of-curvature method, measure channel curvature at a series of points to define a metric that is known to scale to bend migration rate (Nanson & Hickin, 1983). Although these approaches have merit, their implementation means that a subset of irregular meander shapes are not accounted for.

Some quantitative methods to aid prediction of channel pattern have been developed for specific rivers: for example, the angle measuring technique (AMT), (Andrle, 1994) was developed on a confined reach of the Shenandoah River, Virginia, USA, and the curve-fitting method (Brice 1973; 1974) was refined through analysis of a reach spanning six meanders of the White River, Indiana, USA. Other quantitative methods have been developed for specific types of rivers, such as perennial (Van De Berg, 1995) and gravel-bed rivers (Gustavson, 1978). The main limitation of these methods is that they work most effectively for the river reaches for which they were developed, and are difficult to apply universally.

Commonly, meander shape is related to the form of associated scroll bars (Ielpi & Ghinassi, 2014; Frascati & Lanzoni, 2010; Bridge, 2003). Scroll bars are a surface record of migrating bedforms, which are defined as ridges and swales present within meander bends (Nanson, 1980). They serve to record evolutionary changes in meander shape, migration direction, bend evolution, and sedimentary architecture

(Allen, 1965; Daniel 1971; Hickin & Nanson, 1975; Bridge, 2003; Miall, 2006; Chen & Duan, 2006), which is preserved in the geological record as coarsening upwards, metre-scale, inclined beds (Ielpi & Ghinassi, 2014). The preserved stratigraphic record of meander-bend deposits is, in almost all cases, incomplete due to issues related to preservation potential and sediment reworking (Fielding & Crane, 1987; Colombera *et al.*, 2017).

The aim of the present paper is to introduce a novel methodology for quantifying the relationship between meander shape and scroll-bar pattern. This methodology has been designed for application to stratigraphic problems, notably the reconstruction of ancient meander forms preserved in the rock record. Observations from aerial imagery show that the relationship between meander shape and scroll-bar pattern is highly variable, and quantification of this relationship provides improved understanding of the controls on the development of meandering reaches in modern systems and criteria for recognition and interpretation of their preserved deposits in ancient successions.

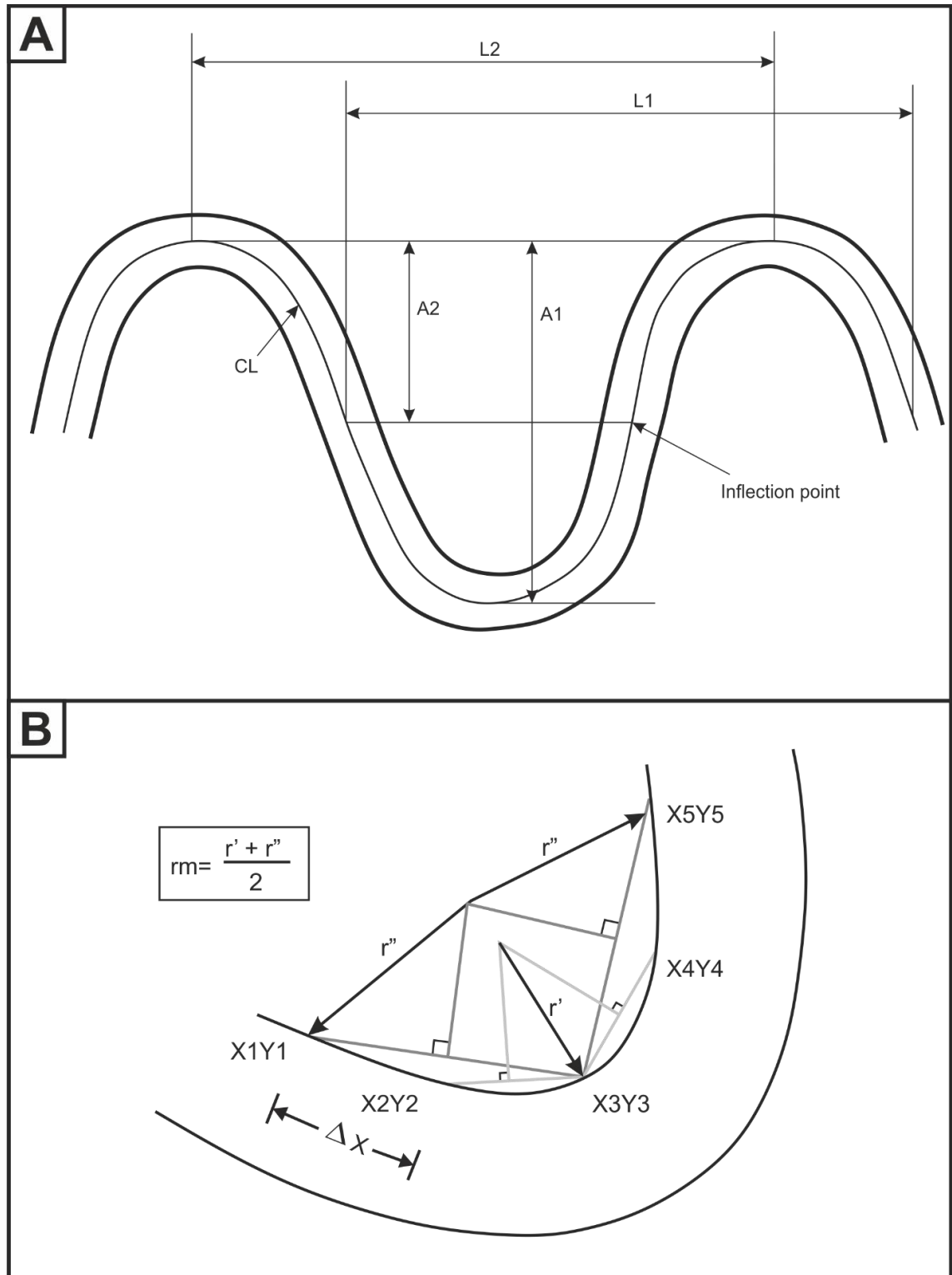
Specific research objectives are: (i) to review the strengths and weaknesses of existing methods used to describe meander form; (ii) to devise a novel, quantifiable and generically applicable method, which is straightforward and repeatable in its application, for comparison of meander shapes and related scroll-bar migration directions in fluvial systems; (iii) to show how the new method can be applied to reduce the reliance on subjective measures for the characterization of meander shape; and (iv) to demonstrate one of the many practical applications of the new method by comparing meander shapes from multiple fluvial systems in a quantitative manner. The method can be applied to stratigraphic problems, notably the reconstruction of ancient meander forms preserved in the rock record, though discussion of this is beyond the scope of this paper.

## 2.3 Background

A range of nomenclature is used to describe morphological variables describing meander shape (Hooke, 1997). “Simple” refers to scroll-bar deposits indicative of unidirectional accretion and meander bends with a sine-wave-like shape. “Compound” refers to meander bodies that possess two or more bend components and multiple phases of scroll-bar migration. “Regular” means to be recurring at uniform spatial intervals and arranged in a non-varying pattern with regard to the spacing of scroll-bar elements within a single meander or the spacing of meanders along a river reach. “Irregular” means to be uneven or unbalanced in shape or arrangement with regard to the arrangement of scroll-bars within a meander or the shape of a meander bend. These terms have been used interchangeably in some older literature (cf. Brice, 1974; Hooke, 1977b; Allen, 1982; Rosgen, 1994), which has led to a lack of clarity in the description of meander shape and scroll-bar pattern. There is further confusion in the literature regarding usage of the terms wavelength and amplitude in application to the study of the form of fluvial meanders (Fig. 2.1A). Bend amplitude is measured as a straight line in a direction perpendicular to the mean direction of flow of the river, as seen in plan-view. It can then either be measured from peak to trough of the meander (Leopold & Wolman, 1960; Allen, 1965; Bhattacharya *et al.*, 2015), or as half of this (Khatsuria, 2008 – Fig. 2.1A). Wavelength is measured either as the straight-line distance from peak-to-peak or trough-to-trough of a meander seen in plan-view (Williams, 1986; Bhattacharya, 2015 – Fig. 2.1A), or from inflection point to inflection point (Leopold & Wolman, 1960; Carlston, 1965). Practical attempts to measure these variables in natural examples can yield different values, depending on the technique employed. The complexity of real systems is such that, even when these terms are defined, they can be difficult to use reliably in practice. The following sections highlight



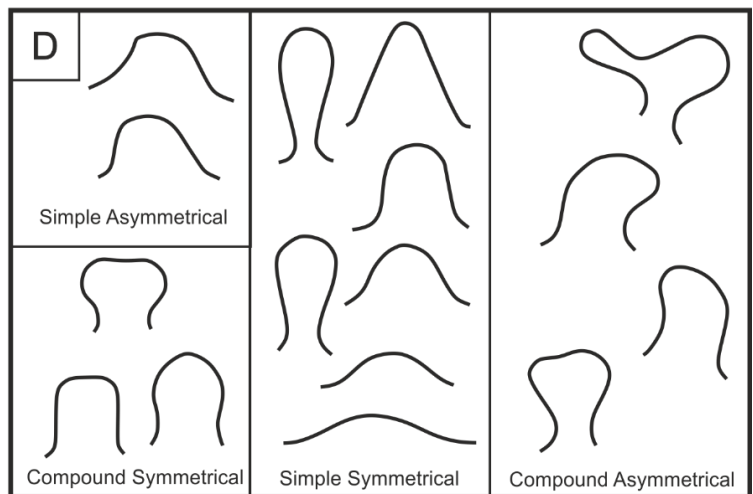
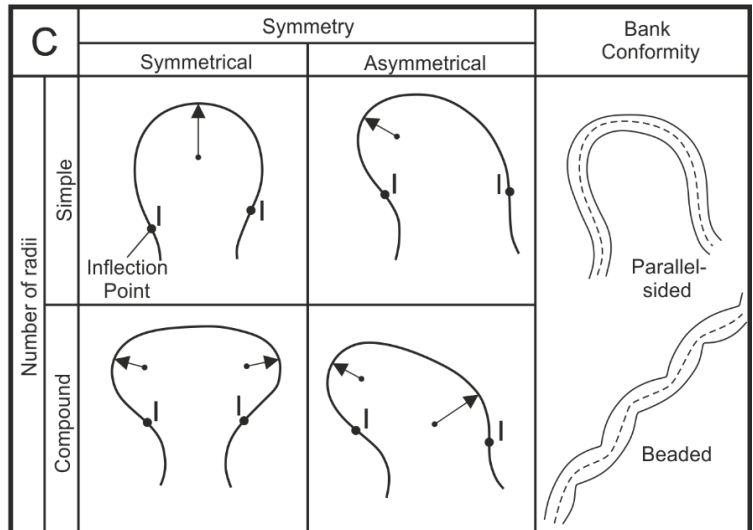
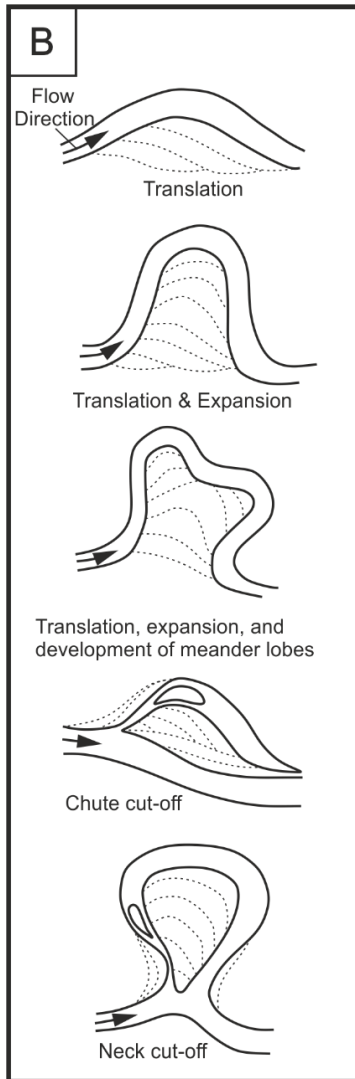
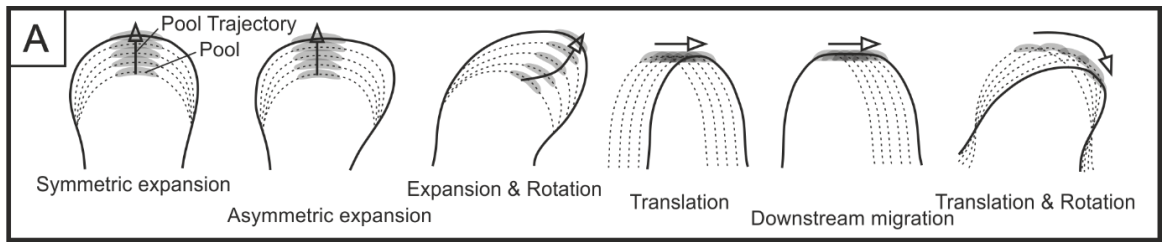
the need for a universal terminology and a quantifiable approach to the description of meander form.



**Figure 2.1 - A) A demonstration of the variety of meaning for wavelength and amplitude in the literature. A1 - Leopold and Wolman 1960, Allen 1965, Bhattacharya et al. 2015; A2 - Katsuria 2008; L1 - Leopold and Wolman 1960, Carlston 1965; L2 - Williams 1986, Bhattacharya et al. 2015; CL - Chen and Duan 2006; B) Nanson and Hickin's (1983), redefinition of Mean Radius of Curvature ( $r_m$ ) for a Meander Bend.**

### *2.3.1 The description of meander form: Subjective shape classification*

Visual classification schemes based on subjective criteria are well established (e.g. Brice, 1974; Allen, 1982; Bridge, 2003; Ielpi & Ghinassi, 2014) (Fig. 2.2). Brice (1974) identified 16 shapes in his classification scheme (Fig. 2.2D), based on the understanding that meanders become increasingly sinuous over time in cases where they eventually cut-off at their neck or chute. However, such methods lack a unified quantitative approach to measurement (Hooke, 1997), especially where irregular meander shapes are studied, such that a meander might be reasonably assigned to multiple categories. The visual approach may thus require multiple classification schemes to adequately describe and classify a single meander shape.



**Figure 2.2 - Meander classification schemes modified from A) Ielpi and Ghinassi (2014), B) Bridge (2003), C) Allen (1982), D) Brice (1974). Each of these can qualitatively identify features of a meander.**

### 2.3.2 *The description of meander form: Simplified sine-generated type curves*

Historically, numerical models developed to represent fluvial systems used simplified analytical forms to fit channel geometries (Jefferson, 1902; Leopold & Langbein, 1966; Chitale, 1973; Ferguson, 1975), that may evolve in shape over time (Hooke, 1977b; Willis & Tang, 2010). These principles are used to replicate patterns in a fluvial reach for the purposes of determining morphometric parameters (Camporeale *et al.*, 2005), such as upstream and downstream skewness (Seminara *et al.*, 2001), and meanders composed of multiple loops (Hooke & Harvey, 1983). Fluvial reaches characterised by near-symmetrical, sinusoidal meander forms are commonly selected for study and comparison (Andrle, 1994), despite such forms being only one of many possible planform configurations. These approaches can be difficult to apply more generally because they are developed for case-specific purposes (Andrle, 1994; Chen & Duan, 2006), and need to be better constrained with more case studies (Miall, 2006). The applicability of such methods is limited because not all fluvial systems can be compared directly.

### 2.3.3 *The description of meander form: Radius of Curvature*

Radius-of-curvature is a widely used quantifiable parameter with which to assess the morphological properties of a meander. It has been correlated with bend migration rate (Hickin & Nanson, 1984; Hudson & Kesel, 2000) and used to reconstruct bank-full channel widths and depths (Williams, 1986; Bhattacharya *et al.*, 2015). Leopold and Wolman (1960) calculate the radius of curvature as the distance from the central point of a meander to the centreline of the channel. The central point of a meander can be difficult to locate in asymmetric forms, so Nanson & Hickin (1983), refined the method (Fig. 2.1B) by using multiple points between two inflection points for the purpose of measurement, and then averaging the resultant numbers ( $r'$  and  $r''$ ). This method is difficult to apply in cases where a meander exhibits more than two inflection points.

Williams (1986) developed an equation for calculating a radius of curvature using sinuosity and wavelength as the variables. The application of the empirical relationship (Williams, 1986) works well if the meander is of a simple shape; however, many meander shapes are more complicated and irregular in form, especially those that have developed to a bulbous shape which would not be recognised through use of the methodology. The practical difficulties of applying the radius-of-curvature methodology make it difficult to compare reaches characterised by meanders with marked morphological diversity.

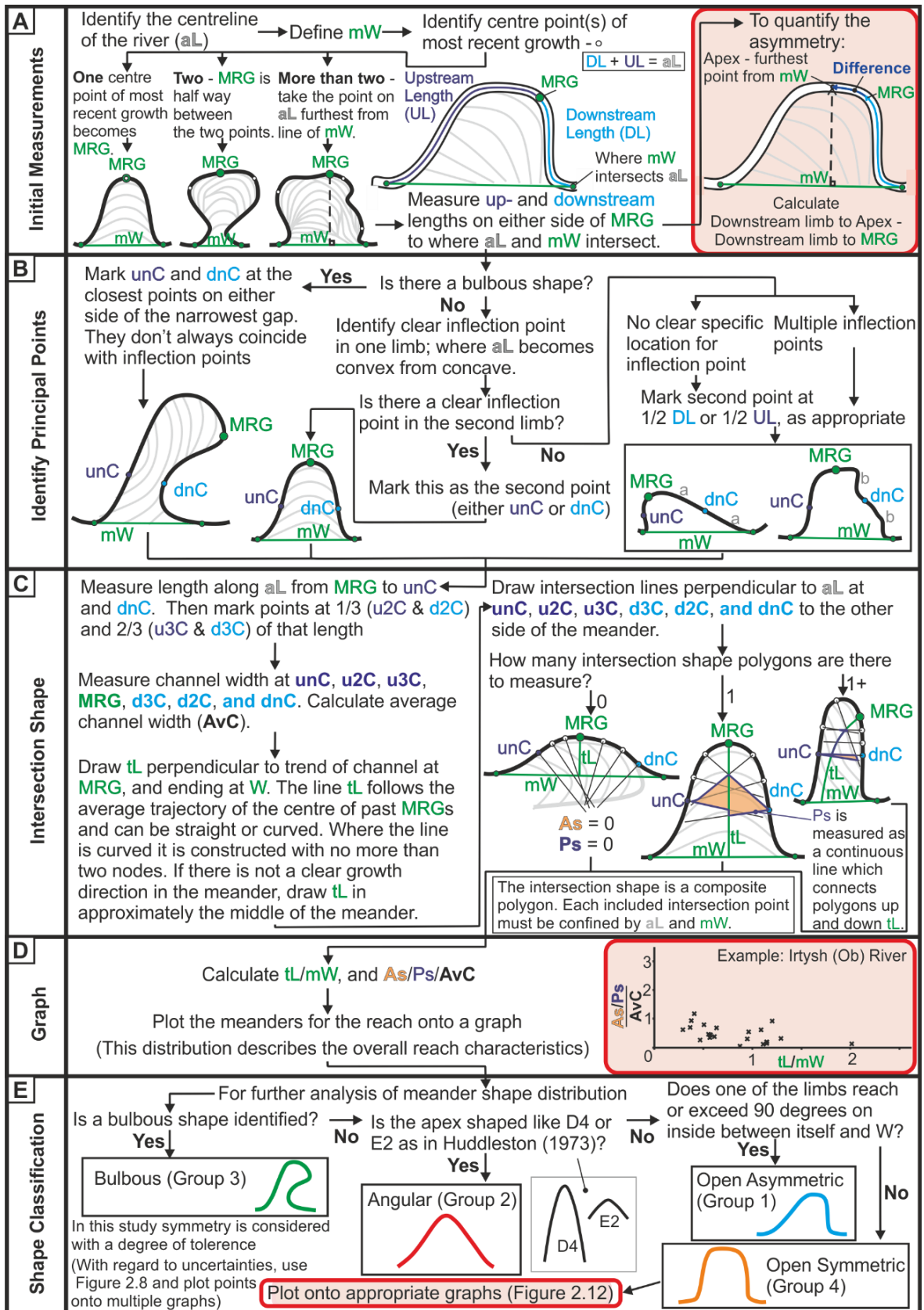
#### *2.3.4 The description of meander form: Bend Asymmetry*

Meander-bend asymmetry is measured through quantitative analysis of meander skew (Parker *et al.*, 1983; Posner & Duan, 2012). Skew is most commonly upstream-directed (Gilvear *et al.*, 2000; Seminara, 2001; Xu *et al.*, 2011), but may also occur in the downstream direction (Zolezzi & Seminara, 2001; Seminara, 2006; Perucca *et al.*, 2007). Overall assessment of these characteristics are difficult to define unequivocally because neighbouring meanders may skew either up- or downstream and individual meanders may behave differently at different times during their evolution. To quantify the variability of asymmetry in a reach, a clear definition of the upstream and downstream parts of a single meander bend is required. Parker *et al.* (1982) defines upstream and downstream based on where a meander changes from dominantly erosional (pools) to accretionary (riffles), because a riffle commonly coincides with a point of inflection and a pool commonly coincides with a bend apex. However, coupling pools with apices, and riffles with inflection points is inconsistent across river types such as the River Elan which is an underfit stream and seems to bounce somewhat against the valley walls, so the pool-riffle sequence is out of phase with the bends (Richards, 1982). Also, a composite meander, as accreted from the same point-bar (Fig. 2.2B), is comprised of multiple bends, therefore forming multiple pool-riffle

sequences. This makes the identification of which change from pool to riffle demarcates the upstream and downstream ends difficult, and at least partly subjective.

## **2.4 Data and methods**

Previous methods used to describe meander form do not consider the full range of morpho-types of meander morphology. The “Intersection Shape” methodology outlined below is a refined approach to the assessment of meander morphology. Application of the method primarily results in the definition of two metrics that describe the relationship between meander shape and scroll-bar pattern. Incorporation of analysis of scroll-bar pattern into the “Intersection Shape” methodology allows a deeper understanding of causative effects of meander shape evolution. The method also serves to quantify meander-bend asymmetry. A workflow for application of the methodology is detailed in Figure 2.3 and discussed further below:



**Figure 2.3 - A step-by-step guide for completion of the Intersection Shape methodology with each of the three outputs highlighted with a red box. The method is broken down into 5 major phases labelled A-E: A) Initial measurements provide the outline for the Intersection Shape methodology. Through using these measurements, skew can be calculated; B) Identification of unC and dnC provides the points between the divisions for the remainder of the methodology to occur; C) The intersection lines can be constructed and the intersection shape formed between these points of intersection; D) The values for the graph axes are calculated to allow for an initial plot of the reach; E) If further analysis of the shapes is required, then the appropriate group may be identified for each shape and this division can allow for further analysis.**

#### A) Initial Measurements (Fig. 2.3A)

The in-channel water level varies between high and low flow stage on a seasonal basis, and that imagery is acquired from different seasons and flow states, or during flood and drought events. To ensure consistency in determining channel width, the active channel is defined to comprise both the waterway and any exposed banks (cf. Hooke, 1995; 2007). The centreline of the channel (aL) is the midpoint between the two channel banks; it is possible for the centreline to be outside of the water-filled part of a channel in some cases. The distance between the two banks provides an estimate for bank-full width. The channel centreline (aL) connects the start and end points of 'mW'. A straight line tangent from the channel centreline (aL), connects two points on the immediately up- and down-stream meanders across the meander being studied (Fig. 2.4A), which defines the limits of a meander bend. A superimposed meander can occur within (or upon) another meander in a compound form. A compound meander (cf. Allen, 1982) (Fig. 2.4C) becomes two distinct meanders where it may be divided by multiple tangents (Fig. 2.4D).



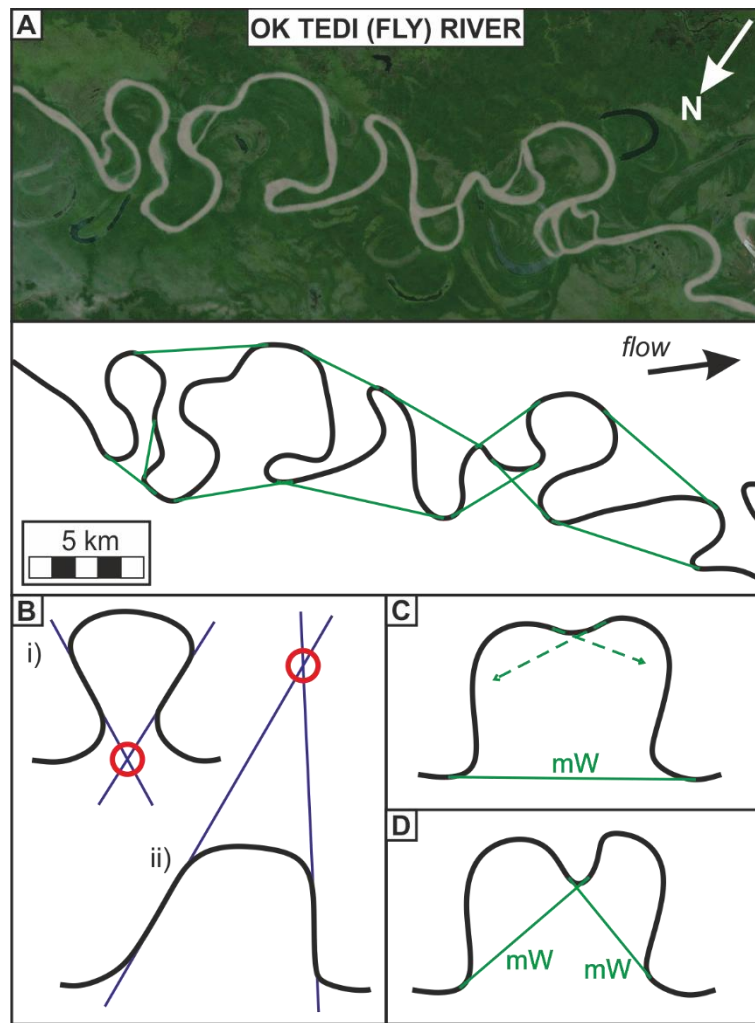


Figure 2.4 - A) A demonstration of the definition of a meander within a reach of the Ok Tedi (Fly) River, Papua New Guinea; B) To identify bulbous shapes, a centreline should be extended through where mW intersects with aL along each limb of the meander. If the centreline extensions intersect inside the shape, it is bulbous, whereas if they intersect outside the shape or run parallel, it is open; C) A demonstration of a compound meander that would be defined as one meander; D) A demonstration of where a compound meander becomes two meanders.

Parameter mW is not analogous to wavelength because wavelength connects two consecutive apices on the same side of the channel-belt axis, (Williams, 1986; Bhattacharya *et al.*, 2015), or from one inflection point on a meander limb to an adjoining inflection point (Leopold & Wolman, 1960). Measurements of wavelength

made using these approaches are not necessarily consistent because naturally occurring meanders are inconsistent and do not reflect the regular form of a sine-wave. By contrast, the method described here for the determination of mW is repeatable, non-limiting, and gives consistent results, because parameter mW isn't confined by the connection of consecutive apices and may be applied to any shape.

For a single meander, scroll bar surface morphology is used to locate the point of most recent growth (MRG), (Fig. 2.5). This can be determined by identifying the point on the inner bank where the most recent scroll bar is widest. Typically, this is indicated in planform by the widest point of a sand bar, but does not necessarily coincide with the point of maximum curvature of the meander. For vegetated point-bars, the most recently accreted part of a bar is typically characterised by a below average vegetation density relative to the surrounding channel belt (Allen, 1965; Daniel, 1971). Typically in compound bends (cf. Allen, 1965: Fig. 2.6C), there are multiple points of recent deposition; in such situations, the mid-point between two identified points of MRG is selected. If there are more than two points of MRG, then the shape apex is used. The bend apex is defined as the point along the centreline that is furthest from mW (Fig. 2.3).

The along-channel distances of MRG from the points where aL and mW intersect are labelled UL (upstream length) and DL (downstream length), respectively (Fig. 2.3A). Bend asymmetry may also be defined as the along-channel distance between MRG and the bend apex (referred to as difference in Fig. 2.3A). These metrics are included later in the Intersection Shape methodology and allow for quantification of geometric skew.

**B) Identify Principal Points (Fig. 2.3B)**

Identify the positions of unC and dnC, which are markers for finding the position of the Intersection Shape. If the shape is bulbous (e.g., see Fig. 2.4B) then unC and dnC are placed on the meander centreline (aL) on either side of the narrowest gap that forms a neck to the meander loop. These points do not necessarily coincide with inflection points. If the shape is not bulbous, then a clear inflection point is identified on either the up- or downstream limb, and this will define either unC or dnC, respectively. If there is a clear inflection point on the other limb, then this will define the second point (either unC or dnC). If the other limb has no clear inflection point, or has multiple inflection points, then the second point is placed at  $\frac{1}{2}$  DL or  $\frac{1}{2}$  UL, as appropriate.

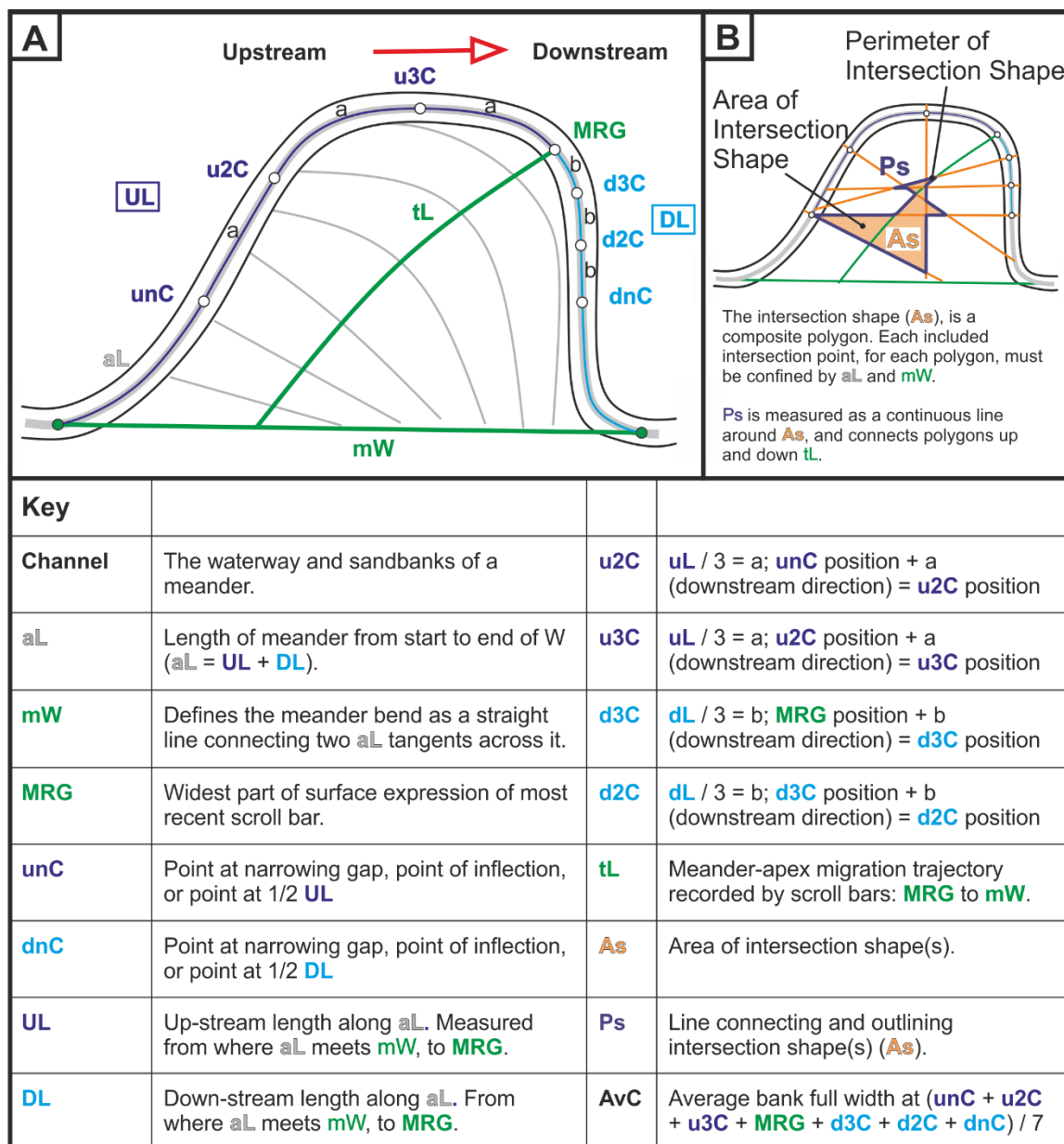


Figure 2.5 - A) The morphometric parameters measured in each meander for this study;

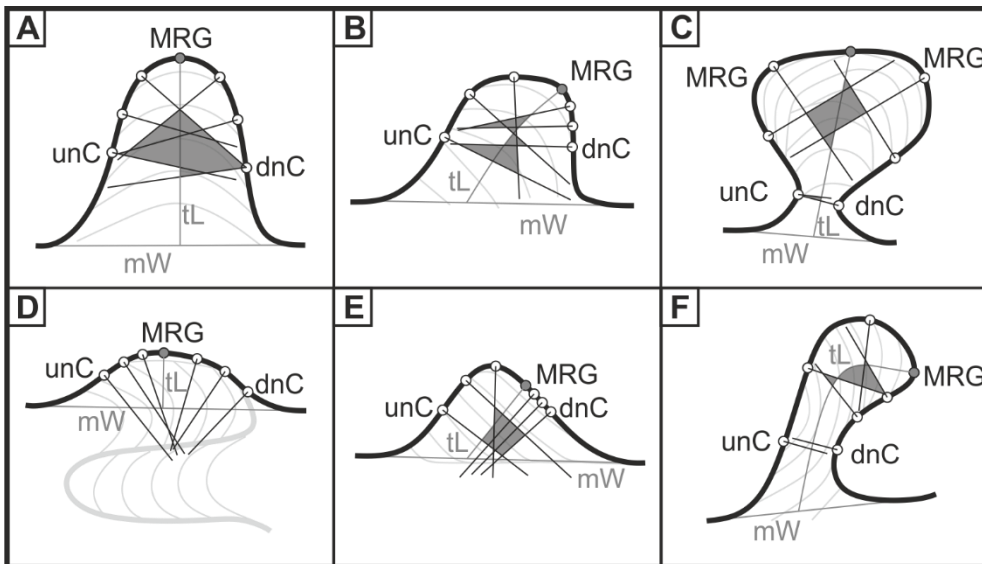
B) the terminology of the “Intersection Shape” methodology.

C) Intersection Shape (Fig. 2.3C)

Measure the along-channel distance from MRG to both  $unC$  and  $dnC$ . Mark points at  $1/3$  and  $2/3$  of each length and label  $u2C$ ,  $u3C$ ,  $d2C$  and  $d3C$  as appropriate at each point (Fig. 2.5A). Because channel width is not constant and varies as a function of curvature and stage (Seminara, 2006), channel width is measured at seven points

(unC, u2C, u3C, MRG, d3C, d2C, and dnC), to find the average channel width (AvC). Channel width is measured perpendicular to the meander centreline and is measured assuming a bank-full width (see above).

The line expressed as tL is defined by the length of the trajectory of meander-apex migration as recorded in the scroll bars through time from mW to MRG and can be straight or curved (Fig. 2.5A). Where scroll bars have become fragmented by erosion or overprinting, the meander-apex migration is traced as far as possible and the remainder of the line is then constructed close to the middle of the meander to terminate at the point where it meets mW. From the other 6 points, (unC, u2C, u3C, d3C, d2C, and dnC), straight intersection lines are constructed at right angles to the river centre-line (aL) into the meander body. The intersection shape is a composite shape comprised of multiple polygons defined where these intersection lines overlap. Each polygon must have every corner enclosed within the meander shape (defined as being within aL and mW). The polygons generated by this method are compiled to form an intersection shape for which the area (As) and perimeter (Ps) are measured (Fig. 2.5B). The resultant composite intersection shape may be one polygon (Fig. 2.6A) or multiple polygons detached from one another (Fig. 2.6C). The line Ps is measured first and is constructed around the complete enclosed polygon. Where the intersection shape is two detached polygons, the line Ps is constructed down the line tL to the other polygon, around the second polygon and then back up the line tL to the starting point. The same principle is applied if there are more than two intersection shapes. For some meander forms, notably those with low curvature, there may be no intersection shape; in such cases both As and Ps are zero.



**Figure 2.6 - A) A classic meander shape; B) An example where tL is curved because MRG does not coincide with the apex; C) A bulbous shape where a narrowing gap is observed. The intersection shape is also in two parts with triangle near “unC” being connected by “Ps” along tL; D) An example where there is no intersection in the meander shape confined by the meander centreline and “mW”, therefore there is no intersection shape; E) An example demonstrating how “mW” confines the intersection shape; F) An example where tL is curved because of the position of MRG. tL is approximated through the middle of the meander body as the scroll bar fragments become more obscure.**

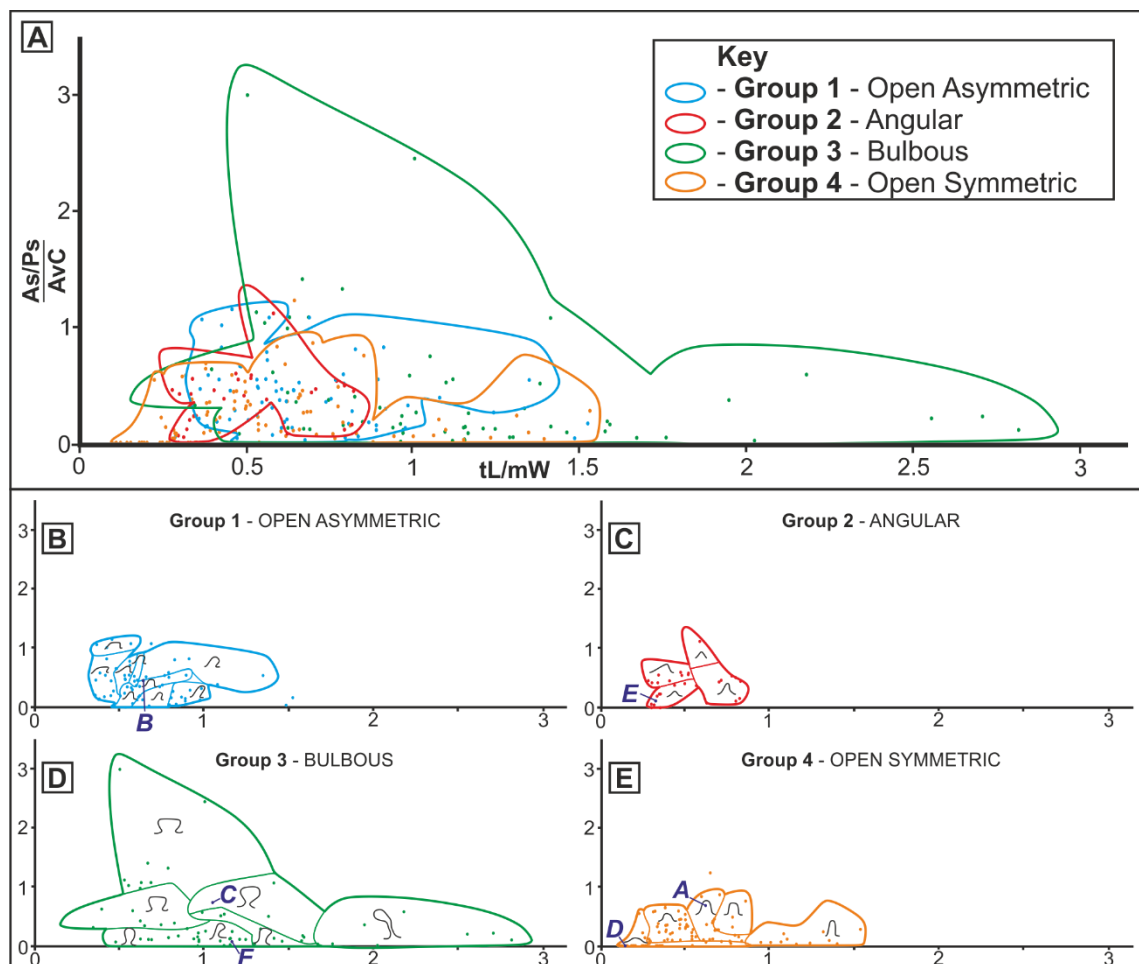
#### D) Graph (Fig. 2.3D)

The principal output of the “Intersection Shape” methodology is a bivariate plot that includes values of (i) the area and (ii) the perimeter of the intersection shape, (iii) the length of trajectory and (iv) the width of the channel. These data are converted into ratios; on the y-axis,  $((As/Ps)/AvC)$ , the ratio of the area ( $As$ ) and perimeter ( $Ps$ ) of the intersection shape, which is normalised using average channel width ( $AvC$ ) to counteract the effect of scale dependence (cf. Nanson and Hickin, 1983; 1986); and on the x-axis ( $tL/mW$ ), the ratio of the length of trajectory of the meander pool ( $tL$ ) and the

meander width (mW). The resultant graph provides a measure of the spatio-temporal relationship of the meander shape to the scroll-bar pattern.

### E) Shape Classification (Fig. 2.3E)

Further analysis of the meander shapes reveals more information concerning the variability of morphology in a meander reach. Manual intervention is required in part for the attribution of meander shapes to their parent groups for clearer visual analysis, the criteria for which are described in this section. Twenty-five meander shapes have been identified (Fig. 2.8) that represent sub-groups within the four parent groups: open asymmetric, open symmetric, open angular and bulbous (Fig. 2.7).



**Figure 2.7 - Four groups of meander and their associated shapes on bivariate plots. On each graph, the y-axis is As / Ps divided by average channel width, and the x-axis is tL /**

**mW. The four small graphs show the shape envelopes and an outline of all of the envelopes is seen on the large graph. The polygons overlying the envelopes represent the shape which sits in each envelope. Group 1: Open Asymmetric, Group 2: Angular, Group 3: Bulbous, Group 4: Open Symmetric. The purple italicised letters A-F indicate the positions of the meander bends depicted in figure 2.8.**

In this study, a wide variety of naturally occurring meander shapes are considered and each shape should be easily incorporated into an easily attributable common category. Naturally occurring perfect symmetry is rare and so through the adoption of tolerance thresholds, a “near-symmetrical” class is defined. Open asymmetric is defined as open (Fig. 2.4Bii) where the angle between one limb and mW is  $90^\circ$  or greater, as measured on the line of the limb tangent (Fig. 2.8; Group 1); angular is defined as being an open (Fig. 2.4Bii) triangular-shaped meander where the apex of a meander is shape D4 or E2 in Huddleston’s (1973) classification (Fig. 2.8; Group 2). Bulbous is defined as where tangents, drawn from the limbs to the channel inflection points from the side closest to MRG, meet inside the meander (Fig. 2.4Bi), i.e., displaying meander tightening (Fig. 2.8; Group 3). Open symmetric (sine-wave-like) meanders (Fig. 2.4Bii) are defined where the angle between one limb and mW is less than  $90^\circ$ , as measured on the line of the limb tangent (Fig. 2.8; Group 4). Within these groups sub-categories are identified. The code attributed to each meander shape is composed of three parts: the prefix “S” refers to it being a meander shape; the number 1 to 4 refers to the parent group to which the meander belongs; the lower-case suffix (“a” to “i”) further qualifies the shape of the meander (Fig. 2.8).



		CODE	OUTLINE	DESCRIPTION	APPX. RATIO tL:W	SHAPE AT APEX (Huddleston 1973)
Group 1	OPEN ASYMMETRIC	S1a		One limb perpendicular to width of meander.	1:1	B2  B3
		S1b		One limb perpendicular to width of meander	2:3	C4
		S1c		One limb perpendicular to width of meander. Box-like.	1:2	B2
		S1d		One limb perpendicular to width of meander.	1:2	D2
		S1e		Overtured. Limbs are approximately parallel.	2:1	B4
		S1f		Overtured.	1:1	B3
		S1g		Recumbent.	1:2	A2  B4
		S1h		Overtured. Limbs are approximately parallel.	1:1	B4
		S1i		Recumbent. Rounded apex.	1.5:1	B3  B4
		Group 2	ANGULAR	S2a		Top is typically 'pinched'.
S2b				Symmetrical. Close to 90°.	1:1	E2
S2c				Most commonly asymmetrical.	0.5:1	E2
S2d				Most commonly symmetrical. Pronounced point.	0.5:1	E2
Group 3	BULBOUS	S3a		Not overturned. Rounded apex.	2:1	B3
		S3b		Sometimes overturned.	1:1	B2
		S3c		Not overturned.	2:3	B1  B2
		S3d		Sometimes asymmetric. Rounded shape at apex.	2:1	C3
		S3e		Typically slight asymmetry.	2:1	B2
		S3f		Recumbent. Typically one straight limb.	2:1	B3
		S3g		Overtured. Rounded shape at apex. Irregular.	3:1	C3
Group 4	OPEN SYMMETRIC	S4a		Elongate. Limbs are approximately parallel.	3:1	B4
		S4b		Limbs are approximately parallel.	1:1	B3  B4
		S4c		Typically rounded apex.	1:1	B3  B4
		S4d		Typically skewed.	0.5:1	B3
		S4e		Typically not skewed.	0.25:1	D1

**Figure 2.8 - Graphical table of shape properties showing the characteristics by which each type of meander is defined.**

The sub-groups (Fig. 2.8) are defined through visual classification of: (i) apex shape, which has been determined using the method of Huddleston (1973); (ii) relative

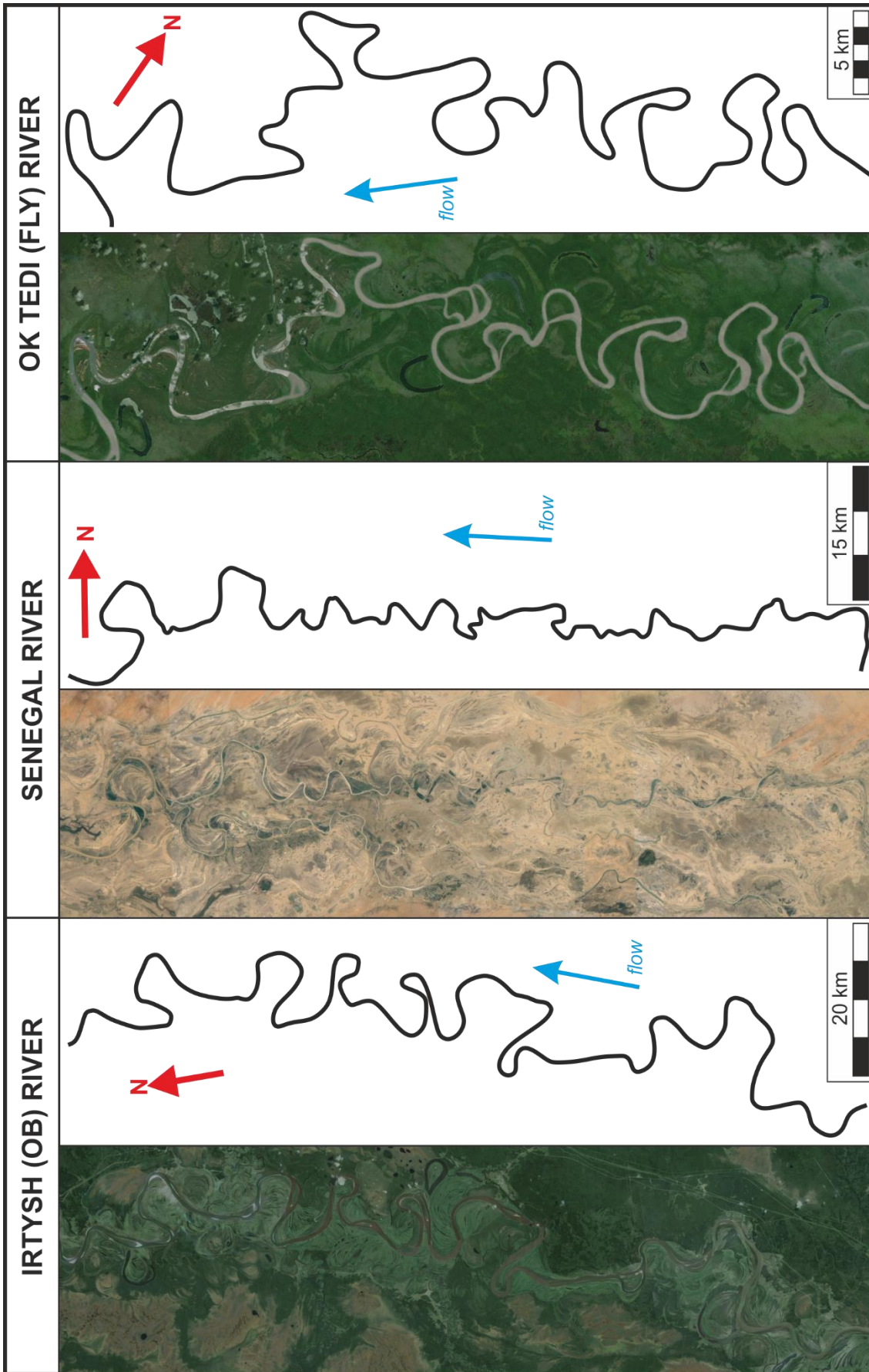
character of the limbs (e.g. one limb may be straight whereas the other is sinuous and curves towards the first limb, creating a narrower gap); (iii) asymmetry, where one limb is perpendicular to line mW, or overturned; (iv) average aspect ratio ( $tL / mW$ ) for the sub-group; and (v) other descriptive terms such as “pinched” (Fig. 2.8). Each data point represents one meander; each grouping allows for the proportion of that shape to be assessed on one of four graphs; each of the four graphs represents a parent group (Fig. 2.7). Therefore, these subdivisions enable a more comprehensive analysis than is possible by solely undertaking visual analysis of each reach.

Once the meanders are assigned to a parent group, a sketch of the shape of the meander was overlain on its point on the graph, and envelopes were constructed around morphometrically corresponding shapes to form an envelope (Fig. 2.7). If a meander has plotted in an envelope that is clearly incorrect, figure 2.8 should be consulted to better inform the parent group classification. This method represents a straightforward way to quantifiably and objectively characterise the spatio-temporal relationship of the meander shape and scroll-bar characteristics in a way that can be implemented universally for all river types.

## **2.5 Application and results**

To develop and test the method, 13 alluvial rivers have been studied from different latitudes and climate regimes. Analytical tools embedded in Google Earth Pro have been used to measure values of length and area. Twenty meanders from each river were measured, totalling 260 meander bends. These active bends have been analysed using the “Intersection Shape” methodology to classify the morphology of each meander shape in its group and sub-group. To demonstrate the applicability of the “Intersection Shape” methodology, results of the analysis of reaches from three meandering alluvial rivers are presented here: the Irtysh (Ob) River, Russia, the

Senegal River, Senegal, and the Ok Tedi (Fly) River, Papua New Guinea (Fig. 2.9). These rivers have been selected as they are physiographically different, i.e. they possess meanders with markedly different morphologies, and are located in contrasting climate zones, as defined by the Köppen-Geiger Climate Classification (Peel *et al.*, 2007): cold, dry, and humid, respectively. In addition, these reaches have readily identifiable scroll patterns visible in aerial imagery. The Ok Tedi (Fly) River is in a tropical rainforest setting, with precipitation during the driest month around  $\geq 60$  mm, the Senegal River is in a hot desert setting, with a mean annual precipitation of  $< 5$  mm and temperature of  $\geq 18^\circ\text{C}$ ; the Irtysh (Ob) River is in a cold climate setting, without a dry season and a cold summer, defined by a summer with a mean temperature  $\leq 22^\circ\text{C}$ , a winter which has mean temperatures  $> -38^\circ\text{C}$ , and  $\leq 4$  months with mean temperatures above  $10^\circ\text{C}$  (Peel *et al.*, 2007). The Ok Tedi (Fly), Senegal and Irtysh (Ob) rivers have the following characteristics: low gradients (ratio of vertical fall / length of valley slope along the river) of  $6.06473 \times 10^{-5}$ ,  $1.87582 \times 10^{-5}$ ,  $8.89561 \times 10^{-6}$ , respectively; discharge rates (Q) of  $1.56 \times 10^{10}$ ,  $1.47 \times 10^{10}$  and  $7.562 \times 10^{10}$  m<sup>3</sup> / annum, respectively (Meybeck & Ragu, 2012); and sinuosities in the studied reaches of 3.06, 1.77 and 2.28, respectively.



**Figure 2.9 - Planform outlines of the three rivers investigated in this paper; the Senegal River, the Irtysh (Ob) River and the Ok Tedi (Fly) River.**

The principal output of the “Intersection Shape” methodology is a graph (Fig. 2.7), which plots  $(A_s / P_s) / AvC$ , against the ratio of length of trajectory of the meander pool (tL) to meander width (mW). Box-like and wide meander shapes have a greater  $A_s / P_s$  value and therefore plot high on the ordinate (y-axis). Elongate or bulbous meander shapes with high aspect ratio (length of growth trajectory (tL) / meander width (mW)) have a high (x-axis) value.

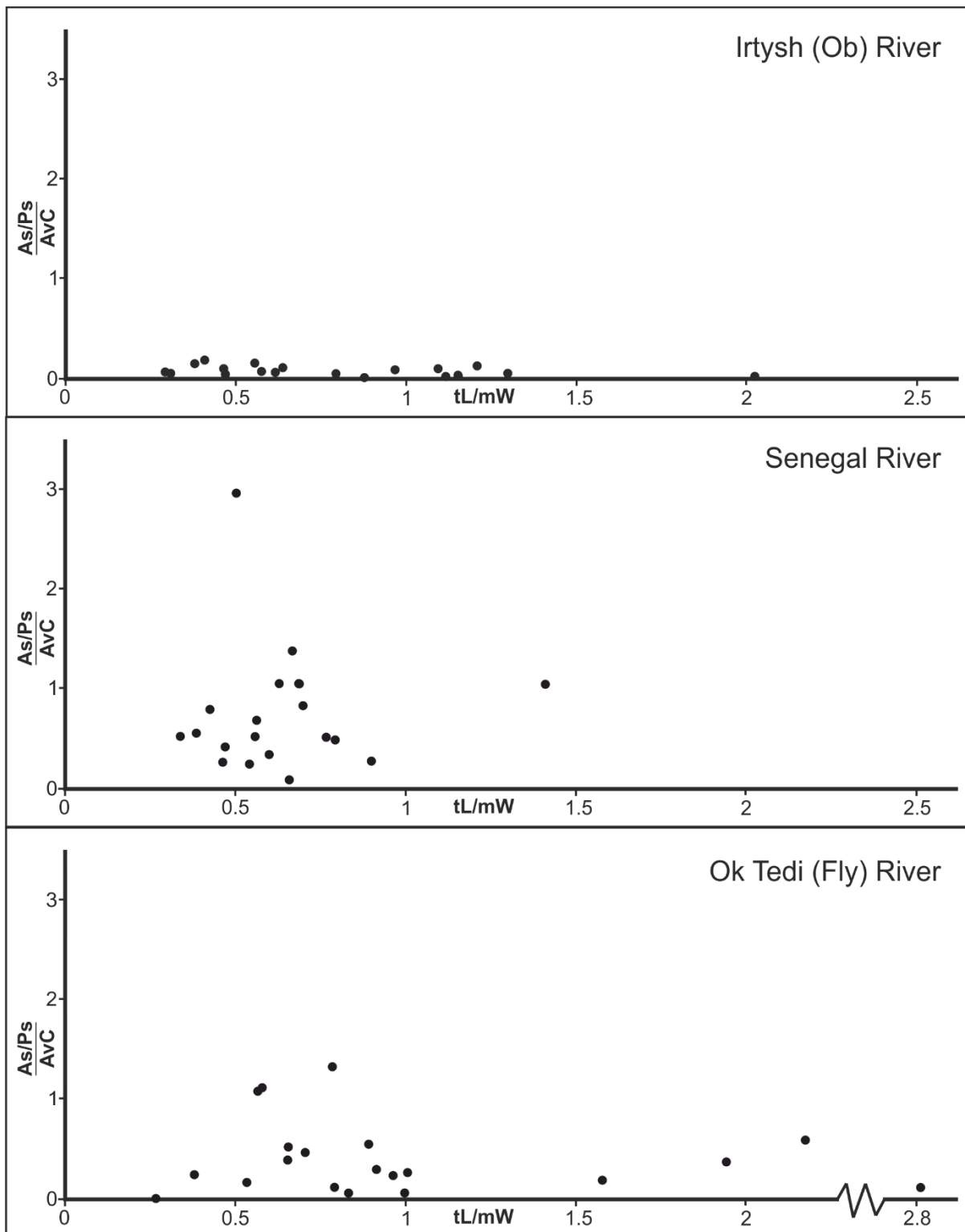


Figure 2.10 - Twenty meanders for each of the meandering reaches, Irtysh (Ob) River, Senegal River and Ok Tedi (Fly) River, have been plotted onto these three graphs to show over-arching trends can be seen. One data point represents one meander.

Data from the Irtysh (Ob) River plots close to the x-axis ( $tL / mW$ ), and 80% of meanders fall into two clusters. The clusters are defined by different aspect ratios (length of meander trajectory “ $tL$ ” / meander width “ $mW$ ”), (0.2 to 0.7, and 1.0 to 0.4). Data from the Senegal River plot with a wider distribution, and 95% of the meanders exhibiting an aspect ratio  $< 0.9$ . The Ok Tedi (Fly) River has one meander of high aspect ratio, plotting  $> 2$  on the x-axis ( $tL / mW$ ); the remaining 95% are  $< 1.5$  on the x-axis ( $tL / mW$ ), as also seen in the Senegal River (Fig. 2.10). The sub-classification scheme (Fig. 2.8) identifies marked morphological differences in the meander forms of the Senegal River and the Irtysh (Ob) River (Fig. 2.11; Table 2.1).

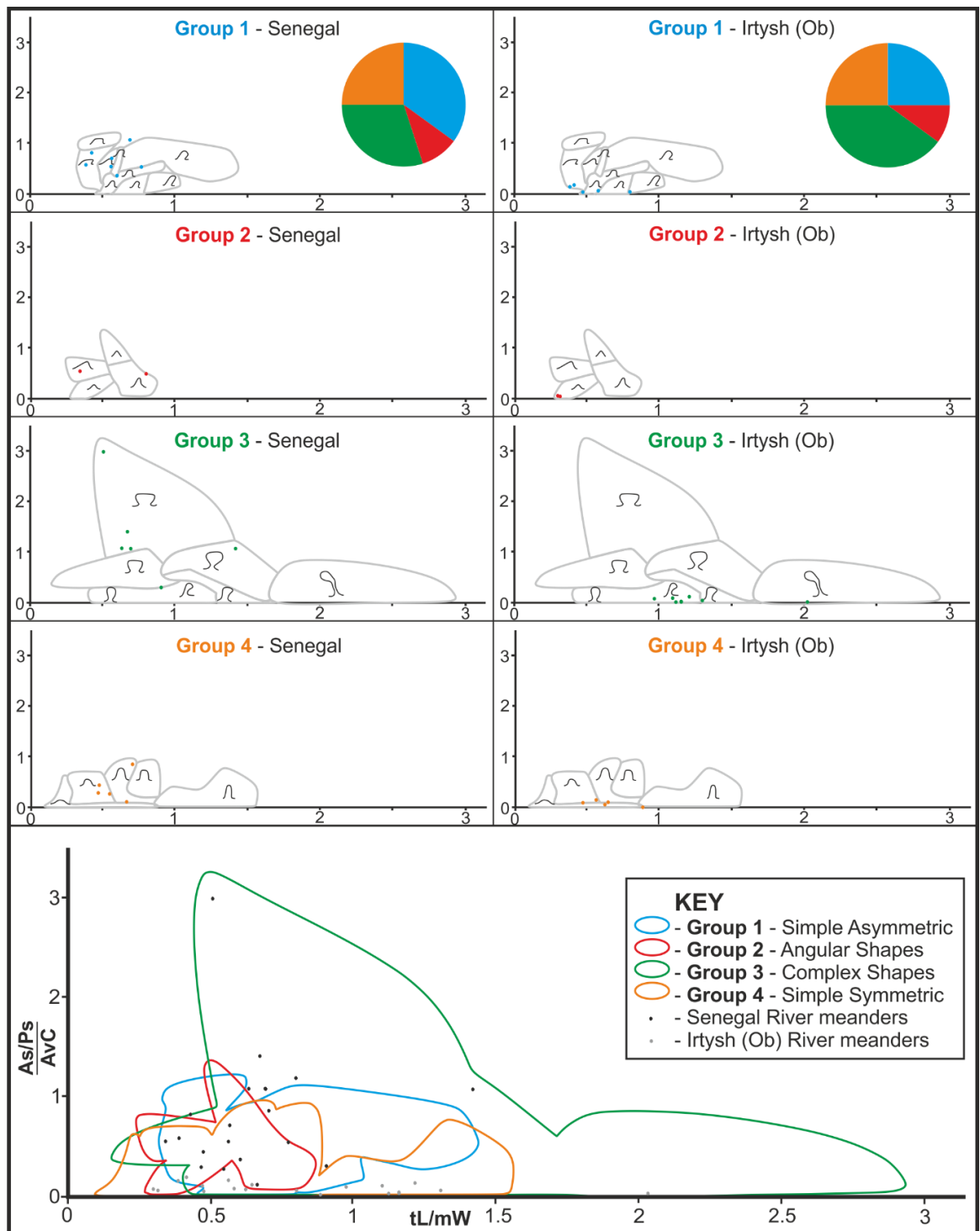
	<b>Senegal River</b>	<b>Irtysh (Ob) River</b>
<b>Regular Asymmetric</b> (Group 1)	7 (35 %)	5 (25 %)
<b>Angular</b> (Group 2)	2 (10 %)	2 (10 %)
<b>Bulbous</b> (Group 3)	6 (30 %)	8 (40 %)
<b>Symmetrical Bulbous</b>	6/6 (100%)	1/8 (13%)
<b>Asymmetrical Bulbous</b>	0/6 (0%)	7/8 (87%)
<b>Regular Symmetric</b> (Group 4)	5 (25 %)	5 (25 %)
<b>Number of different meander shapes</b>	11	11
<b>Number of shapes occurring only once</b>	5	5
<b>Most common shapes</b>	S3c (4x) and S4c (3x)	S3f (5x)

**Table 2.1 - Summary of results depicted as pie-charts in Figure 11 Through comparison of the wide variety of forms in the Senegal and Irtysh (Ob) rivers, similarities and differences are revealed and quantified.**

The Senegal River has almost equal proportions of regular asymmetric, bulbous and regular symmetric shapes (Groups 1, 3 and 4 respectively), notably S3c (occurring 4 times), and S4c (occurring 3 times), (Figs 2.8 and 2.11). Bulbous shapes which are S3b, and S3c, are box-like and symmetrical in form, and compose 25% of the meander shapes seen in this reach. There are two outliers, both are Group 1 open asymmetric shapes. Meander 6 sits outside of the envelopes, it belongs to category S1d, though due to its unusual box-like shape, both the x- and y-axis values are higher than is typical causing it to be an outlier. Meander 25 sits in envelope S1d, it belongs to category S1i, though its form also loosely resembles S1d, so it has plotted as an outlier from S1i, in the S1d envelope.

The Irtysh (Ob) River is dominated by bulbous shapes (Group 3), with equal proportions of open symmetric (Group 4) and open asymmetric (Group 1), notably S3f (occurring 5 times), (Figs 2.8 and 2.11). This reach reveals 87 % of bulbous shapes as asymmetrical in form. There is one outlier in this data set that is a bulbous meander (Group 3). Meander 25 sits in envelope S3f, though it belongs to category S3e. This could be because the channel width is proportionally higher to the point-bar size in the Irtysh (Ob) River, so the intersection shape proportions have been over-normalised giving lower y-axis values.



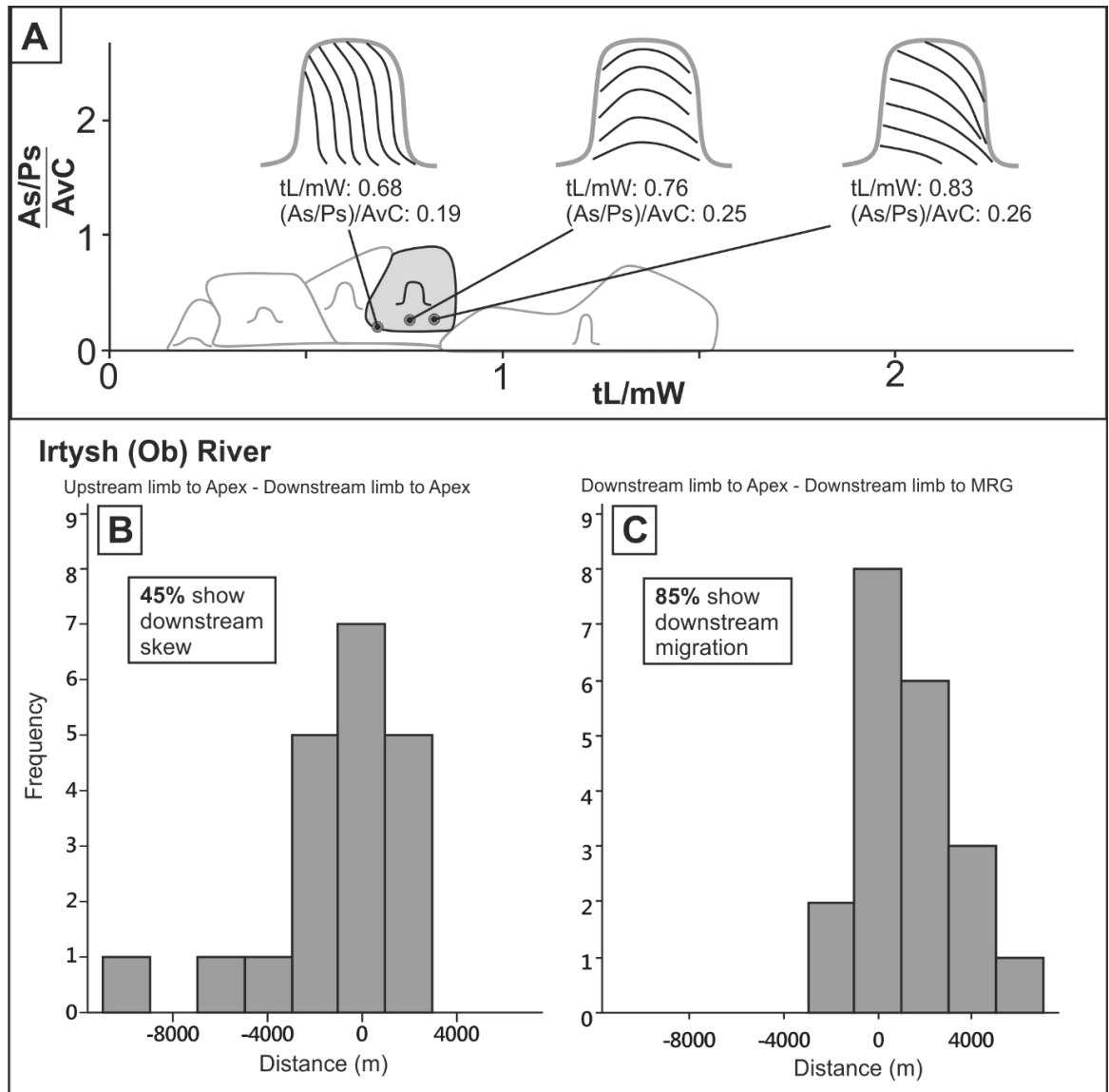


**Figure 2.11 - A comparison of meander shapes in their Groups between the Senegal and Irtysch (Ob) rivers.**

The variability of meander shape and scroll-bar pattern can be identified by plotting end-member models onto a bivariate plot (Fig. 2.12A). Type S4b (Fig. 2.8) has been

selected because it demonstrates the principle effectively. For meanders of this type, 3 data points plot within the envelope of shape S4b with values of  $tL/mW$  ranging from 0.68 to 0.83, and  $(As/Ps)/AvC$  ranges from 0.19 to 0.26. Meanders associated with downstream translation return the lowest values of both  $tL/mW$  and  $(As/Ps)/AvC$ , whereas meanders undergoing expansion and rotation give higher values. This shows how the “Intersection Shape” methodology is applicable regardless of significant variability in scroll-bar pattern for any given shape.

Figures 2.12B and C shows two histograms representing 20 meanders in the Irtysh (Ob) River. Figure 2.12B shows equal-interval class widths of the (ideally normalised) difference between the lengths of the upstream and downstream portions of bends relative to bend apices (Fig. 2.3A); positive values indicate upstream asymmetry while negative values indicate downstream asymmetry. Figure 2.12C shows equal-interval class widths of the (ideally normalised) difference between the length of the downstream portion of bends relative to bend apices and DL (which is measured relative to MRG) (Fig. 2.3A). The histograms reveal that 55% of the meanders assessed in the Irtysh (Ob) River have a downstream limb longer than the upstream limb, indicating slight upstream asymmetry. Therefore, this reach may be assigned to the sub-resonant [ $\beta < \beta_r$ ] morphodynamic regime (cf. Blondeaux & Seminara, 1985; Abad & Garcia, 2009). Consideration of the path of meander growth trajectory indicates that 85% of meanders in the Irtysh (Ob) River are migrating downstream.



**Figure 2.12 - A) Three end member models of scroll bar pattern (translation, expansion, and rotation and expansion), within shape S4b to show how these variable relationships distribute within the relevant envelope on the graph for open symmetric shapes (Group 4). B) Histograms representing the distribution of upstream and downstream asymmetry / resonance (Upstream limb to Apex - Downstream limb to Apex), C) Histogram representing upstream and downstream migration (Downstream limb to Apex - Downstream limb to MRG) respectively. The numbers 45% and 85% have been determined by counting the number of positive results from the calculation, and the proportion of meanders that migrate downstream and of bars that are skewed downstream reflects deviation from the model.**

## 2.6 Discussion

The primary use of the Intersection Shape methodology is to enable quantitative analysis of the variability of meander form between different reaches of the same river, or of different rivers, to be assessed. The abscissa (x-axis) (Fig. 2.7), reflects the spatio-temporal relationship between the meander shape and the orientation of scroll-bar growth by defining the length of the trajectory of meander-apex migration as recorded in the scroll bars through time to MRG ( $tL / mW$ ), (Fig. 2.5A).

The meanders in the studied reach of the Senegal River cluster on the bivariate plot (Fig. 2.10). This occurs because there is limited morphological variability in the reach when the imagery was captured: 70% of the meanders are found to be open. The Irtysh (Ob) River has more bulbous shaped meanders with than the Senegal River (Fig. 2.11). Because the value  $tL / mW$  is on average lower for the Senegal than the Irtysh (Ob) River (0.63 and 0.82, respectively), it could be that the meanders of the Senegal River are less mature in terms of their stage of development. In satellite imagery of the Senegal River (Fig. 2.9), evidence of avulsion events is clearly visible. This could imply that, within this river reach, less time may have elapsed in shaping the active channel, which likely explains the comparatively lower number of bulbous shapes since this river reach is at a relatively early stage of meander-loop development. Alternatively, it could be that low rates of sediment reworking at the surface provide extensive exposure of older channels. Furthermore, 87% of the bulbous shaped (Group 3) meanders of the Irtysh (Ob) River have an asymmetric form, whereas in the Senegal River, 100% of the bulbous shaped (Group 3) meanders are symmetric in form (Fig. 2.12), potentially reflecting the variability of floodplain erosion (Hooke, 2004; Guneralp & Marston, 2012). In Figure 2.10, the Senegal and Ok Tedi (Fly) Rivers show similar distributions of aspect ratio (x-axis), in most shapes, with the exception of five high aspect-ratio meander shapes. This suggests that the mean sinuosity of the reach has been raised

by these five high aspect ratio meanders and therefore the variability of shape might be lower than it initially appears.

Analysis of skew is used to determine a sub-resonant [ $\beta < \beta_r$ ] or super-resonant [ $\beta > \beta_r$ ] morphodynamic regime (Blondeaux & Seminara, 1985, Abad & Garcia, 2009), where  $\beta$  represents bank-full aspect ratio and  $\beta_r$  represents the Exner sediment balance equation – which is an equation implying that meanders resonate at specific values – (Frascati & Lanzoni, 2010). Frascati & Lanzoni (2010) describe two distinct regimes; i) a sub-resonant regime where meanders are skewed upstream and migrate downstream and ii) a super-resonant regime where meanders are skewed downstream and migrate upstream. In nature, sub- and super-resonant regimes are not as distinct as described here; the method developed here enables the extent of variability to be accounted for.

The skew of the studied meandering reaches in the Irtysh (Ob) River is most commonly upstream (Perucca *et al.*, 2007), which indicates a sub-resonant [ $\beta < \beta_r$ ] regime (Frascati & Lanzoni, 2010). However, not all of the meanders in the studied reach of the Irtysh (Ob) River (Fig. 2.12B) have upstream skew and downstream migration. This could be because the reach is highly irregular (Fig. 2.9) and there are several meanders developed to a bulbous form. As a meander neck closes, there can be growth upstream on the downstream limb of the closing neck due to the increasing centrifugal force from an increasingly sinuous meander (Schumm & Khan, 1972).

Through using the “Intersection Shape” methodology, the amount and direction of skew and migration can be constrained to reduce the reliance on subjective measures in the characterization of the relationship between meander shape and scroll-bar pattern.

Brice (1974) identified 16 shapes in a subjective classification scheme (Fig. 2.1D). This only accounts for 11 of the shapes identified in the 25 sub-groups of the Intersection Shape methodology (i.e, only 44% of types of meander form). More specifically, only

11% and 25% of open asymmetric (Group 1) and angular (Group 2) shapes are accounted for respectively, whereas 71% of bulbous (Group 3) shapes, and 80% of open symmetric (Group 4) shapes are included. Thus, older classification schemes, such as that of Brice (1974) might have unintentionally introduced bias in our understanding of the potential range of meander shape variability, whereby simple symmetrical (Group 4) and bulbous (Group 3) shapes are represented preferentially.

Preserved scroll-bar patterns record aspects of the evolutionary behaviour of a meander and so can be used to identify the present direction of growth for a meander. New to this study, the point of most recent growth (MRG) can be used to define up- and downstream portions of a meander which aids in assessing meander asymmetry. The Irtysh (Ob) River fits the common sub-resonant [ $\beta < \beta_r$ ] morphodynamic regime of upstream skew and downstream migration (Seminara *et al.*, 2001; Frascati & Lanzoni, 2010). However, almost half (45%) of the meanders are skewed asymmetrically downstream in the direction of migration, and 15% of the meanders are migrating upstream. Therefore, these meanders do not fit the sub-resonant [ $\beta < \beta_r$ ] model well. The “Intersection Shape” methodology offers quantification of the “grey area” between these two definitions by assessing the value of downstream skew compared with downstream migration. Analysis of the variability of a reach of the Irtysh (Ob) River from this model reveals this reach to be weakly super-resonant (Fig. 2.12B). Through better understanding such variability in meander shape and its relationship with scroll-bar pattern, the parameters that control a river reach with meander bends (Rosgen, 1994) may be better determined and understood (Fig. 2.12).

Limitations of the ‘Intersection Shape’ methodology are as follows: (i) it retains a degree of subjectivity because of the wide variety of meander shapes which need to be accounted for; (ii) once the parent group is established through partially manual analysis (Fig. 2.3E), the sub-groups are defined through the construction of envelopes,

that are not mathematically constrained (cf. Allen, 1965; Nanson & Hickin, 1986), although the positions of envelopes will be further refined through the collection of additional data, and may be constrained more tightly; and (iii) the division of shapes into groups (Fig. 2.11) is informed by Figure 2.8 and partly subjective, though this subjectivity has been reduced to a minimum

The main strengths of the “Intersection Shape” methodology are as follows: (i) it allows for river reaches with markedly contrasting morphologies to be quantitatively compared in a manner that accounts for the inherent natural complexity and variability in form, notably the irregular Ok Tedi (Fly) river can be assessed; (ii) it plots data onto a bivariate plot enabling visual analysis of results and direct comparisons to be made for the purpose of interpretation; (iii) it reduces the subjective nature of meander shape classification; (iv) 242 of the 260 meanders analysed (93.08%) plot within the confines of a geometrically correct envelope (Fig. 2.7); and (v) by incorporating meander migration trajectory (tL) into the method a more powerful spatio-temporal dataset can be derived. As a result, the value  $tL / mW$  is broadly an indicator of the stage of meander growth from initiation to abandonment. This is especially useful when interpreting ancient meander successions preserved in the stratigraphic record, for which scroll-bar patterns can commonly be discerned, for example where they are exhumed (Smith, 1987; Ielpi & Ghinassi, 2014; Wu *et al.*, 2015; Bhattacharya *et al.*, 2015; Ghinassi & Ielpi, 2015) or observable in reflection seismic data (e.g. Hubbard *et al.*, 2011).

## 2.7 Conclusions

A novel “Intersection Shape” methodology provides an easily implemented workflow that can be applied to all meandering fluvial systems that allow for direct comparison of the morphological form of any fluvial system to be made across different river reaches.

It can permit a higher level of objectivity in shape classification than is available through previously applied shape-matching methods. The meander shape classification (Fig. 2.8) is able to account for a wider variety of shapes than previous methodologies, and therefore presents a less biased and more comprehensive characterisation of meandering reaches. The data can be derived from the direct measurement of publically available, remotely sensed imagery, enabling large datasets to be amassed in a time-efficient manner.

Application of the method has been illustrated through analysis of the Ok Tedi (Fly), Senegal and Irtysh (Ob) rivers. New insights into the differences in morphological form have been identified, thereby enabling a wider understanding of potential formative processes. The studied rivers exhibit distinctly different migration styles during development of their meanders. Meander bends of the Irtysh (Ob) River may alternate between bulbous and open meander shapes. By contrast, meander bends of the Senegal River have evolved more open forms, and bulbous shapes are not as common. The Ok Tedi (Fly) River is characterised by meanders that possess an irregular morphology that may still be quantified through the “Intersection Shape” methodology. The Irtysh (Ob) River exhibits a sub-resonant morphodynamic regime but there are significant deviations from the expected model of upstream skew and downstream migration (Frascati & Lanzoni, 2010), due to the presence of mature meander loops that approach a bulbous state. In this regard, the “Intersection Shape” methodology has enabled deviation from an expected model to be quantified.

Through understanding meander inter-relationships, the path and history of fluvial point-bar evolution and growth can be discerned and used to establish links between alluvial form, process and preserved stratigraphic product. Although only active river reaches have been considered in this study, the generic approach outlined here allows for quantification of the history and morphology of relic and partially overprinted



meanders, including those preserved in the ancient stratigraphic record. The “Intersection Shape” methodology can be employed to consider the role of various autogenic processes (e.g., lateral accretion and avulsion) in determining plan-form patterns in the ancient record. Notably, this method can be applied to ancient meanders preserved in the subsurface and imaged in seismic datasets where the plan-form morphology of architectural elements can be discerned (Fachmi & Wood, 2005; Hubbard *et al.*, 2011).

### **3 Prediction of lithological heterogeneity in fluvial point-bar deposits from analysis of meander morphology and scroll-bar pattern**

#### **3.1 Chapter Summary**

Meandering fluvial reaches exhibit a wide range of morphology, yet published interpretations of ancient meander-belt deposits do not reflect the stratigraphic complexity known to be associated with such variability. An improved understanding of processes that generate stratigraphic heterogeneity is important to improve predictions in sedimentary facies distributions in sub-surface settings. Quantification and classification of planform geomorphology of active fluvial point bars and their recently accreted deposits enables determination of spatio-temporal relationships between scroll-bar behaviour and resultant meander shape. Scroll bars are laterally accreted deposits that reflect how the meander has grown incrementally over time. Analysis of 260 active meander bends, from 13 different rivers, classified by a range of parameters including climatic regime, gradient and discharge, has been undertaken. Assessment of scroll-bar morphology and growth trajectory has been achieved using remotely sensed imagery in Google Earth Pro. Twenty-two distinct styles of meander scroll-bar pattern are recognised, and grouped into 8 types that reflect growth via combinations of expansion, extension and translation. A novel technique for predicting the variable distribution of heterogeneity in fluvial point-bars integrates meander-shape and meander scroll-bar pattern. The basis for relative heterogeneity prediction is the observation that deposited sediments fine downstream around a meander bend, and outwards as a barform grows due to bend expansion. Observations of these trends are seen in experimental models, modern fluvial systems, and in the ancient record at both outcrop and in the sub-surface. This trend permits the planform geometries to be

overlain with distributions of bar-deposit lithological types. The method has been applied to predict heterogeneity distribution from seismic data of the McMurray Formation (Alberta, Canada) and tested by comparison of predicted heterogeneity to trends known from analysis of gamma-ray data from densely distributed well-logs. This novel method constrains heterogeneity predictions in fluvial point-bar deposits for which direct lithological observations are not possible or are limited. This method therefore provides the basis of a predictive tool for improving understanding of a fragmentary geological record, including lithological heterogeneity from outcrops of limited spatial extent, or from subsurface seismic datasets.

Keywords: fluvial, morphology, heterogeneity, point-bar, scroll-bar, river

### **3.2 Introduction**

Fluvial point bars that develop on river bends accumulate as laterally discontinuous architectural elements (e.g. Allen, 1965; Fielding & Crane, 1987; Mackey & Bridge, 1995; Donselaar & Overeem, 2008; Colombera *et al.*, 2017), and are internally characterised by complicated distributions of lithofacies (e.g. Thomas *et al.*, 1987; Tye, 2004; Miall, 2006; Durkin *et al.*, 2015; Ghinassi *et al.*, 2016). Architectural elements of point bars that are preserved, are typically sand-rich (Allen, 1965), though packages of mud-prone strata (i.e. with clay and/or silt) may also commonly be present, and these can influence permeability pathways by acting as baffles to fluid flow (Fielding & Crane, 1987; Miall, 1988; Tye, 2004). Quantifying and understanding the formation of this lithological variability is important because the distribution of intra-point-bar mud-prone strata influences oil and gas production from such reservoirs (e.g. Brown & Fisher, 1980; Putnam & Oliver 1980; Mossop & Flach, 1983; Hubbard *et al.*, 2011). In point-bar deposits, mud-prone deposits commonly alternate with sand-prone deposits forming couplets (Thomas *et al.*, 1987: Fig. 3.1), which can take a variety of forms: (i) laterally

continuous, and vertically continuous from top-set to bottom-set; (ii) laterally continuous and vertically discontinuous, i.e. only present in the top-set or bottom-set of strata; (iii) laterally and vertically discontinuous (Thomas *et al.*, 1987; Miall, 1988).

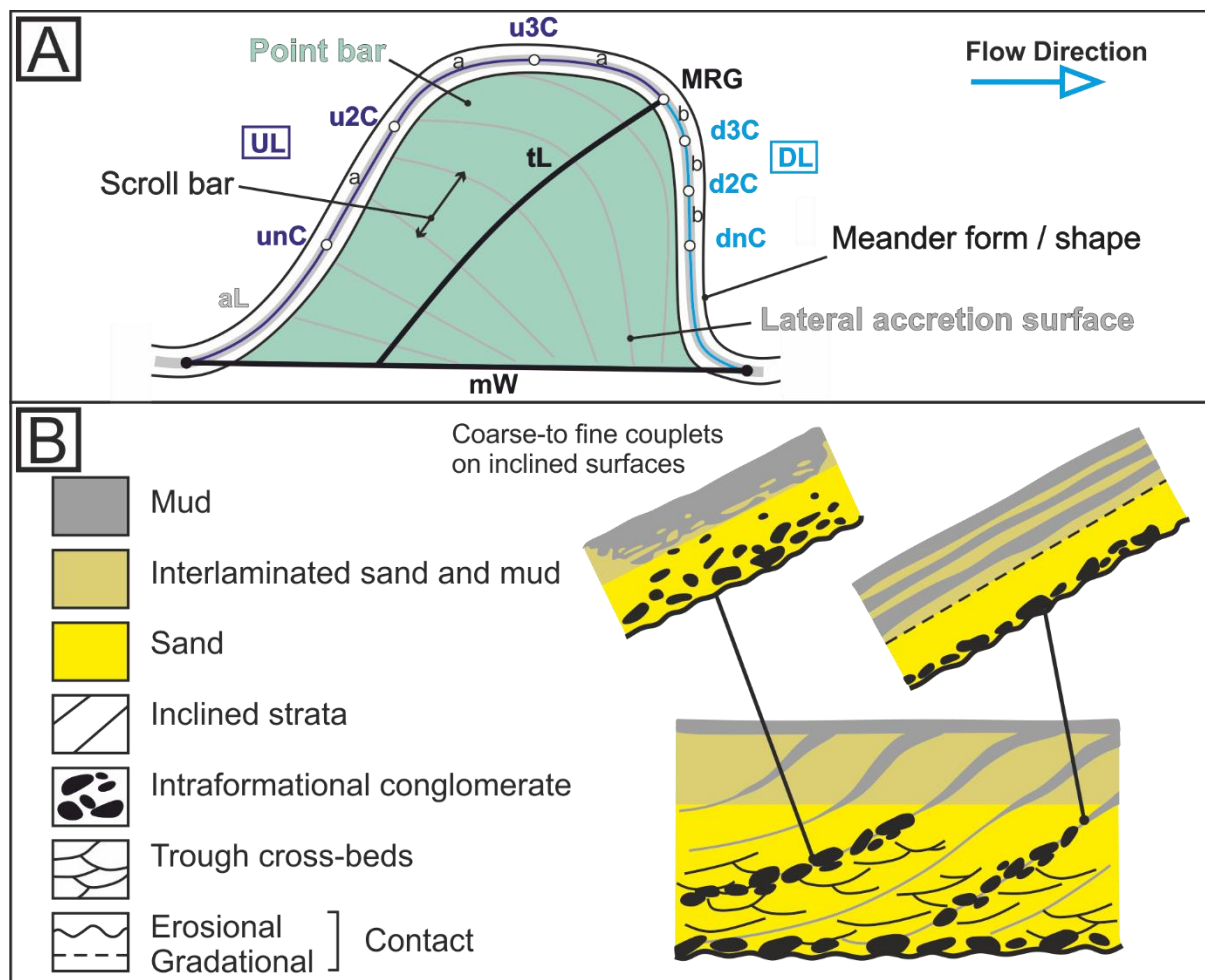
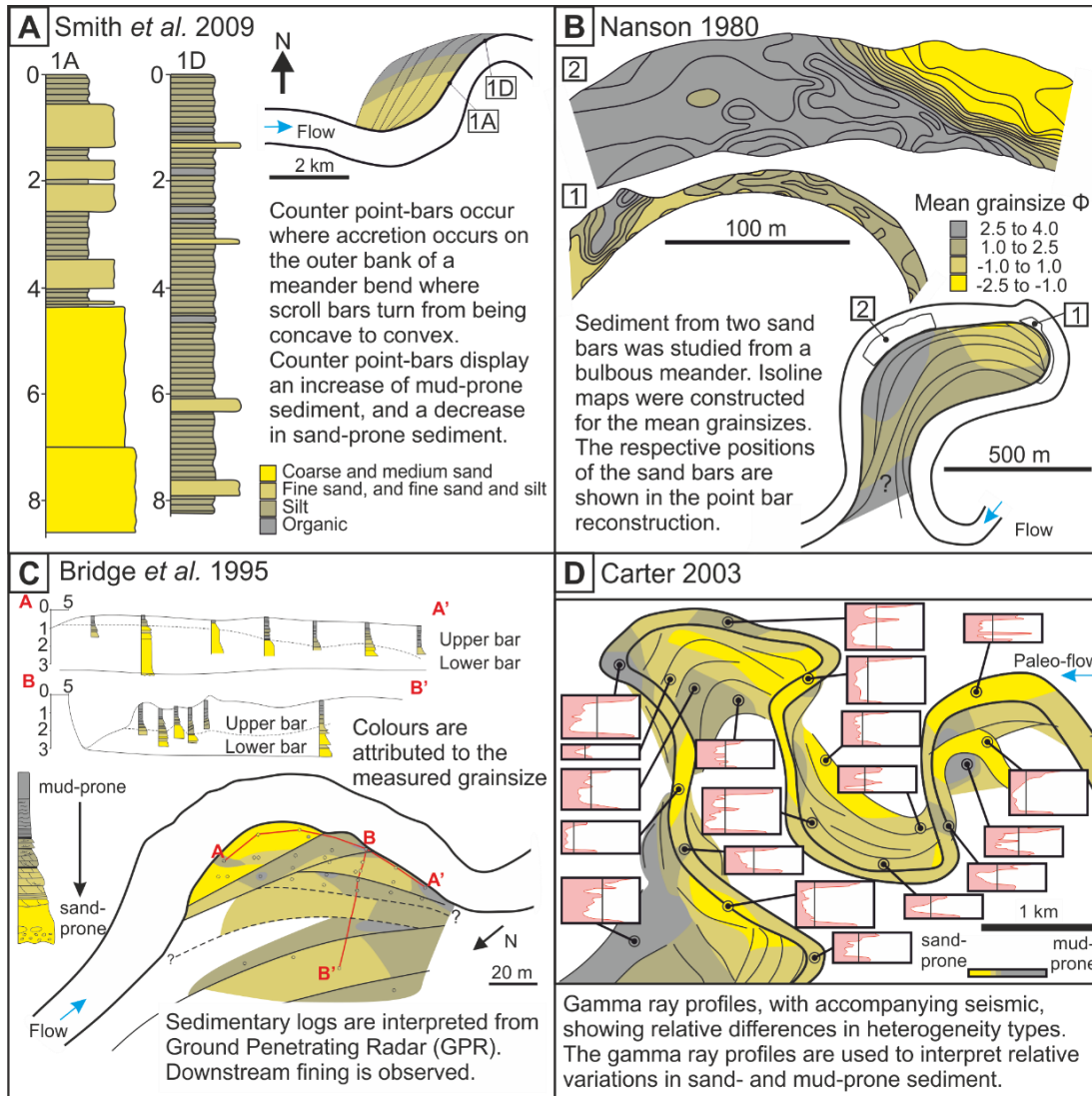


Figure 3.1 - A) Terminology used in the description of fluvial point-bars modified from Chapter 2; B) Inclined Heterolithic Strata (IHS), modified from Thomas *et al.*, (1987).

Geological models, which inform reservoir models, typically simplify or even ignore the variability of heterogeneity in point-bar deposits (Fielding & Crane, 1987; Jordan & Pryor, 1992; Pranter *et al.*, 2009; Hassanpour *et al.*, 2013). As such, a disparity exists between the lithological complexity documented from meandering fluvial systems and the relative simplicity of facies models developed for successions of such deposits (Miall, 2006). To improve prediction of this inherent stratigraphic complexity it is

important to understand the formative processes that give rise to meanders with particular morphological traits, across a range of physiographic settings (Rosgen, 1985; Gutierrez & Abad, 2014). Studies of modern fluvial systems are useful as a way to inform rock record interpretations (Tye, 2004) because they enable observation of meander-shape variability (Allen, 1965; Hooke, 1984), and the surface expression of meander scroll bars (Daniel, 1971; Thompson, 1986; Ielpi *et al.*, 2014; Ghinassi *et al.*, 2016). Scroll bars accrete over time to reflect growth increments of a meander (Allen, 1965; Ielpi *et al.*, 2014); they form a series of ridges and swales on the point-bar surface (Nanson, 1980; Durkin *et al.*, 2015), (Fig. 3.1A), as a result of the primary flow eroding the outer bank and deposition on the inner bank, in turn driving channel migration by bar pull (Van de Lageweg *et al.*, 2014). The geometry of the meander-bend apex causes the channel to change direction, which itself causes the helical flow within the channel to strengthen (Roberts, 2014). This leads to turbulent bursting, which in turn results in vertical anisotropy of fluvial velocity (Jackson, 1976). Differences in fluvial velocity are also observed laterally across the channel in the region of the meander-bend apex (e.g. Nanson, 1980), whereby a strong helical flow is observed at the outer bank, and a weaker secondary helical flow is observed at the inner bank (Leopold & Wolman, 1960; Nanson, 1980; Thompson, 1986; Roberts, 2014). This leads to deposition of material on the down-stream limb of the meander bend, which is relatively finer grained than the material deposited elsewhere on the inner bank of the point-bar deposit (Jackson, 1976; Fustic *et al.*, 2012). This predictable relationship may be harnessed to infer mud- and sand-prone zones. Also, if downstream accretion is occurring, may form a counter point-bar on concave banks (Smith *et al.*, 2009; Fig. 3.2A). Farther downstream, erosion occurs where the thalweg meets the outer bank. The distance downstream from the bend apex where erosion on the outer bank occurs is dependent on the geometries of adjoining meander shapes in the reach. Extensive data have been collected from meandering fluvial reaches that

recognise down-stream fining relationships (e.g. Leopold & Wolman, 1960; Jackson, 1975; Bridge & Jarvis, 1982; Thomas *et al.*, 1987; Labrecque *et al.*, 2011; Fustic *et al.*, 2012). Through use of the scroll-bar geometries and the observed relationships between sediment size and meander geometry, past meander shapes can be determined, and enable prediction of the expected distribution of heterogeneity from plan-view observation of morphology alone.



**Figure 3.2 - Literature summary of heterogeneity data in point-bars: A) An interpreted summary of a counter point bar in a meander from the Peace River, Alberta, Canada (Smith *et al.* 2009). Colours were attributed to defined grainsize, and the logs 1A and 1D**

were used to interpret relative overall planform heterogeneity of the point-bar; B) An interpreted summary of a point-bar from the Beatton River, British Columbia, Canada (Nanson 1980). Colours were attributed to the defined mean grainsize and sand bars 1 and 2 were coloured accordingly. The relative overall planform heterogeneity of the point-bar was then estimated; C) Sedimentary logs taken alongside Ground Penetrating Radar (GPR), data were used to interpret the relative overall planform heterogeneity of the point-bar by analysing each log for average grain-size and plotting an appropriately coloured point on the planform map (Bridge *et al.* 1995). Two lines with their associated logs are depicted (A-A' and B-B'), and show an increasing proportion of mud-prone sediment downstream around the point-bar; D) An interpreted summary of the overall planform heterogeneity of the interpreted seismic from the Widuri field, Java Sea (Carter 2003). The reservoir depth is 1000 – 1200 m subsea, and is an arenite sandstone. The mean relative grainsize, as indicated by vertical black lines, was interpreted from the gamma-ray profiles, where high values are more mud-prone, and low values are more sand-prone. These were then used to mark heterogeneity types onto the interpreted seismic, which were in turn used to determine relative sand:mud ratios.

The aim of this study is to develop a method by which the relationship between point-bar morphology and the resultant stratigraphic heterogeneity of modern fluvial meandering reaches can be determined. Specific research objectives are as follows: (i) to document the extensive variability of both meander shape and scroll-bar pattern known from presently active meandering fluvial systems; (ii) to develop a novel scroll-bar classification scheme that is independent of meander shape; (iii) to demonstrate how understanding of variability of scroll bar pattern can be used to constrain and predict patterns of lithological heterogeneity in accumulated point-bar deposits; and (iv) to discuss the utilisation of this approach to predict the internal lithological composition of fluvial point-bar elements from reflection seismic time slices and from exhumed successions of limited lateral or areal extent.

### 3.3 Background

In modern systems, a broad variety of parameters may be monitored to assess spatial and temporal changes in meander dynamics, including the occurrence of pools and riffles (Thompson, 1986), and changes in flow velocity, discharge, and grain size (Erskine *et al.*, 1992). Of these parameters, only grain size data can be measured directly from the rock record, and this has historically been used as the basis for extrapolation of palaeohydraulic parameters such as mean annual discharge, mean annual flood discharge, and grain transport mechanisms (Visher, 1964; Schumm, 1968; 1969; Schumm & Khan, 1972; Miall, 1976; Middleton, 1976; Wu *et al.*, 2015). Commonly, active modern fluvial systems are employed as analogues to explain and account for depositional architecture (Bridge & Tye, 2000; Reijenstein *et al.*, 2011; Ghinassi, 2011; Durkin *et al.*, 2015; Ghinassi *et al.*, 2016) and to constrain parameters for geological models used for reservoir modelling (Fielding & Crane 1987; Tye, 2004; Yan *et al.*, 2017). However, current methods for quantifying this variability in modern systems and applying it to ancient successions remain inadequate (Tye, 2004; Miall, 2006). Although meandering processes can be similar between reaches of different rivers (Leopold & Wolman, 1960), autogenic and allogenic influences (Rosgen, 1985; Blum & Törnqvist, 2002; Ghinassi *et al.*, 2016), lead to extensive variability in sedimentary architecture and distributions of heterogeneity (Thomas *et al.*, 1987; Durkin *et al.*, 2015). The complex interaction of autogenic and allogenic processes governs morphological and lithological variability in freely meandering fluvial systems (Rosgen, 1985; Miall, 1988). Therefore, through assessing meander morphologies, controls that govern the formative processes can be better understood. Two principal morphologies (meander shape, and the surface expression of the associated scroll-bar accretion direction) are studied in order to develop an approach to compare fluvial geometries.



### 3.3.1 Meander shape

Quantification and classification of a static meander shape (i.e. its present form) is difficult because the natural form is highly variable and not straightforward to define objectively (Phillips, 2003; Miall, 2006). Existing approaches include shape matching (e.g. Brice, 1974; Allen, 1982; Bridge, 2003; Ielpi & Ghinassi, 2014), measuring sinuosity (Hooke, 2004), measuring radius-of-curvature (Nanson & Hickin, 1983; Hudson & Kessel, 2000; Sambrook Smith *et al.*, 2016), and using the Intersection Shape methodology (Chapter 2). This study uses the Intersection Shape methodology because it is a repeatable and semi-quantifiable method for classifying the full range of meander shapes. The method identifies the direction of bend asymmetry (Xu, *et al.*, 2011; Chapter 2), and dominant migration direction (Frascati & Lanzoni, 2010; Ghinassi *et al.*, 2016). The Intersection Shape methodology also enables studied meanders to be ordered by relative complexity (i.e., immature to mature forms), which in turn aids understanding of meander formative processes (Chapter 2).

### 3.3.2 Scroll-bar pattern

Historic episodes of meander growth are recorded within point bar deposits (Allen, 1965; Thompson, 1986; Ielpi *et al.*, 2014) and are expressed as scroll-bar deposits. Scroll-bar deposits represent the incremental growth (accretion) of point bars through bend expansion, translation, rotation, or combinations thereof (Daniel, 1971). Such growth behaviour results in the development of consecutively laterally accreted packages called scroll bars (Schumm, 1963; Allen, 1965; e.g. Bridge, 2003; Fig. 3.3C, Ielpi *et al.* 2014; Fig. 3.3A). Widely applied point-bar facies models (Schumm, 1963; Allen 1964; 1965; 1983; McGowen & Garner, 1970) do not account for the large variability in form observed in modern systems. Typically, accumulated point-bar elements comprise multiple scroll-sets, which are themselves groups of genetically related scroll-bars with a common direction of growth (Ghinassi *et al.*, 2016). Widely

used models typically depict the most recent episode of meander growth; many such models commence with an already established sinusoidal shape (e.g., Leopold & Wolman, 1960; Daniel, 1971; Willis & Tang, 2010). Few models depict initiation of point-bar growth from a relatively straight reach (Lewin, 1976; Thompson, 1986).

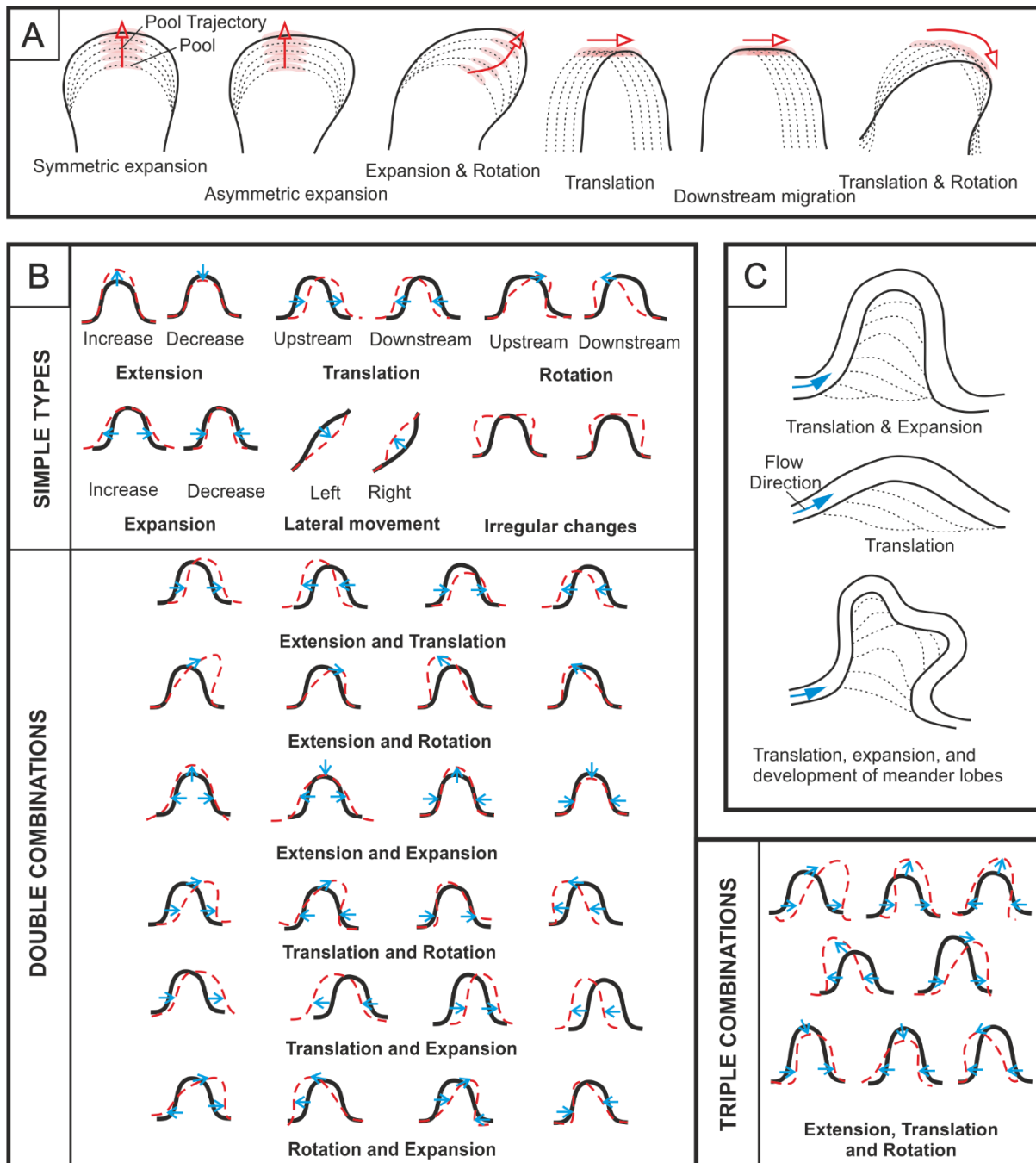


Figure 3.3 - A figure to show examples of the literature where meander shape change is depicted; A) Ielpi *et al.* (2014); B) Hooke (1977); C) Bridge (2003).

### 3.3.3 Point-bar heterogeneity

Understanding the history of evolution of a meander is essential for improved prediction of lithofacies distribution within its accumulated deposits. Inclined heterolithic strata (IHS) are packages of strata composed of alternating mudstone and sandstone beds, commonly found in fluvial point-bar deposits (Thomas, 1987; Fig. 3.1), for example those of the Cretaceous McMurray Formation, Alberta (Strobl *et al.*, 1997; Labrecque *et al.*, 2011; Brekke, 2015; Jablonski & Dalrymple, 2016). Packages of IHS can act as permeability baffles to fluid-flow pathways within reservoir rock units, and form volumes with highly variable petrophysical properties. Producing hydrocarbons from fluvial point-bar deposits characterised internally by packages of IHS is challenging. Therefore, prediction of the spatial distribution of occurrence of IHS is important to reservoir geologists and engineers (Miall, 1988; Pranter *et al.*, 2000; Labrecque *et al.*, 2011).

The stratigraphic heterogeneity of a point bar deposit is described by the proportion of sand and mud. This can be identified in the subsurface through observation of IHS in the signatures of gamma-ray logs obtained from well logs, which in turn enables “gamma radiation contour mapping” (Hubbard *et al.*, 2011; Labrecque *et al.*, 2011). Where this approach is not available, predictive models are produced that typically simplify the degree of heterogeneity (Hohn *et al.*, 1997; Ramon & Cross, 1997; Webb & Davis, 1998; Pranter *et al.*, 2000; Tye, 2004). An alternative approach focuses on prediction of the expected downstream-fining of deposited sediment (Labrecque *et al.*, 2011; Fustic *et al.*, 2012), and upstream fining of counter point-bars (Smith *et al.*, 2009). Downstream-fining occurs because flow moves at different speeds around a meander bend (Thompson, 1986, Leopold & Wolman, 1960). Sediment deposited on the inner banks of meander bends is commonly characterised by a change in grain size, whereby sediment calibre decreases downstream. This trend has been attributed primarily to a change in flow dynamics at the meander-bend apex (Jackson, 1976).

Specifically, the geometry of the meander-bend apex causes the channel to change direction which causes the helical flow within the channel to strengthen (Roberts, 2014). This leads to turbulent bursting, which in turn results in vertical anisotropy of fluvial velocity (Jackson, 1976). Differences in fluvial velocity are also observed laterally across the channel in the region of the meander-bend apex (e.g. Nanson, 1980), whereby a strong helical flow is observed at the outer bank, and a weaker secondary helical flow is observed at the inner bank (Leopold & Wolman, 1960; Nanson, 1980; Thompson, 1986; Roberts, 2014). Differences in flow velocities are recorded in the distribution of sand- and mud-prone sediment in the resultant point-bar deposits (Jackson, 1976; Thompson, 1986; Bridge & Jarvis, 1982; Thomas et al., 1987; Fustic et al., 2012; Sambrook-Smith et al., 2016). The weaker secondary helical flow caused by the change in flow direction from the meander-bend apex, causes the deposition of material on the down-stream limb of the meander bend, which is relatively finer grained than the material deposited elsewhere on the inner bank of the point-bar deposit (Jackson, 1976; Fustic et al., 2012). This leads to the proportion of sand-prone sediment to be observed to decrease downstream, whereas mud-prone sediment is observed to increase in proportion downstream (Bridge et al., 1995; Fustic *et al.*, 2012). Observations of point-bar deposits may be undertaken in the field through use of cores and ground-penetrating radar (e.g. Bridge et al., 1995), as well as trenches and examination of natural cliff-forming outcrops. Data from Bridge et al. (1995), the conceptual, quantitative model by Willis (1989), and physical modelling of meandering systems (Peakall et al., 2007) identify the coarsest sediment as having been deposited at the meander-bend apex where the flow is most turbulent; Jackson (1976) demonstrates a similar trend.

Willis (1989) argues that variations in channel geometry, channel orientation, and channel position each act as a control on the sedimentology of point-bar deposits.

However, the wide variety of modes of growth is not considered in detail in Willis' study. It is important to consider modes of meander growth because they determine where accretion may occur on the meander limbs. This is important because the calibre of sediment deposited is influenced by the energy of the flows in the meander channel, and consequently the calibre of sediment that may be preserved at a point on the up- or down-stream limbs. The models by Jackson (1976) and Willis (1989) only consider growth by extension. Meanders observed by Bridge *et al.* (1995), and Peakall *et al.* (2007), are notably regular in shape and also dominantly accreted via extension. However, there is a greater degree of variation than is accounted for in these studies. Counter point bars represent the fine-grained distal end of a point bar where the scroll bars turn from being concave to convex, and may present a sharp contact between sand- and mud-prone sediment (Smith *et al.*, 2009). Figure 3.2A represents a counter point-bar, which is undertaking downstream accretion, and this contrasts with Figure 3.2C (from Bridge *et al.*, 1995), which represents a bar undertaking extension with punctuated rotation (cf. Durkin *et al.*, 2015). Figure 3.2C depicts the expected downstream fining of sediments in each scroll bar. Downstream around the meander, mud-prone upper bar sediments become more dominant than the sand-prone lower bar sediments (Fig. 3.2C A-A'). Downstream fining is also seen the interpreted seismic and gamma-ray profiles from the Widuri field, Java Sea (Carter, 2003; Fig. 3.2D). Counter point-bars are also interpreted in Fig. 3.2D; more extreme shapes show increased deposition of relatively mud-prone sediment on the downstream limb (Fig. 3.2D). Downstream fining has been recognised extensively in exhumed successions (e.g. Fustic *et al.*, 2012; Durkin, 2015; Wu *et al.*, 2015; Ghinassi *et al.*, 2016), and in the sub-surface (Hubbard *et al.*, 2011; Labrecque *et al.*, 2011).

Therefore, a more inclusive, and generally applicable model of heterogeneity distribution on a point-bar deposit is required that considers other meander shapes, and other mechanisms of growth (e.g. translation and rotation; Daniel 1971).

### **3.4 Methodology**

Here, the static form of 20 consecutive meander bends and their associated scroll bars in a single reach is studied from each of 13 globally distributed meandering river reaches (Table 3.1). The rivers chosen for study are from different physiographic locations (Fig. 3.4; Table 3.1). They have been assessed using Landsat imagery from Google Earth Pro (2001). This approach enables the development of a classification that encompasses a wide range of possible meander shapes. Aspects of the studied rivers are summarised in Table 3.1. Climate, gradient, and river size each influence how the deposits of meandering rivers accumulate (Shanley, 2004; Schwab, 1976; Ouchi, 1985; Table 3.1). The relationships between meander shape and scroll-bar pattern are quantified through use of the Intersection Shape methodology (Chapter 2). The surface expression of scroll-bar pattern is considered separately (Fig. 3.5).

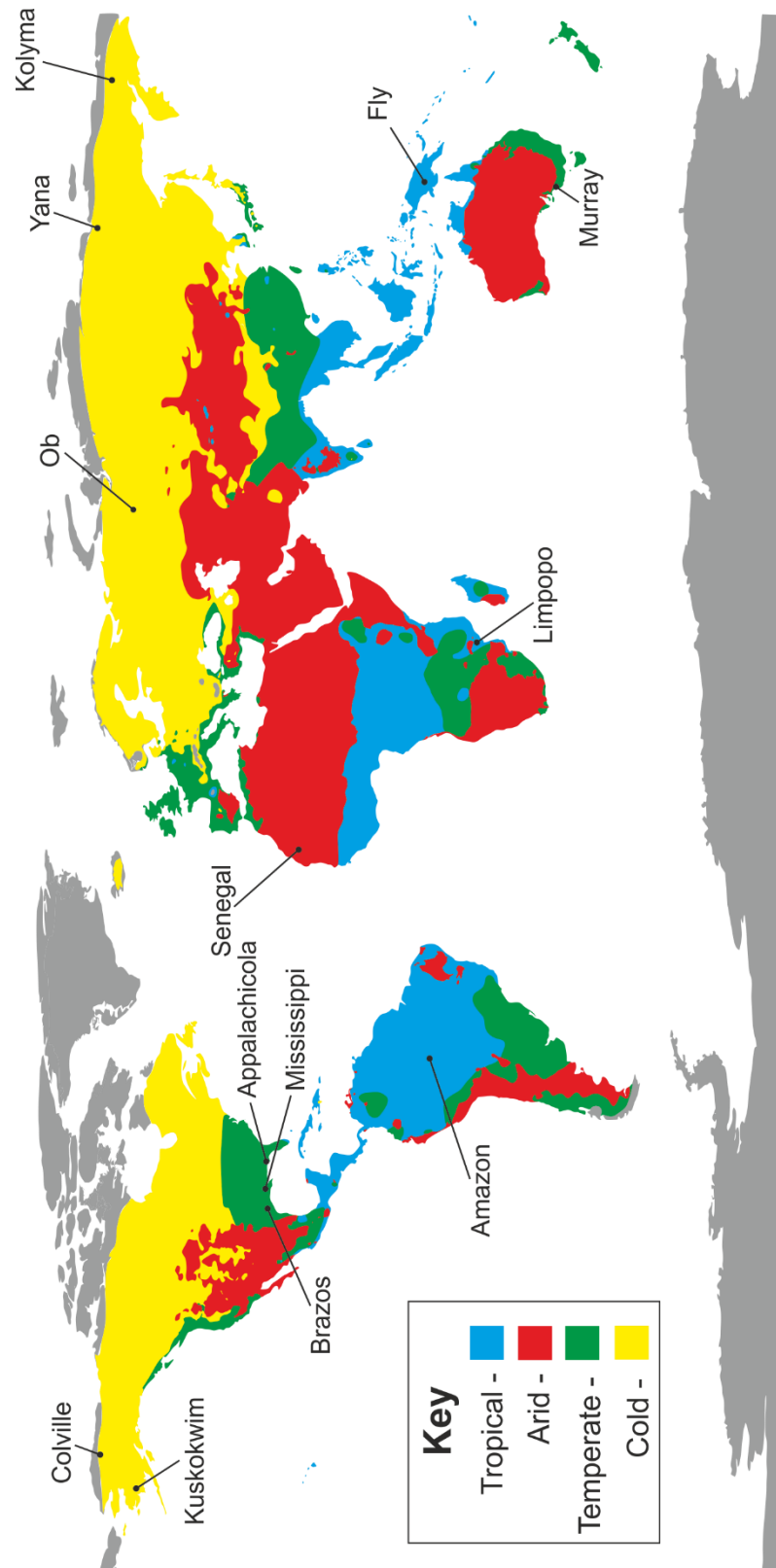


Figure 3.4 - A map of the simplified climate zones modified from (Peel *et al.* 2007). The rivers selected for this study are plotted.

### 3.5 River Selection

The selected freely meandering river reaches encompass a broad range of meander shape and surface expression of scroll-bar pattern.

The regional climate for each system is determined with consideration of the Köppen-Geiger climate classification (Peel *et al.*, 2007; Fig. 3.4). Studied rivers have been selected from 4 climate zones: tropical (temperature of the coldest month  $\geq 18^{\circ}\text{C}$ ); arid (mean annual precipitation  $< 10 \times P_{\text{threshold}}$  cf. Peel *et al.*, 2007); temperate (temperature of the hottest month  $> 10^{\circ}\text{C}$  &  $0^{\circ}\text{C} <$  temperature of the coldest month  $< 18^{\circ}\text{C}$ ); and cold (temperature of the hottest month  $> 10^{\circ}\text{C}$  & temperature of the coldest month  $\leq 0^{\circ}\text{C}$ ) (Peel *et al.*, 2007). River locations are plotted onto a world map with climate zones (Peel *et al.*, 2007; Fig. 3.4).

Gradient has been determined by measuring the length of the measured reach along the river, and recording the average of 10 measurements of elevation within the river channel at both the upstream and downstream extents of the measured reach. On average, 10 measurements per reach are collected to increase accuracy of observations from satellite imagery (Google Earth, 2001). The elevation difference is divided by the along the channel centre line length of the reach to determine the channel gradient.

River size is determined by annual discharge ( $\text{m}^3/\text{yr}$ ) using data from Meybeck & Ragu (1997), Swales *et al.*, (2000), and Bobrovitskaya *et al.*, (1996). In the two cases (The Colville and Kolyma Rivers), where a tributary is used (as opposed to the main channel), the empirical relationship ( $w = 3.15 Q^{0.49}$ ) from Nixon *et al.*, (1959) of channel width ( $w$ , in metres) and bankfull discharge ( $Q$  in  $\text{m}^3 \text{s}^{-1}$ ) is used to yield the metric for the tributary measured in the study.



RIVER	COUNTRY	CLIMATE (Peel <i>et al.</i> 2007)	LATITUDE	LONGITUDE	REACH LENGTH (m)	REACH GRADIENT (UPSTREAM ELEVATION / DOWNSTREAM ELEVATION)	MEAN ANNUAL RIVER DISCHARGE ( $Q=m^3s^{-1}$ )
OK TEDI (FLY)	Papau New Guinea	A Af	-8.5	143.6833	148399	6.06473E-05	983 <sup>i</sup>
SENEGAL	Senegal	B BWh	16.0167	-16.5	159930	1.87582E-05	773 <sup>ii</sup>
MURRAY	Australia	B Bsk	-35.3667	139.3667	42467	9.41908E-05	250 <sup>ii</sup>
YANA	Russia	D Dfd	71.5167	136.5333	102316	6.84155E-05	1087 <sup>ii</sup>
COLVILLE TRIBUTARY	USA	D Dfc	70.4167	-150.5	22391	0.00053593	202 <sup>iii</sup>
KUSKOKWIM	USA	D Dfc	60.2833	-162.45	179915	4.44654E-05	1902 <sup>ii</sup>
MISSISSIPPI	USA	C Cfa	28.95	-89.4	298013	4.36223E-05	16769 <sup>ii</sup>

<b>PURUS (AMAZON)</b>	Brazil	<b>A</b>	<b>Af</b>	0.1667	-49	304250	2.95809E-05	28266 <sup>iii</sup>
<b>IRTYSH (OB)</b>	Russia	<b>D</b>	<b>Dfd</b>	66.75	69.5	224830	8.89561E-06	2125 <sup>iv</sup>
<b>KOLYMA TRIBUTARY</b>	Russia	<b>D</b>	<b>Dfc</b>	68.5667	160.9667	116920	8.55286E-06	26368 <sup>iii</sup>
<b>BRAZOS</b>	USA	<b>C</b>	<b>Cfa</b>	29.5833	-95.75	61690	6.48403E-05	160 <sup>ii</sup>
<b>MWENEZI (LIMPOPO)</b>	Mozambique	<b>B</b>	<b>BSh</b>	-25.25	33.5	55407	0.000631689	409 <sup>iii</sup>
<b>APPALACHICOLA</b>	USA	<b>C</b>	<b>Cfa</b>	30.7	-85.8667	9493	0.000210682	679 <sup>ii</sup>

Table 3.1 - A table to show the rivers selected for this study. Data for reach length and gradient is measured from satellite imagery. Climate data is derived by visual comparison of maps by Peel *et al.* (2007) and the reach location. River discharge data has been collated from the literature; (i) Swales *et al.* 2000; (ii) Meybeck and Ragu 1997; iv) Bobrovitskaya *et al.* 1996. Where the mean annual discharge data was unavailable, it was calculated using the empirical relationship ( $w=3.15 Q^{0.49}$ ) from Nixon *et al.* (1959), using a channel width measured from satellite imagery (iii).

### 3.5.1 *Planform morphometry*

Amalgamated and cannibalised deposits represent a fragmented and partly preserved record of older abandoned point bars in channel belts (Fielding & Crane, 1987; Mackey & Bridge, 1995; Miall, 2006). Images of detailed planform morphology effectively highlight important morphological features, including abandoned-channel geometry, active-meander shape, and the surface expression of scroll-bar forms. This enables the characteristics of a fluvial system to be assessed. A planform image is compiled by tracing the outlines of features that would have high preservation potential in the geological record. First, active channels and lakes are delineated. Abandoned channels are then outlined alongside the surface expression of the scroll bars. In the case of oxbow lakes, both water body and abandoned-channel form are delineated individually and, as the lake is typically smaller, it is placed over the abandoned-channel shape so it is visible. Finally, vegetated areas are classed as high (dense trees or bushes are seen), sparse (colouration and shadows are seen indicating vegetation is present and there are obvious gaps between trees and bushes), or non-vegetated (no evidence of vegetation), and are colour coded accordingly. The result is a visual map of meandering-system variability, which readily enables visual recognition of trends and features relevant to the investigation.

### 3.5.2 *Classification of the surface expression of scroll bar pattern*

Observations of the surface expression of scroll-bar pattern (Google Earth, 2001), show wide variability in the direction(s) of scroll-bar migration. The surface expression of scroll-bar pattern has been assessed independently of meander shape, to enable an objective comparison between channel shape and scroll-bar pattern. The classification scheme developed identifies eight Types into which similar formational processes are grouped. Each type has further sub-divisions, yielding 22 patterns in total (Table 3.2; Fig. 3.5). The classification scheme is flexible and is able to encompass the full variability of scroll pattern. The formative processes of the point-bar deposit are similar within each type and differences are highlighted by the sub-divisions. If a point-bar

deposit is not an accurate visual match it may be categorised into the correct type based on the identified accretion direction(s) (Table 3.2). The code attributed to each scroll bar pattern is composed of three parts: the prefix “T” refers to it being a scroll bar type (i.e., pattern); the number 1 to 8 refers to the parent type of scroll bar pattern; the number after the decimal subdivides the scroll bar pattern to describe more variability (Table 3.2; Fig. 3.5).

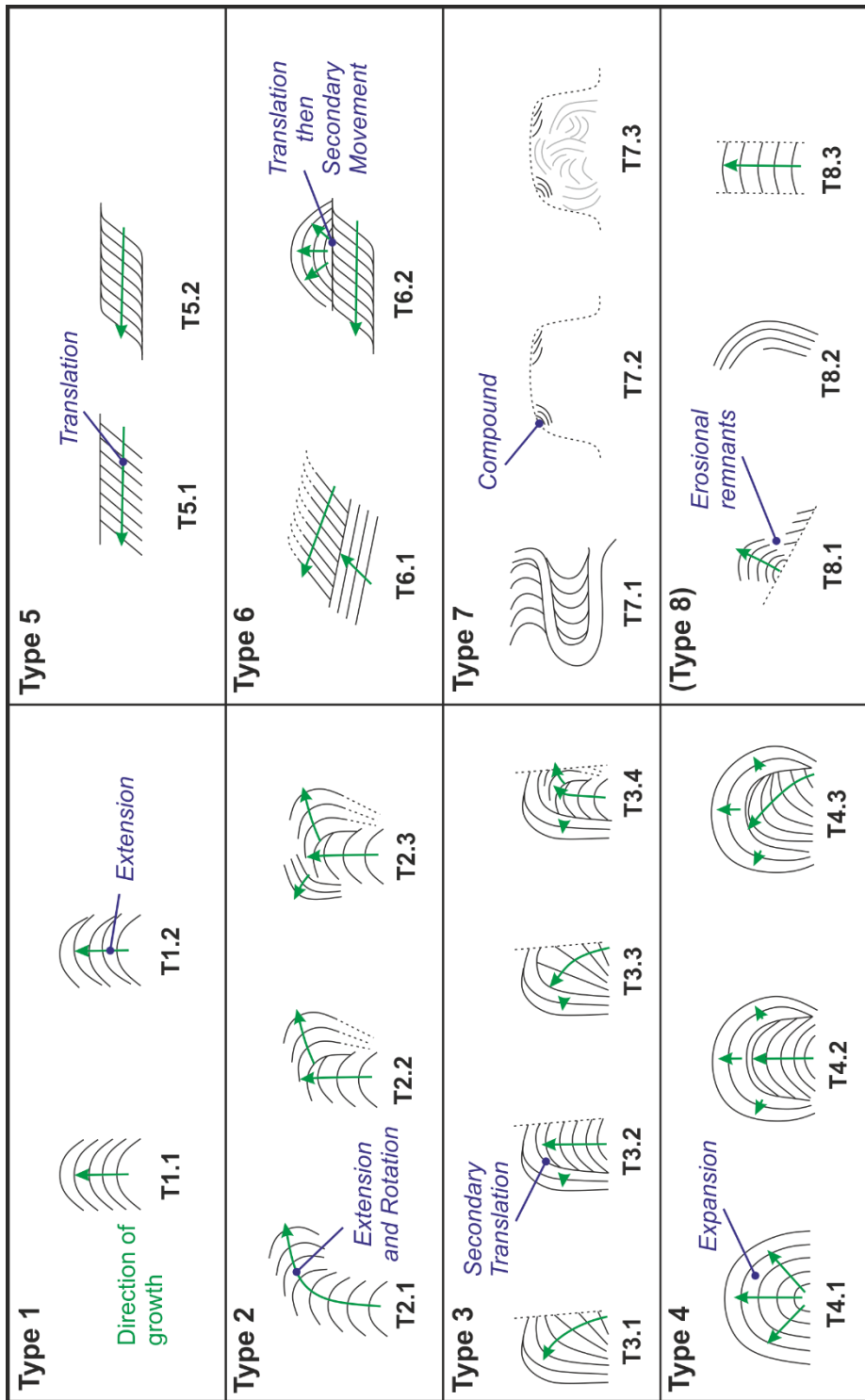


Figure 3.5 - A classification of the surface expression of scroll bar pattern. 8 Types have been defined (Table 3.2); 22 sub-types were defined by identifying variations in the overall process described by the Type category.

Type	Type sub-division	Description
1	1.1	<b>Extensional</b> (cf. Knighton 1998)
1	1.2	<b>Extensional</b> punctuated rotation (cf. Durkin <i>et al.</i> , 2015)
2	2.1	Smooth <b>extension and rotation</b>
2	2.2	<b>Extension and rotation</b> with one major directional change
2	2.3	<b>Extension and rotation</b> with more than one major directional change
3	3.1	<b>Rotation</b> (cf. Daniel 1971) progressing to <b>downstream translation</b>
3	3.2	<b>Extension</b> then <b>downstream translation</b>
3	3.3	<b>Rotation</b> then <b>downstream translation</b>
3	3.4	<b>Extension and rotation</b> then one major directional change, then <b>downstream translation</b>
4	4.1	<b>Expansion</b>
4	4.2	<b>Extension</b> , then <b>expansion</b> is the most recent phase of growth
4	4.3	<b>Rotation</b> , then <b>expansion</b> is the most recent phase of growth
5	5.1	<b>Translation</b> with a straight form (cf. Daniel 1971)
5	5.2	<b>Translation</b> with a curved form (cf. Daniel 1971)
6	6.1	Initial <b>translation</b> then secondary <b>translational</b> movement in a different direction
6	6.2	Initial <b>translation</b> then secondary <b>expansional</b> movement in a different direction
7	7.1	Point-bar composed of <b>recently abandoned</b> point-bar remnants
7	7.2	Only minor movement is visible from surface expression
7	7.3	Point-bar composed of a complex of <b>previously abandoned</b> point-bar remnants

8	8.1	Selection of anomalous <b>remnants</b> of a variety of growth styles
8	8.2	<b>Remnant</b> where the length of the scroll bar is dominantly preserved over migration direction
8	8.3	<b>Remnant</b> where the migration direction is dominantly preserved over the length of the scroll bar

**Table 3.2 - Descriptions of the classifications of scroll-bar styles identified in this study**

### 3.5.3 Meander-shape classification

In this study, the Intersection Shape methodology (Chapter 2) is used to quantify the relationship between meander shape and scroll-bar pattern, because it assesses the full range of meander shapes in an easily implemented, repeatable manner. The method classifies meander shapes into 4 groups, and 25 individual shapes therein. The method results in two metrics, which quantify the relationship between meander shape and scroll-bar pattern. To define the metrics, planform images are analysed to characterise individual meanders and the channel centreline is defined. Straight-line tangents are then projected into the meander body from the channel centreline and where they meet as one straight line, define the meander width (mW) (Fig. 3.1A). The point of most recent meander growth (MRG) is identified by observing scroll-bar growth direction, and a line from MRG is drawn through the meander body to the line mW, tracing the approximate direction of growth of the meander (tL). Inflection points (or mid points, see Chapter 2), are identified in the upstream and downstream limbs, respectively. The combination of these geometric definitions identifies the position of intersection lines, which are constructed normal to the channel centreline. Where intersection lines cross within the confines of the line mW and the channel centreline, a corner of a polygon is identified. These polygons are outlined as one shape known as the intersection shape. Two metrics are derived: (i) the area of the intersection shape divided by the perimeter, then normalised by average channel width; and (ii) the length of the meander (tL), divided by the meander width (mW), (Fig. 3.1).

### 3.5.4 Estimating lithological heterogeneity

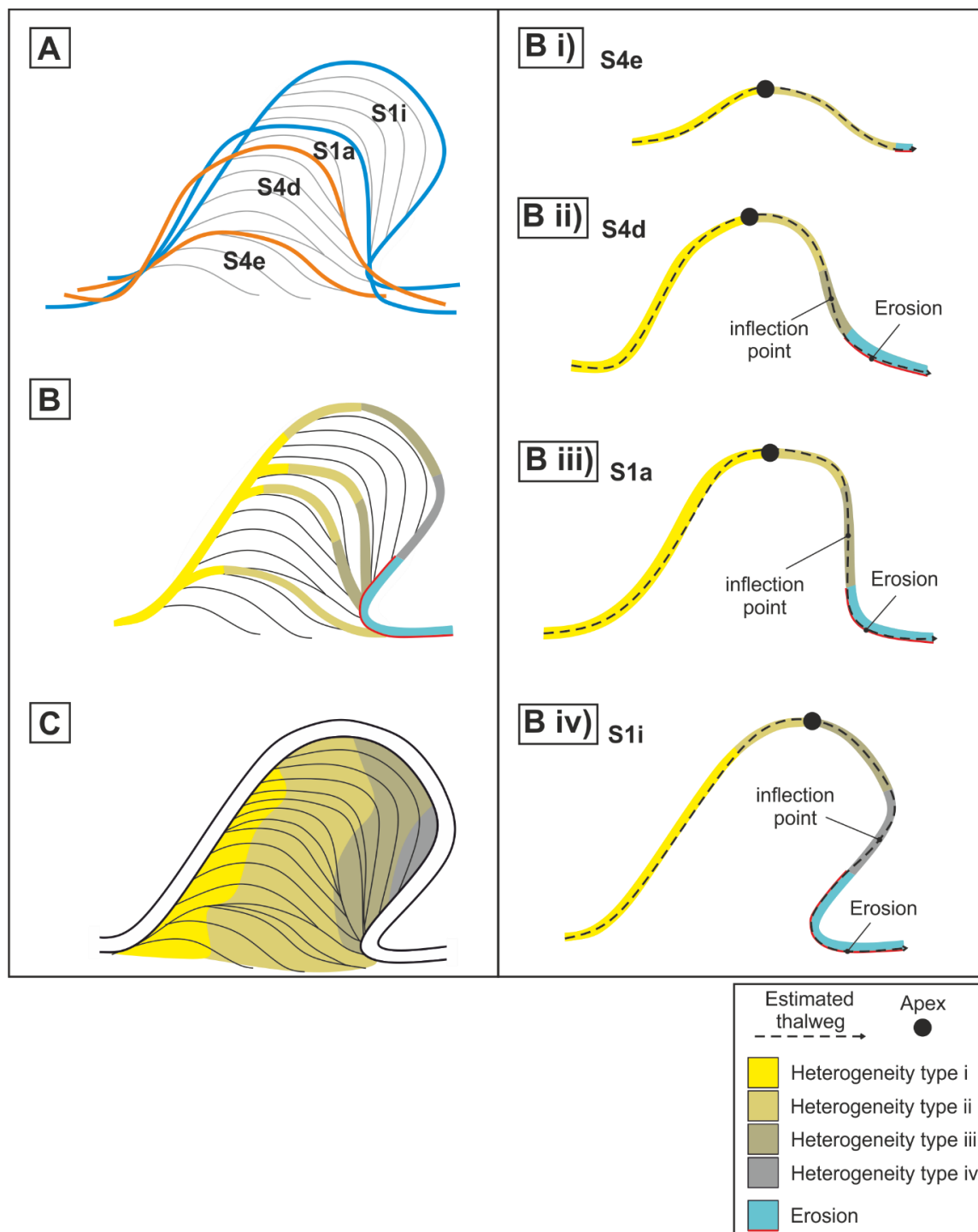
The type of heterogeneity can be estimated by using meander shape and surface expression of scroll-bar pattern through the application of known patterns and trends. Grainsize distribution has been shown to be variable throughout individual accumulated point-bar elements (Labreque *et al.*, 2011; Fustic, 2012; Durkin *et al.*, 2015). To qualify this, the sand: mud ratio is considered under four categories, which are on a relative continuum from sand-prone (type i), to mud-prone (type iv). Wightman & Pemberton (1997), Smith and Ashley (1985), Wood (1989), and Fustic *et al.*, (2012) present models where sediment calibre fines downstream in a point-bar deposit; such trends are observed in many modern meandering rivers (McGowen & Garner, 1970; Jackson, 1975; Bridge & Jarvis, 1982; Smith *et al.*, 2009). Typically, down-stream sediment fining is embodied by an overall increase in IHS in downstream limb deposits (Thomas *et al.*, 1987), whereas abrupt fining on the outer bank may be embodied by counter point bars (Smith *et al.*, 2009). These observed trends are also recognised in outcrop studies that identify increased occurrence of IHS downstream of a bend apex (Pranter, 2007; Ghinassi, 2011; Labreque *et al.*, 2011; Ielpi, 2014; Durkin, 2015; Fig. 3.2). The visual output for this study shows heterogeneity types, as relative to each other, in planform rather than placing absolute sand: mud ratios as this will be system specific; i.e. the sand: mud ratios, classed under types i-iv, can vary depending on the composition of the sediment supply. In a point-bar deposit, where there is a sand-prone sediment supply, type iv may be fine sand with no mud, whereas if there is a mud-prone sediment supply, type iv may be mud dominated.

Meanders vary considerably in planform shape, overall lithological heterogeneity of related bars, and temporal evolution. To aid understanding and enhance interpretation of relative heterogeneity, the simplest meander forms are considered first in each meandering reach. One meandering reach is considered at a time, within which 20 active adjoining meanders are examined. The upstream and downstream limbs are divided by the meander apex (Chapter 2), and a cross-over point is identified where the



thalweg crosses the channel centreline. The meanders within a reach are ordered by length ( $tL$ ), which is the distance from the point of most recent growth to the line representing the meander width ( $mW$ ), (cf. Chapter 2). This is done because meanders with low  $tL$  measurements, relative to the river size, will typically arise from simpler and more immature meanders than those with higher  $tL$  measurements. The meanders with the lowest  $tL$  values are considered first, and once the growth history and relative heterogeneity of the more simple forms is constructed, the trends can be carried forwards to more complex and irregular forms in the reach being assessed. Figure 3.6 illustrates the analysis and interpretation of the heterogeneity in a complex shape. The first step in attributing the relative lithological heterogeneity to a point-bar deposit is to determine the previous channel trajectories of the meander (Fig. 3.6A). The preceding channel form is deduced through i) observation of the geometries of the surface expression of the scroll-bar deposits (e.g. Durkin 2016), and ii) analysis of the meander shape data for the rest of the reach. The shapes identified through use of the Intersection Shape methodology (Chapter 2), are overlain onto the surface expression of the scroll-bar deposits (Fig. 3.6) by initially fitting a low sinuosity shape, and then shapes with increasing sinuosity until the shape of the active reach is achieved. Each of the fitted meander shapes are drawn separately and the apex of the shape (the point furthest from the line  $mW$ , Chapter 2), is constructed (Figs 3.6B i-iv). The fitted meander shapes are predicted through assessment of the likelihood of each shape (as defined by Chapter 2), as considered quantitatively by the frequency of its occurrence in the reach, combined with a visual judgement to join meander scroll-bar shape with meander shape. Next, the downstream inflection point is identified where a riffle, or cross-over, likely existed (cf. Leopold & Wolman, 1957; Allen, 1965; 1982). Where this cross-over occurred, the area of the most mud-prone sediment is identified (Smith, 2009). Where the thalweg is projected to have met the outer bank on the downstream limb, erosion occurred. For individual meander shapes (Figs 3.6B i-iv), the reach is subdivided into areas of predicted types of lithological heterogeneity (types i-iv). The resolution of the estimation is reliant on the amount to which the fundamental principles

of downstream fining can be applied and resolved; volumes of sediment typically span, and can cross-cut, multiple unit bars.



**Figure 3.6 - A demonstration of the construction of a model of heterogeneity from a meander planform image. A) Estimated meander trajectories through which the most recent shape has transitioned; B) a compilation of the interpretations of heterogeneity made in B i)-iv); C) a map of estimated relative grain sizes for the most recent meander form.**

The justifications for the positioning of relative types of lithological heterogeneities around a meander bend, are based on trends described in published literature (Fig. 3.2). Each of Figures 3.2A-D is drawn so lithological heterogeneity is relative within each image. This means that the modelled heterogeneity will be different to that depicted in the examples in Figure 3.2, even for cases where meander shapes are similar. The following method produces models of the relative lithological heterogeneity of point-bar deposits, which itself might vary across bars in an active reach. There are two assumptions taken in this methodology: (i) at least one meander in the reach will exhibit a phase that is not downstream accretion; (ii) at least one meander in the reach will equal or exceed a sinuosity of 2.5. These assumptions allow the rules for the relative distribution of the lithological heterogeneity for the whole reach to be better constrained, for two reasons. Firstly, as assumed by this method, a meander in the reach that is not downstream accreting will likely provide more sand-prone sediment than those that are downstream accreting (Bridge *et al.*, 1995; Smith *et al.*, 2009); therefore heterogeneity type i will be reserved for use in scroll-bars that are not downstream accreting. Secondly, a meander in the reach that displays sinuosity equal to or greater than 2.5 will have sediment on the downstream limb that is more mud-prone than sediment on the same limb of a lower sinuosity meander (Jackson, 1976); therefore heterogeneity type iv will be reserved for use on the downstream limb in shapes with a sinuosity  $>2.5$ .

To construct a model that maps relative heterogeneity types, the following methodology is undertaken. Each heterogeneity type (as constructed onto the meander shapes in 6 Bi-iv), should be adjacent to the next one up or down the expected heterogeneity sequence (see key for Figure 3.6) because changes in heterogeneity type are gradational. For an open asymmetric, angular, or open symmetric meander shape (Groups 1, 2, and 4), heterogeneity types i and ii may record accretion on the upstream limb, and heterogeneity type i may not occur on the downstream limb. Heterogeneity type ii will occur past the upstream cross-over and will vary in its downstream extent

based on the geometry of the meander shape, and mode of accretion of the point bar. If downstream accretion is occurring, there will be no deposition on the upstream limb, so heterogeneity type i will not be observed, and counter point-bars will be observed where the accreting bar turns from being concave to convex (Smith *et al.*, 2009). Counter point-bars will be constructed using heterogeneity types iii and iv, where type iv is furthest from the inflection point. Point-bars not accumulated through downstream accretion are seen to have a larger proportion of heterogeneity types i and ii than point-bars accreted through downstream accretion (Smith *et al.*, 2009; Bridge *et al.*, 1995; Figs 3.6A and C). In a point-bar that is not downstream accreting in an open asymmetric, angular, or open symmetric meander shape (Groups 1, 2, and 4), heterogeneity type iii will not be predicted to occur on the downstream cross-over until a sinuosity greater than 2.5 is measured. This is because the heterogeneity should be relative along the whole reach, and more sinuous shapes that are not downstream accreting have more mud-prone sediment on the downstream limb compared to less sinuous shapes. If the meander shape has a sinuosity of  $>3$ , because of expansional fining (Jackson, 1976), heterogeneity type iv is expected from the cross-over downstream, because this is the fine end-member heterogeneity type for mud-prone strata, and so should be used in the most extreme areas on the downstream limb (Bridge *et al.*, 1995; Carter, 2003). Bulbous shapes (Group 3), can have more than two inflection points so there may be multiple points of most recent growth (cf. Chapter 2), which themselves display grainsize fining around each (Carter, 2003; Fig. 3.2D). The upstream limb may present a range of heterogeneity types depending on the geometry (Nanson *et al.*, 1980; Fig. 3.2B). Multiple zones of relative heterogeneity types i-iv should be used if necessary in a complex, multi-phased combination, such as in a bulbous shape (Nanson *et al.*, 1980; Fig. 3.2B). Next, a map of relative heterogeneity type can be compiled by replacing the lines of the reconstructed meander shapes (Fig. 3.6A) with heterogeneity types (Fig. 3.6B i-iv). The direction of growth of the scroll bars and other information, such as marked changes in direction of scroll-bar accretion and cross-cutting relationships, are used to predict the distribution of heterogeneity types

between the reconstructed lines, and thereby to compile the final map (Fig. 3.6C).

Cross-cutting relationships on the inner bank of the upstream side of meanders are carefully assessed for evidence of upstream erosion. Truncation of scroll-bars may be evident, and there will likely be a decreased proportion of the accumulation of heterogeneity types i and ii (Jackson, 1976). Mud-prone heterogeneity type iv should be reserved for the flood plains and abandoned channels when they are included in the assessment of a whole river reach.

### **3.6 Results**

Each of the 260 meanders have been measured using the Intersection Shape methodology to categorise meander shape into one of four Groups (open asymmetric, angular, bulbous, or open symmetric; cf. Chapter 2, and subsequently into one of 25 sub-groups (Table 3.3, Table 3.1). The surface expression of scroll-bar patterns have been subjectively evaluated and categorised accordingly by Type (1-8), and then into one of 22 sub-classifications. This is achieved through observation of the meander morphometry; the surface expression of scroll-bar pattern can be visually compared to a model in Figure 3.5; otherwise, the point-bar growth history can be determined to enable identification of the scroll bar pattern (Table 3.2).

FLY	SENEGAL		MURRAY		YANA		COLVILLE		KUSKOKWIM		MISSISSIPPI		AMAZON		OB		KOLYMA		BRAZOS		LIMPOPO		APPALACHICOLA		
	Shape	Scroll	Shape	Scroll	Shape	Scroll	Shape	Scroll	Shape	Scroll	Shape	Scroll	Shape	Scroll	Shape	Scroll	Shape	Scroll	Shape	Scroll	Shape	Scroll	Shape	Scroll	
3f	2.2	3c	7.2	3f	2.3	2a	2.2	(3e)	2.3	4d	3.2	4a	2.2	1f	3.1	2d	3.1	4a	3.1	3c	2.3	4d	3.3	(1c)	7.3
1c	3.1	3a	4.2	(4b)	3.1	1g	6.2	1b	3.3	2c	3.4	1h	6.2	2d	6.2	1e	3.3	4a	3.2	3a	2.3	4e	3.1	3d	3.1
4a	2.2	3c	7.3	4e	6.2	1e	3.3	4a	2.2	2c	7.3	4d	3.2	3f	8.2	3f	2.3	(1e)	3.1	3g	2.2	4e	5.2	4d	3.1
2b	3.3	3c	3.1	4b	3.2	1e	3.4	1f	3.4	4a	7.1	4d	6.2	3f	8.2	1g	3.4	1e	3.1	4e	3.3	4e	3.3	2c	3.1
1e	3.2	(1d)	3.2	3c	8.2	3b	2.3	3f	3.4	1h	3.2	2a	3.4	3a	8.1	3f	2.2	4c	3.3	1h	6.2	4e	1.2	4c	3.1
4c	3.1	2a	5.1	3e	3.1	4e	7.1	3g	2.1	4b	3.4	(1f)	3.4	1f	3.1	3e	2.3	1d	3.2	1i	3.1	2d	3.2	3d	3.2
4e	5.1	1i	6.2	4c	3.2	2d	3.1	4d	6.1	1h	3.4	(4b)	3.2	3e	3.4	3f	4.2	4a	3.1	2d	3.4	4d	3.1	3f	2.2
4d	6.2	4c	3.1	4c	6.2	4c	3.1	4d	3.3	1g	3.2	4d	3.1	1e	3.1	4c	2.2	2d	6.2	4e	5.1	1d	3.1	1g	2.2
2a	4.1	2d	6.2	(4c)	2.2	3e	3.4	1b	3.1	2d	3.3	2d	3.4	3d	8.2	3f	3.4	3d	8.2	4b	6.2	4e	5.2	4c	3.2
1i	2.1	4d	6.1	1e	6.2	4d	6.2	1b	3.3	1b	3.4	4e	6.2	3c	6.2	3g	4.1	3d	3.4	4e	4.2	1c	7.2	4d	3.1
3f	1.1	1d	3.3	1g	3.1	1g	2.1	2a	3.3	1h	2.2	4c	3.1	4e	3.3	4a	8.2	3f	4.2	4e	6.2	4d	3.1	4e	3.1
3a	2.1	1f	6.1	(1f)	7.2	4e	6.2	4e	3.1	4c	3.3	(4d)	3.3	3e	3.1	3f	8.2	4d	6.2	1c	6.2	4d	3.2	2c	3.2
1a	3.1	3b	2.3	3b	2.2	3b	4.2	4a	2.2	4c	2.2	4c	3.3	3g	4.2	1b	3.1	1i	4.2	3d	6.1	4d	3.1	4d	3.1
1e	4.1	4c	3.1	3d	6.1	4c	3.1	3c	7.1	4d	4.1	4d	7.1	4c	2.2	(1d)	4.1	4c	3.1	4b	3.2	4e	5.2	1e	4.3
2a	8.2	4d	3.1	3e	8.2	4d	7.1	2a	2.1	4d	7.1	4e	5.2	4d	3.1	4c	3.4	1i	2.1	4c	3.1	4e	3.3	(1b)	3.1

3g	8.2	4c	6.2	3e	3.3	3b	7.1	1i	2.3	2c	7.1	2b	5.2	4e	5.1	(3e)	2.3	1c	6.2	3e	3.3	4e	5.2	1g	3.1
3c	2.3	(1i)	3.2	1d	3.3	(1g)	3.2	4a	2.1	1g	2.2	2d	7.1	2a	5.1	4d	3.2	3b	2.3	1i	8.1	4e	5.2	4d	1.2
4d	7.1	3c	6.1	4d	7.3	3f	2.1	1i	7.3	1h	3.1	4e	5.2	3f	2.2	2d	6.1	4d	3.2	1e	3.2	1h	3.1	(3f)	3.1
3g	2.3	1g	3.3	1g	3.2	1i	3.1	3d	2.2	4d	5.2	4d	7.3	3a	2.2	4d	6.2	4d	7.3	4a	3.3	2b	3.1	4d	3.1
3g	6.1	1g	6.1	4a	8.2	1i	3.3	2a	5.1	4e	7.1	4e	5.2	1a	3.1	1g	7.3	4d	2.2	(1e)	3.3	2d	1.2	(3d)	3.2

**Table 3.3 - Meander shape and scroll-bar pattern observed for the 20 meanders studied in each of the 13 meandering reaches studies. A shape reference in brackets indicates that it is an outlier.**

### 3.6.1 *Meander shape*

Through use of the Intersection Shape methodology, four Groups and 25 shapes are identified in the 13 assessed river reaches. Open asymmetric, angular, bulbous and open symmetric shapes (Groups 1, 2, 3 and 4), represent 26, 11, 24 and 39 % of the 260 meander shapes assessed, respectively (Table 3.3, Fig. 3.7). Open symmetric (Group 4) shapes are the most prevalent with at least 4 in each assessed reach. Occurrence of angular and bulbous shapes (Groups 2 and 3) is more variable. For example, there are no bulbous shapes in the reach of the Kuskokwim River, but 10 in the reach of the Purus (Amazon) River. The most common shapes in each of Groups 1 through 4 are S1g, S2d, S3e, and S4d respectively (cf. Chapter 2), (Table 3.3, Fig. 3.7).



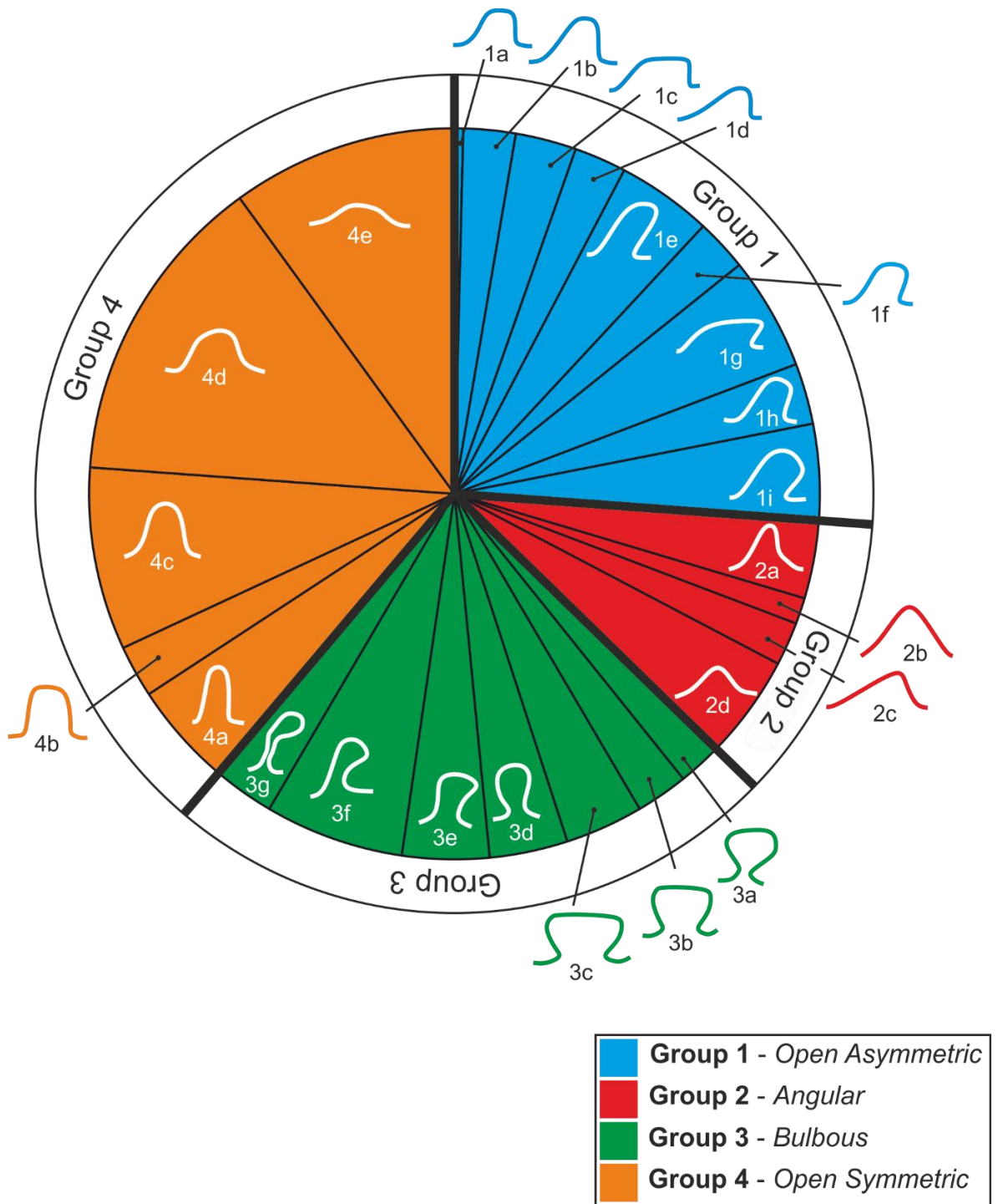


Figure 3.7 - A pie chart showing the proportion of each shape in the 260 meander shapes studied.

### *3.6.2 Surface expression of scroll-bar pattern*

Eight Types and 22 sub classifications are identified through use of the classification of the surface expression of scroll bar pattern on the 13 river reaches assessed (Table 3.3, Figs 3.5 and 8). Multi-phased migration (Type 2) and downstream accretion with translation as a secondary phase (Type 3) is present in every river. Type 3 is the most abundant (45.5%) with 6 or more meanders exhibiting this surface expression of scroll-bar pattern in each river. The least consistent scroll-bar pattern identified is translation followed by a secondary movement (Type 6). Seven meanders exhibit this style in the Senegal reach, but none in the Kuskokwim reach. The most common shapes in each of Types 1 through 8 are T1.1, T2.2, T3.1, T4.1 and T4.3, T5.1, T6.2, T7.1, and T8.2 (Table 3.3, Figs 3.5 and 3.9).

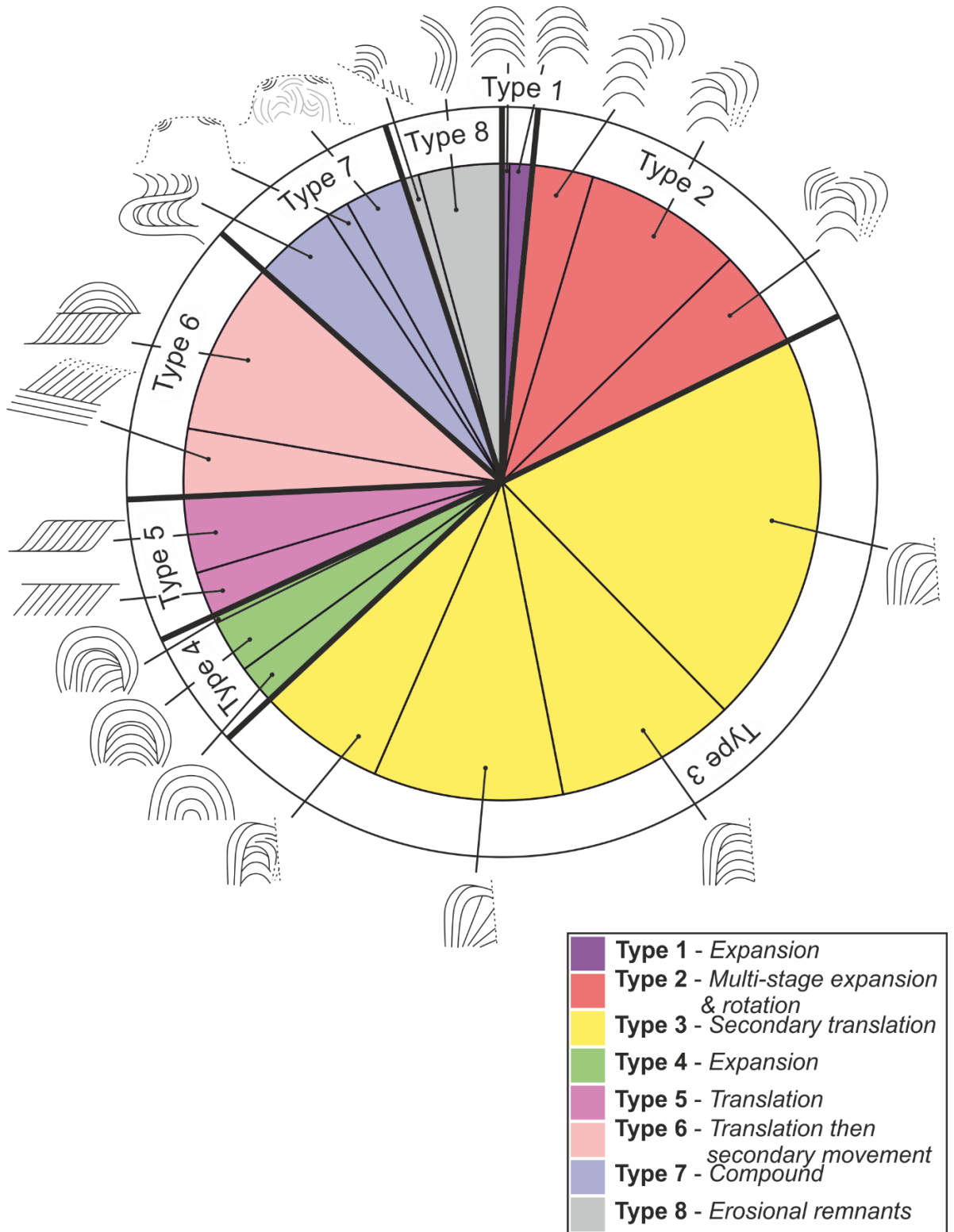


Figure 3.8 - A pie chart showing the proportion of each scroll bar type in the 260 meander shapes studied.

### 3.6.3 Relationships between the data sets

Each of the four meander shape groups exhibit a wide variety of scroll-bar patterns (Fig. 3.9). Bulbous shapes (Group 3) have markedly different trends than Groups 1, 2, and 4 (Table 3.4). They show the least amount of downstream accretion (Types 3, 5 and 6). Fifty-two per cent of scroll-bar patterns are multi-stage rotation (Type 2), or fragmented remnants (Type 8).

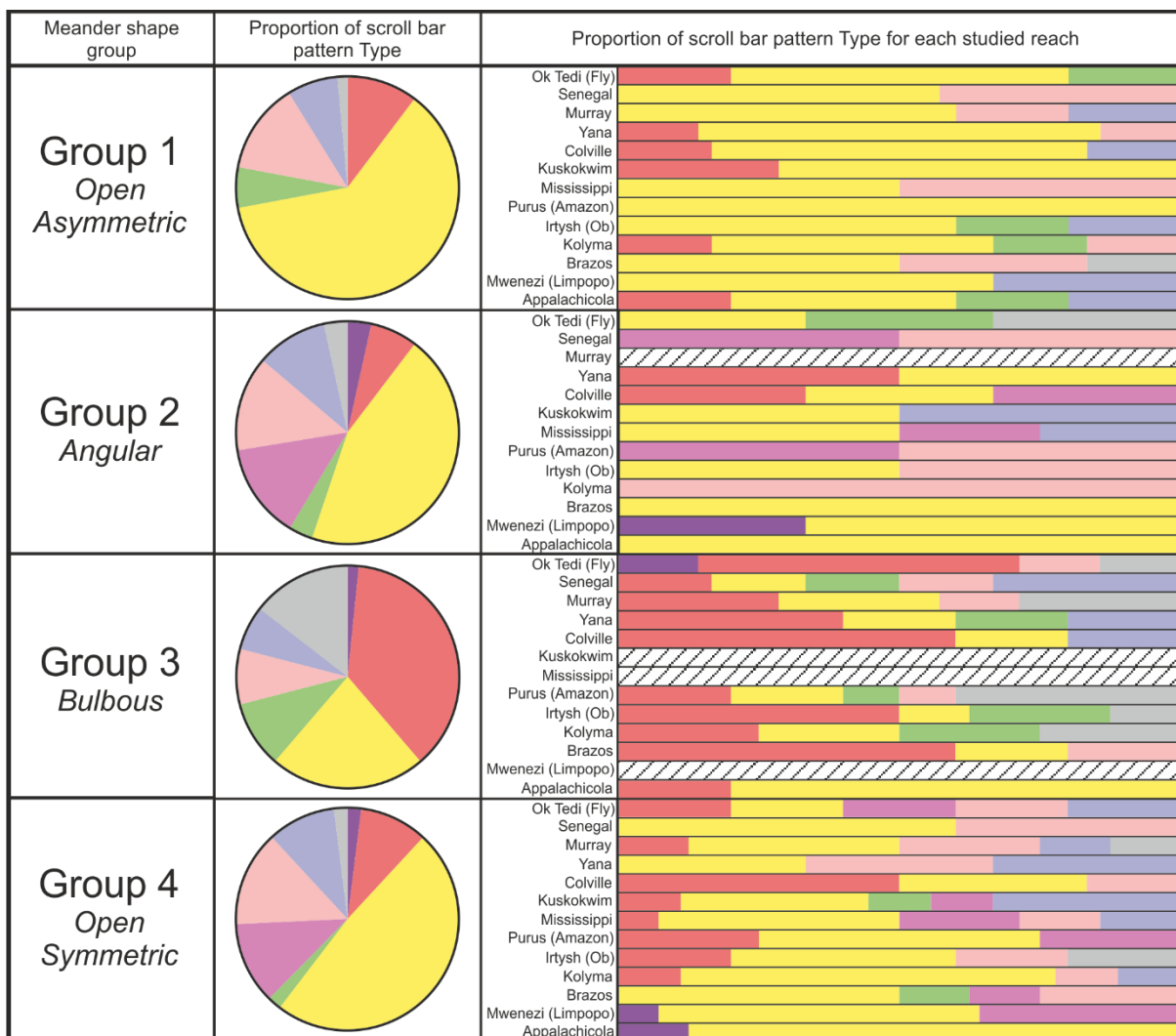


Figure 3.9 - A graph showing the variety of scroll bar patterns in each meander shape group overall, and for each river studied.

	Open Asymmetric (Group 1)	Angular (Group 2)	Bulbous (Group 3)	Open Symmetric (Group 4)
Secondary migration style of downstream translation (Type 3)	62%	45%	23%	49%
Translation (Types 5 and 6)	13%	28%	8%	26%
<b>Downstream accretion (Types 3, 5 and 6)</b>	<b>75%</b>	<b>73%</b>	<b>31%</b>	<b>75%</b>
Multi-stage rotation (Type 2)	10%	7%	37%	10%
Fragmented remnants (Type 8)	2%	3%	15%	2%
Sum of multi-stage rotation (Type 2), and fragmented remnants (Type 8)	<b>12%</b>	<b>10%</b>	<b>52%</b>	<b>12%</b>

**Table 3.4 - A table to demonstrate the markedly different trends seen in Group 3 compared with Groups 1, 2, and 4.**

#### *3.6.4 Observations from planform morphometric constructions*

Reaches from the Ok Tedi (Fly), Senegal, Murray and Irtysh (Ob) Rivers have been drawn as planform morphometric maps (Figs 3.10 and 3.11). The dominant shapes and modes of migration are markedly different, and, when combined, mark a style, or character, for each reach. The reaches selected for visual and quantitative analysis are subject to different sets of environmental influences (Table 3.1).

### *Ok Tedi (Fly) River*

Meander shapes appear to be mostly open symmetrical (Group 4) with multi-phased growth (Type 2). Analysis of the quantified data reveals an even balance of meander shape between open asymmetric and open symmetric, and bulbous shapes make up the majority of meanders (40%). Meander scroll-bar growth shows gradual and punctuated directional change, with major directional changes occurring episodically. Style of meander growth is dependent on size (meander area): larger meanders typically expand, whereas smaller meanders typically rotate. The quantified data show that there is a wide variety of scroll-bar growth direction. Chute cut-off occurs sequentially in sections, and abandoned loops on the floodplain overlap each other in a pattern that varies from regular to irregular. Figure 3.12A shows a complex and fragmented assemblage of point-bar remnants. There are many sections of scroll-bar that are not obviously related to any active reaches, making it difficult to assign a heterogeneity type. Where heterogeneity can be assigned, it is constructed as fining downstream in point-bar deposits exhibiting scroll-bars that are undertaking rotation (Type 3.1), and punctuated rotation (Type 1.2).

### *Senegal River*

All four groups of meander shape are represented in this reach, with open asymmetric type being the most common (35%). Through visual assessment of the reach, scroll-bar growth occurs through expansion and translation in co-sets identifiable by gradual directional changes. Scroll-bar styles that represent downstream accretion (Types 3, 5 and 6), collectively represent 80% of the scroll styles in the reach. More pronounced changes in direction are seen in compound forms, and vegetation density increases towards the active reach. Figure 3.12B shows the main active reach to be dominantly undertaking rotation and expansion; this leads to segregation of the sediment whereby relatively mud-prone sediments occur downstream of relatively sand-prone sediments

as depicted in previous models (e.g., Fustic *et al.* 2012). In the planform map, there is no evidence of bulbous shapes in the active channel, which could explain why the abandoned reaches are less sinuous than other reaches studied.

#### *Murray River*

Meander shapes increase in irregularity and complexity as they increase in area. Meander shapes with a relatively smaller point-bar area exhibit one scroll pattern (most commonly Type 3 or Type 6), and meander shapes with a relatively larger point-bar area exhibit punctuated growth in scroll-bar sets. There are no angular shapes in this reach, and there is markedly less variation in scroll-bar pattern and meander shape than is typical. Growth by secondary translation (Type 3) is most common (40%). The character of abandoned reaches indicate chute channel cut-off to be the dominant mode of meander-loop abandonment. Where avulsion occurs, long and narrow channels remain connecting parts of the main reach (Fig. 3.11 (5)). Figure 3.12C shows point-bars that vary in size and complexity. There are large expanses of irregularly shaped mud-prone sediment, which relate to channel remnants abandoned by cut-off mechanisms. Large abandoned point-bar deposits record incremental growth, whereas smaller point-bars record downstream accretion, dominantly as rotation and translation.

#### *Irtys (Ob) River*

The most common meander shape group in the studied reach is bulbous (40%), and open symmetric and open asymmetric are present in equal proportion (25% each). The principal style of meander growth is translation and rotation (Types 3 and 6), though expansion and multi-phased rotation are both also common (Types 4 and 2). Point bars have grown through incremental rotation and occur in scroll-bar sets of 2-6. Many abandoned loops are bulbous in shape indicating neck cut-off occurred in the past. In these loops, the scroll bars are oriented orthogonal to the point of palaeo cut-off. Figure

3.12D shows a section of the studied area that represents an irregular active reach, and regular-shaped abandoned loops. Each point-bar is depicted with deposits fining downstream, and growth to have occurred through extension then expansion (Type 4.2), or rotation (Type 3.1). Compared with the other examples in Figure 3.12, the scroll-bar patterns are the most continuous in this example, enabling a comparatively more confident reconstruction.



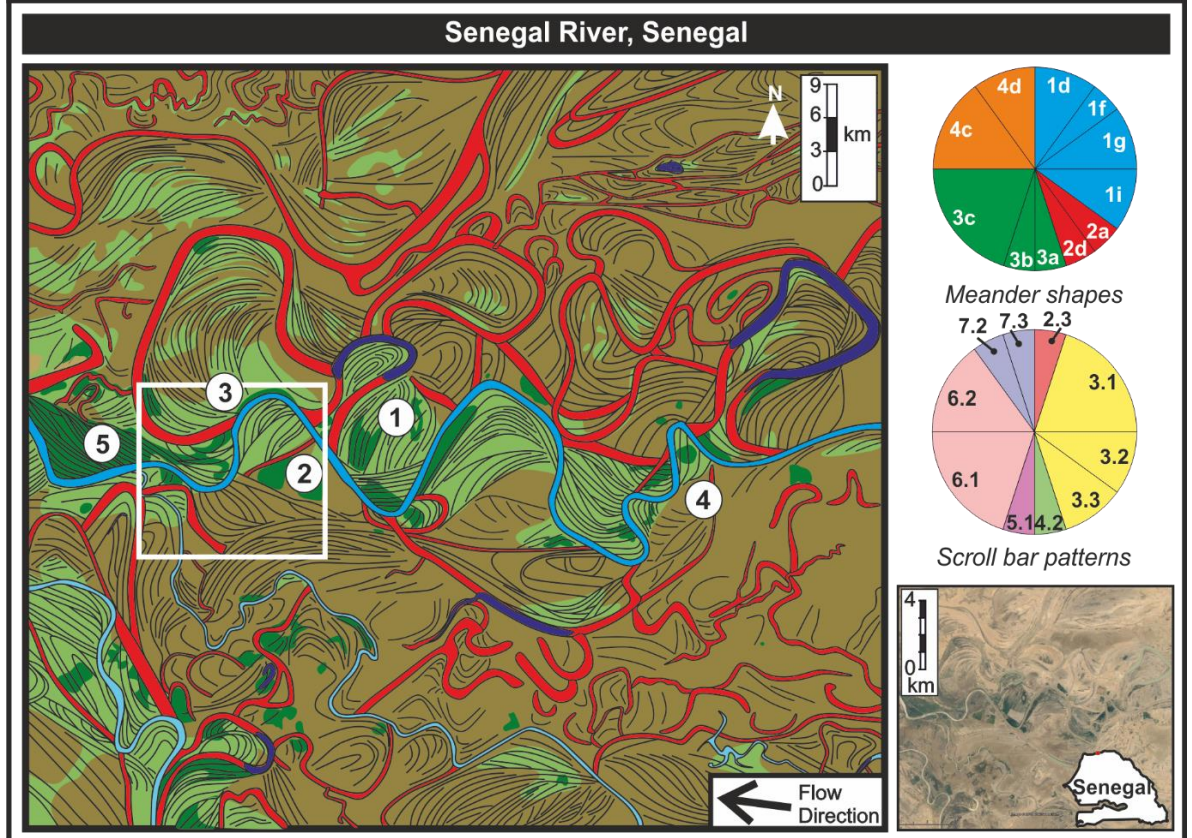
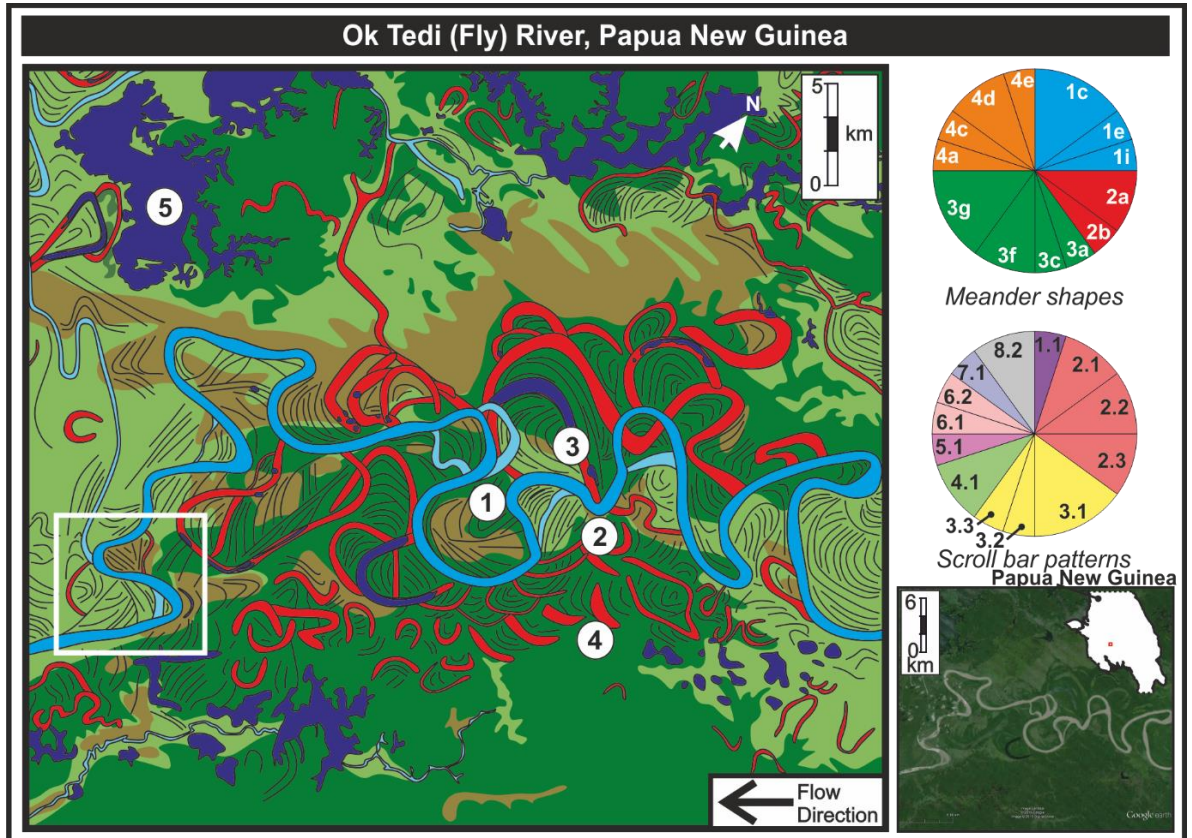


Figure 3.10 - Pie charts of the proportions of features seen in fluvial meandering systems are shown with planform morphology maps for the Ok Tedi (Fly) River, Papua New Guinea, and the Senegal River, Senegal. The white boxes show the sections which are interpreted in Figure 3.12. In the Ok Tedi (Fly) River the following features are noted: (1) larger meanders growth through expansion; (2) smaller meanders typically rotate; (3) meanders on the same side of the channel undertake chute cut-off sequentially; (4) abandoned loops to the south east overlap; (5) lacustrine environments. In the Senegal River, the following features are noted: (1) meander shapes are commonly both open asymmetric and open symmetric, with occasional bulbous and angular shapes; (2) Meander scroll-bar growth is typically through expansion and translation; (3) clear changes in growth direction are seen in compound forms; (4) vegetation is most dense directly on point bars by the active channel; (5) interestingly, the most closely spaced scroll bars are on the most vegetated point bar.



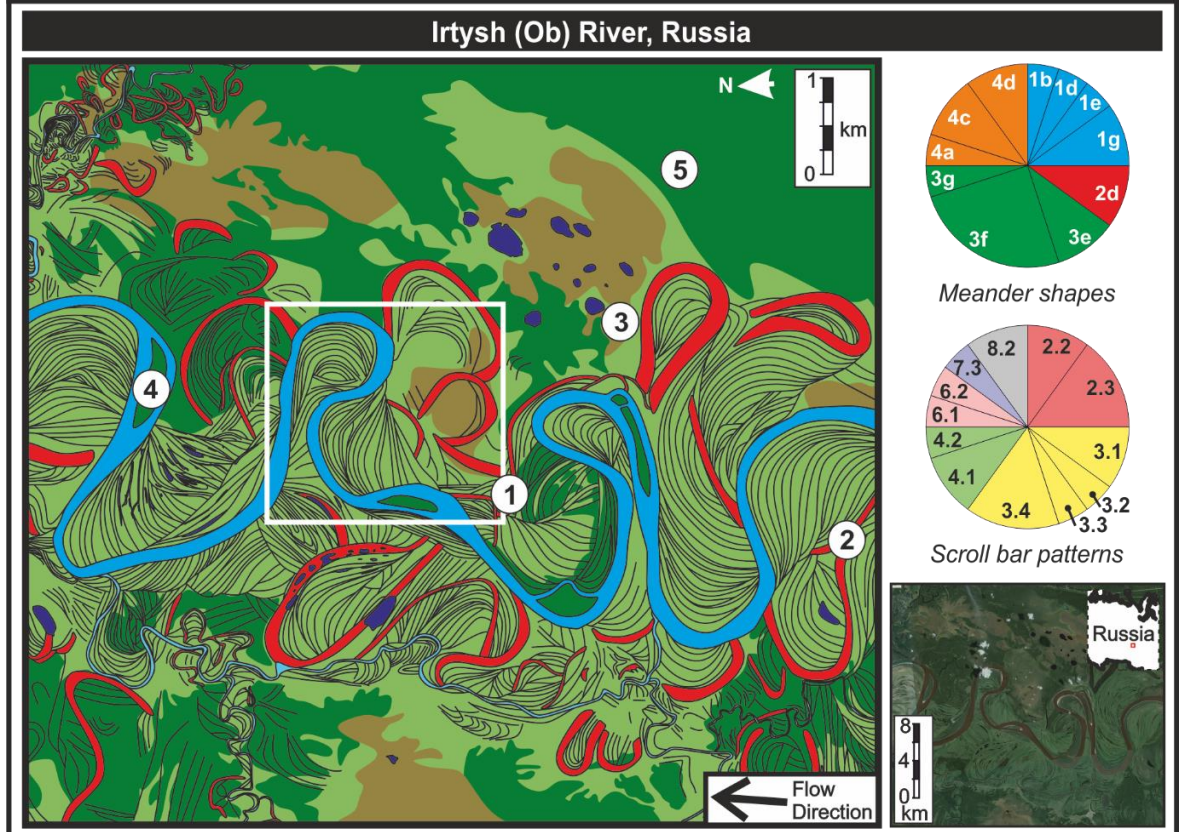
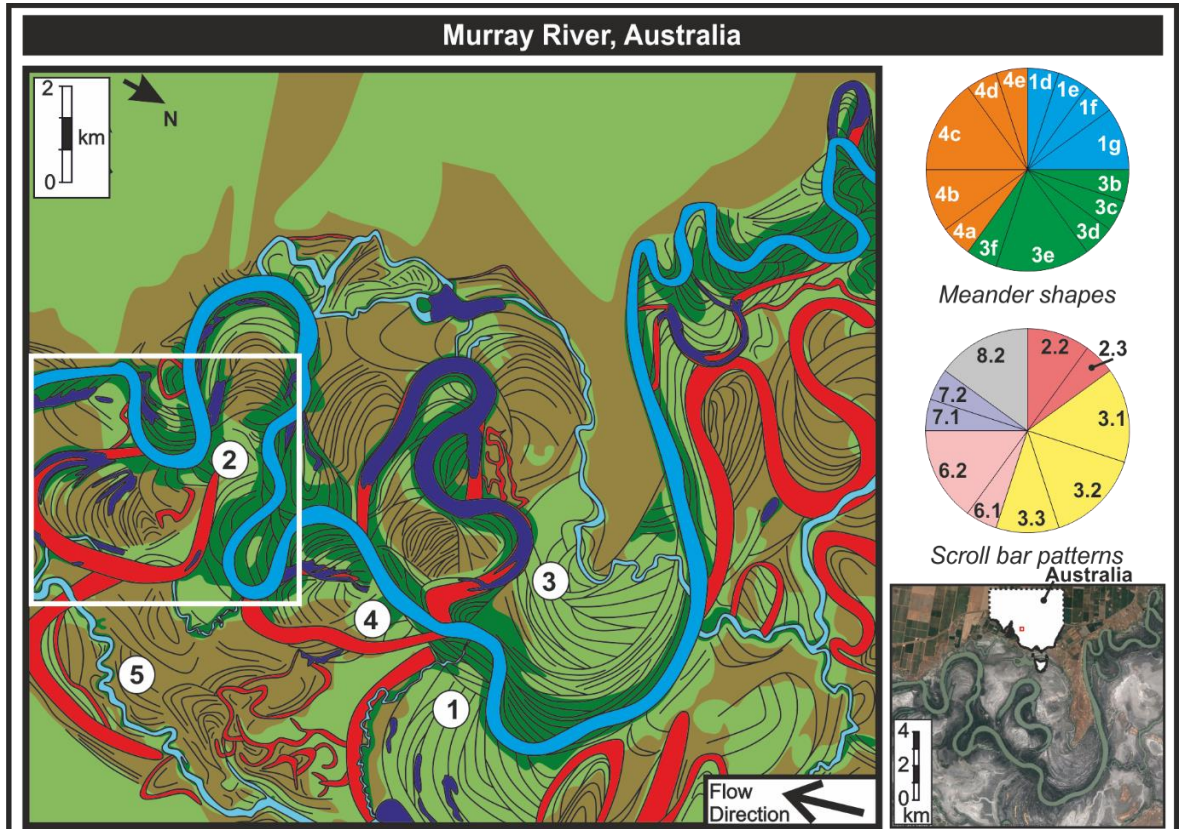
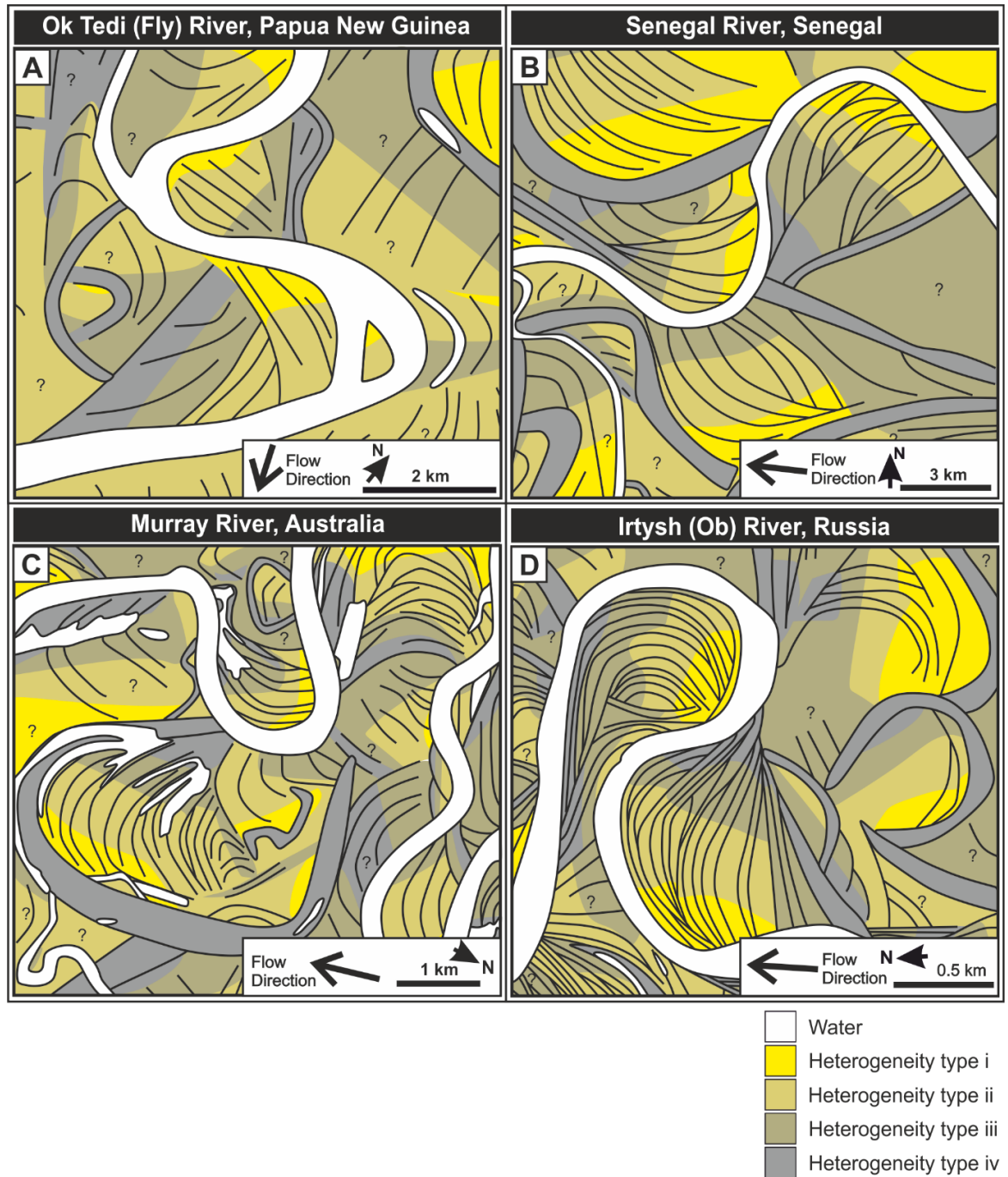


Figure 3.11 – Pie charts of the proportions of features seen in fluvial meandering systems are shown with planform morphology maps for the Murray River, Australia, and the Irtysh (Ob) River Russia. The white boxes show the sections which are interpreted in Figure 3.12. In the Murray River, the following features are noted: (1) meander shapes are either small and regular or large and irregular; (2) punctuated growth occurs in co-sets of approximately five; (3) translation and expansion is typical; (4) chute cut-off is indicated by the character of abandoned loops (5) channels connect parts of the main reach. In the Irtysh (Ob) River the following features are noted: (1) meander shape appears to be typically either bulbous, or open symmetric and the principal style of meander growth is translation and rotation; (2) point bars grow in co-sets of 2-6 and undertake incremental rotation; (3) Abandoned loops are sometimes bulbous in nature; (4) Vegetation is most dense on mid-channel bars (5) and on the floodplain beyond the active channel.



**Figure 3.12 - Interpretations of the heterogeneity types for modern systems in planform;**  
**A) Ok Tedi (Fly) River, Papua New Guinea; B) Senegal River Senegal; C) Murray River,**  
**Australia; D) Irtysh (Ob) River, Russia.**



## 3.7 Discussion

Assessment of the spatial distribution of lithologic zones with variable grain size in fluvial point-bar deposits is important to determine sub-seismic architecture, and therefore the fluid-flow rates and pathways in reservoir bodies hosted in such deposits (Fielding & Crane, 1987; Miall, 1988). Observation of meander form through seismic imagery enables the geometries of a stratigraphic deposit to be evaluated.

### 3.7.1 *Application of heterogeneity prediction to the sub-surface*

A study of the Cretaceous McMurray Formation, Alberta, Canada, is used here to demonstrate the applicability of these methods. Characteristics exhibited by preserved point-bar architectural elements of this ancient meandering fluvial succession (Fig. 3.13A; Smith 2009) include neck cut-off, translation and rotation. Scroll bars are oriented at approximately 90° to the point where meander cut-off occurs (i.e. point bars 1 and 3, Fig. 3.13A). This character is similar to that seen in the Irtysh (Ob) River, (Figs 3.11 and 3.15), and Figure 3.12D shows two meander shapes and scroll-bar combinations that are commonly observed in this imaged reach of the Irtysh (Ob) River. Due to this similarity in character, comparisons can be drawn to inform the interpretation of the sub-surface data depicted in Figure 3.13A. Therefore, by considering a modern system with similar observed characteristics in scroll-bar pattern and meander form, the interpretation regarding the progression of a meander shape can be informed (Fig. 3.13E). Examination of the incremental progression of meander growth aids understanding of the possible grain-size distribution in the reach (Fig. 3.13B).

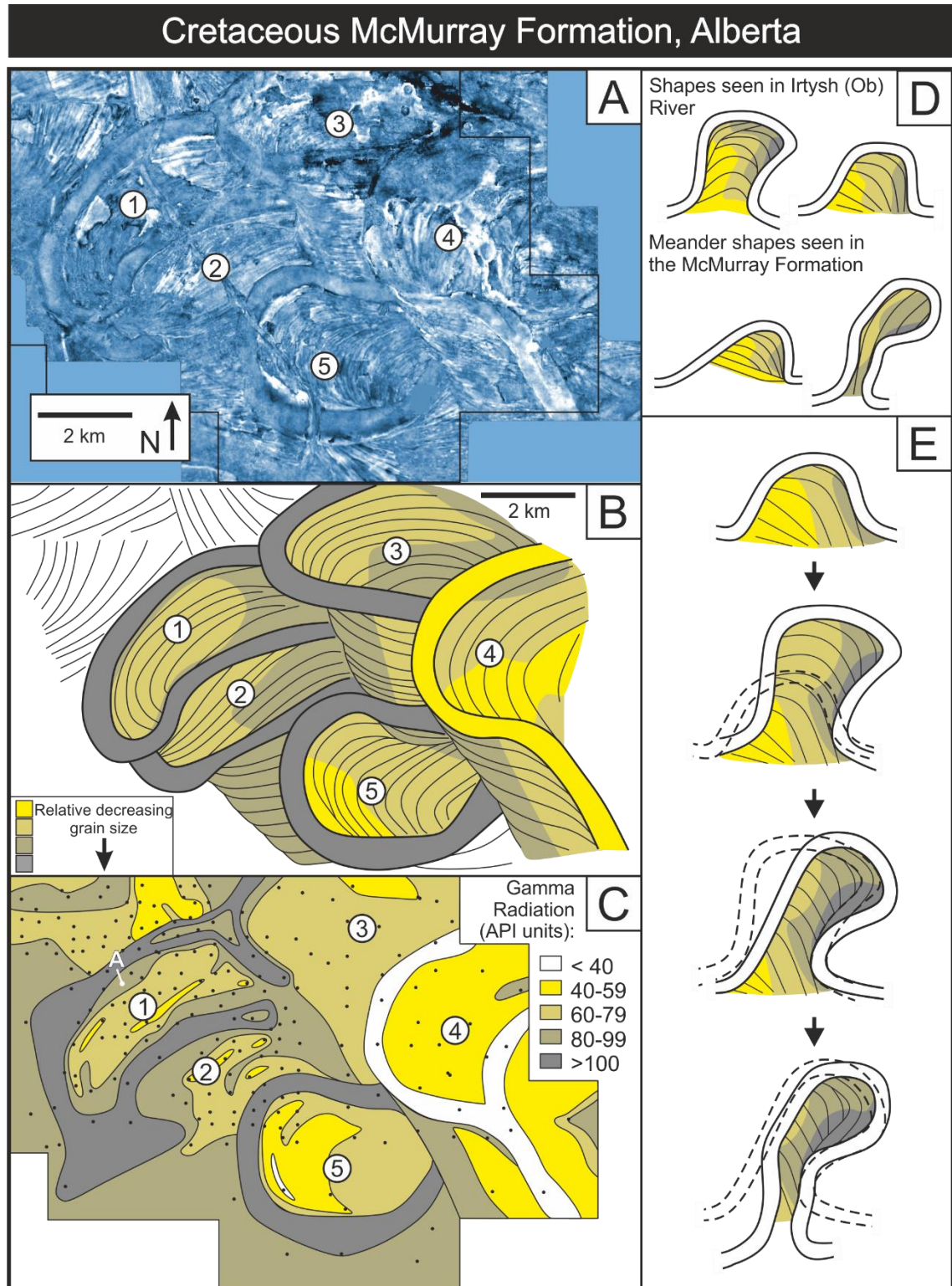


Figure 3.13 - A comparison of the interpretation of a seismic time slice from the Cretaceous McMurray Formation, Alberta between data compiled with this study, and the interpretation modified from Hubbard *et al.* (2011). The image is from Nexen's property lease of Lower Cretaceous meandering fluvial-dominated tidal estuary channel deposits

(Smith *et al.* 2009). A) Seismic data modified from Smith *et al.*, (2009); B) an interpretation of the data in A) made with use of data in this study; C) a gamma ray contour map constructed with data from 213 wells, modified from Hubbard *et al.* (2011). 'A' marks a location of mud clast facies as defined by Labrecque *et al.* (2011); D) common shapes seen in both the Irtysh (Ob) River and the seismic data of the Cretaceous McMurray Formation; E) An interpretation of the typical route by which a meander might grow in this system.

In Figure 3.13B, preserved point-bar architectural elements 1, 2 and 3 were interpreted to have scroll bar deposits oriented at angles, which are approximately 90° to where meander cut-off occurs, so were annotated as having a higher proportion of fines.

Preserved point-bar architectural elements 4 and 5 are extensional, and are annotated with a lower proportion of fines. Counter-point bars for meander loops 3 and 4 were constructed as fine-grained, heterogeneity types iii and iv (Smith *et al.*, 2009).

Meanders that underwent neck cut-off or chute cut-off experienced a different abandonment process to that of avulsion or channel abandonment, so they have been modelled with different lithologies. A neck- or chute cut-off results in oxbow lake development and the progressive filling of such lakes by fine sediment (heterogeneity types iii and iv); such bodies are modelled as relatively mud prone. A channel that infills due to chute cut-off or avulsion will contain a waning flow, therefore enabling sand-prone (heterogeneity types i and ii), asymmetric accretion (Toonen *et al.*, 2012), and when the flow ends, concentric filling of mud-prone sediment is observed (Schumm, 1960; Harms, 1982).

Figure 3.13C is a gamma ray contour map of the Cretaceous McMurray Formation, Alberta, constructed with data from 213 wells (Hubbard *et al.*, 2011). By comparing the measured data (Fig. 3.13C), with the predicted data (Fig. 3.13B), the strengths and weaknesses of the technique can be assessed. Figure 3.13B (predicted) shows a narrower fine-grained margin for preserved point-bars 1 and 3 than is seen in the



measured data. The measured data (Fig. 3.13C) shows small areas of less mud-prone material on the up- and downstream ends of the preserved abandoned channel of point-bar 1. This potentially indicates a slow abandonment process, which included the development of mid-channel bars, and a higher-than-expected proportion of channel-adjacent fine-grained material, though Labrecque *et al.*, (2011) recorded a mud-clast facies at label "A" (Fig. 3.13C), which would have offset the gamma-ray recording. This shows the new approach to be effective as it is able to help mitigate the effects of mud clasts and enable the overall heterogeneity to be revealed. Counter point-bars of preserved meanders 3 and 4 have different sand to mud ratios. The heterogeneity for preserved point bar 2 was predicted as analogous to preserved point bar 1 because the level of fragmentation and reworking does not enable a more refined analysis; for this reason the prediction for preserved point bar 2 uncertain. This assessment method provides a straightforward and cost-effective approach for predicting sub-surface heterogeneity.

### **3.7.2** *Limitations and future development*

The limitations of this study are that: (i) relative, rather than absolute, grain size is interpreted; (ii) the scroll-bar classification scheme is subjective in nature, though it is difficult to quantify and the method used has been shown to be widely applicable; and (iii) heterogeneity prediction (Fig. 3.6) contains a subjective (user) element, and although the rules have been clearly constrained, uncertainties for predictive models remain in relation to natural variability and limited knowledge thereof; these uncertainties may be reduced thanks to insight from future studies. However, this paper presents a novel, conceptual model which provides numerical modellers with a testable hypothesis.

### 3.8 Conclusions

A new approach to the assessment of meander morphology provides quantified metrics that enable the past and future growth of a point bar deposit to be inferred. This enables relative grain size to be predicted semi-quantitatively, an advantage over classic facies models. A higher degree of objectivity can be achieved with the application of the Intersection Shape methodology (Chapter 2), and the classification of the surface expression of scroll-bar morphology (Fig. 3.5), than with previous methods of meander shape change (Daniel, 1971; Hooke, 1984). A wider variety of morphometric variability is accounted for that leads to a less biased assessment of fluvial meandering reaches with less subjective comparisons between river reaches, through quantification of system elements. The methods is applied to 260 meanders from 13 globally distributed rivers from different environments. This has provided insights into the formative processes of different morphologies uncovered through assessment of migration styles and shape morphologies. Morphometric planform analysis (Figs 3.10 and 3.11) has allowed key features of a meandering reach to be better constrained.

Open symmetric (Group 4) shapes are the most abundant (39%), and downstream accretion by translation and rotation is the most typical mode of growth (Type 3.1). Open asymmetric and open symmetric shapes (Groups 1 and 4), are found in every meandering reach studied, whereas angular and bulbous shapes are absent in 8% of rivers studied. There is a very wide distribution of meander scroll type in the 260 studied meander shapes (Fig. 3.8), and the interrelationships of these to meander shape exhibit discernible trends, albeit with wide variability (Fig. 3.9). Identification of this variability can be used to construct a meander model (Fig. 3.6), by combining the shape, as identified using the Intersection Shape methodology, with the surface expression of the scroll-bar pattern, as identified with Figure 3.5. Through

understanding of the complex interrelationships of the meander geometries, the history of point-bar evolution may be reconstructed (Fig. 3.13E) and subsequently used to i) provide an understanding of this template for prediction of a preserved fluvial deposit (Fig. 3.13B), and ii) enable heterogeneity maps to be produced (Fig. 3.12). Each measured point bar may be used to aid in the composition of conceptual reservoir models to enable statistical limitations to be obtained for meandering features. Interpretation of meanders in a fluvial reach using both the Intersection Shape methodology, and the scroll-bar classification scheme, along with the character of a reach, allows a river to be described in a manner that can aid more accurate interpretation of the rock record.

## 4 Implications of the variation of mechanisms for fluvial abandonment on the stratigraphic record

### 4.1 Chapter Summary

Abandonment of meandering river reaches occurs through a variety of mechanisms, as observed in the study of modern fluvial systems. Three main types of river reach abandonment are recognised: (i) neck cut-off, where the up- and down-stream limbs of a meander bend join each other via bend tightening; (ii) chute cut-off, where a cut-through channel joins the up- and down-stream limbs of a meander; and (iii) avulsion, where a channel moves to a new location thereby abandoning its previous reach. Each cut-off type results in the development of an abandoned channel with particular morphological shape characteristics, and sediment infill with a distinctive facies succession. It is important to consider these characteristics when assessing the stacking styles and interconnectivity of accumulated sand-prone deposits of point-bars and channel fills in terms of their potential to act as reservoirs for hydrocarbons. To assess the styles of abandonment, a classification scheme is presented based on observations from 110 abandoned point-bar deposits from 11 different rivers; it includes styles that are documented in the literature, and observations made in this study. This classification divides cut-off types into those that lead to abandonment of an individual meander, and those that lead to abandonment of a reach of multiple meanders. Six types of individual cut-off, and 8 types of group cut-off are identified. The most common individual cut-off type is neck cut-off (52%), and the most common group stacking type is "nodal, unidirectional" (18%). It is found that rounded (1:1) and long (1:<1) shapes are almost equally prevalent in abandoned point-bars, suggesting that long (1:<1) shapes ought to be considered to a greater extent when constructing 3D geological models of ancient fluvial point-bar deposits. Individual reaches are assessed in detail through the methods outlined in this chapter, which enables

comparisons to be made and the relationship of a meander to its resultant point-bar deposit to be better understood. Abandoned point-bar deposits have a higher variability of length and width than active ones, and this variability should be more integrated into models of abandoned fluvial meandering systems.

## 4.2 Introduction

Active meandering fluvial systems are dynamic and episodically undertake substantial readjustments because of meander-loop abandonment (e.g. Fisk, 1947; Allen, 1965; Hooke, 2004; Camporeale *et al.*, 2005). The resulting amalgamated and cannibalised partial record of fluvial point-bar deposits is complex (Fielding & Crane, 1987; Mackey & Bridge, 1995; Miall, 2006), such that interpretation of past processes is not straightforward (Durkin *et al.*, 2015). Fluvial point-bar deposits tend to be sand-prone but with a heterolithic component (e.g. Allen, 1965; Thomas *et al.*, 1987; Gibling, 2006), because the grainsize of the sediment deposited decreases around a meander bend (Fustic *et al.*, 2012; chapter 3). Therefore, understanding and predicting the connectivity of point-bar deposits is important for prediction of reservoir quality and connectivity in hydrocarbon exploration (Fielding & Crane, 1987; Gibling, 2006), (Fig. 4.1A).

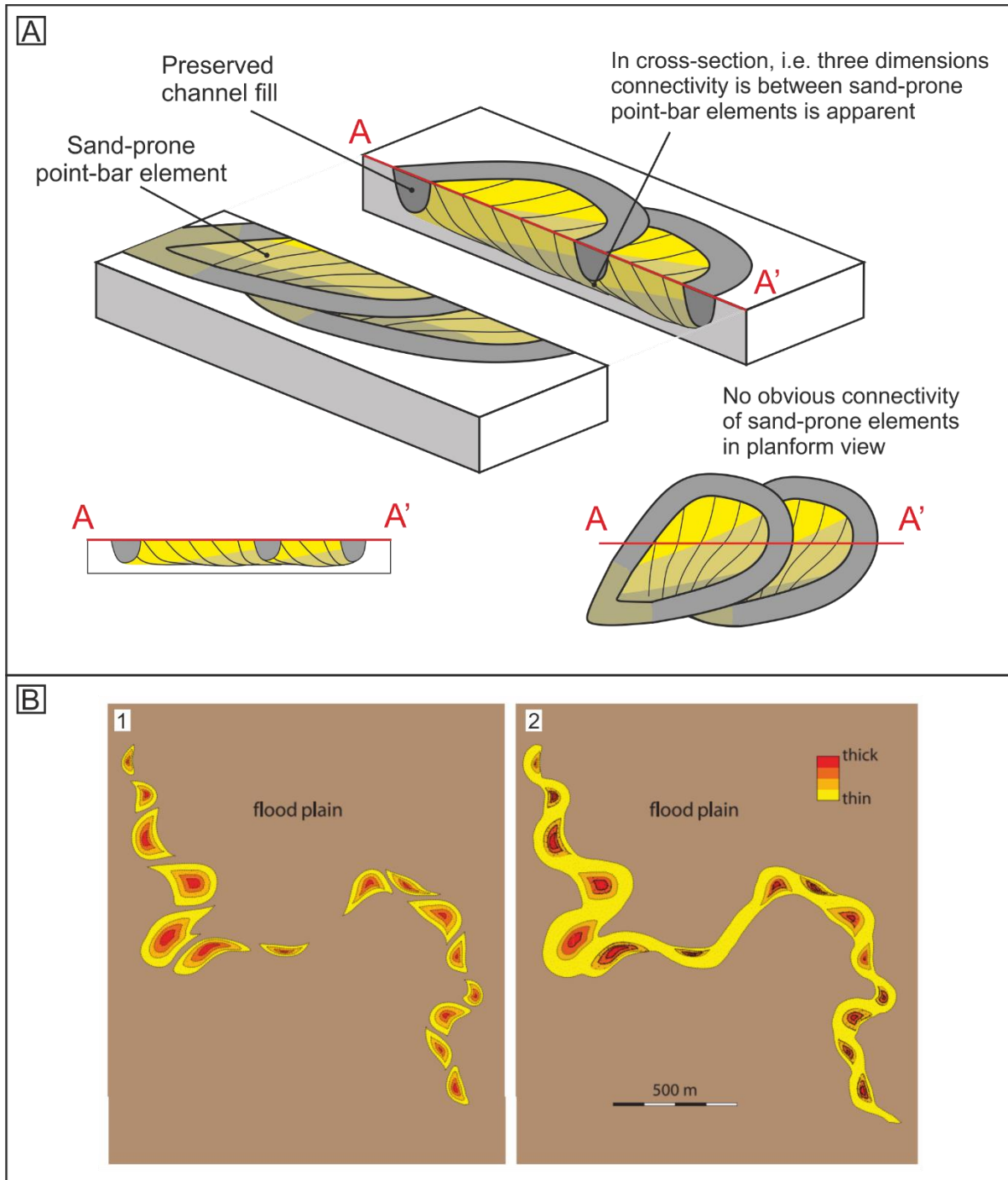
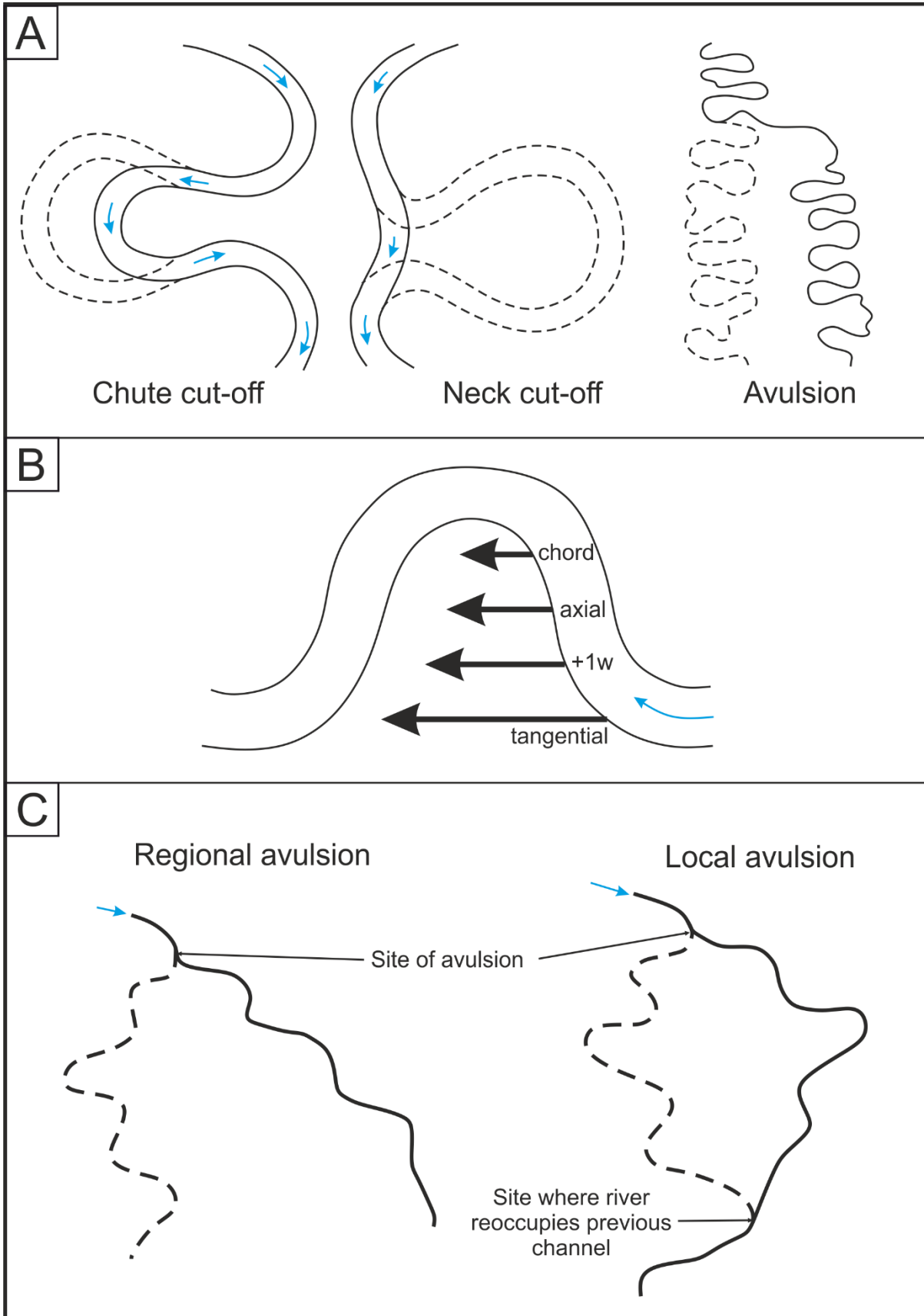


Figure 4.1 - A) A figure to demonstrate connectivity of sand-prone sediment in planform and cross-section; B) An isopach map of two scenarios for the spatial distribution of meandering river sandstone bodies, 1) the fluvial channel is filled with a clay plug when abandoned leading to disconnected sandstone bodies; 2) the fluvial channel floor is a clean, trough-cross-bedded sandstone leading to connected sandstone bodies in a “string-of-beads”(from Donselaar and Overeem 2008).

Modern, active fluvial systems provide a natural laboratory with which to study the processes of meander development and abandonment (Fisk, 1947; Erskine *et al.*, 1992; Gay *et al.*, 1998; Hooke, 2004; 2007). There are three main types of meander abandonment (Fig. 4.2A): (i) neck cut-off, where the inner banks of the up- and down-stream limbs are eroded until they converge and meet via tightening of a meander bend (Fisk, 1947; Mosley, 1976; Allen, 1965); (ii) chute cut-off, where the main channel flow splits and exploits a depression across the point-bar surface as a cut-through (Fisk, 1947; Kulemina, 1973; Brice, 1977; Lewis & Lewin, 1983; Gagalino & Howard, 1984; Hooke, 1984; Gay *et al.*, 1998), for example in response to high-stage flow (Matthes, 1948), or formation of a headcut gully (Gay *et al.*, 1998); and (iii) avulsion, where the meandering reach relocates from a common node (Fisk, 1947; Allen, 1965; Erskine *et al.*, 1992), due to processes that may be allogenic (El-Mowafy & Marfurt, 2016; Maynard, 2006) or autogenic (Aslan & Blum, 1999) in origin. A meander may also undertake bend flattening, which eliminates the meander loop by reducing sinuosity by primarily depositing sediment on the outer bank, rather than the inner bank (Matthes, 1948).





**Figure 4.2 - Prevailing models of cut-off in the literature: A) modified from Allen (1965), shows chute cut-off, neck cut-off and avulsion; B) modified from Lewis and Lewin (1983), shows the four modes of intra-bar cut-off, chord, axial,  $w+1$  (where the new channel is one channel width into the point-bar), and tangential); C) modified from Heller and Paola (1996), shows the two identified modes of avulsion as being local, and regional.**

Assessing the range of heterogeneity produced from combinations of 25 meander shapes (in 4 Groups), and 22 scroll bar patterns (in 8 Types; Chapter 3) allows a better understanding of the processes that have led to the accumulation of complex amalgamated deposits seen in the ancient record (Hubbard *et al.*, 2011). This can be used to estimate the overall lithologic heterogeneity of a point-bar deposit (Chapters 2 and 3), and is achieved by estimating the past positions of the meander apex to identify sand- and mud-prone areas. Where the secondary helical flow weakens on the inner bank (Jackson, 1975; Paola *et al.*, 1992), the proportion of sand-prone sediment tends to decrease downstream, and the proportion of mud-prone sediment tends increase (Bridge *et al.*, 1995; Fustic *et al.*, 2012). These trends may be used to inform predictive models (Chapter 3).

The overall aim of this study is to devise an informed technique for determining the cut-off style, lateral accretion history, and heterogeneity of fluvial point-bar deposits from limited data. Scientific research objectives are as follows: (i) to summarise the current understanding of the range of both individual, and group types of cut-off as discussed in the published literature; (ii) compare styles of cut-off in 11 studied river reaches, to assess the probabilities of occurrence, and to determine potential causative mechanisms; (iii) assess the preservation potential of point-bar deposits which have undertaken cut-off through different mechanisms; and (iv) to predict the likely lithofacies arrangements resulting from different mechanisms of cut-off for different meander, and scroll-bar, types.

## 4.3 Background

The geological record preserves abandoned fluvial point-bar deposits (Allen, 1965), some of which are clearly imaged in the subsurface using seismic methods and others of which are well expressed in outcropping successions (Fachmi & Wood 2005; Hubbard *et al.*, 2011; Ielpi *et al.*, 2014). However, there is a recognised disparity between the dimensions of active river meander loops, and the dimensions of point-bar architectural elements generated via the evolution of such meanders (Lewis & Lewin, 1983; Colombera *et al.*, 2017). This is of significance because point-bar deposits are sand-prone (Allen, 1965), and the process and mechanisms by which meander cut-off occurs influences the resultant shape of the abandoned body, and heterogeneity of the channel fill (Fisk, 1947; Allen, 1965, Erskine *et al.*, 1992, Toonen *et al.*, 2012).

### 4.3.1 Causes of meander cut-off

Meander cut-off is an autogenic process that occurs as a result of continual and progressive geometric adjustments (Fisk, 1947; Erskine *et al.*, 1992; Hooke, 2004), which cause individual meander loops to become overdeveloped and eventually cut-off (Fisk, 1947), such that the river reach episodically straightens. Cut-off processes are influenced by both autogenic and allogenic controls (Fisk, 1947; Rosgen, 1985; Gay *et al.*, 1998). Commonly identified autogenic controls are meander tightening over time, i.e. neck cut-off (Hooke, 2009), meander cut-off (Fisk, 1947), and avulsion (Bernard *et al.*, 1962; Smith *et al.*, 1989). Allogenic controls may be flooding frequency (Knighton, 1998), gradient (Schumm & Khan, 1972), climate (Alford & Holmes, 1985; Blum & Törnqvist, 2002), tectonics (Schwab, 1976; El-Mowafy & Marfurt, 2016; Ghinassi *et al.*, 2016), sediment calibre (Schumm, 1969; 1985), discharge variability (Fisk, 1947; Gay *et al.*, 1998), and subsidence rate (Ouchi, 1985). Meandering reaches may avulse due to dominantly allogenic changes (Blum & Törnqvist, 2002), although autogenic controls remain influential (Fisk, 1947; Allen, 1965), for example, a freely meandering fluvial

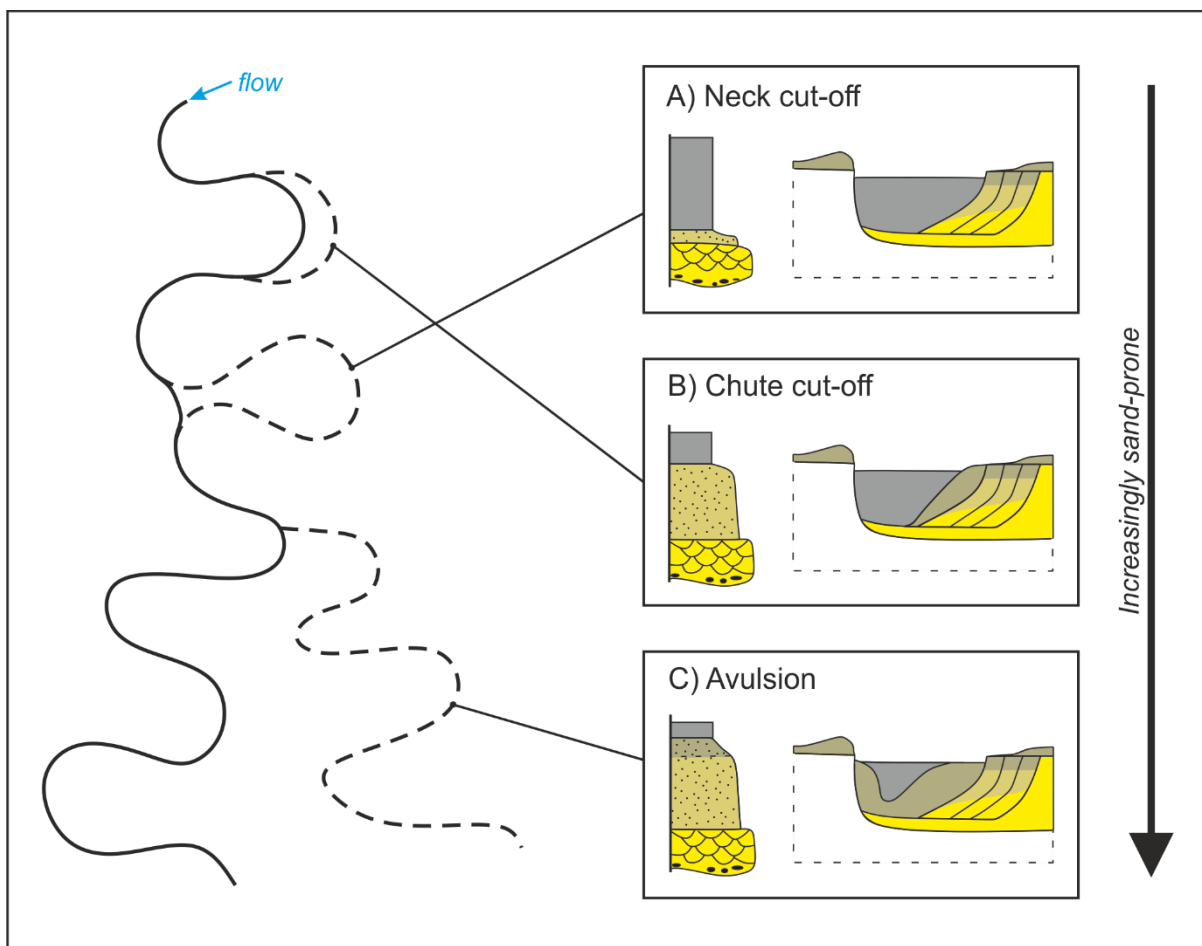
system in an area which is actively subsiding, will still undertake cut-off and meander abandonment due to the autogenic process of meander tightening and neck cut-off over time. When avulsion occurs, meanders in the reach may have previously undertaken individual loop cut-off, so all mechanisms ought to be considered.

Models and simulations of meandering fluvial processes provide valuable insights for understanding cut-off mechanisms (Camporeale *et al.*, 2005; Han & Endreny, 2014). For example, models show how cut-off results in an increase in the local gradient of the river bed (Han & Endreny, 2014), and a decrease in the resistance on the reach, in order to keep the reach as short and efficient as possible (Camporeale *et al.*, 2005). Meander cut-off is common in active fluvial systems across a range of rivers from different environments (Fisk, 1947; Lewis & Lewin, 1983; Hooke, 2004), and recently abandoned deposits are recognised as indicators of former channel conditions (Erskine *et al.*, 1992). Observations from modern rivers can be used to gain insight into the dominant controls that give rise to preserved successions (Bridge, 1993a; Miall, 2006; Engel & Rhoads, 2012; Lotsari *et al.*, 2014).

#### 4.3.2 *Channel fill*

When a meander loop is abandoned, the channel fills with sediment that may be preserved as a channel-fill element, adjacent to associated point-bar elements (Fig. 4.1A). It is important to assess this channel-fill lithology as it may be of varying heterogeneities that affect the connectivity of the sand-dominated point-bars (Donselaar & Overeem, 2008; Willis & Tang, 2010). Channel fills are variable, in terms of element geometry and facies arrangement and composition, in both fluvial successions in the rock record (Hubbard *et al.*, 2011), and in laboratory experiments (Peakall *et al.*, 2007). Channel-fill elements are overall upwards accreting (Davies, 1993), and generally upwards fining (Ielpi *et al.*, 2014), and may commonly transition from relatively “clean” sand at the base, to a mud plug fill at the top (Fisk, 1947; Allen,

1965; Harms, 1982; Erskine *et al.*, 1992; Davies, 1993; Donselaar & Overeem, 2008; Toonen *et al.*, 2012; Fig. 4.3). The channel fill in cross-section may be asymmetric and laterally accreting, or concentric (Gibling, 2006; Toonen *et al.*, 2012), which is dependent on the type of cut-off that occurred. Where a cut-off channel is still partly active and exhibits flow, accretion will tend to occur asymmetrically on one side of the channel (Gibling, 2006; Toonen *et al.*, 2012). Where a river (or meander loop) is subject to waning flow, such as in ephemeral rivers, symmetrical, concentric filling is common (Schumm, 1960; Schumann, 1989; Gibling *et al.*, 1998; Gibling, 2006; Fig. 4.3).



**Figure 4.3 - Solid lines are active channel courses, dashed represent abandoned ones. The log represents the vertical accretion which occurs post cut-off. Figure is a combination of Allen (1965), Harms (1982), Walker and Cant (1984), and Toonen *et al.***

(2012). The cross sections are from Toonen *et al.* (2012) who compiled them under the principles of accretionary phases in active and stagnant water resulting in lateral, or vertical accretion. A) is a generalised section for neck cut-off; B) is a generalised section for chute cut-off; and C) is a generalised section for avulsion.

The rate of channel filling is influenced by the diversion angle (Lindner, 1953; Bridge *et al.*, 1986; Fig. 4.4), i.e. the angle of difference between the old and new channel where the flow splits on the upstream limb. Where the flow splits is known as the flow separation zone where the initially unnatural change of direction leads to a more turbulent flow that loses energy and is prone to sediment deposition. Where the diversion angle is  $\leq 50^\circ$ , the former channel may infill five times faster, than if the diversion angle was  $>70^\circ$  (Kondolf, 2007). This is due to the diversion angle regulating the size of the flow separation zone, which in turn dictates the style of sedimentation in the former channel at the upstream end (Shields & Abt, 1989; Kondolf, 2007).

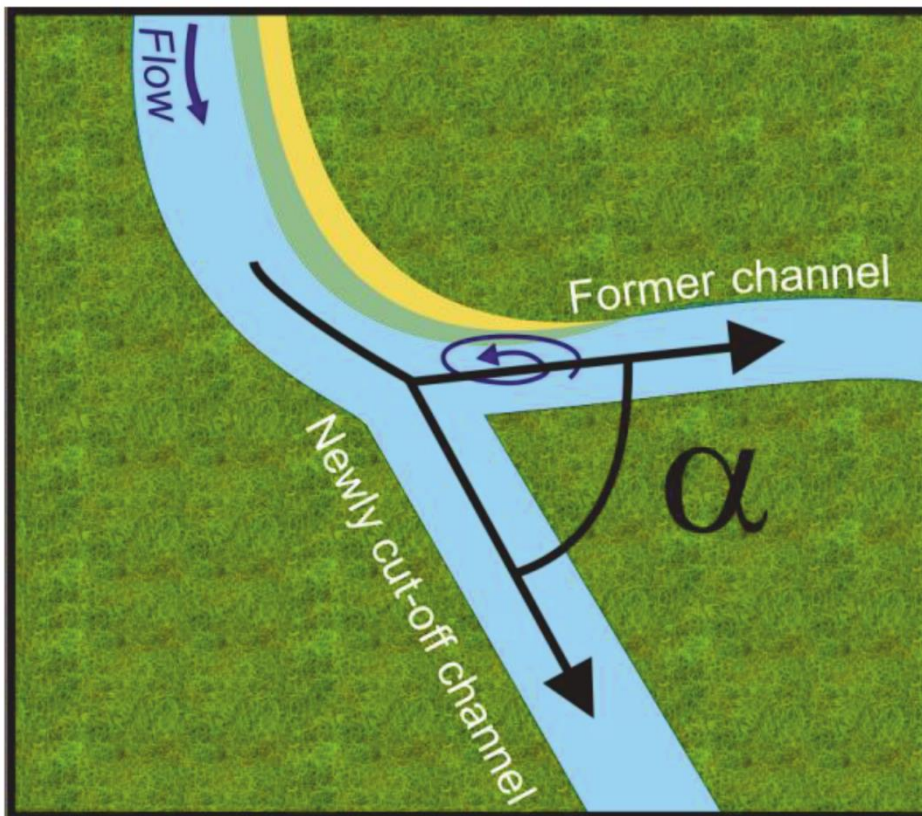


Figure 4.4 - Schematic representation of the diversion angle ( $\alpha$ ). From Dieras (2013), in turn adapted from Constantine *et al.*, (2010). The small flow whirl at the entrance to the former channel indicates the flow separation zone.

Where a diversion angle of  $\leq 50^\circ$  occurs, the channel-fill is typically composed of long bar deposits that grade vertically, and horizontally downstream, from coarse to fine. Where a diversion angle of  $>70^\circ$  occurs, a dominantly fine-grained vertical profile may be observed (Shields & Abt, 1989; Piegay *et al.*, 2002; Kondolf, 2007). Coarser-grained sediment typically accumulates more rapidly; therefore the diversion angle dictates the length of time that passes before cut-off and infill is complete (Fisk, 1947; Allen, 1965; Toonen *et al.*, 2012). With regard to the overall channel infill, persisting flow will tend to result in asymmetric lateral accretion of the channel fill, whereas an abandoned lake will usually be infilled by concentric, vertically accreted mud-prone fill (Toonen *et al.*, 2012). Therefore, where the diversion angle is high ( $>70^\circ$ ), a mud-prone deposit will ensue and take  $>100$  years to become infilled; where the diversion angle is lower

( $\leq 50^\circ$ ), a more sand-prone deposit will ensue and take  $<100$  years to become infilled (Fisk, 1947; Allen, 1965; Harms, 1982; Erskine *et al.*, 1992; Gibling, 2006; Donselaar & Overeem, 2008; Toonen *et al.*, 2012; Dieras, 2013). However, variations in these trends are common and this model is not universally applicable (Erskine *et al.*, 1992), and the timings for complete infill are dependent on the river size, load type, and load volume.

#### 4.3.3 Neck cut-off

Neck cut-off occurs when a meander bend tightens, becoming elongate and overdeveloped (Fisk, 1947; Allen, 1965; Erskine *et al.*, 1992; Toonen *et al.*, 2012). Where erosion on the inner banks of converging meander limbs continues (Mosley, 1976), the up- and down-stream limbs migrate closer together and may join, in some cases by forming a short chute channel that is one channel width long or less (Fisk, 1947; Allen, 1965; Guneralp & Marston, 2012). This process results in a reach with a shorter path and a steeper gradient (Han & Endreny, 2014), as a result of abandonment of the former active meander reach (Fisk, 1947; Crickmay, 1960; Allen, 1965; Erskine *et al.*, 1992). This process is observed in many rivers (Crickmay, 1960; Erskine *et al.*, 1992; Gagliano & Howard, 1984, Fig. 4.2).

##### 4.3.3.1 Abandoned channel shape and fill for neck cut-off

Where a meander undertakes neck cut-off there is typically a high diversion angle  $>70^\circ$ . This encourages rapid cut-off and abandonment of the meander loop (Fisk, 1947, Allen, 1965, Erskine *et al.*, 1992). Sand-prone plugs typically accumulate at either end of the abandoned loop due to the flow separation zone (Fig. 4.4), and the remainder is infilled over time with mud-grade sediment (Fisk, 1947; Allen, 1965; Harms, 1982). The plan-view shape of the channel-fill deposit that arises from a neck cut-off is typically strongly curved and almost forms a complete loop that can isolate the point-bar deposit developed within the central part of the meander loop (Allen, 1965). This can be

observed in modern (i.e. Schwenk *et al.*, 2015), and ancient (Hubbard *et al.*, 2011) fluvial systems (Fig. 4.5).

#### 4.3.4 Chute cut-off

The process of chute cut-off is more common than neck cut-off (Fisk, 1947; Kulemina, 1973; Brice, 1977; Lewis & Lewin, 1983; Gagalino & Howard, 1984; Hooke, 1984; Gay *et al.*, 1998). Chute cut-off arises where a channel path exploits point-bar depressions associated with ridge-and-swale topography on point-bar surfaces (Fisk, 1947; Bridge *et al.*, 1986; Gay *et al.*, 1998; Ghinassi, 2011; Zinger *et al.*, 2013; Van de Lageweg, 2014; Durkin *et al.*, 2015). Ridge-and-swale topography is the surface expression of accreted scroll bars, which form components of the point-bar (Fisk, 1947; Nanson, 1980). Lewis and Lewin (1983) sub-divided types of intra point-bar chute cut-off based their relative position to the meander loop. They may be: (i) tangential; (ii) one channel width into the point-bar from the tangential position ( $w+1$ ); (iii) axial, which cuts approximately midway along the length of the point-bar; or (iv) they may form a chord (Fig. 4.2B). Chute cut-offs typically initiate during high-stage flow (Matthes, 1948) and may form through (i) channel development from a headcut gully (Gay *et al.*, 1998; Moody & Meade, 2014), (ii) deposition of a second confining bank (Moody & Meade, 2014), or (iii) the piling up of water in the up-stream limb of the meander, which raises the water level to allow flow across the point-bar surface and thereby initiating chute channel development (Johnson & Paynter, 1967). As a chute channel evolves and grows, the primary active channel of the meander slowly becomes smaller and narrower as the chute channel becomes dominant (Fisk, 1947; Allen, 1965). Both the main channel and the cut-off channel can remain active for a substantial period of time once cut-off has occurred, because the angle of diversion down the chute channel is typically small, such that the redirection of flow is gradual (Fisk, 1947).



#### 4.3.4.1 Abandoned channel shape and fill for chute cut-off

Where a meander has undertaken chute cut-off, there is typically a low diversion angle  $\leq 50^\circ$ . In cases of chute cut-off, both channels tend to remain active for some time, which may be decades (Fisk, 1947; Allen, 1965; Harms, 1982; Erskine *et al.*, 1992; Toonen *et al.*, 2012). This results in coarse bedload sediment being transported around the chute-channel for longer, producing a sand-prone channel fill that is asymmetric in section view downstream (Fisk, 1947; Allen, 1965; Harms, 1982; Toonen *et al.*, 2012). The shape of the channel-fill deposit from a neck cut-off is typically a horseshoe-shaped loop (Toonen *et al.*, 2012), or an arc (Allen, 1965) that does not fully enclose the point-bar deposit. This can be observed in modern, and ancient (Fachmi & Wood, 2005) fluvial systems (Fig. 4.5).

#### 4.3.5 Avulsion

Avulsion is the process by which part (of a reach), of a meander belt is abandoned for a new course (Fisk, 1947; Allen, 1965; Erskine *et al.*, 1992; Heller & Paola, 1996). Avulsion is well documented in the modern and recent fluvial record (Fisk, 1947; Russell, 1954; LeBlanc & Hodgson, 1959; Anderson, 1961; Bernard *et al.*, 1962; Smith *et al.*, 1989). Avulsion is also well documented in the ancient rock record in the subsurface (Posamentier, 2001; Carter, 2003; Fachmi & Wood, 2005). A newly avulsed channel may be up to 80 km away from the original channel (Fisk, 1944). This has significant implications for the connectivity of larger-scale elements of sand-rich deposits (Heller & Paola, 1996). Through understanding the causative effects of meander avulsion, models can be compiled to enable predictions in stacking patterns and connectivity to be made (Leeder, 1977; Heller & Paola, 1996; Gibling, 2006). Physical requirements for avulsion to occur are a gradient advantage i.e. the river would preferentially flow on the steeper gradient (Davies *et al.*, 1993), and sufficient potential energy for a new path to be initiated and sustained (Lapointe *et al.*, 1998).

Factors that are known to have an influence on these requirements are: (i) growth fault activity (El-Mowafy & Marfurt, 2016); (ii) subsidence rates (Maynard, 2006); (iii) valley filling due to sea-level rise (Blum & Törnqvist, 2002); (iv) active reach movement to reoccupy older channel belts (Aslan & Blum, 1999; Blum & Törnqvist, 2002); (v) stage of bank retreat (Makaske *et al.*, 2012); (vi) rate of sediment accumulation (Heller & Paola, 1996); and (vii) effects of super-elevation of a channel belt (Mohrig *et al.*, 2000).

There are two broad categories defining the nature of an avulsion: regional and local (Heller & Paola, 1996), (Fig. 4.2C). Regional avulsion, or nodal avulsion occurs where the course of a meander belt is changed at a node (Fisk, 1947; Leeder, 1977; Cain & Mountney, 2009). Local avulsion is where a segment of the reach, which may itself be several kilometres in length and encompass multiple meander bends (Kulemina, 1973), avulses to a new area, but rejoins the main channel downstream (Davies *et al.*, 1993, Heller & Paola, 1996). Whether local or regional avulsion occurs is thought to be dependent on the distance and speed by which aggregation of sediment has occurred within the channel (Heller & Paola, 1996). If aggregation of sediment is occurring along the whole reach, as opposed to aggregation over a small area, then regional avulsion will tend to occur in preference to local avulsion (Heller & Paola, 1996). However, readily datable recent deposits need to be studied to test this working hypothesis (Törnqvist *et al.*, 1994). The frequency of avulsion may be measured to compare reaches and monitor change (Mackey & Bridge, 1995; Maynard, 2006; Willis & Tang, 2010), for example using time series aerial photographs. However, such analysis is beyond the scope of this study.

#### 4.3.5.1 Abandoned channel shape and fill for avulsion

If a meandering reach is abandoned through local or regional avulsion, the distribution of shapes and likelihood of different types of scroll-bar pattern will likely be similar to that of a modern active reach (Posamentier, 2001; Carter, 2003; Fachmi & Wood,

2005). Therefore, geometric analyses (such as measuring sinuosity, radius of curvature, meander belt width and channel width) can be undertaken in a similar manner to that which would be carried out on a modern reach (Hooke, 1984; Fachmi & Wood, 2005). Avulsion may be observed in both modern and ancient systems (Gulliford *et al.*, 2014) (Fig. 4.5).

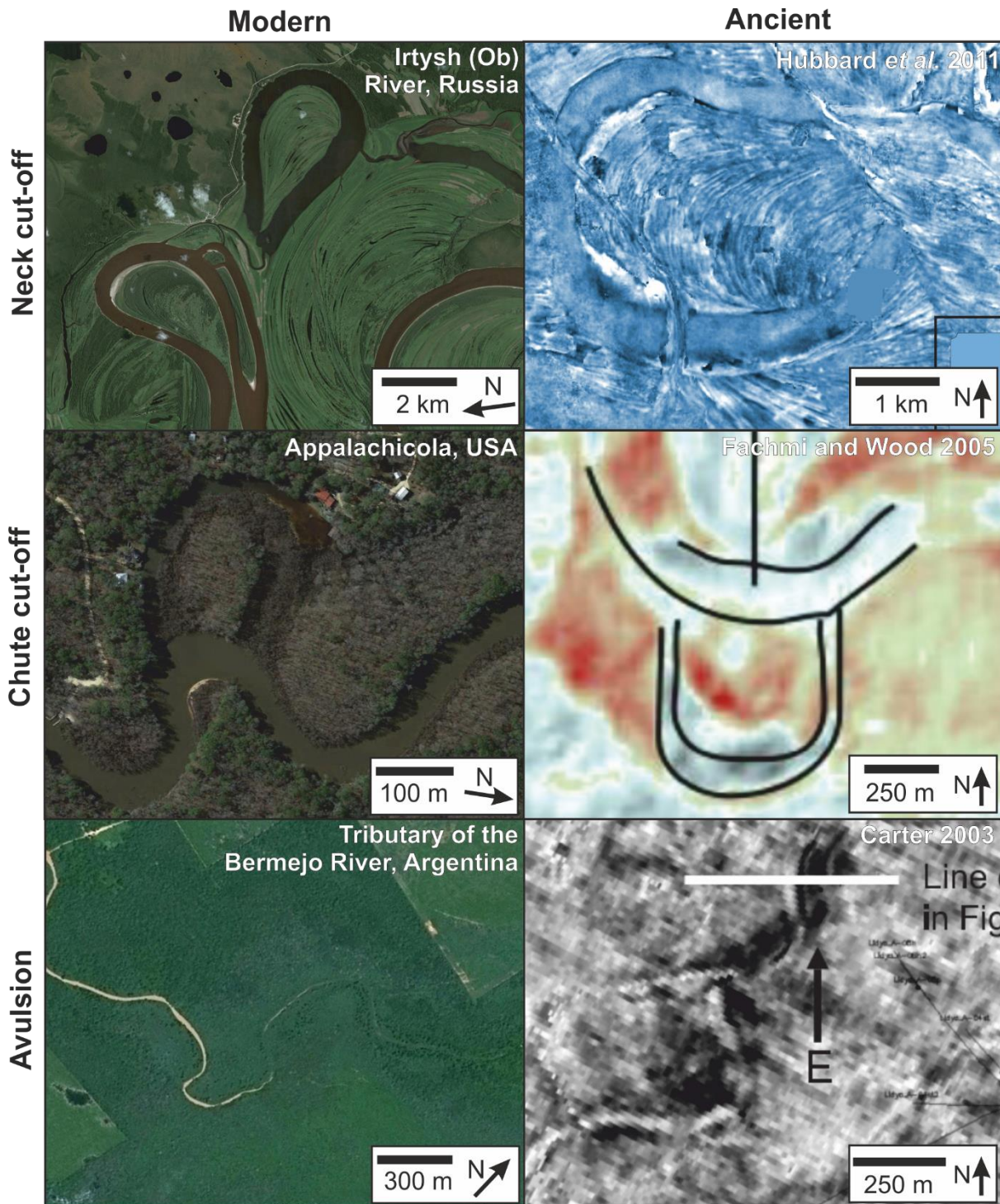


Figure 4.5 - A figure of modern examples of the prevalent mechanisms of cut-off alongside ancient examples of flattened seismic imagery. Imagery is taken from Hubbard *et al.* (2011), Fachmi and Wood (2005), and Carter (2003).

#### 4.3.6 *Styles of sandbody stacking*

Through understanding the lithological heterogeneity and lateral and vertical relational geometries of sand-prone fluvial elements, the reservoir potential of a fluvial deposit can be considered (Fielding & Crane, 1987; Gibling, 2006; Willis, 1993; Willis & Tang, 2010; Labrecque *et al.*, 2011; Colombera *et al.*, 2015). An avulsed, sand-rich channel can enhance inter-point-bar connectivity (Donselaar & Overeem, 2008; Willis & Tang, 2010). However if the abandoned channel is mud-prone, sandy point-bar deposits will be less well connected, as in the so-called “string-of-beads” model (Galloway, 1981; Donselaar & Overeem, 2008; Willis & Tang, 2010; Colombera *et al.*, 2017; Fig. 4.1B).

Meander loops undertake amalgamation and cannibalisation processes leading them to exhibit highly variable lateral and vertical stacking patterns (Mackay & Bridge, 1995; Gibling, 2006). It is useful to consider the stacking style in a point-bar succession because it affects the lateral and vertical connectivity of sand-rich point-bar bodies (Gibling, 2006; Donselaar & Overeem, 2008; Colombera *et al.*, 2015). Lateral and vertical connectivity of sand-prone sediment depends on: (i) style of meander cut-off (Fisk, 1947; Allen, 1965; Erskine *et al.*, 1992); (ii) heterogeneity distribution in the point-bar deposit (Thomas *et al.*, 1987; Fustic *et al.*, 2012; Chapter 3); (iii) heterogeneity of the channel fill (Fisk, 1947; Allen, 1965; Harms, 1982; Erskine *et al.*, 1992; Toonen *et al.*, 2012); (iv) relative positions of the amalgamated point-bar bodies (Thomas *et al.*, 1987; Gibling, 2006; Donselaar & Overeem, 2008); (v) plan-form shape of the point-bar deposit (Shanley, 2004; Chapter 2); (vi) amount of overlap of laterally and vertically adjoining point-bar deposits (Gibling, 2006); and (vii) subsidence rate of the floodplain and fluvial system (Blum & Törnqvist, 2002).

#### 4.3.7 *Lithological heterogeneity of abandoned point-bar deposits*

The heterogeneity of a single point-bar deposit is variable (Labrecque *et al.*, 2011; Fustic *et al.*, 2012; Durkin *et al.*, 2015), and is affected by the mode of growth by which

the body accreted (Chapters 2 and 3). The thickness of a point-bar deposit varies dependent on the mode of growth, as this dictates the position of the most erosive flow (Willis & Tang, 2010). Packages of alternating mudstone and sandstone beds are known as inclined heterolithic strata (IHS), and such packages of strata are common in fluvial point-bar deposits (Thomas *et al.*, 1987). The presence of IHS affects the lithologic heterogeneity of the point-bar element and can markedly influence fluid flow pathways in hydrocarbon production (Thomas *et al.*, 1987; Labrecque *et al.*, 2011).

Prediction of the distribution of heterolithic (mud-prone), and sand-prone deposits in a fluvial point-bar deposit can be achieved through reconstructing past meander shapes by using positions of past meander apices (Chapter 3). This method is based on the assertion that when the meander bend was active, the helical flow strengthened at the bend apex, causing a weaker secondary helical flow on the inner bank (Leopold & Wolman, 1960; Nanson, 1980; Thompson, 1986; Roberts, 2014). The lateral, and vertical anisotropy of fluvial velocity causes the proportion of sand-prone sediment to decrease downstream, whereas the proportion of mud-prone sediment increases downstream (Bridge *et al.*, 1995; Fustic *et al.*, 2012).

In active meandering systems, 25 meander shapes identified and assigned to four Groups, and 22 scroll-bar patterns are identified and assigned to 8 Types (Chapters 2 and 3). These classifications enable known morphologies to be detected and recorded and are valuable for heterogeneity analysis of a fluvial meandering reach. The proportions of meander shape and scroll-bar pattern (Chapter 3), may be directly related to meandering reaches that have been abandoned via avulsion, because an avulsed system maintains a record of its geometry from the time when it was active (Posamentier, 2001; Carter, 2003; Fachmi & Wood, 2005).

## 4.4 Methodology

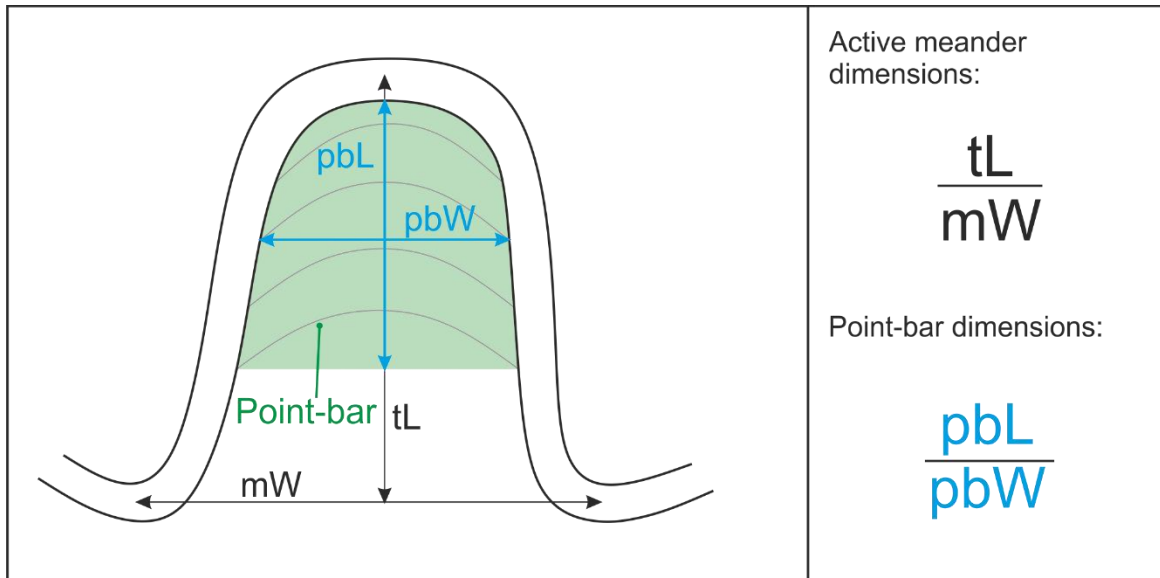
To assess the complexity and variability of planform geometries of abandoned meander point-bar deposits, effective observation must be constrained from a variety of recorded parameters. The primary focus of this work is to determine the dimensions and lithological heterogeneity of point-bar deposits, which have undertaken meander cut-off.

### 4.4.1 Recorded parameters

Measurements of the dimensions of meander shape and the active point-bar are recorded (Lewis & Lewin, 1983; Colombera *et al.*, 2017). For each point-bar deposit, the length and width has been measured, because length and width are metrics that are easily transferable between active, and abandoned point-bar deposits.

#### 4.4.1.1 Active meanders

An active meander is defined as a channel bend within which the primary flow of the river is in its channel. The shape of an individual bend is quantified through use of the Intersection Shape methodology (Chapter 2). In this chapter the ratio of meander width (mW), and meander length (tL), is used to determine the dimension of the meander (Fig. 4.6).



**Figure 4.6 - A description of the dimensions and ratios used in this study; meander width (mW) and meander length (tL), are used to determine meander dimensions; point-bar length (pbL), and point-bar width (pbW), are used to determine point-bar dimensions. The pale grey lines represent scroll-bars that are used to calculate tL.**

#### 4.4.1.2 Active point bars

The inner bank of an active meander bend may comprise previously deposited and partly cannibalised point-bar deposits. The measured point-bar is one that is actively accreting from a meander bend, and may be traced through its accretion process, i.e. the direction and history of the point-bar accretion. The dimensions of the point bar are determined through measurements of the point-bar length (pbL), and point-bar width (pbW), (Fig. 4.6).

#### 4.4.1.3 Abandoned point-bar deposit

An abandoned point-bar deposit is what remains after meander cut-off has occurred. The dimensions of an abandoned point-bar deposit are measured using the same method as for an active point-bar (pbL and pbW, Fig. 4.6). Where a partial point-bar fragment is seen, this is measured in the same way. In order to determine the length (pbL), the direction of cut-off must be resolved through studying other meanders along



the reach that are in the process of abandonment. To define the width (pbW),  $\frac{1}{2}$  pbL is determined, and the width measured across the point-bar deposit at this mid-point of pbL. Where less information is available in ancient successions, informed decisions may be made with regard to interpreting cut-off mechanisms in the ancient record.

#### 4.4.2 *Styles of meander abandonment*

Few previous attempts have been made to classify the complete range of meander cut-off types (Erskine *et al.*, 1992). Effective observation and understanding of planform geometries should be undertaken (Miall, 2006; Engel & Rhoads, 2012; Lotsari *et al.*, 2014) to compile a comprehensive understanding of cut-off mechanisms. This study assesses the mechanism by which meander abandonment occurs, classifies the shape of the reach post cut-off, and identifies its associated characteristics, i.e. the proto-meander, or initial meander shape of the subsequent meander. Most simulations and models of fluvial meandering systems commence with an already established sinusoidal shape (e.g., Leopold & Wolman, 1960; Daniel, 1971; Willis & Tang, 2010), whereas few models commence growth from a relatively straight reach (Lewin, 1976; Thompson, 1986). In modern systems, growth of a meander may initiate from a relatively straight reach, or an already sinuous channel, therefore both proto-meander types are allowed for in this study, i.e. straight and slightly sinuous.

The variety of meander abandonment style impacts the heterogeneity and dimensions of the resultant geological deposit. Therefore, assessing the variety of abandonment forms is critical to understanding these effects. Polarised meander growth (Fig. 4.7D) depicts how a meander can grow in the opposite direction to its previous growth direction, as a result of bend flattening (Matthes, 1948), after meander cut-off.

Polarised meander growth is recorded in the classification, but is not sufficiently common to present substantiated results, and has not been evaluated in this study. In

this classification, individual, and grouped cut-off types are differentiated. This enables the geological impacts to be considered at different scales.

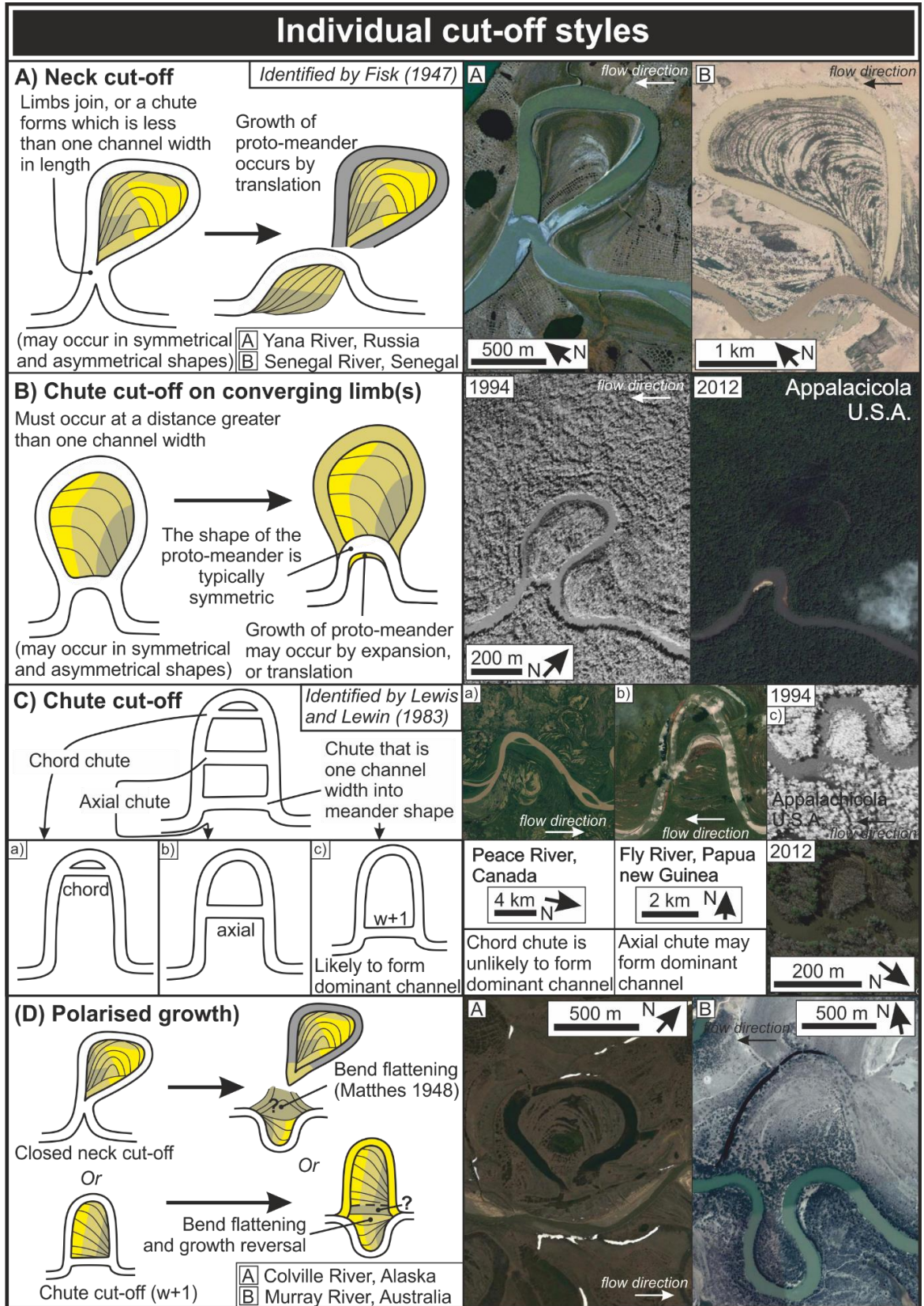


Figure 4.7 - Individual cut-off styles; four referenced examples including their proto-meanders to assess the implications of the variations of growth. The shapes and scroll-bar patterns shown here are simply to demonstrate the principles; a full range of shape and scroll-bar pattern may undertake these cut-off styles, though some are more common than others. The type of heterogeneity associated with bend flattening (D), has been estimated as mud-prone as it forms in a similar process to a counter point-bar.

## 4.4.2.1 Individual cut-off types

Style	Description	Geological significance
Neck cut-off (Fig. 4.7A)	Occurs where the up- and down-stream limbs converge and meet, or a short chute channel forms, which is one channel width long (Fisk, 1947; Allen, 1965; Guneralp & Rhodes, 2012). The proto-meander is typically an angular shape (Group 2), though bend flattening (Matthes, 1948) may occur, forming an open symmetric shape (Group 4). Initial migration of the proto meander is most likely translating.	Neck cut-off forms a high diversion angle ( $>70^\circ$ ) (Kondolf, 2007). The cut off will usually occur rapidly. The neck area will typically be infilled with sand-prone deposits, and the abandoned loop will typically slowly infill with mud-prone deposits. The abandoned point-bar deposit is enclosed by a channel-fill deposit.
Chute cut-off on converging limb(s) (Fig. 4.7B)	Occurs where the up- and downstream limbs converge, and a chute channel forms, which is longer than one channel width. The proto-meander is typically an open symmetric shape (Group 4), and may initially accrete through expansion, though accretion through translation is most common.	There will likely be a diversion angle ( $>70^\circ$ ), as there is a chute cut-off in a bulbous shape. Therefore, the channel fill may be mud-prone. The plan-view shape of the point-bar deposit is more rounded, and the channel fill does not entirely enclose the point-bar deposit, as the neck remains

		open, leaving the point-bar as vulnerable to erosion, as it is sand-prone and near an active channel.
Chute cut-off (Fig. 4.7C)	Occurs where the meander limbs are not converging, and a channel is formed across the point-bar, joining the up-and down-stream limbs. The three types of cut-off considered in this study are: (i) chord chute cut-off; (ii) axial chute cut-off, and; (iii) chute cut-off one channel width into the meander shape. Tangential cut-off is the fourth type of cut-off identified by Lewis and Lewin (1983), (Fig. 4.2B); however, no examples of this are documented in this study.	Different styles of chute cut-off have different geological implications: (i) chord chute cut-off may form a sand-prone deposit, though it is unlikely to become the primary channel; (ii) axial chute cut-off may evolve to be the primary channel, and where it does, may cannibalise the remaining point-bar deposit. The channel fill will typically be sand-prone as there is a low diversion angle between the primary and chute channel flows (Fisk, 1947), and both channels may remain active for some time after initial cut-off; (iii) chute cut-off one channel width into the meander shape ( $w+1$ ) will typically become dominant. It leads to growth from a relatively straight reach, as opposed to continuing growth on an already sinuous reach. The point-bar deposit from chute

		cut-off one channel width into the meander shape (w+1) is more likely to be preserved than axial cut-off. The diversion angle is low; therefore, both channels may remain active for some time following initial cut-off, leading to a sand-prone channel fill (Toonen <i>et al.</i> , 2012; Dieras, 2013).
Polarised growth (Fig. 4.7D)	May occur after cut-off, where the proto-meander grows in the opposite direction after bend flattening where the meander loop is flattened and eliminated (cf. Matthes, 1948), leading to polarisation (i.e. growth in the opposite direction), of the subsequent meander bend growth.	The deposit left by bend flattening may be sand- or mud-prone. More research needs to be undertaken to establish likely facies arrangements.

**Table 4.1 - Definitions of individual cut-off types and their geological implications. Also see Figure 4.7.**

#### 4.4.2.2 Group stacking types

A group stacking style refers to repeated abandonment processes, which lead to sets of abandonment types (i.e. time-consecutive point-bar deposits that were abandoned by the same process). Each mechanism may occur in a variety of shapes and scroll-bar pattern. Here, shapes and scroll-bar patterns have been selected to demonstrate the implications for sand-body connectivity. Some of these types are termed “overlapping”, which means that they partially erode previously deposited point-bar deposits, and now overlay them.

Each of these types may or may not lead to interconnected sand-prone deposits, depending on the type of cut-off undertaken, and the inter point-bar architecture: for example if the meander has become abandoned through neck cut-off, then the channel-fill deposits will likely be mud-prone which will reduce the interconnectivity of the point-bar deposits (Fisk, 1947; Toonen *et al.*, 2012). Also, if the meander has undertaken downstream accretion, then the point-bar deposit will typically be less sand-prone sediment that may be interconnected (Chapter 3).

Each type of development is complex and may be described in terms of overall traits that determine the group growth style; the behaviour of the proto meander is instrumental in these processes. The whole length of a new meander loop may overlap with the genetically related point-bar deposit (Fig. 4.8A), when the proto-meander translates upstream and evolves into a meander that overlaps the one that has been previously deposited. Part of the channel fill is removed in this process. The whole length of a new meander loop may form and not be overlapping a previous point-bar deposit (Fig. 4.8D), when the proto meander is able to translate a sufficient distance that allows for isolated point-bar deposits to occur. Figure 4.8F shows isolated point-bar deposits that are different to figure 4.8D because they are not genetically related; they appear to form discrete units though the vegetation may be obscuring previously

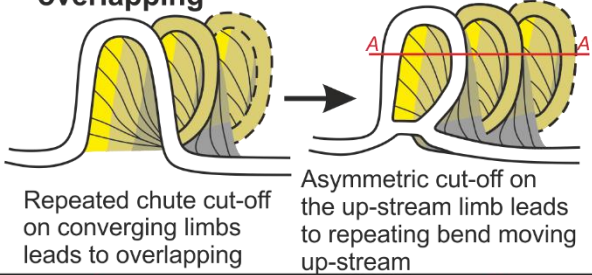


deposited point-bar deposits. Point-bar growth may extend from the meander apex in a multi- or unidirectional manner (Figs 4.8B and C). The differences in these deposits may be due to the distribution of mud- and sand-prone sediment, as sand-prone sediment is more easily eroded. Figure 4.8E shows overlaying, partially cannibalised point-bar deposits that may be thought to be sand-prone because the shapes don't appear limited by differential erosion. Avulsion is a complex process within which there may be a great range of causative processes; therefore regional or local avulsion will occur dependant on the controls at that time.

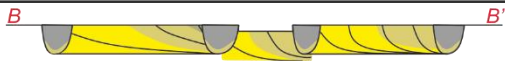
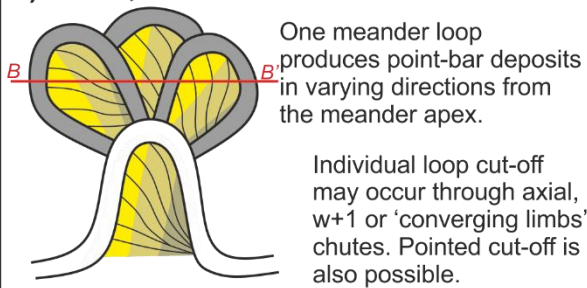
## Group stacking styles

### A) Whole length, overlapping

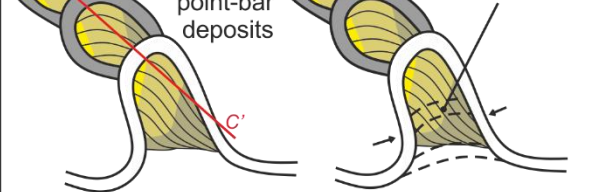
Thomas et al. 1987



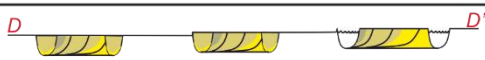
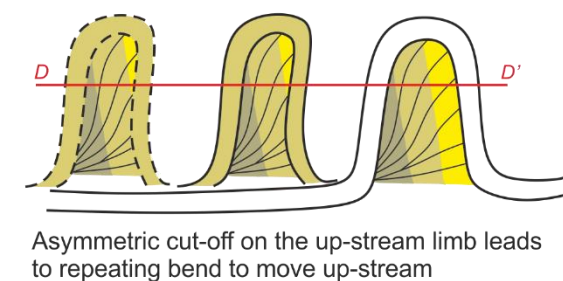
### B) Nodal, multidirectional



### C) Nodal, unidirectional



### D) Whole length, not overlapping





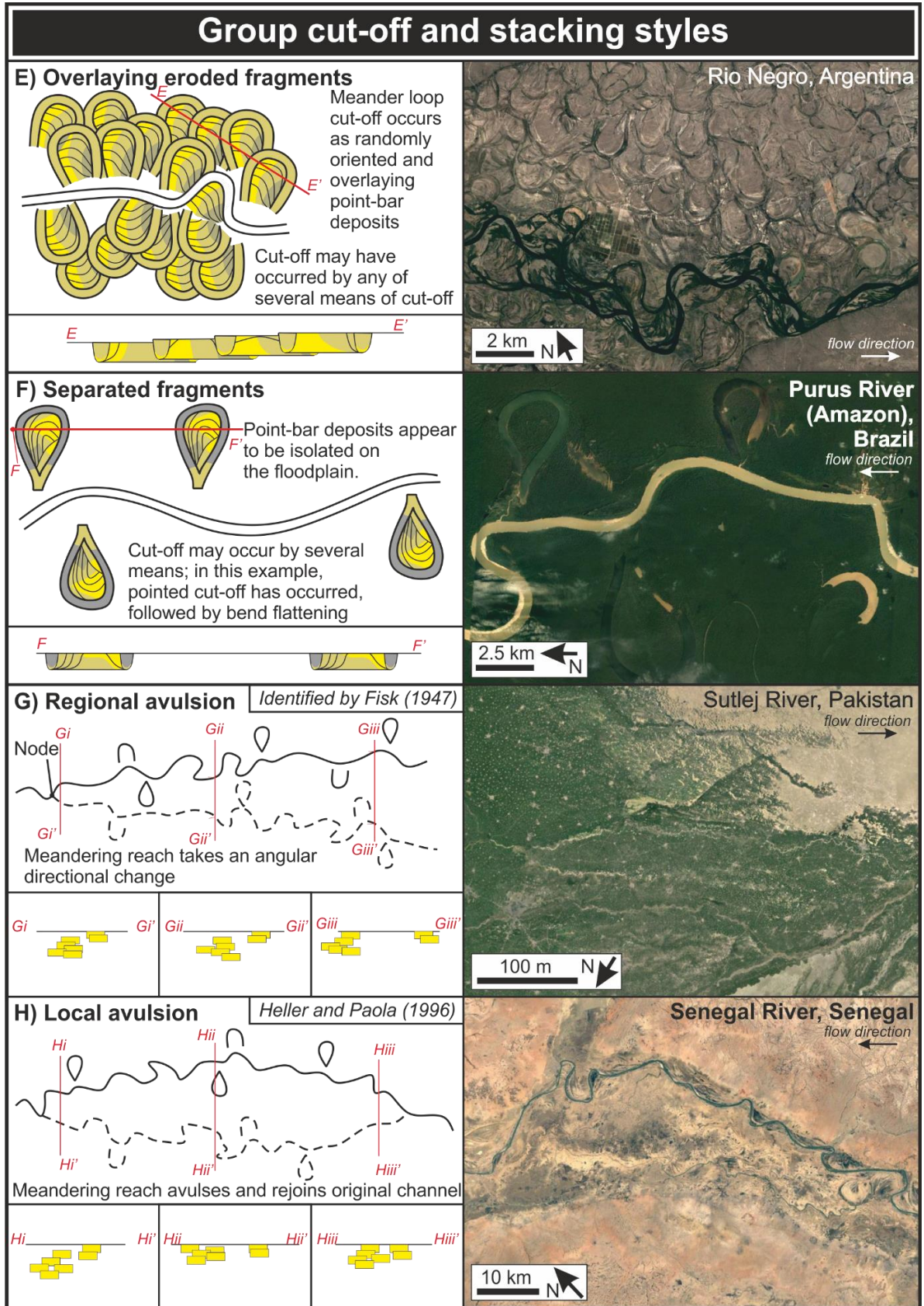


Figure 4.8 - Group cut-off styles; eight referenced examples including hypothetical cross-sections to assess the implications of the variations of style. The shapes and scroll-bar patterns demonstrated here are simply to demonstrate the principles; a full range of shape and scroll-bar pattern may undertake these group cut-off styles, though some are more probable than others.

Style	Description	Geological significance
Whole length, overlapping (Fig. 4.8A)	Where meanders overlap and partially cannibalise previously deposited point-bar deposits along their length. This leads to overlapping lengths.	Depending on the style of cut-off, and the mode of accretion in the point-bar, this style can lead to interconnected sand-prone deposits.  In Fig. 4.8A, chute cut-off on converging limbs has been attributed to scroll-bar pattern T3.1 (Chapter 3).
Nodal, multidirectional (Fig. 4.8B)	Where one meander loop subsequently produces overlapping point-bar deposits, which overlap from the meander apex in different directions in a fan-like pattern.	Depending on the style of cut-off, and the mode of accretion in the point-bar, this group style could lead to interconnected sand-prone deposits.  In Fig. 4.8B, neck cut-off has been attributed to scroll-bar pattern T3.1 (Chapter 3).
Nodal, unidirectional (Fig. 4.8C)	Where one meander loop subsequently produces overlapping point-bar deposits, which overlap in a single direction from the meander apex. This leaves an elongate deposit.	Depending on the style of cut-off, and the mode of accretion in the point-bar, this group style could lead to interconnected sand-prone deposits.

		In Fig. 4.8C, neck cut-off has been attributed to scroll-bar pattern T3.1 (Chapter 3).
Whole length, not overlapping (Fig. 4.8D)	Where meander loops abandon point-bar deposits in a disconnected trail.	This group style is unlikely to lead to interconnected deposits, i.e. the sand-prone point-bar deposits are unlikely to amalgamate. In Fig. 4.8D, w+1 chute cut-off has been attributed to scroll-bar pattern T3.1 (Chapter 3).
Overlaying eroded point-bar deposits (Fig. 4.8E)	Where meander loops overlap each other in a repeatedly cannibalised deposit.	This group style is likely to lead to interconnected sand-prone deposits. Gaining improved understanding of the style(s) of cut-off, and modes of accretion of the point bars, enables the extent of interconnectivity to be better explored. In Fig. 4.8E, chute cut-off has been attributed to scroll-bar pattern T3.1 (Chapter 3).
Separated point-bar deposits	Where meander loops abandon point-bar deposits as lone disconnected point-bar deposits.	There is only a planview image available, so deposits appear to be isolated though this may be due to a rapid accumulation rate and

(Fig. 4.8F)		<p>covering vegetation. The cross-section constructed only depicts what is visible in planform.</p> <p>This group style is unlikely to lead to interconnected deposits, i.e. the sand-prone point-bar deposits are unlikely to amalgamate.</p> <p>In Fig. 4.8F, neck cut-off has been attributed to scroll-bar pattern T6.1 (Chapter 3).</p>
Regional avulsion (Fig. 4.8G)	Where a meandering reach avulses to a new region as an angular adjustment around a node (Fisk, 1947; Leeder, 1978; Heller & Paola, 1996).	The interconnectivity of the sand-prone channel bodies and associated point-bar deposits leads to channel stacking patterns that may be considered at a larger scale (Heller & Paola, 1996; Gibling, 2006).
Local avulsion (Fig. 4.8H)	Where a meandering reach avulses to a new region and grows to re-join the original channel (Fisk, 1947; Heller & Paola, 1996).	The interconnectivity of the sand-prone channel bodies and attributed point-bar deposits is unchanged from normal regional avulsion (Fig. 4.8G), but in the locally altered area, there is a change in vertical stacking pattern (Heller & Paola, 1996).

**Table 4.2 - Definitions of group cut-off types and their geological implications. Also see accompanying Figure 4.8. In Figure 4.8, the scroll-bar and shape variations are selected and used to demonstrate an example, though is important to note that many shape and scroll-bar styles are possible.**



#### 4.4.3 *Scroll-bar type*

The style of scroll-bar pattern is determined through subjective observation using the categories of type outlined and justified in Chapter 3. There are 22 sub-types, which are assigned to 8 Type categories.

### 4.5 Results

The dimensions of 110 abandoned point-bar deposits have been measured and assessed from 11 rivers, with 10 measured from each: Ok Tedi (Fly) River, Papua New Guinea; Senegal River, Senegal; Murray River, Australia; Yana River, Russia; Colville River, Alaska; Kuskokwim River, Alaska; Mississippi River, USA; Amazon River, Peru; Irtysh (Ob) River, Russia; Kolyma River, Russia; Brazos River, USA (Table 4.1, Chapter 3). It is important in this study to consider the geometries of active point-bar deposits, as these are the dimensions that may be seen in avulsed fluvial channels. Measurements of point-bar dimensions were taken from the point-bars studied in Chapter 3. A difference has been found between the planform dimensions of active meanders and active point bars. This relationship is represented in Figure 4.9A where the majority of meander dimensions are wider than they are long ( $1:>1$ ), with fewer longer than they are wide ( $1:<1$ ). The active bars display a wider distribution of dimensions and are dominated by 1:1 shapes with near equal proportions of wide ( $1:>1$ ), and long ( $1:<1$ ) shapes (Fig. 4.10A). Figure 4.9B demonstrates that there is a positive relationship between the dimension of an active meander and its associated point-bar ( $y = 0.2733x + 0.4315$ ). The Pearson correlation R value is 0.5546, which indicates a moderate positive correlation; the Pearson correlation p value is  $<0.00001$  indicating that the correlation is significant at  $p < 0.10$ .

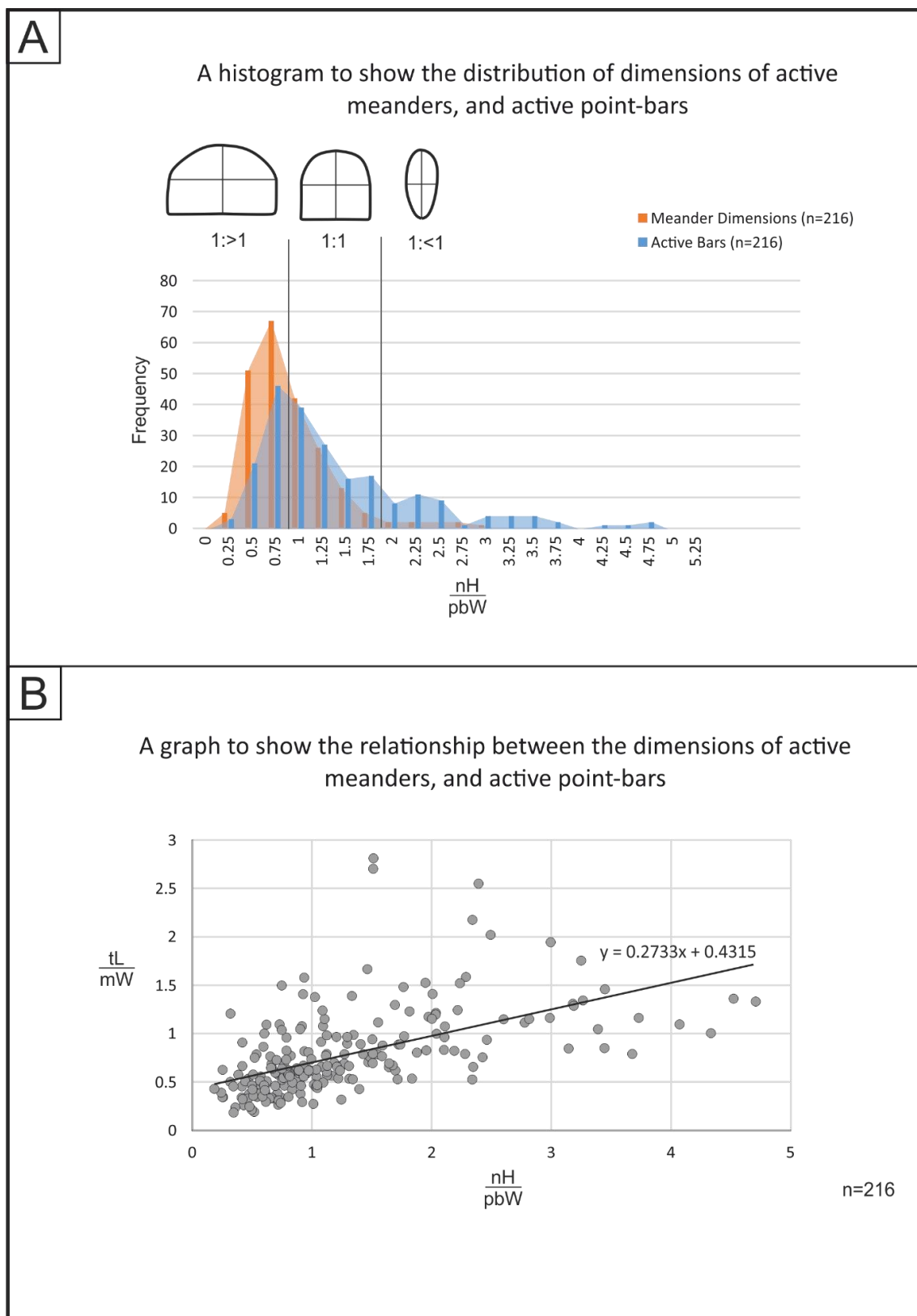


Figure 4.9 - A) A graph showing the comparative distributions of point-bar shape dimensions for 216 meander shapes; B) A graph showing a predictive relationship between the dimensions of an active meander shape, and an active point-bar shape.

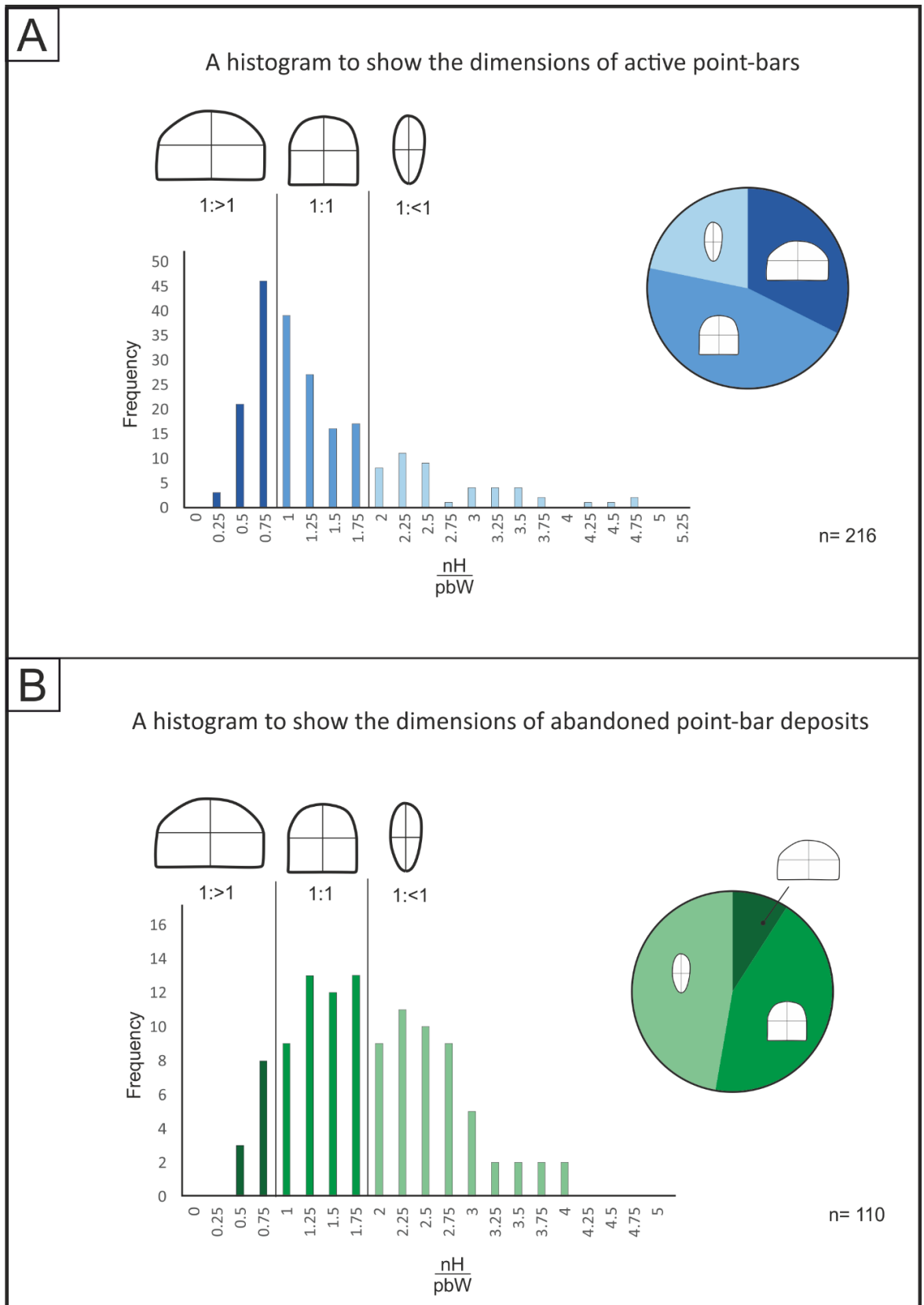


Figure 4.10 - A) A histogram showing the dimensions of active point-bars; B) A histogram showing the dimensions of abandoned point-bar deposits.

Point-bar deposits commonly occur as fragments nested within flood plain deposits, as a result of different styles of meander cut-off and abandonment. The 110 abandoned point-bar deposits measured herein show fewer wide ( $1:>1$ ) shapes than in active meanders and point-bars, and almost equal proportions of round ( $1:1$ ), and long ( $1:<1$ ) shapes (Figure 4.10B). Figure 4.11 shows that the wide abandoned point-bar deposit ( $1:>1$ ) shapes are likely to occur in association with both chute cut-off (both axial and  $w+1$  cut-off), and closed neck cut-off; rounded shapes ( $1:1$ ), are equally likely to occur through avulsion and closed neck cut-off; long ( $1:<1$ ) shapes are most likely to occur through closed neck cut-off. Closed neck cut-off is the dominant style of individual cut-off observed (52%) (Fig. 4.12); local avulsion is the next most abundant (19%); neck cut-off at converging limbs represent 17%. The chute cut-off styles  $w+1$ , and axial cut-off together represent 10%.

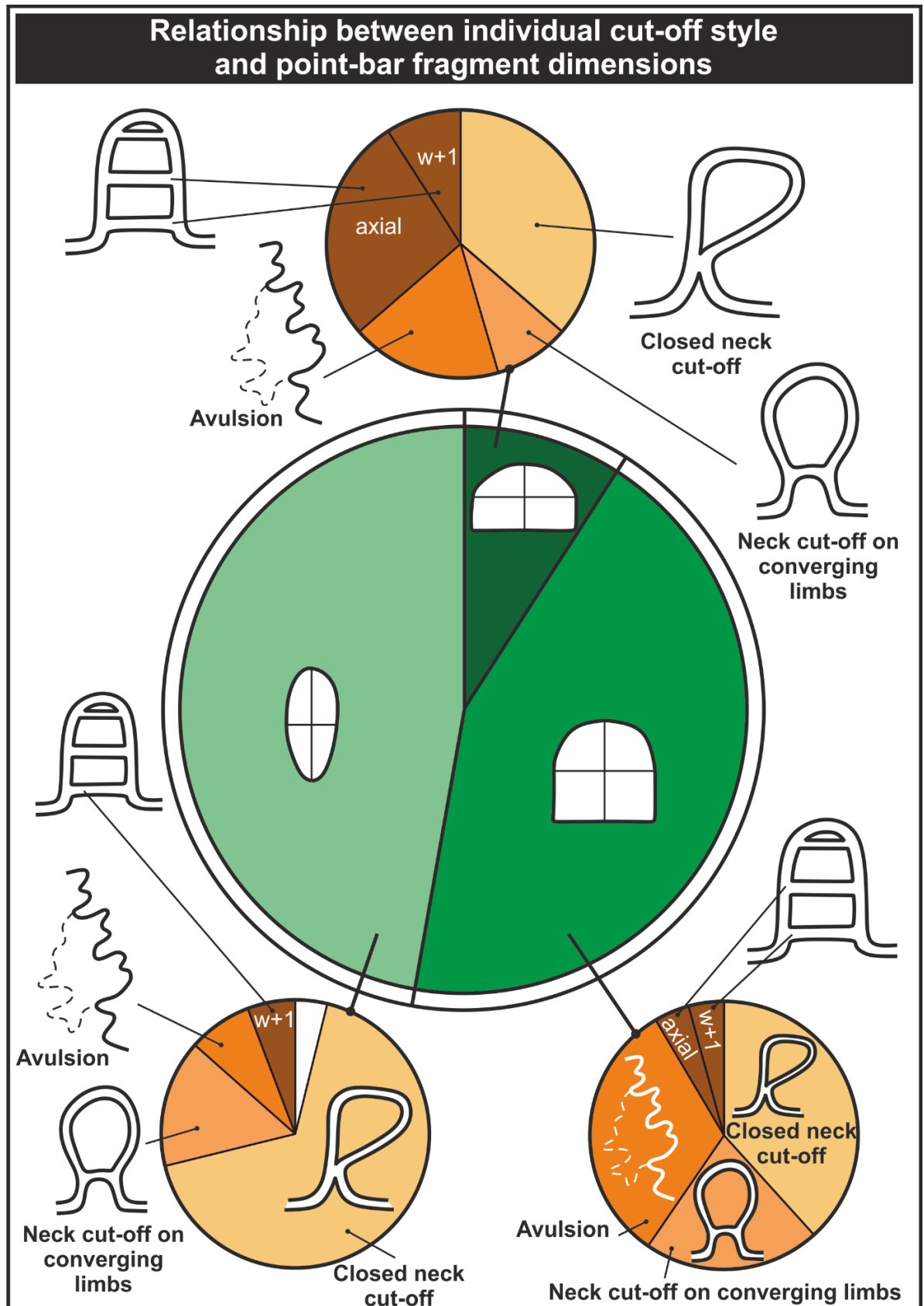
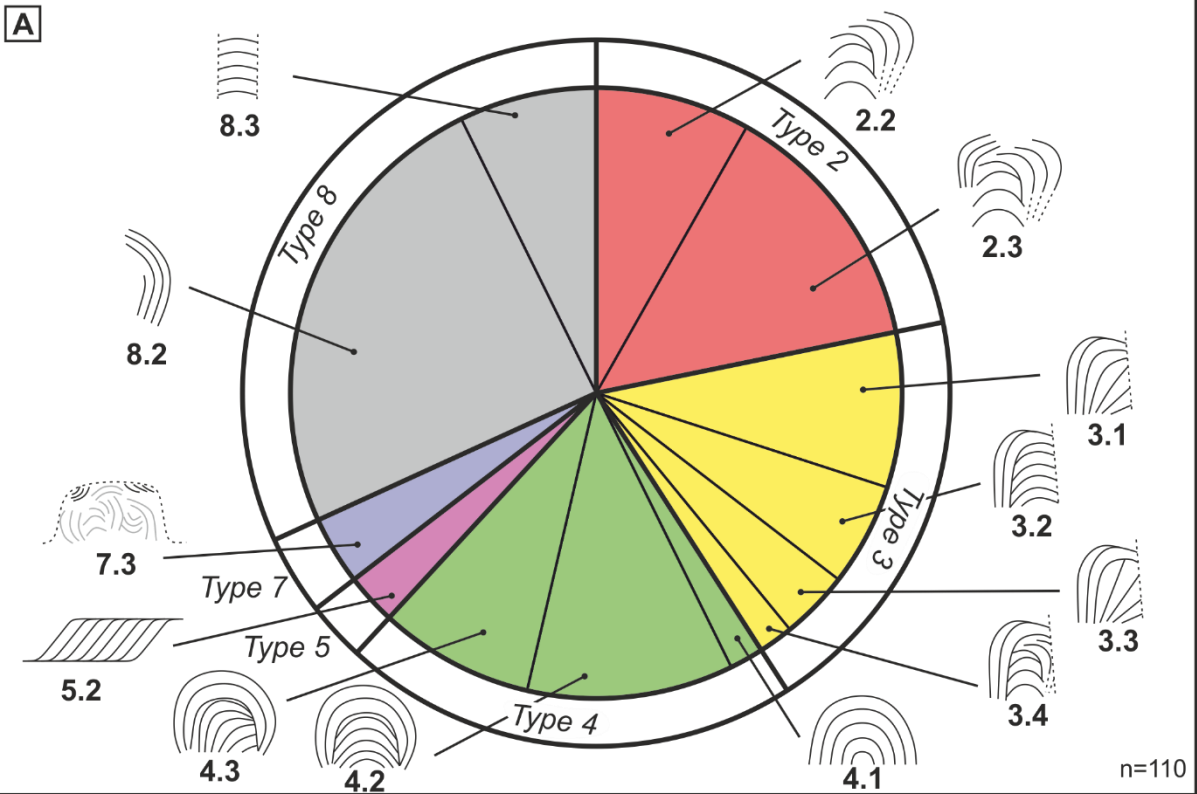


Figure 4.11 – A graph to show the proportions of abandoned point-bar deposits and the individual cut-off style for each.

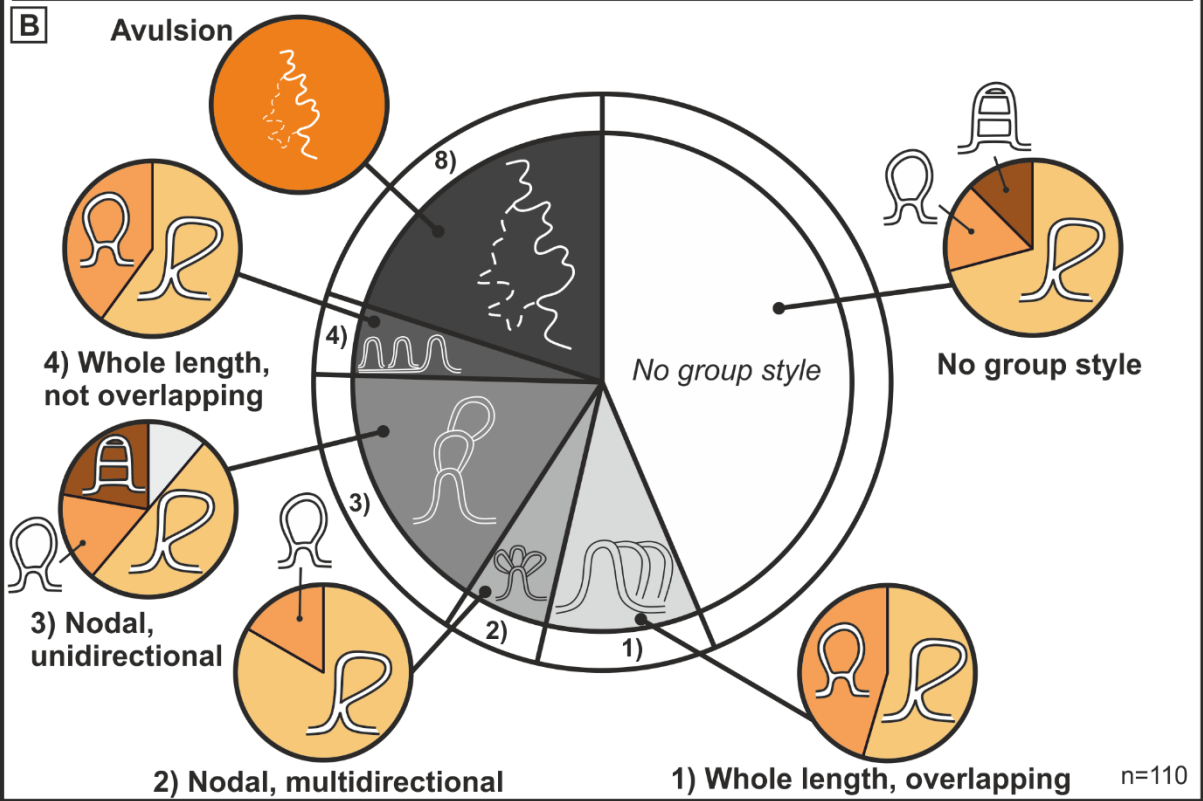


There is a wide variety of scroll-bar patterns seen on point-bar deposits (Fig. 3.13A, for detail on scroll-bar patterns). Partial remnants, of scroll-bars, (Type 8) are dominant (32%), with the remainder of abandoned point-bar deposits represented by extension and rotation with directional changes (22%) (Type 2), downstream translation (19%) (Type 3), or expansion (20%) (Type 4). Translation (Type 5), and compound forms (Type 7) are seen in 3% and 4% of cases, respectively. No examples of extension (Type 1), or translation then secondary growth (Type 6) are observed. Scroll-bars, which are partial remnants, of scroll-bars, (Type 8), are dominant in abandoned point-bar deposits that have undertaken closed neck cut-off (44%). Extension and rotation with directional changes (Type 2), and expansion (Type 4) are both also observed to be of note on shapes that have undertaken closed neck cut-off (28% and 17%, respectively). Neck cut-off of converging limbs is represented by equal proportions of downstream translation (21%) (Type 3), expansion (21%) (Type 4), and partial remnants (26%) (Type 8). Extension and rotation with directional changes (Type 2), and compound (Type 7) are both identified (16% each). Point-bar deposits that have been abandoned through avulsion show dominantly downstream translation (33%) (Type 3), and expansion (33%) (Type 4). Chute cut-off (both w+1 and axial) is dominated by downstream translation (45%) (Type 3), with extension and rotation with directional changes (Type 2), and expansion (Type 4) also being common (27%, and 18%, respectively).

**Proportions of scroll-bar patterns on point-bar fragments**



**Group cut-off styles**





**Figure 4.13 - A) The proportions of scroll-bar patterns observed for the 110 abandoned point-bar deposits observed; B) Group cut-off styles observed, and the individual cut-off styles observed in each case.**

To determine if it is possible to characterize the stacking style of a group of bars, the immediate floodplain is observed for signs of meander scars, i.e. distinctly marked areas that may have lower vegetation density (Fig. 4.8). Of the abandoned point-bar deposits studied, 36% are part of a recurring process, and therefore form a group type (Fig. 4.13B). Nodal, unidirectional abandonment is common (50% of the 36% showing a group cut-off type), and is dominated by an individual cut-off type of closed neck cut-off. Overlapping whole lengths is the next most common (28% of the 36% showing a group cut-off type), and is almost equally represented by both closed neck cut-off, and neck cut-off on converging limbs. The group cut-offs that are “nodal, multidirectional”, and “whole length, not overlapping”, are each observed in 11% of 36% which were part of a recurring process; both are also dominated by the individual cut-off type of closed neck cut-off. Neck cut-off on converging limbs is observed in a significant proportion of the group cut-off style “whole length, not overlapping”, and is less prevalent in “nodal, multidirectional”. Where local avulsion was the mechanism of abandonment, both the individual and group classes are represented as such. Therefore, 100% of the individual cut-off styles are local avulsion, where the group abandonment is local avulsion.

The abandoned point-bar deposits from each river are below considered in turn (Fig. 4.14); notable trends are observed.

#### *Ok Tedi (Fly) River* (Fig. 4.14A)

Closed neck cut-off is dominant; of the abandoned point-bar deposits 70% are part of a repeating cut-off process; the group types include “whole length, overlapping”, “nodal, multidirectional”, and “whole length, not overlapping”. Partial remnants (Type 8) is the dominant type of scroll-bar pattern.

*Senegal River* (Fig. 4.14B)

Local avulsion is the only type of group abandonment, and has occurred for 60% of the abandoned point-bar deposits. Downstream translation (Type 3) is the most dominant (50%), and extension and rotation with directional changes (Type 2) is the next most common (20%).

*Murray River* (Fig. 4.14C)

Long (1:<1) shapes are dominant (70%). There is a variety of individual abandonment styles, where closed neck cut-off, and neck cut-off on converging limbs are represented by 30%, and chute cut-off is represented by 20%. Partial remnants (Type 8), and downstream translation (Type 3), are both present in 30% of the abandoned point-bar deposits.

*Yana River* (Fig. 4.14D)

Long (1:<1) shapes are dominant (60%). Ninety percent of point-bars have undertaken closed neck cut-off, and only one point-bar has undertaken a group cut-off, which is local avulsion. There are only two scroll patterns present, which are extension and rotation with directional changes (Type 2) and expansion (Type 4). These types represent 60% and 40%, respectively.

*Colville River* (Fig. 4.14E)

Long (1:<1) shapes are dominant (80%). Extension and rotation with directional changes (Type 2) is the dominant scroll-bar pattern (50%), and Type 8 is present in 40% of observed abandoned point-bar deposits. Eighty percent of point-bars have undertaken individual closed neck cut-off.

*Kuskokwim River* (Fig. 4.14F)

Sixty percent of the shapes are long (1:<1) and chute-cut off is the most common mode of individual cut-off. Sixty percent of meanders show extension and rotation with directional changes (Type 2), and all of chute cut-off on converging limbs show Type 2.

Group cut-off is dominantly nodal, unidirectional (40%), though whole length, overlapping is also present (30%).

*Mississippi River* (Fig. 4.14G)

Ninety percent of the shapes are long (1:<1), and 50% of the meanders have been abandoned through local avulsion. Expansion (Type 4), is observed in 50% of meander shapes, and the other 50% is comprised of extension and rotation with directional changes (Type 2), downstream translation (Type 3), and partial remnants (Type 8), these are at 20%, 10%, and 20% respectively.

*Purus (Amazon) River* (Fig. 4.14H)

Long (1:<1) shapes are dominant (70%). Scroll-bar patterns showing partial remnants (Type 8), and expansion (Type 4), are most dominant (60% and 30%, respectively). Closed neck cut-off comprises 80% of abandoned point-bar shapes. Four styles of group cut-off are present which are whole length, overlapping, nodal, unidirectional, whole length, not overlapping, and local avulsion.

*Irtys (Ob) River* (Fig. 4.14I)

Rounded (1:1) shapes are dominant (60%). There is a variation of scroll-bar pattern where downstream translation (Type 3) is the most common at (40%), and present in each individual cut-off style. Closed neck cut-off is the most represented at 40%, and local avulsion represents 30%.

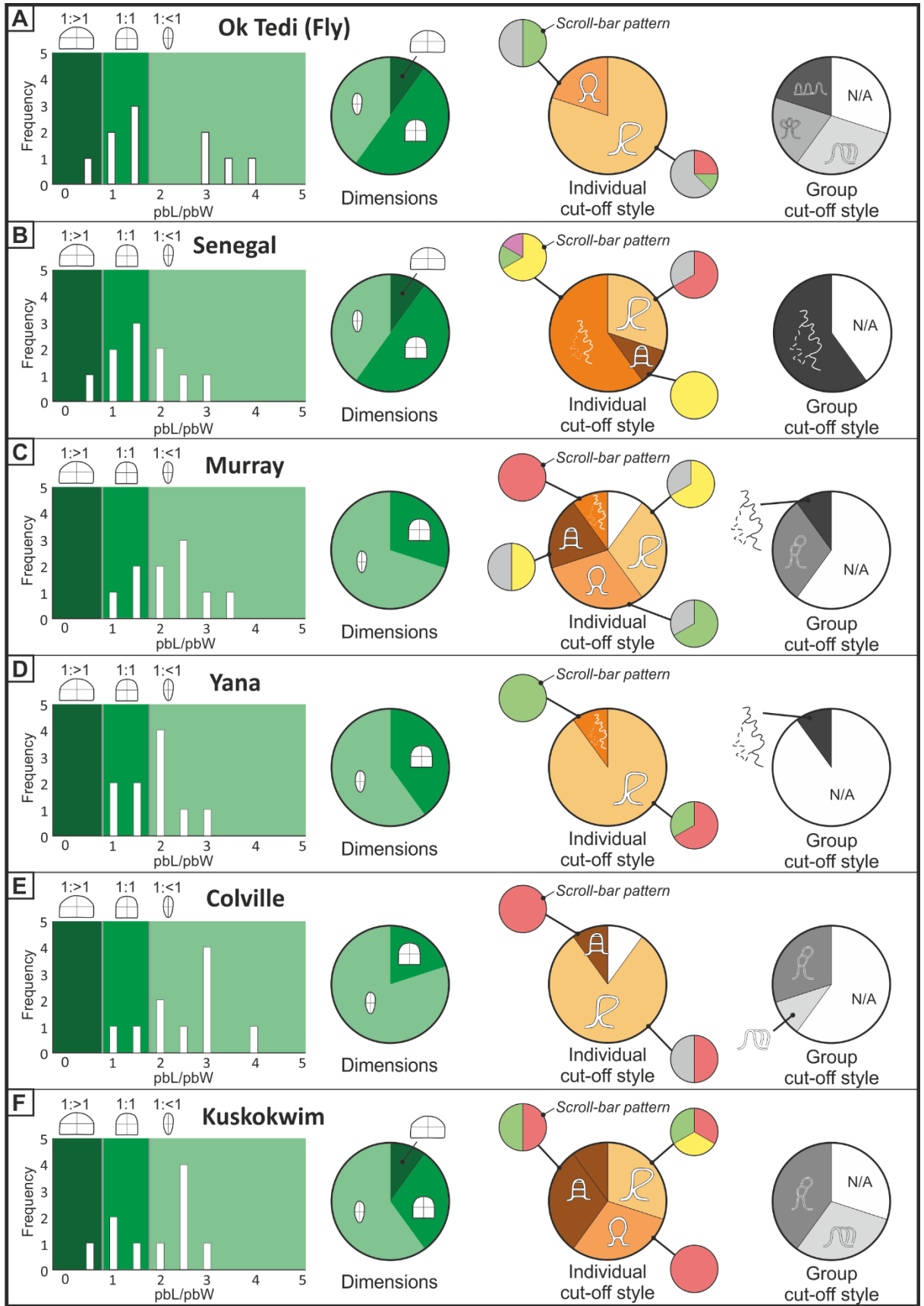
*Kolyma River* (Fig. 4.14J)

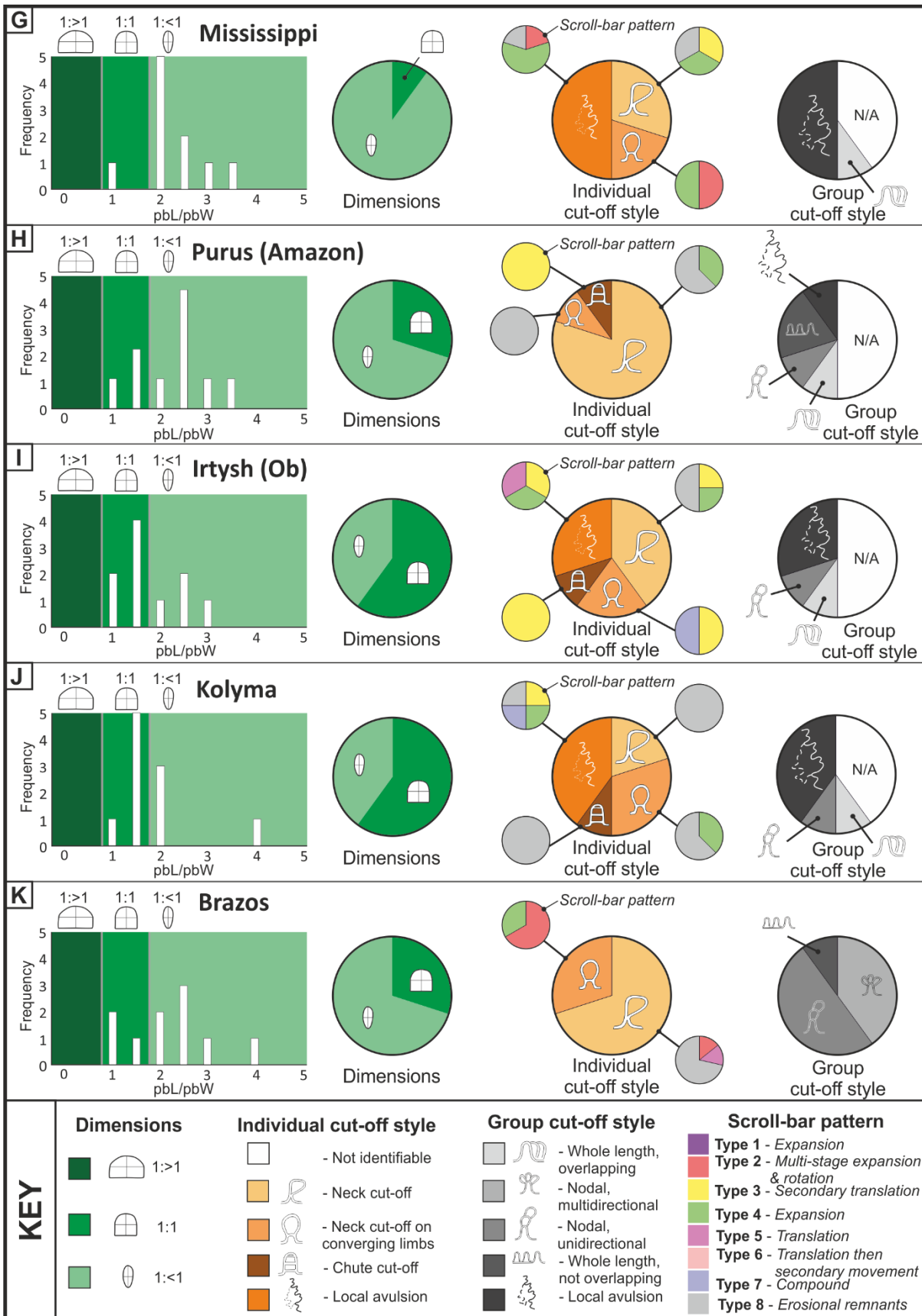
Rounded (1:1) shapes are dominant (60%). Partial remnants (Type 8), is the dominant scroll-bar pattern (60%). The most typical style of individual cut-off is local avulsion (40%), and chute cut-off on converging limbs is observed in 30% of cases.

*Brazos River* (Fig. 4.14K)

Long (1:<1) shapes are dominant (70%). Closed neck cut-off is dominant and is mostly partial remnants (Type 8), whereas chute cut-off on converging limbs is dominantly

extension and rotation with directional changes (Type 2). All individual cut-offs observed are party to a group cut-off where the style “overlapping, unidirectional” is dominant (50%), and multidirectional nodal is significant (40%).





**Figure 4.14 - An assessment of abandoned point-bar deposit dimensions, individual cut-off styles, (with associated scroll-bar patterns), and group cut-off styles, for each of the 11 rivers studied.**

## 4.6 Discussion

Active fluvial meandering systems are widely used to support interpretations of ancient point-bar deposits (Bridge, 1993a; Miall, 2006; Engel & Rhoads, 2012; Lotsari *et al.*, 2014). This has led to an oversimplified approach in reflecting point-bar proportions. One goal of developing an objective model of ancient fluvial systems is to determine the position and proportions of the sand-prone deposits (Allen, 1965; Tye, 2004). Therefore, the size of the point-bar deposit is important to consider appropriately. The classifications of individual and group cut-offs (Figs 4.7 and 4.8) enable fluvial styles to be examined (Fig. 4.14), so improved classifications of meandering reaches can be developed and incorporated into object, and pixel based models.

### 4.6.1 Planform point-bar dimensions

The difference in dimensions between an active meander, and an active point-bar presents a predictable relationship between active meander dimensions and active point-bar dimensions ( $y = 0.2733x + 0.4315$ ,  $R^2=0.3076$ ) (Fig. 4.9). This can be utilised to reconstruct the dimensions of a point-bar deposit where only the shape of the river reach is evident, for example in seismic reflection time-slice images. Where fewer data are available, the dimensions of point-bar deposits are often approximated by round, or similarly equidimensional shapes, in models and calculations (e.g. Gibling, 1981; Colombera *et al.*, 2017; Donselaar & Overeem, 2008). Point-bars whose dimensions result in an approximately equidimensional shape (1:1), are almost equally common in both active point-bar, and abandoned point-bar deposits (Figs 4.7A, and 4.7B). Where avulsion occurs, a higher proportion of rounded (1:1) shapes are seen (Figs 4.14B, 4.14I, and 4.14J), with the exception of the Mississippi (Fig. 4.14G). The shape of an

avulsed channel closely resembles the shape it possessed when active (Fisk, 1947; Makaske *et al.*, 2012). Therefore, use of equidimensional shapes where avulsion is likely to have occurred is acceptable. However, in deposits that comprise abandoned point-bars (Hubbard *et al.*, 2011), long shapes (1:<1) are approximately equally as prevalent as to rounded shapes (1:1) (Fig. 4.10B). Therefore, when fluvial deposits with these characteristics are reconstructed it would be prudent to include long (1:<1) shape dimensions in any such model, e.g. for modelling sand-body connectivity in reservoir models (cf. Colombera *et al.*, 2017).

#### 4.6.2 Controls on cut-off mechanisms

Rivers in different physiographic settings undertake varying cut-off and abandonment processes (Fig. 4.14) in response to variations in autogenic and allogenic influences (Fisk, 1947; Erskine *et al.*, 1992; Hooke, 2004). These factors are therefore influential in meander development and are likely to be reflected in the preserved meander morphology (Ghinassi *et al.*, 2016). The distribution of sand- and mud-prone sediments on the floodplain is known to influence the development of meander shape, as mud-prone sediment tends to be more resistant to erosion than sand-prone sediment (Hooke, 2004; Guneralp & Marston, 2012). Increased vegetation density also increases the resistance of the river bank to erosion processes (Howard, 1984; Wynn & Mostaghimi, 2006). Examples where this may be noticeably influential are: (i) in the frequency of polarised meander growth (Fig. 4.7D), where a highly resistant floodplain may cause a meander to rework the deposit of a preceding meander loop, because it is less resistant; (ii) in the Yana River, Russia, where the floodplain shows signs of frost sorting and rounded pools indicative of permafrost, which would suggest that it is resistant to erosion; the channel is mainly seen to undertake neck cut off, where the proto-meander remains pointed (i.e. angular (Group 2), Chapter 2)) for some time (Fig. 4.7Aa), which could be considered as end-member geometry characteristics where the floodplain is resistant to erosion; and (iii) types of overlapping styles of group cut-off



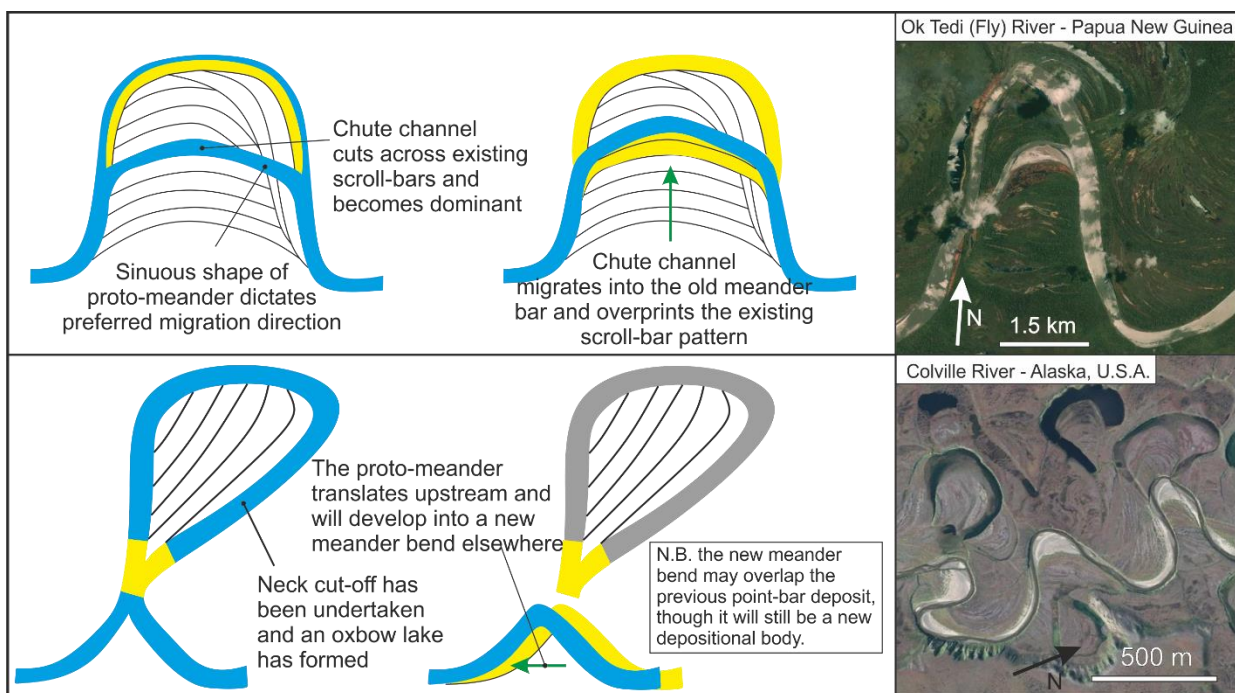
(Figs 8A-C), are influenced by the positions of the previously deposited meanders, which leads to the predictable shape relationships (Fig. 4.8).

The rate of land subsidence affects the rate of accumulation of new sediment on the floodplain, for example, a slow subsidence rate could result in continuous reworking of the floodplain over 1000s of years (Blum & Törnqvist, 2002). Where a group stacking style is seen (Figs 8A-D), the repeating shape rarely occurs more than three or four times. This could be because after four repeats, the point-bar deposits are sufficiently overlain with floodplain deposits to obscure them from aerial observation. More data are required to validate statistically any further trends or relationships.

#### *4.6.3 Preservation potential of point-bar deposits*

The preservation of fluvial point-bar deposits is fragmentary because scouring and cannibalisation of point-bar deposits commonly occurs after abandonment (Thomas *et al.*, 1987, Mackey & Bridge, 1995; Gibling, 2006). Determining the susceptibility of a point-bar deposit to erosion is important to establish its preservation potential, and therefore its interconnectivity where a group cut-off style is seen (Fig. 4.8). Group cut-off styles may belong to one of these three broad categories: (i) amalgamated point-bar bodies with adjoining sand-rich segments; (ii) amalgamated sand-prone point-bar bodies without adjoining sand-rich segments; (iii) point-bar bodies which are not connected. The amount of cannibalisation and reworking may be influenced by the style of cut-off that occurs. Following neck cut-off, the proto-meander is most likely to translate and then begin expansion in a different area up-stream (Figs 4.8A, 4.8D). Following chute cut-off, the proto-meander is limited in growth direction (Fig. 4.7Cb), therefore the amount of cannibalisation and scouring of previously deposited point-bar deposits will likely be greater. The shape and heterogeneity of the channel-fill deposit (Allen, 1965) will also influence preservation potential of a point-bar deposit, (Fig. 4.15); neck cut-off will likely result in a shape with a mud-prone fill (Fisk, 1947; Allen, 1965; Toonen *et al.*, 2012), that encloses its point-bar, protecting it from erosion, whereas

chute cut-off will likely result in a shape with a coarser-grained fill that is more sand-prone and open (Fisk, 1947; Allen, 1965; Toonen *et al.*, 2012), leaving the point-bar at risk of erosion. In modern systems, the process of chute cut-off is more common than neck cut-off (Fisk, 1947; Kulemina, 1973; Brice, 1977; Lewis & Lewin, 1983; Gagalino & Howard, 1984; Hooke, 1984; Gay *et al.*, 1998). However, this study has shown that 52% of the individual cut-off styles observed in the floodplain, represent neck cut-off, whereas only 10% represent axial or “w+1” chute cut-off, which reflects the preservation potential of point-bars abandoned via these mechanisms, or that these mechanisms are not as common as reported.



**Figure 4.15 – Illustration demonstrating the preservational bias of point-bar deposits that are recently abandoned via chute or neck cut-off, as a result of the behaviour of its genetic proto meander.**

This disparity in preservational bias is significant as it shows the importance of accounting for the abandonment process of a point-bar deposit in reconstruction, both from outcrop, and planform. It also highlights the dangers of only considering modern analogues for fluvial systems when reconstructing a fragmented ancient deposit.

To determine where the sand-prone areas in a point-bar may be, the evolutionary history of a point bar can be reconstructed through use of the flowchart depicted in Figure 4.16. The flowchart shows how one shape may evolve into another, and may continue to termination by symmetric or asymmetric cut-off. Assuming that a proto-meander will follow the course of the previously deposited meander, these are the growth patterns that would ensue: (i) a proto-meander resulting from neck cut-off (Fig. 4.7A) may typically be S2d, or S4d, and may grow to terminate by either symmetric or asymmetric closure; (ii) a proto-meander resulting from chute cut-off on converging limbs (Fig. 4.7B) may begin at S4e, S4d, or S1a, and may grow to a bulbous shape; (iii) a proto-meander resulting from w+1 chute cut-off (Fig. 4.7Cc) may be S4e, and may grow to terminate at any phase of maturity in any shape; (iv) a proto-meander resulting from axial chute cut-off (Fig. 4.7Cb) may be S1a, or S4b, and may grow to terminate at any phase of maturity in any shape. These “lineages” can be utilised to interpret the expected mode of growth of a meander, which in turn can be used to determine the likely lithological heterogeneity (Chapter 2). This is important because the dominant style of scroll-bar pattern consists of eroded, partial remnants (Type 8), one of which is otherwise difficult to further interpret. The interpretation of these lineages to determine heterogeneity will be detailed in the Discussion section (Chapter 6).

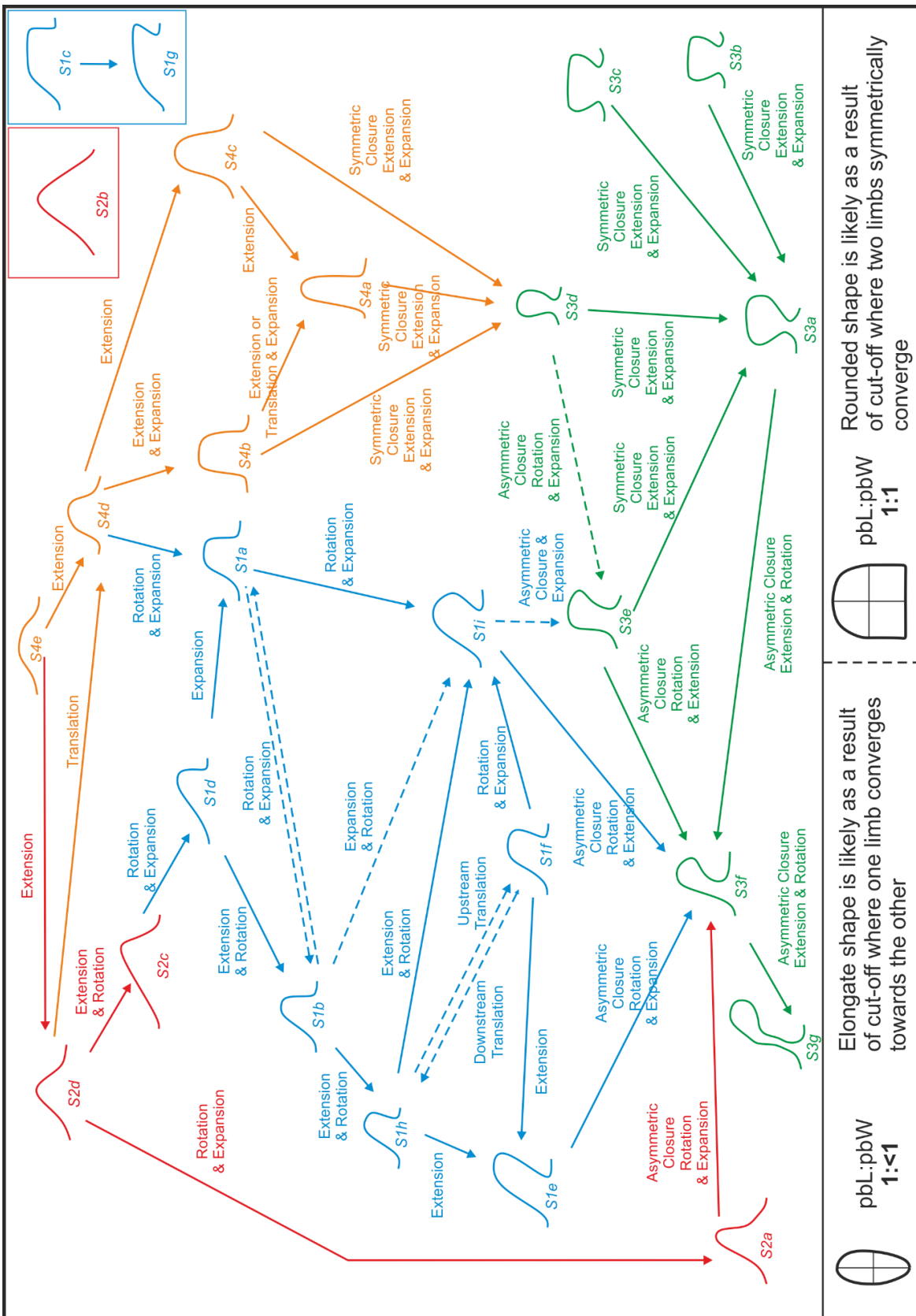


Figure 4.16 - A flowchart demonstrating the relationships between the meander shapes described in Chapter 2, and the resulting abandoned point-bar deposit dimensions

leading from asymmetric or symmetric cut-off. The code attributed to each meander shape related to those attributed in Figure 2.8.

#### 4.6.4 Limitations

The main limitation of this research is that the data set is relatively small. Only 10 cut-offs have been studied from each of 11 river reaches. Through the study of additional examples, better statistical validation of results would be obtained.

### 4.7 Conclusions

There are many meander cut-off types documented in the literature (Fisk, 1947; Allen, 1965; Lewis & Lewin, 1983; Toonen *et al.*, 2012). In this study, these varying principles have been refined into a classification of individual cut-off styles (Fig. 4.7). Group cut-off styles have also been defined and classified (Fig. 4.8), which is an important step towards a better understanding of the interconnectivity of deposits (Gibling, 2006). Active point-bar deposits have variable dimensions (Fig. 4.6), and this variability increases when meander loops undertake abandonment (Fig. 4.10B). Rounded (1:1) and long (1:<1) shapes are almost equally prevalent in abandoned point-bars, suggesting that long (1:<1) shapes ought to be considered when modelling fluvial deposits. Where an abandoned, sinuous reach is seen due to the impedance contrast in a seismic reflection time slice (e.g. Fachmi & Wood, 2005), the relationship shown in Figure 4.6B can be used to determine the approximate dimensions of the point-bar associated with the meander shape dimensions. Neck cut-off is the most prevalent style of individual meander cut-off observed, which could be because mud-prone channel fill is protecting the abandoned point bar from erosion because mud is significantly more difficult to erode than sand (Hooke, 2004). Group cut-off styles occur in 36% of the observed individual meander cut-offs, and local avulsion occurs in 20% of cases (Fig. 4.13B). By attributing a style of group cut-off, stacking patterns may be considered to determine interconnectivity of sand-prone deposits (Fig. 4.8). Scroll-bar

patterns on the 110 abandoned point-bars studied are most commonly partial remnants (32%) (Type 8), then extension and rotation with directional changes (22%) (Type 2). Downstream translation (19%) (Type 3) and expansion at (20%) (Type 4) describe the majority of the other types (Fig. 4.13A). These methods enable the characteristics of individual river reaches to be assessed, enabling better incorporation of cut-off mechanisms and products into models (Fig. 4.14).

## **5 Reconstructing planform point-bar dimensions and palaeo-meander shape from a preserved point-bar deposit in outcrop**

### **5.1 Chapter Summary**

Outcrop data are routinely used to inform reservoir models that seek to characterize subsurface sedimentary architecture to a level of detail that cannot be observed directly from seismic images, or that cannot be determined in three dimensions from available core or well-log data. Therefore, accurate interpretation of outcrop data is important for robust application to develop predictive models with applied significance. Geological aspects of preserved point-bar deposits that can be interpreted from sedimentological and stratigraphical analysis are as follows: i) depositional history and mechanism of accretion; ii) type and distribution of lithological heterogeneity; and iii) dimensions and form of the sandbody element itself. Many published reconstructions of point-bar architecture and shape depict simplistic models that do not necessarily resemble the complex interactions observed from modern systems. Here, a partially preserved ancient point-bar deposit, which crops out in a well-exposed cliff face at Nolton Haven (Carboniferous, Westphalian 318-299 Ma, Pennant Sandstone Formation), Pembrokeshire, UK, has been examined in detail and the methodologies described in Chapters 2-4 have been applied to determine the evolutionary history of development and accumulation of the bar deposit. Through detailed analysis, 17 distinct lithofacies, and 4 commonly occurring facies successions have been identified. Statistical analyses have been undertaken using the FAKTS database, and Markov chain analysis to enable detailed facies transitions to be documented. The point-bar deposit is shown to have exhibited extension and rotation followed by upstream accretion (scroll-bar pattern 2.3), and final abandonment via a mechanism of chute cut-off on converging limbs. Two possible evolutionary paths have been determined; each has a different

accretion history and yields a different estimate of predicted final lateral extent.

Through use of a flow chart (Fig. 4.16), variations in the accretion history have been reconstructed, and expected heterogeneity distribution has been determined for the two proposed evolutionary paths. The approach outlined in this chapter demonstrates how a more complex and varied analysis can be undertaken using data derived from an outcrop exposure of a partially exposed remnant point-bar element than has hitherto been possible.

## 5.2 Introduction

The thicknesses of ancient preserved point-bar deposits in the subsurface can usually be determined from core or wireline log data. However such data cannot usually be used to provide direct measurements of lateral extents of such elements. Yet, determination of the geometry of these elements is required to inform 3D geological models (Tye, 2004). Outcrop data considered to be analogous to subsurface successions of interest have long been used as proxies to predict likely lateral extent (Tye, 2004; Ekeland, 2007; Keogh *et al.*, 2014). However, documenting the geometry of a point-bar element from a two-dimensional cliff exposure in an attempt to determine its lateral extent and its process of palaeo-accretion is challenging (Geehan & Underwood, 1993; Mjøs *et al.*, 1993; Bridge *et al.*, 2000; Tye, 2004; Miall, 2006). It is important to interpret palaeo-accretion in detail and in three-dimensions because it affects the distribution of lithological heterogeneities. Heterogeneity distribution is important because it affects both the permeability of the rock unit, and the flow pathways of hydrocarbon accumulations that are stored in such geological reservoirs (Miall, 1988; Tye, 2004; Keogh *et al.*, 2014). In fluvial point-bar deposits, the distribution of mud-prone sediment accumulations markedly influences hydrocarbon flow properties, and can act as baffles or barriers to fluid flow (Fielding & Crane, 1987; Thomas *et al.*, 1987; Miall, 1988; Pranter *et al.*, 2000; Gibling, 2006; Pranter *et al.*, 2007; Donselaar & Overeem, 2008; Willis & Tang, 2010; Labrecque *et al.*, 2011).

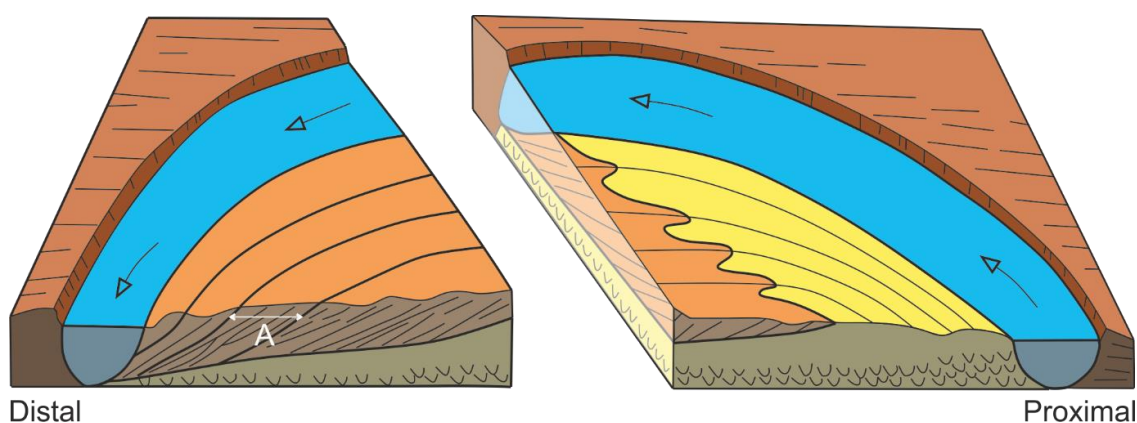


The ability of a geological model to predict subsurface reservoir behaviour depends on the accuracy of the input parameters (e.g. lateral dimensions of the point-bar deposit and its heterogeneity distribution), as based, for example, on data collected from outcrops (Tye, 2004). Traditional – and widely applied – facies models typically depict point bars and their preserved elements as simple, sine-wave-like planforms (Leopold & Wolman, 1960; Allen, 1965), with simple internal characteristics (Allen, 1965; McGowen & Garner, 1970). However, recent advancements have revealed a greater complexity in both planform shape, and accretion process (Ghinassi *et al.*, 2016; Durkin *et al.*, 2015; Moody & Mead, 2014; Labrecque *et al.*, 2011; Hubbard *et al.*, 2011). A point bar may be studied in detail through assessment of its internal facies types and their distribution in relation to likely formative processes, and also through detailed analysis of palaeocurrent indicators (Miall, 1976; 1988). However, because ancient preserved point-bar deposits tend to be laterally discontinuous and internally complex (Moody & Mead, 2014), facies relationships can be difficult to determine, especially in three dimensions.

Markov chain analysis can be used to establish these relationships (Walker, 1979; Gibling & Rust, 1993; Xu & MacCarthy, 1998). Markov chain analysis is a commonly employed statistical test that enables significant facies transitions to be established and predicted (Schwarzacher, 1969; Miall, 1973; 1977). The tools for observing and quantifying fluvial point-bar deposits in order to reconstruct their original form are not well established (Miall, 2006), so modern analogues are commonly utilised to constrain the lateral dimensions (e.g., length and width; Fig. 4.6) of point-bar deposit (e.g. Miall & Tyler, 1991; Dalrymple, 2001; Durkin *et al.*, 2015; Colombera *et al.*, 2017). Where planform outcrops are studied, uncertainty associated with seeking a morphologically equivalent analogue is reduced (Wu *et al.*, 2015; Ghinassi *et al.*, 2016), although not eliminated (Miall, 2006). This is because the planform of the outcrop cannot necessarily be directly related to the planform of an active modern system. Analogues are

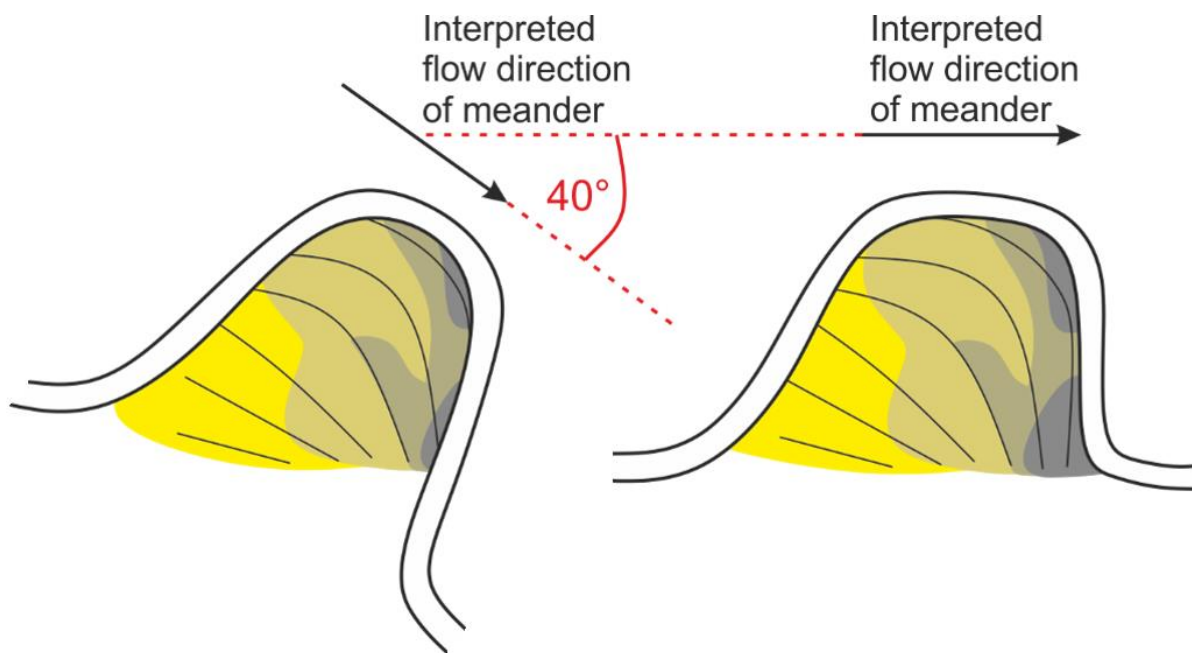
commonly selected from active reaches, and based on subjective visual matching between the meander shapes of modern systems and the exposed scroll-bar patterns of ancient preserved successions; such matching is not necessarily undertaken using a statistically robust approach (Tye, 2004). Direct comparison between active modern meanders and abandoned ancient preserved successions may be problematic because the process of abandonment may alter the dimensions of the preserved succession (Chapter 4). An active reach may be directly compared to an ancient preserved succession if the latter has undertaken abandonment via avulsion because the dimensions of the point-bar deposit may be similar, and so direct comparison may be appropriate in this case. Chute and neck cut-off are more variable and so the process of point-bar growth, and abandonment ought to be considered when undertaking reconstructions though it is rare to see abandonment included in a sequence of meander growth (e.g. Davies *et al.*, 1993; Bhattacharya 2015).

A range of palaeohydraulic parameters (mean and maximum bankfull depth, bankfull width, width to depth ratio, sinuosity, mean annual discharge, mean annual flood, channel slope, meander wavelength, and mean flow velocity) may be estimated given a known thickness of a preserved point-bar element in outcrop, the horizontal length of a lateral accretion surface (e.g. "A" on Fig. 5.1), reconstructed estimates of bankfull width and bankfull depth, and grainsize (Hjulström, 1935; Leopold & Wolman, 1960; Schumm, 1960; 1963; 1972; Carlston, 1965; Leeder, 1973; Ethridge & Schumm 1977; Middleton & Southard, 1978). However, point-bar deposits vary in thickness (Labrecque *et al.*, 2011), grainsize commonly decreases downstream within a single point-bar element (Fustic *et al.*, 2012; Fig. 5.1), and partial erosion of the point-bar deposit can lead to underestimation of its original dimensions (Bhattacharya *et al.*, 2015).



**Figure 5.1 - A figure to demonstrate the downstream fining of sediment on a meander bend (modified from Fustic et al., 2012). Orange represents mud-prone sediment, whilst yellow represents sand-prone.**

An exposed section of a point-bar deposit may represent a portion of the point-bar that was i) deposited exclusively on the downstream limb; ii) deposited exclusively on the upstream limb; iii) deposited on parts of both the up- and downstream limbs. To accurately infer palaeohydraulic parameters, it is necessary to determine the position of the outcrop with respect to its position in an entire preserved point-bar deposit, else the flow direction of the reach may be significantly misinterpreted (Fig. 5.2). Moreover, this same important point also applies in determining values for the other parameters, such as lateral extent. This requires point-bar exposures to be studied in detail and their accumulation histories reconstructed from initiation to abandonment. A procedure to achieve this is outlined in this chapter and builds on the methods described previously in chapters 2 to 4.



**Figure 5.2 - A figure to demonstrate the potential error in interpreting fluvial meander bends in outcrop. Both point-bars shown have the same deposit; the most sand-prone deposits are shown in yellow, and the most mud-prone deposits in grey. The reconstruction on the left is the most likely to be interpreted through use of classic models, the one on the right is most likely based on information acquired from active systems in this study. Each will produce a different interpretation for meander flow direction, therefore accurate interpretation is important.**

A partly preserved point-bar element crops out in cliffs at the west side of the beach at Nolton Haven, Pembrokeshire. This element has been selected as a suitable case study because it is especially well exposed in cliff faces that are accessible for detailed study.

The overarching aim of this chapter is to determine the lateral extent, accumulation history, and heterogeneity of a point-bar element that is studied in outcrop through use of the tools and methods that have been developed in this thesis (Chapters 2-4). Specific research objectives are as follows: (i) to use established numerical methodologies in order to reconstruct palaeohydraulic parameters; (ii) to describe, interpret and understand the type and distribution of lithofacies and their related

heterogeneity; (iii) to deduce facies associations using a quantitative statistical approach; and (iv) to apply the tools devised in Chapters 2-4 to reconstruct the architecture and abandonment history of the point bar that gave rise to the preserved studied element.

### **5.3 Geological background**

The study area is located on the NW cliff of Nolton Haven cove, Pembrokeshire, Wales, UK (Fig. 5.3). The succession is Pennsylvanian (Westphalian) in age: 318-299 Ma (Jenkins, 1962; Hartley & Warr, 1990; Waters *et al.*, 2009; Fig. 5.4). During the Westphalian, the region occupied an equatorial palaeolatitude; the climate was tropical (Waters *et al.*, 2009; Fig. 5.5A); and sediment accumulation occurred during a long-term rise in relative sea level (Ramsbottom, 1984; Hartley, 1993). This controlled the sedimentation of the South Wales Coal Measures Group (Early Westphalian), a succession represented by extensive, basin-wide mud and coal deposits that have been interpreted as preserved peat mires (Hartley & Warr, 1990; Cope *et al.*, 1992; Waters *et al.*, 2009).

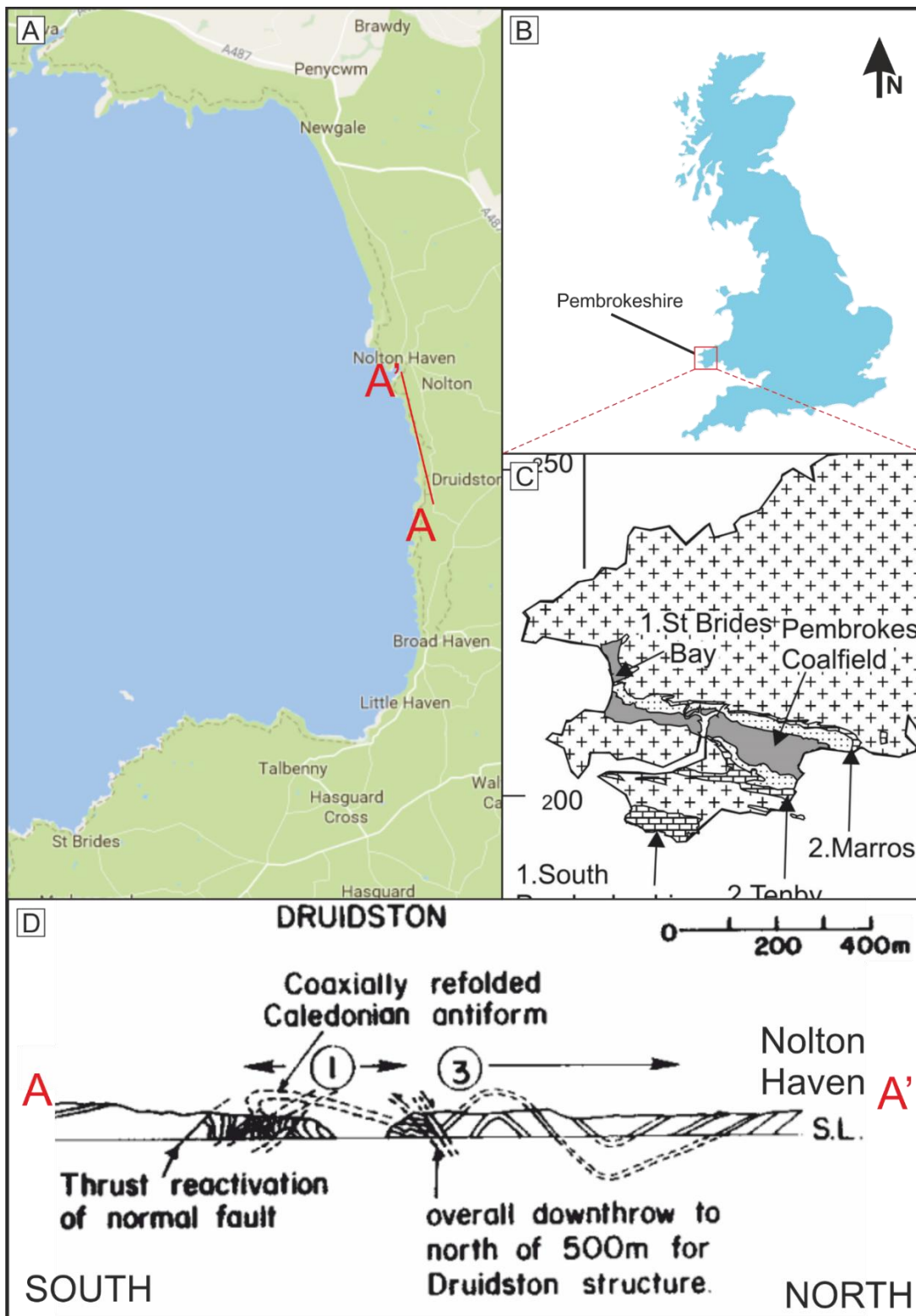
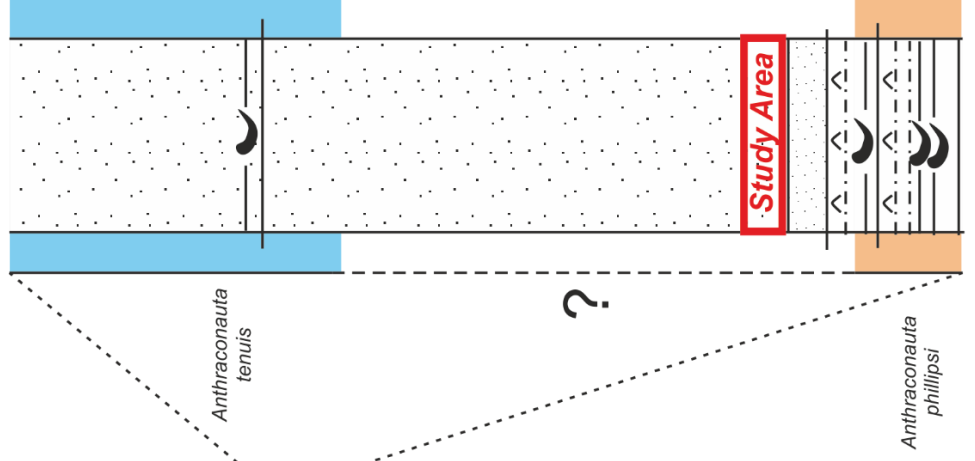


Figure 5.3 - Location maps and geological setting of Nolton Haven cove: A) the location of Nolton Haven on the Pembrokeshire coast line; B) the location of Pembrokeshire in the UK; C) the distribution of the coal fields in Pembrokeshire (from Waters et al., 2009; D) cross-section of the geology at Nolton Haven (as marked as A and A' in Fig. 5.3A), from Smallwood (1985).

Druidston Haven & Nolfon Haven Stratigraphy and Biostratigraphy



Period	International Series	Former European Subperiods	International Stage	European Stages
Carboniferous	Mississippian	Dinantian (Lower Carboniferous)	Silesian (Upper Carboniferous)	Tournaisian
				Viséan
Carboniferous	Pennsylvanian	Silesian (Upper Carboniferous)	Moscovian	Westphalian
				Stephanian
Carboniferous	Pennsylvanian	Silesian (Upper Carboniferous)	Bashkirian	Namurian
				Serpukhovian
Carboniferous	Pennsylvanian	Silesian (Upper Carboniferous)	Kasim-ovian	Langsettian
				Gzhelian
Carboniferous	Pennsylvanian	Silesian (Upper Carboniferous)	Kasim-ovian	Duckmantian
				Bolsovian
Carboniferous	Pennsylvanian	Silesian (Upper Carboniferous)	Kasim-ovian	Asturian
				Langsettian
Carboniferous	Pennsylvanian	Silesian (Upper Carboniferous)	Kasim-ovian	Lower Coal Measures
				Lower Coal Measures
Carboniferous	Pennsylvanian	Silesian (Upper Carboniferous)	Kasim-ovian	South Wales Coal Measures Group
				South Wales Coal Measures Group
Carboniferous	Pennsylvanian	Silesian (Upper Carboniferous)	Kasim-ovian	Warwickshire Group
				Warwickshire Group
Carboniferous	Pennsylvanian	Silesian (Upper Carboniferous)	Kasim-ovian	St. Brides Bay Stratigraphy
				St. Brides Bay Stratigraphy
Carboniferous	Pennsylvanian	Silesian (Upper Carboniferous)	Kasim-ovian	Non-marine bivalve zones
				Non-marine bivalve zones
Carboniferous	Pennsylvanian	Silesian (Upper Carboniferous)	Kasim-ovian	Carbonicola communis
				Carbonicola communis
Carboniferous	Pennsylvanian	Silesian (Upper Carboniferous)	Kasim-ovian	Anthraconaia modiolaris
				Anthraconaia modiolaris
Carboniferous	Pennsylvanian	Silesian (Upper Carboniferous)	Kasim-ovian	'Lower similis- pulchra'
				'Lower similis- pulchra'
Carboniferous	Pennsylvanian	Silesian (Upper Carboniferous)	Kasim-ovian	'Upper similis- pulchra'
				'Upper similis- pulchra'
Carboniferous	Pennsylvanian	Silesian (Upper Carboniferous)	Kasim-ovian	Anthraconauta phillipsi
				Anthraconauta phillipsi
Carboniferous	Pennsylvanian	Silesian (Upper Carboniferous)	Kasim-ovian	Anthraconauta tenuis
				Anthraconauta tenuis

299

310

320

330

340

350

359

**Figure 5.4 - Stratigraphic column combined from work by Waters *et al.*, (2008), Waters *et al.*, (2009; 2011), Jenkins (1962), Hartley and Warr (1990), with ages derived from Gradstein *et al.*, (2004). The red box indicates the stratigraphy studied in this chapter.**

The Pennant Sandstone Formation (part of the Warwickshire Group) overlays the South Wales Coal Measures Group; it reflects a marked change in sedimentation style (Hartley & Warr, 1990). The Pennant Sandstone Formation is approximately 750 m thick (Waters *et al.*, 2011), and its base is diachronous with the underlying coal measures (Waters *et al.*, 2011). The Pennant Sandstone Formation has been interpreted to represent a distributive alluvial environment (Cope *et al.*, 1992), with sediment sourced from the Wales-Brabant High that covered the southern part of Britain (Hartley & Warr, 1990; Waters *et al.*, 2009). Overall, the deposits consist of mostly sandstone with limited mudstone, coal fragments and plant debris (Kelling, 1974; Jones, 1989; Hartley & Warr 1990; Hartley, 1993).



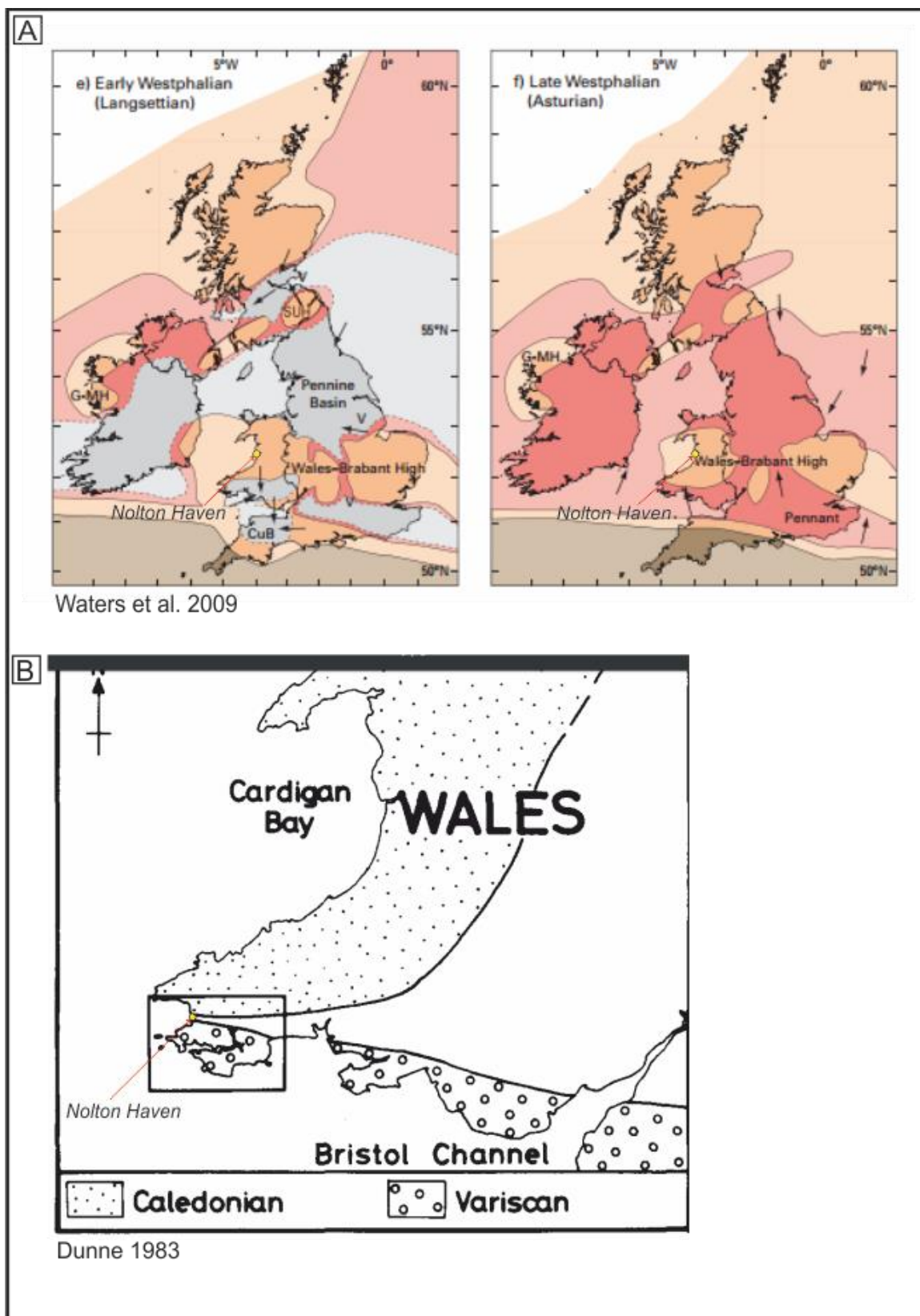


Figure 5.5 – A) Reconstructed palaeoenvironment of the early and late Westphalian (from Waters et al., 2009); B) A map showing the areas of Wales affected by the Caledonian and Variscan orogenies (from Dunne, 1983)

The Carboniferous successions in South Wales have been subject to complex tectonic evolution (Jenkins, 1962; Hancock *et al.*, 1981; Smallwood, 1985; Fig. 5.5B). The Variscan Orogeny (Williams, 1968; Dunne, 1983; Smallwood, 1985; Frodsham & Gayer, 1997) resulted in deformation and displacement of the stratigraphy due to compressional tectonics (Frodsham & Gayer, 1997). Fluvial drainage systems were laterally confined by active E-W trending tectonic structures during the deposition from the Pennant Sandstone Formation (Hartley & Warr 1990), leading to variability in the thickness and facies distributions (Jones, 1989). Subsequently, the rocks exposed along what is now part of the west coast of Wales were subject to widespread faulting and folding (Smallwood, 1985), which has led to difficulty in correlating strata regionally (i.e. across Wales – Jenkins, 1962).

Biozones were established through identification of goniatites (“marine-bands”), and non-marine bivalves (Bisat, 1923; Jenkins, 1960; 1962). This approach of using biozones has effectively yielded otherwise unachievable stratigraphic understanding (Williams, 1968; Hampson *et al.*, 1997; George & Kelling, 1982).

Goniatites are cephalopods from the subclass *Ammonoidea* of the order *Goniatitida* (Hyatt, 1994), that make excellent biozone markers, as they evolved rapidly, creating clear and diagnostic fauna (Hampson *et al.*, 1997). The non-marine bivalves are thick-shelled and easily preserved, and are found alongside fish and ostracodes (Waters *et al.*, 2009). Goniatites are preserved in parts of the succession interpreted as condensed sections: these highly fossiliferous marine bands that are thought to represent maximum flooding surfaces (Hampson *et al.*, 1997). In the Carboniferous, MFS's record eustatic sea-level transgressions driven by Gondwanan glacial cycles (Maynard & Leeder 1992; Hampson *et al.*, 1997). Beds comprising non-marine bivalves are thought to be due to terrestrial flood events and are the resulting condensed beds are used as biomarkers. Both the Goniatite-bearing, and non-marine bivalve-bearing intervals are of significant value in resolving the Westphalian chronostratigraphy; these

intervals can be traced over regional distances and effectively partition the otherwise undistinctive lithostratigraphic units (Ramsbottom, 1978; Hampson, 1997; Waters *et al.*, 2009).

At Nolton Haven, *Anthraconauta phillipsii* (a non-marine bivalve; Fig. 5.4), was observed by Trueman (1934) 19.8 m above the base of the SE cliff, which itself is 86.7 m high (Jenkins, 1962; Fig. 5.4). No further fossiliferous beds are identified at Nolton Haven, which indicates that the succession exposed in the studied cliff face at Nolton Haven lies in part of the succession that is transitional between two non-marine biozones (represented by the dashed line in Fig. 5.4; see biostratigraphy of Jenkins, 1962). The Nolton Haven coal field (north of Nolton Haven cove), is within the *Alethopteris serllei* subzone (Cleal, 1997); this indicates that the study interval is late Bolsovian in age (Waters *et al.*, 2009). *Alethopteris serllei* is a seed fern (Cleal, 1997).

The studied Westphalian succession at Nolton Haven, Pembrokeshire, is exposed as a cliff-forming sand body that is 123 m in length, with a maximum thickness of 4.3 m; the average grain size is 400µm. The sand body displays vertical fining (from 450µm to 350µm on average), as well as overall fining from NNE to SSW. Eight distinct sedimentary packages are identified and are erosionally juxtaposed and overlapping in a south-westerly direction. On average, each package has an exposed apparent horizontal length of 10.9 m, and each is bounded by an erosional surface. Across the outcrop, the succession is composed of seventeen distinct lithofacies: trough cross-bedded sandstone (St); medium grained planar cross-stratified sandstone (Spm); coarse grained planar cross-stratified sandstone (Spc); very coarse grained planar cross-stratified sandstone (Spvc); ripple-laminated sandstone (Srs); planar laminated sandstone (packages of 3 laminations), (Sh3); planar laminated sandstone (packages of 4 laminations), (Sh4); planar laminated sandstone (packages of 5 or more laminations), (Sh5); medium grained low-angle cross-stratified sandstone (Slm); coarse grained low-angle cross-stratified sandstone (Slc); intraformational conglomerate (Sec);

matrix supported conglomerate (Sem); Scour fill (Ss); laminated mudstone/siltstone (Fl); mudstone/siltstone with rootlets (Fm); mudstone/siltstone (Fsc); and coal, carbonaceous sandstone (C). At the SSW end of the outcrop, there is a dominantly mud-prone deposit, the base of which is concave upwards; the dimensions of this mud-prone deposit are 3.4 m thick and 22.7 m in observable lateral extent. The NNW end of the outcrop is characterised by coal (C), and matrix supported conglomerate (Sem); neither of these facies are seen in such abundance elsewhere in the outcrop. The central portion of the outcrop is dominantly sand-prone; abundant facies are planar cross-stratified sandstone (Spm, Spc and Spvc), planar laminated sandstone (Sh3, Sh4 and Sh5), and low-angle cross-stratified sandstone (Slm, Slc). The SSW end of the outcrop is characterised as exhibiting the most mud-prone sediment, and the facies identified are trough cross-bedded sandstone (St), low-angle cross-stratified sandstone (Slm and Slc), ripple-laminated sandstone (Srs), Laminated mudstone/siltstone (Fl), and Mudstone/siltstone with rootlets (Fm).

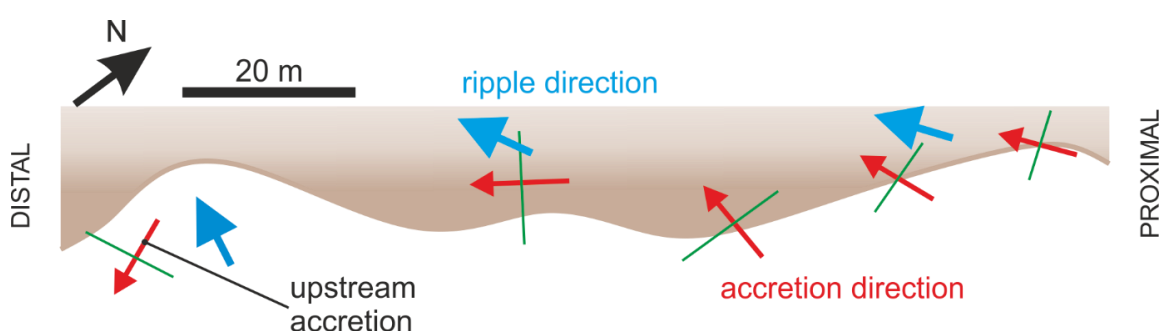
To interpret the outcrop, a range of methodologies have been employed for field data collection and its subsequent analysis. Data collection undertaken included bed thickness, grain size, facies, position of erosional boundaries, and sedimentary structure of 560 beds; this data was presented as 37 sedimentary graphic logs that depicted facies, bed thickness, and total 65.6 m in length.

At the time of this sediment deposition, Nolton Haven was terrestrial as evidenced by the presence of non-marine bivalves (Bisat, 1923; Jenkins, 1960; 1962), fossils of the seed fern *Alethopteris serlii* (Cleal, 1997), as well as palaeogeographic reconstructions (Waters *et al.* 2009 - Fig. 5.5A). The palaeocurrent analysis shows that the sand-body deposit has accreted laterally with the NNE end of the outcrop being proximal, and the SSW end being distal. The overall trend observed is that at the palaeocurrent direction changes from NW to SW from proximal to distal respectively (Fig 5.6). The palaeoflow

direction changes markedly at lateral accretion surfaces, and undertakes upstream accretion at the distal end.

The eight packages that overlap and erode each other are interpreted as lateral accretion packages (cf. Allen, 1984; Miall, 1985; Ghazi and Mountney, 2009). A sand-prone terrestrial body, that may be laterally accreting, is most likely a fluvial bank-attached point bar (Ghazi and Mountney, 2009). Vertical fining trends are noted to be indicative of point-bar deposits (McGowen and Garner, 1970; Allen, 1984), which are observed in this outcrop. Additionally, the mud-prone body observed at the SSW extent of the outcrop, is interpreted as an abandoned channel fill because it is mud-prone and overall upwards accreting (Fisk, 1947; Allen, 1965; Davies, 1993; Toonen *et al.*, 2012). It is also concave upwards and similar in morphology to the channel cross-sections observed by Smith *et al.* (2009). This supports the interpretation that this is a preserved fluvial point-bar deposit.

To assess the character of this sand-prone deposit, palaeocurrent analysis has been undertaken; 2092 measurements were recorded from accretion surfaces, ripple crests, trough axes, channel axes, and cross bedding foresets. Figure 5.6 shows the overall character of the lateral accretion direction and associated ripple direction.



**Figure 5.6-A planform sketch of the outcrop showing the overall accretion direction**

Further assessment of this point-bar deposit will be undertaken in this chapter via analysis of sedimentary graphic logs that have been used to construct 2D and pseudo-3D panels.

## **5.4 Methodology**

This chapter utilises a case study of a single point-bar architectural element. The purpose is to demonstrate the application of the predictive workflows outlined in Chapters 2-4 as a method for the reconstruction and prediction of planform point-bar geometry and internal facies arrangement from primary data sets that are essentially two-dimensional.

### *5.4.1 Lithofacies identification*

Lithofacies are defined by rock properties: grainsize, texture, lithology, colour, sedimentary structures and fossil content (Middleton, 1973; 1978; Lindholm, 1987). In this study, Miall's (1978) well-known and widely applied facies classification scheme has been used; this is also the basis for the facies scheme used in the FAKTS database (Colombera *et al.*, 2013), which itself is employed in a later part of this study.

### *5.4.2 Sedimentary graphic logs*

Thirty seven vertical sedimentary graphic logs were acquired, totalling 65.6 m in length. Five hundred and sixty beds were recorded at a centimetre scale resolution over 35.75 m of point-bar stratigraphy. Vertical facies distributions were recorded as sedimentary graphic logs at a resolution of 1 cm. Logs record grainsize, sedimentary structures, bed thickness, lithology, fossils, and other distinguishable features. Logs were constructed from data recorded between each major lateral accretion bounding surface in the point-bar element. This enables lateral changes in beds to be recorded by virtue of the dipping nature of the outcropping succession (the tectonic dip and strike is between 5

and 10° SW). The locations of the measured sedimentary graphic logs are recorded on field sketches and on a map, and are indicated on Figure 5.7.

#### *5.4.3 Stratigraphic panels*

The sedimentary graphic logs collected were used to construct a series of 2D stratigraphic panels and these have been depicted in a larger overview panel in a style that depicts their arrangement in their relative position in space; this yields a pseudo-3D view. The pseudo-3D view was achieved by using the positions of the logs (Fig. 5.7), and then marking their relative vertical positions to each other on a separate sketch. The two images were then combined using the perspective tool in Corel Draw. Each panel was drawn separately using the sedimentary graphic logs, and placed into the panel individually. A 2D panel informs of interrelationships between adjoining logs in their relative vertical positions; a pseudo-3D panel informs the interpretation of the 3D distribution of facies, which – along with palaeocurrent data (described later) – are used to reconstruct the internal facies anatomy of the point-bar elements.



Figure 5.7 - Positions that the sedimentary graphic logs were taken from at Nolton Haven cove. The numbering system shown on the image refers to the logs that were recorded at



**Nolton Haven cove; the first number refers to the lateral accretion unit, and the second to the number within that unit.**

#### *5.4.4 Palaeocurrent analysis*

Two thousand and ninety two palaeocurrents were measured from accretion surfaces, ripple crests, trough axes, channel axes, and cross bedding foresets, across the 8 recognised lateral accretion packages. The direction of accretion reflects the direction of scroll-bar accretion, thereby enabling the data to aid in reconstructing point-bar accretion processes. They may be collected from accretion surfaces, ripple crests, trough axes, channel axes, and cross bedding foresets.

### **5.5 Data analysis techniques**

The FAKTS database was used for data analysis in this study. FAKTS has been applied to synthesise large volumes of data from this analysis, and to determine trends and relationships in the data (Colombera *et al.*, 2013).

The primary data recorded that was input into FAKTS were the thickness of each bed. These data were linked to their respective logs, enabling analysis of Individual logs, and analysis of the whole point-bar element. Data were input into the FAKTS database by assigning a unique identifier to each facies unit in order to be able to integrate this case study into the system, and thereby enable comparisons to be made to other case studies already in the database. Data outputs from FAKTS used in this study are as follows: i) average bed thickness for each facies; ii) relative proportion of each facies type, at log, and point-bar element scale; and iii) a tally matrix of the number of occurrences of each vertical facies transition.

One objective of point-bar research is to understand and predict facies successions and their related heterogeneity within point-bar deposits (Thomas, 1987; Labrecque *et al.*, 2011; Ghinassi *et al.*, 2016). Markov chain analysis has been employed to statistically assess vertical facies relationships, therefore quantifiably assessing facies

associations (Selly, 1970; Harper, 1984; Lindholm, 1987; Gibling & Rust, 1993; Xu & MacCarthy, 1998). The input for this approach is a tally matrix that accounts for the number of times a particular facies transitions into another facies (Walker, 1979; Harper, 1984; Türk, 1979); the output is typically a facies relationship diagram (cf. De Raaf *et al.*, 1965). Alternative implementations of the Markov chain methodology have been proposed that enable specific studies (Naylor & Woodcock, 1977; Miall & Gibling, 1978; Carr, 1982). However, it is the Walker (1979), and Harper (1984) methods that are most commonly used in sedimentological analyses.

The Walker (1979) methodology uses the tally matrix to calculate a transition probability matrix; a stochastic matrix that shows the probability of one facies transition occurring into another. An independent trials probability matrix is then calculated (a model of randomness against which the probability matrix is tested), by utilising Equation 1:

$$\left( \frac{\text{Total number of beds for facies transitioned to (column total)}}{\text{Total number of transitions for all facies}} - \frac{\text{Total number of beds for facies transitioned from (column total)}}{\text{Total number of beds for facies transitioned from (column total)}} \right)$$

**Equation 1 - Equation for forming the independent trials probability matrix**

Values from the independent trials probability matrix are subtracted from the transition probability matrix to obtain a difference matrix. In the difference matrix, where a value is positive, it suggests that the transition may occur more frequently than would be expected if the arrangement was random (Harper, 1984; Lindholm, 1987; Xu & MacCarthy, 1998). Weaknesses in this method are as follows: i) that the nature of the facies contact is commonly not included (De Raaf *et al.*, 1965; Reading, 1978); ii) the column totals are distorted through calculation of the independent trials probability matrix (Türk, 1982; Carr, 1982), and the rows no longer sum to unity (i.e. the rows totals no longer sum to 1, as they do in the probability matrix); iterative proportional fitting may be undertaken to correct this (Carr, 1982; Turk, 1982; Harper, 1984); and iii)

the independent trials probability matrix is not random because row scaling is not able to preserve the row totals; however, through use of this method, the transitions highlighted by the difference matrix are statistically significant, though if the columns were scaled rather than the rows, different statistical significances would result. The Harper (1984), methodology builds on the Gingerich (1969) method and initially follows the same methodology as Walker (1979), with an additional step at the end to calculate the chi-square value to test for randomness. This test therefore calculates a biased “randomness”, because chi-squared analysis forces the diagonal values to be zero (Xu & MacCarthy, 1998). Harper (1984) uses a binomial probability model to determine statistically significant facies transitions, whereby the number of times a transition occurs is compared to the number of times where that transition does not occur. This is argued to be an improvement over the method of Walker (1979), because it assesses the matrices on a cell-by-cell resolution, as opposed to row-by-row. Transitions may be considered significant at 0.01 (Harper, 1984), or 0.1 may be considered as significant (Xu & MacCarthy 1998).

Usually, embedded transition statistics do not include data for self-transitions, which renders the data set biased. Inclusion of self-transitions, however, can lead to “masking” and/or “swamping” of data, which makes outliers harder to differentiate from significant values (Bradú & Hawkins, 1982; Harper, 1984). This study uses an embedded matrix using the Walker (1979) methodology both with, and without, self-transitions. Inclusion of self-transitions is achieved by not eliminating the tallied self-transitions prior to calculation of the probability matrix. The Harper (1984) methodology is also utilised without self-transitions, considering statistical significance of binomial probabilities at both 0.01 and 0.1.

## 5.6 Point-bar reconstruction

To reconstruct the lateral extent, and palaeo-accretion mechanisms of the point-bar deposit, the interrelationships of meander shape, scroll-bar style and abandonment process (Chapters 2-4) are considered. Specifically these interrelationships are utilised to deduce: (i) the dimensions of the point-bar deposit (Chapter 4), (ii) the mode of accretion it undertook and (Chapter 3), (iii) a set of likely planform shapes; and (iv) the likely cut-off mechanism undertaken (Chapter 4).

## 5.7 Results

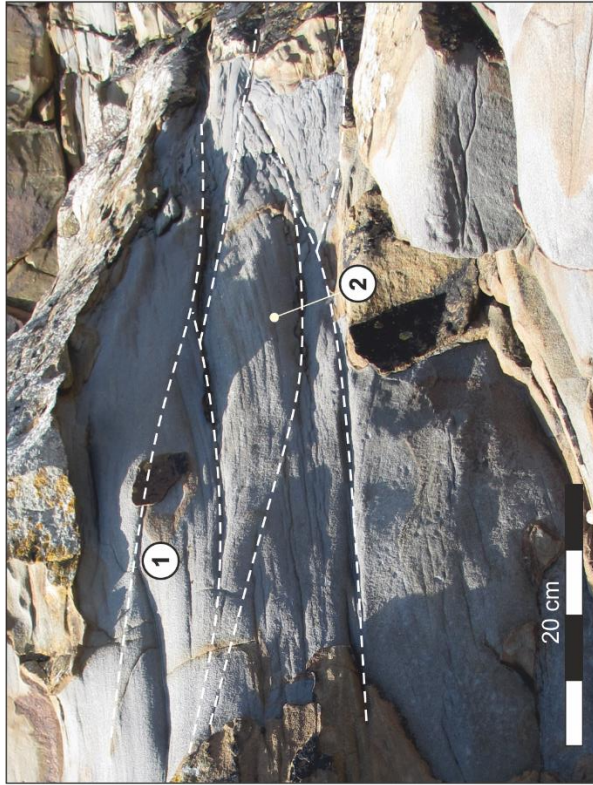
### 5.7.1 Lithofacies

Seventeen distinct lithofacies are recognised in the fluvial point-bar architectural element studied (Figs 5.8.1-5.8.12). They are described through use of a modified and extended version of Miall's (1978), classification scheme (Fig. 5.9). Each recognised lithofacies possesses distinctive sedimentological characteristics (Table 5.1), including lithologic heterogeneity, and the approximate energy that was required for the formation of the sedimentary structures seen (Fig. 5.9).

The lithofacies identified are as follows: Trough cross-bedded sandstone (St); Medium grained planar cross-stratified sandstone (Spm); Coarse grained planar cross-stratified sandstone (Spc); Very coarse grained planar cross-stratified sandstone (Spvc); Ripple-laminated sandstone (Srs); Planar laminated sandstone (packages of 3 laminations), (Sh3); Planar laminated sandstone (packages of 4 laminations), (Sh4); Planar laminated sandstone (packages of 5 or more laminations), (Sh5); Medium grained low-angle cross – stratified sandstone (Slm); Coarse grained low-angle cross – stratified sandstone (Slc); Intraformational conglomerate (Sec); Matrix supported conglomerate (Sem); Scour fill (Ss); Laminated mudstone/siltstone (Fl); Mudstone/siltstone with rootlets (Fm); Mudstone/siltstone (Fsc); and Coal, carbonaceous sandstone (C).

These are translated for integration within the FAKTS database as follows: Trough cross-bedded sandstone (St); Planar cross-stratified sandstone (Sp); Ripple-laminated sandstone (Sr); Planar laminated sandstone (Sh); low-angle cross – stratified sandstone (Sl); Intraformational conglomerate (Gp); Matrix supported conglomerate (Sm); Scour fill (Ss); Laminated mudstone/siltstone (Fl); Mudstone/siltstone with rootlets (Fm); Mudstone/siltstone (Fsm); and Coal, carbonaceous sandstone (C).

# Trough cross-bedded sandstone (St)



## Key Facies Information

Colour	Grey
Grain-size	Medium sandstone
Sorting & Texture	Moderately sorted
Max. Thickness	26 cm
Min. Thickness	3 cm
Average Thickness	9.7 cm

## Key Facies Characteristics

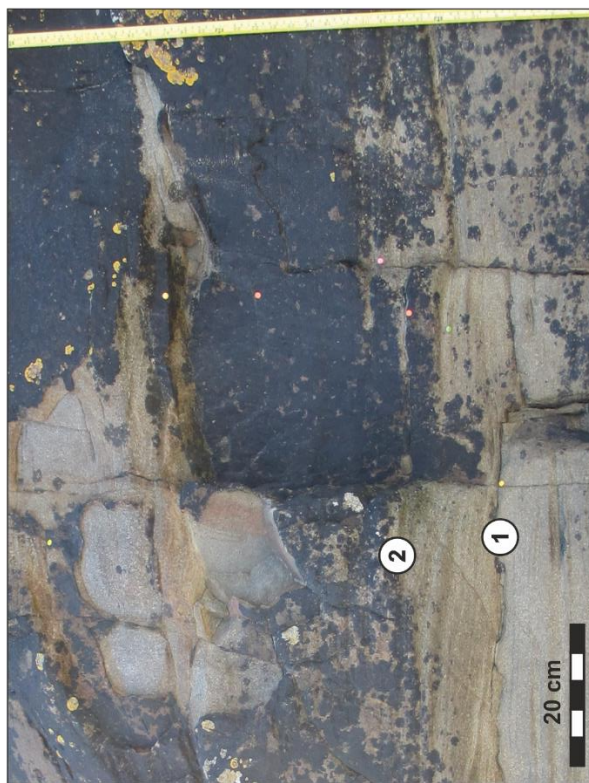
- ① Sets of trough cross-beds erode and cross-cut one another.
- ② Differential erosion on the beds is due to mud-drapes.
- ③ Mud drapes may group and splay / feather
- ④ Mud drapes may be continuous (i.e. 50+ cm)

## Interpretation

Trough cross-bedding formed by uni-directional currents in fluvial channels from migrating three-dimensional dunes in the lower flow regime (Miall 1985), through moderate to high energy traction currents (Adamson et al. 2013). Basal channel lag indicates that these sediments are deposited near the base of the channel.



## Planar cross-stratified sandstone (Sp - Spm, Spc, Spvc)



### Key Facies Information

Colour	Grey to brown
Grain-size	Medium to very coarse
Sorting & Texture	Moderate to well sorted
Max. Thickness	50 cm
Min. Thickness	3 cm
Average Thickness	16.3 cm

- ① Sharp eroded contact at base of bed.
- ② Thick beds displaying clear planar cross-stratification.
- ③ Where a very coarse grain-size is seen, a sharp and irregularly eroded contact is observed.
- ④ Alternating laminations of very coarse, and coarse grain-sizes are observed.

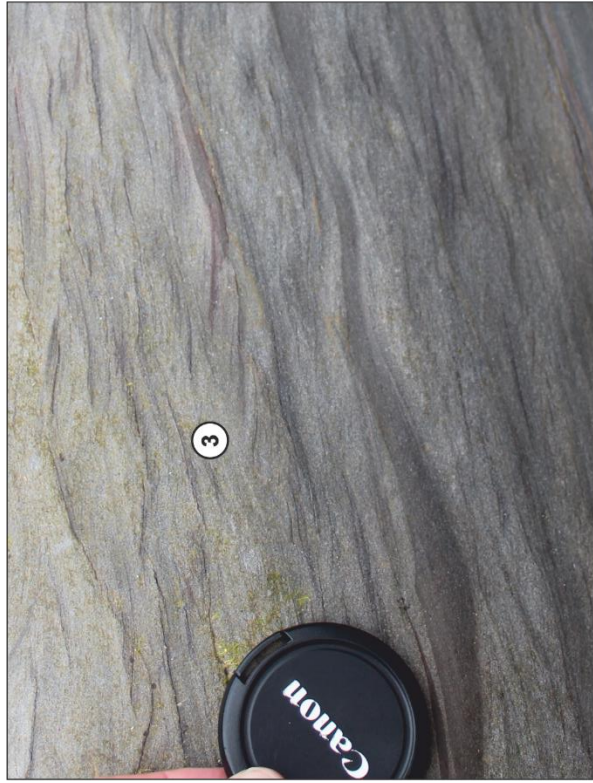
### Key Facies Characteristics

Formed by the downstream migration, or lateral accretion of 2D dunes from a unidirectional flow (Miall 1985, 1988). Within a point-bar, it represents a low-high energy environment (cf. Davies and Ethridge 1975, Donselaar and Schmidt 2010).

### Interpretation

Sharp eroded contact at base of bed.  
 Thick beds displaying clear planar cross-stratification.  
 Where a very coarse grain-size is seen, a sharp and irregularly eroded contact is observed.  
 Alternating laminations of very coarse, and coarse grain-sizes are observed.

## Ripple-laminated sandstone (Sr - Srs)



### Key Facies Information

Colour	Light grey
Grain-size	Medium
Sorting & Texture	Moderate
Max. Thickness	24 cm
Min. Thickness	2 cm
Average Thickness	9.8 cm

### Key Facies Characteristics

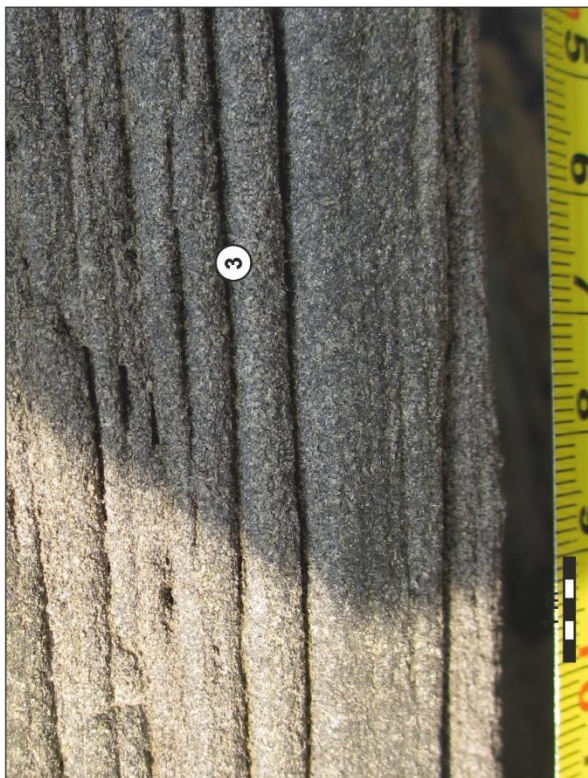
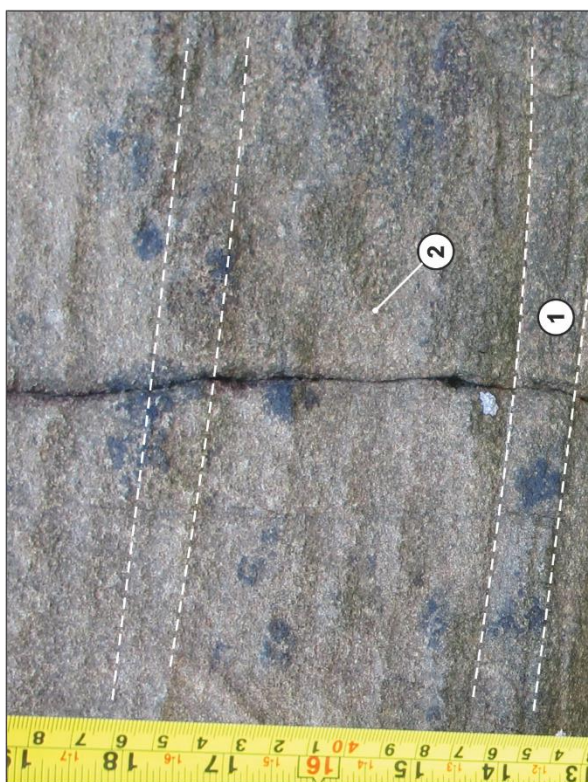
- ① Unclear and gradational boundary at the base of the rippled bed.
- ② Climbing ripples with defined rippleform laminae. They change upwardly from subcritical to supercritical climb.
- ③ Drapes on rippleform laminae. These may be composed of mud, or carbonaceous drapes containing plant fragments, there may also be a mixed composition.

### Interpretation

Lower flow regime deposits, resulting from the downstream migration of small, sand-prone bedforms in a uni-directional (Miall 1985, 1988). Carbonaceous drapes indicate periods of differing energy in the system.



## Planar laminated sandstone (Sh - Sh3, Sh4, Sh5)



### Key Facies Information

Colour	Grey to brown
Grain-size	Fine to medium
Sorting & Texture	Moderate
Max. Thickness	38 cm
Min. Thickness	1 cm
Average Thickness	13 cm

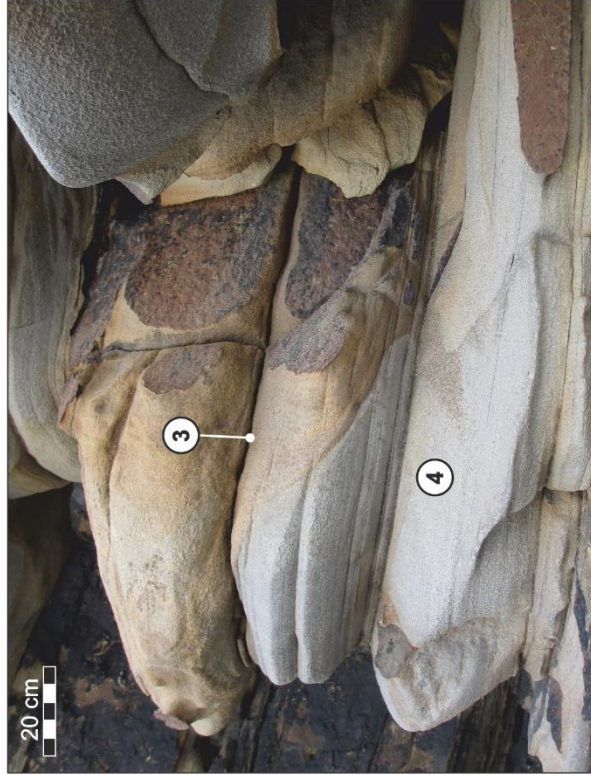
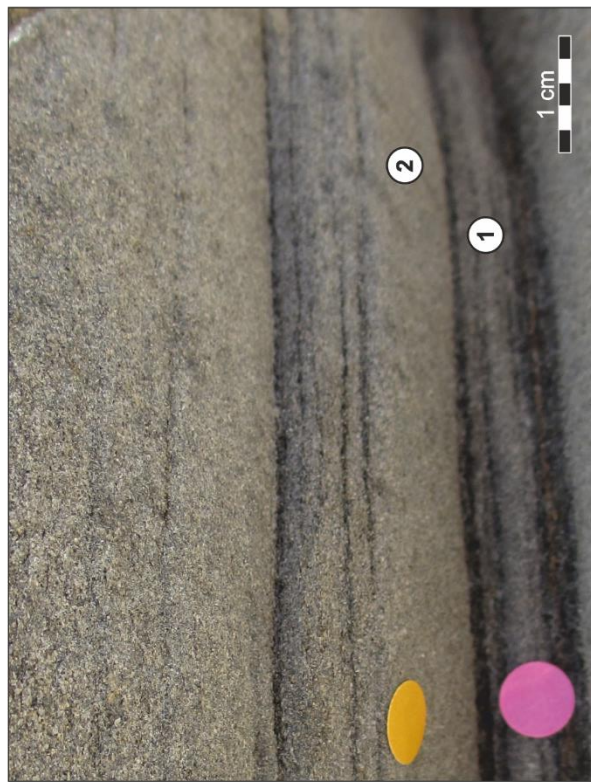
### Key Facies Characteristics

- ① One cm thick coarse-grained beds that define a horizontal lamination package.
- ② Laminations of a coarser grain-size form distinct ridges due to differential erosion.
- ③ This sheet sandstone is the Thompson Canyon Bed and forms a distinctive plateau at this locality.

### Interpretation

Deposited from a waning planar bed flow in the lower or upper flow regime (Miall 1985). Depicted on Figure XXX as upper flat bed, and lower flat bed.

# Low-angle cross-stratified sandstone (Sl - Slm, Slc)



## Key Facies Information

Colour	Grey
Grain-size	Medium to coarse
Sorting & Texture	Moderate
Max. Thickness	80 cm
Min. Thickness	1 cm
Average Thickness	23.3 cm

## Key Facies Characteristics

- ① Carbonaceous drapes and laminations may dominate in places.
- ② Beds with discontinuous drapes are interbedded with beds with continuous drapes.
- ③ Thin mudstone / siltstone beds (Fsc) divide packages of low-angle cross-stratified bed sets.
- ④ There are sections of outcrop where no drapes are seen, therefore the facies is variable in its heterogeneity.

## Interpretation

Formed by a unidirectional flow which is transitional from lower to upper flow regime within a fluvial environment.



## Intraformational conglomerate (Gp - Sec)



### Key Facies Information

Colour	Grey (clasts - various)
Grain-size	Matrix - medium
Sorting & Texture	Very poor
Max. Thickness	18 cm
Min. Thickness	4 cm
Average Thickness	9.8 cm

### Key Facies Characteristics

- 1 Moderately sorted matrix with medium grain size.
- 2 Clasts are aligned with stratification surfaces and often accompanied with carbonaceous drapes.
- 3 Clasts become finer progressively upwards, and the facies makes a gradual transition to St.
- 4 Clasts may be exposed on bedding surfaces. Composition may be of coal, sand, silt, or clay. Clasts range from 4-30 mm in length; average 16 mm.

### Interpretation

Channel lags or scour fills that occurred in a lag at the base of the channel. Clasts are reworked from underlying stratigraphy (coal, sand, and silt clasts), and nearby floodplain deposits (clay clasts).

## Matrix supported conglomerate (Sm - Sem)



### Key Facies Information

Colour	Grey (clasts - various)
Grain-size	Matrix - medium
Sorting & Texture	Very poor
Max. Thickness	120 cm
Min. Thickness	2 cm
Average Thickness	18.2 cm

### Key Facies Characteristics

- 1 Here observed underneath the outcrop as it represents basal channel lag.
- 2 Typically transitions upwards to Sp.
- 3 Within, or overlying, the conglomerate beds, carbonaceous drapes may be observed.
- 4 Clasts are composed of coal, sand, silt, or clay. Clasts range from 4-30 mm in length; average 16 mm.

### Interpretation

Channel lags or scour fills that occurred in a lag at the base of the channel. Clasts are reworked from underlying stratigraphy (coal, sand, and silt clasts), or may be from bank collapse events (Plint 1986), or nearby floodplain deposits (clay clasts).



## Scour fill (Ss)



### Key Facies Information

Colour	Grey
Grain-size	Medium
Sorting & Texture	Moderate
Max. Thickness	10 cm
Min. Thickness	2 cm
Average Thickness	5.3 cm

### Key Facies Characteristics

- ① Clear and erosive base. Internal structure not always able to be observed
- ② Where internal structure is observed, carbonaceous drapes may be seen, indicating a dynamic scouring process.
- ③ Multiple beds of Ss angularly overlay each other as subsequent erosion has occurred.

### Interpretation

Scour fill that occurred in a lag at the base of the channel.

## Laminated mudstone / siltstone (FI)



### Key Facies Information

Colour	Dark grey
Grain-size	Fine
Sorting & Texture	Moderate
Max. Thickness	15 cm
Min. Thickness	1 cm
Average Thickness	5.3 cm

### Key Facies Characteristics

- 1** Interbedded, laminated texture of alternating dark grey and brownish-grey beds.
- 2** Subcritical climb is seen in places, though rippleform laminae are not always observed.
- 3** Occasional bed of fine sand is observed.
- 4** Packages of ~4 mm are themselves internally laminated.

### Interpretation

Overbank, abandoned channel or flood deposit



## Mudstone / siltstone with rootlets (Fm)



### Key Facies Information

Colour	Grey to orange
Grain-size	Fine
Sorting & Texture	Moderate
Max. Thickness	23 cm
Min. Thickness	1 cm
Average Thickness	5.2 cm

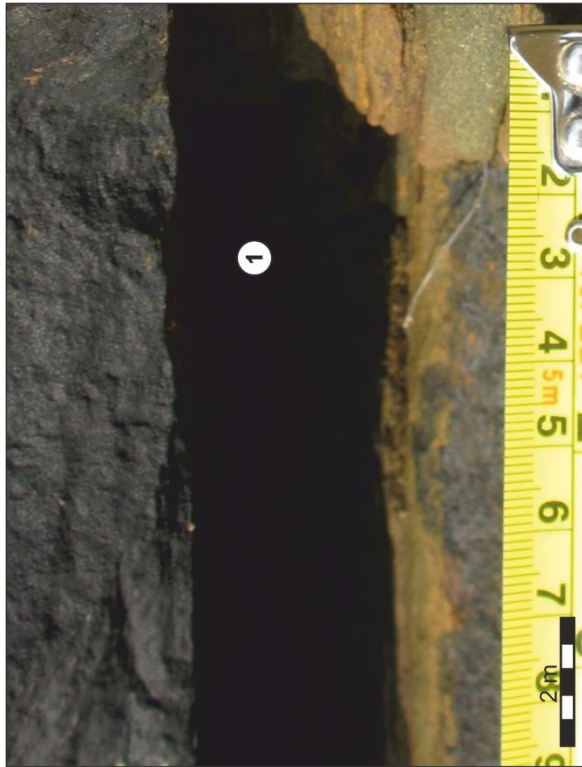
### Key Facies Characteristics

- ① Occurs near the distal end of the point-bar.
- ② Plant fragments are typically tree bark and are oriented from the top to bottom of the image
- ③ Orange colouration is due to iron staining
- ④ Rare clasts (3 cm long max.), are seen amongst the fossilised plant debris.

### Interpretation

Low energy deposits with little/no water flow, likely in the distal parts of the point-bar, or on the floodplain (Fielding 1984). Plant fragments became entrained in the flow prior to deposition, possibly due to a flood event.

# Mudstone / siltstone (Fsm - Fsc)



## Key Facies Information

Colour	Grey
Grain-size	Fine
Sorting & Texture	Well-sorted
Max. Thickness	9 cm in point-bar deposit; 3.6 m in channel fill deposit
Min. Thickness	1 cm in point-bar deposit
Average Thickness	4 cm

## Key Facies Characteristics

- ① Commonly occurs as 1 cm beds throughout the point-bar deposit, through they are typically eroded.
- ② Channel fill is dominantly composed of facies Fsm.
- ③ Above the studied outcrop, Fsm is observed and interpreted as floodplain deposits.

## Interpretation

Low energy deposits with little/no water flow, likely in the distal parts of the point-bar, channel fill (Allen 1965), or on the floodplain.



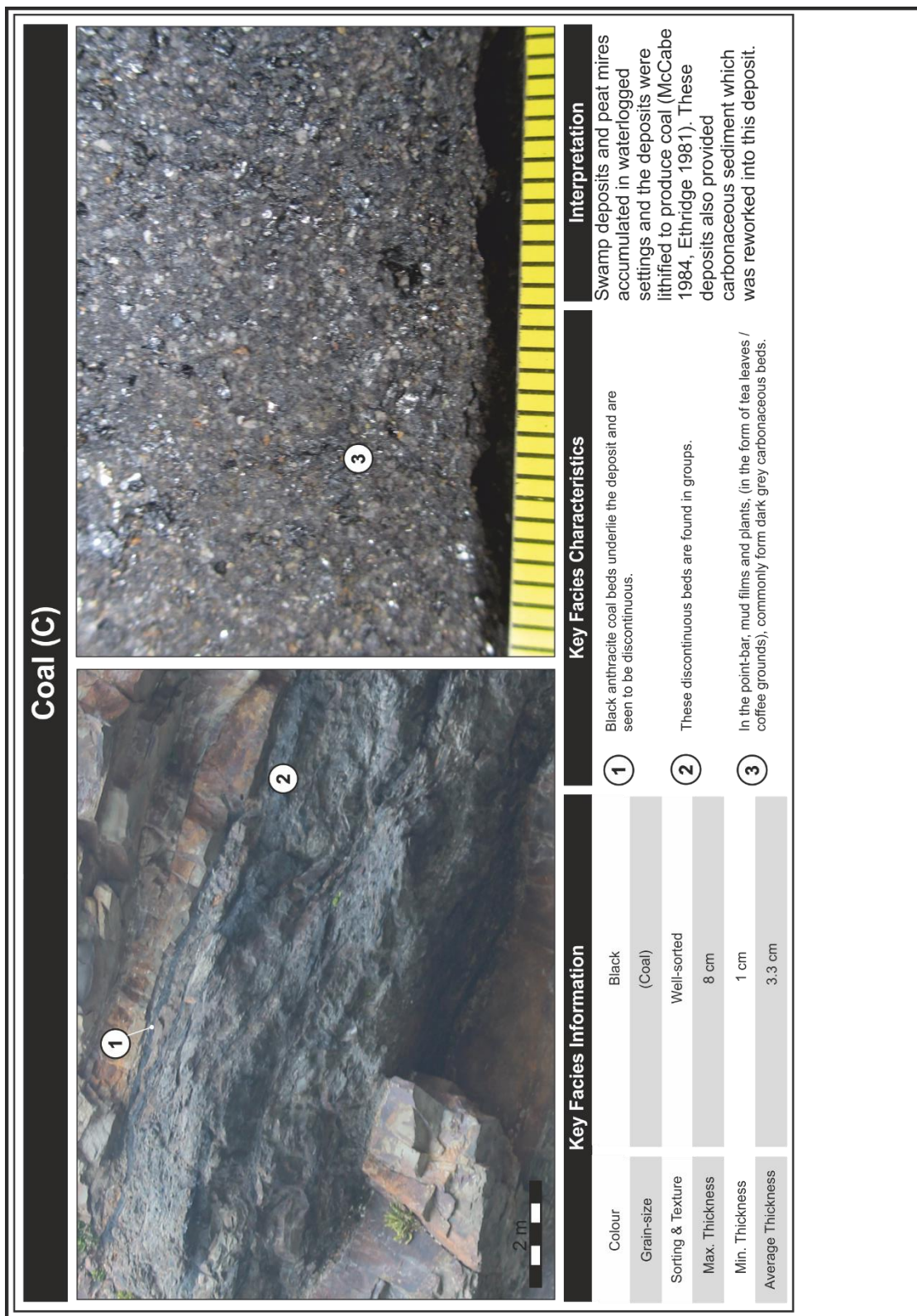


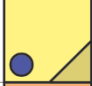

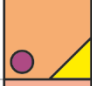

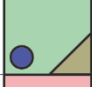
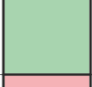
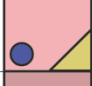
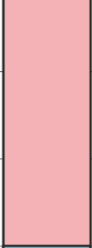

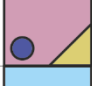



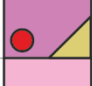
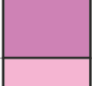




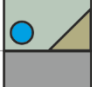

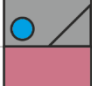







Figure 5.8 - Facies panels describing the facies at the outcrop in detail

### Legend (part 1)

Facies Code	Characteristics	FAKTS facies Code	
St	 Sandy, identifiable from upper surfaces	St	 Trough-cross bedding
Spm	 Cross stratification, medium grain size	Sp	 Planar X-Stratification
Spc	 Cross stratification, coarse grain size		
Spvc	 Cross stratification, very coarse grain size		
Srs	 Ripples in sandy sediment ~ 10cm crest-to-crest	Sr	 Sand Ripples
Sh3	 1-5 cm thick packages of 3 laminations	Sh	 Horizontal Lamination
Sh4	 1-5 cm thick packages of 4 laminations		
Sh5	 1-5 cm thick packages of 5+ laminations		
Slm	 Low-angle cross beds, medium grain size	Sl	 Low-angle X-beds
Slc	 Low-angle cross beds, coarse grain size		
Sec	 Clast supported (crude X-bedding)	Gp	 Erosional Scour Deposits
Sem	 Matrix supported erosional scour	Sm	 Conglomerate
Ss	 Scour fill, X-bedded. Eroded surfaces	Ss	 Scour fill, X-bedded. Eroded surfaces
Fl	 Overbank, coal draped	Fl	 Overbank, coal draped
Fm	 Overbank deposits, includes coal	Fm	 Overbank deposits, includes coal
Fsc	 Laminated or massive silt or mud	Fsc	 Laminated or massive silt or mud
C	 Contains plants / mud films	C	 Contains plants / mud films

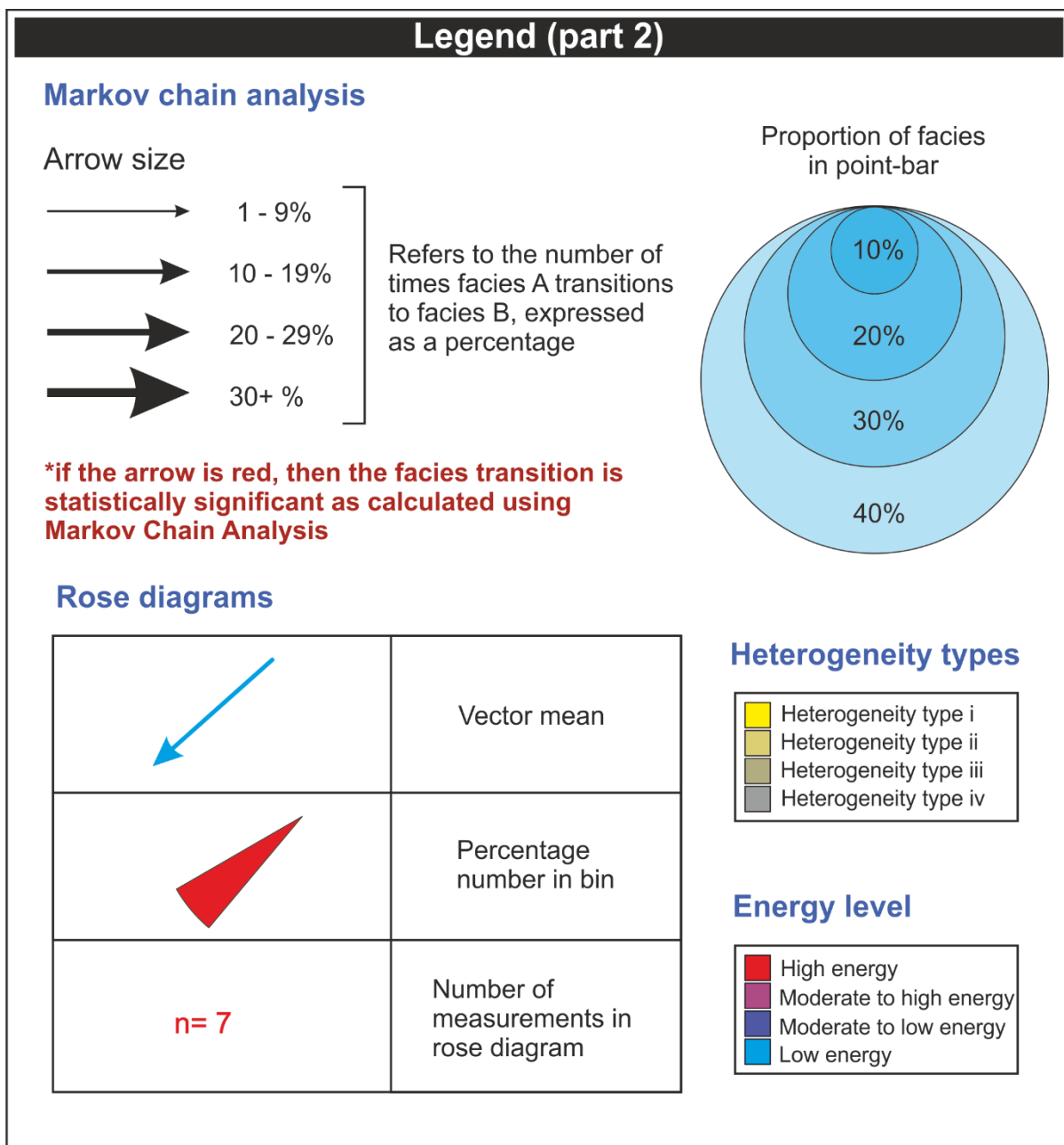


Figure 5.9 - Legends for the following figures. The small triangles on the facies colours represent the average lithologic heterogeneity of the facies. The coloured circles represent the approximate energy that was required for the formation of the sedimentary structures seen.



FAKTS FACIES CODE	FACIES CODE	FACIES	DESCRIPTION	INTERPRETATION
<b>St</b>	St	Trough cross-bedded sandstone	Grey coloured, medium grained sandstone, commonly mud draped. Preserved stacked with reactivation surfaces. Concave down dip with typically 8cm thick and 30-50 cm long. Coarser grained basal channel lag is sometimes present. Beds vary in thickness from 3-26 cm, with an average thickness of 9.7 cm.	Trough cross-bedding formed by unidirectional currents in fluvial channels from migrating three-dimensional dunes in the lower flow regime (Miall 1985), through moderate to high energy traction currents (Adamson <i>et al.</i> 2013). Basal channel lag indicates that these sediments are deposited near the base of the channel.
<b>Sp</b>	Spm	Medium grained planar cross-stratified sandstone	Grey to brown, medium grained sandstone with approximately parallel cross-bedding, and the dip varies from 15-25°. Deposits contain coal granules and carbonaceous drapes and typically fine upwards. Beds	Formed by the downstream migration, or lateral accretion of 2D dunes from a unidirectional flow (Miall 1985, 1988). Within a point-bar, it represents a

			often have erosive bases, and themselves contain second order bedding surfaces. Beds vary in thickness from 3-48 cm, with an average thickness of 14.5 cm.	relatively low-energy environment (cf. Davies and Ethridge 1975, Donselaar and Schmidt 2010).
<b>Sp</b>	Spc	Coarse grained planar cross-stratified sandstone	Grey to brown, coarse grained sandstone with approximately parallel cross-bedding, and the dip varies from 15-25°. Deposits contain coal granules and carbonaceous drapes and typically fine upwards. Beds often have erosive bases, and themselves contain second order bedding surfaces. Beds vary in thickness from 3-50 cm, with an average thickness of 15.2 cm.	Formed by the downstream migration, or lateral accretion of 2D dunes from a unidirectional flow (Miall 1985, 1988). Within a point-bar, it represents a relatively higher-energy environment than that which deposits Spm (cf. Davies and Ethridge 1975, Donselaar and Schmidt 2010).
<b>Sp</b>	Spvc	Very coarse grained planar cross-stratified sandstone	Grey to brown, very coarse grained sandstone with approximately parallel cross-bedding, and the dip varies from 15-25°. Well-sorted, clean, sand grains which typically fine upwards. Beds often have erosive bases, and themselves contain second order bedding	Formed by the downstream migration, or lateral accretion of 2D dunes from a unidirectional flow (Miall 1985, 1988). Within a point-bar, it represents a high-energy environment (Fisher and

			surfaces. Beds vary in thickness from 13-23 cm, with an average thickness of 19.3 cm.	McGowen 1963, Davies and Ethridge 1975, Donselaar and Schmidt 2010).
<b>Sr</b>	Srs	Ripple-laminated sandstone	Light grey fine to medium sandstone within which mud and carbonaceous drapes are common. Beds vary in thickness from 2-24 cm, with an average thickness of 9.8 cm.	Lower flow regime deposits, resulting from the downstream migration of small, sand-prone bedforms in a uni-directional (Miall 1985, 1988).  Carbonaceous drapes indicate periods of differing energy in the system.
<b>Sh</b>	Sh3	Planar laminated sandstone (packages of 3 laminations)	Grey to brown, interlaminated fine- and medium-grained sandstone in packages of 3 laminations. The base of the bed may be erosive, or gradational, and the beds themselves contain second order bedding surfaces. Beds vary in thickness from 1-38 cm, with an average thickness of 10.4 cm.	Deposited from a waning planar bed flow in the lower or upper flow regime (Miall 1985).

<b>Sh</b>	Sh4	Planar laminated sandstone (packages of 4 laminations)	Grey to brown, interlaminated fine- and medium-grained sandstone in packages of 4 laminations. The base of the bed may be erosive, or gradational, and the beds themselves contain second order bedding surfaces. Beds vary in thickness from 2-30 cm, with an average thickness of 10.8 cm.	Deposited from a waning planar bed flow in the lower or upper flow regime (Miall 1985).
<b>Sh</b>	Sh5	Planar laminated sandstone (packages of 5 or more laminations)	Grey to brown, interlaminated fine- and medium-grained sandstone in packages of 5 or more laminations. The base of the bed may be erosive, or gradational, and the beds themselves contain second order bedding surfaces. Beds vary in thickness from 12-25 cm, with an average thickness of 18 cm.	Deposited from a waning planar bed flow in the lower or upper flow regime (Miall 1985).
<b>SI</b>	Slm	Medium grained low-angle cross – stratified sandstone	Medium grained sandstone dipping at <math><15^\circ</math>, with a grey colouration. Contain coal granules and carbonaceous drapes. Beds vary in thickness from 1-80 cm, with an average thickness of 11.0 cm.	Formed by a unidirectional flow which is transitional from lower to upper flow regime within a fluvial environment.



<b>SI</b>	Slc	Coarse grained low-angle cross – stratified sandstone	Coarse grained sandstone dipping at <math><15^\circ</math>, with a grey colouration. Contain coal granules and carbonaceous drapes. Beds vary in thickness from 3-30 cm, with an average thickness of 12.3 cm.	Formed by a unidirectional flow which is transitional from lower to upper flow regime within a fluvial environment.
<b>Gp</b>	Sec	Intraformational conglomerate	Medium-grained sandstone containing gravel-sized clasts composed of coal, sand, silt, or clay, which may be sideritised and orange coloured. Clasts may be 4-30mm in length with an average of 16mm. Clast line scour surfaces and are aligned to cross-bed surfaces. Mostly clast-supported. Beds vary in thickness from 4-18 cm, with an average thickness of 9.8 cm.	Channel lags or scour fills that occurred in a lag at the base of the channel. Clasts are reworked from underlying stratigraphy (coal, sand, and silt clasts), and nearby floodplain deposits (clay clasts).
<b>Sm</b>	Sem	Matrix supported conglomerate	Light-brown to grey, coarse to medium-grained sandstone containing gravel-sized clasts composed of coal, sand, silt, or clay, which may be sideritised and orange coloured. Clasts are sub-rounder and typically lenticular, and may be 4-30mm in length with an	Channel lags or scour fills that occurred in a lag at the base of the channel. Clasts are reworked from underlying stratigraphy (coal, sand, and silt clasts), or may be from bank collapse

			average length of 16mm. Clast line scour surfaces and are aligned to cross-bed surfaces. Mostly matrix supported. Beds vary in thickness from 2-120 cm, with an average thickness of 18.2 cm.	events (Plint 1986), or nearby floodplain deposits (clay clasts).
<b>Ss</b>	Ss	Scour fill	Fine sand forming broad, shallow scour fills. Beds vary in thickness from 2-10 cm, with an average thickness of 5.3 cm.	Scour fill that occurred in a lag at the base of the channel.
<b>Fl</b>	Fl	Laminated mudstone/siltstone	Dark grey, laminated and interbedded mudstone and siltstone, sometimes containing ripples. Beds vary in thickness from 1-15 cm, with an average thickness of 5.3 cm.	Overbank, abandoned channel or flood deposit
<b>Fm</b>	Fm	Mudstone/siltstone with rootlets	Massive silt/mud, grey to orange in colour, often with roots and bioturbation, wood fragments, up to 15cm in length, and coal granules. Beds vary in thickness from 1-23 cm, with an average thickness of 5.2 cm.	Low energy deposits with little/no water flow, likely in the distal parts of the point-bar, or on the floodplain (Fielding 1984).

<b>Fsm</b>	Fsc	Mudstone/siltstone	May be laminated or massive. Well lithified beds vary in thickness from 1-9 cm, with an average thickness of 4.0 cm within the point bar; channel fill is 3.6 m thick.	Low energy deposits with little/no water flow, likely in the distal parts of the point-bar, channel fill (Allen 1965), or on the floodplain.
<b>C</b>	C	Coal, carbonaceous sandstone	Black discontinuous beds of anthracite, though more commonly, mud films and plants, (in the form of tea leaves/coffee grounds), form dark grey carbonaceous beds. Beds vary in thickness from 1-8 cm, with an average thickness of 3.3 cm.	Swamp deposits and peat mires accumulated in waterlogged settings and the deposits were lithified to produce coal (McCabe 1984, Ethridge 1981). These deposits also provided carbonaceous sediment which was reworked into this deposit.

**Table 5.3 – Description of facies characteristics in the deposits of the studied point-bar element at Nolton Haven.**

### 5.7.2 Facies successions

Markov chain analysis enables the assessment of vertical facies relationships to be quantitatively assessed (Selly, 1970; Walker, 1979; 1984; Harper, 1984; Lindholm, 1987). The initial analysis has been undertaken using the Walker (1979) methodology.

A facies code was adopted; in this study, the FAKTS adaptation of the Miall (1973) code is used so that the data might more easily be compared with other areas in future studies. The numbers of transitions were tabulated to generate a tally matrix (Table 5.4). These data were output from the FAKTS database. The number of transitions per row is totalled in the right-hand column.

TALLY	C	Fl	Fm	Fsm	Gp	Sh	Sl	Sm	Sp	Sr	Ss	St	Total
C						1	1	2	1	1		1	7
Fl		6	1				4			1		2	14
Fm							4	1	5				10
Fsm							2					2	4
Gp					1							10	11
Sh		1		1	1	23	15		7	2	1	1	52
Sl	2	4	7	2		21	99	3	30	8	1	5	182
Sm	2		1			1	3	1	3			1	12
Sp	2		2			6	33	1	57	4	1	1	107
Sr	1	3				2	4	1	5	14		2	32
Ss							1		1		1		3
St	1	2		2	8	2	9	2	1	1		98	126
<b>Total</b>	<b>8</b>	<b>16</b>	<b>11</b>	<b>5</b>	<b>10</b>	<b>56</b>	<b>175</b>	<b>11</b>	<b>110</b>	<b>31</b>	<b>4</b>	<b>123</b>	<b>560</b>

**Table 5.4-Tally matrix for the data considered in this study**

A probability matrix was constructed through dividing the number of transitions between two facies (Table 5.5), by the total number of transitions that the facies

undertakes; i.e. for facies Fm, the observed transition probabilities are 0.4 (4/10), to Sl; 0.1 (1/10), to Sm; and 0.5 (5/10), to Sp. Each row will total 1.

PROB	C	Fl	Fm	Fsm	Gp	Sh	Sl	Sm	Sp	Sr	Ss	St	Total
C	0.0000	0.0000	0.0000	0.0000	0.0000	0.1429	0.1429	0.2857	0.1429	0.1429	0.0000	0.1429	1
Fl	0.0000	0.4286	0.0714	0.0000	0.0000	0.0000	0.2857	0.0000	0.0000	0.0714	0.0000	0.1429	1
Fm	0.0000	0.0000	0.0000	0.0000	0.0000	0.0000	0.4000	0.1000	0.5000	0.0000	0.0000	0.0000	1
Fsm	0.0000	0.0000	0.0000	0.0000	0.0000	0.0000	0.5000	0.0000	0.0000	0.0000	0.0000	0.5000	1
Gp	0.0000	0.0000	0.0000	0.0000	0.0909	0.0000	0.0000	0.0000	0.0000	0.0000	0.0000	0.9091	1
Sh	0.0000	0.0192	0.0000	0.0192	0.0192	0.4423	0.2885	0.0000	0.1346	0.0385	0.0192	0.0192	1
Sl	0.0110	0.0220	0.0385	0.0110	0.0000	0.1154	0.5440	0.0165	0.1648	0.0440	0.0055	0.0275	1
Sm	0.1667	0.0000	0.0833	0.0000	0.0000	0.0833	0.2500	0.0833	0.2500	0.0000	0.0000	0.0833	1
Sp	0.0187	0.0000	0.0187	0.0000	0.0000	0.0561	0.3084	0.0093	0.5327	0.0374	0.0093	0.0093	1
Sr	0.0313	0.0938	0.0000	0.0000	0.0000	0.0625	0.1250	0.0313	0.1563	0.4375	0.0000	0.0625	1
Ss	0.0000	0.0000	0.0000	0.0000	0.0000	0.0000	0.3333	0.0000	0.3333	0.0000	0.3333	0.0000	1
St	0.0079	0.0159	0.0000	0.0159	0.0635	0.0159	0.0714	0.0159	0.0079	0.0079	0.0000	0.7778	1

**Table 5.5-A probability matrix for the data considered in this study**

These probabilities were used to construct a facies relationship diagram (Fig. 5.10).

The percentage probability of each transition is indicated by arrow thickness (cf.

Walker, 1979) and its associated number. To assess the significance of the transitions,

an independent trials probability matrix was constructed, which is a model of

randomness against which the transition statistics (Table 5.6) are tested:

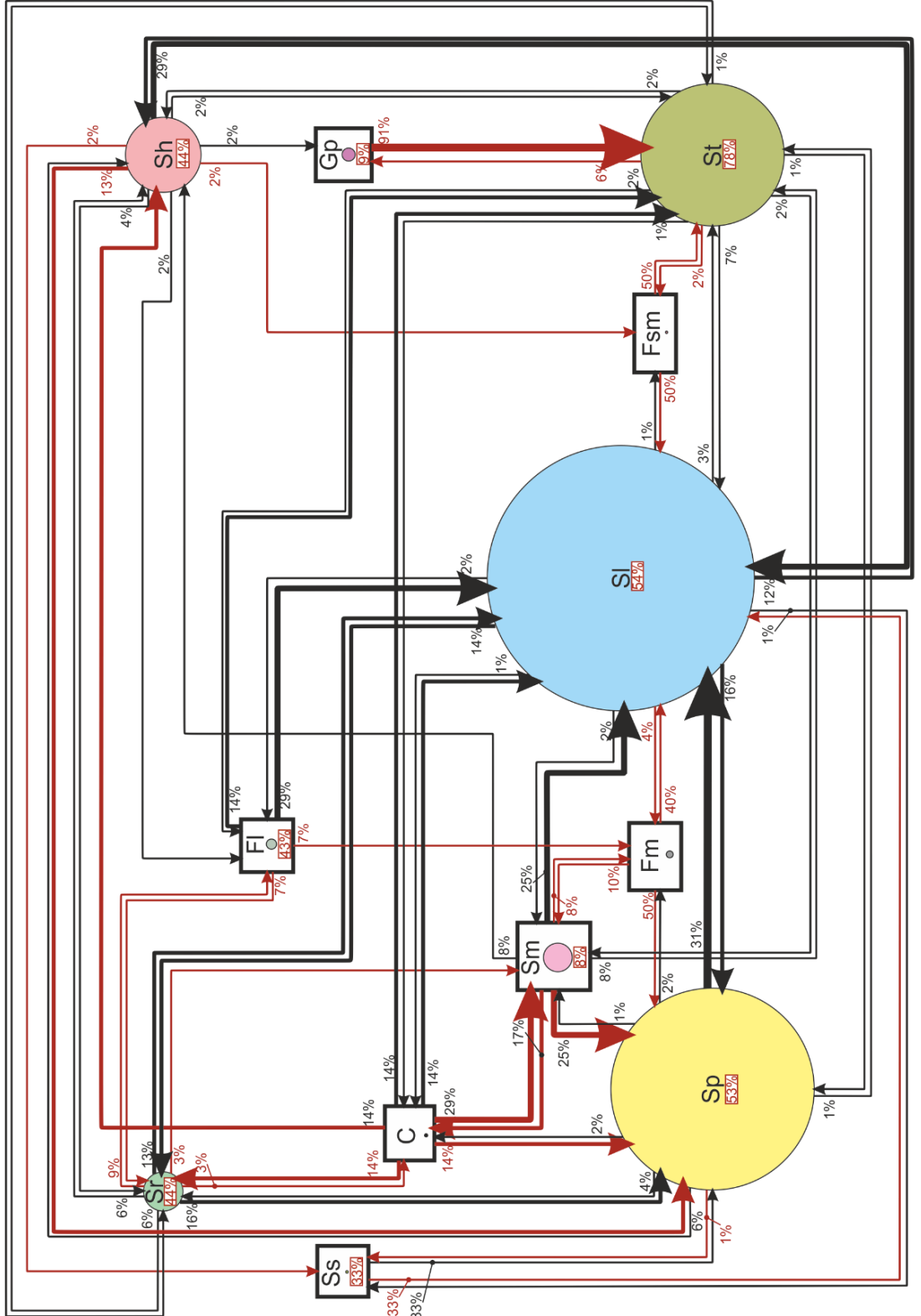
$$\left( \frac{\text{Total number of beds for facies transitioned to (column total)}}{\text{Total number of transitions for all facies}} - \frac{\text{Total number of beds for facies transitioned from (column total)}}{\text{Total number of beds for facies transitioned from (column total)}} \right)$$

**Equation 2 - Equation for forming the independent trials probability matrix**

ITPM	C	Fl	Fm	Fsm	Gp	Sh	Sl	Sm	Sp	Sr	Ss	St	Total
<b>C</b>	0.0145	0.0290	0.0199	0.0091	0.0181	0.1014	0.3170	0.0199	0.1993	0.0562	0.0072	0.2228	1.0145
<b>Fl</b>	0.0147	0.0294	0.0202	0.0092	0.0184	0.1029	0.3217	0.0202	0.2022	0.0570	0.0074	0.2261	1.0294
<b>Fm</b>	0.0146	0.0291	0.0200	0.0091	0.0182	0.1020	0.3188	0.0200	0.2004	0.0565	0.0073	0.2240	1.0200
<b>Fsm</b>	0.0144	0.0288	0.0198	0.0090	0.0180	0.1009	0.3153	0.0198	0.1982	0.0559	0.0072	0.2216	1.0090
<b>Gp</b>	0.0145	0.0291	0.0200	0.0091	0.0182	0.1018	0.3182	0.0200	0.2000	0.0564	0.0073	0.2236	1.0182
<b>Sh</b>	0.0159	0.0317	0.0218	0.0099	0.0198	0.1111	0.3472	0.0218	0.2183	0.0615	0.0079	0.2440	1.1111
<b>Sl</b>	0.0208	0.0416	0.0286	0.0130	0.0260	0.1455	0.4545	0.0286	0.2857	0.0805	0.0104	0.3195	1.4545
<b>Sm</b>	0.0146	0.0291	0.0200	0.0091	0.0182	0.1020	0.3188	0.0200	0.2004	0.0565	0.0073	0.2240	1.0200
<b>Sp</b>	0.0178	0.0356	0.0244	0.0111	0.0222	0.1244	0.3889	0.0244	0.2444	0.0689	0.0089	0.2733	1.2444
<b>Sr</b>	0.0151	0.0302	0.0208	0.0095	0.0189	0.1059	0.3308	0.0208	0.2079	0.0586	0.0076	0.2325	1.0586
<b>Ss</b>	0.0144	0.0288	0.0198	0.0090	0.0180	0.1007	0.3147	0.0198	0.1978	0.0558	0.0072	0.2212	1.0072
<b>St</b>	0.0183	0.0366	0.0252	0.0114	0.0229	0.1281	0.4005	0.0252	0.2517	0.0709	0.0092	0.2815	1.2815

**Table 5.6-An independent trials probability matrix for the data considered in this study**

Markov chain analysis - Walker method with self-transitions



**Figure 5.10 – Depiction of the probabilities and statistical significance of facies relationships through use of the Walker (1979) methodology. This method also describes independent proportions of each facies in the point-bar deposit exposure.**

A difference matrix was then calculated by subtracting the number calculated in the independent trials probability matrix (Table 5.4), from the probability as calculated from the tally matrix (Table 5.6). All values will fall between +1.0 and -1.0. Negative values indicate that the transition may occur randomly, but a positive value shows the transition may occur more frequently than randomness would account for (Selley, 1970; Walker, 1979). The positive values are highlighted in Table 5.7 with a yellow cell, and in the facies relationship diagram (Fig. 5.10), by a dark red arrow.

DIFF	C	Fl	Fm	Fsm	Gp	Sh	Sl	Sm	Sp	Sr	Ss	St
C	-0.0145	-0.029	-0.0199	-0.0091	-0.0181	<b>0.04141</b>	-0.1742	<b>0.26579</b>	-0.0564	<b>0.0867</b>	-0.0072	-0.08
Fl	-0.0147	<b>0.3992</b>	<b>0.0512</b>	-0.0092	-0.0184	-0.1029	-0.036	-0.0202	-0.2022	<b>0.01444</b>	-0.0074	-0.0832
Fm	-0.0146	-0.029	-0.02	-0.0091	-0.0182	-0.102	<b>0.08124</b>	<b>0.07996</b>	<b>0.29964</b>	-0.0565	-0.0073	-0.224
Fsm	-0.0144	-0.029	-0.0198	-0.009	-0.018	-0.1009	<b>0.18468</b>	-0.0198	-0.1982	-0.0559	-0.0072	<b>0.27838</b>
Gp	-0.0145	-0.029	-0.02	-0.0091	<b>0.0727</b>	-0.1018	-0.3182	-0.02	-0.2	-0.0564	-0.0073	<b>0.68545</b>
Sh	-0.0159	-0.013	-0.0218	<b>0.0093</b>	-0.0006	<b>0.3312</b>	-0.0588	-0.0218	-0.0836	-0.023	<b>0.01129</b>	-0.2248
Sl	-0.0098	-0.02	<b>0.0099</b>	-0.002	-0.026	-0.0301	<b>0.08941</b>	-0.0121	-0.1209	-0.0366	-0.0049	-0.292
Sm	<b>0.1521</b>	-0.029	<b>0.0633</b>	-0.0091	-0.0182	-0.0187	-0.0688	<b>0.0633</b>	<b>0.04964</b>	-0.0565	-0.0073	-0.1407
Sp	<b>0.0009</b>	-0.036	-0.0058	-0.0111	-0.0222	-0.0684	-0.0805	-0.0151	<b>0.28827</b>	-0.0315	<b>0.00046</b>	-0.264
Sr	<b>0.0161</b>	<b>0.0635</b>	-0.0208	-0.0095	-0.0189	-0.0434	-0.2058	<b>0.01046</b>	-0.0517	<b>0.3789</b>	-0.0076	-0.17
Ss	-0.0144	-0.029	-0.0198	-0.009	-0.018	-0.1007	<b>0.01859</b>	-0.0198	<b>0.13549</b>	-0.0558	<b>0.32614</b>	-0.2212
St	-0.0104	-0.021	-0.0252	<b>0.0044</b>	<b>0.0406</b>	-0.1123	-0.329	-0.0093	-0.2438	-0.063	-0.0092	<b>0.49631</b>

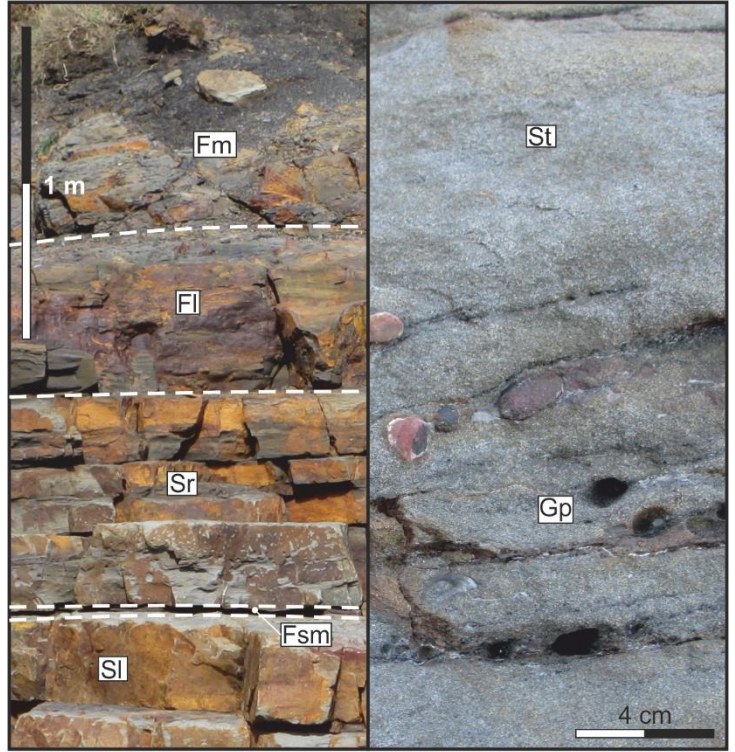
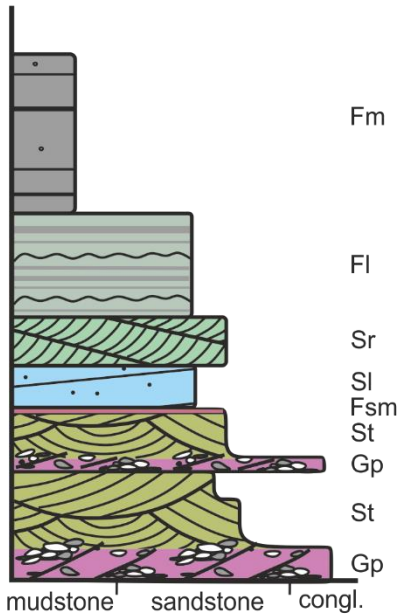
**Table 5.7 - A difference matrix between the independent trials probability matrix, and the probabilities calculated from the tally matrix. Yellow cells highlight numbers that are statistically significant**

Despite the weaknesses of this method (Walker, 1979), it is still of value, and may be used to aid in the observation of trends (Lindholm, 1987).



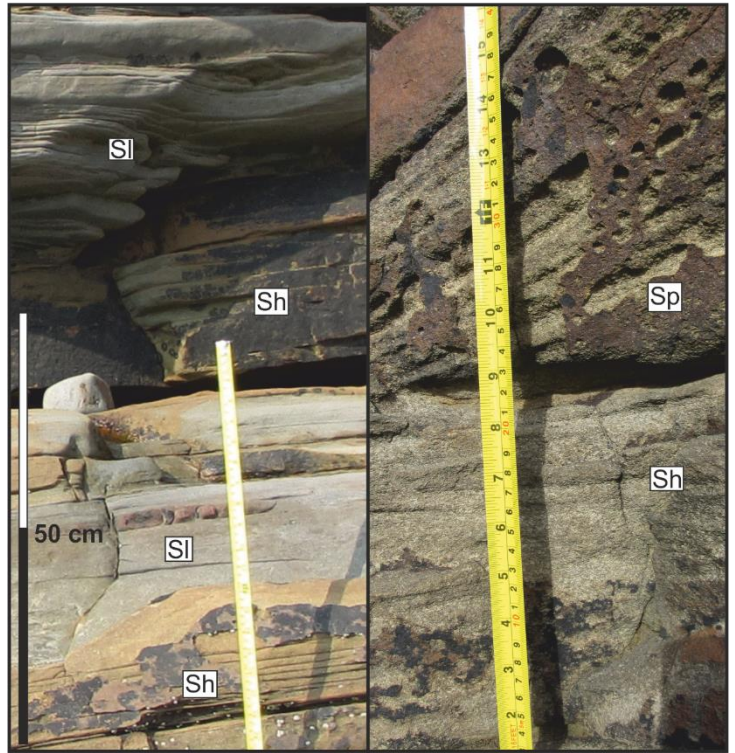
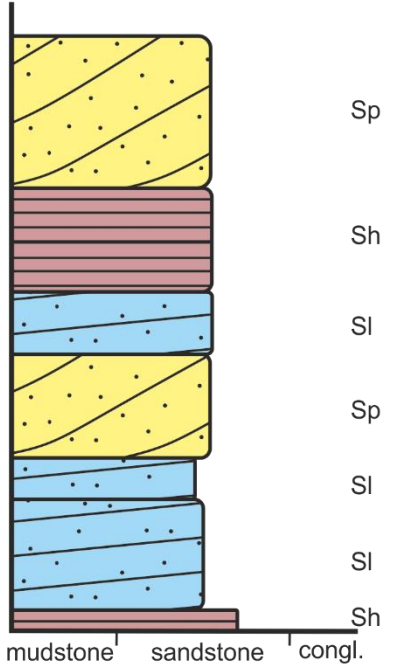
### A Facies Succession 1

**Constituent facies**  
Gp, St, Fsm, Sl, Sr, Fl, Fm



### B Facies Succession 2

**Constituent facies**  
Sh, Sl, Sp

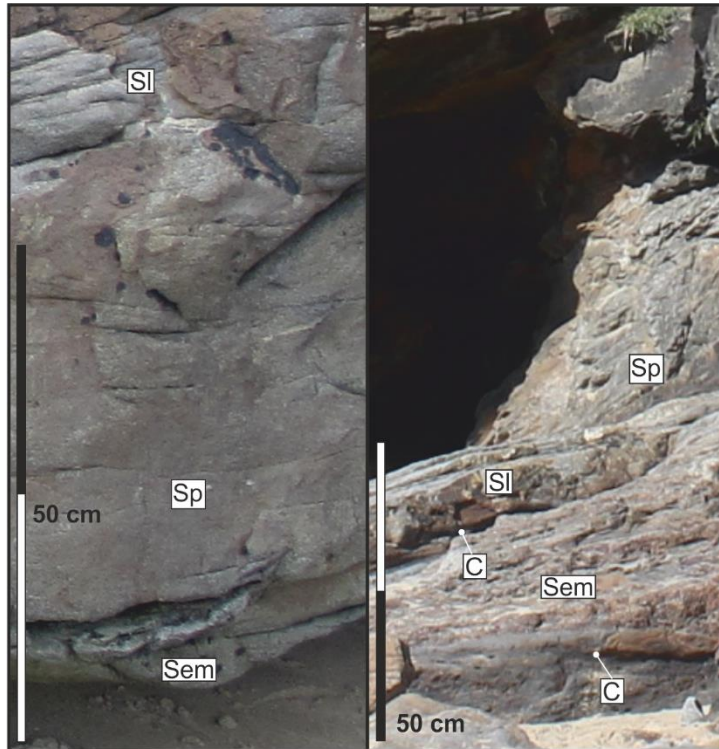
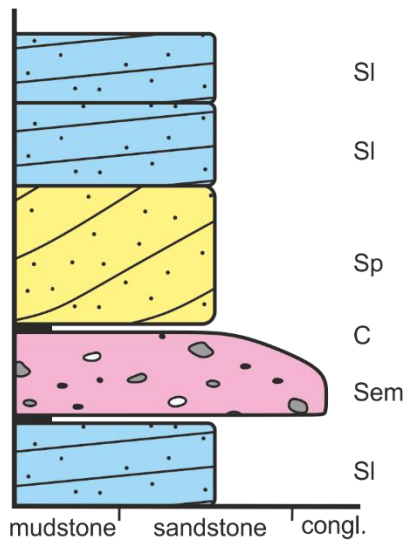




**C**

**Facies Succession 3**

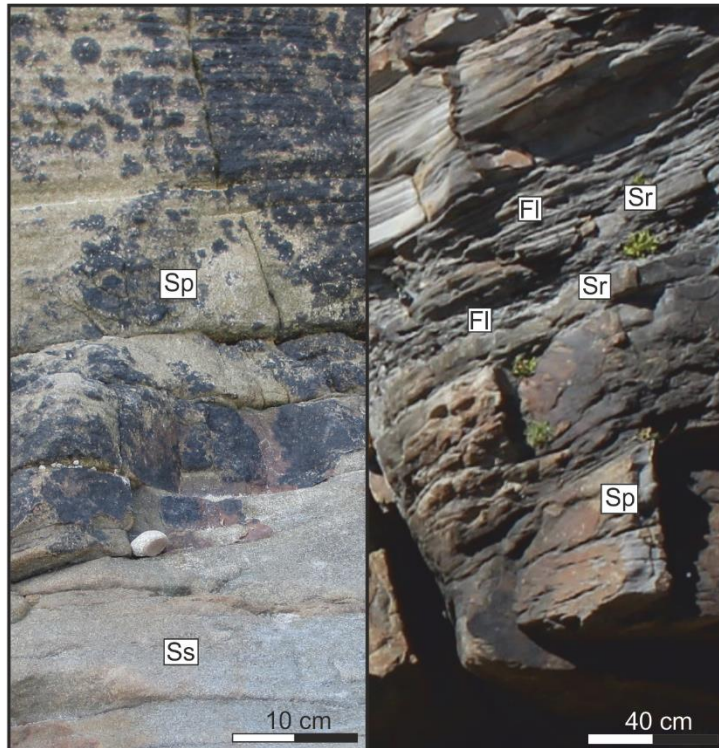
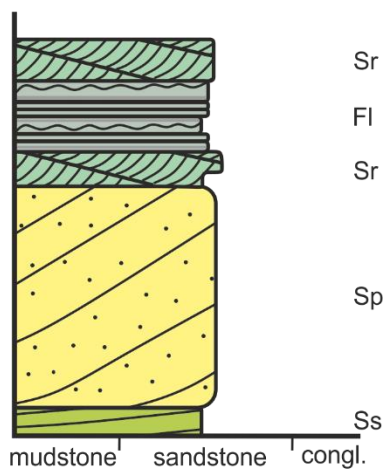
**Constituent facies**  
Sl, Sem, C, Sp



**D**

**Facies Succession 4**

**Constituent facies**  
Ss, Sp, Sr, Fl



**Figure 5.11 – Figures showing sketch logs, and outcrop examples, of the facies successions identified in this study through use of the Markov chain analyses undertaken.**

#### 5.7.2.1 Facies Succession 1 (Fig. 5.11A)

All of the facies transitions included in facies succession 1 (except for the SI to Sr transition) are marked as statistically significant by the Walker (1979) methodology. The SI to Sr transition has been included because it is observed, though in some cases there is a thin bed of Fsm between SI and Sr. The strongest association in this data is Gp to St, and Sr to FI is also seen often.

The base of the facies succession is typically eroded, and infilled with facies Gp. Facies Gp transitions to St which itself may display inter-erosion (Fig. 5.10). Facies Fsm is typically either observed above or below facies SI, so either Fsm or SI may be next in the succession, though SI is not always observed. The final three facies are Sr, FI and Fm, which display an overall fining upwards trend.

The facies succession displays an overall decrease in energy from high-energy erosive facies (Gp, and St), to low energy more mud-prone facies (Fm) (Fig. 5.12), thereby describing an environment where variations in flow energy are marked.

#### 5.7.2.2 Facies Succession 2 (Fig. 5.11B)

The transitions that are included in facies succession 2 are commonly seen together on the sedimentary graphic logs, though are not considered as statistically significant by either the Walker (1979) methodology. This is because the individual facies transitions are not unique to each other making the transition likelihood less; i.e. although the probability that the transition may occur is high (Fig. 5.10), the transition is not sufficiently unique for it to be reported as statistically significant. Facies Sh, SI, and Sp

are seen to be associated in the sedimentary graphic logs (Appendix C); their relationships are seen to have high probabilities of occurrence (Fig. 5.10).

The base of where these associated facies initiate, is typically eroded, and there are further erosion surfaces between, and within, each bed. Facies Sh, Sl, and Sp are interbedded, and may commonly undertake self-transitions (Fig. 5.10). Across the overall point-bar deposit from proximal to distal occurrences of Facies Succession 2, Sh is observed the most at the proximal end of the point-bar deposit, Sp then becomes dominant and is interbedded with Sl, Sl becomes more frequent, then Sh becomes more dominant again.

Across this facies succession, there is a uniform grainsize of 400-500  $\mu\text{m}$ , and variance in flow is expressed by the different bedforms. The grainsize indicates that these sediments were deposited by a moderate, to high-energy flow.

#### 5.7.2.3 Facies Succession 3 (Fig. 5.11C)

The Walker (1979) methodology marks Sm to C, C to Sm, C to Sp, and Sm to Sp as significant where self-transitions are considered (Fig. 5.10). There is a strong inter-relationship observed from C to Sm.

The base of facies succession 3 is typically erosional. The scour is then infilled with either Sem, or Sl, and C is commonly deposited on either side of Sem. Sem will transition up to sand-prone facies such as Sp and Sl.

The flow that deposited facies succession 3 demonstrates fluctuating energy, as C which is associated with low energy, is observed adjacent to Sem which is associated with high energy. It represents channel lag, and slump / bank collapse deposits.

#### 5.7.2.4 Facies Succession 4 (Fig. 5.11D)

The Walker (1979) methodology marks Ss to Sp, Sp to Ss, Sr to Fl, Fl to Sr as significant where self-transitions are considered (Fig. 5.10); Sr to Fl is markedly significant. Transitions between Sp and Sr are also probable, but not statistically significant. Where self-transitions are not considered, the same significant relationships are observed.

The base of facies succession 4 is erosional and is infilled by Ss. Facies Sp then typically follows Ss, and Sr is seen to overlay sand-prone facies. Sr and Fl have a strong interrelationship and this is due to the common interbedding of these two facies.

The flow that deposited facies succession 4 shows an overall decrease in energy. It begins with a high-energy scour, and then migrating dunes produce Sp. The flow velocity then decreased significantly, and sustained a low energy level that transitions between low energy (depositing Sr), and no movement (depositing Fl).

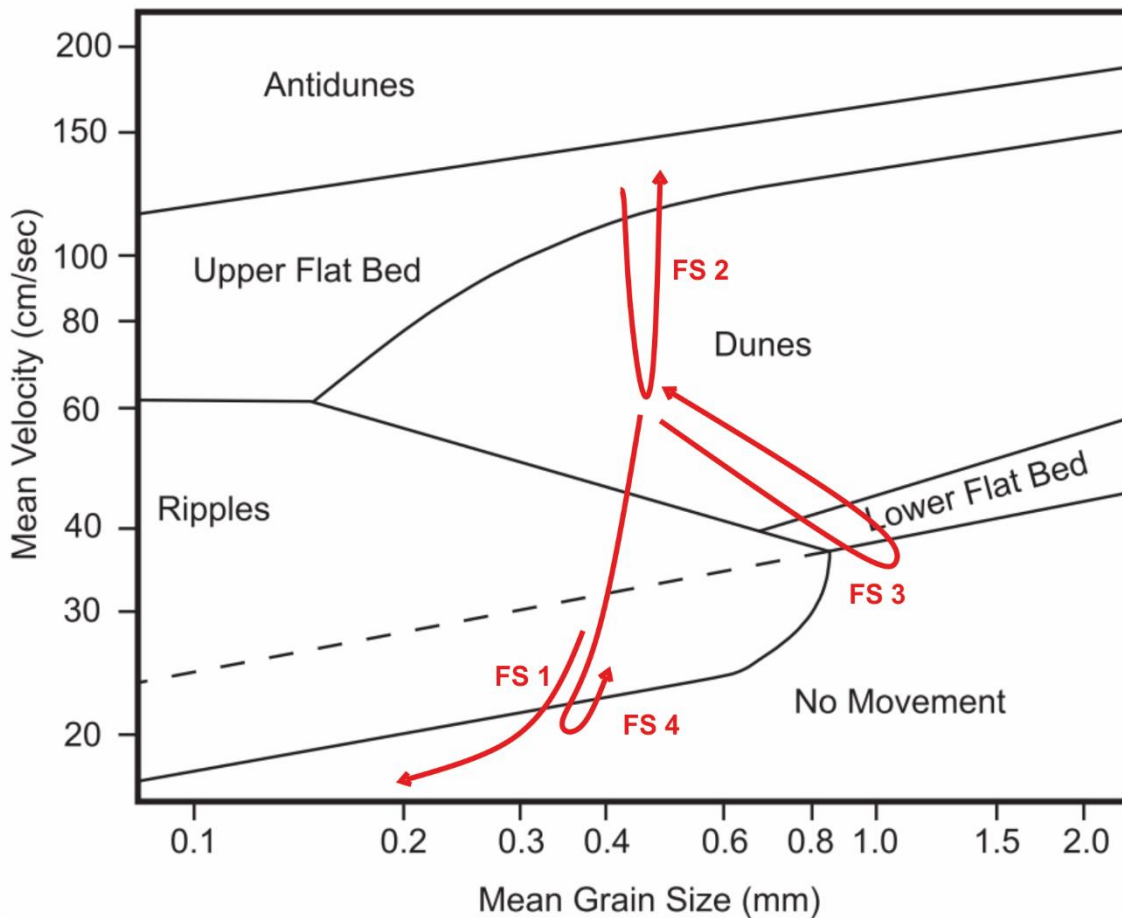


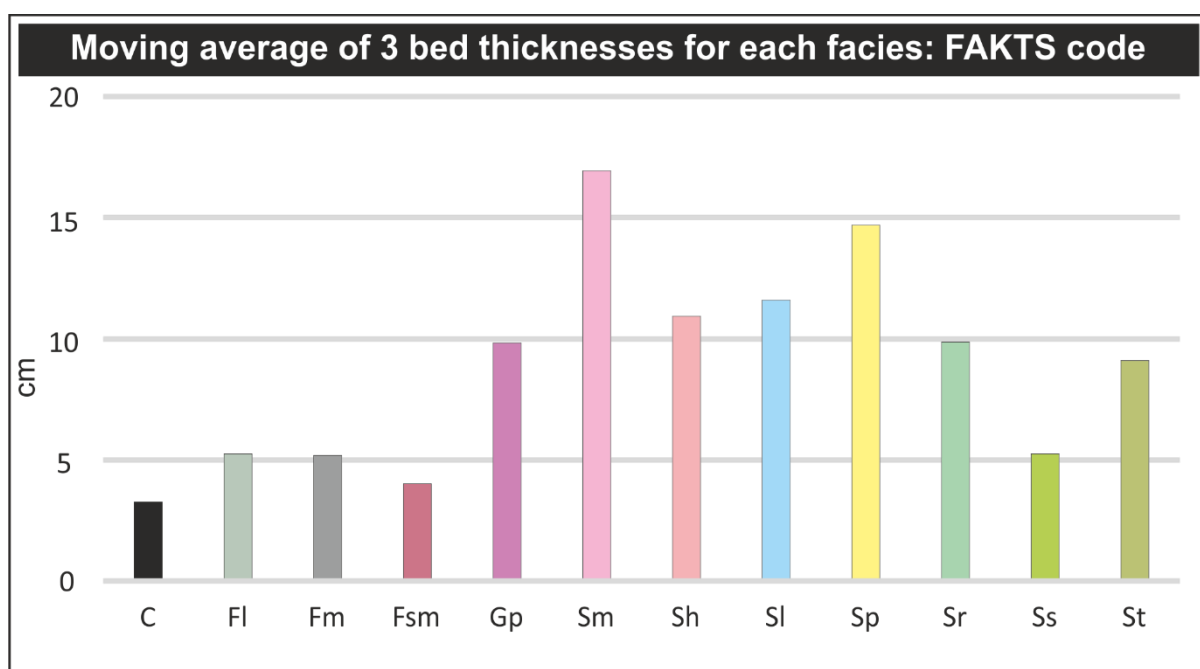
Figure 5.12 – A bedform phase diagram that relates the mean grainsize to the mean flow velocity. Each facies succession is approximately positioned on the graph (from Ellison 2004, in turn modified from Middleton & Southard 1978). Note that the values on this figure are derived from a certain range of flood depths therefore velocities may not be read directly from this graph.

### 5.7.3 FAKTS analysis

The bed number, facies types and bed thickness for 560 beds were input and analysed using the FAKTS database (Colombera *et al.*, 2013). The 12 facies codes used in this analysis are the FAKTS facies codes; they group some sub-divisions in this study (Fig. 5.9 legend B). The outputs from this analysis were: i) thickness of the moving average

of 3 beds (Fig. 5.13); ii) the relative proportion of each facies type to others in the point-bar deposit; and iii) a tally of the occurrences of each facies vertical transition (Fig. 5.14A).

The average bed thickness for each facies (Fig. 5.13) reveals that the facies that exhibit the thickest beds are matrix-supported conglomerate (Sm), and planar cross-stratified sandstone (Sp). The key finding from this graph is that, with the exception of scour fill (Ss), facies that are of medium sand grainsize or above, on average occur in beds of thickness greater than 8 cm; all fine-grained sediment recorded occurs in beds that are on average less than 6 cm thick (coal, C), laminated mudstone / siltstone (Fl), mudstone / siltstone with rootlets (Fm), mudstone / siltstone (Fsm)), mudstone / siltstone (Fsm)).

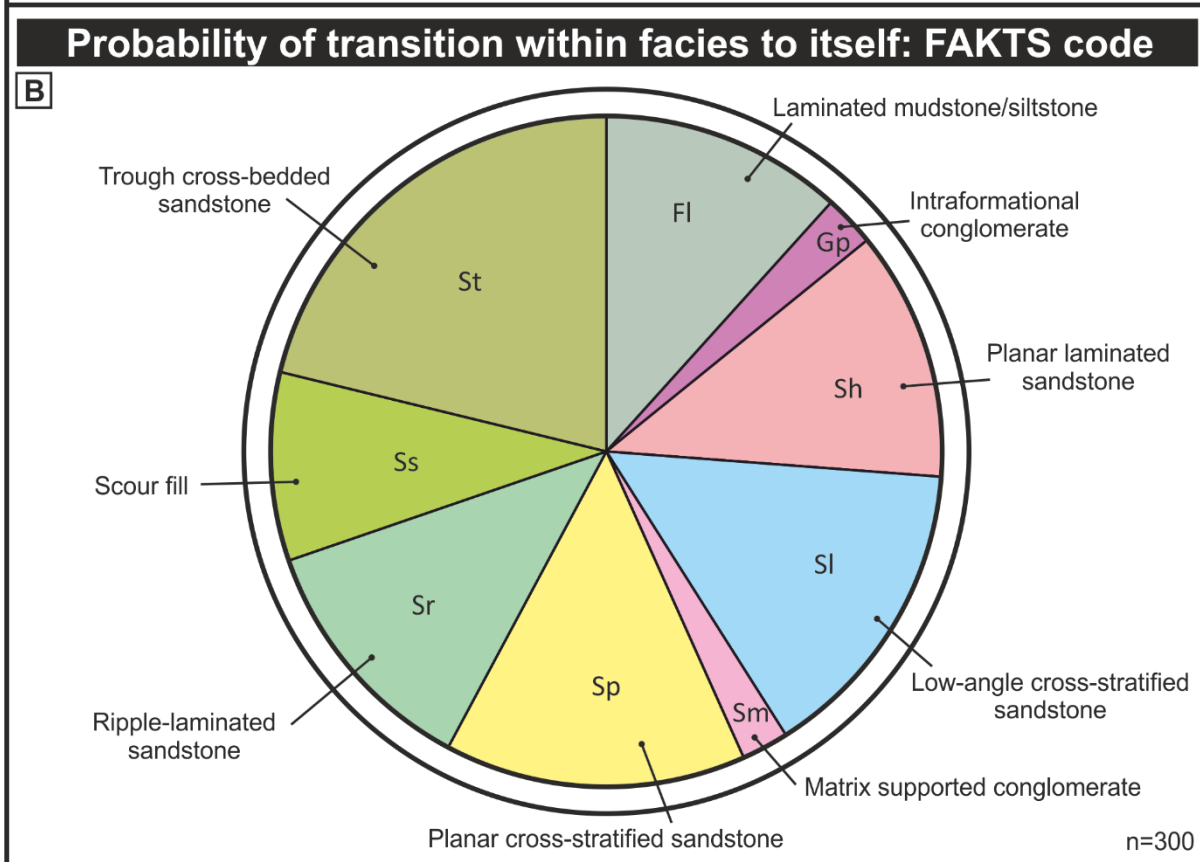
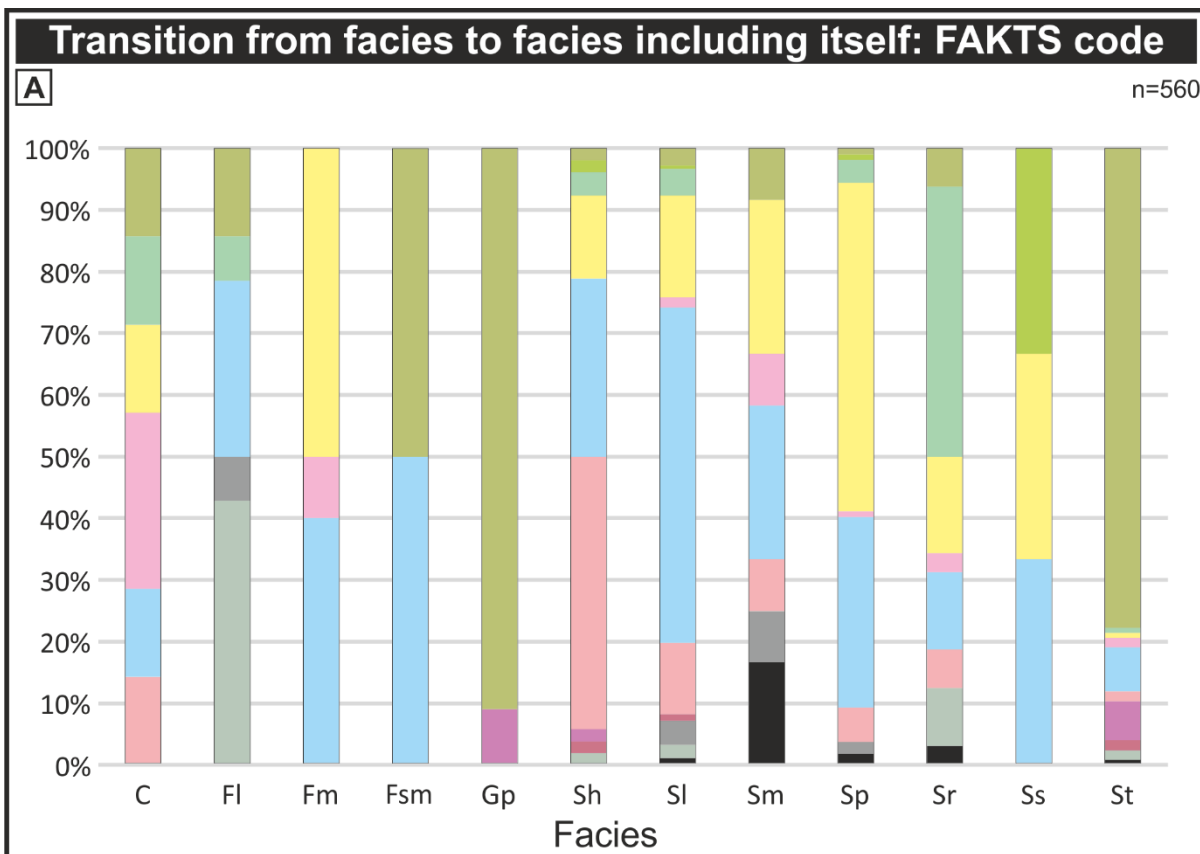


**Figure 5.13 - A figure to show the average bed thicknesses for a 3 bed thick moving average of each facies.**

Figure 5.14A is a stacked column to illustrate the proportion of occurrences of a facies transitioning to another derived from the probability matrix (Table 5.5). Each facies may

transition vertically upward into a variety of other facies, although it is worth noting that trough cross-bedded sandstone (St) transitions to itself 78% of the time, and intraformational conglomerate (Gp) transitions to trough cross-bedded sandstone (St) 91% of the time. Intraformational conglomerate (Gp) is also the only facies that is not observed to transition to low-angle cross stratified sandstone (Sl). Figure 5.13B shows the relative probability that a facies will transition to itself. Of the 12 FAKTS facies codes, 3 do not self-transition (Fm, Fsm, and C). Trough cross-bedded sandstone (St) is the most likely to self-transition, whilst matrix supported conglomerate (Sm), and intraformational conglomerate (Gp), are the least likely to self-transition.





**Figure 5.14 - A) A stacked column to show the probabilities of transition between facies; B) A pie chart describing the probability of each facies transitioning to itself vertically upward.**

#### 5.7.4 Panels

Sedimentary graphic logs have been constructed into panels to enable more complex observations to be undertaken. The image shown in Figure 5.15A is of the exposure studied; a pseudo three-dimensional panel has been constructed. Figure 5.15B shows the detailed facies (Fig. 5.9 legend A), and the pie charts show average three bed thickness for each log. This figure shows that the facies exhibiting the thickest bed is not necessarily the dominant facies in the log. Figure 5.15C shows the FAKTS facies (Fig. 5.9, legend B), with erosional surfaces marked. There is a decreasing density of erosional surfaces towards the south. Rose diagrams indicate the change in accretion direction changes from trending NW at the north-most end of the point-bar, to trending SW at the south-most end of the point-bar (Fig. 5.15C). Figure 5.15D displays the generalised heterogeneity of the point-bar exposure. It is seen to be most sand-prone in the central portion. Figure 5.16B is the estimated energy required for the formation of each facies. Estimations are derived from Fisher and McGowen (1963), Allen (1965), Davies and Ethridge (1975), Ethridge (1981), Fielding (1984), McCabe (1984), Miall (1985), Donselaar and Schmidt (2010), and Adamson *et al.* (2013). From Figure 5.16B, it can be observed that facies categorised as high-energy deposits are few, and facies categorised as moderate- to high-energy deposits are common.

**Figure 5.15 - A) A field photo of the exposure studied at Nolton Haven; B) a pseudo-3D panel of the detailed facies described in Table 5.1; C) a pseudo-3D panel of the simplified facies according to the FAKTS classification scheme overlain with the erosional surfaces seen, and rose diagrams; D) a pseudo-3D panel of the average lithologic heterogeneity across the point-bar deposit.**

**Figure 5.16 - A) A field photo of the exposure studied at Nolton Haven; B) a pseudo-3D panel of the relative energy required to deposit each bed, interpreted using Table 5.3 and Figure 5.12; C) a pseudo-3D panel of the interpreted facies successions.**













## 5.8 Discussion

Here, outcrop data are assessed to establish the lateral extent, and the palaeo-accretion history of the point-bar. This is achieved in three stages; i) use of established palaeohydraulic methodologies; ii) use of facies and derived facies successions; iii) consideration of the internal architecture and data established in Chapters 2-4.

### 5.8.1 Application of established methodologies

The studied outcrop lends itself to numerical analysis as it is well exposed. A list of parameters and their associated equations has been compiled from the literature (Leopold & Wolman, 1960; Schumm, 1960; 1963; Carlston, 1965; Schumm, 1972; Leeder, 1973; Ethridge & Schumm, 1977; Collinson, 1978; Osterkamp & Hedman, 1982; Williams, 1984; Bridge & Mackey, 1993; Bhattacharya *et al.*, 2015; Table 5.9). In order to undertake these analyses, the parameters listed in Table 5.8 are required.

<b>Length of outcrop</b> (straight line outcrop length measured from satellite imagery)	123 m
<b>Thickness of point-bar (Dt)</b> (Maximum thickness recorded)	4.3 m
<b>Average grainsize</b>	400 $\mu\text{m}$
<b>Horizontal length of a lateral accretion surface (Wla)</b>	10.9 m
<b>Channel width (W)</b>	22.7 m
<b>Channel depth (D)</b>	3.4 m

Table 5.8 - A table of the parameters used in the calculations

There is a selection of calculations for each parameter, the most commonly used have been selected (Table 5.9). With regard to discharge there is a selection of options, all of which are based on differing data (Peakall, 1995). The equation proposed by Williams (1984; modified from Schumm, 1972), has been selected as it is commonly used; the equation proposed by Osterkamp and Hedman (1982), has been selected because it is derived from a large dataset. The abandoned channel exposed at the outcrop does not represent the maximum depth of the channel because the maximum thickness of the point-bar deposit exceeds that of the abandoned channel deposit (Table 5.8). For this reason, the equation from Williams, (1984) modified from Schumm, (1972), for average daily discharge; the measurement for the thickest part of the point-bar ( $D_t$ ), has been used in place of the parameter  $D_{max}$ .

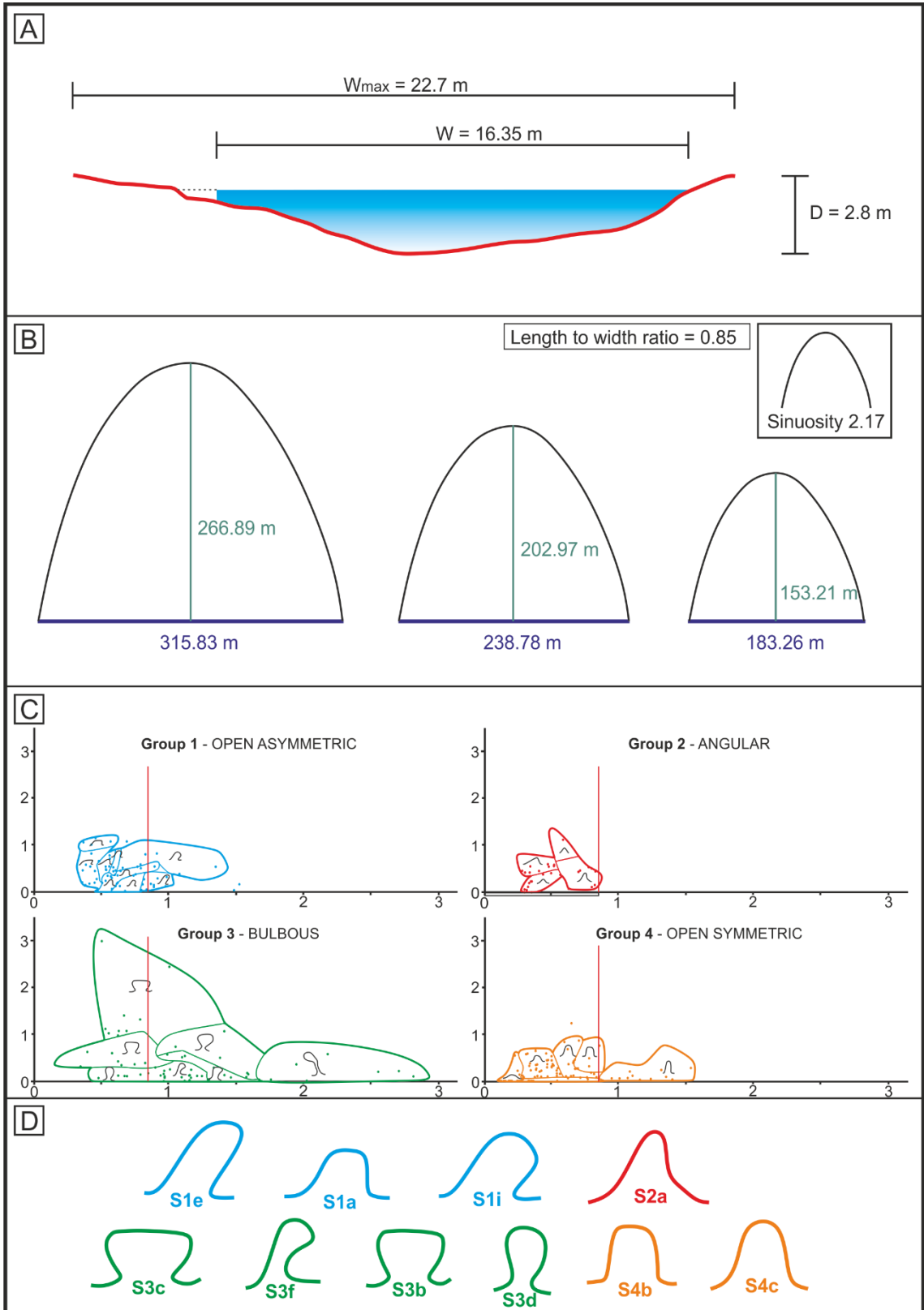
Parameter	Symbol	Unit	Equation	Result
<b>Average flow velocity</b> (Middleton & Southard, 1978)	U	cm/s <sup>-1</sup>	Achieved through observation of Figure 5.14	0.60-0.75 m/s
<b>Mean Bankfull Depth</b> (Ethridge & Schumm, 1977)	D	m	$D = 0.585D_t/0.9$	2.80 m
<b>Mean Bankfull Width</b> (Ethridge & Schumm, 1977)	W	m	$W = 1.5W_l a$	16.35 m
(Leeder, 1973)			$W = 6.8D^{1.54}$	33.11 m

<b>Width to Depth ratio of channel</b> (Schumm, 1960)	F	--	$F = W/D$	5.85
<b>Sinuosity</b> (Schumm, 1963)	P	--	$P = 3.5F^{-0.27}$	2.17
<b>Discharge (unspecified)</b> (Bhattacharya, 2015)	Q	m <sup>3</sup> /s	$Q = U*(D*W)$	2746.8 m <sup>3</sup> /s to 3433.5 m <sup>3</sup> /s
<b>Average daily discharge</b> (Williams, (1984) modified from Schumm, (1972))	Qm	m <sup>3</sup> /s	$Qm = 0.029W^{1.28}D_{max}^{1.10}$	6.06 m <sup>3</sup> /s
(Osterkamp & Hedman, 1982)			$Qm = 0.027W^{1.71}$	5.63 m <sup>3</sup> /s
<b>Mean annual flood</b> (Schumm, 1972)	Qma	m <sup>3</sup> /s	$Qma = 16(W^{1.56}/F^{0.66})$	389.68 m <sup>3</sup> /s
<b>Channel slope</b> (Schumm, 1972)	S	m/km	$S = 30(F^{0.95}/W^{0.98})$	6.24 m/km
<b>Meander wavelength</b> (Schumm, 1972)	$\lambda_m$	m	$L = 18 (F^{0.53}W^{0.69})$	315.83 m

(Leopold & Wolman, 1960)			$L = 10.9W^{1.01}$	183.26 m
(Carlston, 1965)			$L = 106Qm^{0.46}$	238.79 m
<b>Meander-belt (channel belt) width</b> (Bridge & Mackey, (1993) modified from Collinson, (1978)	$W_m$	m	$W_m = 65.6*D^{1.57}$	330.33 m

**Table 5.9 - A table of the parameters and associated equations used in this study.**

A moderate velocity of 0.60-0.75 m/s is tenuously calculated through observation of Figure 5.12 where an average grainsize of 400  $\mu\text{m}$  is considered, and seen to dominantly produce dunes. The average bankfull depth and average bankfull width are calculated by the equations proposed by Ethridge and Schumm (1977) (Fig. 5.17A). The equation proposed by Leeder (1973) considerably over-estimates the preserved bankfull width, so is discounted. The equations for average daily discharge ( $Q_m$ ) give similar results from Williams (1984, modified from Schumm, 1972), and Osterkamp and Hedman (1982) that average at 5.84  $\text{m}^3/\text{s}$ .



**Figure 5.17 – A visual summary of the numerical deductions that were undertaken using the equations in Table 9**

The sinuosity has been derived through use of the equation proposed by Schumm (1963), and found to be 2.17 (Table 5.9) The sinuosity may be expressed as a sine-wave shape, and scaled to suit the wavelength parameters deduced through use of the equations proposed by Schumm (1972), Leopold and Wolman (1960) and Carlston (1965) (Fig. 5.17B). Each wavelength measurement may be considered as possible as the outcrop is 123 m in length, and the minimum length value calculated is 153.21 m (Fig. 5.17B). The ratio of the length to meander width values (as defined in Chapter 2), may be expressed as the ratio 0.85. The ratio was plotted onto the graphs derived through use of the Intersection Shape methodology (Chapter 2), and found to intersect with 10 possible shapes from Groups 1 to 4 (Figs 5.17C and D). These shapes present a wide range of lateral extent. Therefore the approach provided through use of the equations is insufficient for determining the lateral extent of a point-bar deposit. However, due to the limited extent of the outcrop, these equations are able to provide estimations of otherwise unattainable characteristics, such as channel slope, and meander belt width.

The main weakness of utilising the equations in Table 5.9 is the aggradation of extrapolated values. Every result presented is derived from the thickness of the point-bar deposit, and the distance between lateral accretion surfaces. Both of these parameters are variable, and may differ considerably depending on the position of the outcrop in the point-bar being studied. Also, the parameters attained reconstruct the meander assuming avulsion occurred i.e. as if it is active. Where avulsion has not occurred, the resulting dimensions of the point-bar deposit will be different (Chapter 4), therefore these approaches are not always appropriate. Another weakness it that the

shapes derived through use of the Intersection Shape methodology are active shapes, however, they are able to place on the flowchart and enable dynamic processes to be considered, and from deducing a planform shape (or selection thereof), the lateral accretion history may be more accurately determined.

### *5.8.2 Application of facies and facies successions*

The facies in a point-bar are laterally discontinuous and variable (Labreque *et al.*, 2011; Moody & Mead, 2014; Shiers *et al.*, in review). The facies divisions that have been identified and utilised in this study have provided a useful framework from which facies successions have been interpreted. Detail in this analysis has been particularly aided by facies sub-divisions based on grainsize, as they have enabled the variability of bedforms, grainsize and heterogeneity to be observed (Fig. 5.8). The facies were mapped onto a pseudo-3D panel that was recoloured with facies properties to more easily enable integrated visual comparisons (Figs 5.15 and 5.16). Identifying and assessing the distribution of facies and facies successions enables: (i) the position of an outcrop in a point-bar to be approximately determined; (ii) the interpretation of the accretion history, and morphological history of the point-bar to be validated with bedform characteristics; and (iii) identification of predictable trends to achieve testable hypotheses. The panels highlight that the distal end of the point-bar is to likely be to the SSW, because this is where mud-prone sediment deposited by low energy flow is seen most consistently (Fig. 5.16). This is substantiated through observation of the lateral accretion surfaces that are also angled towards SSW. It may be noted that trough-cross bedding (St) occurs where there is a marked change in the direction of lateral accretion (Fig. 5.15C). Overall, the distribution of the facies is varied, and this is reflected in the panels showing the related heterogeneity and depositional energy of the deposits (Figs 5.15 and 5.16). The individual facies trends are complex, therefore

to aid the interpretation of further predictable relationships, facies groups have been established.

In order to place facies into groups, an assemblage should be observed that shows a restricted range of inter-relationships. These facies associations are commonly cyclic, and interpreted to be characteristic of a particular environment (Middleton and Southard, 1978; Lindholm, 1987). The facies associations observed act as a framework and predictive tool for future observations (Walker, 1979). However, the exposure studied is one point-bar and its lateral discontinuity limits the extent of cyclicity that may occur so identifying predictive relationships is challenging. Markov chain analysis was therefore undertaken to aim to find cyclic, and predictable relationships.

Markov chain analysis enables a quantitative assessment of facies transitions, and enables facies successions to be derived, as opposed to associations. The Walker (1979) methodology shows statistically significant transitions. There are many relationships marked as significant, and so facies successions were derived through using this data alongside a visual analysis of the sedimentary graphic logs, and 3D panels (Figs 5.15 and 5.16). Through using these datasets together, observations were statistically qualified and 4 facies successions derived (Fig. 5.11).

Figure 5.16C shows the distribution of the facies successions in the outcrop where facies successions 1 and 2 are dominant; facies 3 and 4 are dominantly seen at the proximal end of the point-bar. Facies successions 1, 3 and 4 may typically be observed following a major erosional surface, though this is not always the case. Facies succession 1 represents a fining-upwards trend due to decreasing energy. The base may be conglomeratic and consist of trough-cross bedding that marks a directional change in lateral accretion. Facies succession 2 is formed from moderate to high, and



moderate to low-energy facies that has resulted in dominantly sand-prone deposits. Facies succession 3 represents either pebble-lag scour fill, or bank collapse. Facies succession 4 infills high-energy scours and decreases in energy, depositing laminated and rippled sandstone deposits. All of these facies successions interfinger, generating a complex deposit, within which facies successions are seen to change along lateral accretion surfaces (Fig. 5.16C). Overall, the facies successions reveal that there were successive scouring episodes (facies successions 3 and 4) that lessened, and point-bar deposition became more stable and consistently sand-prone (facies succession 2). There was a change in accretion direction highlighted by facies St, (affiliated with facies succession 1), and then deposition became stable again (facies succession 2). A second change in accretion direction occurred (facies succession 1), and meander loop abandonment followed.

Each facies succession demonstrates trends in changing velocity (Fig. 5.12) that impacts its overall heterogeneity and sedimentary structures. The facies successions derived are sufficient to attain a testable hypothesis, although this may not be used in isolation, as interpreting the internal architecture of the point-bar is critical to this reconstruction process.

### *5.8.3 Application of architectural derivations*

The architecture and facies of the abandoned channel provide information regarding the cut-off mechanism (Chapter 4), and its position in the meander bend. Figure 5.18 is a panel of the abandoned channel fill at the distal SSW end of the outcrop. It shows a three stage infill process; the first contains comparatively more silt than is observed in stages 2 and 3, though all three are of facies Fsm. Figure 5.18B i) shows the channel fill architecture corrected from effects of tectonic tilting. The mode of accretion can be

seen as lateral in the first stage, then aggradational in a concentric manner in the second and third stages. Figure 4.3 shows the resultant facies accumulation, and architecture, from each of the three main modes of cut-off (modified from Allen, 1965; Harms, 1982; Walker & Cant, 1984; Toonen *et al.*, 2012). Because the channel fill is identified as fine-grained (Fsm), this would indicate a diversion angle of  $>70^\circ$  (Shields & Apt, 1989; Piegay *et al.*, 2002; Kondolf, 2007). In turn, this would indicate the mechanism of cut-off to be neck cut-off (Fig. 4.3A). However, the lateral accretion seen in stage 1, suggests that the cut-off mechanism could be chute cut-off (Fig. 4.3B), although the grain size is not indicative of this mechanism. Erskine *et al.*, (1992) identified that the established models often show variability, therefore despite the lateral accretion, the mode of cut-off may be neck cut-off, though remains too fine-grained for chute cut-off to be considered. Figure 4.7B, introduced a cut-off mechanism of chute cut-off on converging limbs within which the diversion angle may be  $>90^\circ$  that would produce mud-prone channel fill (Shields and Abt 1989). Flow may continue for some time as it is a variation on the mechanism of chute cut-off, though this would require a field study to justify. The mechanism of abandonment was likely either neck cut-off, or chute cut-off on converging limbs.

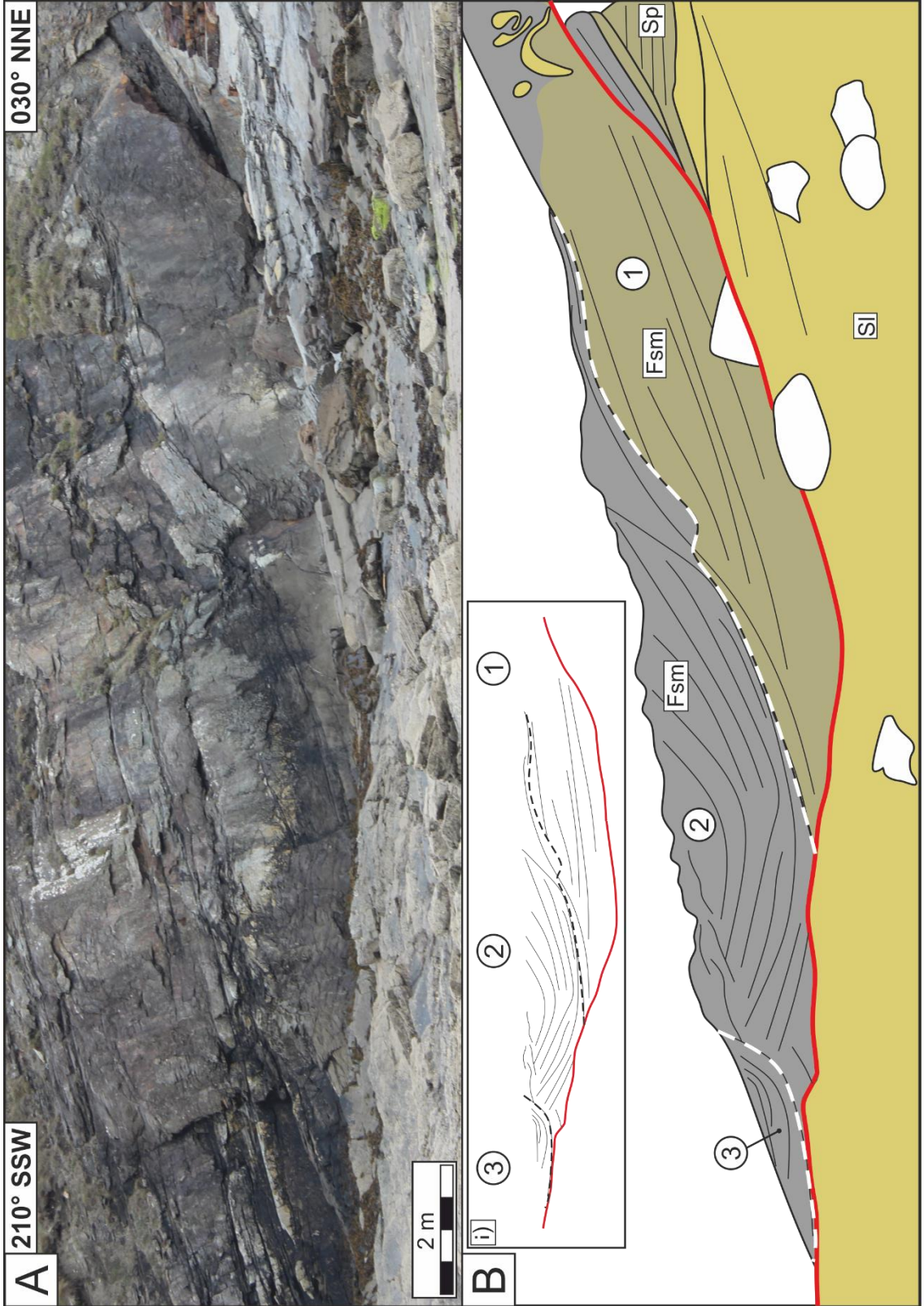
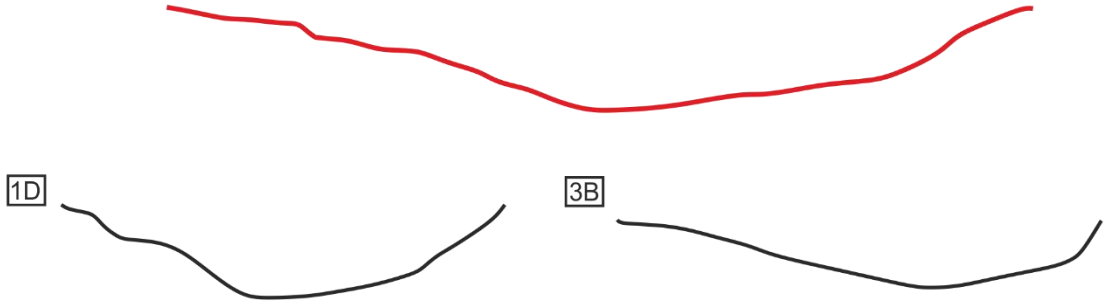


Figure 5.18 - A) A panel of the abandoned channel exposure; B) interpretation of the abandoned channel fill exposure

### Channel cross-section shape

Channel shape observed in outcrop studied



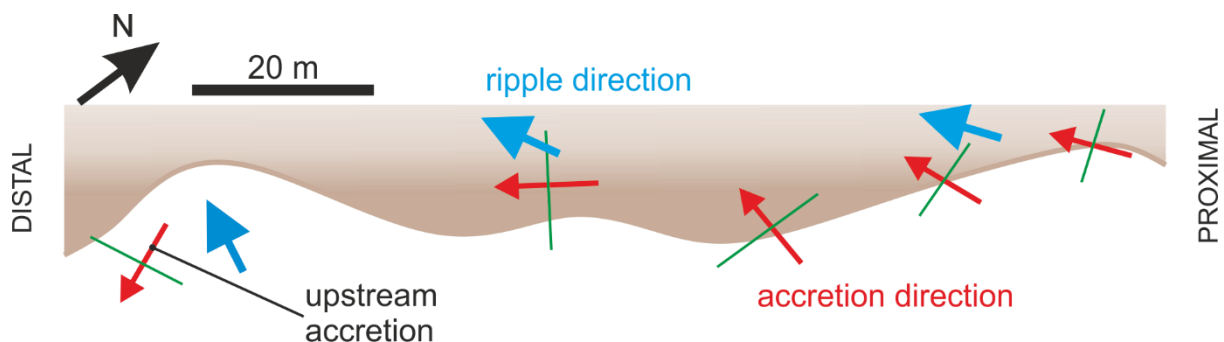
Peace River, Alberta



**Figure 5.19 - A figure to show the abandoned channel shape exposed at Nolton Haven cove, compared to data from Smith et al., (2009)**

The shape of the channel cross-section seen in outcrop is asymmetric and shallow (Figure 5.19). When the outcrop architecture is compared to cross-sections measured in the Peace River, Alberta (Smith *et al.*, 2009), it is subjectively observed to be similar to two sections. Both of these sections are on the up-stream limbs of meander bends. The greatest resemblance is seen with section 3B, though section 1D also shows comparable asymmetry. This suggests that the channel section exposed at the outcrop is from the upstream limb of a meander bend, though more evidence is required to validate this.

The direction of lateral accretion has been simplified from Figure 5.15C to indicate the overall directions of accretion, in relation to the outcrop (Fig. 5.20). It shows the disparity between ripple direction and accretion direction to increase towards the distal end of the outcrop.

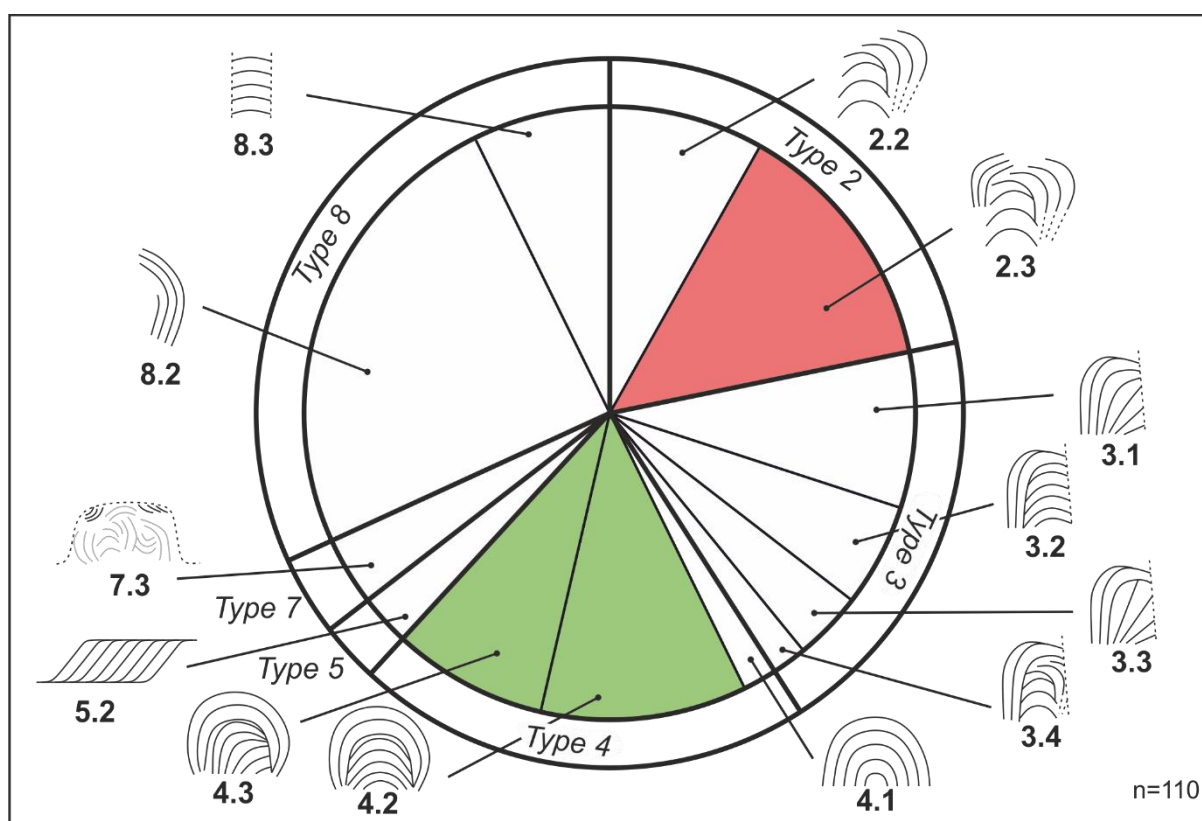


**Figure 5.20 - A planform sketch of the outcrop with accretion direction, and flow direction marked on. Outcrop is 123 m long**

There is an overall change in accretion direction from SW to SSE. It is evident from the flow direction and architecture of the outcrop (Fig. 5.15C), that the distal part of the outcrop reflects upstream accretion. This observation supports the hypothesis that the



channel section exposed at the outcrop is from the upstream limb of the point-bar deposit because this is where upstream accretion would be most evident. Figure 5.21 shows a modified version of Figure 4.13A that highlights the scroll-bar patterns exhibiting upstream accretion that are present in abandoned point-bar deposits: extension and rotational with directional changes (Type 2; 2.3), and expansion (Type 4; 4.2, and 4.3).





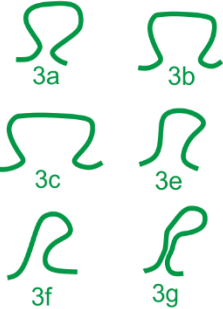


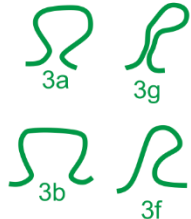



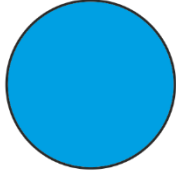
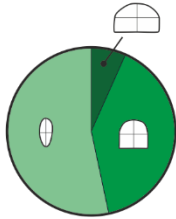
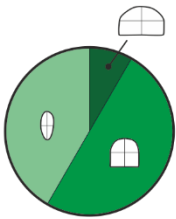
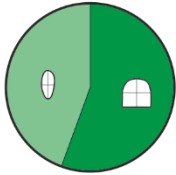
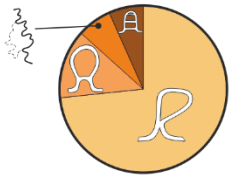
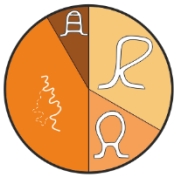
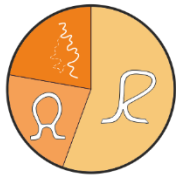


**Figure 5.21 - An edited version of Figure 4.13A, showing the accretionary styles that exhibit upstream accretion.**

Each of these scroll-bar styles has been assessed in order to determine the active meander shapes, and dimensions and cut-off styles of the abandoned shapes that exhibit them (Fig. 5.22). Overall where these scroll-bar patterns are seen in active meandering reaches, bulbous shapes are dominantly observed. A bulbous shape

supports the suggestions for the style of cut-off that was identified through study of the channel fill (Fig. 5.18), as a bulbous shape must occur prior to abandonment by neck cut-off, and chute cut-off on converging limbs. Each of the scroll-bar patterns 2.3, 4.2, and 4.3 are observed in abandoned point-bar deposits 15, 12, and 9 times respectively. Of these, the two cut-off mechanisms under consideration occur 87% (13/15), 50% (6/12), and 78% (7/9), times respectively. The variability of the dimensions of the abandoned shape is similar in all cases whereby the majority of the pie is composed of equidimensional, and long shapes. All three scroll-bar patterns (2.3, 4.2, and 4.3), may be correct. However, it is the aim of this study to deduce the most likely accretion history, so a decision must be sought with regard to the scroll-bar study to be pursued. Scroll-bar pattern 2.3 is the most commonly seen in both modern, and ancient systems, and has the greatest chance of undertaking abandonment via a suitable mechanism, therefore it will be the only pattern considered in the remainder of this study.

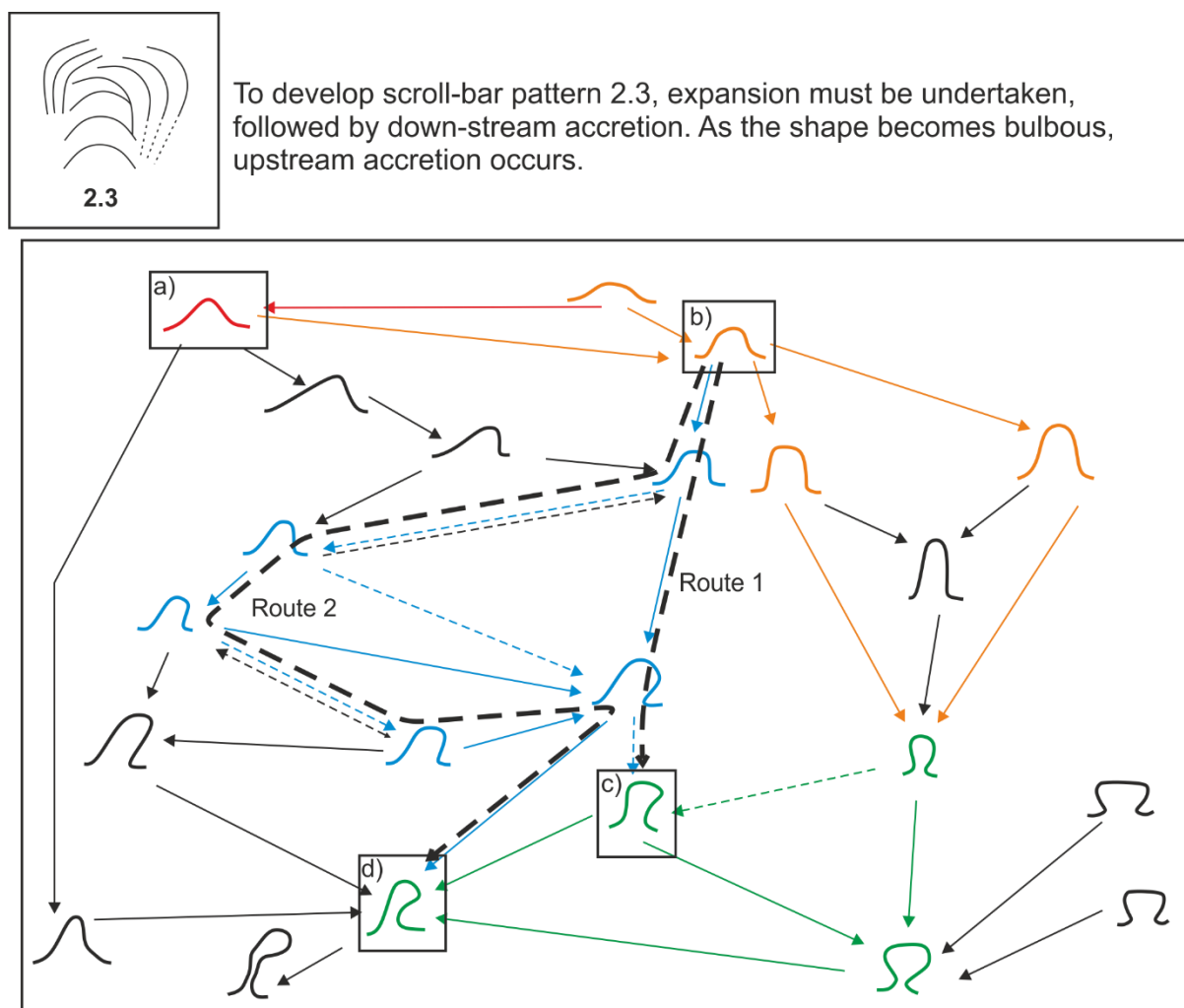


Scroll-bar pattern	 <p style="text-align: center;"><b>2.3</b></p>	 <p style="text-align: center;"><b>4.2</b></p>	 <p style="text-align: center;"><b>4.3</b></p>																														
Active shapes	<p>3c x 2 3g 3b x 3 3f x 2 3e x 3 1i 3a</p> <p><b>Open Asymmetric</b></p>  <p><b>Bulbous</b></p>  	<p>3a 3b 3g 3f x 2 1i 4e</p> <p><b>Open Asymmetric</b></p>  <p><b>Bulbous</b></p>  <p><b>Open Symmetric</b></p>  	<p>1e</p> <p><b>Open Asymmetric</b></p>  																														
Abandoned shapes																																	
Cut-off mechanism	 <table border="1" data-bbox="368 1682 735 1845"> <tr> <td>Neck cut-off</td> <td>11</td> </tr> <tr> <td>Cut-off on converging limbs</td> <td>2</td> </tr> <tr> <td>Avulsion</td> <td>1</td> </tr> <tr> <td>Axial chute cut-off</td> <td>1</td> </tr> <tr> <td>w+1 chute cut-off</td> <td>0</td> </tr> </table>	Neck cut-off	11	Cut-off on converging limbs	2	Avulsion	1	Axial chute cut-off	1	w+1 chute cut-off	0	 <table border="1" data-bbox="756 1682 1123 1845"> <tr> <td>Neck cut-off</td> <td>4</td> </tr> <tr> <td>Cut-off on converging limbs</td> <td>2</td> </tr> <tr> <td>Avulsion</td> <td>5</td> </tr> <tr> <td>Axial chute cut-off</td> <td>1</td> </tr> <tr> <td>w+1 chute cut-off</td> <td>0</td> </tr> </table>	Neck cut-off	4	Cut-off on converging limbs	2	Avulsion	5	Axial chute cut-off	1	w+1 chute cut-off	0	 <table border="1" data-bbox="1139 1682 1506 1845"> <tr> <td>Neck cut-off</td> <td>5</td> </tr> <tr> <td>Cut-off on converging limbs</td> <td>2</td> </tr> <tr> <td>Avulsion</td> <td>2</td> </tr> <tr> <td>Axial chute cut-off</td> <td>0</td> </tr> <tr> <td>w+1 chute cut-off</td> <td>0</td> </tr> </table>	Neck cut-off	5	Cut-off on converging limbs	2	Avulsion	2	Axial chute cut-off	0	w+1 chute cut-off	0
Neck cut-off	11																																
Cut-off on converging limbs	2																																
Avulsion	1																																
Axial chute cut-off	1																																
w+1 chute cut-off	0																																
Neck cut-off	4																																
Cut-off on converging limbs	2																																
Avulsion	5																																
Axial chute cut-off	1																																
w+1 chute cut-off	0																																
Neck cut-off	5																																
Cut-off on converging limbs	2																																
Avulsion	2																																
Axial chute cut-off	0																																
w+1 chute cut-off	0																																

**Figure 5.22 - A collation of data relating to each scroll-bar pattern that exhibits upstream accretion.**

The flowchart proposed in Figure 4.15 has been modified to aid in the interpretation of the accretion history that would lead to scroll-bar pattern 2.3. The shapes considered in this next stage of the interpretation, are those that occur multiple times: 3c, 3b, 3f, and 3e; it is worth noting that these bulbous shapes were also isolated by using the ratio 0.85 derived in Figure 5.17 – except 3e. Shapes 3c and 3b are typically derived through composite accretion, therefore they do not have a route by which they may form on the flow chart which makes it difficult to determine an accretion history, and these two shapes are therefore discounted. The outcrop shows a relatively continuous growth, therefore 3c and 3b are discounted because they are typically composite and not easily traced. More data on the complex evolution of composite point-bar deposits would need to be collected to validate the accretion histories of these shapes for future studies. Starting positions a) and b) are proposed because if chute cut-off on converging limbs had occurred, then the proto-meander would be shape S4d (a), and if neck cut-off had occurred, then the proto-meander would be shape S2d (b). Positions c) and d) are potential finishing positions, as they correlate with the most commonly observed meander shapes that exhibit scroll-bar pattern 2.3. On Figure 5.23, any coloured route, may be undertaken from a start to finishing position. Any of these routes are possible; the routes have been decided though studying the active shapes that the scroll-bar style is seen in, and considering the mechanism by which it must occur. In order to develop scroll-bar pattern 2.3, expansion must be undertaken, followed by down-stream accretion. Downstream accretion may be seen in both symmetric, and asymmetric shapes (Chapter 3), so any route is possible. As the shape becomes bulbous, upstream accretion occurs. There are two outcomes identified: i) if

the meander shape was isolated at c), chute cut-off on converging limbs would have occurred, and the point-bar deposit dimensions would be approximately equidimensional; ii) if the meander shape was isolated at d), chute cut-off on converging limbs would have occurred, and the point-bar deposit dimensions would be “long”.



**Figure 5.23 - A flowchart that shows the possible routes that may be taken to develop scroll-bar pattern 2.3. Routes in colour are the most probable.**

Two routes were considered and are labelled on Figure 5.23. The meander shapes encountered on each route were compiled and assessed. The morphology and

heterogeneity of the resultant point-bar deposits from both routes 1 and 2 were constructed using the methodology outlined in Chapter 3 (Fig. 5.24).

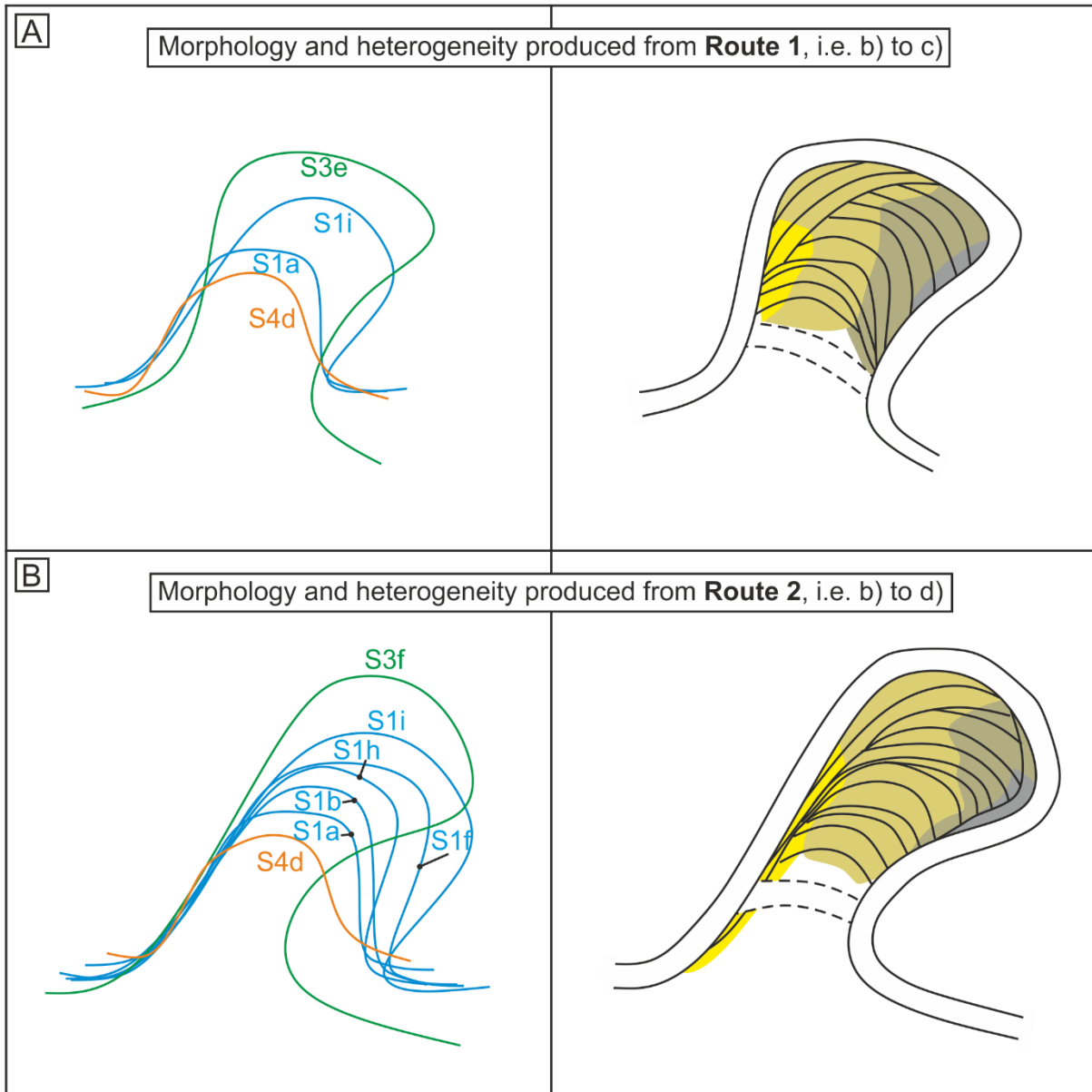
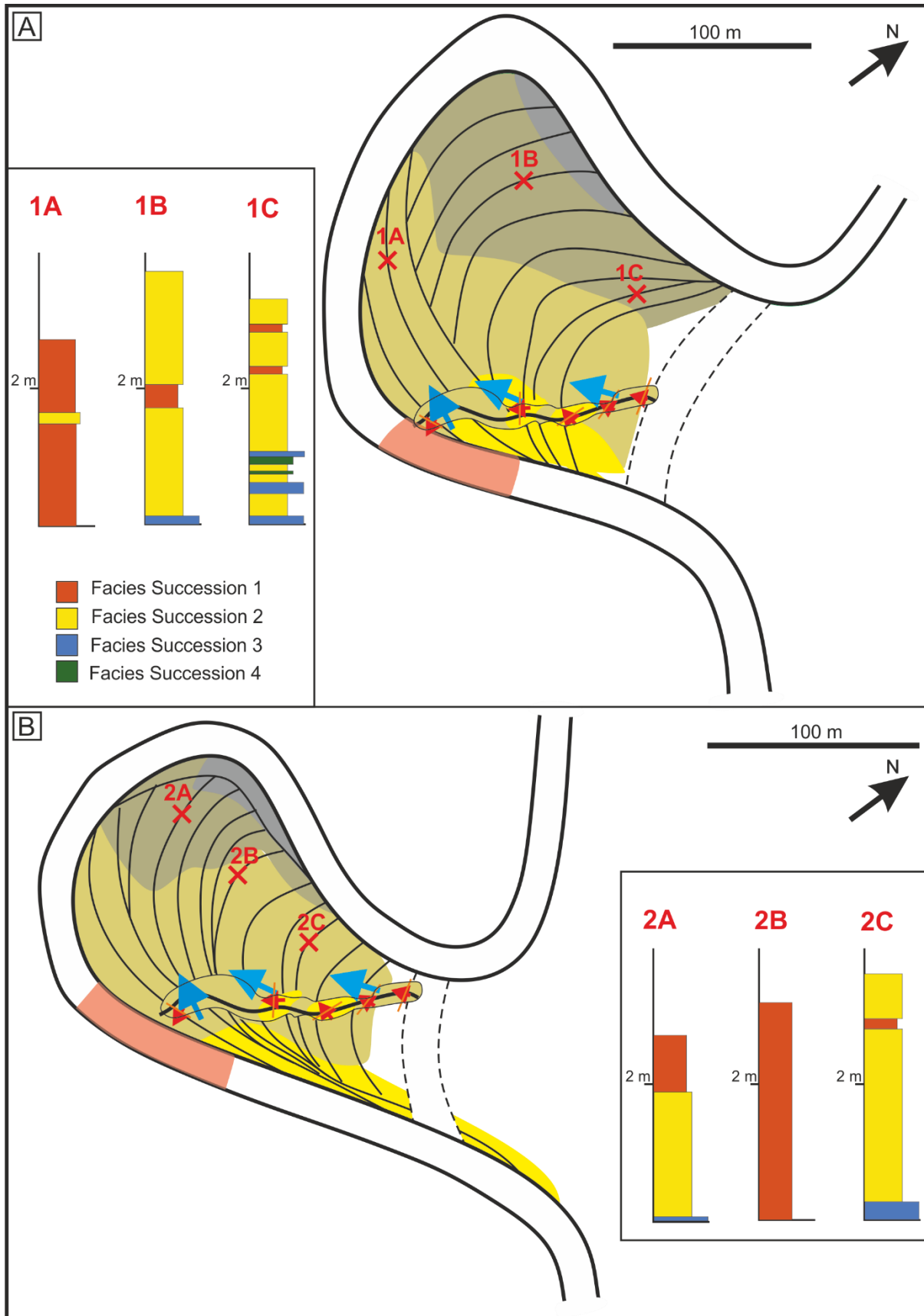


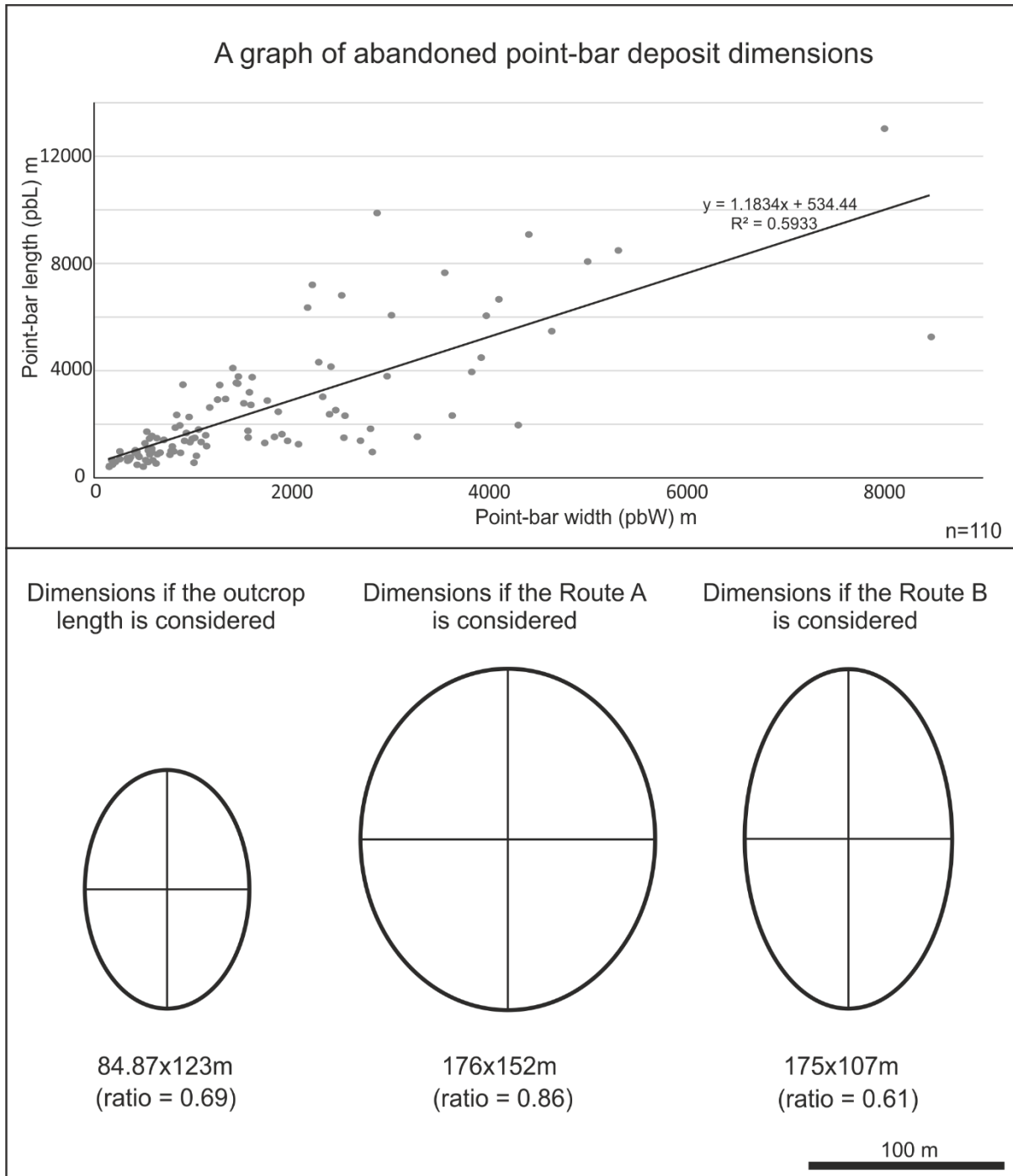
Figure 5.24 - A) the morphology and relative lithologic heterogeneity that would hypothetically be formed if the meander accreted via. Route 1; B) the morphology and relative lithologic heterogeneity that would hypothetically be formed if the meander accreted via. Route 2

Figure 5.25 shows the best fit for the outcrop in each point-bar deposit, taking into account the estimated position of the abandoned channel, the heterogeneity, and the accretion directions. The information derived regarding the causative processes of the facies successions seen in the outcrop, has enabled hypothetical sketch logs to be constructed (Fig. 5.25). In Figure 5.21, both shapes are suggested to have undertaken abandonment via chute cut-off on converging limbs, therefore this has been deduced as the preferred cut-off mechanism, though neck cut-off is still also a likely scenario. This may be supported by facies succession 3, for which a potential causative mechanism is bank collapse, which in turn, may have occurred as a result of chute cut-off, or neck cut-off. Figure 5.15B highlights chute cut-off deposits, therefore indicating that the floodplain substrate is amenable for enabling chute channels to occur.



**Figure 5.25 - The reconstructions and predicted facies successions for the two point-bar deposit reconstructions constructed in Figure 5.26. The pink section of channel is the estimated position of the abandoned channel shape (Fig. 5.21).**

Figure 5.26 shows a graph of the length and width of the abandoned point-bar deposits that were measured in Chapter 4. If the length of the outcrop was taken as the definitive length of the point-bar, then the first ellipse would be the lateral dimensions concluded for the point-bar deposit, though use of the relationship identified in the graph of point-bar deposit dimensions. Through the analysis undertaken in this study, the two larger ellipses have been derived; Route A (Fig. 5.23), results in a point-bar deposit that is almost equidimensional; Route B (Fig. 5.23), results in a point-bar deposit that is elongate. The ratio derived from the point-bar deposit of Route B is close to the ratio that is derived from the graph (Fig. 5.26). The wavelengths (i.e. meander width – mW), measured from the two reconstructions (Fig. 5.25), are 266 m (via Route 1), and 278 m (via Route 2). These measurements sit within the range of wavelengths derived through use of published equations (Table 5.9; Fig. 5.17).



**Figure 5.26 - A graph of abandoned point-bar deposit dimensions. The first ellipse is constructed through use of the relationship depicted on the graph. The second and third ellipses are measured from the reconstructions in Fig. 5.27.**



#### 5.8.4 Limitations

The main limitation of these interpretations is that there are so many scenarios that could account for the preserved stratigraphy. In order to combat this more effectively in future, a larger data set should be derived that will enable derivations to be made with stronger statistical support to reduce the range in a repeatable and quantifiable manner.

### 5.9 Conclusions

It is difficult to establish links between active sedimentary processes and the preserved alluvial architecture (Miall, 2006), and remains so. The methodologies that have been applied in this chapter have sought to take a step towards appreciating the vast range of possible morphologies that the point-bar deposit may form. This study has achieved its aim in forming a stronger appreciation for the lateral extent of an exposed point-bar deposit. There has previously not been a procedure to enable this data to be interpreted in this detail (Wood, 1989; Bhattacharya *et al.*, 2015; Brekke, 2015). Now that this procedure has been determined, more possibilities for accretion histories may be considered. A reconstruction of a point-bar accretion history ought to be a story board (e.g. Wu *et al.*, 2015), that ends in meander abandonment. This is because abandonment must occur prior to lithification, and is an important control on the dimensions of the resultant deposit (Chapter 4).

Seventeen distinct lithofacies have been identified and found to comprise 4 facies successions via statistical analysis. The use of Markov chain analysis methodologies from Walker (1979) and Harper (1984) has revealed that they are independently unsuitable for use in a laterally discontinuous and varied deposit such as the point-bar studied here. Future work could entail separating the data into the respective facies

successions, and running the analysis on each succession in turn. This would reveal any trends and analyses that are currently undiscovered by the methodology undertaken. Also in this detailed approach, the analysis could consider the type of contact at each facies transition (Miall & Gibling, 1978).

Facies succession 1 was found to be associated with a change in direction in the point-bar deposit. This is of use because it has direct morphological implications of the reconstruction of the point-bar accretion history. Facies succession 2 has been found to be the most sand-prone. Because this is associated with continued growth in a similar direction, this may aid interpretation of sand-prone areas in point-bar deposits from seismic reflection data. The use of palaeohydraulic parameters was of interest, though of little use in reconstructing the morphological history of the point-bar deposit. A vast amount of variability remains, however this methodology provides the basis for a more refined method, and generates models that are testable hypotheses for geological models.

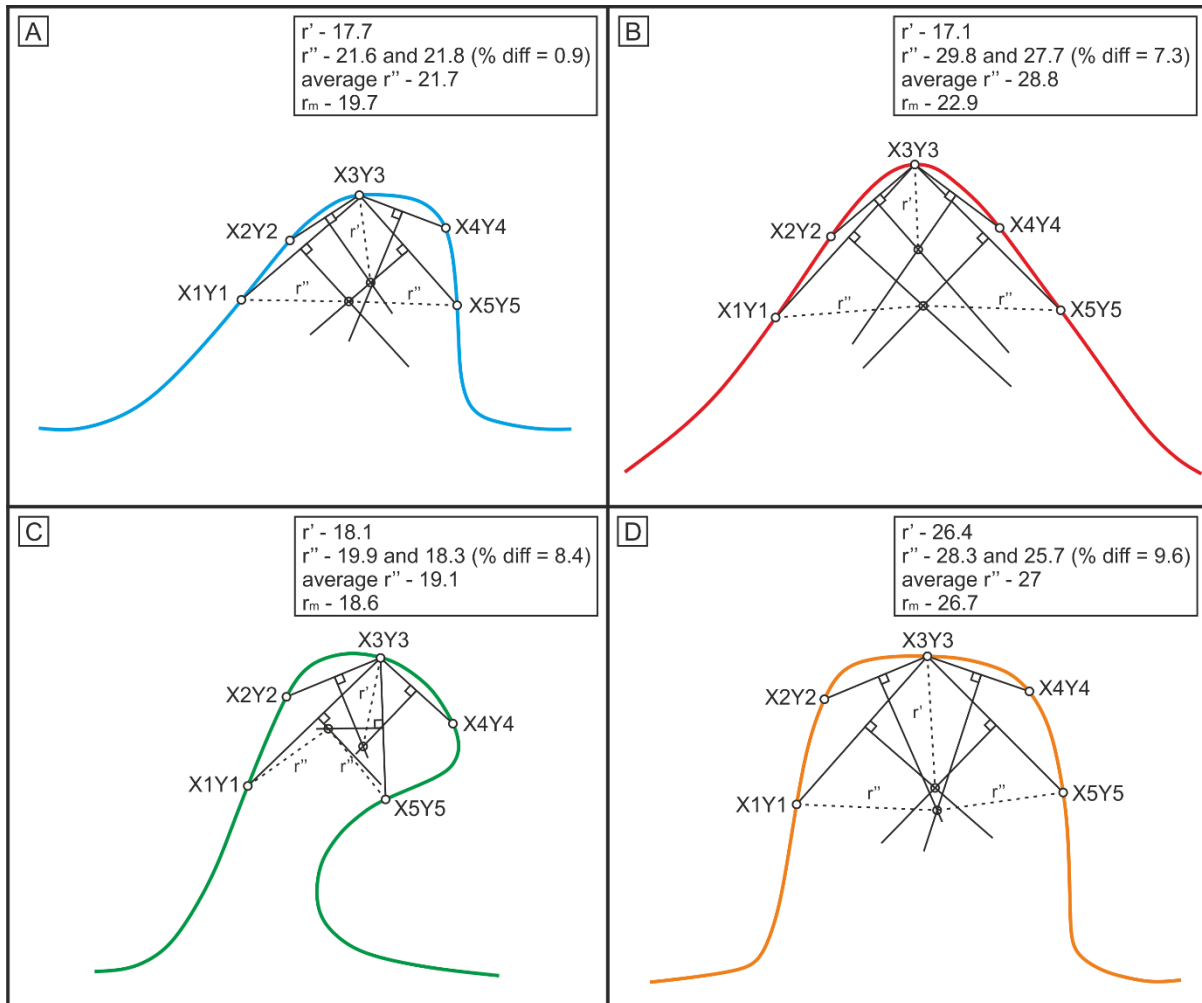
## 6 Discussion

This chapter integrates all results from the preceding Chapters (2-5), and presents a wider discussion.

### 6.1 Research Question 1

*How can meander shapes be geometrically classified, in order to be compared universally, in a repeatable, quantifiable manner?*

For meaningful interpretation of the ancient record of meandering fluvial systems it is critical to assess the morphological features of modern systems using a repeatable and quantifiable method to enable improved comparison of different fluvial reaches, and to establish formative processes (Miall, 2013; Lotsari *et al.*, 2014). Quantitative studies of modern fluvial systems utilise metrics such as sinuosity (Howard & Hemberger, 1991; Hooke, 2007), and radius of curvature (Nanson & Hicken, 1983). These metrics are limited in their ability to express the natural variability of active and abandoned meander shape. The radius-of-curvature methodology (Nanson & Hicken, 1983; Fig. 2.1B) has been applied to classify a range of meander shapes from each parent group identified in Chapter 2 (Fig. 2.8). However, several limitations are identified in using this established and widely used method (Fig. 6.1).



**Figure 6.1 - A demonstration of the application of the radius-of-curvature methodology for analysis of a variety of meander shapes identified in this study; A) meander shape S1b; B) meander shape S2b; C) meander shape S3f; and D) meander shape S4b (Figure 2.8).**

The two measurements of the parameter  $r''$  (the distance between X1Y1 and an intersection point, and X5Y5 and the same intersection point; the intersection point is the one formed by the perpendicular lines, in turn, drawn from the lines connecting X3Y3 to X1Y1, and X5Y5), should be the same. However In implementation of the method (Fig. 2.1B), the two values are found to vary; in experimental implementations of the method, parameter  $r''$  varied up to 9.6 % (Fig. 6.1D). Furthermore, the angular

(Group 2) shapes studied have a small radius of curvature with two near-straight limbs (e.g. Fig. 6.1B); the resultant measurement ( $r_m$ ) is 22.9. This value is greater than that determined for the bulbous shape (Group 3), where  $r_m$  is 18.6 (Fig. 6.1C). A visual comparison of these two shapes indicates that this is incorrect because the bulbous shape shows a broader curve than the angular shape, yet has a smaller value. Twenty-nine (11 % of 260 when rounded up), of the meander shapes assessed in this study are angular (Group 2), therefore this inaccuracy has significant implications for the value of quantitative assessments that are based on the application of this method. The accuracy and diversity of the range of shapes that may be recorded by the radius-of-curvature method is limited by its simplicity: it does not account for symmetry or asymmetry in shape, scroll-bar accretion direction, or maturity. The principal application of the radius-of-curvature methodology (Nanson & Hickin, 1983) was solely to quantify the curvature of the actively aggrading inner bank of meander bends (Fig. 2.1B); in order to achieve this, the meander apex is assessed. In this study, 64% (166 of 260) of meander shapes considered are downstream accreting (Table 3.4). Therefore, measuring the radius of curvature at the meander apex to ascertain the rate of accretion may not always be appropriate. An alternative method for determination of radius-of-curvature of a meander bend is the equation devised by Williams (1986):

$$Rc = (\lambda_m * [\text{sinuosity}]^{1.5}) / 13 * [\text{sinuosity} - 1]^{0.5}$$

The two variables in the equation are sinuosity and wavelength; each can be measured in multiple ways (Fig. 2.1A). Therefore, results may be inconsistent between studies. The variability of these parameters becomes increasingly problematic in highly irregular, sinuous reaches. Neither the original nor the modified (Nanson & Hicken, 1983; Williams, 1986), methodology for determining the radius of curvature provides an effective tool for the universal, system-independent assessment of the complexity and

diversity of meander shapes. However, both methods are commonly used as proxies for meander shape, and for the reconstruction of estimates of bank-full channel width and depth for meandering river elements accumulated and preserved in the rock record (e.g., Williams, 1986, Bhattacharya *et al.*, 2015). Such use of these methods requires caution.

A second widely employed approach to meander shape assessment is a subjective shape classification (Brice, 1974; Bridge 2003). It is unlikely that this type of assessment is repeatable because the results will vary between individual studies and between observers. Also, an outcome of this study has been that, in the commonly applied Brice (1974) classification (Fig. 2.2D), only 44% of the meander shapes identified in this study (Fig. 3.8), are accounted for. Most notably only 11% (of 68) of open asymmetric (Group 1) shapes were classified.

The limitations and shortcomings of the radius-of-curvature and subjective shape assessment methodologies are largely resolved by the Intersection Shape methodology developed by this research (Chapter 2, Fig. 2.3). This novel method reduces the reliance on subjective approaches to the classification of meander form and permits quantitative assessment and classification of the morphological form of the full range of fluvial meander shapes that is well suited to system-independent comparisons. The Intersection Shape method utilises data derived from direct measurement of publically available remotely sensed images, thereby allowing disparate data sets to be compiled for direct comparison (Table 3.3). The Intersection Shape methodology presents a quantifiable and repeatable approach for assessing modern systems. The majority of measurements (93.08%; 242 of 260) plot accurately, allowing a more discrete description of meander shapes that occurred through the

accretion history of a point-bar deposit. This becomes important when aiming to predict heterogeneity in the fluvial point-bar deposit (Fig. 3.6).

The Intersection Shape methodology provides many advantages and improvements over other widely used methods for meander shape assessment and classification. It uses the most recent point bar growth as opposed to pools and riffles (Parker *et al.*, 1982) to differentiate between the up- and downstream limbs of a meander. This is an improvement because evidence for pools and riffles are not commonly present in the lithified ancient record. However, direction of accretionary growth can be established from outcropping successions (by measuring palaeo-accretion directions using a compass-clinometer), and from subsurface geophysical data (by observing the general accretion direction from seismic reflection data). Where there are multiple areas of most recent growth, the parameter  $tL$  is measured from the meander apex which still enables the meander shape to be plotted in the correct envelope (Fig. 2.12A).

The Intersection Shape methodology is designed for application to the stratigraphic record. In images derived from reflection seismic data detailing meandering reaches that have been cut-off by avulsion, accretion direction may be discernible. If this is the case, then the Intersection Shape methodology may be directly applied, and the presence or absence of scroll-bars does not impact the accuracy of the results. However, if the imagery is of low resolution such that individual scroll-bars are not discernible, the Intersection Shape methodology may still be directly applied by measuring the length ( $tL$ ) from the meander apex (Fig. 2.3A), and it will plot in the same envelope (Fig. 2.12A). This consistency in methodology means that meander shapes recorded in both the modern and ancient record may be robustly compared and suitable analogues for subsurface successions may be identified. The irregularity of a reach does not provide a limitation because the tangent ( $mW$ ), of the meander loop is

used (Figure 2.4A). This is an improvement on identifying meander wavelengths because there are different ways that meander wavelength can be defined (Fig. 2.1A). The method of using tangents of meandering reaches is easy to apply universally and in a repeatable manner where an irregular reach is assessed. The Intersection Shape methodology is largely a quantitative approach meaning that the limitations of subjective assessment techniques to shape-fitting methodologies are eliminated.

Limitations to the Intersection Shape methodology include the subjective step of sorting the shapes into their parent groups (Groups 1-4; Figure 2.7), where part of the process requires subjective decision making. However, the process is well constrained (Fig. 2.3E), and although this might introduce inconsistency, overall, the method is more effective at quantitatively recording meander shape than previous methodologies.



## 6.2 Research Question 2

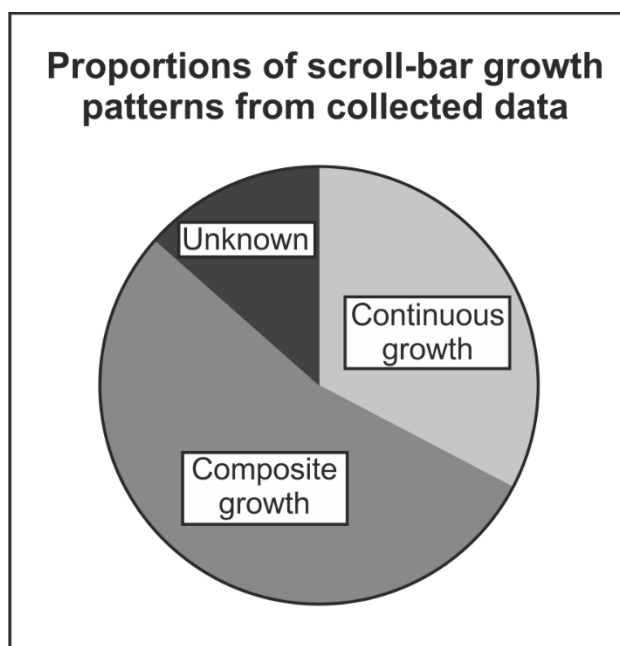
*How does the geometry of a meander and scroll-bar pattern of the point-bar, relate to the heterogeneity of a point-bar deposit?*

Where fluvial point-bar deposits form important petroleum reservoirs, for example in the Cretaceous McMurray Formation, Alberta (Hubbard *et al.*, 2011), determining the position and orientation of production wells is significantly influenced by the distribution of inclined heterolithic strata (IHS) within point-bar elements. Many point-bar deposits are dominantly sand-prone (Allen, 1965), yet mud-prone packages of IHS can still significantly influence the connectivity of the sand-prone compartments in the point-bar deposit (Thomas *et al.*, 1987). The deposition of sand- and mud-prone deposits occurs in a predictable distribution around meander bends (e.g. Fustic *et al.*, 2012; Fig. 5.1), based on a collation of observations from published data (Fig. 3.2). However, fluvial point-bar deposits can have highly complex accretion histories. Previous methodologies for assessing meander accretion direction, typically only attend to the most recent change in form (e.g. Daniel, 1971; Hooke, 1977b (Fig. 3.3B); Bridge, 2003 (Fig. 3.3C); Ielpi *et al.*, 2014 (Fig. 3.3A)). Assessing changes in form from the initiation of a meander is challenging. In this study, the surface expression of scroll-bar patterns has been used to interpret the accumulation history of a point-bar deposit. By determining the accumulation history, the up- and down-stream division of the meander bend may be derived, and by identifying the position of most recent growth (Fig. 2.3A) a relative heterogeneity distribution can be predicted.

Assessing the surface expression of a scroll-bar pattern is straightforward to achieve, and enables an improved analysis of scroll-bar pattern variability that enables an empirical dataset on the proportions of meander shapes with specific scroll-bar

patterns to be collated (of which there are 22 categories in 8 Types; Fig. 3.5). The overall accretion history may be assessed (Fig. 3.5). Significantly, it has been found that downstream accretion through translation or secondary translation (Groups 5, 6 and 3) accounts for ~75% of open asymmetric, open symmetric and angular meander shapes. Classic point-bar facies models (e.g. Schumm, 1963; Allen, 1965; McGowen & Garner, 1970) typically depict open symmetric shapes (Group 4) that develop through expansional growth (Type 1); yet, expansional growth (Type 1) is only seen in only 1.5% of scroll-bar patterns studied.

The scroll-bar patterns identified in Figure 2.8 may be broadly grouped into 3 categories: i) continuous, whereby point-bar accretion is unidirectional, and directional change is gradational; ii) composite, whereby point-bar accretion is multidirectional, and directional change during meander evolution was apparently abrupt as discerned by sharp changes in scroll-bar patterns; and iii) unknown, whereby the accretion history may not be easily determined. Continuous growth is observed in 33 % of the point-bar deposits assessed, composite growth is observed in 54 % (Table 3.3; Fig. 6.2).



**Figure 6.2 - Pie chart depicting the types of growth observed in 260 active point-bar deposits studied.**

Understanding and interpreting the variability of fluvial, meandering systems has been limited to-date by over reliance on “classic” and widely applied facies models.

Application of this novel approach means that the accretionary history of a meander may be estimated for any point-bar deposit, independent of meander shape.

There are 550 possible combinations of scroll-bar pattern, and meander shape. The relative lithological heterogeneity distribution may be modelled for any instance. To achieve this, the overall accretion history may be broken down into its constituent historic forms (Fig. 3.6), by dividing the accretion history into phases of growth (using the shapes defined in Fig. 2.8). The relative lithological heterogeneity may be assessed at each stage, and then combined into a relative lithological heterogeneity map (Fig. 3.6C).

The key strengths and improvements that are offered by this methodology are as follows. Firstly, the rivers selected for the study are distributed globally, and are from a range of physiographic and climatic configurations, so a wide range of styles are accounted for. Secondly, the scroll-bar is independently assessed from the meander shape such that a varied combination of meander shape and scroll-bar pattern may be considered. This enables a greater variability in interpretations to be attained where they are combined (i.e. Fig. 3.3C), and it enables more flexibility in a reconstruction where either the meander shape or scroll-bar pattern are unknown or only partially reveal by a fragmentary data set the most likely combination may be modelled. Thirdly, the principles of the methodology may be used robustly on both modern, and ancient fluvial systems, enabling disparate datasets to be directly compared and analogues to be quantifiably identified based on morphological similarities.

Limitations of this approach are that the overall accretion history is derived through subjective visual analysis of planform image of the point-bar deposit, which is then compared to the scroll bar classification (Fig. 3.5). This is not ideal, and a future recommended research avenue is to geometrically model meander growth and scroll-bar development so as to capture and assess the probability of different migration scenarios. Also, the methods by which the heterogeneity is predicted (cf. Fig. 3.6) is based on a limited set of assumptions derived from the published understanding of known sediment distributions (Thompson, 1986; Leopold & Wolman, 1960; Jackson, 1975; Nanson, 1980; Bridge *et al.*, 1995; Carter, 2003; Smith *et al.*, 2009; Fustic *et al.*, 2012). For example, the data interpreted for the point bar in Figure 2.2C reveal a contrast to Figure 3.2A, despite a similar planform meander shape. This could be because the meander in Figure 3.2A has developed through translation, whereas the meander in Figure 3.2C is interpreted to have developed through expansion and

rotation. This principle is also supported by tests that have been undertaken to assess the flow dynamics (Bagnold, 1960; Sakalowsky, 1974; Jackson, 1975; Thompson, 1986; Leopold & Wolman, 1960). These data highlight differences in heterogeneity type distribution for point bars associated with expansion (Fustic *et al.*, 2012, Durkin *et al.*, 2015), and downstream accretion (Smith *et al.*, 2009). The resultant predicted heterogeneity, however, is not absolute, and the results inevitably oversimplify the variability of the heterogeneity and accretion history. This could be refined in the future with process-based numerical modelling and/or rules-based modelling (cf. Yan *et al.*, 2017).

Many of the currently active river reaches assessed in this study are not in subsiding sedimentary basins, and therefore have a low chance of being preserved to the rock record. For this reason, appropriate caution should be taken in directly relating proportions of meander shape and scroll-bar pattern recorded in this study (Figs 3.7 and 3.8), to the rock record (cf. Miall, 2006). Currently popular models like the DFS model (Hartley *et al.*, 2010), argue that fluvial systems are preferentially preserved in subsiding basins, largely as distributive channel networks. However, incised valley deposits are also important and form numerous major fluvial reservoir intervals (e.g. McMurray Formation; Hubbard *et al.*, 2011; and the Mungaroo Formation; Stuart, 2014).

Counter point-bars (also known as out bank benches or eddy accretion deposits; Smith *et al.*, 2009) have not been included in this study. This presents a weakness, as they are important with regard to the distribution of mud-prone sediment. Counter point bars make up 15-20% of some preserved meandering successions: like the McMurray and Dinosaur Park (Hubbard *et al.*, 2011; Durkin *et al.*, 2015; Durkin, 2016). They have not been included as they accrete via a different mechanism to point bars, i.e. counter

point-bars form on the outer bank of meander bends and form concave-shaped deposits, as opposed to point-bars that form on the inner bank, and form convex-shaped deposits. These important and increasingly recognised elements could be incorporated into the assessment methodologies developed here; this provides scope for future work.

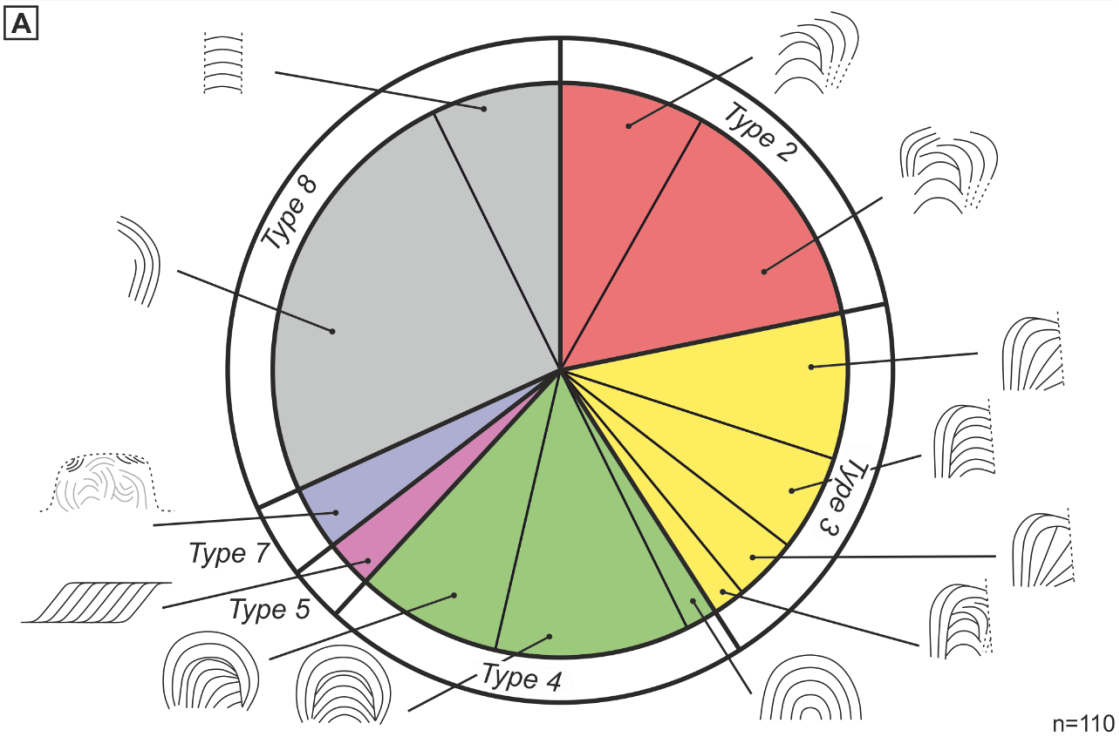
### 6.3 Research Question 3

*What is the impact of the timing and mechanism of channel abandonment on geometries of preserved point-bar deposits?*

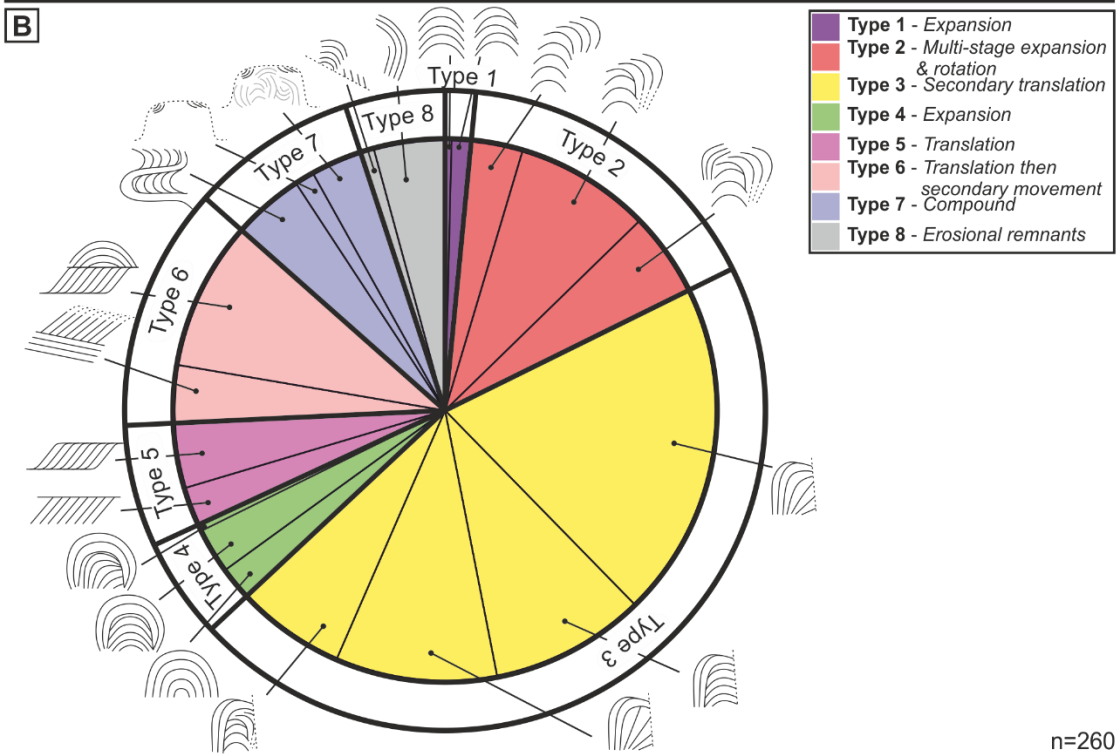
Active systems are useful to fluvial studies because they enable observation and demonstration of a range of characteristics and processes that may occur in fluvial meandering reaches (e.g. Fisk, 1947; Allen, 1965; Schumm, 1985; Erskine *et al.*, 1992; Gay *et al.*, 1998; Bridge, 2003; Phillips, 2003; Hooke, 2004; 2007; Smith *et al.*, 2009; Ghinassi *et al.*, 2016). However, active meanders have developed to different stages of maturity; their form and scroll-bar pattern cannot necessarily be compared directly to those of abandoned systems where channel cut-off has already occurred. This should be a significant consideration when comparing active versus relic systems (Miall, 2006).

Observations made on active fluvial reaches have not been found to adequately reflect the abandoned record (Tye, 2004; Miall, 2006). The two main disparities between active and abandoned point-bar deposits are that the overall geometries (Fig. 4.10): rounded (1:1) and long (1:<1) shapes are almost equally prevalent in abandoned point-bars, suggesting that both shapes ought to be considered when constructing 3D geological models of ancient fluvial point-bar deposits; and planform morphology of scroll-bars are different (Fig. 6.3). Current modelling approaches typically only consider circular target bodies because data sets are collected from active modern analogues (e.g. Colombera *et al.*, 2017).

**Proportions of scroll-bar patterns on point-bar fragments**



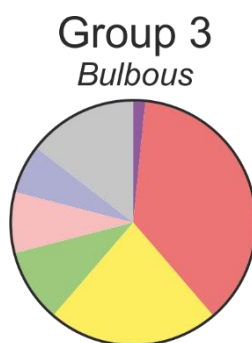
**Proportions of scroll-bar patterns on active point-bars**





**Figure 6.3 - A) Pie chart to illustrate the proportions of scroll-bar pattern in abandoned point-bar deposits; B) Pie chart to show the proportions of scroll-bar pattern in active point-bar deposits.**

There are many differences in the proportions of scroll-bar pattern between active and abandoned point-bar deposits (Fig. 6.3). Notably, down-stream accretion (Type 3) is dominant in active systems, whereas partial scroll-bar remnants (Type 8) is dominant in abandoned systems. The exception is if the reach has avulsed (Fig. 4.5), in which case the active preserved morphometries may be similar, i.e. meanders that cut off by reach avulsion may be preserved at various states of evolution. The pie chart presented for active bulbous shapes (Group 3), in Figure 3.9 (replicated as Figure 6.4), is compared with Figure 6.3. It is found to resemble abandoned proportions (Fig. 6.3A) more closely than active proportions (Fig. 6.3B). This suggests that both scroll-bars and meander shapes have quantifiably progressive immature and mature phases, i.e. active, to bulbous, to abandoned.



**Figure 6.4 –Pie chart showing proportions of scroll-bar style observed in active bulbous deposits (see also Figure 3.9). Key is the same as in Figure 6.3. n=62.**

Meander loops may become abandoned by neck cut-off, chute cut-off, or avulsion (Fisk 1947, Allen 1965, Kulemina, 1973; Brice, 1977). It is important to consider these mechanisms because the resultant channel fill may be mud- or sand-prone (Fisk, 1947;

Allen, 1965; Toonen *et al.*, 2012; Fig. 4.3). In a petroleum basin, if the channel-fill is sand-prone then it may form a reservoir unit, and may also connect point-bar deposits and crevasse splay deposits if the reach has avulsed (e.g. Donselaar & Overeem, 2008), and may improve vertical connectivity to overlying point-bar deposits (Fig. 4.8A). Avulsion (Figs 4.8G and 4.8H) is most likely to leave a sand-prone channel-fill deposit in a single thread (Allen, 1965, Mackey & Bridge, 1995; Toonen *et al.*, 2012; Fig. 4.3C). It may occur at any phase of meandering and the resultant preserved deposit is morphologically similar to its active form (Fig. 4.5). Chute cut-off (Fig. 4.7C) is likely to leave a channel-fill deposit that is less sand-prone than avulsion, and the shape of the abandoned deposit is open and curved (Fisk, 1947; Allen, 1965; Erskine *et al.*, 1992; Toonen *et al.*, 2012; Figs 4.2, 4.3B, and 4.7C). This mode of cut-off may occur when the meander is at any phase prior to maturing to a bulbous shape (Group 3; Fig. 2.8). The distinct sub-category of chute cut-off that is chute cut-off on converging limbs (Fig. 4.7B), was introduced in this study, and so the resulting channel fill is suggested to be a combination of features from neck cut-off, and chute cut-off. Meander loop abandonment via the mechanism chute cut-off on converging limbs, occurs when the meander loop has matured into a bulbous shape (Group 3; Fig. 2.8). Neck-cut-off (Fig. 4.7A) is likely to leave a mud-prone channel fill deposit that forms a loop that may, or may not, be closed (Fisk, 1947; Allen, 1965; Harms, 1982). The potential array of channel-fill heterogeneities and geometries highlight the importance of considering the cut-off mechanism. The mechanism of meander abandonment also has an impact on the preservation potential of the point-bar deposit; if the meander undertakes chute cut-off, the point-bar deposit may be consequently eroded because it is not entirely encased by a mud-prone plug that resists erosion. If the meander undertakes neck cut-off, the point-bar deposit may have a mud-prone perimeter making it more likely to be

preserved on the floodplain, and consequently in the rock record. Also, chute cut-off will tend to leave a proto meander that is a suitable shape for growth into the point-bar resulting in erosion of the recently abandoned point-bar deposit.

Due to the disparities between active and abandoned point-bar deposits, it is suggested that for an ancient (non-avulsed), meandering system), suitable analogues should ideally be limited to those containing abandoned meander loops (e.g. Ielpi *et al.*, 2014), as opposed to active ones (Hubbard *et al.*, 2011, Durkin *et al.*, 2015). This insight ought to be considered when conditioning reservoir models, as typically only equidimensional shapes are currently considered (e.g. Colombera *et al.*, 2017). A strength of the data set compiled for Chapter 4 is that it is entirely from abandoned point-bar deposits. This has enabled a comparative analysis of active, and abandoned settings so that they may be quantitatively characterised; the morphological complexities of active, and abandoned settings may better understood independent of one another. In addition, the methods by which the active, and abandoned point-bar deposits are measured are similar. This means that statistically significant and robust comparisons may be undertaken through use of the methodologies outlined in Chapters 2, 3 and 4 to enable the most appropriate analogues to be obtained. By understanding the mechanisms of meander abandonment, and the cut-off style that occurred: i) potential geometries and associated scroll-bar patterns may be deduced; ii) the sequence of accretion over time may be constrained; and iii) the lithologic heterogeneity of the point-bar deposit may be predicted.

Weaknesses of this study are as follows: (i) only 10 point-bar deposits are assessed, for analysis of cut-off type, from each meandering fluvial reach so more data would strengthen the statistical trends derived; (ii) the scroll-bar pattern evident in the studied point-bar deposits have been subjectively determined (Fig. 3.5); and (iii) future erosion

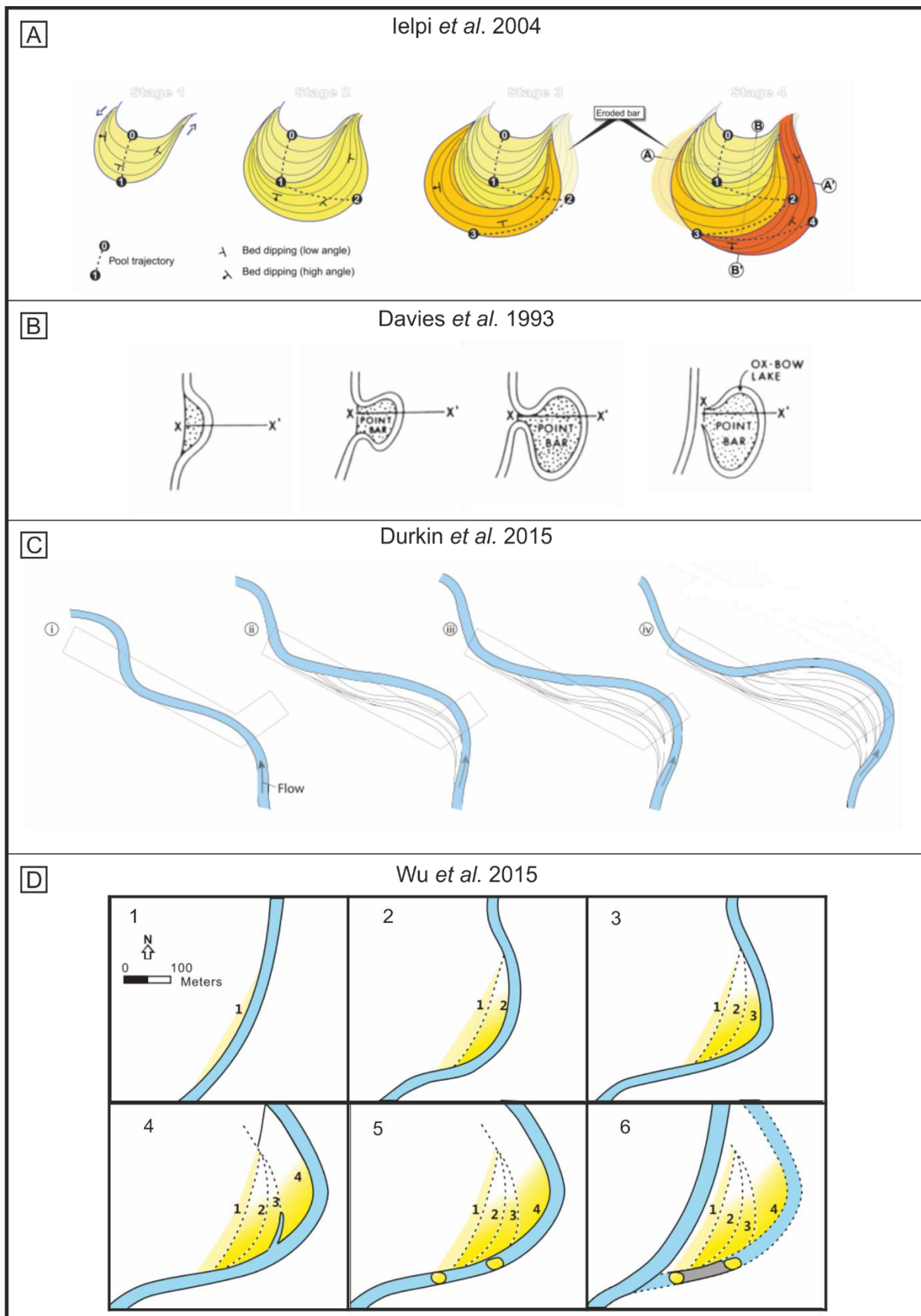
may occur that would alter the dimensions of the abandoned channels observed in this study. However, the considerations of this study are novel, and provide the framework for a more substantial analysis in the future.

## 6.4 Research Question 4

*How can planform point-bar dimensions and palaeo meander shape be reconstructed from an exposure of a preserved point-bar deposit.*

Where point-bar deposits are considered in outcrop, their limited exposure typically requires some form of reconstruction to accurately interpret the broader geometry (size and shape) of the studied element, its internal lithofacies distribution and heterogeneity, and its accumulation history. From an applied standpoint, it is important that the geological data are interpreted as accurately as possible because the suitability of geological models to predict subsurface reservoir behaviour depends on the accuracy of the input data (Tye, 2004). Pragmatically, models tend to be of limited complexity for the maintenance of accuracy and processing speed. Thus, their ability to capture subtle spatio-temporal changes in lithological heterogeneity within deposits will be limited. However, refinement of estimates of geometry (shape and lateral extent) is comparatively simple and may have a significant impact on the accuracy of the model. There are two broad categories of fluvial point-bar outcrop successions: those exposed in cross sectional (e.g. Ekeland, 2007; Donselaar & Overeem, 2008; Shiers *et al.*, in review), and those evident in planform (e.g. Wu *et al.*, 2015), though sometimes both cross sectional, and planform are available at the same outcrop (Ielpi *et al.*, 2014, Ghinassi *et al.*, 2015; 2016). Even in rare cases where point-bar deposits are observed in planform, only part of the larger element is usually evident as a partial remnant (e.g. Ghinassi *et al.*, 2016). Analogues are identified to find mutually agreeable morphologies between modern and ancient systems (Tye, 2004; Colombera *et al.*, 2017). In turn this may be used to determine similarities in scale, climate, latitude and basin type (Colombera *et al.*, 2013). This is a commonly adopted approach which has

been successful in supporting interpreted reconstructions of formative processes (e.g. Smith *et al.*, 2009; Fustic *et al.*, 2012; Durkin *et al.*, 2015; Ghinassi *et al.*, 2016). However, this approach is often used to “match” morphologies between active and abandoned deposits (e.g. Posamentier, 2004; Hubbard *et al.*, 2011; Durkin *et al.*, 2015). There are rare exceptions whereby recently abandoned point-bar deposits are studied (Shanley, 2004; Ielpi *et al.*, 2014). It can be problematic to compare active and abandoned point-bar deposits because active point-bars are dynamic and will likely undertake further adjustments prior to abandonment and potential lithification.

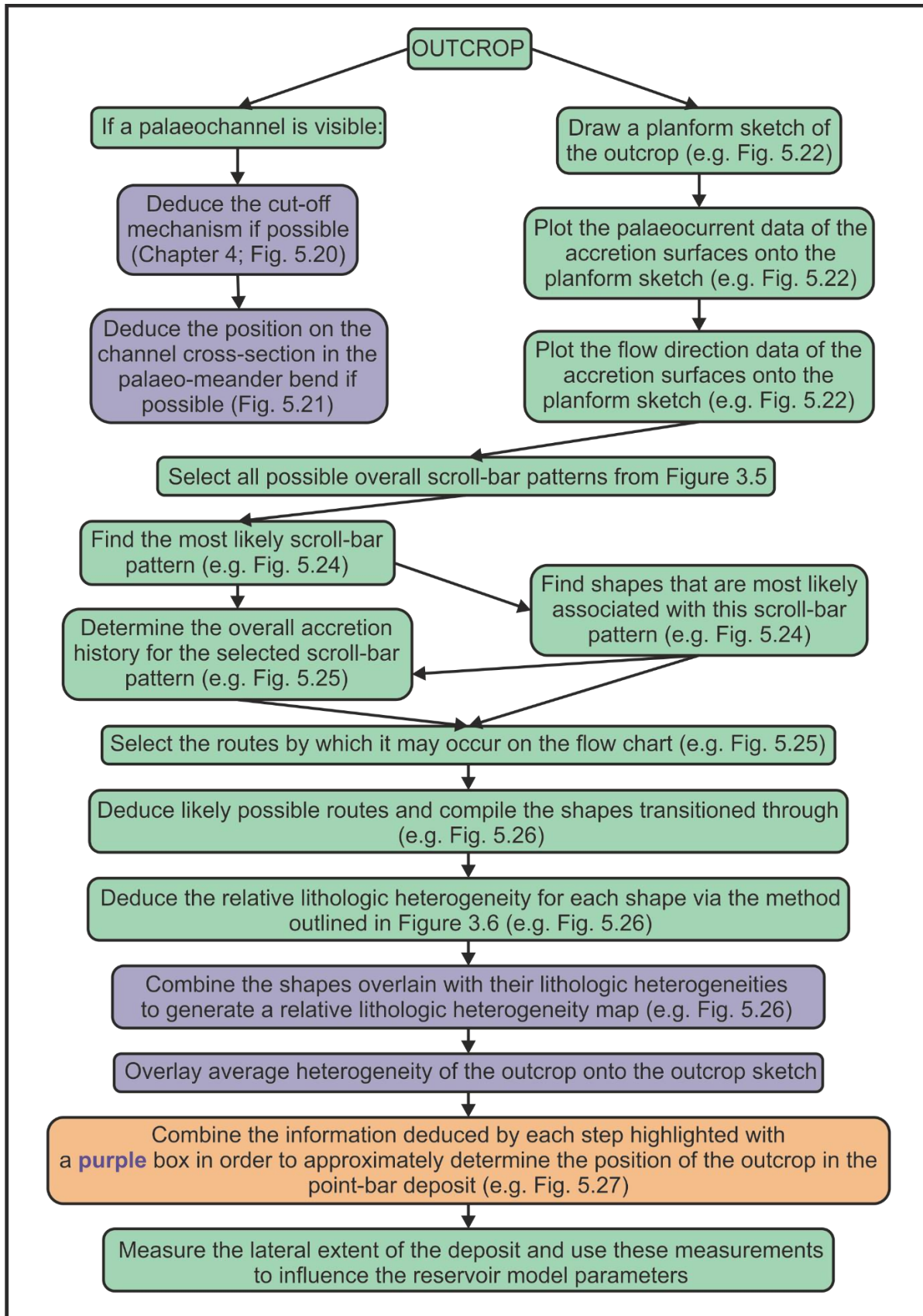


**Figure 6.5 – A) an idealised diagram of a point bar that evolves via expansion and downstream translation resulting in a bulbous shape, based on one exposed at Cromer Point, in the Jurassic Scalby Formation, UK (from Ielpi *et al.*, 2014); B) the sequential development of channel deposits and abandonment based on studies of the Lower Cretaceous Travis Peak Formation, East Texas, USA (from Davies *et al.*, 1993); C) the planform interpretation of lateral accretion packages studied between Willow Creek, and Red Deer River, in the Late Cretaceous Bearpaw Formation, Alberta, Canada (from Durkin *et al.*, 2015); D) a model for the channel bend migration of an interpreted point-bar deposit in the Cretaceous Ferron Sandstone Formation, Utah, USA), including its abandonment, (from Wu *et al.*, 2015).**

Time sequences are an effective way to convey likely past and future evolutionary accretion histories for point-bar deposits. Davies *et al.*, (1993) and Ielpi *et al.*, (2014), provide hypothetical accretion histories (Figs 6.5A and B); both of these systems evolve from a low-sinuosity open symmetrical shape (S4e or S4d), to a symmetrical bulbous shape (S3a). This contrasts with the outcrop reconstructions by Durkin *et al.*, (2015), and Wu *et al.*, (2015); both of these systems evolve from a low-sinuosity open symmetrical shape (S4e), to an open symmetrical shape with a slightly higher sinuosity (S4d). Ekeland (2007) provides a diverse consideration of sinuosity and accretion direction in fluvial point-bar deposits. However, meander shapes are reconstructed as symmetrical, and as if they are active, even when neck-cut off is interpreted. Varying lithologic heterogeneity across a point-bar deposit is not considered (as in Fig. 5.1), therefore the models may be improved by additionally considering parameters outlined in this study. This disparity between complex hypothetical reconstructions, and less complex outcrop reconstructions, suggests that a methodology is required to better reconstruct point-bar exposures in a manner that is statistically justified and sensitive to potential complexities. Outcrops may be either 2D planform, 2D outcrop, or 2D with



some pseudo-3D control (for example where cliff faces are arranged in various orientations); it is important for all types of exposure to be able to be analysed because exceptional planform outcrops are comparatively rare (e.g. Ielpi *et al.*, 2014; Ghinassi *et al.*, 2015, 2016). It is far more common for point-bar deposits in ancient fluvial systems that are documented and accessible, to be two dimensional cross-sections. This study has outlined a methodology by which a point-bar deposit may be reconstructed where a certain minimum fraction of the entire point-bar body is exposed (Fig. 6.6).



**Figure 6.6 – A flowchart of the recommended methodology to assess the range of possible reconstructions of a point-bar deposit. References to “planform” do not imply that the outcrop must be planform, it means that the analysis at that stage of the reconstruction requires a bird’s eye view sketch, or map, or image (e.g. Fig. 5.22)**

Through the application of this methodology for interpreting point-bar deposits at outcrop, complex, bulbous shapes have been reconstructed from a 2D outcrop (Fig. 5.27), demonstrating the application of methodologies outlined in Chapters 2 to 4. The shapes defined by the Intersection Shape methodology (Fig. 2.8), and the data set acquired, enabled the likelihood of shape occurrence, and likelihood of coincidence with the range of scroll-bars to be assessed. The proportions of scroll-bar patterns determined for both active (Fig. 3.8), and abandoned point-bar deposits (Fig. 4.13A), enable the most likely possibilities of scroll-bar pattern, and therefore accretion history, to be deduced for the point-bar deposit (Fig. 5.24). The flowchart of the development of a meander shape (Fig. 4.16) enables a route to be determined from initiation to abandonment of a meander bend. This understanding of the processes enables the heterogeneity to be mapped for the whole accumulation history, and for multiple processes to be considered.

The main strength of this approach is that it is able to provide a variety of potential reconstructions of point-bar deposits. These possible evolutionary histories and resultant reconstructions of final shape are deduced using likelihoods that have been measured from real-world data. Previously reconstructed point-bar accretion histories may be revisited to consider possible alternative interpretations. Here, the two models shown in Figures 6.5C (Durkin *et al.*, 2015), and 6.5D (Wu *et al.*, 2015), are reassessed and discussed in terms of the differences from the original interpretations, and how these differences are relevant.

The model presented by Durkin *et al.*, (2015; Fig. 6.5C), shows a low-sinuosity open symmetrical meander shape (S4e), to evolve, via punctuated rotation, to an open symmetrical shape with a slightly higher sinuosity (S4d), whereby it presumably undertook abandonment via avulsion. Through using the classifications and methods developed in this study, it may be suggested that this point-bar deposit represents fragmented scroll-bar remnants (Type 8; Fig. 3.5), that may have occurred as a result of neck cut-off (Fig. 4.12). This is significant because, by assessing the accretion history of the point-bar deposit as accurately as possible, the distribution of mud-prone sediment may be more accurately predicted. In turn, this has significant implications for the petroleum industry, as the proposed reconstruction displays a similar morphology to the point-bar deposits imaged in Figure 3.13 (Hubbard *et al.*, 2011). Therefore the proposed reconstruction could identify valuable information for more efficient hydrocarbon extraction.

The model presented by Wu *et al.*, (2015; Fig. 6.5D), shows a low-sinuosity open symmetrical meander shape (S4e), to evolve to an open symmetrical shape with a slightly higher sinuosity (S4d), whereby it undertook abandonment via w+1 chute cut-off. The reconstruction in Figure 6.5D is not dynamic because erosional processes are not considered; accretion surfaces 1, 2, and 3 appear truncated and their associated upstream deposits are fine-grained. Through using the classifications and methods developed in this study, it may be suggested that the accretion history was somewhat different. It is unlikely that this growth occurred without erosion, and so it is proposed that as stage 4 occurred (Fig. 6.5D), erosion of the upstream sand-prone sediment on accretion surfaces 1, 2, and 3 was undertaken. This would account for the truncated appearance of accretion surfaces 1, 2, and 3, and for the upstream fine-grained deposits that were recognised in the study. This is significant because it enables a

more accurate view of the character of the ancient meandering reach to be established, enabling other less well-exposed deposits to be more accurately interpreted. It may also provide information that allows for a wider appreciation of the fluvial system and its palaeoenvironment to be established.

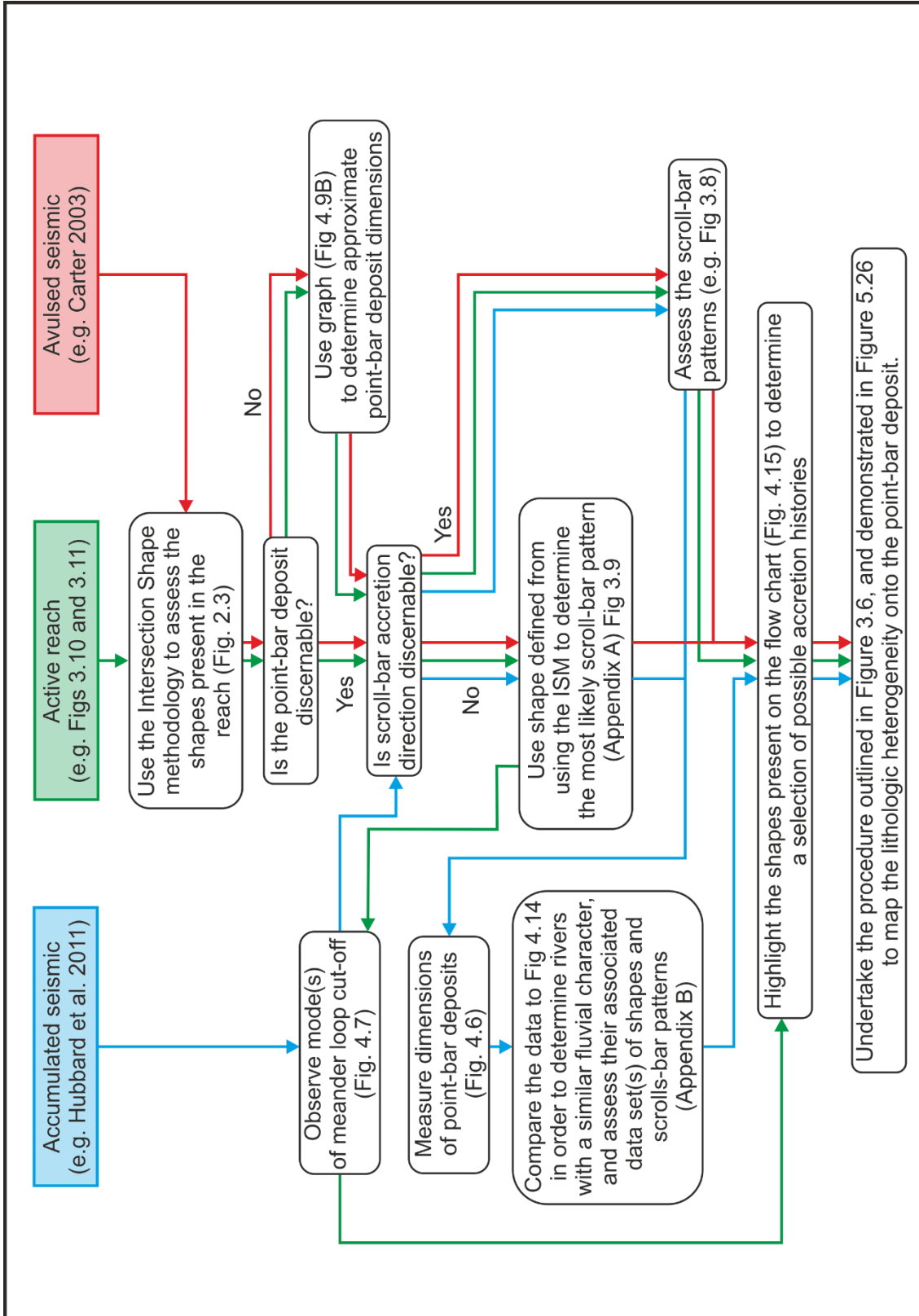
The principal limitation of this approach is that there are a large number of options provided and narrowing them down is largely subjective, even though statistical likelihoods have been deduced. More data are required from a more varied set of river systems to constrain the natural variability between meander shape and meander scroll-bar pattern in different environmental settings. This is because there are relationships implied by classic models (e.g. Bridge, 2003), that are not consistent with the variabilities observed in this study. The variability of results presented in an analysis is complex and varied, though this could be lessened in the future by collecting a larger data set as common trends will emerge that can form the mainstay of future interpretations. However, the presentation of a single meander bend for the reconstruction of the evolutionary histories of ancient preserved point-bars is misleading given the available data. Therefore, carrying multiple alternatives forward strengthens the approach because carrying this uncertainty is preferred to presenting false accuracy.

## 6.5 Research Question 5

*How can the internal stratigraphic architecture, and geomorphic variability, be predicted from surface morphology, or flattened seismic timeslices?*

When assessing a clearly imaged, fluvial meandering system in planform (e.g. Hubbard *et al.*, 2011; Alqahtani *et al.*, 2015; 2017) – whether it be from imagery of modern systems, from outcrop or from seismic data – the lateral extent (both length and width), of each point-bar deposit may be directly measured (i.e. Fig. 4.6). It is most challenging to determine the accretion history and heterogeneity of the point-bar deposit, so only the lateral extent is determined here as the full shape currently holds too much uncertainty with the available data. It is important to predict point-bar characteristics because the mud-prone (IHS) sediment can act as a baffle to fluid flow (Fielding & Crane, 1987; Miall, 1988; Tye, 2004). Therefore predicting its distribution is of use to reservoir engineers (Tye, 2004). In modern systems, no two meandering reaches are exactly the same. Therefore matching an ancient system with an active modern system may be considered limiting in its capacity to be of use. Analogues are most commonly used as a means to deduce the missing attributes of a preserved meandering fluvial system (e.g. Posamentier *et al.*, 2004; Colombera *et al.*, 2013; 2017). In this study, the similarities between modern and ancient point-bar deposit morphologies is compartmentalised into constituent morphological features, so they may be separately assessed, and the adaptive methodologies constructed in this study (Chapters 2-4), may improve the understanding of stratigraphic architecture and heterogeneity distribution. This can be achieved because the approach taken herein captures the robust interrelationship of point-bar properties, between modern and ancient, that helps

to better interpret reflection seismic data (e.g. Fig. 3.13). This is done by using an accessible data set of modern systems to reduce uncertainty and gaps in knowledge. Figure 6.7 shows how the active, modern system data (green), may be integrated in analysis, to provide support to the interpretation of both accumulated, and avulsed fluvial systems that may be evident in reflective seismic studies.





**Figure 6.7 - A flow chart to describe the methodologies for determining the lateral accretion history and heterogeneity for active modern systems, and both accumulated and avulsed seismic reflection imagery.**

This approach enables the lateral accretion history and lithological heterogeneity of a fluvial point-bar deposit to be determined, and therefore the mud- and sand-prone areas may be estimated. This approach is an improvement on past approaches for the following reasons: (i) it lessens the direct dependency on modern active fluvial reaches used as analogues that might not necessarily be entirely appropriate; (ii) it enables independent analysis for each reach, and each point-bar deposit; (iii) it establishes the appreciation that one point-bar deposit ought to not be considered in isolation, but as part of a dynamic set of processes in a dynamic geomorphic system; (iv) it draws data from active and abandoned fluvial meandering reaches together to identify common characteristics from each; (v) it enables multiple possibilities to be considered at each stage; and (vi) it allows additional information to be introduced into a fluvial reservoir model from this study, such as point-bar dimensions (Fig. 4.10) and outcrop interpretations (Figs. 5.27 and 5.28). Most importantly, through use of this approach, models that have sparse or poor-quality data (e.g. only limited borehole information or 2D seismic, or which only poorly image point-bar plan form shape, for example at great subsurface depth), may be populated with likely shape and/or scroll-bar combinations and further refined if environmental constraints (e.g. climate, basinal setting), are deduced. This may be achieved by filtering the data set collected to make use of only that subset of data considered most appropriate (cf. Colombera *et al.*, 2013).

The principal limitation of this approach is that it is not yet proven. The variability of the model outputs may be too high for this outlined approach to be of use; there might be insufficient data to adequately deduce from a variety of eventualities. More data should

be collected to improve this and the resultant enhanced and augmented data set ought to be able to produce better substantiated results.

## 7 Conclusions and Future Work

### 7.1 Conclusions

The principle conclusions arising from the research documented in this thesis are outlined below:

- Two-hundred-and-sixty active meander bends, from 13 river reaches, and 10 abandoned point-bar deposits from 13 river reaches, have been subject to detailed morphometric analysis to determine the pattern of lithofacies heterogeneity distribution within preserved deposits from analysis of meander shape, scroll-bar pattern, and cut-off mechanism.
- The Intersection Shape methodology provides a quantitative, novel, repeatable approach that can be readily implemented for the morphometric analysis of individual meanders in any meandering river system, and which allows for direct comparison of any two meandering reaches using data from: (i) remote sensing; (ii) seismic time slices; (iii) outcrop plan forms; (iv) meanders reconstructed from outcrop sections; (v) core or well log data (of sufficient coverage to enable tentative assessment). It may be applied to a wider range of meander shapes than previous, older methods.
- Due to the quantitative nature of the Intersection Shape methodology, it permits a level of objectivity that is more accurate than previously developed applied shape matching methods (e.g. Brice, 1974; Allen, 1982), and more accurate than the semi-quantitative radius-of-curvature methodology (Nanson & Hickin, 1983). Therefore, a more comprehensive characterisation of fluvial meandering reaches is possible.

- Twenty-five meander shapes are identified that are divided into 4 parent groups: open asymmetric (Group 1), angular (Group 2), bulbous (Group 3), and open symmetric (Group 4). These parent groups represent 26, 11, 24 and 39 % of the 260 meander shapes assessed, respectively.
- New insights into the controls that influence the differences in the morphology of fluvial meander form have been identified. These insights enable a wider understanding of controls and formative processes that govern meandering river development and associated bar accumulation. For example, in the Senegal and Irtysh (Ob) Rivers, similar proportions of open asymmetric, angular, bulbous, and open symmetric meander shapes are observed. However, the bulbous shapes are shown to possess a symmetrical form in the Senegal River compared to an asymmetric form in those of the Irtysh (Ob) River. This is significant in terms of improving our understanding of the behaviours of these (and other) rivers, because by assessing the morphologies objectively, trends may arise enabling more insight into the behaviours, patterns, and controlling mechanisms of meandering fluvial systems.
- The surface expression of a fluvial point-bar deposit may be classified using 22 scroll-bar patterns established in 8 parent groups: extension (Type 1), multi-stage expansion and rotation (Type 2), secondary translation (Type 3), expansion (Type 4), translation (Type 5), translation then secondary movement (Type 6), compound (Type 7), erosional remnants of scroll-bar deposits (Type 8). This classification scheme describes a more complete range of scroll-bar types than existing widely used classifications.

- The accretion history of point bars developed as a consequence of meander-loop evolution may be established through observation of the scroll-bar pattern. From this, the relative grainsize deposited may be predicted for each meander shape (as recognised by the Intersection Shape methodology). This is done by fitting the meander shapes to the scroll-bar pattern observed, and estimating the relative heterogeneities that may be present on each shape as grain-size fines downstream (cf. Fustic, 2012). Images are then overlain and heterogeneity types are joined in order to construct a heterogeneity map.
- The most commonly occurring scroll-bar pattern in the point-bar deposits of studied active fluvial meanders is secondary downstream accretion (Type 3). The most commonly occurring scroll-bar pattern in the abandoned fluvial point-bar deposits studied, is fragmented remnants (Type 8).
- Reservoir models are developed based on observed relationships known to occur in nature, and are usually scaled to appropriate analogue data from one or more comparable systems to the type of system being modelled. Data from this study may be incorporated into such models, and therefore enable statistical limitations to be incorporated; i.e. the dimensions of the point-bar deposits may be used to constrain modelled dimensions.
- A more accurate interpretation of the origin, evolutionary history and internal facies distribution of meanders in an active fluvial reach may be attained by using the Intersection Shape methodology, and the scroll-bar classification schemes in combination.
- Abandoned point-bar dimensions are expressed as length:width. Rounded (1:1) and long (1:<1) shapes are almost equally prevalent in abandoned

point-bars (43 and 47% respectively), whereas wide ( $1:>1$ ) shapes are less prevalent (10%). This demonstrates that long ( $1:<1$ ) shapes ought to be considered when constructing 3D geological models of ancient fluvial point-bar deposits.

- Neck cut-off is the most prevalent style of individual meander cut-off observed in the floodplains of the studied active fluvial reaches. This could be because mud is significantly more difficult to erode than sand (Hooke, 2004). Therefore, mud-prone channel fills deposited as a consequence of neck cut-off may protect abandoned point bars from erosion.
- Where a cut-off type repeats, a group cut-off style may be described. Such relationships have implications for the connectivity of abandoned point-bar deposits. Group cut-off styles are seen in 36% of the observed individual meander cut-offs. Local avulsion is defined as when part of a meandering reach avulses and re-joins the channel; it is observed in 20% of the abandoned point-bar deposits studied.
- Consideration of the characteristics of abandoned fluvial point-bar deposits enables a more complete and objective assessment of river characteristics. This is because, by assessing a fluvial meandering reach from initiation to abandonment, the whole process of sedimentation in that reach may be reconstructed.
- Application of the methodologies presented in Chapters 2 to 4 enable a step towards appreciating the large range of possible morphologies that the point-bar elements may form and become preserved.

- The accretion history of a point-bar deposit may be more accurately reconstructed, and presented as a sequential evolutionary history that culminates in meander abandonment (e.g. Wu *et al.*, 2015).
- An exposed point-bar architectural element of Pennsylvanian age exposed in cliff sections at Nolton Haven cove (Pembrokeshire, Wales, UK) has been examined in detail. Seventeen distinct lithofacies have been identified and these are arranged into commonly repeating associations in 4 facies successions, as demonstrated by the results of statistical analysis, for which Markov chain analysis methodologies from Walker (1979) and Harper (1984) were used.
- Facies succession 1 is associated with a change in migration direction in the point-bar deposit. Facies succession 2 is associated with continued growth in a similar direction. Facies succession 3 represents either pebble-lag scour fill, or bank collapse. Facies succession 4 infills high-energy scours and decreases in energy, depositing laminated and rippled sandstone deposits. Through interpreting the formative processes of each of these facies successions, the outcrop succession may be more accurately interpreted and sand-prone areas observed.
- The combination of the novel methodologies developed as a primary outcome of this research presents a powerful, and refined approach for prediction of the lateral extent, geometry, accretion history, and internal lithofacies heterogeneity distribution of fluvial point-bar deposits for which not all of these parameters are known or can be constrained from available data. The results of this thesis are able to provide the framework from which testable hypotheses for geological models may be constructed.

## 7.2 Future Work

A primary objective of future work should be to determine the key controls on meander form. In turn this will require the collection of more data from both modern systems and ancient outcrop successions. Potential ideas for future data collection are: (i) more specific studies of longer reaches, so that the source-to-sink process may be better understood; (ii) targeting fluvial systems that have marine influence, so that the influence of tides on the morphology of tidally-influenced, meandering fluvial systems may be better understood; (iii) targeting fluvial systems in subsiding basins that are responding to the controls that will likely enable long-term preservation, so that the morphologies that have preservation bias may be better constrained. The acquisition of more data and its application using the analytical approach devised here, will mean that individual classifications of meander shape, scroll-bar pattern, and mode of abandonment will likely be modified as the classifications become more robustly supported. Independent use of the Intersection Shape methodology provides much scope for future work: (i) typical meander growth trajectories may be visually described on a bivariate plot to help determine shapes that may be associated in the ancient record; (ii) the skew of the meander and position of meander growth may be more specifically analysed to help determine the relative amount of mud- and sand-prone sediment that might be expected in a reach; (iii) environmental controls may be determined through a more extensive study of modern systems and, by achieving this, the understanding of the environmental controls on the morphology will become more informed; and (iv) the methods applied could be developed and applied to other environments, i.e. sinuous deep water channels (Peakall and Sumner, 2015), and sinuous deposits on Mars (Burr *et al.*, 2013), to determine similarities, and differences in form. Key research questions for the next decade are in testing the relative



influences of climate, gradient, vegetation type, vegetation density, sediment calibre, river size, and basin setting in modern systems. There may also be influences induced by palaeolatitude, and age in ancient systems. All of these controls will likely be reflected in the fluvial morphology. By quantitatively, and objectively, assessing fluvial reaches in modern and ancient successions via the methods outlined in this study, answers to these questions may be discerned. Heterogeneity prediction may be more robustly justified through acquisition of piston cores taken from modern systems to ground truth and test the proposed models. These piston cores ought to be taken from different positions on both active and abandoned point-bars and infilled channel deposits. Core data that are substantiated by flattened reflection seismic imagery should be incorporated into the understanding, and consequently the resulting geologic models. This is important to ensure that the models may be as accurate as possible. The applied importance of this work is such that it may be used to improve understanding and build models for hydrocarbon reservoirs that are both shallow and well imaged (e.g. McMurray Formation; Hubbard *et al.*, 2011), and deeper, and less well imaged (e.g. Mungaroo Formation; Stuart, 2014).

Further work with regard to the studied outcrop at Nolton Haven, and many other similar outcropping successions, could entail separating the data into the respective facies successions, and running Markov chain analysis on each succession in turn. This would reveal further trends and analyses within each substantiated group. Further analysis of this type may also consider the type of contact at each facies transition (Miall & Gibling, 1978).

However, these methodologies have broader applications, and may be developed further on 3D outcrops, and outcrops supported by core, to revolutionise the way in which we interpret the significance of the ancient rock record. The procedure outlined

for the interpretation of the exposure at Nolton Haven may be used to determine potential meander shapes prior to the Palaeozoic facies shift, and compared to now to determine if there has been an evolution of meander architecture, and shape, over geological time.

However, the surface morphology of fluvial point-bars is highly variable, and its relationship with the internal architecture has only been established on a small case-specific scale. More data are required to better establish these morphological relationships so that key surfaces in the rock record may be translated into geological models effectively.

The combination of these approaches will enable: (i) rules based modelling of heterogeneity that may be used in object-based, or pixel-based models; (ii) numerical modelling of meander growth constrained by statistically defined morphometric rules; (iii) the likelihood of the frequencies of occurrence of different meander shapes in different fluvial reaches; and (iv) forward modelling of active fluvial systems to predict a future geological deposit.

A larger, longer-term research plan that might significantly advance the state-of-the-science is to make sedimentology more quantitative so that it may be integrated meaningfully with large datasets, such as those of FAKTS (Colombera *et al.*, 2013); the methodologies outlined in this thesis could be used to contribute the sedimentary architecture of point-bar deposits in both modern, and ancient settings. However, there is scope for these data to form their own global, or open, database that others might contribute data to; it could include meander shape, and scroll-bar pattern data, depositional environment, palaeolatitude, gradient, and mode of meander loop abandonment. Such a database should be designed so that it can be queried to

discern allogenic and autogenic controls on fluvial architecture, a long-lived and fundamental science research question in sedimentary geology. There would also be potential for the database to be developed as a commercial tool, and may become a plug-in for Schlumberger Petrel. The broader, applied significance of developing the approach outlined in this thesis is that it will enable a clearer, understanding of the flow dynamics in a heterolithic body. This has implications for the hydrocarbon industry, assessment of groundwater aquifers, and assessment of potential sites for underground CO<sub>2</sub> storage.

Overall, there is significant potential scope for this research to be continued to provide new insights into both modern and ancient fluvial deposits.

## 8 List of References

- Abad, J.D. and Garcia, M.H. (2009) Experiments in a high-amplitude Kinoshita meandering channel: 2. Implications of bend orientation on bed morphodynamics. *Water Resources Research*, **45**, 1-14.
- Abbe, T.B. and Montgomery, D.R. (2003) Patterns and processes of wood debris accumulation in the Queets river basin, Washington. *Geomorphology*, **51**, 81–107.
- Abernethy, B. and Rutherford, I.D. (1998) Where along a river's length will vegetation most effectively stabilise stream banks? *Geomorphology*, **23**, 55–75.
- Adamson, K.R., Lang, S.M., Marshall, N.G., Seggie, R., Adamson, N.J. and Bann, K.L. (2013) Understanding the Late Triassic Mungaroo and Brigadier Deltas of the Northern Carnarvon Basin, North West Shelf. In: *The Sedimentary Basins of Western Australia IV*: (Eds M. Keep and S.J. Moss), Proceedings of the Petroleum Exploration Society of Australia Symposium, Perth, WA. p. 1
- Alford, J.J. and Holmes, J.C. (1985) Meander scars as evidence of major climate change in southwest Louisiana. *Annals of the Association of American Geographers*, **75**, 395-403.
- Allen, J.R.L. (1965) A review of the origin and characteristics of recent alluvial sediments. *Sedimentology*, **5**, 89-191.
- Allen, J.R.L. (1964) Studies in Fluvial Sedimentation: Six Cyclothems from the Lower Old Red Sandstone, Anglowelsh Basin. *Sedimentology*, **3**, 163–98.
- Allen, J.R.L. (1982) *Sedimentary structures: Their Character and Physical Basis, Volume 1. Developments in Sedimentology* 30. Elsevier Science Publishers, **30**, 285-94.

Allen, J.R.L. (1983) Studies in fluvial sedimentation: bars, bar-complexes and sandstone sheets (low-sinuosity braided streams) in the brownstones (L. Devonian), Welsh borders. *Sedimentary Geology*, **33**, 237–93.

Alqahtani F.A., Johnson H.D., Jackson C.A-L. and Som M.R.B. (2015) Nature, origin and evolution of a Late Pleistocene incised valley-fill, Sunda Shelf, Southeast Asia. *Sedimentology*, **62**, 1198-1232.

Alqahtani F.A., Jackson C.A-L., Johnson H.D. and Som M.R.B. (2017) Controls on the geometry and evolution of humid-tropical fluvial systems: insights from 3D seismic geomorphological analysis of the Malay basin, Sunda shelf, southeast Asia. *Journal of Sedimentary Research*, **87**, 17-40.

Anderson, G.C., Barnes, C.A., Budinger, T.F., Love, C.M., and McManus, D.A. (1961) The Columbia River discharge area of the northeast Pacific Ocean. *A literature survey. University of Washington, Department of Oceanography, Seattle.*

Andrie, R. (1994) The angle measure technique: a new method for characterizing the complexity of geomorphic lines. *Mathematical Geology*, **26**, 83-97.

Ashworth, P.J. and Ferguson, R.I. (1986) Interrelationships of channel processes, changes and sediments in a proglacial braided river. *Geografiska Annaler. Series A. Physical Geography* **68**, 361–71.

Aslan, A. and Blum, M.D. (1999) Contrasting styles of Holocene avulsion, Texas Gulf coastal plain, USA. In: *Fluvial sedimentology* (Ed. by N.D. Smith and J. Rodgers), International Association for Sedimentologists, **6**, 193-209.

Bagnold, R.A., (1960) Some aspects of river meanders: United States Geological Survey Professional Paper **282-E**, 10 p.

Bernard, H.A., Leblanc, R.J. and Major, D.J. (1962) Recent and Pleistocene geology of southeast Texas. In: *Geological Society of America Guidebook for 1962 Annual Meeting* (Eds E.H. Rainwater and R.P. Zingula), p. 175-224.

Bhattacharya, P., Bhattacharya, J.P. and Khan, S.D. (2015) Paleo-channel reconstruction and grain size variability in fluvial deposits, Ferron Sandstone, Notom Delta, Hanksville, Utah. *Sedimentary Geology*, **325**, 17-25.

Bisat, W. S. (1923) The Carboniferous goniatites of the north of England and their zones. *Proceedings of the Yorkshire Geological Society*, **20**, 40-124.

Bledsoe, B.P. and Watson, C.C. (2001) Logistic analysis of channel pattern thresholds: meandering, braided, and incising. *Geomorphology*, **38**, 281–300.

Blondeaux, P. and Seminara, G. (1985) A unified bar–bend theory of river meanders. *Journal of Fluid Mechanics*, **157**, 449-470.

Blum, M.D. and Törnqvist, T.E. (2002) Fluvial Responses to Climate and Sea-Level Change: A Review and Look Forward. *Sedimentology* **47**, 2–48.

Bobrovitskaya, N.N., Zubkova, C. and Meade, R.H. (1996) Discharges and yields of suspended sediment in the Ob and Yenisey Rivers of Siberia. In: *Erosion and Sediment Yield: Global and Regional Perspectives* (Ed. by D.E. Walling, B.W. Webb), *IAHS Publications-Series of Proceedings and Reports-Int. Assoc. Hydrological Sciences*, **236**, 115-124.

Bradu, D. and Hawkins, D.M. (1982) Location of multiple outliers in two-way tables, using tetrads. *Technometrics*, **24**, 103-108.

Brekke, H. (2015) Cretaceous forensic podiatry: big game tracking with a microresistivity image log on a McMurray Formation scroll bar. *Bulletin of Canadian Petroleum Geology*, **63**, 225–42.

Brice, J.C. (1973) Meandering pattern of the White River in Indiana - an analysis. In: *Fluvial Geomorphology; Proceedings of the Binghamton Symposium* (Ed M. Morisawa), p. 178-200.

Brice, J.C. (1974) Evolution of Meander Loops. *Geological Society of America Bulletin*, **85**, 581–586.

Brice, J.C. and Blodgett, J.C. (1978) Countermeasures for hydraulic problems at bridges. *Federal Highway Administration Report FHWA-RD-78-162*, Vols. 1, 2, Washington, DC.

Bridge, J.S. and Mackey, S.D. (1993) A theoretical study of fluvial sandstone body dimensions, In: *The geological modelling of hydro-carbon reservoirs* (Eds S. Flint and I.D. Bryant), International Association of Sedimentologists Special Publication **15**, 213–236.

Bridge, J.S. (1993) The interaction between channel geometry, water flow, sediment transport and deposition in braided rivers. In: *Braided Rivers* (Ed. by Best, J.L., Bristow, C.S.) Geology Society, London, –71. Bridge, J.S., Smith, N.D., Trent, F., Gabel, S.L. and Bernstein, P. (1986) Sedimentology and morphology of a low-sinuosity river: Calamus River, Nebraska Sand Hills. *Sed70*.

Bridge, J.S. (1993a) The Interaction between Channel Geometry, Water Flow, Sediment Transport and Deposition in Braided Rivers, In: *Braided Rivers* (Eds J.L. Best and C.S. Bristow), *Geological Society, London, Special Publications*, **75**, 13–71.

Bridge, J.S. (1993b) Description and Interpretation of Fluvial Deposits: A Critical Perspective. *Sedimentology*, **40**, 801–10.

Bridge, J.S. (2003) *Rivers and Floodplains*. Blackwell, Oxford. 491 pp.

Bridge, J.S. and Jarvis, J. (1982) The Dynamics of a River Bend: A Study in Flow and Sedimentary Processes. *Sedimentology*, **24**, 499–541.

Bridge, J.S. and Tye, R.S. (2000) Interpreting the Dimensions of Ancient Fluvial Channel Bars, Channels, and Channel Belts from Wireline-Logs and Cores. *American Association of Petroleum Geologists Bulletin*, **84**, 1205–28.

Bridge, J.S., Alexander, J., Collier, R.E., Gawthorpe, R.L. and Jarvis, J. (1995) Ground-penetrating radar and coring used to study the large-scale structure of point-bar deposits in three dimensions. *Sedimentology*, **42**, 839-852.

Brooks, A.P., Brierley, G.J. and Millar, R.G. (2003). The long-term control of vegetation and woody debris on channel and flood-plain evolution: insights from a paired catchment study in southeastern Australia. *Geomorphology*, **51**, 7-29.

Brown, L.F. and Fisher, W.L. (1980) Seismic Stratigraphic Interpretation and petroleum exploration: *American Association of Petroleum Geologists Department of Education: AAPG Course Notes* 16. 181 p.

Burns, C.E., Mountney, N.P., Hodgson, D.M. and Colombera, L. (2017) Anatomy and dimensions of fluvial crevasse-splay deposits: Examples from the Cretaceous Castlegate Sandstone and Neslen Formation, Utah, USA. *Sedimentary Geology*, **351**, 21-35.



- Burr, D.M., Enga, M.T., Williams, R.M.E., Zimbelman, J.R., Howard, A.D. and Brennand, T.A. (2009) Pervasive aqueous paleoflow features in the Aeolis / Zephyria Plana region, Mars. *Icarus*, **200**, 52–76.
- Burr, D.M., Williams, R.M., Wendell, K.D., Chojnacki, M. and Emery, J.P. (2010) Inverted fluvial features in the Aeolis/Zephyria Plana region, Mars: Formation mechanism and initial paleodischarge estimates. *Journal of Geophysical Research: Planets*, **115** (E7 20pp).
- Burr, D.M., Perron, J.T., Lamb, M.P., Irwin, R.P., Collins, G.C., Howard, A.D., Sklar, L.S., Moore, J.M., Ádámkóvics, M., Baker, V.R., Drummond, S.A. and Black, B.A. (2013) Fluvial features on Titan: Insights from morphology and modelling. *Geological Society of America Bulletin*, **125**, 299-321.
- Cain, A.C. and Mountney, N.P. (2009) Spatial and temporal evolution of a terminal fluvial fan system: the Permian Organ Rock Formation, South-east Utah, USA. *Sedimentology*, **56**, 1774–1800.
- Camporeale, C., Perona, P., Porporato, A. And Ridolfi, L. (2005) On the long-term behavior of meandering rivers. *Water Resources Research*, **41**, AR W12403.
- Carlston, C.W. (1965) The relation of free meander geometry to stream discharge and its geomorphic implications. *American Journal of Science*, **263**, 864-885.
- Carr, T.R. (1982) Log-linear models, Markov chains and cyclic sedimentation. *Journal of Sedimentary Petrology*, **52**, 905-912.
- Carter, D.C. (2003) 3-D seismic geomorphology: Insights into fluvial reservoir deposition and performance, Widuri field, Java Sea. *AAPG Bulletin*, **87**, 909-934.

Chen, D. and Duan, J.G. (2006) Modeling width adjustment in meandering channels. *Journal of Hydrology*, **321**, 59-76.

Chitale, S.V. (1973) Theories and relationships of river channel patterns. *Journal of Hydrology*, **19**, 285-308.

Church, M. (2006) Bed material transport and the morphology of alluvial river channels. *Annual Review of Earth and Planetary Sciences*, **34**, 325-354.

Cleal, C.J. (1997) The palaeobotany of the upper Westphalian and Stephanian of southern Britain and its geological significance. *Review of Palaeobotany and Palynology*, **95**, 227–253.

Collinson, J. D. (1978) Vertical sequence and sand body shape in alluvial sequences. In: *Fluvial sedimentology* (Ed A.D. Miall), Canadian Society of Petroleum Geologists Memoir **5**, p. 577–586.

Colombera, L., Mountney, N.P. and McCaffrey, W.D. (2013) A quantitative approach to fluvial facies models: Methods and example results. *Sedimentology*, **60**, 1526–1558.

Colombera, L., Mountney, N.P. and McCaffrey, W.D. (2015) A meta-study of relationships between fluvial channel-body stacking pattern and aggradation rate: implications for sequence stratigraphy. *Geology*, **43**, 283–286.

Colombera, L., Mountney, N.P., Russell, C.E., Shiers, M.N. and McCaffrey, W.D. (2017) Geometry and compartmentalization of fluvial meander-belt reservoirs at the bar-form scale: quantitative insight from outcrop, modern and subsurface analogues. *Marine and Petroleum Geology*, **82**, 35-55.

Constantine J.A., Dunne, T., Piégay, H. and Kondolf, G.M. (2010) Controls on the alluviation of oxbow lakes by bed-material load along the Sacramento River, California. *Sedimentology*, **57**, 389–407.

Cope, J.C.W., Ingham, J.K., and Rawson, P.F. (1992) Atlas of palaeogeography and lithofacies. Memoir of the Geological Society of London, No. 13

Crickmay, C. H. (1960). Lateral activity in a river of northwestern Canada. *The Journal of Geology*, **68**, 377-391.

Dalrymple, M. (2001) Fluvial reservoir architecture in the Staffjord Formation (northern North Sea) augmented by outcrop analogue statistics. *Petroleum Geoscience*, **7**, 115–122.

Daniel, J.F. (1971) Channel Movement of Meandering Indiana Streams. *U.S. Geological Survey Professional Paper*, **A18**, 443-512.

Davies, D.K. and Ethridge, F.G. (1975) Sandstone composition and depositional environment. *AAPG Bulletin*, **59**, 239-264.

Davies, D.K., Williams, B.P. and Vessell, R.K. (1993) Dimensions and quality of reservoirs originating in low and high sinuosity channel systems, Lower Cretaceous Travis Peak Formation, East Texas, USA. In: Characterization of fluvial and aeolian reservoirs (Ed. by C. P. North and D. J. Prosser), *Geological Society, London, Special Publications*, **73**, 95-121.

Davies, N.S. and Gibling, M.R. (2011) Evolution of fixed-channel alluvial plains in response to Carboniferous vegetation. *Nature Geoscience*, **4**, 629-633.

- Davies, N.S., Gibling, M.R. and Rygel, M.C. (2011) Alluvial facies evolution during the Palaeozoic greening of the continents: case studies, conceptual models and modern analogues. *Sedimentology*, **58**, 220-258.
- Davies, N.S., Gibling, M.R., McMahon, W.J., Slater, B.J., Long, D.G.F., Bashforth, A.R., Berry, C.M., Falcon-Lang, H.J., Gupta, S., Rygel, M.C. and Wellman, C.H. (2017) Discussion on 'Tectonic and environmental controls on Palaeozoic fluvial environments: reassessing the impacts of early land plants on sedimentation'. *Journal of the Geological Society, London*, first published online April 17, 2017
- De Raaf, J.F.M., Reading, H.G. and Walker, R.G. (1965) Cyclic sedimentation in the lower Westphalian of north Devon, England. *Sedimentology*, **4**, 1–52
- Dieras, P.L. (2013) The Persistence of Oxbow Lakes as Aquatic Habitats: an Assessment of Rates of Change and Patterns of Alluviation Unpublished PhD these, Cardiff University, Wales. 177 pp.
- Donselaar, M.E. and Schmidt, J.M. (2010) The application of borehole image logs to fluvial facies interpretation. In: *Dipmeter and Borehole Image Log Technology* (Eds M. Pöppelreiter, C. García-Carballido and M. Kraaijeveld). *AAPG Memoir*, **92**, 145–166.
- Donselaar, M.E. and Overeem, I. (2008) Connectivity of fluvial point-bar deposits: An example from the Miocene Huesca fluvial fan, Ebro Basin, Spain. *AAPG Bulletin*, **92**, 1109-1129.
- Dunne, W.M. (1983) Tectonic evolution of SW Wales during the Upper Palaeozoic. *Journal of the Geological Society, London*, **143**, 257–265.
- Durkin, P. (2016) The Evolution of Fluvial Meander Belts and Their Product in the Rock Record,. Unpublished PhD thesis, University of Calgary, Canada. 245 p.

Durkin, P.R., Hubbard, S.M., Boyd, R.L. and Leckie, D. A. (2015) Stratigraphic Expression of Intra-Point-Bar Erosion and Rotation. *Journal of Sedimentary Research*, **85**, 1238–57.

Eaton, B.C. and Giles, T.R. (2009) Assessing the effect of vegetation-related bank strength on channel morphology and stability in gravel-bed streams using numerical models. *Earth Surface Processes and Landforms*, **34**, 712–724

Ekeland, A. (2007) Sedimentology and geomodelling of small scale fluvial architecture from the Lourinha Formation., Central Portugal. Unpublished MSc thesis, University of Bergen, Norway. 96 p.

Ellison, A.I. (2004) Numerical modelling of heterogeneity within a fluvial point-bar deposit using outcrop and LIDAR data: Williams Fork Formation, Piceance Basin, Colorado. Unpublished MSc thesis, University of Colorado, Boulder, 225 p.

El-Mowafy, H.Z. and Marfurt, K.J. (2016). Quantitative seismic geomorphology of the middle Frio fluvial systems, south Texas, United States. *AAPG Bulletin*, **100**, 537-564.

Engel, F.L. and Rhoads, B.L. (2012) Interaction among Mean Flow, Turbulence, Bed Morphology, Bank Failures and Channel Planform in an Evolving Compound Meander Loop. *Geomorphology* **163–164**, 70–83.

Erskine, W., McFadden, C. and Bishop, P. (1992) Alluvial Cutoffs as Indicators of Former Channel Conditions. *Earth Surface Processes and Landforms*, **17**, 23–37.

Ethridge, F.G. and S.A. Schumm, (1977) Reconstructing paleochannel morphologic and flow characteristics: methodology, limitations, and assessment. In: *Fluvial sedimentology* (Ed A.D. Miall), *Canadian Society of Petroleum Geologists Memoir*, **5**, 703-722

- Ethridge, F.G., Wood, L.J. and Schumm, S.A. (1998) Cyclic variables controlling fluvial sequence development: problems and perspectives. In: *Relative Role of Eustasy, Climate and Tectonism in Continental Rocks* (Eds P.J McCabe and K.W. Shanley). *SEPM, Special Publication* **59**, 17–29.
- Fachmi, M. and Wood, L.J., (2005) Seismic geomorphology: a study from West Natuna Basin, Indonesia. In: Indonesian Petroleum Association, 30th Annual Convention Proceedings, **1**, 163-178.
- Fenneman, N.M. (1906) Floodplains produced without floods. *American Geographical Society Bulletin*, **38**, 89-91.
- Ferguson, R.I. (1975) Meander bulbosity and wavelength estimation. *Journal of Hydrology*, **26**, 315-333.
- Fielding, C.R. (1984) Upper delta plain lacustrine and fluviolacustrine facies from the Westphalian of the Durham coalfield, NE England. *Sedimentology*, **31**, 547-567.
- Fielding, C.R. and Crane, R.C. (1987) An application of statistical modelling to the prediction of hydrocarbon recovery factors in fluvial reservoir sequences. In: *Recent Developments in Fluvial Sedimentology* (Eds F.G. Ethridge, R.M. Flores and M.D. Harvey), *Society of Sedimentary Geology, SEPM Special Publication*, **39**, 321-327.
- Fisher, W.L. and J.H. McGowen, (1967) Depositional systems in Wilcox Group (Eocene of Texas) and their relation to occurrences of oil and gas. *Gulf Coast Association Geological Society Transactions*, **17**, 105-125.
- Fisk, H.N., (1944) Geological investigation of the alluvial valley of the lower Mississippi River. U.S. Army Corps of Engineers, Mississippi River Commission, Vicksburg, 78 p.

Fisk, H.N. (1947) Fine-grained alluvial deposits and their effects on Mississippi River activity. Vols 1 & 2. Mississippi River Commission, Vicksburg, MS.

Frascati, A. and Lanzoni, S. (2010) Long-term river meandering as a part of chaotic dynamics: A contribution from mathematical modelling. *Earth Surface Processes and Landforms*, **35**, 791-802.

Frodsham, K. and Gayer, R.A. (1997) Variscan compressional structures within the main productive coal-bearing strata of South Wales. *Journal of the Geological Society, London*, **154**, 195–208

Fuller, I.C., Large, A.R.G. and Milan, D.J. (2003) Quantifying channel development and sediment transfer following chute cut-off in a wandering gravel-bed river. *Geomorphology*, **54**, 307–323.

Fustic, M., Hubbard, S.M., Spencer, R., Smith D.G., Leckie, D.A., Bennett, B. and Larter, S. (2012) Recognition of down-valley translation in tidally influenced meandering fluvial deposits, Athabasca Oil Sands (Cretaceous), Alberta, Canada. *Marine and Petroleum Geology*, **29**, Elsevier Ltd: 219–32.

Gagliano, S.M. and Howard, P.C. (1984) The neck cutoff oxbow lake cycle along the Lower Mississippi River. In: *River Meandering* (Ed C.M. Elliott), pp. 147–158. Proceedings of the Conference Rivers '83, American Society of Civil Engineers

Galloway, W.E. (1981) Depositional architecture of Cenozoic Gulf Coastal Plain fluvial systems. In: *Recent and ancient nonmarine depositional environments* (Eds F.G. Ethridge and R.M. Flores). *SEPM Special Publication*, **31**, 127-156

Gay, G.R., Gay, H.H., Gay, W.H., Martinson, H.A., Meade, R.H. and Moody, J.A. (1998) Evolution of Cutoffs across Meander Neck in Powder River, Montana, USA. *Earth Surface Processes and Landforms*, **23**, 651–62.

Geehan, G. and Underwood, J. (1993) The use of length distributions in geological modelling. In: *The geological modelling of hydrocarbon reservoirs and outcrop analogs* (Eds S.S. Flint and I.D. Bryant). *International Association of Sedimentologists Special Publication*, **15**, 205–212.

George, G.T. and Kelling, G. (1982) Stratigraphy and sedimentology of Upper Carboniferous sequences in the coalfield of south-west Dyfed. In: *Geological excursions in Dyfed, south-west Wales* (Ed M.G. Bassett), *National Museum of Wales, Cardiff*, 174–201.

Ghazi, S. and Mountney, N.P. (2009) Facies and architectural element analysis of a meandering fluvial succession: The Permian Warchha Sandstone, Salt Range, Pakistan. *Sedimentary Geology*, **221**, 99-126.

Ghinassi, M. (2011) Chute Channels in the Holocene High-Sinuosity River Deposits of the Firenze Plain, Tuscany, Italy. *Sedimentology*, **58**, 618–42.

Ghinassi, M. and Ielpi, A. (2015) Stratal architecture and morphodynamics of downstream-migrating fluvial point bars (Jurassic Scalby Formation, UK). *Journal of Sedimentary Research*, **85**, 1123-1137.

Ghinassi, M., Ielpi A., Aldinucci, M. and Fustic, M. (2016) Downstream-Migrating Fluvial Point Bars in the Rock Record. *Sedimentary Geology*, **334**, 66–96.



Gibling, M.R. (2006) Width and thickness of fluvial channel bodies and valley fills in the geological record: a literature compilation and classification. *Journal of Sedimentary Research*, **76**, 731-770.

Gibling, M.R. and Rust, B.R. (1993) Alluvial ridge-and-swale topography: A case study from the Morien Group of Atlantic Canada. In: Alluvial sedimentation (Eds M. Marzo and C. Puigdefabregas), *International Association of Sedimentologists, Special Publication* **17**, 133–150.

Gibling, M.R., Nanson, G.C. and Maroulis, J.C. (1998) Anastomosing river sedimentation in the Channel Country of central Australia. *Sedimentology*, **45**, 595-619.

Gilvear, D., Winterbottom, S. and Sichingabula, H. (2000) Character of channel planform change and meander development: Luangwa River, Zambia. *Earth Surface Processes and Landforms*, **25**, 421-436.

Gingerich, P.D. (1969) Markov analysis of cyclic alluvial sediments. *Journal of Sedimentary Petrology*, **39**, 330-332.

Gorycki, M.A. (1973) Hydraulic drag: a meander-initiating mechanism. *Geological Society of America Bulletin*, **84**, 175-86.

Gradstein, F. and Ogg, J. (2004) Geologic time scale 2004—why, how, and where next! *Lethaia*, **37**, 175-181.

Güneralp, I. and Rhoads B.L. (2011) Influence of floodplain erosional heterogeneity on planform complexity of meandering rivers. *Geophysical Research Letters*, **38**, L14401

Güneralp, İ. and Marston, R.A. (2012) Process–form linkages in meander morphodynamics: Bridging theoretical modeling and real world complexity. *Progress in Physical geography*, **36**, 718-746.

Gustavson, T.C. (1978) Bed forms and stratification types of modern gravel meander lobes, Nueces River, Texas. *Sedimentology*, **25**, 401-426.

Gutierrez, R.R. and Abad, J.D. (2014) On the Analysis of the Medium Term Planform Dynamics of Meandering Rivers. *Water Resources Research*, **50**, 3714–33.

Hampson, G J. (1997) A sequence stratigraphic model for deposition of the Lower Kinderscout Delta, an Upper Carboniferous turbidite-fronted delta. *Proceedings of the Yorkshire Geological Society*, **51**, 273–296.

Han, B. and Endreny, T.A. (2014) Detailed river stage mapping and head gradient analysis during meander cutoff in a laboratory river. *Water Resources Research*, **50**, 1689-1703.

Hancock, P.L., Dunne, W.M. and Tringham, M.E. (1981) Variscan structures in southwest Wales. *Geol. Mijnbouw*, **60**, 81-8

Harms, J.C., Southard, J.B. and Walker, R.G. (1982) Fluvial deposits and facies models. *Structure and Sequence in Clastic Rocks (SEPM, Short Course 9)*, 1-26.

Harper Jr, C.W. (1984) Facies models revisited: An examination of quantitative methods. *Geoscience Canada*, **11**, 203-207.

Hartley, A.J. (1993) Silesian sedimentation in SW Britain: sedimentary responses to the developing Variscan Orogeny. In: *Rhenohercynian and Subvariscan Fold Belts* (Eds R.A. Gayer, R.O. Greieing and A.K. Vogel), Vieweg Publishing, Braunschwcig, 159-196.

Hartley, A.J. and Warr, L.N. (1990) Upper Carboniferous foreland basin evolution in SW Britain. *Proceedings of the Ussher Society*, **7**, 212-216.

- Hartley, A.J., Weissmann, G.S., Nichols, G.J. and Warwick, G.L. (2010) Large distributive fluvial systems: characteristics, distribution, and controls on development. *Journal of Sedimentary Research*, **80**, 167-183.
- Hartley, A.J., Owen, A., Swan, A., Weissmann, G.S., Holzweber, B.I., Howell, J., Nichols, G. and Scuderi, L. (2015) Recognition and importance of amalgamated sandy meander belts in the continental rock record. *Geology*, **43**, 679-682.
- Hassanpour, M.M., Pyrcz, M.J. and Deutsch, C.V. (2013) Improved Geostatistical Models of Inclined Heterolithic Strata for McMurray Formation, Alberta, Canada. *AAPG Bulletin*, **97**, 1209–24.
- Heller, P.L. and Paola, C. (1996). Downstream changes in alluvial architecture: an exploration of controls on channel-stacking patterns. *Journal of Sedimentary Research*, **66**, 297-306.
- Hickin, E.J. and Nanson, G. (1975) The character of channel migration on the Beatton River, northeast British Columbia, Canada. *Geological Society of America Bulletin*, **86**, 487-494.
- Hickin, E.J. and Nanson, G. (1984) Lateral migration rates of river bends. *Journal of Hydraulic Engineering*, **110**, 1557-1567.
- Hjulstrom, F. (1935) Studies of the morphological activity of rivers as illustrated by the River Fyris. *Bulletin Geological Institute Uppsala*, **25**, 221-527.
- Hohn, M.E., McDowell, R.R., Matchen, D.L. and Vargo, A.G. (1997) Heterogeneity of Fluvial-Deltaic Reservoirs in the Appalachian Basin: A Case Study from a Lower Mississippian Oil Field in Central West Virginia. *AAPG Bulletin*, **81**, 918–36.

Hooke, J.M. (1977a) An Analysis of Changes in River Channel Patterns. Unpublished PhD thesis, University of Exeter.

Hooke, J.M. (1977b) The distribution and nature of changes in river channel patterns: The example of Devon. In: *River Channel Changes* (Ed. by Gregory, K.J.), Wiley, Chichester 265-280.

Hooke, J.M. (1984) Changes in river meanders a review of techniques and results of analyses. *Progress in Physical Geography*, **8**, 473-508.

Hooke, J.M. (1995) River channel adjustment to meander cutoffs on the River Bollin and River Dane, northwest England. *Geomorphology*, **14**, 235-253.

Hooke, J.M. (1997) Styles of channel change. In: *Applied Fluvial Geomorphology for River Engineering and Management* (Ed. by Thorne, C.R., Hey, R.D., Newson, M.D.) Wiley, Chichester, 237-268.

Hooke, J.M. (2004) Cutoffs Galore!: Occurrence and Causes of Multiple Cutoffs on a Meandering River. *Geomorphology*, **61**, 225–38.

Hooke, J.M. (2007) Complexity, self-organisation and variation in behaviour in meandering rivers. *Geomorphology*, **91**, 236-258.

Hooke, J.M. and Harvey, A.M. (1983) Meander changes in relation to bend morphology and secondary flows. In: *Modern and ancient fluvial systems*. (Eds J.D. Collinson and J. Lewin), Blackwell, Oxford, 121-132.

Howard, A.D. and Hemberger, A.T. (1991) Multivariate characterization of meandering. *Geomorphology*, **4**, 161–186.

Howard, A.D., Knutson, T.R., (1984) Sufficient conditions for river meandering: a simulation approach. *Water Resources Research*, **20**, 1659–1667.

Howell, J.A., Martinius, A.W. and Good, T.R. (2014) The application of outcrop analogues in geological modelling: A review, present status and future outlook. In: Sediment-Body Geometry and Heterogeneity (Ed. by. Martinius, A.W., Howell, J.A and Good, T.R.), *Geological Society, London, Special Publications*, **387**, 1-25.

Hubbard, S.M., Smith, D.G., Nielsen, H., Leckie, D.A., Fustic, M., Spencer, R.J. and Bloom, L. (2011) Seismic geomorphology and sedimentology of a tidally influenced river deposit, Lower Cretaceous Athabasca oil sands, Alberta, Canada. *AAPG Bulletin*, **95**, 1123-1145.

Huddleston, P.J. (1973) Fold morphology and some geometrical implications of theories of fold development. *Tectonophysics*, **16**, 1-46.

Hudson, P.F. and Kesel, R.H. (2000) Channel migration and meander-bend curvature in the lower Mississippi River prior to major human modification. *Geology*, **28**, 531-534.

Ielpi, A. and Ghinassi, M. (2014) Planform Architecture, Stratigraphic Signature and Morphodynamics of an Exhumed Jurassic Meander Plain (Scalby Formation, Yorkshire, UK). *Sedimentology*, **61**, 1923–60.

Ielpi, A., Gibling, M.R., Bashforth, A.R., Lally, C., Rygel, M.C. and Al-Silwadi, S. (2014) Role of vegetation in shaping Early Pennsylvanian braided rivers: architecture of the Boss Point Formation, Atlantic Canada. *Sedimentology*, **61**, 1659-1700.

Ikeda, S., Parker, G. and Sawai, K. (1981) Bend theory of river meanders: part I, Linear development. *Journal of Fluid Mechanics*, **112**, 363–377.

Jablonski, B.V.J. and Dalrymple, R.W. (2016) Recognition of strong seasonality and climatic cyclicity in an ancient, fluvially dominated, tidally influenced point bar: middle

McMurray formation, lower Steepbank River, north-eastern Alberta, Canada. *Sedimentology*, **63**, 1-34

Jackson, R.G. (1975) Velocity-Bed-Form-Texture Patterns of Meander Bends in the Lower Wabash River of Illinois and Indiana. *Bulletin of the Geological Society of America*, **86**, 1511–22.

Jackson, R.G. (1976) Depositional model of point bars in the lower Wabash River. *Journal of Sedimentary Petrology*, **46**, 579-594.

Jefferson, M. (1902) Limiting width of meander belts. *National Geographic Magazine*, **13**, 373-384.

Jenkins, T.B.H. (1960) Non-marine lamellibranch assemblages from the Coal Measures (Upper Carboniferous) of Pembrokeshire, West Wales. *Palaeontology*, **3**, 104-123.

Jenkins, T.B.H. (1962) The sequence and correlation of the Coal Measures of Pembrokeshire. *The Quarterly Journal of the Geological Society of London*, **118**, 65-101.

Jenkins, G.M. and Watts, D.G. (1968) *Spectral analysis and its applications*, Holden-Day, San Francisco, 525 pp.

Johnson, R.H. and Paynter, J. (1967) The development of a cutoff on the River Irk at Chadderton, Lancashire. *Geography*, **52**, 41-49.

Jones, J.A. (1989) Sedimentation and tectonics in the eastern part of the South Wales Coalfield. Unpublished PhD thesis, University of Wales, Cardiff.

Jordan, D.W. and Pryor, W.A. (1992) Hierarchical Levels of Heterogeneity in a Mississippi River Meander Belt and Application to Reservoir Systems. *AAPG Bulletin*, **76**, 1601-1624.

Kelling, G. (1974) Upper Carboniferous sedimentation in south Wales. In: *The Upper Palaeozoic and post-Palaeozoic rocks of Wales* (Ed T.R. Owen), University of Wales Press, Cardiff, 185–244.

Keogh, K.J., Leary, S., Martinius, A.W., Scott, A.S., Riordan, S., Viste, I., Gowland, S., Taylor, A.M. and Howell, J. (2014) Data capture for multiscale modelling of the Lourinhã Formation, Lusitanian Basin, Portugal: An outcrop analogue for the Staffjord Group, Norwegian North Sea. In: *Sediment-body geometry and heterogeneity: Analogue studies for modelling the subsurface* (Ed. by A. W. Martinius, J. A. Howell, and T. R. Good), *Geological Society, London, Special Publications*, **387**, 27-56.

Khatsuria, R.M. (2008) Experimental study of transition and skimming flows on stepped spillways in RCC dams: qualitative analysis and pressure measurements. *Journal of Hydraulic Research*, **46**, 175-176.

Knighton, D. (1998) *Fluvial forms and processes*. Edward Arnold, London, 377 p

Kondolf, M. (2007) Sacramento River Ecological Flows Study: Off-Channel Habitat Study Final Report. Chico, California: for The Nature Conservancy

Konsoer, K.M., Rhoads, B.L., Langendoen, E.J., Best, J.L., Ursic, M.E., Abad, J.D. and Garcia, M.H. (2016) Spatial variability in bank resistance to erosion on a large meandering, mixed bedrock–alluvial river. *Geomorphology*, **252**, 80–97.

Kulemina, N.M. (1973) Some characteristics of the process of incomplete meandering of the channel of the Upper Ob River. *Soviet Hydrology*, **12**, 518–534.

Labrecque, P.A., Jensen, J.L., Hubbard, S.M. and Nielsen, H. (2011) Sedimentology and Stratigraphic Architecture of a Point-bar Deposit, Lower Cretaceous McMurray Formation, Alberta, Canada. *Bulletin of Canadian Petroleum Geology*, **59**, 147–71.

Lapointe, M.F., Secretan, Y., Driscoll, S.N., Bergeron, N. and Leclerc, M. (1998) Response of the Ha! Ha! River to the flood of July 1996 in the Saguenay region of Quebec: Large-scale avulsion in a glaciated valley. *Water Resources Research*, **34**, 2383-2392.

LeBlanc, R.F., and Hodgson, W.D. (1959) Origin and development of the Texas shoreline. *Gulf Coast Association Geological Society Transactions*, **9**, 197-220.

Leeder, M.R. (1973) Fluvial fining upward cycles and the magnitude of palaeochannels. *Geological Magazine*, **110**, 265-276.

Leeder, M.R. (1977) A quantitative stratigraphic model for alluvium, with special reference to channel deposit density and interconnectedness. In: *Fluvial Sedimentology* (Ed A.D. Miall), *Canadian Society of Petroleum Geologists Memoir*, **5**, 587-596.

Leighly, J. (1936) Meandering arroyos of the dry southwest. *Geographical Review*, **26**, 270-282.

Leopold, L.B. and Langbein, W.B. (1966) River meanders. *Scientific American*, **214**, 60-70.

Leopold, L.B. and Wolman, M.G. (1957) River channel patterns: braided, meandering, and straight. *United States Geological Survey, Professional Paper* **282-B**, 39–84.

Leopold, L.B. and Wolman, M.G. (1960) River meanders. *Geological Society of America Bulletin*, **71**, 769-793.



Lewin, J. (1976) Initiation of Bedforms and Meanders in Coarse-Grained Sediment. *Geological Society of America Bulletin*, **87**, 281–85.

Lewis, G.W. and Lewin, J. (1983) Alluvial cutoffs in Wales and the Borderlands. In: *Modern and ancient fluvial systems* (Eds J.D. Collinson and J. Lewin) Special Publications of the International Association of Sedimentologists, **6**, 145-154.

Lindholm, R.C. (1987) A Practical Approach to Sedimentology. *Allen and Unwin, London*, 276 pp.

Lindner, C.P. (1953) Diversions from alluvial streams. *Transactions of the American Society of Civil Engineers*, **118**, 245-288

Lotsari, E., Vaaja, M., Flener, C., Kaartinen, H., Kukko, A., Kasvi, E., Hyyppä, H., Hyyppä, J. and Alho, P. (2014) Annual bank and point bar morphodynamics of a meandering river determined by high-accuracy multitemporal laser scanning and flow data. *Water Resources Research*, **50**, 5532-5559.

Lunt, I.A., and Bridge, J.S. (2004) Evolution and deposits of a gravelly braid bar, Sagavanirktok River, Alaska. *Sedimentology*, **51**, 415-432.

Mackey, S.D. and Bridge, J.S. (1995) Modelling Alluvial Stratigraphy in 3D with Maths. *Journal of Sedimentary Research*, **B65**, 7-31.

Makaske, B., Maathuis, B.H., Padovani, C.R., Stolker, C., Mosselman, E. and Jongman, R.H. (2012) Upstream and downstream controls of recent avulsions on the Taquari megafan, Pantanal, south-western Brazil. *Earth Surface Processes and Landforms*, **37**, 1313-1326.

Matthes, G.H. (1948) Mississippi River cutoffs. *Transactions of the American Society of Civil Engineers*, **113**, 1–15.

Maynard, J.R. and Leeder, M.R. (1992) On the periodicity and magnitude of Late Carboniferous glacio-eustatic sea-level changes. *Journal of the Geological Society, London*, **149**, 303-311.

Maynard, J.R. (2006) Fluvial response to active extension: evidence from 3D seismic data from the Frio Formation (Oligo-Miocene) of the Texas Gulf of Mexico Coast, USA. *Sedimentology*, **53**, 515-536.

McCabe, P.J. (1984) Depositional environments of coal and coal-bearing strata. In: *Sedimentology of Coal and Coal-bearing Sequences* (Eds R.A. Rahmani and R.M. Flores) *Special Publications of the International Association of Sedimentologists*, **7**, 13-42.

McGowen, J.H. and Garner, L.E. (1970) Physiographic Features and Stratification Types of Coarse-Grained Point bars: Modern and Ancient Examples. *Sedimentology*, **14**, 77-111.

Meybeck, M. and Ragu, A. (1997) Presenting the GEMS-GLORI, a Compendium of World River Discharge to the Oceans. *International Association of Hydrological Sciences Publication*, **243**, 3-14.

Miall, A.D. (1973) Markov chain analysis applied to an ancient alluvial plain succession. *Sedimentology*, **20**, 347-364.

Miall, A.D. (1976) Palaeocurrent and palaeohydraulic analysis of some vertical profiles through a Cretaceous braided stream deposit Banks Island, Arctic Canada. *Sedimentology*, **23**, 459-483.

Miall, A.D., (1977) A review of the braided river depositional environment. *Earth Science Reviews*, **13**, 1-62.

Miall, A.D. (1978) Lithofacies types and vertical profile models in braided river deposits: a summary. In: *Fluvial Sedimentology* (Ed A.D. Miall), *Canadian Society of Petroleum Geologists Memoir*, **5**, 597-604.

Miall, A.D. (1985) Architectural-element analysis: a new method of facies analysis applied to fluvial deposits. *Earth-Science Reviews*, **22**, 261–308.

Miall, A.D. (1988) Reservoir Heterogeneities in Fluvial Sandstones: Lesson from Outcrop Studies. *AAPG Bulletin*, **72**, 682–97.

Miall, A.D. (2006) Reconstructing the Architecture and Sequence Stratigraphy of the Preserved Fluvial Record as a Tool for Reservoir Development: A Reality Check. *AAPG Bulletin*, **90**, 989–1002.

Miall, A. (2013) *The Geology of Fluvial Deposits: Sedimentary Facies, Basin Analysis, and Petroleum Geology*. Springer, Toronto, 581 p.

Miall, A.D., & Gibling, M.R. (1978) The Siluro-Devonian clastic wedge of Somerset Island, Arctic Canada, and some regional paleogeographic implications. *Sedimentary Geology*, **21**, 85-127.

Miall, A.D. and Tyler, N. (1991) The three-dimensional facies architecture of terrigenous clastic sediments, and its implications for hydro- carbon discovery and recovery. *Society of Economic Paleontologists and Mineralogists, Concepts in Sedimentology and Palaeontology*, **3**. 309 pp.

Middleton, G.V. (1973) Johannes Walther's law of the correlation of facies. *Geological Society of America Bulletin*, **84**, 979-988.

Middleton, G.V. (1976) Hydraulic interpretation of sand size distributions. *The Journal of Geology*, **84**, 405-426.

- Middleton, G.V. and Southard, J.B. (1978) Mechanics of sediment movement. *SEPM Short Course* no. 3, 244 p.
- Millar, R.G. and Quick, M.C. (1993) Effect of bank stability on geometry of Gravel Rivers. *Journal of Hydraulic Engineering*, **119**, 1343-1363.
- Mjø̆s, R., Walderhaug, O. and Prestholm, E. (1993) Crevasse splay sandstone geometries in the Middle Jurassic Ravenscar Group of Yorkshire, UK. In: *Alluvial sedimentation* (Eds M. Marzo and C. Puigdefábregas) *International Association of Sedimentologists Special Publication*, **17**, 167–184.
- Mohrig, D., Heller, P.L., Paola, C. and Lyons, W.J. (2000) Interpreting avulsion process from ancient alluvial sequences: Guadalupe-Matarranya system (northern Spain) and Wasatch Formation (western Colorado). *Geological Society of America Bulletin*, **112**, 1787–1803.
- Moody, J.A. and Meade, R.H. (2014). Ontogeny of point bars on a river in a cold semi-arid climate. *Geological Society of America Bulletin*, **126**, 1301-1316.
- Mosley M.P. (1976) An experimental study of channel confluences. *Journal of Geology* **84**: 535–562.
- Mossop, G.D. and Flach, P.D. (1983) Deep Channel Sedimentation in the Lower Cretaceous McMurray Formation, Athabasca Oil Sands, Alberta. *Sedimentology*, **30**, 493–509.
- Nanson, G.C. (1980) Point Bar and Floodplain Formation of the Meandering Beatton River, Northeastern British Columbia, Canada. *Sedimentology*, **27**, 3–29.
- Nanson, G.C. and Hickin, E.J., (1983) Channel migration and incision on the Beatton River. *Journal of Hydraulic Engineering*, **109**, 327-337.

Nanson, G.C. and Hickin, E.J. (1986) A statistical analysis of bank erosion and channel migration in western Canada. *Geological Society of America Bulletin*, **97**, 497-504.

Naylor, M.A. and Woodcock, N.H., (1977) Transition analysis of structural sequences. *Geological Society of America Bulletin*, **88**, 1488-1492.

Ndiaye, M. (2007) *A multipurpose software for stratigraphic signal analysis*.

Unpublished PhD thesis, Université de Genève, Genève: <https://archive-ouverte.unige.ch/unige:717>

Nixon, M. (1959) A study of the bank-full discharges of rivers in England and Wales. *Proceedings of the Institution of Civil Engineers*, **12**, 157-174.

Osterkamp, W.R. and Hedman, E.R. (1982) Perennial streamflow characteristics related to channel geometry and sediment in the Missouri River basin. *United States Geological Survey Professional Paper*, **1242**, 39 pp.

Ouchi, S. (1985) Response of Alluvial Rivers to Slow Active Tectonic Movement. *Geological Society of America Bulletin*, **96**, 504–15.

Parker, G., Diplas, P. and Akiyama, J. (1983) Meander bends of high amplitude. *Journal of Hydraulic Engineering*, **109**, 1323-1337.

Parker, G., Sawai, K. and Ikeda, S. (1982) Bend theory of river meanders. Part 2. Nonlinear deformation of finite-amplitude bends. *Journal of Fluid Mechanics*, **115**, 303-314.

Peakall, J. (1995) *The influences of lateral ground-tilting on channel morphology and alluvial architecture*. Unpublished PhD thesis, University of Leeds, UK, 333 pp.

- Peakall, J., Ashworth, P.J. and Best, J.L. (2007) Meander-bend evolution, alluvial architecture, and the role of cohesion in sinuous river channels: a flume study. *Journal of Sedimentary Research*, **77**, 197–212.
- Peakall, J. and Sumner, E.J. (2015) Submarine channel flow processes and deposits: A process-product perspective. *Geomorphology*, **244**, 95-120.
- Peel, M.C., Finlayson, B.L. and McMahon, T.A. (2007) Updated world map of the Köppen-Geiger climate classification, *Hydrology and Earth System Sciences*, **11**, 1633–1644.
- Perucca, E., Camporeale, C. and Ridolfi, L. (2007) Significance of the riparian vegetation dynamics on meandering river morphodynamics. *Water Resources Research*, **43**, 1-10.
- Phillips, J.D. (2003) Sources of Nonlinearity and Complexity in Geomorphic Systems. *Progress in Physical Geography*, **27**, 1–23.
- Piegay, H., Bornette, G. and Grante, P. (2002) Assessment of silting-up dynamics of eleven cut-off channel plugs on a free-meandering river (Ain River, France). In: *Applied Geomorphology* (Ed R.J. Allison), John Wiley and Sons, New York, pp. 227-247.
- Posamentier, H.W. (2001). Lowstand alluvial bypass systems: incised vs. unincised. *AAPG Bulletin*, **85**, 1771-1793.
- Posamentier, H.W. (2004) Seismic geomorphology: imaging elements of depositional systems from shelf to deep basin using 3D seismic data: implications for exploration and development. In: *3D Seismic Technology: Application to the Exploration of Sedimentary Basins* (Ed. by R.J. Davies, J. Cartwright, S.A. Stewart, J.R. Underhill and M. Lappin), *Geological Society, London, Memoirs*, **29**, 11-24.

Posner, A.J. and Duan, J.G. (2012) Simulating river meandering processes using stochastic bank erosion coefficient. *Geomorphology*, **163**, 26-36.

Pranter, M.J., Cabrera-Garzón, R., Blaylock, J.J., Davis, T.L. and Hurley, N.F. (2000) Use of multicomponent seismic for the static reservoir characterization of the San Andres formation at Vacuum Field, New Mexico. *Society of Exploration Geophysicists, Technical Program Expanded Abstracts 2000*, 1548-1551.

Pranter, M.J., Cole, R.D., Panjaitan, H. and Sommer, N.K. (2009) Sandstone-Body Dimensions in a Lower Coastal-Plain Depositional Setting: Lower Williams Fork Formation, Coal Canyon, Piceance Basin, Colorado. *AAPG Bulletin*, **93**, 1379–1401.

Pranter, M.J., Ellison, A.I., Cole, R.D. and Patterson, P.E. (2007) Analysis and modelling of intermediate-scale reservoir heterogeneity based on a fluvial point-bar outcrop analog, Williams Fork Formation, Piceance Basin, Colorado. *AAPG Bulletin*, **91**, 1025-1051.

Putnam, P.E. and Oliver, T.A. (1980) Stratigraphic traps in channel sandstones in the Upper Mannville (Albian) of east-central Alberta. *Bulletin of Canadian Petroleum Geology*, **28**, 489-508.

Ramón, J.C. and Cross, T. (1997) Characterization and Prediction of Reservoir Architecture and Petrophysical Properties in Fluvial Channel Sandstones, Middle Magdalena Basin, Colombia. *CT Y F - Ciencia, Tecnología Y Futuro*, **1**, 19–46.

Ramsbottom, W.H.C. (1984) Developments from faunal studies in the Carboniferous of Wales. *Proceedings of the Geologists' Association*, **95**, 365-371.

Reading, H.G. (Ed.), (1978) *Sedimentary Environments and Facies*. Blackwell, 557 pp.

Reijenstein, H.M., Posamentier, H.W. and Bhattacharya, J.P. (2011) Seismic Geomorphology and High-Resolution Seismic Stratigraphy of Inner-Shelf Fluvial,

Estuarine, Deltaic, and Marine Sequences, Gulf of Thailand. *AAPG Bulletin*, **95**, 1959–90.

Richards, K. (1982) *Rivers: Form and Process in Alluvial Channels*, Methuen, London. 358 pp.

Robert, A. (2014) *River processes: an introduction to fluvial dynamics*. Routledge, London.

Rosgen, D.L. (1985) *A Stream Classification System. Riparian Ecosystems and Their Management: Reconciling Conflicting Uses*, USDA Forest Service General Technical Report, **RM 120**, 91–95.

Rosgen, D.L. (1994) A classification of natural rivers. *Catena*, **22**, 169-199.

Rowntree, K.M. and Dollar, E.S. (1999) Vegetation controls on channel stability in the Bell River, Eastern Cape, South Africa. *Earth Surface Processes and Landforms*, **24**, 127-134.

Russell, R.J. (1954) Alluvial morphology of Anatolian rivers. *Annals of the Association of American Geographers*, **44**, 363-391.

Sakalowsky, P.P. (1974) Theories of Stream Meander Causation: A Review and Analysis. *Earth Science Reviews*, **10**, 121–38.

Sambrook-Smith, G.H., Best, J.L., Leroy, J.Z. and Orfeo O. (2016) The Alluvial Architecture of a Suspended Sediment Dominated Meandering River: The Río Bermejo, Argentina. *Sedimentology*, **63**, 1187–1208.

Santos, M.G.M., Mountney, N.P. and Peakall, J. (2017a) Tectonic and environmental controls on Palaeozoic fluvial environments: reassessing the impacts of early land plants on sedimentation. *Journal of the Geological Society, London*, **174**, 393-404.



- Santos, M.G., Mountney, N.P., Peakall, J., Thomas, R.E., Wignall, P.B., & Hodgson, D.M. (2017b). Reply to Discussion on 'Tectonic and environmental controls on Palaeozoic fluvial environments: reassessing the impacts of early land plants on sedimentation'. *Journal of the Geological Society, London, in press*, 31-33.
- Schumann, R.R. (1989) Morphology of Red Creek, Wyoming, an arid-region anastomosing channel system. *Earth Surface Processes and Landforms*, **14**, 277-288.
- Schumm, S.A. (1960) The effect of sediment type on the shape and stratification of some modern fluvial deposits. *American Journal of Science*, **258**, 177-184.
- Schumm, S.A. (1963) Sinuosity of Alluvial Rivers on the Great Plains. *Bulletin of the Geological Society of America*, **74**, 1089–1100.
- Schumm, S.A. (1968) Speculations concerning paleohydrologic controls of terrestrial sedimentation. *Geological Society of America Bulletin*, **79**, 1573-1588.
- Schumm, S.A. (1969) River Metamorphosis. *Journal of the Hydraulics Division*, **95**, 255–74.
- Schumm, S.A. (1985) Patterns of Alluvial Rivers. *Annual Review of Earth and Planetary Sciences*, **13**, 5–27.
- Schumm, S.A. and Khan H.R. (1972) Experimental Study of Channel Patterns. *Geological Society of America Bulletin*, **83**, 1755–70.
- Schumm, S.A., Harvey, M.D. and Watson, C.C. (1984) Incised Channels: Morphology, Dynamics, and Control. Water Resources Publications, Littleton, CO.
- Schwab, F.L. (1976) Modern and Ancient Sedimentary Basins: Comparative Accumulation Rates. *Geology*, **4**, 723–27.

Schwarzacher, W. (1969) The use of Markov chains in the study of sedimentary cycles. *Mathematical Geology*, **1**, 17-39.

Schwenk, J., Lanzoni, S. and Fofoula-Georgiou, E. (2015) The life of a meander bend: Connecting shape and dynamics via analysis of a numerical model. *Journal of Geophysical Research: Earth Surface*, **120**, 690-710.

Selly, R. C., (1970) Ancient sedimentary environments. *Chapman and Hall, London*, 237 pp.

Seminara, G. (2006) Meanders. *Journal of Fluid Mechanics*, **554**, 271-297.

Seminara, G., Zolezzi, G., Tubino, M. and Zardi, D. (2001) Downstream and upstream influence in river meandering. Part 2. Planimetric development. *Journal of Fluid Mechanics*, **438**, 213-230.

Shanley, K.W. (2004) Fluvial Reservoir Description for a Giant, Low-Permeability Gas Field : Jonah Field, Green River Basin, Wyoming, U. S. A., *AAPG Studies in Geology 52 and Rocky Mountain Association of Geologists 2004 Guidebook*, 159–82.

Shanley, K.W. and McCabe P.J. (1994) Perspectives on the Sequence Stratigraphy of Continental Strata: report of a working group at the 1991 NUNA Conference on High Resolution Sequence Stratigraphy. *American Association for Petroleum Geology Bulletin*, **74**, 544-568.

Shields, F.D.J. and Abt, S.R. (1989) Sediment Deposition in cutoff meander bends and implications for effective management. *Regulated Rivers: Research and Management*, **4**, 381-396.

Shiers, M.N., Mountney, N.P., Hodgson, N.M and Colombera L. (*in review*) Controls on the depositional architecture of fluvial point-bar elements in a coastal plain succession.

*International Association of Sedimentology Special Publication* **48**.

Smallwood, S. (1985) A thin-skinned thrust model for Variscan Pembrokehire, Wales. *Journal of Structural Geology*, **7**, 683-687.

Smith, G.A. (1987) Sedimentology of volcanism-induced aggradation in fluvial basins: examples from the Pacific Northwest, U.S.A.. In: *Recent Developments in Fluvial Sedimentology* (Eds F.G. Ethridge, R.M. Flores and M.D. Harvey), *SEPM Special Publication* **39**, 217–228.

Smith, D.G., Hubbard, S.M., Leckie, D.A. and Fustic, M. (2009) Counter Point Bar Deposits: Lithofacies and Reservoir Significance in the Meandering Modern Peace River and Ancient McMurray Formation, Alberta, Canada. *Sedimentology*, **56**, 1655–69.

Smith, N.D. and Ashley G.M. (1985) Proglacial lacustrine environment. In: *Glacial sedimentary environments* (Eds G.M. Ashley, J. Shaw and N.D. Smith), *Society of Economic Paleontologists and Mineralogists*, Short Course 16: 135–215.

Smith, N.D., Cross, T.A., Dufficy, J.P. and Clough, S.R. (1989) Anatomy of an avulsion. *Sedimentology*, **36**, 1-23.

Strobl, R.S., Muwais, W.K., Wightman, D.M., Cotterill, D.K. and Yuan, L-P. (1997) Geological modeling of McMurray Formation reservoirs based on outcrop and subsurface analogues. In: *Petroleum geology of the Cretaceous Mannville Group, Western Canada* (Ed. by Pemberton, S. G. and James, D. P.) Canadian Society for Petroleum Geologists, *Memoirs* **18**, 292–311.

- Stuart, J.Y. (2014) *Subsurface architecture of fluvial-deltaic deposits in high- and low-accommodation settings*. Unpublished PhD thesis , University of Leeds, UK. 347 pp.
- Sundborg, A. (1956) The River Klarälven. *Geograf. Annaler*, **38**, 125-316
- Swales, S., Storey, A.W. and Bakowa, K.A. (2000) Temporal and spatial variations in fish catches in the Fly River system in Papua New Guinea and the possible effects of the Ok Tedi copper mine. *Environmental Biology of Fishes*, **57**, 75-95.
- Sweet, I.P. (1988) Early Proterozoic stream deposits: Braided or meandering— Evidence from central Australia: *Sedimentary Geology*, **58**, 277– 293.
- Sylvester, Z. (2014) *Rivers through time, as seen in Landsat images*, Wordpress, viewed 26 July 2017, <https://hinderedsettling.com/2014/03/16/rivers-through-time-as-seen-in-landsat-images/>
- Thomas, R.G., Smith, D.G., Wood, J.M., Visser, J., Calverley-Range E.A. and Koster E.H. (1987) Inclined Heterolithic Stratification-terminology, Description, Interpretation and Significance. *Sedimentary Geology*, **53**, 123–79.
- Thompson, A. (1986) Secondary Flows and the Pool Riffle Unit: A Case Study of the Processes of Meander Development. *Earth Surface Processes and Landforms*, **11**, 631–641.
- Toonen, W.H., Kleinhans, M.G. and Cohen, K.M. (2012) Sedimentary architecture of abandoned channel fills. *Earth Surface Processes and Landforms*, **37**, 459-472.
- Törnqvist, T.E., Weerts, H.J.T. and Berendsen, H.J.A., (1994) Definition of two new members in the upper Kreftenheye and Twente Formations (Quaternary, the Netherlands): a final solution to persistent confusion? *Geologie en Mijnbouw*, **72**, 251-264

Towl, R.N. (1935) The behaviour history of the "Big Muddy". *Engineering News Record*, **115**, 262-264.

Trueman, A.E. (1938) Erosion Levels in the Bristol District and their Relation to the Development of Scenery. *Proceedings of the Bristol Nature Society*, **8**, pp. 402.

Türk, G. (1979) Transition analysis of structural sequences: Discussion and reply. *Geological Society of America Bulletin*, **90**, 989-991.

Türk, G. (1982) Markov Chain analysis. *Mathematical Geology*, **14**, 539-542.

Tye, R.S. (2004) Geomorphology: An Approach to Determining Subsurface Reservoir Dimensions. *AAPG Bulletin*, **88**, 1123-47.

Van den Berg, J. (1995) Prediction of alluvial channel pattern of perennial rivers, *Geomorphology*, **12**, 259-279.

Van de Lageweg, W.I., van Dijk, W.M., Baar, A.W., Rutten, J. and Kleinhans, M.G. (2014) Bank pull or bar push: What drives scroll-bar formation in meandering rivers. *Geology*, **42**, 319-322.

Vecoli, M., Clément, G. and Meyer-Berthaud, B. (2010) The terrestrialization process: Modelling complex interactions at the biosphere-geosphere interface. In: *Modelling Complex Interactions at the Biosphere-Geosphere Interface: The Terrestrialization Process* (Eds M. Vecoli, G. Clément and B. Meyer-Berthaud), Geological Society, London, Special Publications, **339**, 1-3.

Visher, G.S. (1964) Fluvial Processes as Interpreted from Ancient and Recent Fluvial Deposits. *AAPG Bulletin*, **48**, 116-132.

Walker, R.G. (ed.), (1979) *Facies Models*, Geological Association of Canada Reprint Series 1.

- Walker, R.G.(1984) General Introduction: Facies, facies sequences and facies models. In *Facies models*, (Ed R.G. Walker), 2<sup>nd</sup> edition, Geological Association of Canada, p. 1–9
- Walker, R.G. and Cant, D.J. (1984) Sandy fluvial systems. In: *Facies Models* (Ed R.G. Walker), 2nd edn, pp. 71–90. Geological Association of Canada Reprint Series. Geological Association of Canada, Toronto.
- Waters, C.N., Chisholm, J.I., Benfield, A.C. and O'Beirne, A.M. (2008) Regional evolution of a fluviodeltaic cyclic succession in the Marsdenian (late Namurian Stage, Pennsylvanian) of the central Pennine basin, UK. *Proceedings of the Yorkshire Geological Society*, **57**, 1–28.
- Waters, C.N., Waters, R.A., Barclay, W.J. and Davies, J.R. (2009) A lithostratigraphical framework for the Carboniferous successions of southern Great Britain (Onshore). *British Geological Survey, Research Report RR/09/01*. 184 pp.
- Waters, C.N., Waters, R.A., Barclay, W.J., Davies, J.R., Jones, N.S. and Cleal, C.J. (2011) South Wales. In: *A revised correlation of Carboniferous rocks in the British Isles*, (Ed. by C. Waters) Geological Society of London, 29-36.
- Webb, E.K. and Davis, J.M. (1998) Simulation of the Spatial Heterogeneity of Geologic Properties: An Overview. In: *Hydraulic Models of Sedimentary Aquifers*, (Eds G.S. Fraser and J.M. Davis), *SEPM Concepts in Hydrology and Environmental Geology*, **1**, 1–24.
- Wightman, D.M. and Pemberton, S.G. (1997) The Lower Cretaceous (Aptian) McMurray Formation: an overview of the Fort McMurray area, northeastern, Alberta. In: *Petroleum Geology of the Cretaceous Mannville Group, Western Canada* (Ed. by Pemberton, S.G., and James, D.P.) *Canadian Society of Petroleum Geologists, Memoir* **18** 312–344.

Williams, R.M., Grotzinger, J.P., Dietrich, W.E., Gupta, S., Sumner, D.Y., Wiens, R.C., Mangold, N., Malin, M.C., Edgett, K. S., Maurice, S., Forni, O., Gasnault, O., Ollilia, A., Newsom, H.E., Dromart, G., Palucis, M.C., Yingst, R.A., Anderson, R.B., Herkenhoff, K.E., Le Mouélic, S., Goetz, W., Madsen, M.B., Koefoed, A., Jensen, J.K., Bridges, J.C., Schwenzer, S.P., Lewis, K.W., Stack K.M., Rubin, D., Kah, L.C., Bell, J.F., Farmer, J.D., Sullivan, R., Van Beek, T., Blaney, D.L., Pariser, O. and Deen, R.G. (2013) Martian fluvial conglomerates at Gale crater. *Science*, **340**, 1068-1072.

Williams, P.F. (1968) The sedimentation of Westphalian (Ammanian) measures in the Little Haven-Amroth coal- field, Pembrokeshire, *Journal of Sedimentary Petrology*, **38**, 332-362.

Williams, G.P. (1984) Paleohydrological methods and some examples from Swedish fluvial environ- ments; II -- river meanders. *Geogr. Ann.*, **66A**, 8-102.

Williams, G.P. (1986) River meanders and channel size. *Journal of Hydrology*, **88**, 147-164.

Willis, B.J. (1989) Palaeochannel reconstructions from point bar deposits: a three-dimensional perspective, *Sedimentology*, **36**. 757–766.

Willis, B.J. (1993) Evolution of Miocene fluvial systems in the Himalayan foredeep through a two kilometer-thick succession in northern Pakistan, *Sedimentary Geology*, **88**, 77–121.

Willis, B.J. and Tang, H. (2010). Three-dimensional connectivity of point-bar deposits. *Journal of Sedimentary Research*, **80**, 440-454.

Wood, J.M. (1989) Alluvial architecture of the Upper Cretaceous Judith River Formation, Dinosaur Provincial Park, Alberta, Canada. *Bulletin of Canadian Petroleum Geology*, **37**, 169-181.

Woodland, A.W., Evans, W. B. and Stephens, J. V. (1957) Classification of the Coal Measures of South Wales with Special reference to the Upper Coal Measures. *Bulletin of the Geological Survey of Great Britain*, **13**, 39-60.

Wu, C. and Bhattacharya J.P. (2015) Paleohydrology and 3D Facies Architecture of Ancient Point Bars, Ferron Sandstone, Notom Delta, South-Central Utah. *Journal of Sedimentary Research*, **85**, 399–418.

Wu J.Y., Shi S.M., Feng X., Wu X.X., Du X.L. and Bao Y. (2015) Internal architecture analysis and modeling of point-bar—a case study of P12 formation, X area. In: Energy and Environmental Engineering. In: Proceedings of the 2014 International Conference on Energy and Environmental Engineering (ICEEE 2014), September 21-22, 2014, Hong Kong (Vol. 1, p. 149). CRC Press.

Wynn, T. and Mostaghimi, S. (2006) The effects of vegetation and soil type on streambank erosion, southwestern Virginia, USA. *Journal of the American Water Resources Association*, **42**, 69-82.

Xu, H. and MacCarthy, I.A.J. (1998) Markov chain analysis of vertical facies sequences using a computer software package (SAVFS): Courtmacsherry Formation (Tournaisian), Southern Ireland. *Computers & Geosciences*, **24**, 131-139.

Xu, D., Bai, Y., Ma, J. and Tan, Y. (2011) Numerical investigation of long-term planform dynamics and stability of river meandering on fluvial floodplains. *Geomorphology*, **132**, 195-207.



Yan, N., Mountney, N.P., Colombera, L. and Dorrell, R.M. (2017) A 3D forward stratigraphic model of fluvial meander-bend evolution for prediction of point-bar lithofacies architecture. *Computers & Geosciences*, **105**, 65-80.

Zinger, J.A., Rhoads, B.L., Best, J.L. and Johnson, K.K. (2013) Flow Structure and Channel morphodynamics of meander bend chute cutoffs: a case study of the Wabash River, USA. *Journal of Geophysical Research: Earth surface* **118**, 2468-2487.

Zolezzi, G. and Seminara, G. (2001) Downstream and upstream influence in river meandering. Part 2. Planimetric development. *Journal of Fluid Mechanics*, **438**, 183-211.

## 9 Appendix

A – Meander shape and scroll-bar data – all measurements are in metres and metres squared.

B – Data from abandoned point-bar deposits – all measurements are in metres and metres squared.

C – Sedimentary graphic logs collected from Pembrokeshire; vertical axes in cm.

Facies code may be found as Figure 5.8. The location of each log is shown in planform on Figure 5.6; horizontal relationships are shown in Appendix E.



APPENDIX A

Ok Tedi (Fly)											
	Latitude	Longitude	Ps	As	AvC	tL	mW	(As/Ps)/AvC	tL/mW	Shape	Scroll
1	7°23'59.49"S	141°29'30.82"E	5768	455868	303.0476	5743	5712	0.2608	1.0054	3f	2.2
2	7°24'4.77"S	141°31'10.03"E	7610	2484788	303.0476	3325	5883	1.0774	0.5652	1c	3.1
3	7°21'53.75"S	141°31'32.87"E	7776	131476	303.0476	4803	4818	0.0558	0.9969	4a	2.2
4	7°22'56.24"S	141°33'13.25"E	7333	2472383	303.0476	3944	6818	1.1126	0.5785	2b	3.3
5	7°21'2.53"S	141°33'52.11"E	2502	41565	303.0476	3623	4355	0.0548	0.8319	1e	3.2
6	7°20'31.18"S	141°35'3.29"E	4279	500290	303.0476	2073	3174	0.3858	0.6531	4c	3.1
7	7°19'54.56"S	141°34'27.75"E	0	0	303.0476	747	2808	0.0000	0.2660	4e	5.1
8	7°19'12.20"S	141°35'10.95"E	1345	97361	303.0476	1535	4053	0.2389	0.3787	4d	6.2
9	7°18'12.08"S	141°35'4.34"E	7343	1027881	303.0476	3182	4516	0.4619	0.7046	2a	4.1
10	7°16'45.55"S	141°36'31.14"E	7260	1139031	303.0476	4178	6378	0.5177	0.6551	1i	2.1
11	7°15'55.62"S	141°39'12.28"E	10175	711056	303.0476	5492	5702	0.2306	0.9632	3f	1.1
12	7°17'17.42"S	141°39'53.24"E	6836	379933	303.0476	5739	3637	0.1834	1.5779	3a	2.1
13	7°16'11.43"S	141°41'23.46"E	5419	895515	303.0476	2448	2746	0.5453	0.8915	1a	3.1
14	7°15'2.74"S	141°42'33.50"E	3117	275921	303.0476	4154	4545	0.2921	0.9140	1e	4.1
15	7°15'0.94"S	141°43'34.18"E	1519	52033	303.0476	5651	7146	0.1130	0.7908	2a	8.2
16	7°14'29.74"S	141°44'17.91"E	3661	650959	303.0476	7327	3369	0.5867	2.1748	3g	8.2
17	7°14'13.97"S	141°46'0.08"E	10312	4133921	303.0476	3603	4591	1.3228	0.7848	3c	2.3
18	7°13'13.07"S	141°47'34.48"E	1461	71674	303.0476	2060	3866	0.1619	0.5329	4d	7.1
19	7°11'44.40"S	141°47'34.05"E	5044	562020	303.0476	5574	2869	0.3677	1.9428	3g	2.3
20	7°12'17.51"S	141°48'53.11"E	6924	232583	303.0476	5382	1915	0.1108	2.8104	3g	6.1

APPENDIX A

		Senegal								Shape	Scroll
	Latitude	Longitude	Ps	As	AvC	tL	mW	(As/Ps)/AvC	tL/mW		
1	16°35'59.25"N	15° 7'5.31"W	8028	1484080	171.2000	5653	9023	1.0798	0.6265	3c	7.2
2	16°38'59.44"N	15° 5'13.57"W	11039	2027275	171.2000	7185	5102	1.0727	1.4083	3a	4.2
3	16°39'23.78"N	15° 1'35.97"W	20915	10709187	171.2000	5808	11606	2.9909	0.5004	3c	7.3
4	16°40'8.49"N	14°58'37.60"W	9505	1756258	171.2000	7046	10306	1.0793	0.6837	3c	3.1
5	16°39'5.95"N	14°56'8.21"W	9415	1735588	171.2000	3789	5529	1.0768	0.6853	(1d)	3.2
6	16°38'14.26"N	14°55'0.39"W	4428	368437	171.2000	3032	3833	0.4860	0.7910	2a	5.1
7	16°38'57.73"N	14°52'6.94"W	3261	302236	171.2000	2702	3535	0.5414	0.7644	1i	6.2
8	16°38'36.84"N	14°52'40.11"W	8144	1196393	171.2000	3029	4350	0.8581	0.6963	4c	3.1
9	16°39'1.29"N	14°50'20.47"W	3090	291030	171.2000	1582	4711	0.5501	0.3358	2d	6.2
10	16°38'37.49"N	14°49'45.72"W	3320	252259	171.2000	1282	2742	0.4438	0.4675	4d	6.1
11	16°38'33.90"N	14°48'47.45"W	4563	555811	171.2000	2463	4400	0.7115	0.5598	1d	3.3
12	16°38'29.94"N	14°45'52.83"W	5874	369303	171.2000	3384	5672	0.3672	0.5966	1f	6.1
13	16°38'2.37"N	14°44'39.78"W	4243	219207	171.2000	4062	4527	0.3018	0.8973	3b	2.3
14	16°37'38.64"N	14°43'51.22"W	1636	76201	171.2000	879	1631	0.2721	0.5389	4c	3.1
15	16°38'7.01"N	14°43'50.37"W	1331	66135	171.2000	875	1900	0.2902	0.4605	4d	3.1
16	16°38'22.39"N	14°43'22.69"W	1977	38580	171.2000	1480	2256	0.1140	0.6560	4c	6.2
17	16°38'31.16"N	14°39'0.49"W	4370	409745	171.2000	3934	7083	0.5477	0.5554	(1i)	3.2
18	16°37'46.48"N	14°38'19.87"W	6015	1449124	171.2000	2650	3985	1.4072	0.6650	3c	6.1
19	16°38'12.03"N	14°25'22.82"W	3051	428260	171.2000	2210	5230	0.8199	0.4226	1g	3.3
20	16°38'20.05"N	14°24'8.46"W	2549	254127	171.2000	1611	4208	0.5823	0.3828	1g	6.1

APPENDIX A

			Murray							Shape	Scroll
	Latitude	Longitude	Ps	As	AvC	tL	mW	(As/Ps)/AvC	tL/mW		
1	34°15'1.36"S	140°43'9.18"E	833	16028	148.2714	1125	980	0.1298	1.1480	3f	2.3
2	34°14'43.59"S	140°43'2.89"E	351	1968	148.2714	837	1098	0.0378	0.7623	(4b)	3.1
3	34°14'23.59"S	140°42'59.37"E	0	0	148.2714	349	1346	0.0000	0.2593	4e	6.2
4	34°14'15.43"S	140°43'23.65"E	1331	34477	148.2714	1016	1292	0.1747	0.7864	4b	3.2
5	34°13'54.58"S	140°43'50.78"E	3275	500542	148.2714	1065	1929	1.0308	0.5521	3c	8.2
6	34°13'34.75"S	140°44'18.04"E	521	6885	148.2714	1157	794	0.0891	1.4572	3e	3.1
7	34°13'34.69"S	140°44'38.29"E	2242	88401	148.2714	958	1410	0.2659	0.6794	4c	3.2
8	34°11'48.97"S	140°45'23.49"E	2516	252050	148.2714	1317	2148	0.6756	0.6131	4c	6.2
9	34°11'28.54"S	140°45'54.70"E	1602	567	148.2714	934	1745	0.0024	0.5352	(4c)	2.2
10	34°10'10.06"S	140°45'48.32"E	4101	77278	148.2714	2657	2730	0.1271	0.9733	1e	6.2
11	34° 9'3.57"S	140°46'24.76"E	1463	100401	148.2714	1408	3924	0.4628	0.3588	1g	3.1
12	34° 8'15.32"S	140°46'43.51"E	1597	111534	148.2714	924	1735	0.4710	0.5326	(1f)	7.2
13	34° 7'38.95"S	140°46'31.07"E	2493	233843	148.2714	862	2193	0.6326	0.3931	3b	2.2
14	34° 7'5.68"S	140°46'33.13"E	1665	29775	148.2714	1648	2464	0.1206	0.6688	3d	6.1
15	34° 6'41.26"S	140°47'13.42"E	3826	24212	148.2714	3353	2012	0.0427	1.6665	3e	8.2
16	34° 6'26.31"S	140°45'41.97"E	1277	56077	148.2714	1373	1032	0.2962	1.3304	3e	3.3
17	34° 5'57.64"S	140°45'43.00"E	2719	194803	148.2714	1235	2327	0.4832	0.5307	1d	3.3
18	34° 4'56.45"S	140°45'12.55"E	260	2569	148.2714	577	2008	0.0666	0.2874	4d	7.3
19	34° 4'13.01"S	140°48'12.23"E	1243	36004	148.2714	1208	2401	0.1954	0.5031	1g	3.2
20	34° 3'59.26"S	140°48'41.86"E	1168	11059	148.2714	875	827	0.0639	1.0580	4a	8.2

APPENDIX A

			Yana							Shape	Scroll
	Latitude	Longitude	Ps	As	AvC	tL	mW	(As/Ps)/AvC	tL/mW		
1	71°28'19.12"N	136°17'12.67"E	4644	121094	334.4762	3272	5282	0.0780	0.6195	2a	2.2
2	71°27'28.88"N	136°13'27.00"E	9967	2187779	334.4762	2921	6061	0.6563	0.4819	1g	6.2
3	71°25'52.50"N	136°11'6.96"E	5543	277942	334.4762	3208	3619	0.1499	0.8864	1e	3.3
4	71°25'24.81"N	136° 9'0.81"E	1738	63226	334.4762	2384	2690	0.1088	0.8862	1e	3.4
5	71°23'57.76"N	136°10'4.76"E	6688	965952	334.4762	2505	4033	0.4318	0.6211	3b	2.3
6	71°19'55.37"N	136° 7'48.55"E	0	0	334.4762	1254	3656	0.0000	0.3430	4e	7.1
7	71°19'58.56"N	136° 3'53.98"E	3756	290560	334.4762	1385	3992	0.2313	0.3469	2d	3.1
8	71°16'53.57"N	135°41'59.22"E	2422	216754	334.4762	1395	2023	0.2676	0.6896	4c	3.1
9	71°18'33.84"N	136° 2'51.91"E	7275	1261883	334.4762	3986	3639	0.5186	1.0954	3e	3.4
10	71°17'8.32"N	136° 3'32.85"E	2519	166583	334.4762	2026	4997	0.1977	0.4054	4d	6.2
11	71°16'18.47"N	136° 7'40.91"E	1887	86825	334.4762	1869	4985	0.1376	0.3749	1g	2.1
12	71°14'27.37"N	135°55'56.91"E	0	0	334.4762	1462	7660	0.0000	0.1909	4e	6.2
13	71°14'53.83"N	136° 8'52.08"E	7504	995230	334.4762	3095	3767	0.3965	0.8216	3b	4.2
14	71°14'2.65"N	136° 9'23.32"E	2757	73821	334.4762	2619	3168	0.0801	0.8267	4c	3.1
15	71°13'0.08"N	136° 7'51.19"E	5269	769140	334.4762	2437	4928	0.4364	0.4945	4d	7.1
16	71°10'26.91"N	136° 8'33.69"E	4751	510685	334.4762	3018	8798	0.3214	0.3430	3b	7.1
17	71°11'2.32"N	135°55'53.67"E	8935	1621543	334.4762	3692	6987	0.5426	0.5284	(1g)	3.2
18	71° 8'35.67"N	136° 9'7.39"E	7061	193797	334.4762	6698	5769	0.0821	1.1610	3f	2.1
19	71° 9'25.86"N	135°57'19.61"E	6185	936696	334.4762	3316	5199	0.4528	0.6378	1i	3.1
20	71° 7'53.53"N	136° 3'55.35"E	14934	4101277	334.4762	11352	12499	0.8211	0.9082	1i	3.3

APPENDIX A

Colville (tributary)											
	Latitude	Longitude	Ps	As	AvC	tL	mW	(As/Ps)/AvC	tL/mW	Shape	Scroll
1	69°55'24.20"N	151°43'58.87"W	1374	47280	98.2381	1100	1703	0.3503	0.6459	3e	2.3
2	69°55'12.96"N	151°44'32.31"W	1025	33856	98.2381	707	1246	0.3362	0.5674	1b	3.3
3	69°54'26.49"N	151°45'58.73"W	1350	11698	98.2381	843	628	0.0882	1.3424	4a	2.2
4	69°54'11.99"N	151°45'47.26"W	1813	93667	98.2381	843	1440	0.5259	0.5854	1f	3.4
5	69°53'46.86"N	151°45'36.25"W	1912	30558	98.2381	1210	1262	0.1627	0.9588	3f	3.4
6	69°53'36.35"N	151°44'54.39"W	2198	9609	98.2381	2372	1352	0.0445	1.7544	3g	2.1
7	69°53'9.82"N	151°47'28.11"W	988	33220	98.2381	520	1376	0.3423	0.3779	4d	6.1
8	69°53'1.43"N	151°48'11.61"W	832	25676	98.2381	457	921	0.3141	0.4962	4d	3.3
9	69°52'50.24"N	151°48'42.21"W	1364	46560	98.2381	505	929	0.3475	0.5436	1b	3.1
10	69°52'27.07"N	151°48'49.53"W	1169	40860	98.2381	543	880	0.3558	0.6170	1b	3.3
11	69°52'15.69"N	151°48'30.32"W	1515	66114	98.2381	845	1033	0.4442	0.8180	2a	3.3
12	69°51'54.50"N	151°48'25.46"W	0	0	98.2381	475	1993	0.0000	0.2383	4e	3.1
13	69°51'21.33"N	151°48'19.42"W	1941	44574	98.2381	1704	1304	0.2338	1.3067	4a	2.2
14	69°51'7.97"N	151°49'37.88"W	2769	267615	98.2381	1079	1740	0.9838	0.6201	3c	7.1
15	69°51'22.68"N	151°51'35.46"W	1685	25852	98.2381	1128	1387	0.1562	0.8133	2a	2.1
16	69°51'5.40"N	151°52'20.06"W	2140	113515	98.2381	1315	978	0.5400	1.3446	1i	2.3
17	69°50'44.20"N	151°53'16.64"W	725	1817	98.2381	830	723	0.0255	1.1480	4a	2.1
18	69°50'28.57"N	151°52'37.44"W	1108	49007	98.2381	729	1140	0.4502	0.6395	1i	7.3
19	69°50'13.75"N	151°53'17.99"W	1010	9741	98.2381	767	488	0.0982	1.5717	3d	2.2
20	69°50'1.00"N	151°52'57.14"W	1146	41812	98.2381	506	907	0.3714	0.5579	2a	5.1



APPENDIX A

Kuskokwim										Shape	Scroll
	Latitude	Longitude	Ps	As	AvC	tL	mW	(As/Ps)/AvC	tL/mW		
1	60°39'24.68"N	162° 0'43.83"W	6405	1076073	512.9048	4718	9271	0.3276	0.5089	4d	3.2
2	60°40'54.22"N	161°55'43.45"W	4959	1067328	512.9048	4234	12779	0.4196	0.3313	2c	3.4
3	60°44'38.31"N	161°47'33.18"W	14840	4424908	512.9048	7471	14590	0.5813	0.5121	2c	7.3
4	60°45'49.88"N	161°42'49.67"W	8730	895029	512.9048	5907	5501	0.1999	1.0738	4a	7.1
5	60°47'51.46"N	161°42'4.09"W	7429	90111	512.9048	5455	8106	0.0236	0.6730	1h	3.2
6	60°48'37.41"N	161°36'48.30"W	10700	2641623	512.9048	8221	10646	0.4813	0.7722	4b	3.4
7	60°50'23.02"N	161°31'22.57"W	19746	3836686	512.9048	8994	11975	0.3788	0.7511	1h	3.4
8	60°49'6.28"N	161°25'34.93"W	7804	1113008	512.9048	2611	5642	0.2781	0.4628	1g	3.2
9	60°51'0.15"N	161°28'34.09"W	3856	457026	512.9048	1927	5665	0.2311	0.3402	2d	3.3
10	60°50'4.24"N	161°23'5.96"W	3910	482306	512.9048	1631	3087	0.2405	0.5283	1b	3.4
11	60°50'55.79"N	161°21'33.60"W	2604	170356	512.9048	1500	2490	0.1275	0.6024	1h	2.2
12	60°53'10.71"N	161°21'2.37"W	8883	672639	512.9048	4569	5653	0.1476	0.8082	4c	3.3
13	60°54'32.94"N	161°14'40.83"W	11469	2446554	512.9048	4193	6380	0.4159	0.6572	4c	2.2
14	60°55'41.58"N	161°10'11.16"W	6522	1949143	512.9048	3476	7660	0.5827	0.4538	4d	4.1
15	61°16'23.63"N	160°41'37.34"W	1855	101020	512.9048	4706	12090	0.1062	0.3892	4d	7.1
16	61°19'40.69"N	160°39'11.30"W	6272	1461642	512.9048	5169	18779	0.4544	0.2753	2c	7.1
17	61°24'37.05"N	160°34'29.59"W	8350	1922688	512.9048	3366	7500	0.4489	0.4488	1g	2.2
18	61°25'31.95"N	160°32'43.80"W	6561	603564	512.9048	2464	4030	0.1794	0.6114	1h	3.1
19	61°25'56.16"N	160°30'11.13"W	1178	48698	512.9048	1627	5674	0.0806	0.2867	4d	5.2
20	61°27'25.36"N	160°28'0.13"W	0	0	512.9048	1023	5573	0.0000	0.1836	4e	7.1

APPENDIX A

	Mississippi										
	Latitude	Longitude	Ps	As	AvC	tL	mW	(As/Ps)/AvC	tL/mW	Shape	Scroll
1	30°31'31.15"N	91°14'21.66"W	2122	204045	859.9095	6650	6078	0.1118	1.0941	4a	2.2
2	30°32'50.11"N	91°16'30.07"W	13030	3943211	859.9095	6110	8304	0.3519	0.7358	1h	6.2
3	30°35'20.62"N	91°17'19.59"W	10437	4725672	859.9095	5084	10308	0.5265	0.4932	4d	3.2
4	30°37'51.55"N	91°18'49.02"W	4794	931973	859.9095	3486	10268	0.2261	0.3395	4d	6.2
5	30°46'50.14"N	91°29'16.69"W	20171	9222115	859.9095	16592	21612	0.5317	0.7677	2a	3.4
6	30°52'17.39"N	91°32'26.15"W	17302	4479004	859.9095	11993	20889	0.3010	0.5741	(1f)	3.4
7	30°57'24.24"N	91°36'23.38"W	23827	25091452	859.9095	12295	19174	1.2246	0.6412	(4b)	3.2
8	31° 2'56.09"N	91°36'28.87"W	9300	2848986	859.9095	7755	16784	0.3562	0.4620	4d	3.1
9	31° 7'44.49"N	91°35'4.63"W	4941	832109	859.9095	4840	14783	0.1958	0.3274	2d	3.4
10	31°10'57.43"N	91°37'1.63"W	0	0	859.9095	4909	14195	0.0000	0.3458	4e	6.2
11	31°14'25.12"N	91°36'10.88"W	14811	3290266	859.9095	9569	14323	0.2583	0.6681	4c	3.1
12	31°28'28.90"N	91°27'53.83"W	0	0	859.9095	7379	22395	0.0000	0.3295	(4d)	3.3
13	32° 6'21.03"N	91° 3'55.23"W	22215	7789096	859.9095	8165	12398	0.4077	0.6586	4c	3.3
14	32° 9'15.57"N	91° 2'28.04"W	20732	10339966	859.9095	6242	19765	0.5800	0.3158	4d	7.1
15	32°15'46.22"N	90°55'53.23"W	0	0	859.9095	1741	14502	0.0000	0.1201	4e	5.2
16	32°19'13.76"N	90°58'30.85"W	19656	10055796	859.9095	9817	21074	0.5949	0.4658	2b	5.2
17	32°22'31.89"N	90°57'34.63"W	3573345	9627	859.9095	4640	13430	0.0000	0.3455	2d	7.1
18	32°24'35.01"N	91° 1'49.81"W	1434	46816	859.9095	4059	14429	0.0380	0.2813	4e	5.2
19	32°29'49.05"N	91° 4'38.48"W	4379	415376	859.9095	5290	18925	0.1103	0.2795	4d	7.3
20	32°33'48.98"N	91° 8'22.18"W	0	0	859.9095	2701	13537	0.0000	0.1995	4e	5.2

APPENDIX A

Purus (Amazon)											
	Latitude	Longitude	Ps	As	AvC	tL	mW	(As/Ps)/AvC	tL/mW	Shape	Scroll
1	5°41'41.92"S	63°31'30.36"W	11963	3109876	584.8476	5232	8922	0.4445	0.5864	1f	3.1
2	5°43'38.23"S	63°32'59.31"W	0	0	584.8476	2610	8870	0.0000	0.2943	2d	6.2
3	5°42'53.32"S	63°37'36.94"W	5550	825013	584.8476	9793	8424	0.2542	1.1625	3f	8.2
4	5°41'51.70"S	63°40'16.92"W	2332	186233	584.8476	11378	9872	0.1365	1.1526	3f	8.2
5	5°38'48.48"S	63°39'51.73"W	15006	1378048	584.8476	14225	8968	0.1570	1.5862	3a	8.1
6	5°38'26.89"S	63°47'36.55"W	8563	2315801	584.8476	4521	7500	0.4624	0.6028	1f	3.1
7	5°38'18.66"S	63°50'38.82"W	14828	5009424	584.8476	9865	10008	0.5776	0.9857	3e	3.4
8	5°35'44.48"S	63°52'27.29"W	24268	4558020	584.8476	12607	12850	0.3211	0.9811	1e	3.1
9	5°36'54.88"S	64° 2'46.13"W	10023	1052059	584.8476	12281	14535	0.1795	0.8449	3d	8.2
10	5°36'42.55"S	64° 5'24.55"W	17070	11205984	584.8476	6459	12253	1.1225	0.5271	3c	6.2
11	5°38'37.20"S	64° 8'12.60"W	0	0	584.8476	3007	9331	0.0000	0.3223	4e	3.3
12	5°37'40.45"S	64°11'7.88"W	3633	295606	584.8476	9981	7083	0.1391	1.4091	3e	3.1
13	5°35'17.08"S	64° 9'42.13"W	15141	2001309	584.8476	9919	3671	0.2260	2.7020	3g	4.2
14	5°34'38.07"S	64°12'40.24"W	10443	5048658	584.8476	4657	7908	0.8266	0.5889	4c	2.2
15	5°35'30.49"S	64°14'37.52"W	4818	1235681	584.8476	3537	7708	0.4385	0.4589	4d	3.1
16	5°34'49.43"S	64°17'15.96"W	0	0	584.8476	2040	11076	0.0000	0.1842	4e	5.1
17	5°36'49.26"S	64°19'1.06"W	17130	4334758	584.8476	8997	12995	0.4327	0.6923	2a	5.1
18	5°40'20.03"S	64°19'52.52"W	16751	458324	584.8476	11348	8825	0.0468	1.2859	3f	2.2
19	5°40'19.66"S	64°22'25.73"W	14373	4271154	584.8476	8685	6307	0.5081	1.3770	3a	2.2
20	5°43'13.48"S	64°22'55.62"W	10713	3187612	584.8476	6555	8301	0.5088	0.7897	1a	3.1

APPENDIX A

			Irtysk (Ob)							Shape	Scroll
	Latitude	Longitude	Ps	As	AvC	tL	mW	(As/Ps)/AvC	tL/mW		
1	59°13'50.17"N	68°47'58.92"E	6475	970290	3092.0580	3103	10036	0.0485	0.3092	2d	3.1
2	59°10'28.97"N	68°49'4.00"E	3279	458122	3092.0580	8154	10279	0.0452	0.7933	1e	3.3
3	59° 9'0.11"N	68°52'23.95"E	14693	4280776	3092.0580	8178	7487	0.0942	1.0923	3f	2.3
4	59° 4'27.59"N	68°52'4.83"E	20773	9270695	3092.0580	5827	15350	0.1443	0.3796	1g	3.4
5	59° 1'30.91"N	68°50'27.18"E	9410	2433188	3092.0580	8851	9163	0.0836	0.9660	3f	2.2
6	58°59'31.73"N	68°47'25.72"E	4745	697785	3092.0580	11253	8683	0.0476	1.2960	3e	2.3
7	58°56'39.50"N	68°50'29.10"E	9493	480128	3092.0580	6819	6119	0.0164	1.1144	3f	4.2
8	58°56'15.26"N	68°47'24.78"E	10853	1928063	3092.0580	3971	6453	0.0575	0.6154	4c	2.2
9	58°53'0.64"N	68°44'1.94"E	10543	950126	3092.0580	6348	5517	0.0291	1.1506	3f	3.4
10	58°51'54.23"N	68°46'52.28"E	6855	384591	3092.0580	9086	4499	0.0181	2.0196	3g	4.1
11	58°50'1.74"N	68°44'40.40"E	8242	144113	3092.0580	8043	9174	0.0057	0.8767	4a	8.2
12	58°46'49.16"N	68°35'27.84"E	3668	232669	3092.0580	9025	7843	0.0205	1.1507	3f	8.2
13	58°45'28.42"N	68°34'15.40"E	6179	749013	3092.0580	3292	7012	0.0392	0.4695	1b	3.1
14	58°38'1.87"N	68°34'47.48"E	13374	2764439	3092.0580	5244	9114	0.0668	0.5754	(1d)	4.1
15	58°35'59.07"N	68°33'44.41"E	10964	3561985	3092.0580	5635	8836	0.1051	0.6377	4c	3.4
16	58°30'54.53"N	68°33'35.73"E	13050	4932639	3092.0580	12201	10113	0.1222	1.2065	(3e)	2.3
17	58°29'14.53"N	68°26'48.18"E	12778	5946943	3092.0580	5544	9978	0.1505	0.5556	4d	3.2
18	58°28'23.25"N	68°21'29.42"E	3172	606324	3092.0580	2732	9313	0.0618	0.2934	2d	6.1
19	58°26'14.20"N	68°21'40.84"E	8426	2476615	3092.0580	3905	8411	0.0951	0.4643	4d	6.2
20	58°22'53.58"N	68°17'32.64"E	24280	13561289	3092.0580	6732	16468	0.1806	0.4088	1g	7.3

APPENDIX A

Kolyma (tributary)											
	Latitude	Longitude	Ps	As	AvC	tL	mW	(As/Ps)/AvC	tL/mW	Shape	Scroll
1	68°28'16.65"N	160°55'53.31"E	15560	211581	310.4429	7281	5925	0.0438	1.2289	4a	3.1
2	68°26'46.36"N	160°55'46.75"E	12163	1037630	310.4429	7604	4983	0.2748	1.5260	4a	3.2
3	68°25'20.53"N	160°55'8.21"E	10720	552358	310.4429	5060	3329	0.1660	1.5200	(1e)	3.1
4	68°24'37.14"N	160°56'47.12"E	5165	263191	310.4429	2967	3692	0.1641	0.8036	1e	3.1
5	68°23'52.40"N	160°58'32.82"E	4319	601094	310.4429	2151	3234	0.4483	0.6651	4c	3.3
6	68°22'49.98"N	160°58'15.33"E	5584	1351966	310.4429	2994	5362	0.7799	0.5584	1d	3.2
7	68°21'16.18"N	160°59'29.79"E	6630	65986	310.4429	5410	3895	0.0321	1.3890	4a	3.1
8	68°20'46.94"N	161° 3'35.75"E	886	31752	310.4429	1872	5873	0.1154	0.3187	2d	6.2
9	68°19'29.18"N	161°13'20.33"E	7739	313497	310.4429	5504	5879	0.1305	0.9362	3d	8.2
10	68°20'1.31"N	161°17'14.80"E	6734	229982	310.4429	5433	5621	0.1100	0.9666	3d	3.4
11	68°19'43.58"N	161°20'24.68"E	1219	44928	310.4429	6265	5042	0.1187	1.2426	3f	4.2
12	68°19'35.77"N	161°22'40.25"E	1629	41190	310.4429	1144	4031	0.0814	0.2838	4d	6.2
13	68°21'41.14"N	161°23'46.51"E	2027	163952	310.4429	5995	4843	0.2605	1.2379	1i	4.2
14	68°21'39.26"N	161°27'39.25"E	3518	83195	310.4429	3416	4517	0.0762	0.7563	4c	3.1
15	68°21'8.51"N	161°30'34.65"E	4245	509838	310.4429	4639	4312	0.3869	1.0758	1i	2.1
16	68°19'13.27"N	161°35'10.57"E	8778	3130867	310.4429	3615	7963	1.1489	0.4540	1c	6.2
17	68°17'59.70"N	161°40'12.45"E	11347	2131819	310.4429	3837	6661	0.6052	0.5760	3b	2.3
18	68°16'29.14"N	161°43'29.35"E	3296	111618	310.4429	1510	2832	0.1091	0.5332	4d	3.2
19	68°15'53.71"N	161°44'33.58"E	3576	387992	310.4429	1020	2636	0.3495	0.3869	4d	7.3
20	68°15'29.32"N	161°46'55.04"E	2599	179617	310.4429	1055	1984	0.2226	0.5318	4d	2.2

APPENDIX A

	Brazos										
	Latitude	Longitude	Ps	As	AvC	tL	mW	(As/Ps)/AvC	tL/mW	Shape	Scroll
1	29°56'7.81"N	96° 7'13.89"W	4752	1316044	111.6519	2065	2063	2.4450	1.0010	3c	2.3
2	29°56'55.66"N	96° 6'34.77"W	3885	337287	111.6519	2550	2435	0.7429	1.0472	3a	2.3
3	29°57'36.42"N	96° 6'58.27"W	3943	104176	111.6519	2626	1030	0.2094	2.5495	3g	2.2
4	29°58'29.13"N	96° 5'58.57"W	0	0	111.6519	924	2581	0.0000	0.3580	4e	3.3
5	29°59'27.46"N	96° 5'38.82"W	533	13522	111.6519	2103	3400	0.2016	0.6185	1h	6.2
6	30° 0'15.90"N	96° 5'29.71"W	3392	315918	111.6519	1786	2168	0.8049	0.8238	1i	3.1
7	30° 1'19.12"N	96° 5'57.51"W	808	31346	111.6519	1151	2677	0.3787	0.4300	2d	3.4
8	30° 2'8.84"N	96° 6'39.24"W	0	0	111.6519	655	1872	0.0000	0.3499	4e	5.1
9	30° 4'14.56"N	96° 8'17.12"W	3021	229343	111.6519	1130	1331	0.7506	0.8490	4b	6.2
10	30° 4'36.48"N	96° 8'17.50"W	0	0	111.6519	387	1573	0.0000	0.2460	4e	4.2
11	30° 4'53.27"N	96° 8'38.69"W	315	3408	111.6519	673	1616	0.0918	0.4165	4e	6.2
12	30° 5'28.47"N	96° 9'7.77"W	2335	274139	111.6519	1174	2773	1.0109	0.4234	1c	6.2
13	30° 6'11.75"N	96° 9'27.64"W	3898	62734	111.6519	1906	2421	0.1516	0.7873	3d	6.1
14	30° 6'13.66"N	96°10'8.14"W	2696	96394	111.6519	1370	1776	0.3125	0.7714	4b	3.2
15	30° 6'26.14"N	96°10'36.50"W	1952	83356	111.6519	1155	1866	0.3563	0.6190	4c	3.1
16	30° 6'42.52"N	96°11'2.05"W	1393	86948	111.6519	1414	1267	0.5462	1.1160	3e	3.3
17	30° 7'18.70"N	96°11'6.52"W	1592	86054	111.6519	1192	1513	0.5885	0.7878	1i	8.1
18	30° 8'7.73"N	96°11'4.58"W	4139	74308	111.6519	2048	2370	0.1760	0.8641	1e	3.2
19	30° 8'29.84"N	96°10'42.84"W	2832	18928	111.6519	1747	1860	0.0571	0.9392	4a	3.3
20	30° 8'57.80"N	96°10'35.29"W	4515	22093	111.6519	2666	1801	0.0388	1.4803	(1e)	3.3

APPENDIX A

			Limpopo							Shape	Scroll
	Latitude	Longitude	Ps	As	AvC	tL	mW	(As/Ps)/AvC	tL/mW		
1	22°36'55.71"S	31°48'32.57"E	2090	98807	147.3300	1050	3194	0.3209	0.3287	4d	3.3
2	22°36'20.20"S	31°47'52.03"E	865	27602	147.3300	744	3074	0.2166	0.2420	4e	3.1
3	22°35'11.90"S	31°47'38.03"E	0	0	147.3300	428	4003	0.0000	0.1069	4e	5.2
4	22°34'12.65"S	31°46'44.95"E	534	10591	147.3300	1402	5484	0.1346	0.2557	4e	3.3
5	22°33'35.12"S	31°44'37.51"E	0	0	147.3300	625	2553	0.0000	0.2448	4e	1.2
6	22°33'2.65"S	31°44'0.76"E	3083	183853	147.3300	1160	2368	0.4048	0.4899	2d	3.2
7	22°33'3.64"S	31°43'18.25"E	1584	68392	147.3300	989	2000	0.2931	0.4945	4d	3.1
8	22°32'27.36"S	31°43'4.47"E	3560	345734	147.3300	2029	4245	0.6592	0.4780	1d	3.1
9	22°30'1.41"S	31°43'12.95"E	0	0	147.3300	365	2063	0.0000	0.1769	4e	5.2
10	22°29'37.04"S	31°42'27.61"E	8585	1341165	147.3300	2647	7275	1.0604	0.3638	1c	7.2
11	22°28'48.15"S	31°41'18.74"E	4956	499064	147.3300	1690	4499	0.6835	0.3756	4d	3.1
12	22°28'52.48"S	31°39'59.36"E	2465	231386	147.3300	1499	3995	0.6371	0.3752	4d	3.2
13	22°27'31.75"S	31°39'14.16"E	1758	147702	147.3300	1539	5045	0.5703	0.3051	4d	3.1
14	22°27'1.68"S	31°37'38.65"E	0	0	147.3300	939	6240	0.0000	0.1505	4e	5.2
15	22°25'14.80"S	31°36'40.03"E	1704	135695	147.3300	1402	6335	0.5405	0.2213	4e	3.3
16	22°24'40.80"S	31°35'50.50"E	0	0	147.3300	498	3570	0.0000	0.1395	4e	5.2
17	22°23'46.40"S	31°36'9.73"E	0	0	147.3300	531	3006	0.0000	0.1766	4e	5.2
18	22°23'35.15"S	31°35'23.76"E	3077	58585	147.3300	1733	2731	0.1292	0.6346	1h	3.1
19	22°22'36.01"S	31°34'54.29"E	3667	293945	147.3300	1396	2955	0.5441	0.4724	2b	3.1
20	22°22'48.84"S	31°33'47.05"E	1940	119868	147.3300	964	3246	0.4194	0.2970	2d	1.2

APPENDIX A

Appalachicola											
	Latitude	Longitude	Ps	As	AvC	tL	mW	(As/Ps)/AvC	tL/mW	Shape	Scroll
1	30°36'13.91"N	85°54'44.99"W	64.4	130	41.4100	211	742	0.0487	0.2844	(1c)	7.3
2	30°36'21.87"N	85°54'37.01"W	319	1690	41.4100	260	418	0.1279	0.6220	3d	3.1
3	30°36'30.50"N	85°54'36.67"W	474	4293	41.4100	176	421	0.2187	0.4181	4d	3.1
4	30°36'47.98"N	85°54'30.54"W	533	12262	41.4100	291	570	0.5556	0.5105	2c	3.1
5	30°36'52.66"N	85°54'32.27"W	177	518	41.4100	193	273	0.0707	0.7070	4c	3.1
6	30°36'54.46"N	85°54'36.01"W	431	2072	41.4100	244	355	0.1161	0.6873	3d	3.2
7	30°37'1.48"N	85°54'39.06"W	1207	507	41.4100	496	517	0.0101	0.9594	3f	2.2
8	30°37'10.06"N	85°54'40.61"W	790	17818	41.4100	235	566	0.5447	0.4152	1g	2.2
9	30°37'19.86"N	85°54'34.85"W	229	926	41.4100	164	273	0.0976	0.6007	4c	3.2
10	30°37'23.95"N	85°54'42.70"W	296	3247	41.4100	171	449	0.2649	0.3808	4d	3.1
11	30°37'33.74"N	85°54'39.46"W	70	106	41.4100	221	801	0.0366	0.2759	4e	3.1
12	30°37'46.77"N	85°54'43.83"W	673	12596	41.4100	261	652	0.4520	0.4003	2c	3.2
13	30°37'54.41"N	85°54'42.48"W	134	469	41.4100	118	319	0.0845	0.3699	4d	3.1
14	30°38'7.24"N	85°54'46.44"W	611	6875	41.4100	393	483	0.2717	0.8137	1e	4.3
15	30°38'15.72"N	85°54'47.67"W	562	4663	41.4100	186	416	0.2004	0.4471	(1b)	3.1
16	30°38'17.24"N	85°54'36.48"W	511	4378	41.4100	178	501	0.2069	0.3553	1g	3.1
17	30°38'31.11"N	85°54'32.47"W	322	4971	41.4100	279	835	0.3728	0.3341	4d	1.2
18	30°38'31.48"N	85°54'18.61"W	370	1184	41.4100	311	654	0.0773	0.4755	(3f)	3.1
19	30°38'47.43"N	85°54'13.71"W	492	7260	41.4100	332	662	0.3563	0.5015	4d	3.1
20	30°38'46.77"N	85°53'57.82"W	928	14178	41.4100	461	620	0.3689	0.7435	(3d)	3.2



## APPENDIX A

APPENDIX B

**Ok Tedi (Fly) River**

	Latitude	Longitude	Scroll-bar pattern	Individual cut-off style	Group cut-off style	Length (nH)	Width (pbW)	Ratio (nH/pbW)
1	7°22'35.28"S	141°30'5.31"E	8.2	neck	length NOL	1725	533	3.2364
2	7°20'43.18"S	141°31'13.23"E	2.2	neck	nodal multidir.	882	640	1.3781
3	7°20'27.41"S	141°32'10.22"E	8.3	neck	nodal multidir.	1001	778	1.2866
4	7°15'39.79"S	141°37'47.65"E	4.2	conv. chute	length OL	1753	1558	1.1252
5	7°9'45.06"S	141°50'25.78"E	2.3	neck	none	967	2817	0.3433
6	7°7'44.75"S	141°52'41.80"E	4.3	neck	length OL	1386	2697	0.5139
7	7°6'20.19"S	141°56'0.32"E	8.2	conv. chute	length NOL	3479	899	3.8699
8	7°7'18.68"S	141°56'27.13"E	8.2	neck	length OL	1255	2069	0.6066
9	7°3'0.15"S	141°58'18.09"E	8.2	neck	none	2348	836	2.8086
10	7°0'23.23"S	141°58'43.28"E	8.2	neck	none	1566	584	2.6815

**Senegal River**

	Latitude	Longitude	Scroll-bar pattern	Individual cut-off style	Group cut-off style	Length (nH)	Width (pbW)	Ratio (nH/pbW)
1	16°39'32.82"N	14°47'39.23"W	8.2	neck	none	1957	867	2.2572
2	16°40'33.85"N	14°46'11.70"W	2.3	neck	none	2782	1515	1.8363
3	16°40'16.79"N	14°48'2.79"W	3.1	avulsion	avulsion	1629	1902	0.8565
4	16°40'5.50"N	14°41'54.01"W	2.3	neck	none	3782	1460	2.5904
5	16°40'7.65"N	15°8'44.02"W	3.4	w+1 chute	avulsion	1834	2799	0.6552
6	16°42'8.78"N	14°51'54.74"W	3.1	avulsion	avulsion	2469	1865	1.3239
7	16°41'48.11"N	14°50'9.88"W	5.2	avulsion	avulsion	1967	4295	0.4580
8	16°40'8.12"N	14°44'43.05"W	3.1	avulsion	avulsion	1331	971	1.3708
9	16°40'24.73"N	14°44'1.04"W	3.1	avulsion	avulsion	1339	1084	1.2352
10	16°37'50.63"N	14°39'34.54"W	4.3	avulsion	avulsion	934	874	1.0686

**Murray River**

	Latitude	Longitude	Scroll-bar pattern	Individual cut-off style	Group cut-off style	Length (nH)	Width (pbW)	Ratio (nH/pbW)
1	34°12'21.78"S	140°47'43.14"E	8.2	neck	nodal unidir.	1024	547	1.8720
2	34°11'27.02"S	140°47'22.95"E	2.2	avulsion	avulsion	1416	705	2.0085
3	34°11'49.70"S	140°48'4.08"E	8.2	unclear	nodal unidir.	970	433	2.2402
4	34°3'8.99"S	140°49'52.15"E	8.3	conv. chute	nodal unidir.	595	191	3.1152
5	34°2'44.64"S	140°50'12.48"E	3.2	neck	none	1292	514	2.5136
6	34°2'7.23"S	140°48'41.64"E	4.3	conv. chute	none	1304	1727	0.7551
7	34°2'29.53"S	140°50'41.20"E	3.2	neck	none	1093	582	1.8780
8	34°0'34.38"S	140°51'10.16"E	4.3	conv. chute	none	659	522	1.2625
9	34°0'42.95"S	140°52'15.49"E	3.3	w+1 chute	none	865	767	1.1278
10	33°59'17.57"S	140°52'1.48"E	8.2	w+1 chute	none	741	334	2.2186

**Yana River**

	Latitude	Longitude	Scroll-bar pattern	Individual cut-off style	Group cut-off style	Length (nH)	Width (pbW)	Ratio (nH/pbW)
1	71°20'16.69"N	136°8'35.84"E	2.2	neck	none	1471	560	2.6268
2	71°23'38.09"N	136°26'21.94"E	4.2	avulsion	avulsion	2318	2540	0.9126
3	71°21'31.69"N	136°24'5.95"E	4.3	neck	none	2722	1587	1.7152
4	71°16'46.84"N	136°30'7.17"E	4.2	neck	none	655	594	1.1027
5	71°16'36.88"N	136°18'46.97"E	2.3	neck	none	822	1036	0.7934
6	71°18'49.37"N	136°10'42.96"E	2.2	neck	none	705	357	1.9748
7	71°17'28.54"N	136°23'53.93"E	2.3	neck	none	823	448	1.8371
8	71°10'48.96"N	136°17'41.57"E	2.3	neck	none	989	807	1.2255
9	71°7'4.78"N	136°22'14.41"E	2.3	neck	none	1800	1058	1.7013
10	71°5'48.61"N	136°16'14.23"E	4.3	neck	none	1484	634	2.3407

## APPENDIX B

## APPENDIX B

### Colville River

	Latitude	Longitude	Scroll-bar pattern	Individual cut-off style	Group cut-off style	Length (nH)	Width (pbW)	Ratio (nH/pbW)
1	69°54'58.00"N	151°45'43.73"W	2.3	neck	none	590	546	1.0806
2	69°54'39.40"N	151°44'25.82"W	8.3	neck	none	414	153	2.7059
3	69°54'14.32"N	151°46'36.03"W	2.3	neck	length OL	670	352	1.9034
4	69°53'4.57"N	151°45'36.47"W	8.3	neck	nodal unidir.	640	340	1.8824
5	69°52'54.64"N	151°46'39.94"W	8.3	unclear	nodal unidir.	699	259	2.6988
6	69°52'54.08"N	151°47'26.62"W	8.3	neck	nodal unidir.	494	186	2.6559
7	69°51'54.54"N	151°47'12.71"W	2.2	w+1 chute	none	1030	416	2.4760
8	69°51'50.29"N	151°49'5.68"W	8.2	neck	none	440	154	2.8571
9	69°51'22.66"N	151°49'51.40"W	2.3	neck	none	536	628	0.8535
10	69°51'38.74"N	151°51'41.95"W	2.2	neck	none	663	178	3.7247

### Kuskokwim River

	Latitude	Longitude	Scroll-bar pattern	Individual cut-off style	Group cut-off style	Length (nH)	Width (pbW)	Ratio (nH/pbW)
1	60°51'41.96"N	161°12'16.13"W	3.1	neck	none	3522	1454	2.4223
2	61° 4'54.29"N	160°52'12.00"W	4.2	neck	length OL	3190	1573	2.0280
3	60°40'56.24"N	161°44'21.60"W	2.2	neck	none	3791	2967	1.2777
4	60°58'10.86"N	160°57'23.66"W	2.2	conv. chute	length OL	7655	3550	2.1563
5	61° 2'11.70"N	160°53'4.13"W	4.1	axial chute	nodal unidir.	1505	1559	0.9654
6	61° 1'58.55"N	160°55'51.75"W	2.3	axial chute	nodal unidir.	1499	2529	0.5927
7	61° 4'4.43"N	160°51'22.61"W	8.3	conv. chute	length OL	4093	1404	2.9152
8	61°14'46.30"N	160°42'20.68"W	4.2	axial chute	nodal unidir.	1533	3274	0.4682
9	61°21'42.52"N	160°45'10.86"W	2.2	w+1 chute	nodal unidir.	2270	961	2.3621
10	61°25'52.06"N	160°25'23.72"W	2.3	conv. chute	none	2886	1753	1.6463

### Mississippi River

	Latitude	Longitude	Scroll-bar pattern	Individual cut-off style	Group cut-off style	Length (nH)	Width (pbW)	Ratio (nH/pbW)
1	31°51'18.58"N	91°27'42.71"W	4.2	avulsion	avulsion	8071	4999	1.6145
2	31°54'39.81"N	91°26'49.32"W	2.3	avulsion	avulsion	9882	2865	3.4492
3	31°54'18.28"N	91°22'53.89"W	4.3	avulsion	avulsion	5262	8478	0.6207
4	31°55'39.21"N	91°20'34.90"W	4.2	avulsion	avulsion	4313	2275	1.8958
5	31°58'55.56"N	91°13'23.07"W	4.3	neck	none	6052	3971	1.5240
6	32° 3'3.97"N	91° 7'23.17"W	4.2	conv. chute	none	6809	2507	2.7160
7	31° 3'17.56"N	91°51'19.16"W	8.2	avulsion	avulsion	13032	8006	1.6278
8	31°11'42.29"N	91°53'12.30"W	2.3	conv. chute	none	8483	5309	1.5979
9	31°20'42.87"N	91°54'47.35"W	3.2	neck	length OL	9081	4402	2.0629
10	31°29'34.40"N	91°43'4.28"W	8.2	neck	none	3542	1439	2.4614

### Amazon River

	Latitude	Longitude	Scroll-bar pattern	Individual cut-off style	Group cut-off style	Length (nH)	Width (pbW)	Ratio (nH/pbW)
1	5°32'10.75"S	64° 9'11.69"W	4.2	neck	none	5475	4634	1.1815
2	5°37'27.23"S	64°17'10.76"W	4.2	neck	none	6664	4100	1.6254
3	5°47'6.70"S	64°19'35.37"W	8.2	conv. chute	length NOL	7202	2210	3.2588
4	5°32'29.86"S	63°58'26.14"W	8.2	neck	length NOL	2922	1250	2.3376
5	5°29'55.69"S	64° 1'34.16"W	3.1	avulsion	avulsion	3026	2316	1.3066
6	5°28'17.62"S	64° 4'41.94"W	8.2	neck	none	1871	822	2.2762
7	5°40'19.76"S	64°25'26.09"W	3.3	axial chute	none	2326	3627	0.6413
8	5°36'51.01"S	64°22'16.23"W	8.2	neck	none	2628	1170	2.2462
9	5°54'6.17"S	64°30'2.06"W	8.2	neck	length OL	3468	1272	2.7264
10	6° 0'27.73"S	64°22'19.55"W	4.3	neck	nodal unidir.	6069	3012	2.0149

## APPENDIX B

APPENDIX B

**Irtysh (Ob) River**

	Latitude	Longitude	Scroll-bar pattern	Individual cut-off style	Group cut-off style	Length (nH)	Width (pbW)	Ratio (nH/pbW)
1	59°11'34.22"N	68°44'51.40"E	3.3	neck	none	4150	2399	1.7299
2	59° 8'49.89"N	68°45'22.52"E	3.2	avulsion	avulsion	1527	1825	0.8367
3	59° 6'33.94"N	68°53'32.14"E	4.1	neck	none	4490	3920	1.1454
4	59° 5'55.18"N	68°46'14.77"E	3.3	conv. chute	length OL	3952	3824	1.0335
5	58°56'53.95"N	68°41'50.65"E	8.2	neck	none	6352	2161	2.9394
6	58°55'0.57"N	68°40'53.75"E	7.3	conv. chute	none	2525	2446	1.0323
7	58°50'9.25"N	68°50'52.43"E	8.2	neck	nodal unidir.	3757	1601	2.3467
8	59°13'3.86"N	68°52'0.32"E	3.1	axial chute	none	1590	1130	1.4071
9	59° 6'35.34"N	68°42'15.22"E	5.2	avulsion	avulsion	2944	1331	2.2119
10	59° 3'34.22"N	68°41'35.68"E	4.2	avulsion	avulsion	2371	2384	0.9945

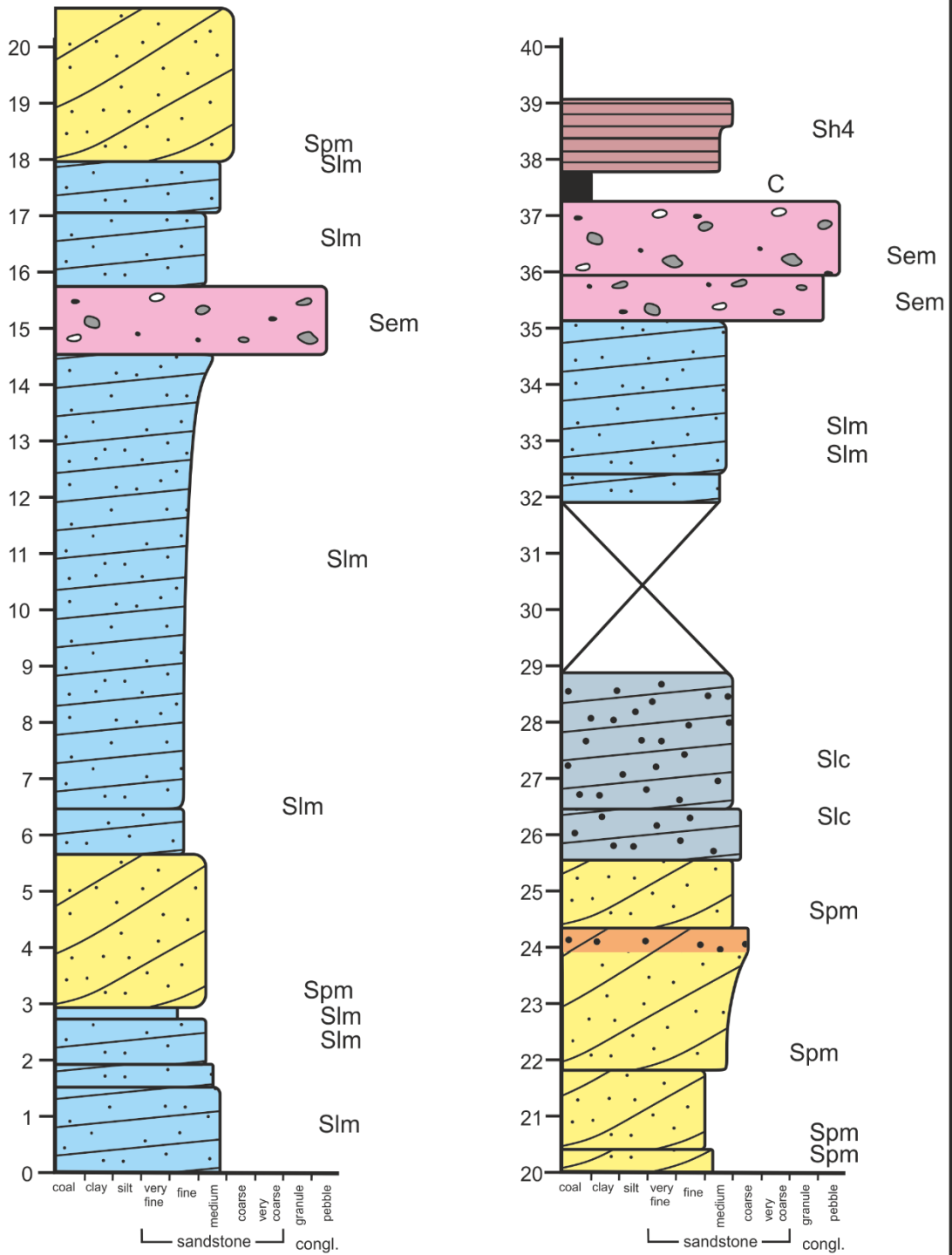
**Kolyma River**

	Latitude	Longitude	Scroll-bar pattern	Individual cut-off style	Group cut-off style	Length (nH)	Width (pbW)	Ratio (nH/pbW)
1	68°16'37.06"N	161°33'27.63"E	3.1	w+1 chute	none	1491	1019	1.4632
2	68°20'14.52"N	161°35'27.09"E	3.2	conv. chute	none	1675	934	1.7934
3	68°16'1.57"N	161°29'49.47"E	4.2	avulsion	avulsion	1171	791	1.4804
4	68°15'26.97"N	161°27'18.08"E	8.2	neck	nodal unidir.	940	668	1.4072
5	68°15'38.49"N	161°29'27.24"E	8.3	avulsion	avulsion	1005	581	1.7298
6	68°14'41.61"N	161°41'52.70"E	7.3	conv. chute	length OL	1383	1958	0.7063
7	68°15'30.33"N	161°38'42.83"E	7.3	conv. chute	none	1380	915	1.5082
8	68°15'1.54"N	161°37'17.22"E	3.2	avulsion	avulsion	1183	1138	1.0395
9	68°15'24.10"N	161°41'1.51"E	8.2	neck	none	653	185	3.5297
10	68°15'56.14"N	161°41'55.41"E	7.3	avulsion	avulsion	1456	993	1.4663

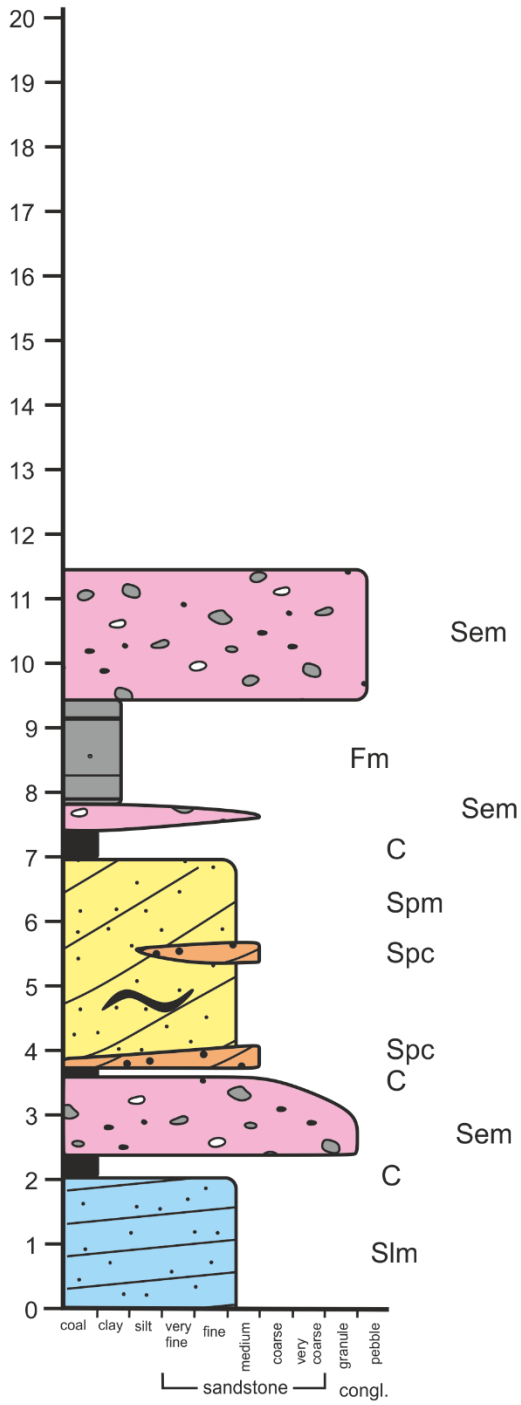
**Brazos River**

	Latitude	Longitude	Scroll-bar pattern	Individual cut-off style	Group cut-off style	Length (nH)	Width (pbW)	Ratio (nH/pbW)
1	30° 1'11.44"N	96° 6'18.51"W	8.2	neck	length NOL	990	259	3.8224
2	30° 4'18.23"N	96° 8'49.99"W	8.2	neck	nodal unidir.	763	366	2.0847
3	30° 6'45.34"N	96° 9'58.28"W	8.2	neck	nodal unidir.	936	415	2.2554
4	29°50'33.53"N	96° 4'5.78"W	5.2	neck	nodal multidir.	874	563	1.5524
5	29°50'31.79"N	96° 4'54.46"W	8.2	neck	nodal multidir.	784	455	1.7231
6	29°50'45.31"N	96° 5'56.95"W	8.2	neck	nodal multidir.	599	216	2.7731
7	29°51'23.33"N	96° 5'51.48"W	3.1	conv. chute	nodal multidir.	487	435	1.1195
8	29°53'56.01"N	96° 6'22.60"W	3.4	conv. chute	nodal unidir.	418	498	0.8394
9	30°10'24.59"N	96°10'3.25"W	8.2	conv. chute	nodal unidir.	1417	706	2.0071
10	30°11'9.60"N	96°10'16.25"W	2.3	neck	nodal unidir.	566	1011	0.5598

# LOG 1.1



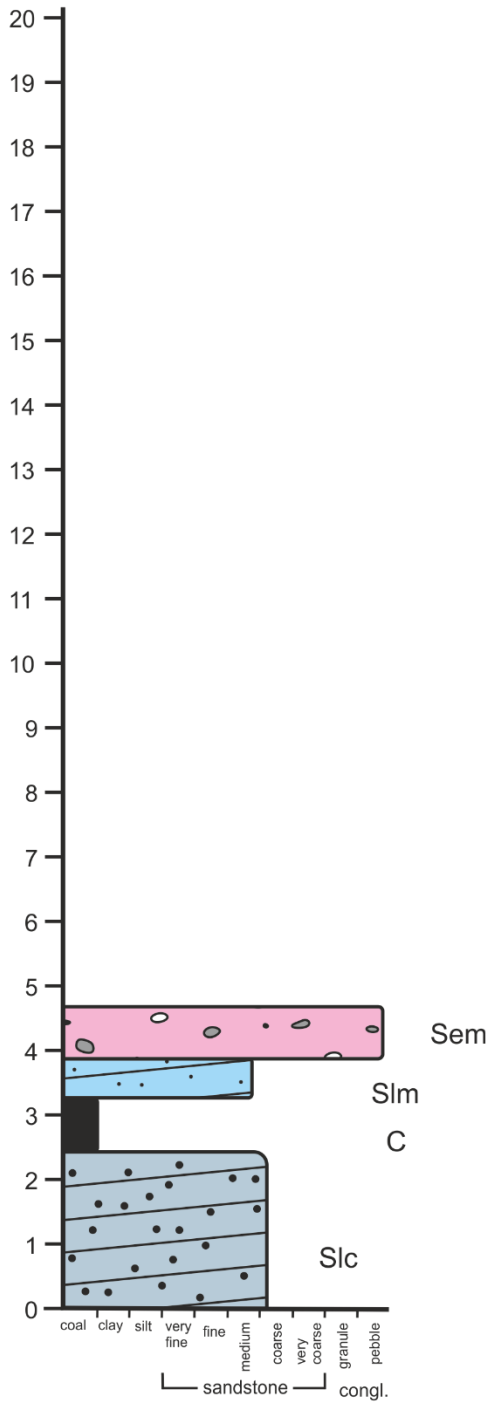
# LOG 1.2



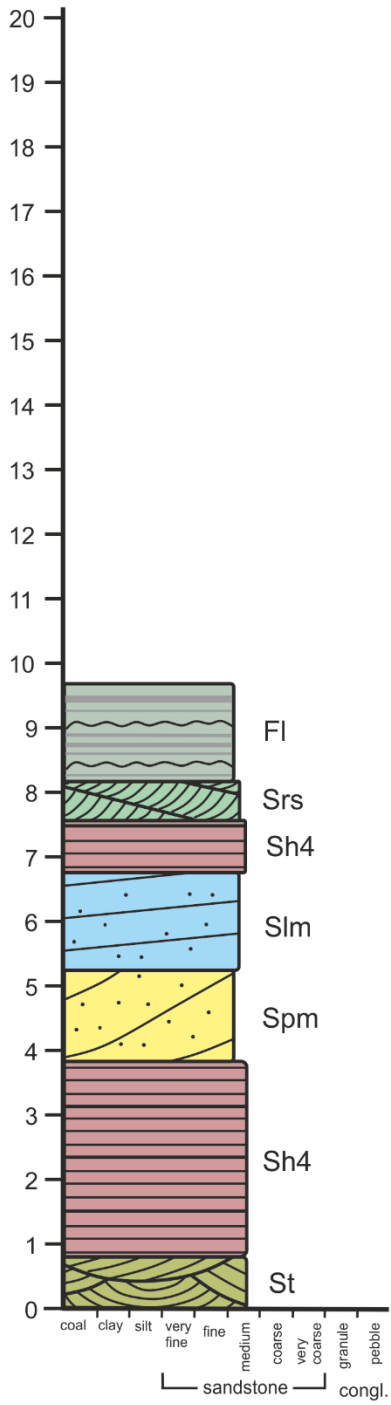


APPENDIX C

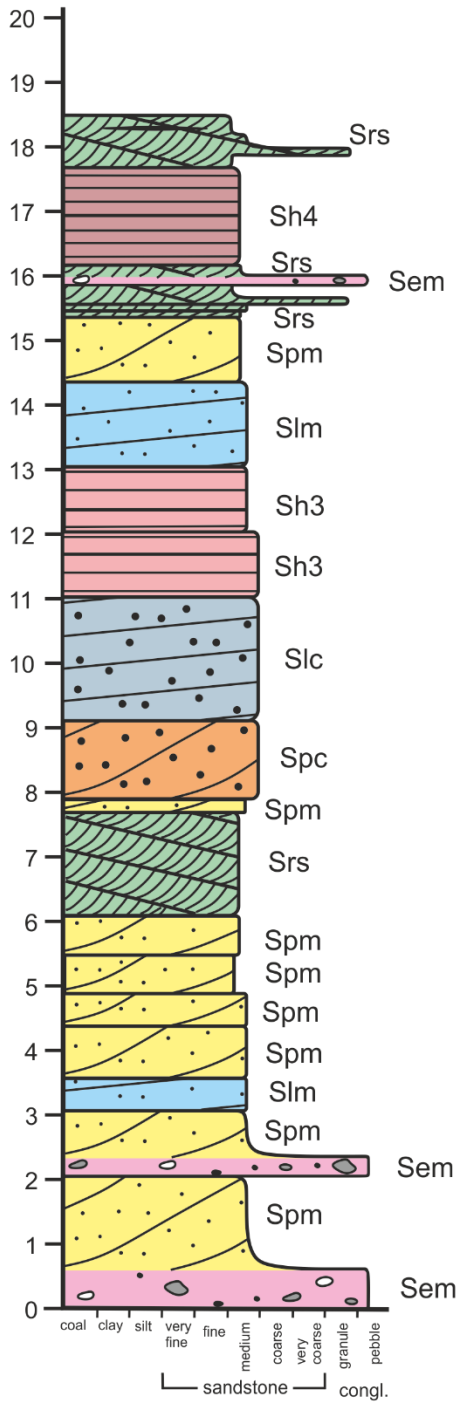
# LOG 1.3



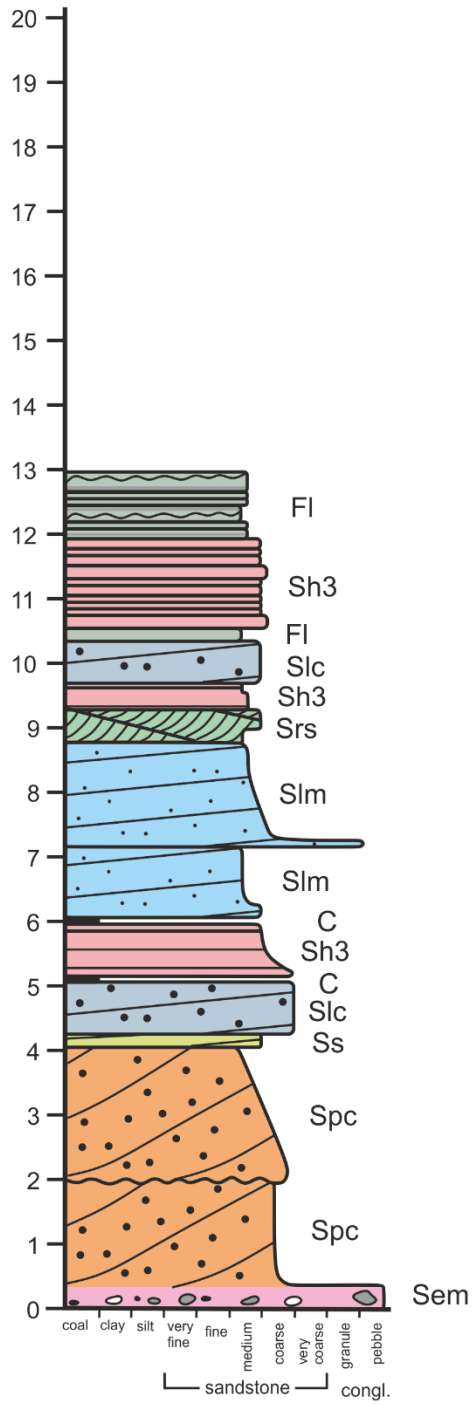
# LOG 2.0



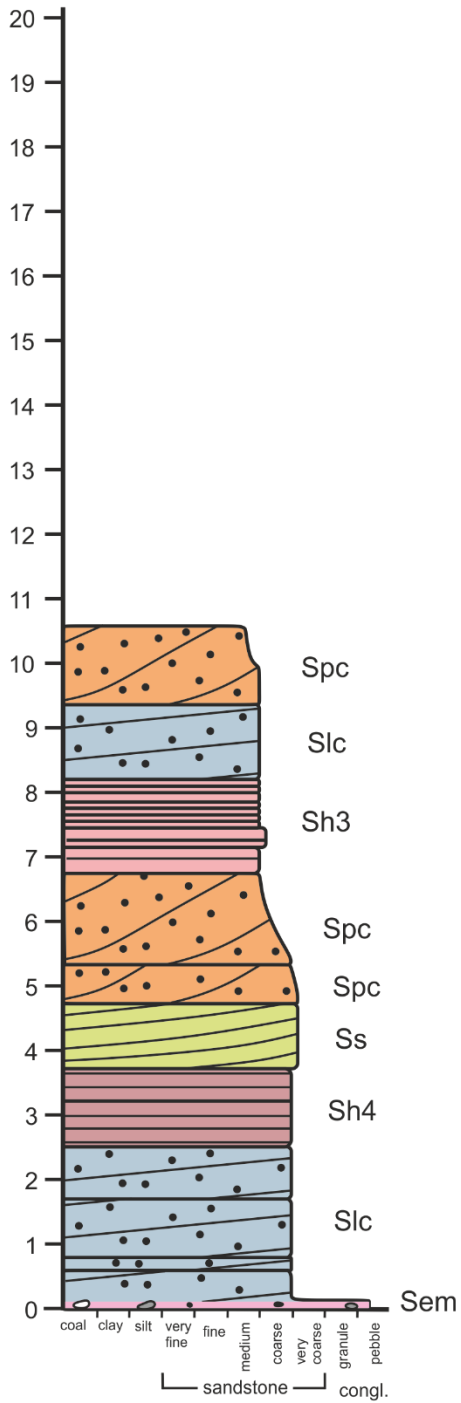
# LOG 2.1



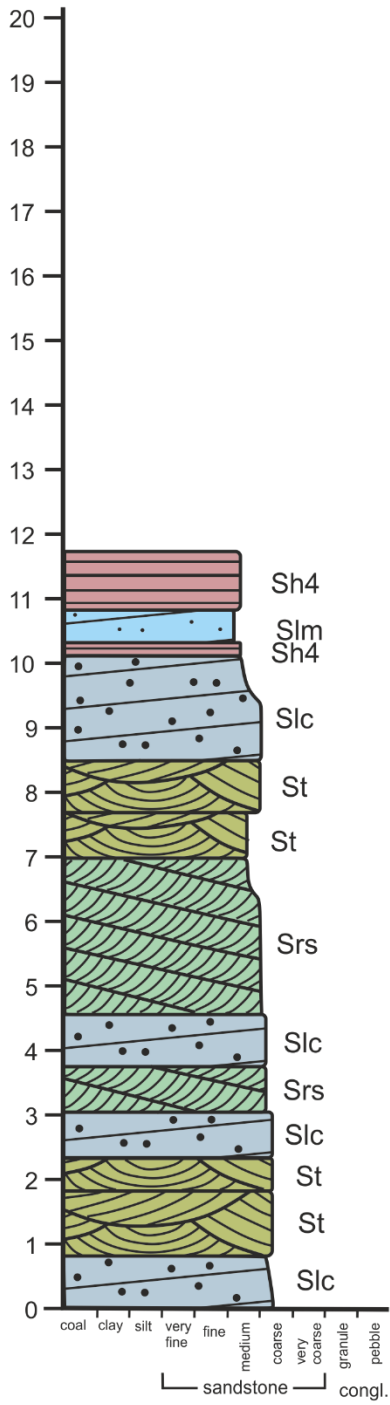
# LOG 2.2



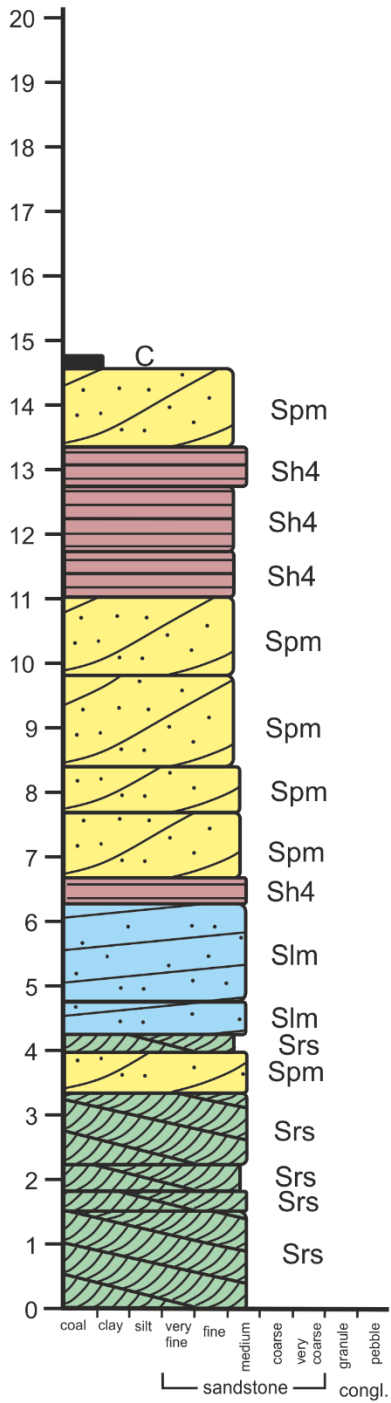
# LOG 2.3a



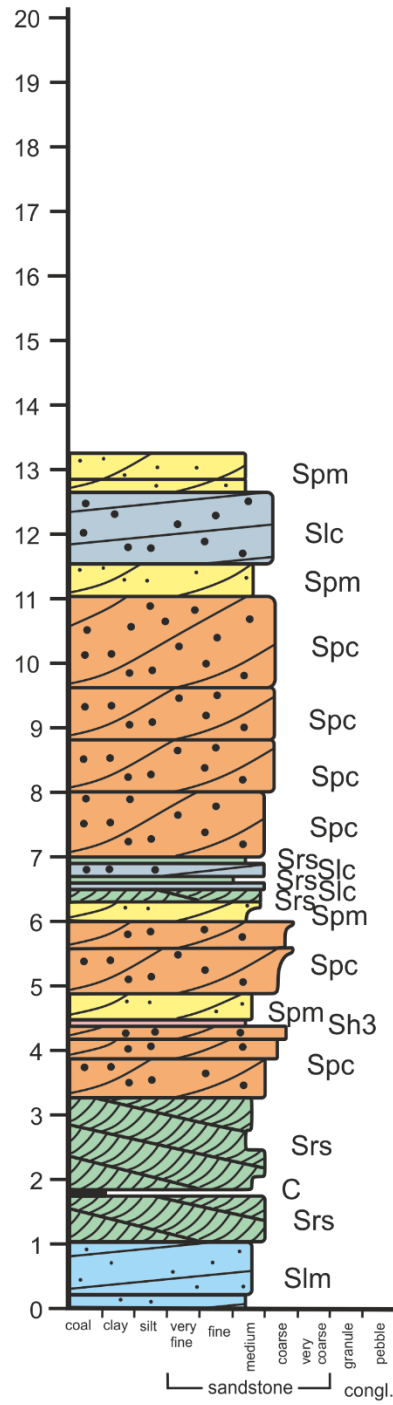
# LOG 2.3b



# LOG 3.1

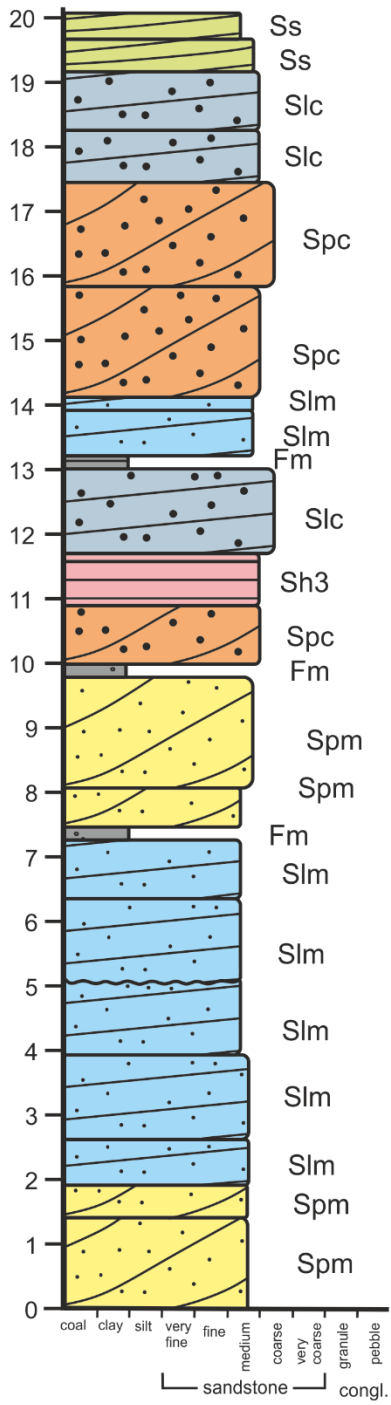


# LOG 3.2

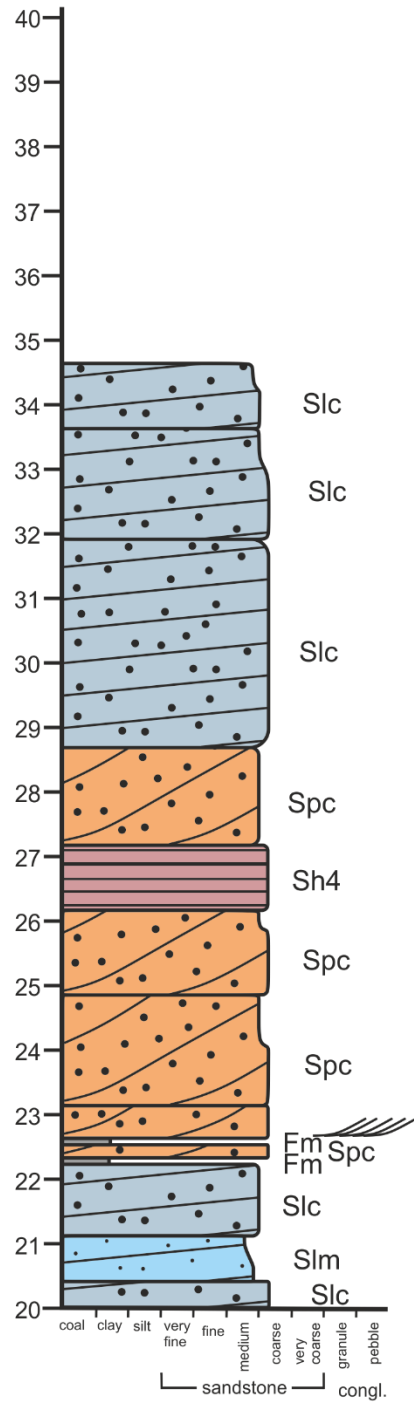
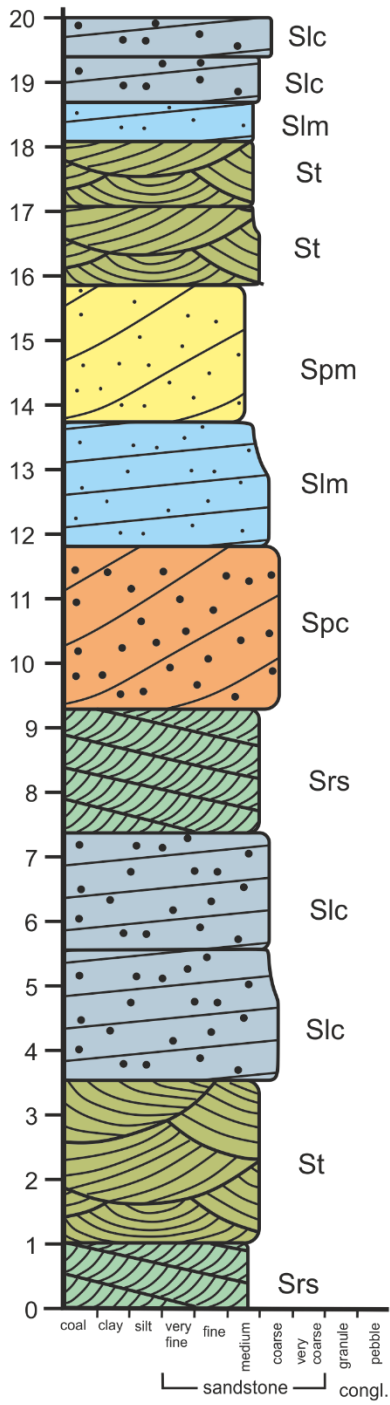




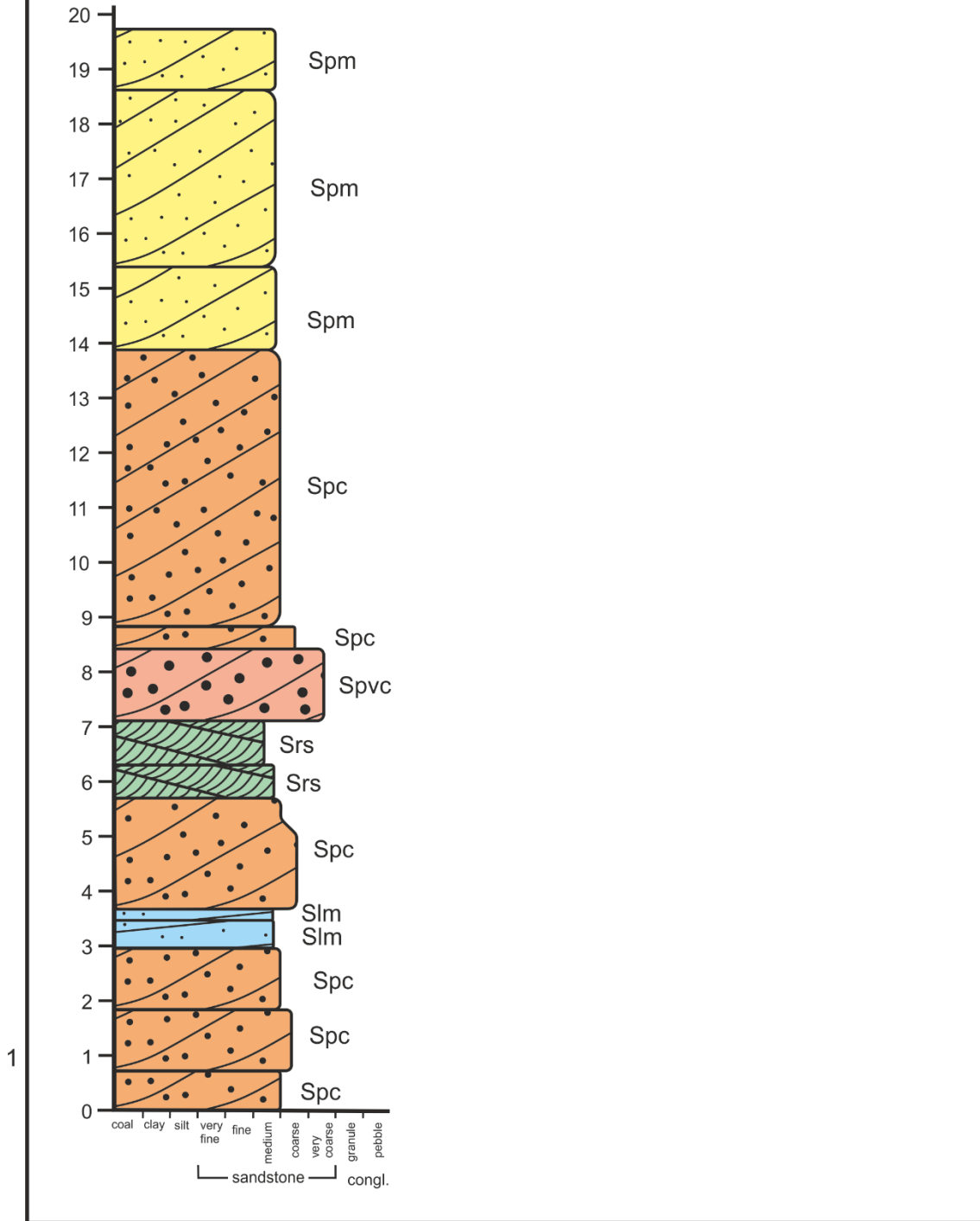
# LOG 4.0



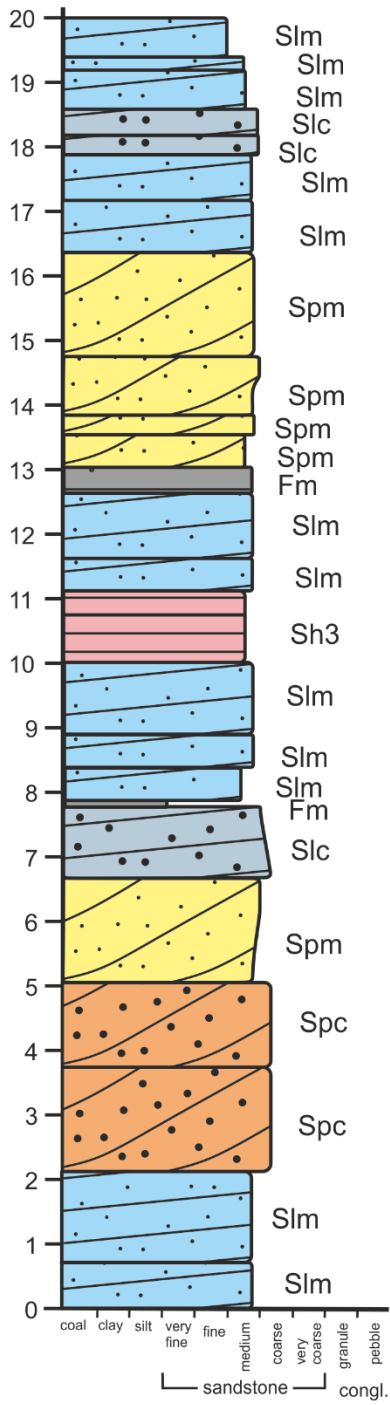
# LOG 4.1



# LOG 4.2

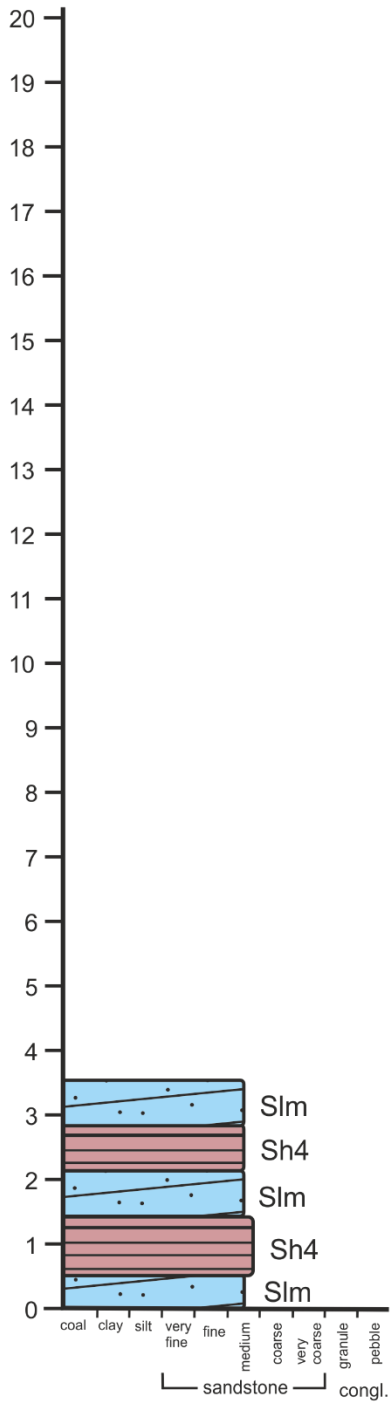


# LOG 5.0

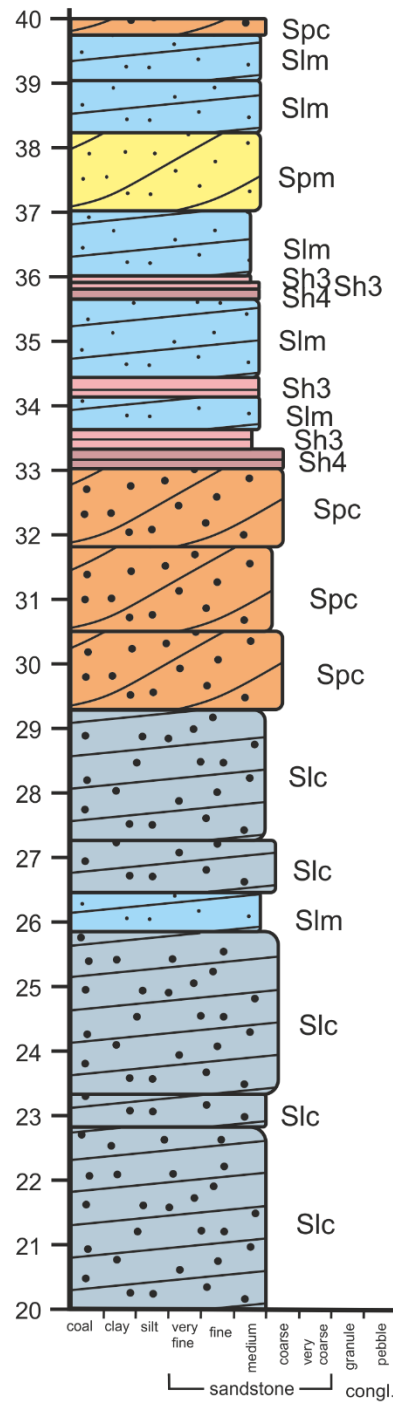
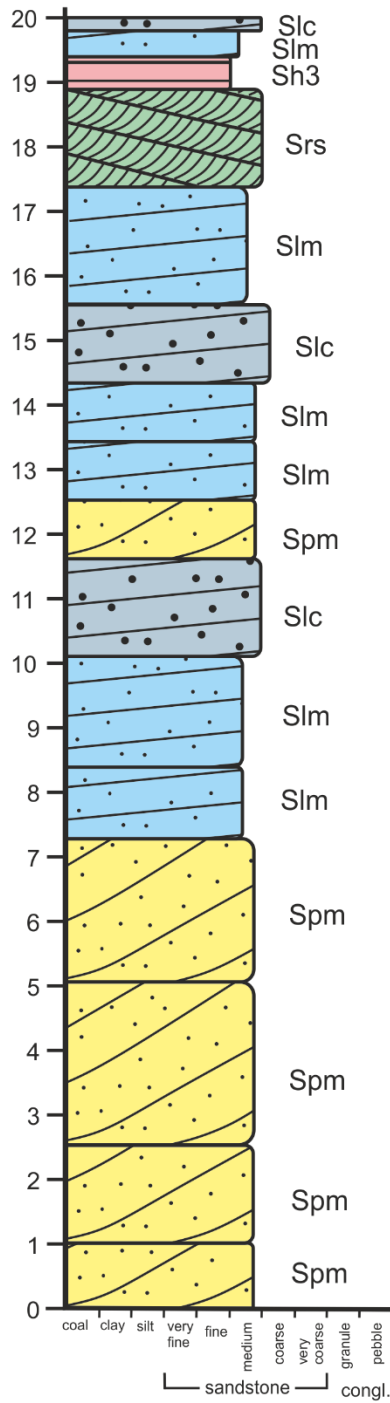


APPENDIX C

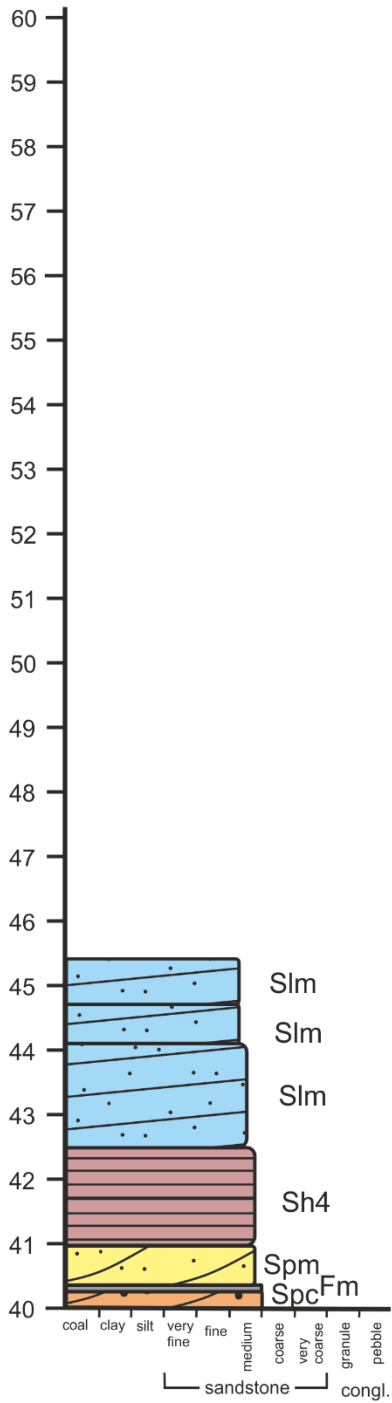
# LOG 5.1b



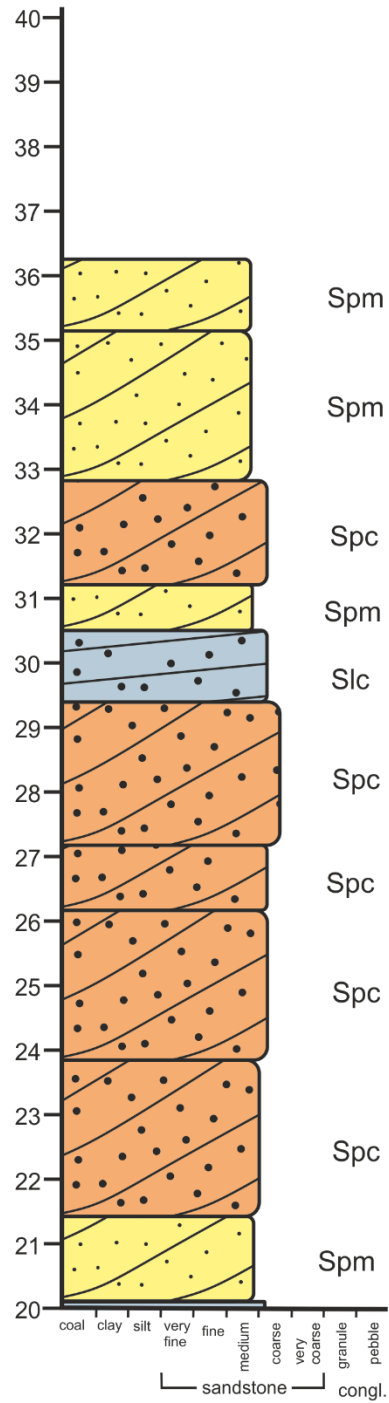
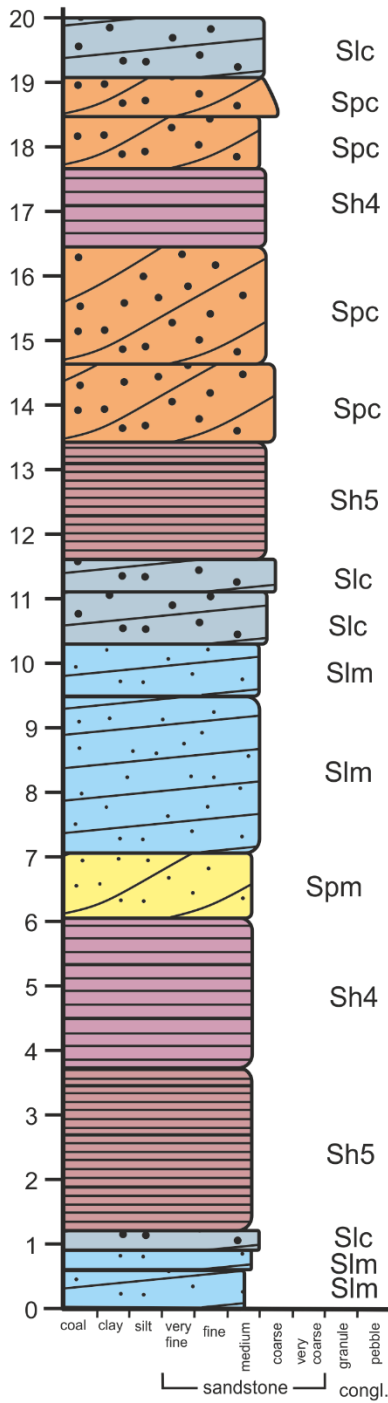
# LOG 5.1 (part 1)



# LOG 5.1 (part 2)

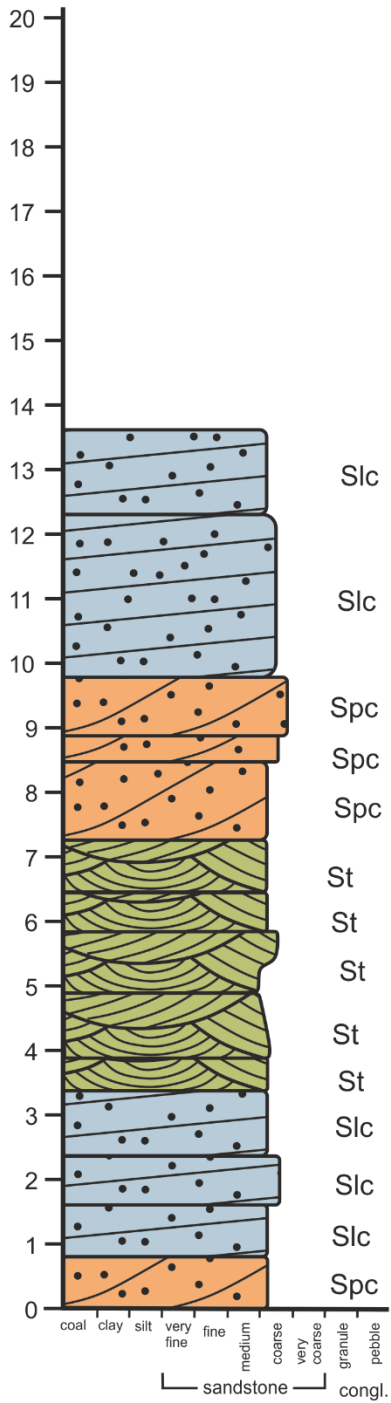


# LOG 5.2

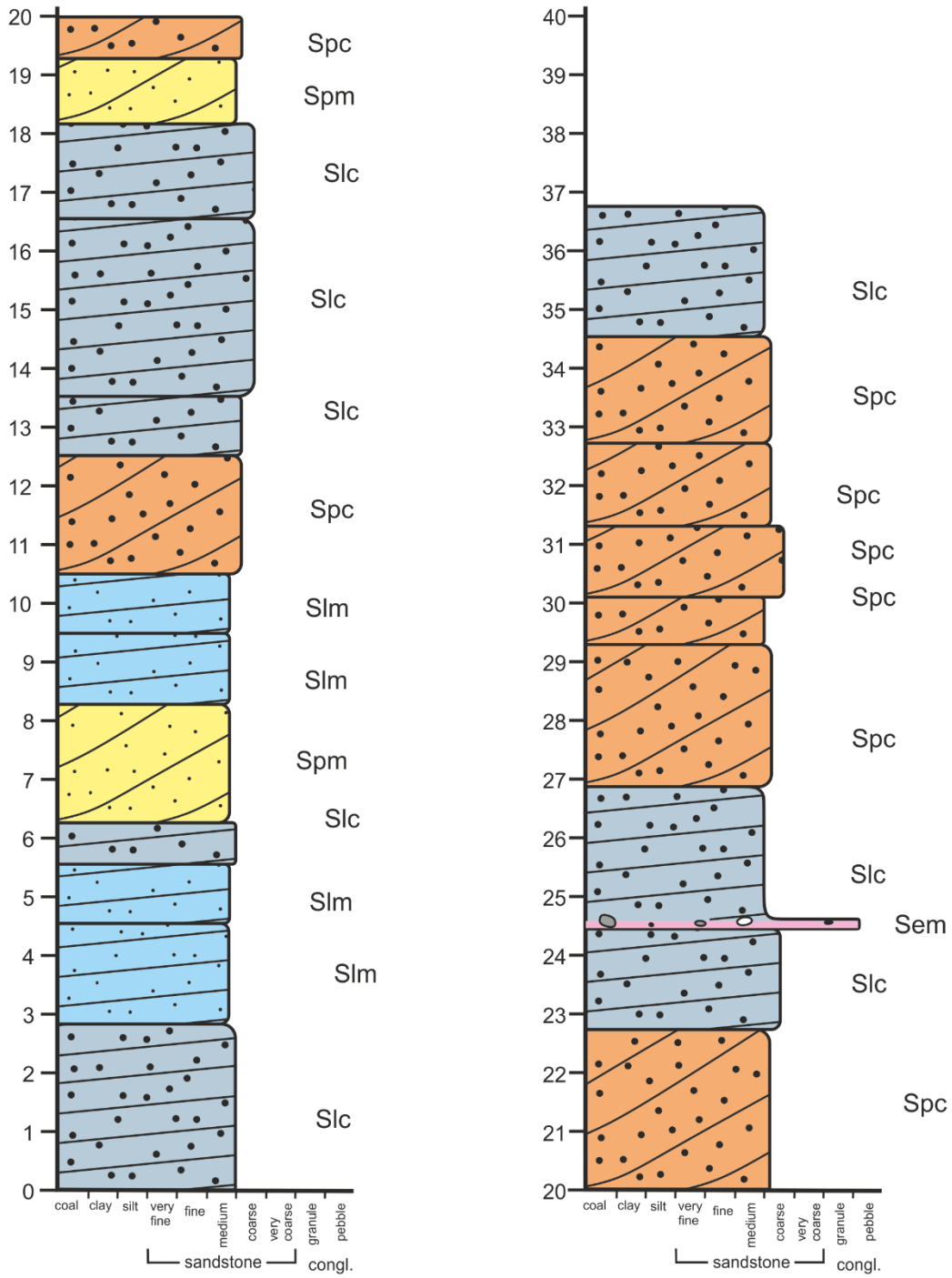




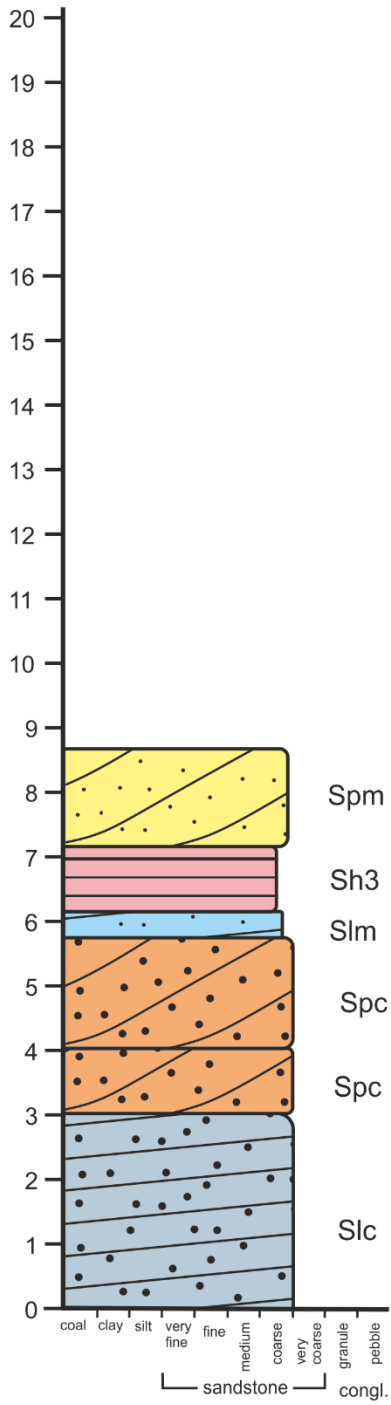
# LOG 5.2b



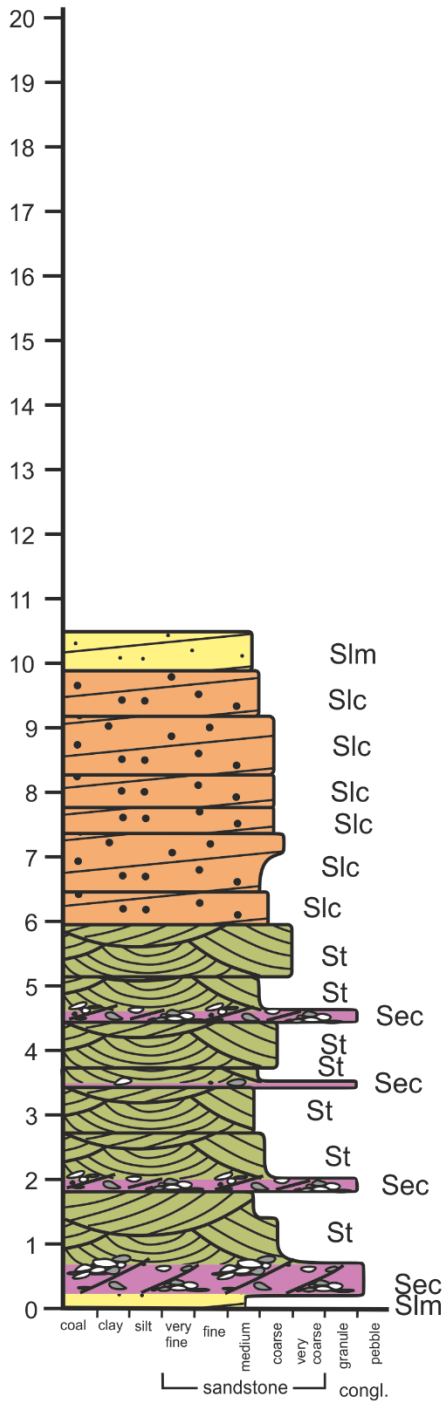
# LOG 5.3a



# LOG 5.3b

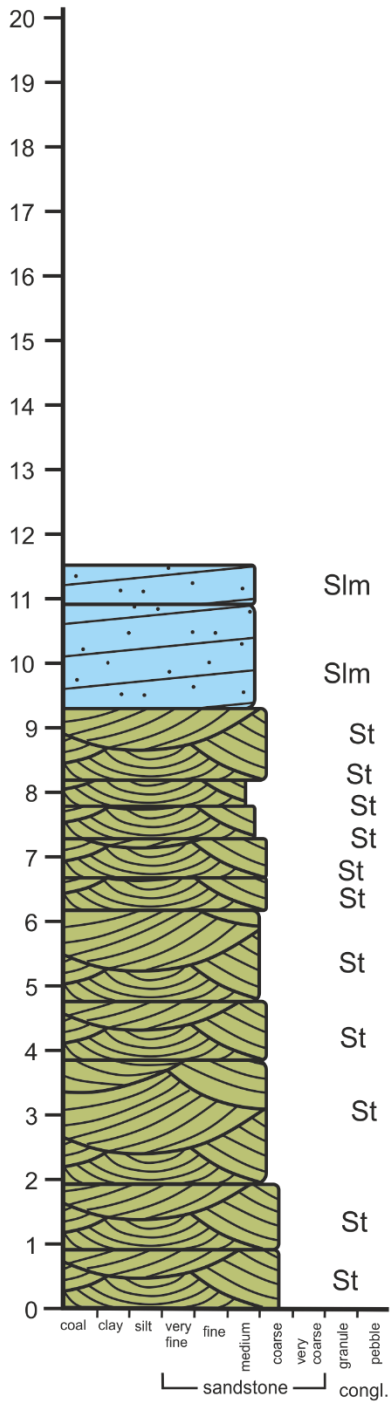


# LOG 6.1



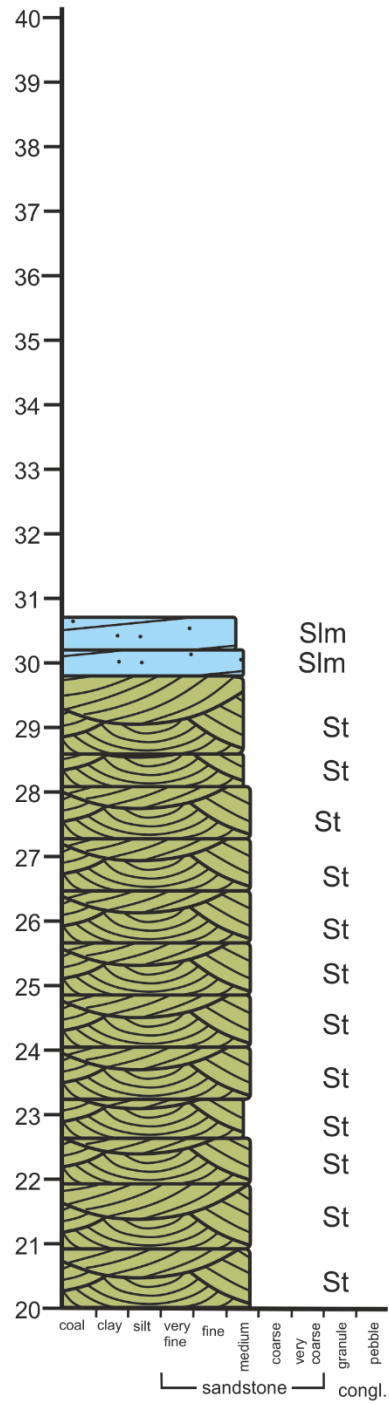


# LOG 6.4

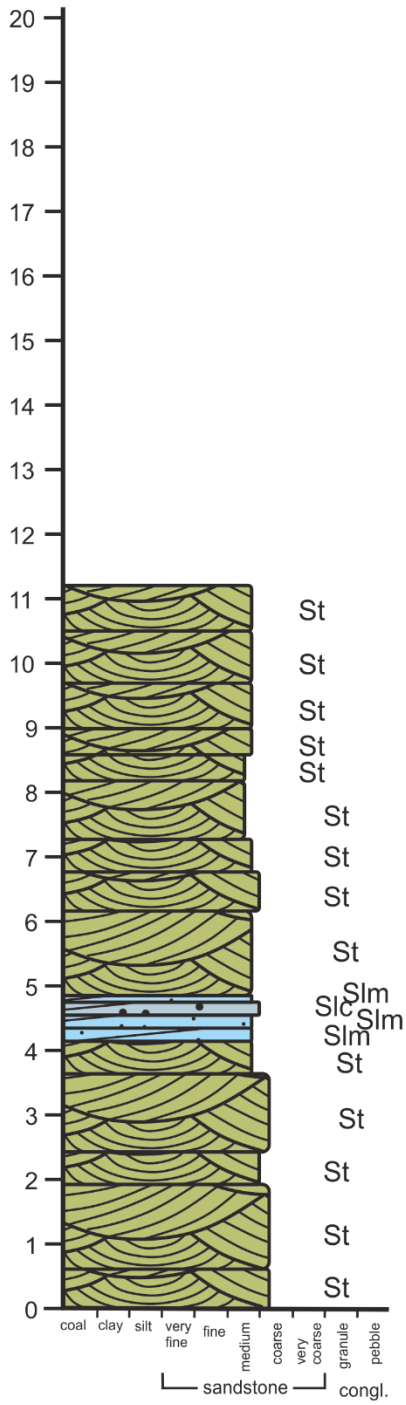


APPENDIX C

# LOG 6.7

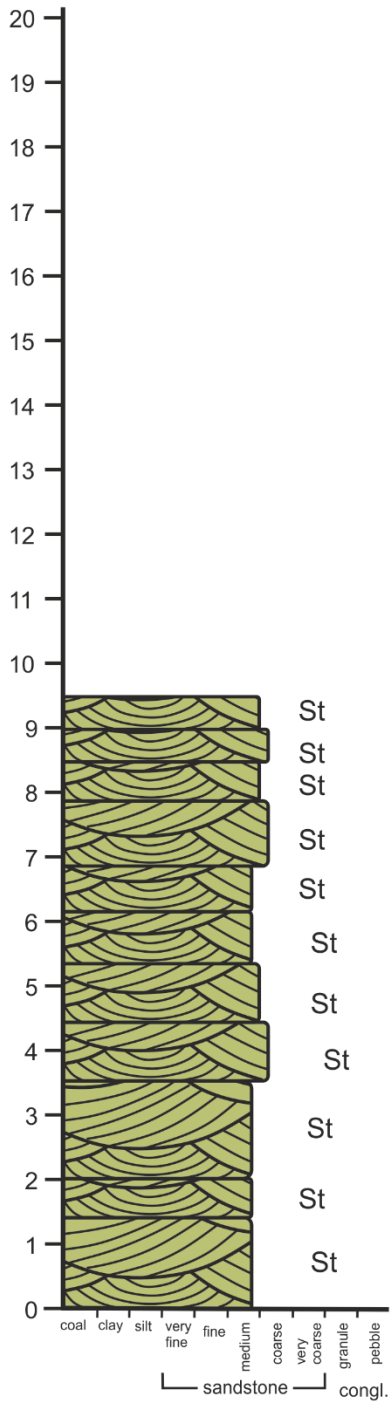


# LOG 6.9

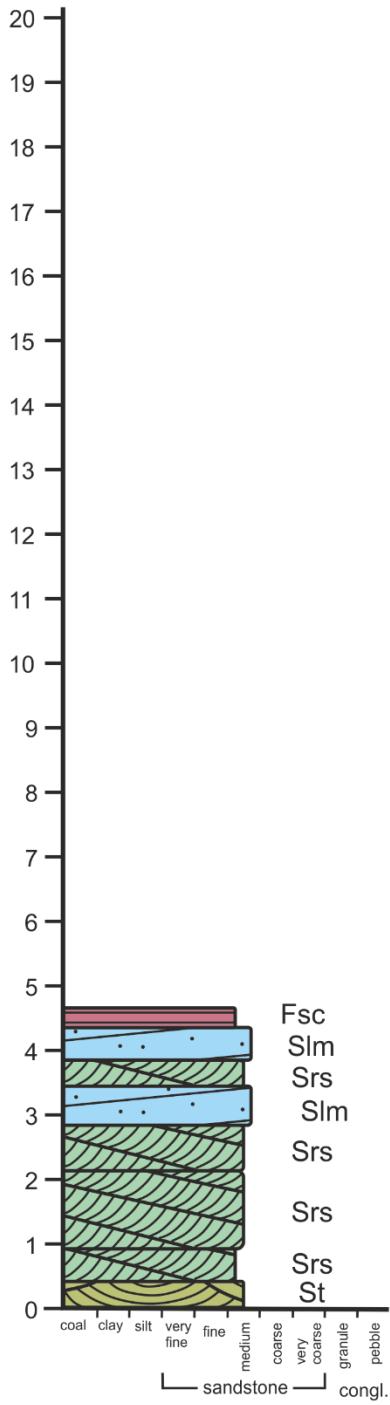




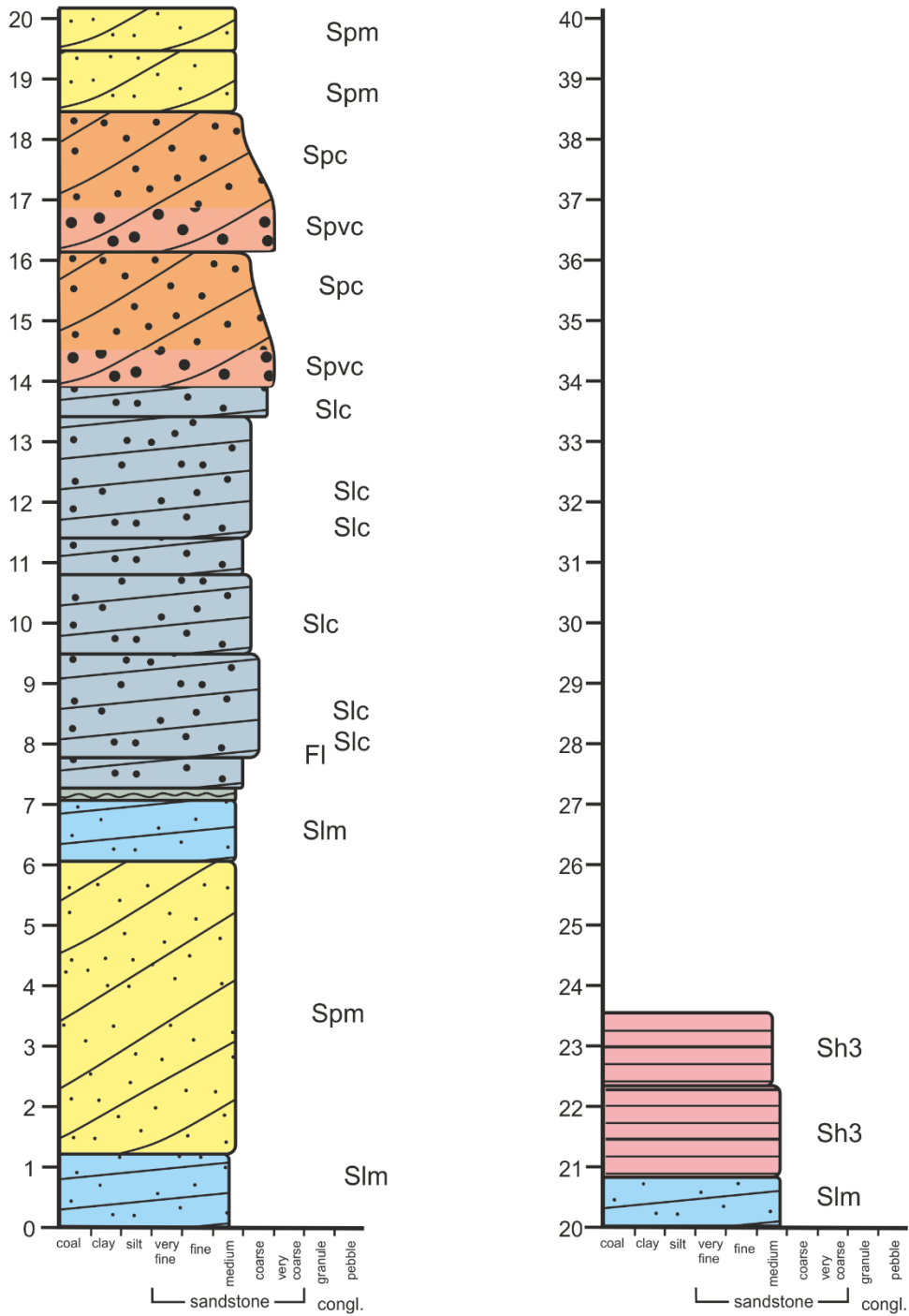
# LOG 6.11



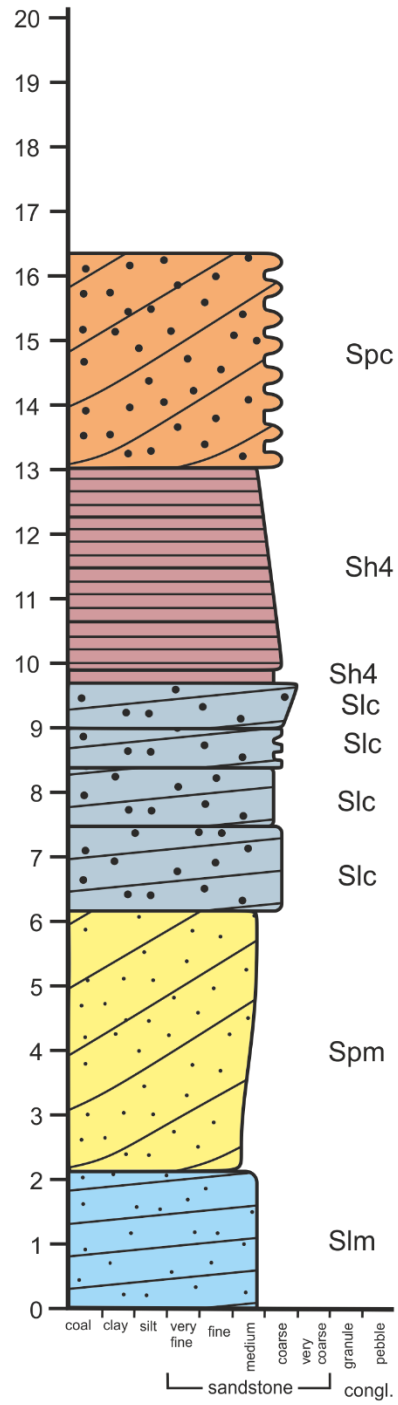
# LOG 6.12



# LOG 7.1a

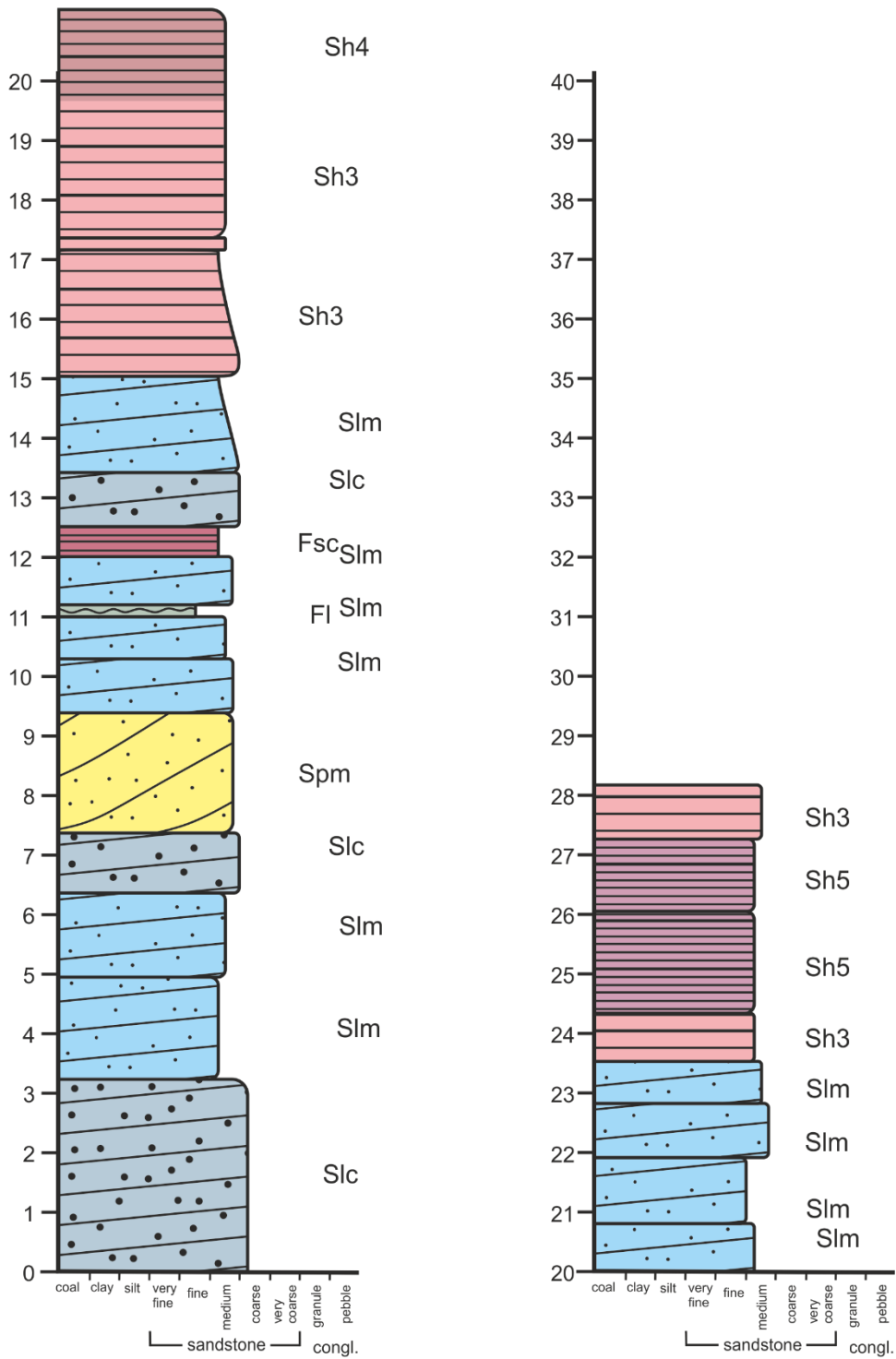


# LOG 7.1b

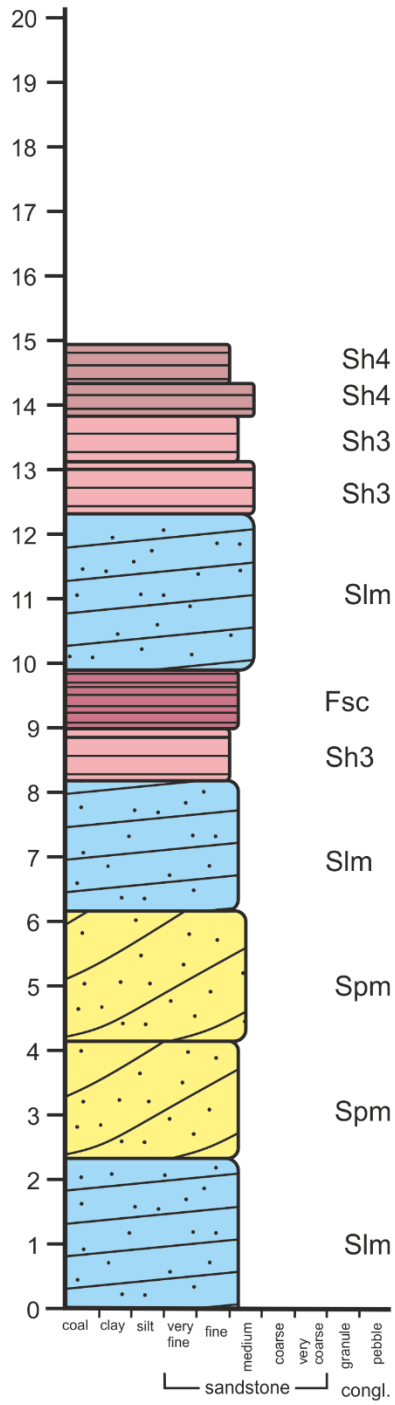


APPENDIX C

# LOG 7.2

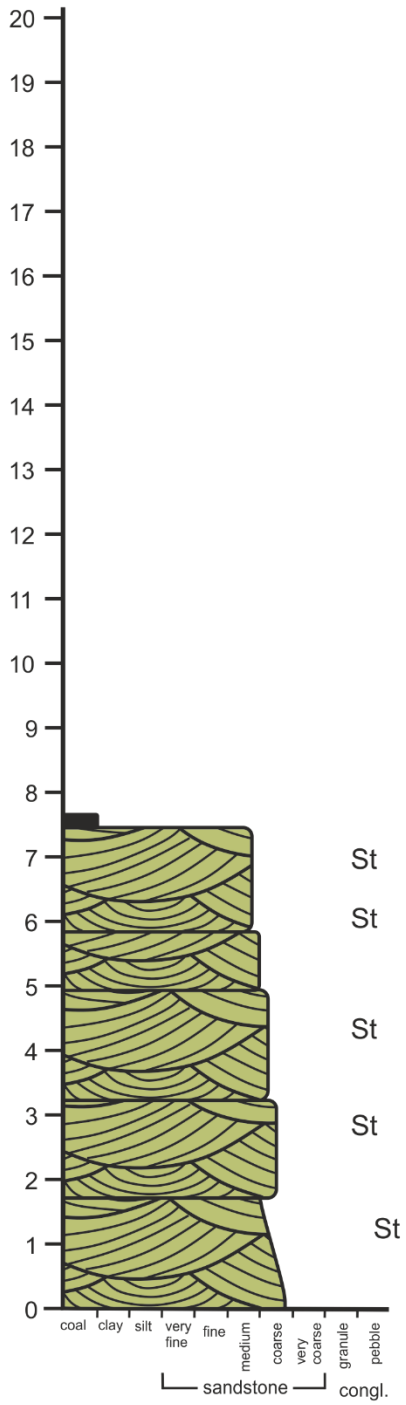


# LOG 7.3

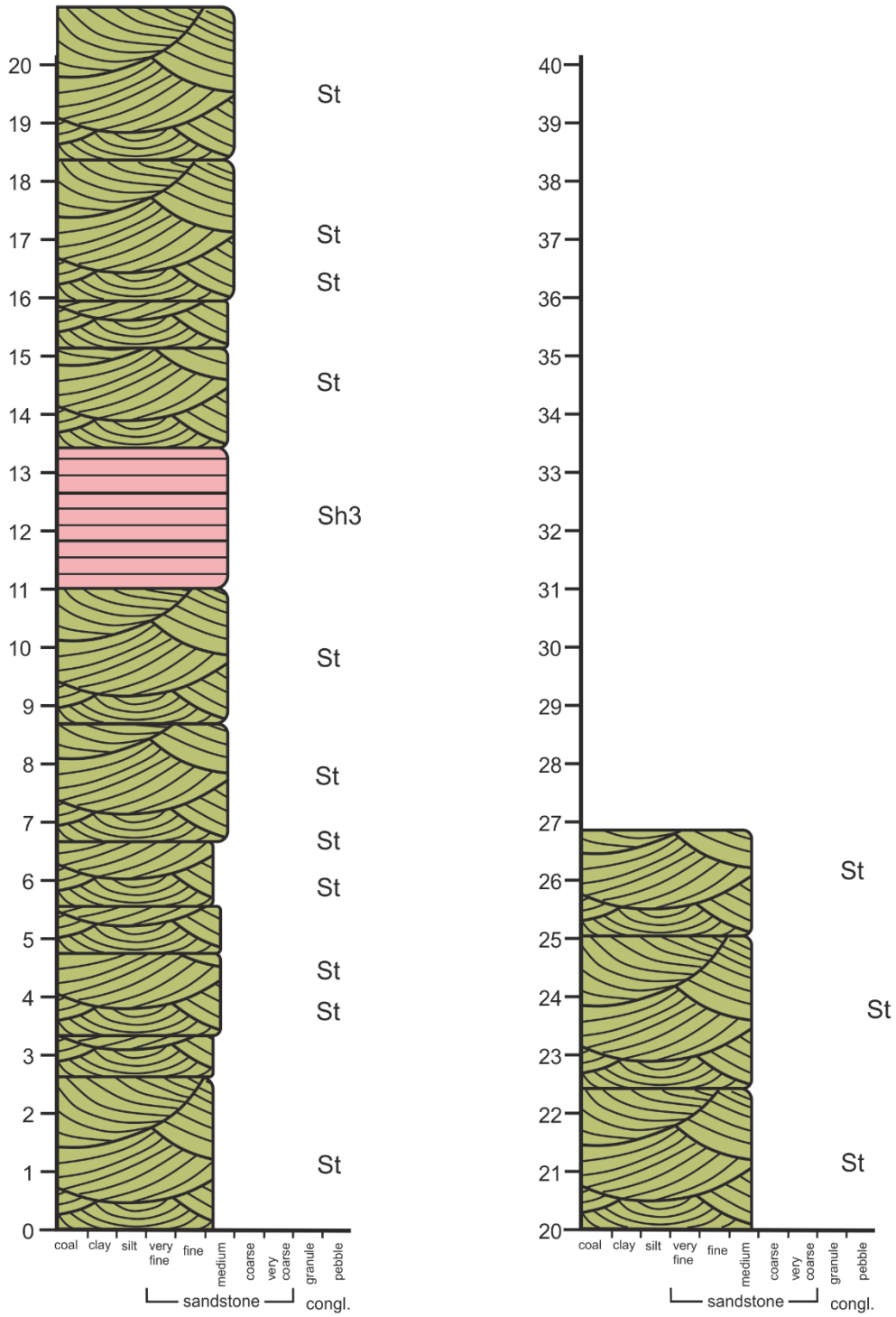


APPENDIX C

# LOG 8.0



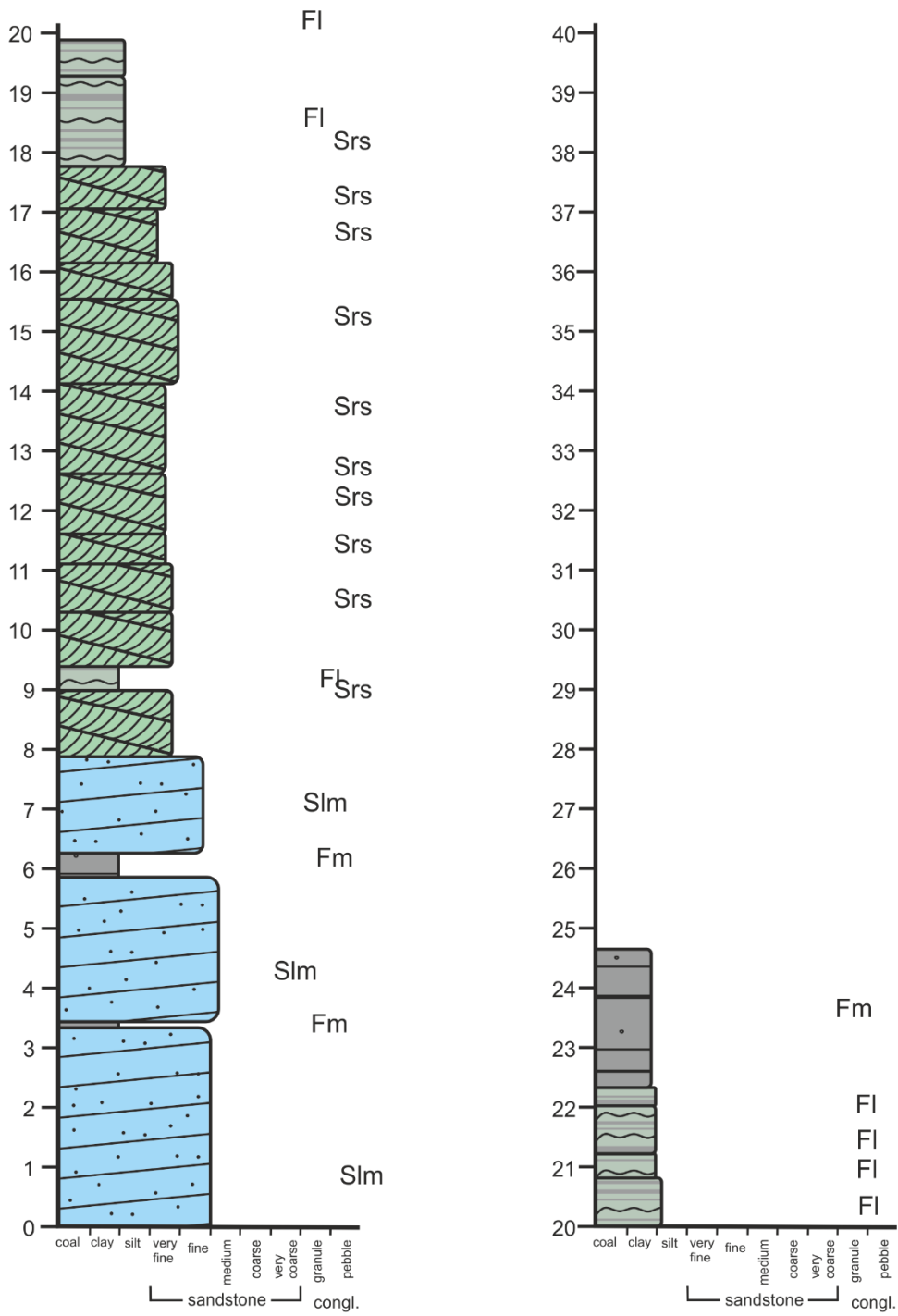
# LOG 8.1



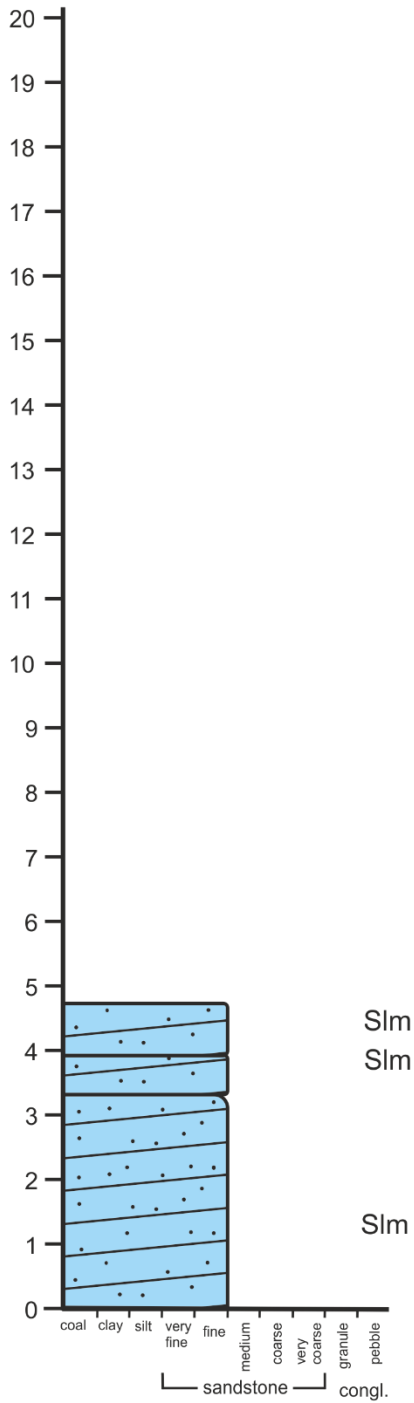


APPENDIX C

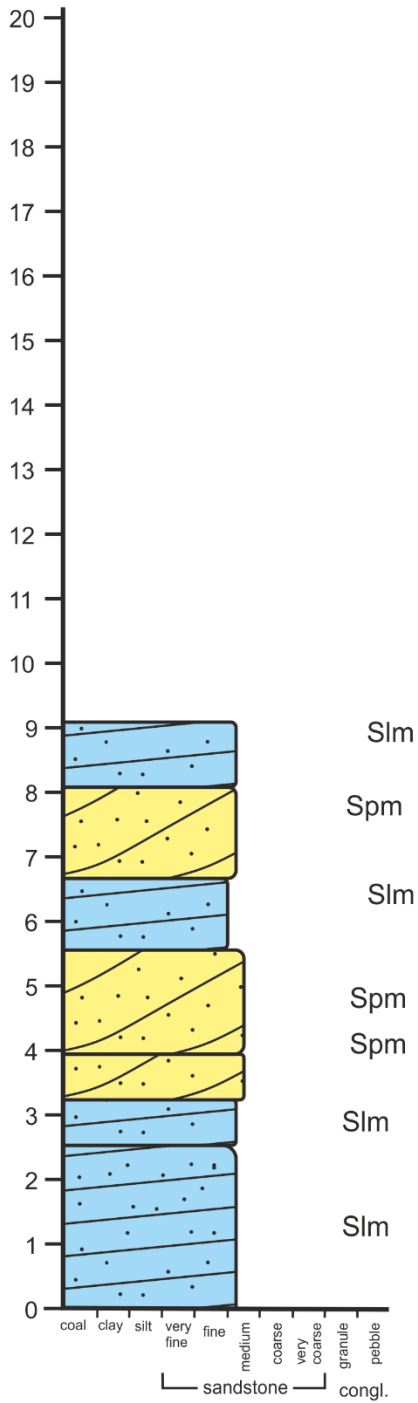
# LOG 8.2



# LOG 8.3 R1



# LOG 8.4 R2



# LOG 8.5 R3

